AN INVESTIGATION INTO THE LINK BETWEEN ANOMALOUS PGE CONCENTRATIONS AND CHROMITE COMPOSITION IN CHROMITITES WITHIN OPHIOLITES

Christopher Paul Brough

Submitted in partial fulfilment of the requirements for the degree of Ph.D.

May 2011

UMI Number: U567105

All rights reserved

INFORMATION TO ALL USERS
The quality of this reproduction is dependent upon the quality of the copy submitted.

In the unlikely event that the author did not send a complete manuscript
and there are missing pages, these will be noted. Also, if material had to be removed,
a note will indicate the deletion.

UMI U567105
Published by ProQuest LLC 2013. Copyright in the Dissertation held by the Author.
Microform Edition © ProQuest LLC.
All rights reserved. This work is protected against
unauthorized copying under Title 17, United States Code.

ProQuest LLC
789 East Eisenhower Parkway
P.O. Box 1346
Ann Arbor, MI 48106-1346

DECLARATION

This work has not previously been accepted in substance for any degree and is not concurrently submitted in candidature for any degree.

Signed ..... (candidate)
Date 06/06/2011

STATEMENT 1

This thesis is being submitted in partial fulfilment of the requirements for the degree of Ph.D.

Signed ..... (candidate)
Date 06/06/2011

STATEMENT 2

This thesis is ~~being~~ the result of my own independent work/investigation, except where otherwise stated

Signed ..... (candidate)
Date 06/06/2011

STATEMENT 3

I hereby give consent for my thesis, if accepted, to be available for photocopying and for inter-library loan, and for the title and summary to be made available to outside organisations.

Signed ..... (candidate)
Date 06/06/2011

Soli Deo Gloria

Abstract

Platinum-group element (PGE) concentrations within podiform chromitites in ophiolites may be extremely erratic, with reported totals varying from below detection limit to several 10s of ppm. This study has investigated three ophiolites, with previously identified high PGE concentrations, to test three main questions; (1) whether there is a link between the geochemistry of the chromite within the chromitites and the associated PGE concentrations of those chromitites, (2) what the presence, or absence, of a link reveals about the mechanism of PGE concentration and therefore (3) why some chromitite pods are highly PGE-enriched. The three ophiolites are located near Al 'Ays in Saudi Arabia, Unst and Fetlar on the northernmost of the Shetland Islands and Berit in south-central Turkey.

Within the Al 'Ays ophiolite there is a link between the chromite composition of chromitite and the PGE concentration. In this ophiolite, a plot of Cr# vs. Mg# can be used to distinguish both the high-PGE chromitites as well as the likelihood of the high-PGE chromitites being relatively enriched in IPGE or PPGE (i.e. containing high or low (Pt + Pd)/Ir)). The link exists because changes in chromite composition and the onset of sulphur saturation are both caused by fractionation, where fractionation is defined as the cumulative effects of the separation of chromite and olivine crystals from the melt, and melt-rock reaction.

In contrast to the Al 'Ays ophiolite, the chromitite samples from the Shetland ophiolite show little geochemical variation. However, both the IPGE-rich chromitites at Harold's Grave and the PPGE-rich chromitites (and dunites) at Cliff display distinctive geochemical characteristics. The PPGE-rich Cliff chromitite deposit is shown to display several complex geochemical trends, one of which contains both the PPGM-rich dunite samples and the PPGE-rich chromitite samples. This key trend is decreasing Cr# with increasing TiO_2. Within Shetland this trend is unique to the Cliff chromitite pod and is interpreted as the product of localized fractionation by water immiscibility leading eventually to sulphur saturation and PGE-enrichment. The IPGE-rich Harold's Grave chromitites contain elevated trace element (TiO_2, V_2O_5 & Zn) values and lower Mg#. The evolved geochemistry of the Harold's Grave deposit, together with the large dunite pod, suggest that the IPGE enrichment has been caused by prolonged reaction with trapped intercumulus melt where chromite has acted as a collector for IPGE, producing an IPGE-rich chromitite deposit.

Within the Berit ophiolite no link between chromite major and trace element geochemistry and PGE concentration has been found, but it was observed that PPGE enrichment was only associated with chromitites containing Cu-bearing sulphides. This was also found in Al 'Ays and Shetland suggesting that PPGE enrichment is dependent upon the separation of Cu-bearing sulphides from melts rising through the mantle. This observation, together with the different textural associations of the IPGM and PPGM previously reported from all three ophiolites, and the apparent independence of IPGE from sulphide saturation, suggests that IPGE and PPGE enrichment may be decoupled processes within ophiolites. A further insight from the Berit ophiolite is the observation of exsolution textures within chromite grains, which extends the miscibility gap previously reported.

For all three ophiolites, variations in chromitite major and trace element geochemistry occur on several different scales. At the smallest scale, single thin sections of chromite may sometimes display large variations in composition. At the next scale, intrapod chemical variation can be extensive, though predominantly displaying an inverse correlation between Cr# and Mg#. Finally, interpod variation, and its relationship to stratigraphic height, changes a great deal between ophiolites, sometimes providing an apparently continuous change with height (e.g. Al 'Ays) and in other places (e.g. Shetland) varying discontinuously with height. These differences can provide important clues to the processes controlling chromite composition. They suggest that multiple controls may sometimes be involved including, the number of phases crystallizing, post-solidus re-equilibration, fractionation, melt-rock reaction and volatile unmixing.

Acknowledgements

I would like to first say a big thank you to my supervisors Hazel Prichard, Chris Neary and Julian Pearce for their help and advice over the past 3 and a half years. In particular, a huge debt of gratitude is owed to Chris Neary for coming out of retirement to co-supervise the project and for making a huge amount of time and resources available towards its completion, as well as to Hazel Prichard for pertinent advice throughout the course of the PhD.

Many people must be thanked for their help with sample collection. In particular, Bob Finch and Gary Keech are thanked for providing repeated access to the Al 'Ays samples housed at Leeds University. For the Shetland ophiolite sample collection thanks go to Hazel Prichard for providing a detailed tour of the ophiolite as well as providing access to samples collected from previous thesis investigations. Thanks also go to my wife Sarah for help in all of the Shetland fieldwork. For the Berit ophiolite thanks goes to Hatice Kozlu and Aydin Goklaglu for providing access and time towards the collection of samples and to the kindness of the local farmer who provided food and water when we were lost and directions towards the Dereagzi chromitite quarry (which providentially he initially discovered).

Data collection would have been impossible without the help of Peter Fisher (on the SEM) and Iain McDonald (on the Laser ICP-MS) who efficiently and patiently helped me throughout all my questioning and mistakes. Lawrence Badham and Peter Greatbatch are also gratefully acknowledged for the numerable polished thin sections and polished blocks that they produced – often under short notice. Genalysis are thanked for their whole-rock PGE analyses. Andy Tindle from the OU is also gratefully acknowledged for his help on their electron microprobe and for answering numerous questions in the aftermath.

My colleagues Kerry Howard, Caroline Johnson, Matthew Minifie and Iain Neill, and latterly Jake Ciborowski and Rhian Jones are gratefully thanked for their kindness to me and for many pertinent talks related to the project. This project is indebted to detailed conversations with Caroline Johnson on all things chromite and to Iain Neill for help with the vagaries of Scottish tectonics. Thanks also go to the original 'Rolling Stones' football team (Tom Gregory, James Griffiths, Matthew Minifie, Ben Rabb, Luca Traverso and Ivan Westley) and latterly to Scott Butler for organising the squash, both of which provided a welcome break from the thesis.

All those at Highfields are gratefully acknowledged for their love and support, particularly Hugo Cosh, Hugh and Maddie Saunders, Adam Fairman, Geoff and Jo Cresswell, and Saturday football. Thanks also go to Tamar Pollard and the 5-2-6 crew (of all ages) for controlled insanity and great fun on a Friday evening.

The natural environmental research council (NERC) are gratefully acknowledged for funding the project as are the mineral deposits studies group (MDSG) and the 11th International Platinum Symposium (IPS) who provided additional travel grants to attend conferences.

My Mum and Dad are thanked for their unquestioning love and support over numerous years, as are Chris and Elaine Dunstone in more recent times.

As well as assisting in the fieldwork my wife Sarah has been a source of unceasing support, kindness, love and patience over many years. You have, as ever, all my love.

Table of Contents

List of Figures

List of Tables

Chapter 1

Literature Review

An overview of the main theories surrounding ophiolite origin, the generation of their chromitite deposits and their associated PGE concentrations.

Aims and scope of project

Chromitite deposits, whether stratiform or podiform, nearly always contain increased concentrations of platinum-group elements relative to their host silicate rocks. Within ophiolitic chromitite deposits the level of upgrading is highly unpredictable and currently poorly understood. The aim of this research is to investigate the following;

1. The variation in chromite geochemistry across an ophiolite, focusing on intrasample, intrapod and interpod scales and whether there is a common link between magmatic chromite geochemistry and bulk PGE concentrations in all or only some ophiolites?
2. What the presence, or absence, of a link reveals about the mechanism of PGE mineralization? For example, if there is a link, is it due to a mutually dependent relationship or to both variables being dependent on another variable (e.g. degree of mantle melting).
3. Why some pods are highly PGE enriched and others very close by are not?

1 Literature Review

1.1 Introduction

The term 'ophiolite' derives from the Greek *ophis*, meaning snake or serpent. The first monograph on the rock-associations of an ophiolite were mentioned as early as 1821 by Brongniart who described the now classical four-fold association of ultrabasics, gabbros, spillites and chert (Amstutz, 1980). This was further developed by Steinmann (1856-1929) who suggested their origin as 'differentiated magmatic rocks evolved on the ocean floor' (Dilek 2003a & references therein). The term 'ophiolite' now relates to terrestrial fragments of oceanic lithosphere emplaced at fossil constructive margins. The evolution of thought with respect to ophiolite analogues within the ocean crust can be divided into three main periods (Pearce, 2003). For the first (1963-1972) all ophiolites were thought to be terrestrial analogues of mid-ocean ridge oceanic crust, and this culminated in the development of the 'Penrose' type ophiolite (Figure 1.1) in 1972.

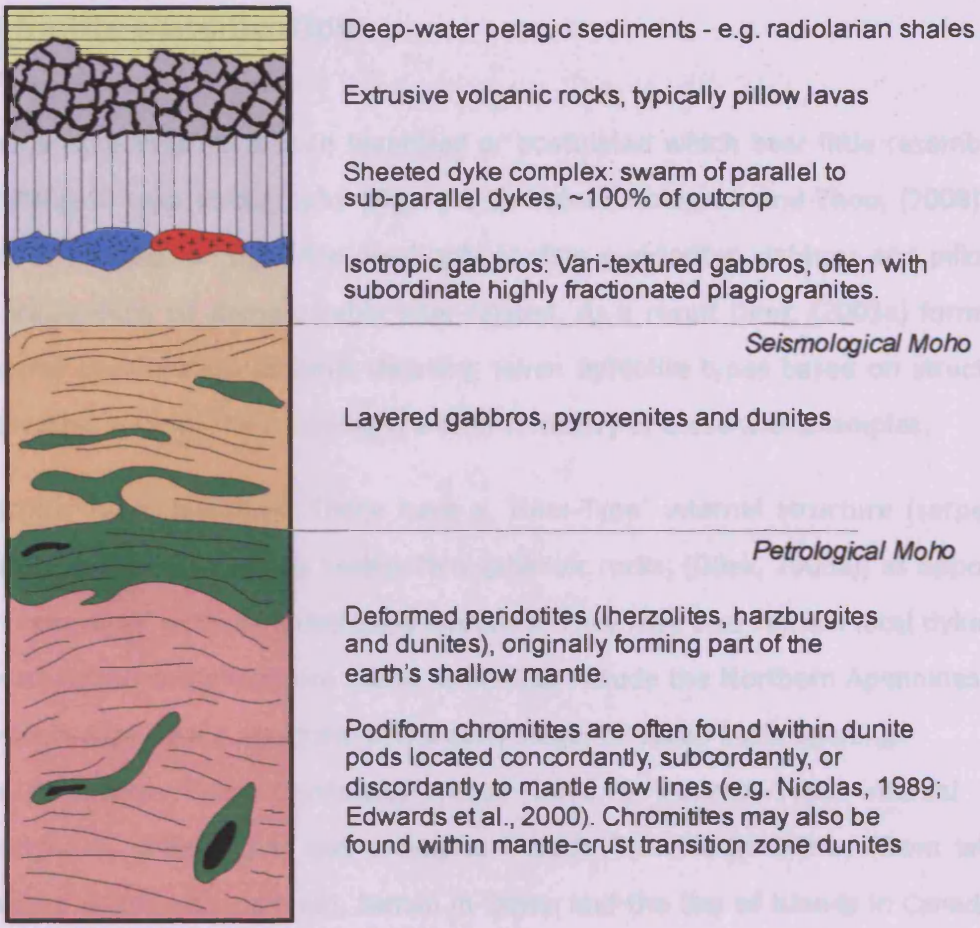

Figure 1.1: *Idealised stratigraphic column of an ophiolite ('Penrose Type', Anonymous, 1972).*

For the second period (1972-1984), there was a paradigm shift away from mid-ocean ridge analogues to the view that the majority of ophiolites were formed above subduction zones (either fore-arc or back-arc type oceanic lithosphere), and these were subsequently termed supra-subduction zone (SSZ) ophiolites (Pearce, 2003). This view, that most ophiolites are SSZ related, has been reinforced by the identification of boninites and island arc volcanic material located within such bodies. Nevertheless, it is apparent that several ophiolites contain no evidence of an influence from subduction related fluids. These were more appropriately considered remnants of intra-continental basins which have been telescoped on land during orogenic activity (e.g. Tribuzio *et al.*, 2004), rather than fully developed mid-ocean ridges. The third period (since 1984) has focused on exactly how SSZ and intra-continental ophiolites form, and what, if any, are their modern analogues.

1.2 Ophiolite classification

Today, many ophiolites have been identified or postulated which bear little resemblance to the ideal Penrose type stratigraphy (Figure 1.1); indeed Robinson and Zhou, (2008) suggest that to be convincing, an ophiolite need only contain peridotites, gabbros and pillow lavas, and that these must be demonstrably inter-related. As a result Dilek, (2003a) formulated a new ophiolite classification scheme, detailing seven ophiolite types based on structure and inferred tectonic setting. The following is a brief summary of these with examples.

i) *Ligurian Type Ophiolites:* These have a 'Hess-Type' internal structure (serpentinised peridotite capped by lavas and/or thin gabbroic rocks, (Dilek, 2003a)) as opposed to a 'Penrose-type' pseudostratigraphic structure. They may also contain local dykes but no sheeted dyke complexes are found. Examples include the Northern Apennines and the Western Alps. These may form in the early stages of ocean basin opening.

ii) *Mediterranean Type Ophiolites:* These have a Penrose-Type internal pseudo-stratigraphy (Figure 1.1) and examples include Troodos in Cyprus (from which the Penrose model was derived), Semail in Oman and the Bay of Islands in Canada. These ophiolites may form in a wide range of tectonic settings from intra-oceanic subduction beneath mid-ocean ridges, to subduction influenced oceanic spreading centres.

iii) *Sierran Type Ophiolites:* These have complex, multi-stage evolutionary paths, and typically occur around the Pacific Rim (e.g. Japan, Philippines, and Cuba). They may contain 'volcanic, plutonic and hypabyssal rocks and locally well developed dyke swarms.' Tectonically, they represent island arc ophiolites, with older oceanic basement and overlying younger volcanic arc assemblages.

iv) *Chilean Type Ophiolites:* The type locality for these are the Rocas Verdes ophiolites in South America. These contain 'mafic volcanic rocks (2-3 km thick) composed of pillow lavas and volcanic breccias, a sheeted dyke complex (300-500m thick), massive diabase and coarse grained gabbros. Tectonically they represent ophiolites formed in extensional back-arc basins. These are different from Mediterranean type ophiolites due to MORB type signatures in the volcanic rocks, and relative autochthoneity in their current location. They are different from Sierran type ophiolites because they don't possess a polygenetic evolution, that is - the basement is no older than the crustal region.

v) *Macquarie Type Ophiolite:* This is a unique 'ophiolite', located within the Southern Ocean at Macquarie island. This island represents oceanic crust, which has been uplifted due to transpressional deformation at the Australian-Pacific plate boundary. Although similar to the Penrose type pseudostratigraphy, and uplifted, this 'ophiolite' has not yet been emplaced on a continental margin and thus its status as an ophiolite is a moot point.

vi) *Caribbean Type Ophiolites:* These represent oceanic crustal assembleges of Large Igneous Provinces (LIP), with the Caribbean ophiolites being the best examples. The internal structures of these are highly heterogeneous, but may contain the main ophiolitic subunits (e.g. pillow lavas, layered gabbros, gabbronorites). Sheeted dyke complexes appear to be missing.

vii) *Franciscan Type Ophiolites:* These are 'associated with accretionary complexes of active margins.' They consist of a complicated intercalation of melanges and high pressure metamorphic (blueschist) rocks and may also contain abyssal peridotites, gabbros and basalts. The high pressure rocks may be exhumed though either erosion of the forearc thrust front at a subduction zone or as a result of 'syn-subduction extensional collapse of the accretionary complex.

1.3 Ophiolite obduction

The obduction or emplacement of an ophiolite occurs during closure of either the continental rift basin or the subduction zone, usually during orogenic activity. Stern (2004) reviewed obduction mechanisms for ophiolites and concluded that most ophiolite fragments on land were supra-subduction related. He provided a comparison between the feasibility of obduction of back-arc ophiolites, fore-arc ophiolites and mid-ocean ridge or incipient intra-continental oceanic crust (Figure 1.2). The exception to the difficulty of emplacing MORB ophiolite is when the initial rifting of intra-continental basins is still incipient, and the resultant uplifted mantle is still warm. In this scenario the intra-continental basin (a modern analogue being the red sea), becomes incorporated into the orogenic event. Ligurian type ophiolites are a good example of this.

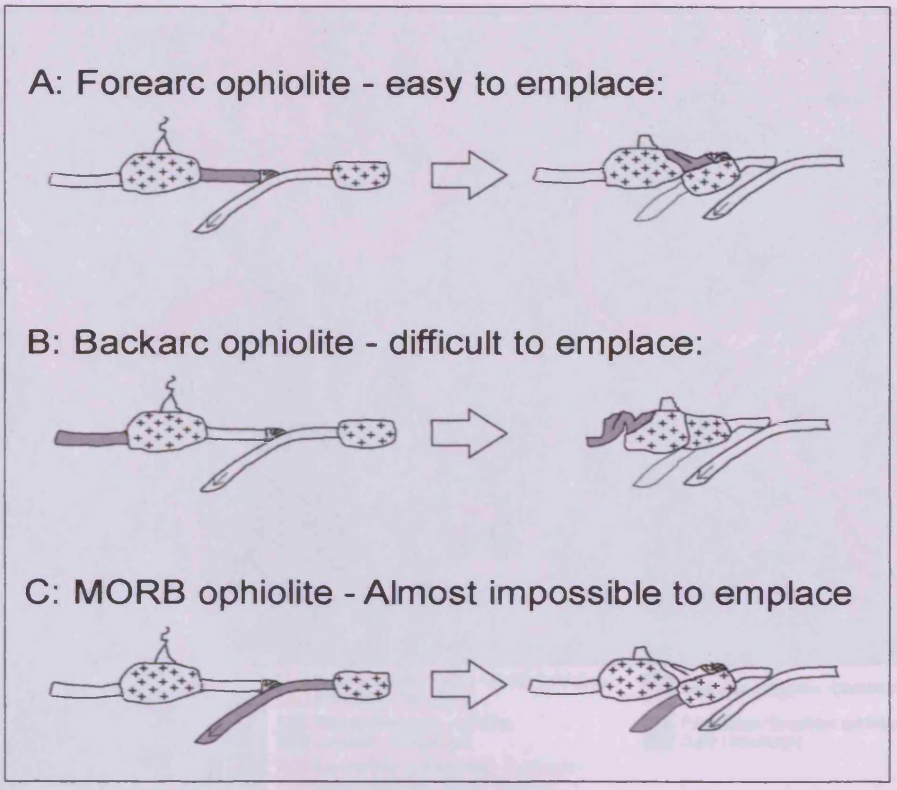

Figure 1.2: *The viability of obducting various types of oceanic lithosphere. In particular it is worth noting that MORB type oceanic lithosphere is considered nearly impossible to obduct, as decollements are not thought to cut deep enough into the subducting lithosphere. Modified from Stern (2004).*

1.4 Ophiolite distribution in space and time

From the different types of ophiolite stratigraphy it is obvious that they vary considerably in terms of formation and emplacement history. Nevertheless their distribution around the world shows distinct patterns (Figure 1.3), that are probably related to large-scale tectonic events such as the formation and break-up of large continents (e.g. Pangea and Rodinia). This review of ophiolites is restricted to the Neoproterozoic and Phanerozoic eons as information on Archaean ophiolites is patchy and currently the subject of debate (e.g. Kusky *et al.*, 2001, 2004; Zhao *et al.*, 2007). In particular, podiform chromitite deposits within Archaean settings have been interpreted as komatiite-hosted rather than ophiolite hosted (e.g. Prendergast, 2008; Mukherjee *et al.*, 2010). Ophiolites are confined to orogenic belts, usually aligned with major thrust or suture zones (Stowe, 1987a) (Figure 1.3).

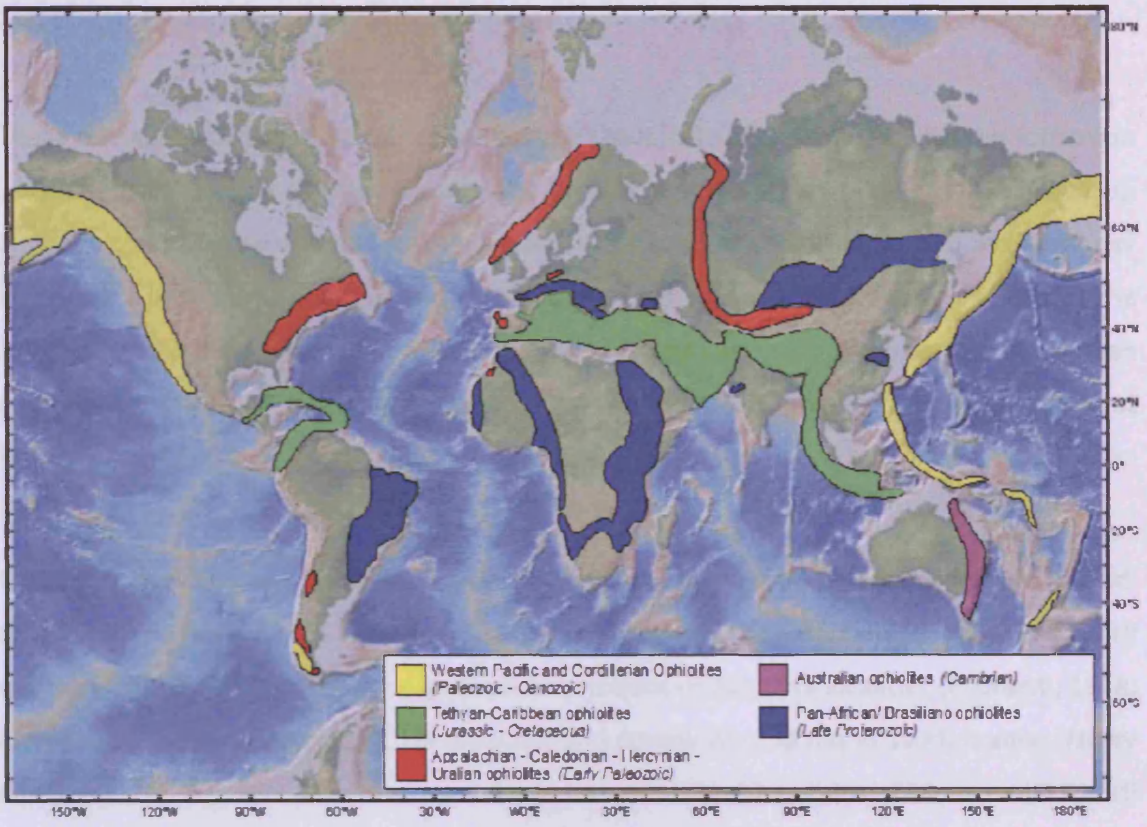

Figure 1.3: *Global distribution of Proterozoic and Phanerozoic ophiolite belts. Modified from Dilek, 2003b and references therein. Similar coloured belts indicate regions which were formed and emplaced in similar time periods during correlated tectonic events. Base map from GeoMapApp,(2009).*

Ophiolites containing chromitites are thought to be restricted to SSZ type tectonic settings (which can include Mediterranean, Sierran, Franciscan, Caribbean or Chilean type). As such they form a subset of the total world ophiolite outcrop. Chromitite occurrence within ophiolites can be both economic and sub-economic. Where economic, these chromitite occurrences have usually been, or are being (e.g. Urals), exploited by mining companies.

1.4.1 Pan-African and Brasiliano ophiolites

These late-Proterozoic (<870 Ma) ophiolites are thought to be associated with the formation of ocean basins during the aftermath of the Rodinia supercontinent break-up (Dilek, 2003b). They are therefore widespread, with occurrences in South America, Africa and Asia and may represent a range of formation and emplacement histories. In particular, ophiolites in the Arabian-Nubian shield represent a diverse range of types, including Ligurian, Mediterranean and Sierran (Dilek, 2003b). The presence of this variation of ophiolitic types indicates that Wilson type opening (Wilson, 1968), narrowing and closing of ocean basins was in operation by 1 Ga.

Chromitite deposits are found extensively in Egypt, north-east Sudan, and north-west Saudi Arabia where there are a series of Neoproterozoic outcrops containing abundant small ophiolitic chromitite deposits. (e.g. general descriptions of ophiolite localities (Al-Shanti, 1988; Ahmed *et al.*, 2001; Ahmed and Hariri, 2008) and specifically - Al'Ays in Saudi Arabia; (Neary and Brown, 1979)). The Bou Azzer ophiolite in the Anti-Atlas Mountains of Morocco (El Ghorfi *et al.*, 2008) and the Hoggar Ophiolites in Nigeria (Stowe, 1987a) have also been reported to contain chromitite deposits. Within Brazil there are chromitite deposits located at Quatipuru & Morro do Agostinho, Campo Morro, Complexo Piraporo and Faixa Dom Feliciano (Suita *et al.*, 2004).

1.4.2 Eastern Australia ophiolites

These Cambrian ophiolites developed along the eastern fringe of Gondwana in a complex arc – back arc system (530-485 Ma). The collapse of this system, and subsequent accretion to the Gondwanan continental margin may have been related to far-field stresses associated with the assembly of Greater Gondwana itself (Dilek, 2003b). Chromitite deposits are restricted to the Great Serpentine Belt and Tasmania (Stowe, 1987a).

1.4.3 Appalachian, Caledonian, Hercynian and Uralian ophiolites

Aside from isolated cases in South America, Africa and Europe, these early Paleozoic ophiolites occur mainly along the Appalachians in America, the Caledonides in Scotland/ Scandinavia and the Urals in Russia. The Appalachians and Caledonides represent SSZ ophiolites which formed on the margins of the Iapetus ocean, and were accreted to the continental margins during the closure of the Eastern Iapetus Ocean between North America and Baltica-Avalonia. The Uralides were derived from the Pleionic ocean which closed in the late Permian with the collision of Baltica with Siberia. The Uralides record Ligurian and Mediterranean type ophiolites in contrast to the Appalchian or Caledonian ophiolites (which are mostly Mediterranean type) (Dilek, 2003b).

Within the Uralides, (which extends from the Ice Sea in the polar circle to the northern tip of Kazakhstan), there are several well known ophiolitic podiform chromitite deposits. These include the Ray-Iz and Voikar-Sininsky on the northern edge and the Kempirsai Massif in Kazakhstan (Melcher *et al.*, 1997) on the southern edge. The giant podiform deposits (>100 Mt) of Kazakstan are the largest known ophiolitic chromitite deposits in the world, from which there is the potential to recover PGE as a by-product (Distler *et al.*, 2008). The surface chromitite outcrops have been mined but subsurface ores e.g. Voskhod, are only now being exploited and others are yet to be mined. Within the Appalachians and the Caledonides there are several well-studied chromitite deposits including the Bay of Islands and Thetford in North America (Stowe, 1987a), and the Unst ophiolite in the Shetland Islands (Prichard *et al.*, 1989)

1.4.4 Tethyan - Caribbean ophiolites

Tethyan ophiolites developed in Palaeo- and Neo-Tethyan ocean settings, between Gondwana and Eurasia. Ophiolites west of the Aegean Sea tend to be Ligurian type and Jurassic in age. Ophiolites east of the Aegean Sea tend to be Mediterranean type, Cretaceous in age (getting progressively younger to the east) and show abundant evidence for having being involved in subduction zone processes (e.g. include depleted harzburgites and boninites). The Caribbean ophiolites belong to a separate ophiolite type (*Caribbean type*) and have been generated by mantle plume activity and so they include fragments of LIP generated oceanic crust (Dilek, 2003b).

There are several ophiolites within these mountain belts which also contain appreciable podiform chromitite deposits. These include: Mirdita – Albania, (e.g. Economou-Eliopoulus, 1996), Pindos, Othrys, Vourinos – Greece, (e.g. Roberts *et al.*, 1988), Troodos – Cyprus, (e.g. Greenbaum, 1977). Several in northern and central Turkey (e.g. Berit, Robertson *et al.*, 2006), Iran (Ghazi *et al.*, 2004) Semail - Oman-U.A.E, (e.g. Ahmed and Arai, 2002) and the Luobusa ophiolite - Tibet (Zhou *et al.*, 1996). Within the Caribbean ophiolites, the most notable chromitite deposits are located on Mayari Baracoa – Cuba (Proenza *et al.*, 1999) although there are also some on Haiti, as well as the Villa de Cura ophiolite in Venezuela (Stowe, 1987a).

1.4.5 Western Pacific and Cordillerian ophiolites

These ophiolites range from the Palaezoic to the Cenozoic and are usually associated with subduction-accretion prisms. There is a wide range of ophiolite types developed within these ophiolite chains, including Ligurian (e.g. Banda Arc), Sierran (e.g. Philippino ophiolites) and Franciscan (e.g. Japan) (Dilek, 2003b). Major chromitite deposits are associated with several of the islands, including Zambales in the Philippines (Yumul Jr *et al.*, 2003), New Caledonia (Moutte, 1982), Sangun – Japan (Arai, 1999), Several of the Indonesian Islands (e.g. Sulawesi and NE Borneo) (Burgath, 1988) and Papua New Guinea (Stowe, 1987a). The Cordillerian ophiolites tend to be barren of major chromitite deposits with the possible exception of the Tortuga and Rochas Verdes Ophiolites in Chile (Stowe, 1987a).

1.5 The formation of chromitite pods within ophiolites

1.5.1 The mineral chromite

Chromite belongs to the spinel group, which has the general formula $([X]^{iv})([Y]^{vi})_2O_4$, where X represents cations in tetrahedral co-ordination and the Y represents cations in octahedral co-ordination (Stowe, 1987b). It has high relative density (3.8 – 4.9) and a Moh hardness of ~5.5. Its lattice structure is face-centred cubic and can accommodate a wide variety of transition elements, including Mg, Fe, Cr, Al, Ti, V, Mn, Ni, Co and Zn (Barnes and Roeder, 2001).

Typically Mg and Fe^{2+} fill the X cation sites with Cr, Al and Fe^{3+} forming the bulk of the Y cation sites. Several trace elements may substantially substitute into chromite. Examples of divalent cations substituting into the divalent site are Mn, Co, Zn and Ni (Barnes and Roeder, 2001; Page and Barnes, 2009). Vanadium is usually assigned to a possible $Fe_7V_2O_{12}$ component and Ti is assumed to present as an ulvospinel component (Barnes and Roeder, 2001).

Accumulations of chromite grains to form chromitite deposits are a common feature within the mantle sequence of supra-subduction zone (SSZ) ophiolites (i.e. Mediterranean and some Sierran-type ophiolites). These chromitite segregations are invariably contained within dunite envelopes (Thayer, 1964; Roberts and Neary, 1993; Zhou *et al.*, 1994), which are themselves hosted within depleted harzburgites. Within the mantle and mantle/crust transition zone the composition of the chromite (within these chromitites) can vary enormously, particularly in the Cr/ Al and Cr/ Fe^{2+} ratios. This variation is dependent on the conditions of formation and it has been hypothesized to depend on some or all of the following; the degree of partial melting of the source region, the extent of magmatic fractionation, the composition of the host peridotite and the extent of melt-rock reaction (see Section 1.5.5)(e.g. Zhou *et al.*, 1996; Edwards *et al.*, 2000; Prichard *et al.*, 2008; Page and Barnes, 2009) .

Chromitite deposits are, with the exception of two localities, exclusively located within SSZ ophiolites and are missing or undiscovered from modern oceanic crust. The two exceptions are a very small micropod (approximately a cm across) from Hess Deep discovered by Hazel Prichard in 1996 (Arai and Matsukage, 1998) during ODP leg 147 and micropods discovered in the mid-Atlantic ridge during ODP leg 209 (Takazawa *et al.*, 2007).

1.5.2 Chromitite formation

The large accumulation of chromian-spinel as podiform orebodies within ophiolites is highly enigmatic as it represents bulk crystallization of chromium from a basaltic melt in which chromium has a low solubility (Roeder and Reynolds, 1991). In addition to this, chromitites often preserve features indicative of cumulate type processes – a feature which would seem at odds with their location within residual mantle tectonite (Thayer, 1964, Brown, 1980). Initial ideas suggested that the chromitite deposits originally formed in the crustal cumulates before being incorporated into the peridotite residuum, either by sinking into the peridotite crystal mush (Dickey Jr, 1975) or by being infolded during tectonism (Greenbaum, 1977).

The recognition that olivine and chromite are the earliest fractionates of rising basaltic melt led to the development of the 'magmatic differentiation model' which proposed that the chromitite deposits represented the initial segregations of rising basaltic melt at sites of original palaeo-spreading (Neary and Brown, 1979; Lago *et al.*, 1982; Roberts and Neary, 1993).

Within the 'magmatic differentiation model' several mechanisms for chromite-only precipitation have been proposed. Lago *et al.* (1982) and (Leblanc and Ceuleneer, 1991) postulated that a vertical cavity forms within mantle peridotite, fed by a narrow dyke and with magma flow carried through and injected upstream via another dyke. As magma flows through the cavity a convection cell initiates allowing constant fractional crystallization, with the olivine and the chromite separating out through density contrasts. Chromium may be constantly replenished in such a scenario through constant melt throughput (i.e. an open system) allowing for the formation of podiform chromitite bodies. In such a scenario, discontinuous batch throughput could result in phase layered chromitite and dunite as each subsequent batch forms a new chromitite-dunite sequence.

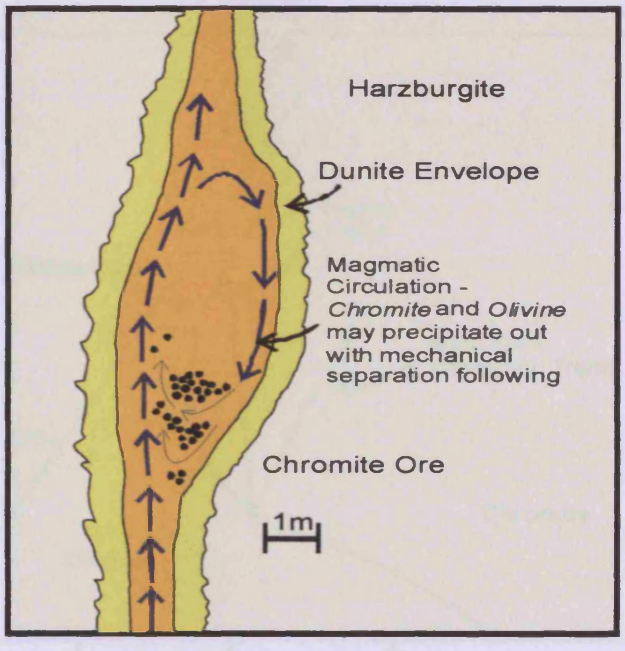

Figure 1.4: *Illustration of a vertical cavity within harzburgite (peridotite). Magma flow circulates through the cavity and chromite and olivine precipitate out of the magma, with chromite concentration occurring through mechanical sorting. Adapted from Lago et al., (1982).*

In contrast, other workers have suggested magma mixing as the essential cause, following the recognition of its potential importance in stratiform chromitite deposits (Irvine, 1977) (Figure 1.5). Ballhaus (1998) suggests the mixing of oversaturated conjugate siliceous and fayalitic melts will result in the nucleation of chromite. This is shown in Figure 1.5 where 'x' represents a siliceous melt and 'a' represents a fayalitic melt. The mixing of 'x' with 'a' produces a liquid 'y' which lies in the chromite only saturation field, resulting in the deposition of monomineralic chromitite deposits. The potential problem with magma mixing is the unlikelihood of two melts of differing composition being present at the same time within a conduit. This was summarized by Edwards *et al.,* (2000) who note that "it is highly unlikely that melts derived from multistage melting will co-exist in the same conduit as the original melt tends to leave a crystalline product rather than a melt". However, if the conduit does remain open, and mixing does occur then a melt/ spinel ratio of ~300-500 is required, implying significant melt focusing is required at the site of deposition (Leblanc and Ceuleneer, 1991). That is as melt travels from the mantle to the crust there may be some junctures within the mantle where melt is particularly focused. Chromitites may form at these locations, which Johan, (1986) postulated to be shear-zones within the mantle harzburgite.

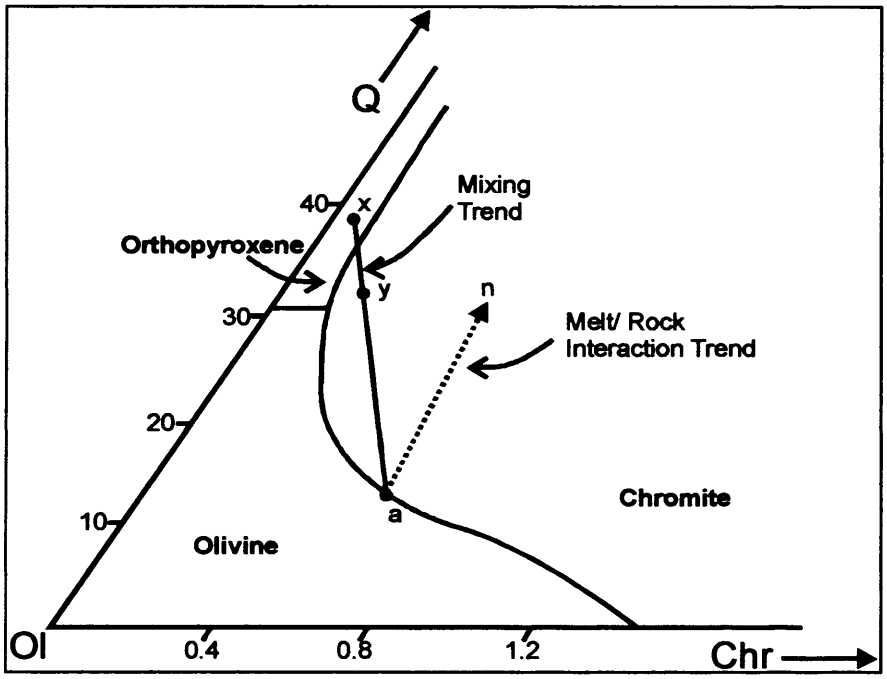

Figure 1.5: *Condensed phase diagram for the system quartz-olivine-quartz (Irvine, 1977). The Mixing Trend 'x-a' is derived from the same work, with the Melt/ Rock Interaction Trend 'a-n' derived from Zhou et al., 1994.*

In addition to the above principal mechanisms, variations in several other physical parameters have been postulated to play an important role, including changes in fO_2 (Murck and Campbell, 1986), total pressure (Lipin, 1993), temperature (Murck and Campbell, 1986) and P_{H2O} (Johan *et al.*, 1983).

More recently the formation of podiform chromitites by melt-rock reaction has been favoured (Zhou *et al.*, 1994). This process was postulated by Kelemen, (1992) to explain the pervasive presence of harzburgite in the mantle sequences of the Trinity ophiolite. Kelemen suggested that the harzburgite was too rich in SiO_2 (in the form of orthopyroxene) to have formed simply as the residuum of partial melting and therefore proposed that melts ascending through the mantle dissolved clinopyroxene and re-precipitated orthopyroxene.

At positions of melt focusing harzburgite may also be converted to dunite through the dissolution of orthopyroxene and re-precipitation of olivine. Zhou *et al.* (1994) further adapted this model to the formation of chromitite deposits by proposing that this dissolution enriches the melt with silica, which therefore moves into the chromite only saturation field along such a line as 'a-n' in Figure 1.5. Within the melt/ rock reaction model the composition of an upwelling melt within the oceanic mantle is thought to be dependent upon the degree of melting of the source region, and the degree of melt to host-rock reaction with fractional crystallization not playing any significant role (e.g. Edwards *et al.*, 2000).

Within the models outlined above, recent research has highlighted the importance of water in the formation of podiform chromitites. Edwards *et al.* (2000) note that the presence of water in the melting regime can increase the Cr solubility through the de-polymerization of the melt. This effect has already been roughly quantified by (Malpas *et al.*, 1997) who report tholeiitic melts as containing ~600 ppm Cr, whereas boninitic melts contain ~1200 ppm Cr. The presence of water during partial melting of SSZ mantle promotes melting to beyond the clinopyroxene-out phase boundary, and although some Cr will be re-partitioned into relict spinels (making them in turn Cr richer) the abundance of Cr-bearing phases decreases. As melting proceeds beyond the transition from lherzolite to harzburgite the dissolution of these chromian-rich spinels will greatly increase the Cr content of the melt.

A secondary role of water in the formation of podiform chromitites is the formation of nodular chromitite with associated orbicular olivine. This texture is unique to ophiolitic chromitite, and was initially attributed to physical processes operating within the magmatic system (e.g. snow-balling of chromite phenocrysts, disruption of plastic chromitite layers or agglomeration of chromite in cavities (Dickey Jr, 1975; Greenbaum, 1977; Lago *et al.*, 1982; Paktunc, 1990)). Recently, the role of water in forming these textures has been emphasized (e.g. Edwards *et al.*, 2000; Matveev and Ballhaus, 2002). Upwelling mantle melts may exsolve an immiscible non-silicate fluid, which separates from the silicate melt (Kamenetsky and Kamenetsky, 2010). From experimental work on this Matveev and Ballhaus (2002) argued that in basalt systems oversaturated with water the olivine will remain in the silicate-melt phase, whilst chromite transfers to the fluid phase. They argued that the fluid phase will exsolve out of the melt using chromite microphenocrysts as nucleation points (driven by the affinity of water-rich fluids for oxide surfaces) (Figure 1.6).

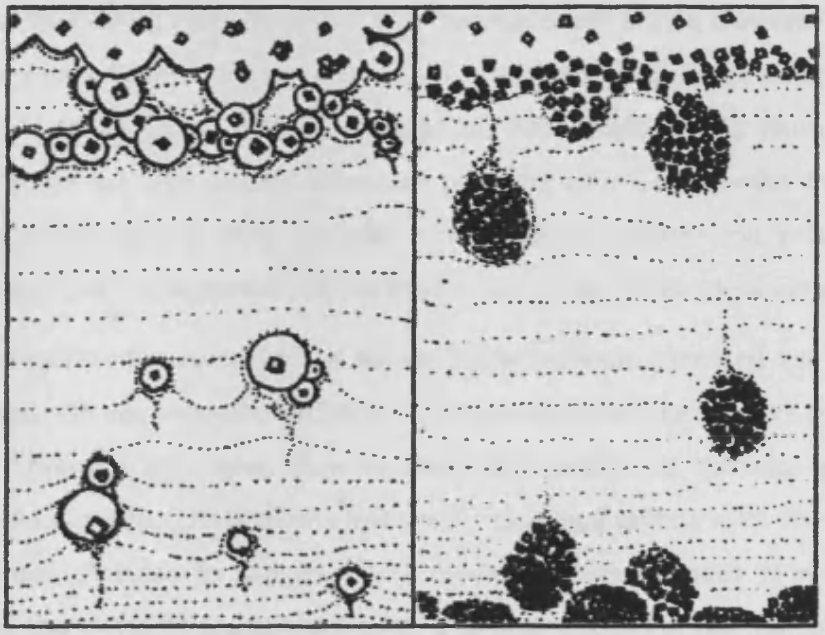

Figure 1.6: *Proposed two-stage model for chromite segregation and nodular chromite formation. This process may be extended to the formation of podiform chromitite deposits. The first stage is the collection of chromite microphenocrysts by an exsolved fluid phase which then rises through the denser silicate melt to the top of the magma column. During the second stage chromite concentrations become dense enough to sink back through the silicate melt forming the typical nodular texture. Diagram taken from Matveev and Ballhaus (2002).*

Initial fluid phase droplets will contain so little chromite that they will be lighter relative to the surrounding silicate melt (Figure 1.6). Such droplets will rise to the top, forming fluid pools in a process analogous to industrial flotation. As more chromite microphenocrysts are gathered they will form a critical mass that then sinks back through the silicate melt to form the typical 'leopard' chromitite deposits (Matveev and Ballhaus, 2002)(Figure 1.6). This concentration process may itself produce podiform chromitite deposits with nodular chromite grains a secondary by-product.

1.5.3 Chromitite alteration

Although chromite grains are refractory and partially resistant to alteration, they are still affected by hydrous alteration and prograde metamorphism, with both being extensively covered in previous investigations (Frisch, 1971; Evans and Frost, 1975; Barnes, 2000; Mellini *et al.*, 2005). There is some confusion about the exact terminology for the alteration product of chromite as two terms ("Cr-magnetite" and "ferritchromit/ ferrian chromite") have been used interchangeably (Barnes, 2000; Mellini *et al.*, 2005) and to describe different products (Peltonen, 1995; Onyeagocha, 1974; Kapsiotis *et al.*, 2007; Khalil, 2007). From the detail it appears that there are two distinct alteration products with Cr-magnetite forming as an overgrowth (e.g. Onyeagocha, 1974; Kapsiotis *et al.*, 2007) and ferritchromit forming as a fine-grained interleaving of Cr-magnetite and Cr-chlorite (Shen *et al.*, 1988; Mellini *et al.*, 2005).

During metamorphism the Fe content of the chromite is greatly increased due to increased Mg-Fe exchange with any neighbouring silicates. This exchange will be far more pronounced in disseminated chromite lithologies, than in chromitite bodies, as chromite grains within chromitite bodies have very little silicate material to exchange cations with. The Cr^{3+} and Al^{3+} contents are not expected to change much, though at higher grades of metamorphism (~amphibolite) the chromite grains are expected to lose aluminium (Barnes, 2000). For the present study no analysis was made of the alteration products of chromite, although the approximate degree of alteration was noted.

1.5.4 Chromitite deformation

Texturally, chromitites are often highly deformed, 'podiform' in shape, and display varying degrees of alteration. The intense deformation is unsurprising, considering the tectonic setting in which they form and the later obduction which they experience. Chromitite pods may be oriented in a discordant, subcordant or concordant manner with respect to tectonised mantle flow lines (Figure 1.7), and their different orientations can often be correlated with different chromitite textures (Figure 1.7, Lago *et al.*, 1982; Christiansen, 1985; Nicolas, 1989; Edwards *et al.*, 2000). After deformation and alteration the ophiolite is then obducted, which will often result in low temperature brittle microfaulting of the chromitite pod.

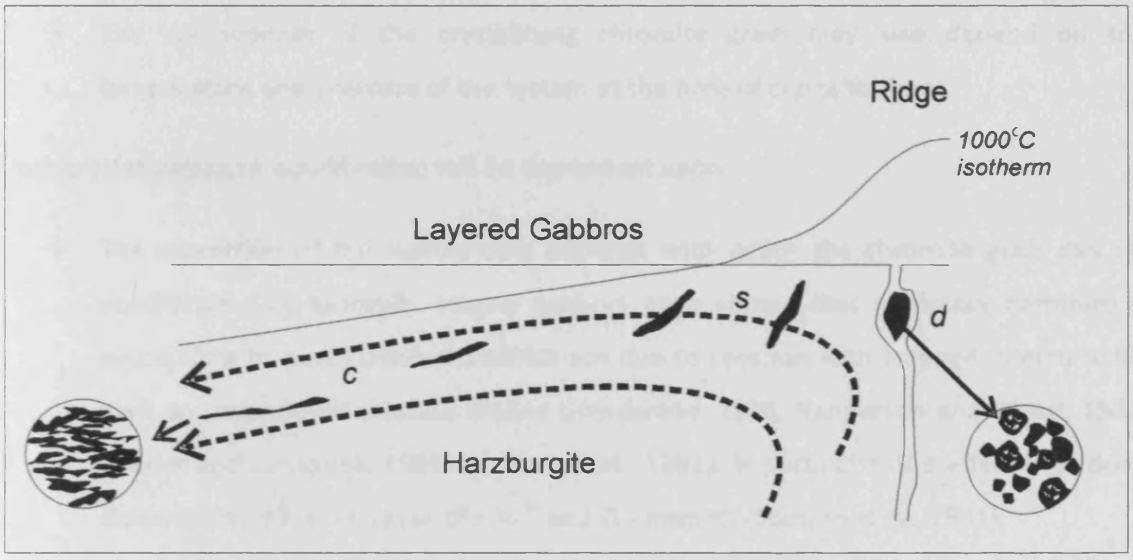

Figure 1.7: *Simplified diagram of the position of discordant, subcordant and concordant chromitite pods, with respect to mantle flow lines. Also shown are the different chromite morphologies expected in discordant and concordant chromitite pods. The 1000°C isotherm represents the likely boundary between the mantle and the crust, which further away from the spreading axis becomes the boundary between the lithosphere and the astenosphere. The diagram is adapted from Lago et al. (1982), Nicolas, (1989) and Edwards et al. (2000).*

1.5.5 Interpreting chromite composition

The final composition of any chromite grain is dependent on the composition of the melt at the time of crystallization and the extent of re-equilibration or alteration experienced by the grain after crystallization. The composition of the liquid from which the grain crystallized will be dependent on four main factors, *viz:*

- The degree of melting of the source region.
- The addition of any phase to the melt (e.g. through reaction with hostrock or reaction with other fluids).
- The separation of any phase from the melt (e.g. crystallization, unmixing of fluids or degassing)
- The composition of the crystallizing chromite grain may also depend on the temperature and pressure of the system at the time of crystallization.

Post-crystallization re-equilibration will be dependent upon:

- The speciation of the surrounding minerals with which the chromite grain can re-equilibrate. For example, several authors have shown that accessory chromite is susceptible to post-cumulus modification due to reaction with trapped intercumulus melt and associated cumulus olivine (Henderson, 1975; Henderson and Wood, 1981; Roeder and Campbell, 1985; Scowen *et al.*, 1991). In particular, the effect is to drive down the Mg# and increase the Fe^{3+} and Ti contents (Scowen *et al.*, 1991).
- The temperature and pressure within the system, the cooling rate, and the presence of fluxes (e.g. the presence of magmatic fluids which may increase the rate of diffusion) may all affect the kinetics of re-equilibration.

Finally, alteration of the chromite grains due to the influx of late stage fluids and serpentinisation may lead to the formation of Cr-magnetite and/or "ferritchromit" rims with a much altered composition.

1.5.5.1 Major trends in chromite compositional space

In a review of the range of spinel compositions within terrestrial mafic and ultramafic rocks Barnes and Roeder identified several trends that regularly reappear, namely; the spinel gap, the Cr-Al trend, the Fe-Ti trend, the kimberlite trend and the Rum trend (Figure 1.8). Two other trends are considered in this review, which are trend A and trend B as defined by Naldrett *et al.* 2009.

The **spinel gap** describes an observed data density minimum between chrome-rich spinels (chromites) and Fe^{3+}-rich spinels (magnetite)(Figure 1.8A). This has two main causes. Firstly there is the extensive solvus within the spinel solid-solution (Sack and Ghiorso, 1991), which occasionally results in the unmixing of spinels (e.g. Loferski and Lipin, 1983; Tamura and Arai, 2005). Secondly, there is the reaction relationship between chromite and Cr-bearing clinopyroxenes. This reaction causes chromite to cease crystallizing followed by a hiatus before magnetite begins to crystallize (Barnes and Roeder, 2001)

The **Cr-Al** trend is particularly well marked in ophiolites and is shown by widely variable Cr# at low Fe# with low concentrations of Fe^{3+} and TiO_2 (Figure 1.8A & 1.8B). There is a slight positive trend with increasing Cr# followed by increasing Fe# (equivalent to a slight inverse trend between Cr# and Mg#). This trend was observed by Irvine in 1967 in the Muskox layered intrusion, who proposed that it arose from the equilibration of chromite with olivine of constant composition at constant temperature. The slope is due to non-ideality within the spinel solid solution and forms the basis for the olivine-spinel geothermometer (Sack and Ghiorso, 1991; Barnes and Roeder, 2001).

The **Fe-Ti** trend describes a positive relationship with Fe^{3+} and Fe^{2+}# increasing and typically accompanied with increasing TiO_2 values (Figure 1.8A-D). This trend is attributed to changes in spinel composition caused by the fractional crystallization of olivine, pyroxene and possibly plagioclase or alternatively reaction with trapped intercumulus melt (Barnes and Roeder, 2001). The low TiO_2 and Fe^{3+} contents of chromite grains within ophiolitic settings means this trend is not observed within ophiolites (Barnes and Roeder, 2001). The **kimberlite** trend is similar to the Fe-Ti trend (Figure 1.8A & C), only differing in the near constant Fe# values over a wide range of Fe^{3+}. As with the Fe-Ti trend, it is not observed within ophiolites, but as its name suggests is commonly observed within kimberlites.

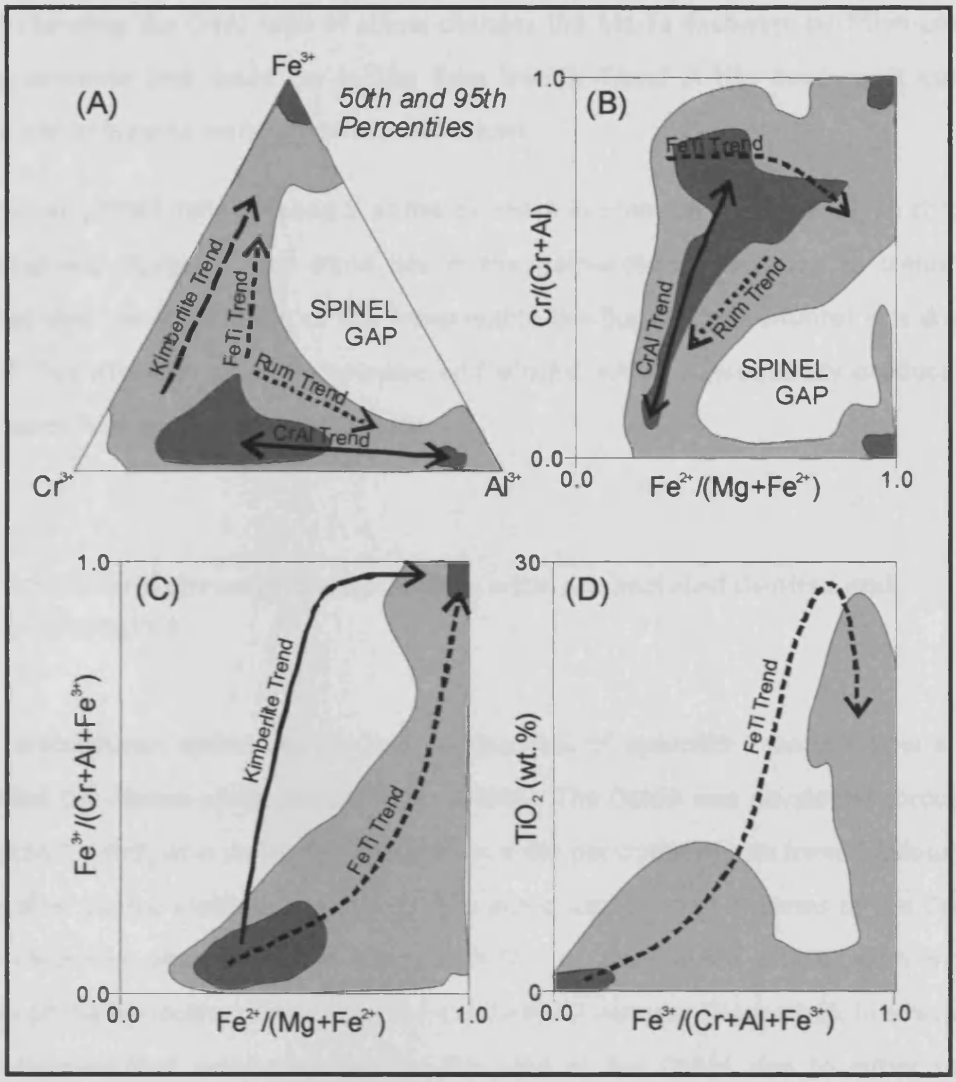

Figure 1.8: *The generalized trends and spinel gap identified within Barnes and Roeder, (2001) from their entire spinel dataset (21, 644 analyses). Figure taken from Barnes and Roeder, (2001).*

The **Rum** trend (Figure 1.8A & B) defined by Barnes and Roeder, (2001). It is similar to the Cr-Al trend but with two differences. The first is that Fe^{3+} values are also expected to increase with increasing Cr# and secondly that the rate of Fe# increases more markedly with increasing Cr# (Figure 1.8B). Barnes and Roeder related it to changes in the exchange partition coefficient of Mg-Fe between chromite and liquid for different Cr# compositions of chromite. It was first recognized in the Rum layered intrusion (Henderson, 1975; Henderson and Wood, 1981).

Trend A (Naldrett *et al.*, 2009) is very similar to the Rum trend as defined by Barnes and Roeder except that there is no change in the Fe^{3+} values with changing Cr#. Naldrett *et al.* relate the trend to changing the melt composition from which chromite is crystallizing and the

fact that changing the Cr/Al ratio of spinel changes the Mg-Fe exchange partition coefficient between chromite and liquid (as in the Rum trend). Trend A has been most commonly recorded within layered mafic-ultramafic intrusions.

Naldrett *et al.* (2009) defined **trend B** as the decrease in both Cr# and Mg# within chromitites in the Bushveld Complex. This trend lies in the perpendicular direction to trend A. It is postulated that the observation of this trend within the Bushveld chromitites was due to the fractional crystallization of orthopyroxene and olivine, which subsequently produced lower Cr# and lower Mg# in crystallizing chromite.

1.5.6 Olivine and chromite compositions within associated dunites and harzburgites

Olivine compositions within dunites and harzburgites of ophiolitic mantle follow a specific trend called the olivine-spinel mantle array (OSMA). The OSMA was developed through work by Arai (1987, 1990) who defined an expected mantle peridotite restite trend (residual source material after partial melting, Figure 1.9). This trend was defined in terms of the Cr# of the residual chromite phase and the associated Fo# of the olivine phase. With increasing depletion of the peridotite restite both Cr# and Fo# will increase (Figure 1.9). In a review, Arai (1994) proposed that peridotites plot to the right of the OSMA due to either fractional crystallization (Figure 1.9), or metasomatism by fluids enriched in incompatible elements. This review included an analysis of several olivine grains from both xenolithic and alpine-type dunites, which plotted both within and outside of the OSMA. It concluded that dunites plotting to the right of the OSMA were likely to be cumulates from relatively primitive basalts but that dunites plotting within the OSMA may be either cumulate in nature or possibly restite in origin. That is, olivine may have either crystallized through orthomagmatic processes from a primitive melt or be a restite phase due to the selective consumption of pyroxenes from harzburgites or lherzolites (e.g. Fisk, 1986). In both scenarios the likely Fo# of the olivine grains would lie within the OSMA, as in the first instance primitive melts would crystallize high Fo# olivine grains and in the second instance olivine is a restite phase so would retain its mantle Fo# composition.

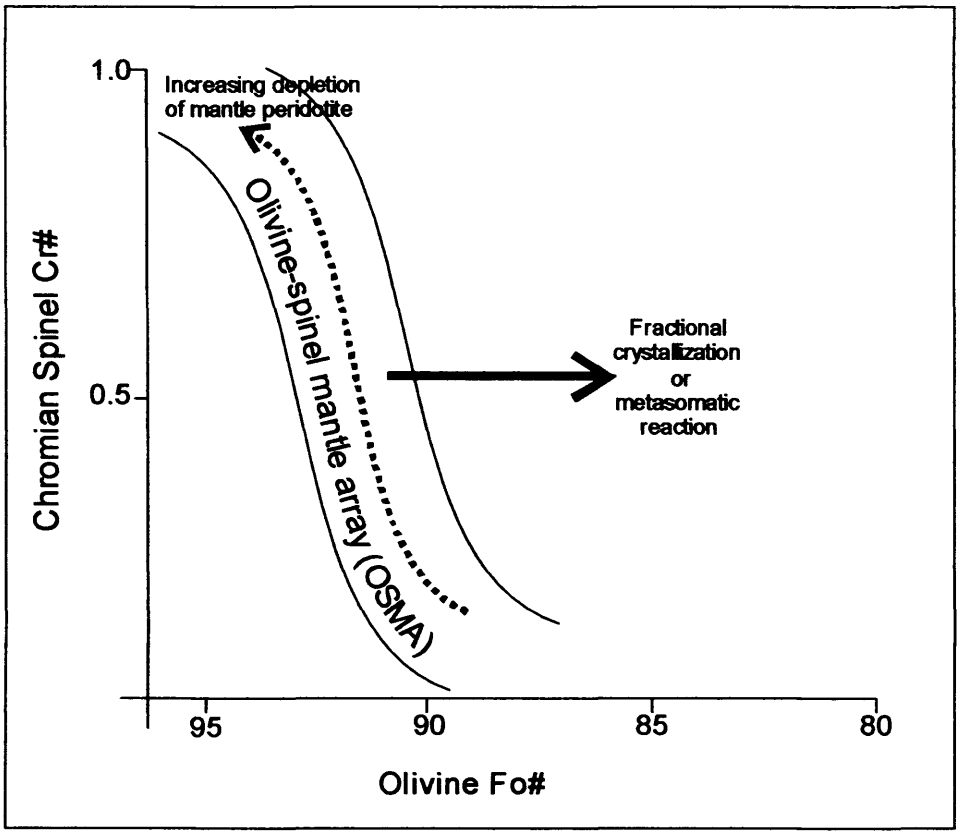

Figure 1.9: *Olivine-spinel mantle array, adapted from Arai, (1987, 1990 & 1994).*

A diagram of Cr# vs. TiO_2 for chromite grains within mantle peridotite samples has been shown to be particularly effective at distinguishing between the effects of partial melting and melt/rock reaction within mantle peridotites (Arai, 1992; Zhou *et al.*, 1996; Pearce *et al.*, 2000) (Figure 1.10). This is because the effect of partial melting on the residual chromite phase is to progressively increase the Cr# whilst decreasing the TiO_2 content. In contrast, the reaction of upwelling melts with residual chromite phases will increase both the Cr# and TiO_2 contents of the chromite grain (Figure 1.10). This is shown using the example of the peridotites from the South Sandwich arc-basin system (Pearce *et al.*, 2000). These peridotites split into two sites – the South Sandwich forearc and the South Sandwich trench fracture zone intersect. Samples from the forearc have experienced greater degrees of partial melting (15-20%) and reaction with boninite melt whereas samples from the trench fracture zone intersect site have experienced relatively little partial melting (<10%) and reaction with MORB like melts (Figure 1.10)

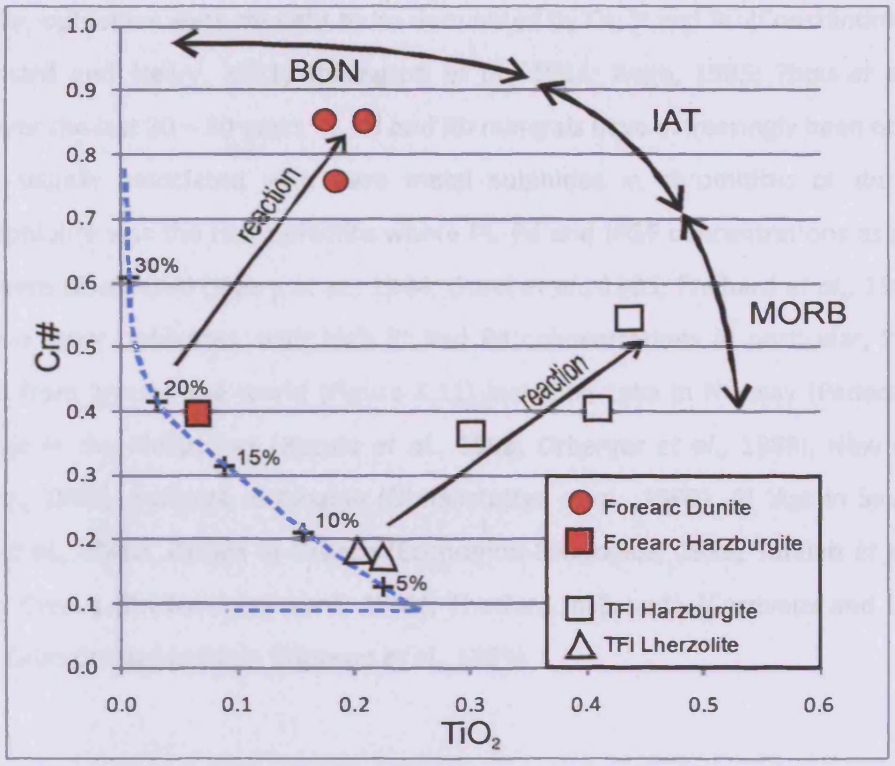

Figure 1.10: *Cr# - TiO_2 plot for chromite from mantle lherzolites, harzburgites and dunites from the South Sandwich arc-basin system. The blue dashed line represents the predicted chromite composition at different degrees of partial melting (adapted from Pearce et al., 2000). Reaction lines for dunites produce a tie-line between expected peridotite host rock composition and the melt which has reacted with the host rock. The expected melt-composition fields and South-Sandwich data are all taken from Pearce et al, 2000. TFI stands for trend-fracture zone intersection.*

1.6 Platinum-group elements

1.6.1 Ophiolites with high PGE concentrations

The six PGE are platinum (Pt), palladium (Pd), rhodium (Rh), iridium (Ir), osmium (Os) and ruthenium (Ru), with the former three referred to as the PPGE and the latter three referred to as the IPGE. They are thought to be concentrate in the mantle at chondritic proportions, reflecting the Earth's early evolution by accretion from chondritic meteorites. Concentration from these mantle proportions is thought to occur through partial melting, whereby PGE are preferentially removed to the melt, before further concentration via a 'carrier phase' in the crystallizing magma chamber (e.g. Mungall and Naldrett, 2008).

Traditionally, ophiolites were thought to be dominated by Os, Ir and Ru (Constantinides *et al.*, 1980; Prichard and Neary, 1981; Talkington *et al.*, 1984; Auge, 1985; Zhou *et al.*, 1998), however over the last 20 – 30 years Pt, Pd and Rh minerals have increasingly been observed in ophiolites, usually associated with base metal sulphides in chromitites or dunites. The Shetland ophiolite was the first ophiolite where Pt, Pd and IPGE concentrations as great as a few ppm were discovered (Neary *et al.*, 1984; Gunn *et al.*, 1985; Prichard *et al.*, 1986). Since then several other ophiolites, with high Pt and Pd concentrations in particular, have been catalogued from around the world (Figure 1.11) including Leka in Norway (Pedersen *et al.*, 1993), Acoje in the Philippines (Bacuta *et al.*, 1988; Orberger *et al.*, 1988), New Caledonia (Auge *et al.*, 1998), Bulquiza in Albania (Ohnenstetter *et al.*, 1999), Al 'Ays in Saudi Arabia (Prichard *et al.*, 2008), Pindos in Greece (Economou-Eliopoulos, 1996; Tarkian *et al.*, 1996), Troodos in Cyprus (Prichard and Lord, 1990), Thetford in Canada (Corrivaux and Laflamme, 1990) and Cabo Ortegal in Spain (Moreno *et al.*, 1999).

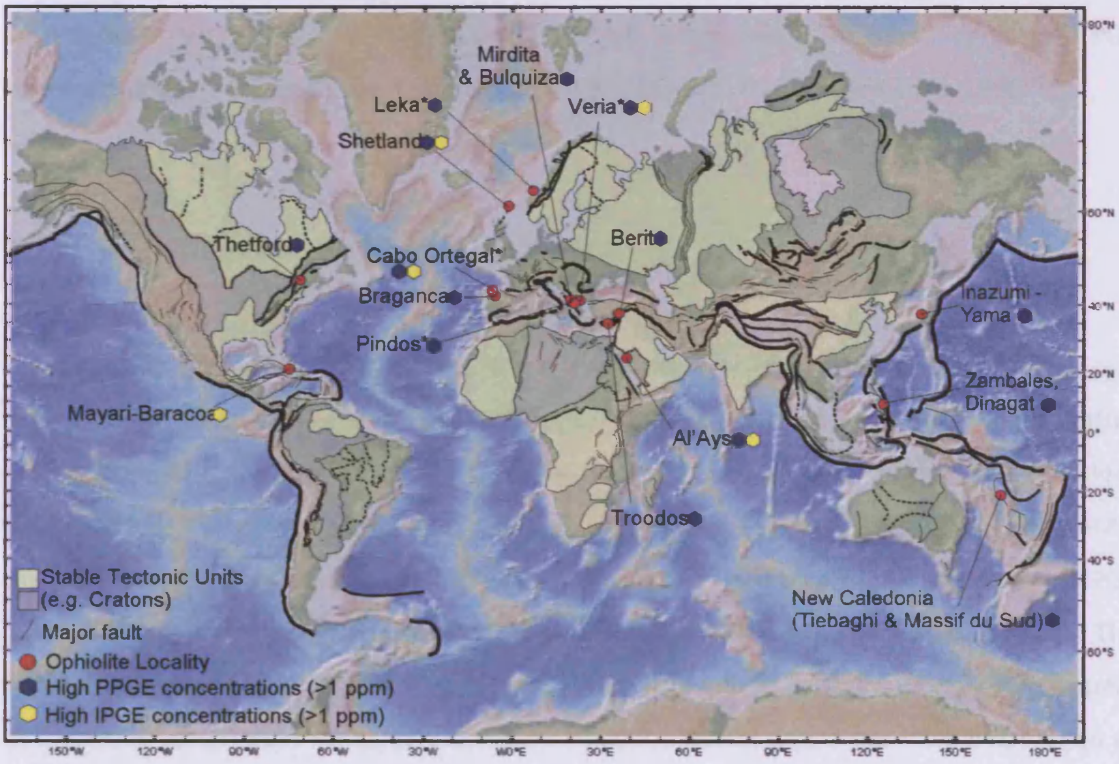

Figure 1.11: *World map showing the location of the major ophiolite deposits which host high (>1 ppm of any single PGE) PGE concentrations. Adapted from Prichard & Brough, (2009).*

1.6.2 The location of high PGE concentrations within ophiolites

Within ophiolites the most common location for PGE is associated with podiform chromitites, though examples have been found of high concentrations within other mafic and ultramafic lithologies including dunites and gabbros (see below for examples). Dunites hosting high PGE concentrations can be associated with podiform chromitites as the surrounding envelope within the mantle sequence, or as layers within the cumulate sequence. When the dunite surrounding podiform chromitites contains high PGE concentrations, these values may either be replicated within the chromitite pods (e.g. Cliff chromitite pod on the Unst ophiolite (Prichard and Tarkian, 1988), or the associated chromitites may be barren (e.g. The Zambales ophiolite where dunites record concentrations up to 14,300 ppb but the associated chromitites are barren, Bacuta *et al.*, 1988). Dunites within the cumulate sequence of ophiolites have also been found to be contain high PGE concentrations, with two notable examples being the cumulate sequence of the Unst ophiolite (Lord and Prichard, 1997) and the cumulate sequence of the Bulquiza ophiolite in Albania (Ohnenstetter *et al.*, 1991; Ohnenstetter *et al.*, 1999). Gabbros have also been found to host significant PGE concentrations as shown by the Troodos ophiolite in Cyprus (Prichard and Lord, 1990).

1.6.3 The extraction of PGE from the mantle

Within the upper mantle PGE are only trace constituents, with concentrations of a few ppb (Barnes *et al.*, 1985; Lorand *et al.*, 1999). Their carrier phase within the mantle is still a matter of considerable debate, in particular whether they are hosted within base metal sulphides (BMS) (Mitchell and Keays, 1981; Alard *et al.*, 2000) or alloys (Barnes *et al.*, 1985). If in BMS, then all the PGE would reside within BMS, but if alloys are also a carrier phase then the IPGE (Os, Ir and Ru) are likely to be hosted by alloys, but the PPGE would be hosted by BMS. The observations that the PPGE and IPGE behave differently during partial melting, often appear to crystallize at different times, and contain different physical properties have been taken as evidence of two different mantle carrier phases in the mantle with IPGE in alloys.

However, direct observation of PGM within mantle sequences has been ambiguous, with most studies of peridotites concluding that the PGM have been produced by small degrees of partial melting, rather than being 'true' residual mantle PGM (e.g. Hutchinson *et al.*, 1999; Luguet *et al.*, 2001). Furthermore, in recent years there has been a consensus towards the PGE being completely hosted by BMS, but with segregation of PPGE and IPGE being caused by incongruent melting of the mantle sulphides (Alard *et al.*, 2000; Luguet *et al.*, 2003; Bockrath *et al.*, 2004; Peregoedova *et al.*, 2004; Lorand *et al.*, 2008). Under incongruent melting the PPGE are concentrated into the Cu sulphide-rich melt, with Os, Ir and Ru concentrated into residual monosulphide solid solution (MSS). With sufficient partial melting the mantle may be stripped of this remaining MSS resulting in the final release of the IPGE. As the IPGE melt out at higher temperatures, they will also be the first to crystallize from the melt as it cools (providing the melt remains as a single phase, i.e. no unmixing). This may explain their common location as inclusions within chromite, whilst the PPGE are usually found within the interstitial space between chromite grains (Prichard and Tarkian, 1988).

BMS may melt over a wide range of partial melting percentages, with the PGE initially being concentrated into the residual BMS. As the degree of partial melting increases the incongruent melting of the residual BMS will release PPGE sulphides into the melt first, with the IPGE being incorporated later. Since all the PGE are likely to hosted within the last BMS to melt, the range of partial melting over which all PGE are removed into the melt is likely to be narrow. If the partial melting was continuous it is predicted that the total PGE content of the mantle source will be removed to the melt at a critical point (O'Hara *et al.*, 2001). With respect to forming economic concentrations of PGE (>3-4 ppm) this partial melting window appears to be very narrow, where too little melting results in not enough PGE and too much melting results in PGE dilution (Prichard *et al.*, 1996).

1.6.4 The crystallization of PGM from the melt – inducing sulphur saturation

Having removed the PGE from the mantle, they are likely to reside in close association with sulphur within the melt, as evidenced by the observation that sulphide-rich melts may contain PGE concentrations 10,000 times higher than sulphide barren silicate melts (Mungall and Naldrett, 2008). In silicate melts sulphur exists as sulphide (S^{2-}) or sulphate (S^{6+}); and the sulphur carrying capacity of the melt increases when both ions are present (Jugo, 2009).

The behavior and likely associations of PGE within the melt may change depending on the likely oxidation state of sulphur within the melt. When sulphide is the dominant phase (fayalite-magnetite-quartz (FMQ) <2), the PGE will reside with the sulphur and in any subsequent immiscible sulphide fluids that exsolve from the melt. However, when sulphate is the dominant phase (FMQ>2), the PGE would reside in the silicate melt, as sulphide phases are not stable (Mungall, 2002; Jugo, 2009). The estimated oxidation state of the mantle wedge above subduction zones is approximately FMQ +0.5 to FMQ +1.7 (Parkinson and Arculus, 1999). These oxidation states would incorporate a significant sulphate phase but would likely mean that the PGE are predominantly residing within sulphide species within the melt.

It is therefore apparent that the crystallization of S-bearing PGM is dependent upon the timing of sulphide saturation (e.g. Mungall and Naldrett, 2008; Prichard *et al.*, 2008). Sulphide saturation may occur through changes in three principle parameters (Li and Ripley, 2005). These include increasing pressure, decreasing temperature or changing the magma composition (specifically a drop in Fe, or an increase in SiO_2, $Na_2O + K_2O$, or MgO). Changes in the fO_2 and fS_2 may have significant effects on the melt (i.e. changing the speciation of sulphur within the melt at high levels of fO_2, or inducing localized PGM crystallization – see Section 1.6.5). However, these are related to changes in temperature and melt composition and at sulphide saturation the fS_2/fO_2 ratio is a predictable function of both (O'Neill and Mavrogenes, 2002; Li and Ripley, 2005).

Although increasing pressure in an ascending melt is unlikely, decreasing temperatures and changing compositions are plausible. For example fractional crystallization within an ascending melt may lead to sulphur saturation through cooling and changes in the melt composition - this is because sulphur does not readily enter any of the initial fractionating minerals (e.g. olivine, chromite, orthopyroxene) and will therefore be progressively concentrated in the residual silicate melt. On reaching sulphur saturation (or slightly superseding), sulphides should crystallize out on mass with their associated PGE tenors. Alternatively, the introduction of crustal rocks (i.e. a cool Si-rich assimilant), will increase the SiO_2 content and lower the temperature of the melt which together lower the sulphur solubility and move the melt towards sulphur saturation. This mechanism is favoured in the petrogenesis of deposits such as the Voisey's Bay Deposit (Naldrett, 1999) but is not likely to happen in ophiolites as there is no continental rock available for contamination (though it is noteworthy that melt/rock reaction does add SiO_2 to the melt).

1.6.5 The role of chromite in concentrating PGM

In addition to the above mechanisms for sulphur saturation it has been postulated that the crystallization of chromite may play an integral role in inducing sulphur saturation. During the crystallization of chromite FeO is removed from the melt, which would increase the likelihood of sulphur saturation (Cawthorn, 2002; Mungall, 2005). The ideal scenario occurs when the melt is close to sulphur saturation before chromite crystallization. In this instance chromite crystallization facilitates sulphur saturation and therefore sulphide crystallization, this in turn draws out the PGE from the melt resulting in PGE enriched chromitite deposits. Prichard *et al.* 2008 hypothesize that for sulphur saturation to occur within the mantle chromitites, there needs to be a critical melting point which stops just after the destruction of the final mantle sulphide carrier phase. In this instance the rising melt will only just be sulphur undersaturated and so will reach sulphur saturation early on in its ascent through the mantle.

It has also been suggested that chromite may act as a collector for PGE *per se* without the need to induce sulphur saturation in the process. Finnigan *et al.* (2008) suggest that the crystallization of chromite within a melt results in a redox gradient at the mineral-melt interface. This is because; during chromite crystallization the melt may be pushed close to PGE saturation, by decreasing temperatures and decreasing fO_2. At this point the nucleation of PGM would be facilitated at the chromite mineral surface. This may also occur if chromite grains which have crystallized in mafic magmas are injected into more primitive magmas (i.e. magmas with higher Cr/ Al ratios). In this instance, the perturbation in fO_2 may be sufficient to extract the PGE from the magma (Finnigan *et al.* 2008). In this instance zoning within the chromite grain may be observed reflecting its initial crystallization from a mafic magma and subsequent overgrowth in a more primitive melt.

1.6.6 The platinum group minerals

In contrast to gold or silver mineralization, platinum-group minerals (PGM) show a great deal of variability, with alloys, sulphides, arsenides, tellurides and oxides particularly common. Although the variety of PGM is large in ophiolites, the majority of IPGE (Os, Ir, Ru) are contained within laurite, erlichmanite and irarsite (e.g. Constantinides *et al.*, 1980; Talkington *et al.*, 1984; Prichard *et al.*, 1986; Tarkian and Prichard, 1987), with the majority of PPGE (Pt, Pd, Rh) contained within sperrylite, geversite, stibiopalladinite and hollingworthite (e.g. Tarkian and Prichard, 1987; Prichard *et al.*, 1994; Auge *et al.*, 1998; Ohnenstetter *et al.*, 1999). PGM occur in several different textural arrangments, including within the chromite grains, within the 'spongey' chromite gain rim, to finally being included interstitial to the chromite grains (Figure 1.12).

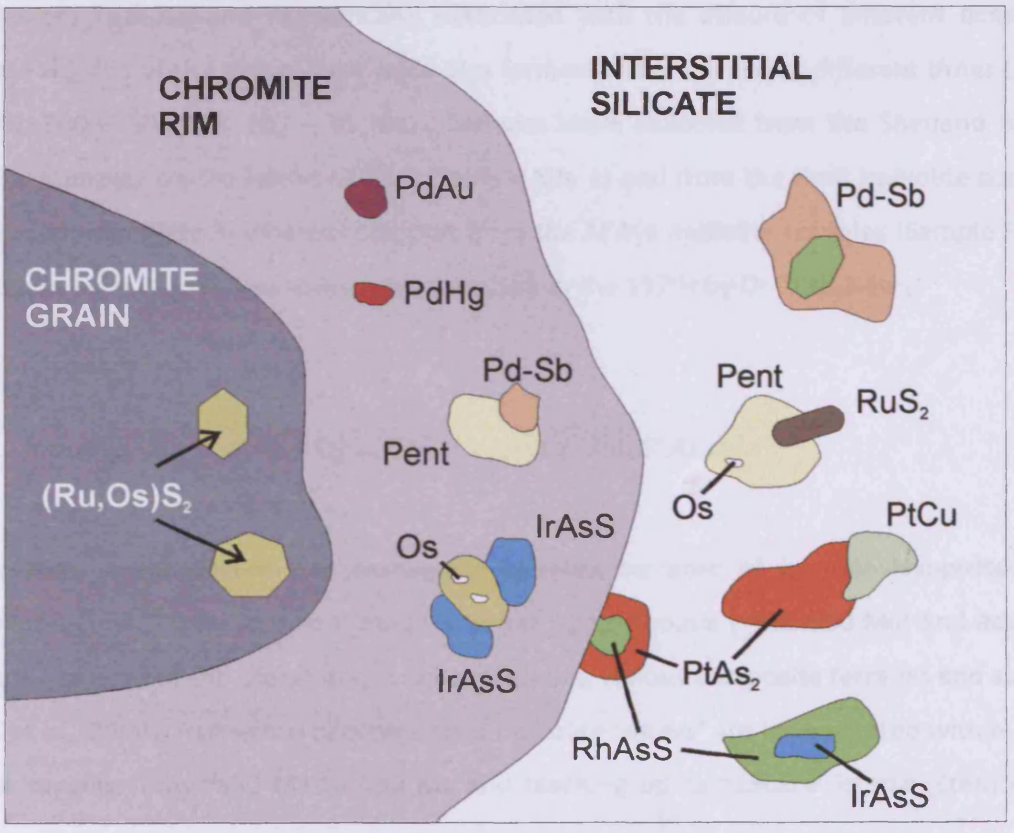

Figure 1.12: *Schematic diagram showing the different textural arrangements of PGM grains (Prichard and Tarkian, 1988; Prichard et al., 1989).*

From these textural relationships it is possible to derive a general order of PGM crystallization (though there may be some variation between specific ophiolite settings). Firstly, euhedral, IPGE-bearing PGM included within chromite, preceded chromite crystallization. Subsequent PGM, found within the spongey rim of chromite grains, formed at an intermediate stage and for the Shetland ophiolite complex included osmium-poor laurite and palladium-bearing PGM. The osmium-poor PGM may have lost Os during alteration and serpentinisation (Tarkian and Prichard, 1987; Prichard and Tarkian, 1988). At the same locality rhodium and platinum are only found within the silicate matrix suggesting they were the last PGE to be made available for crystallization (e.g. Prichard and Tarkian).

1.7 Tectonic Settings

PGE concentrations in chromitites from ophiolite complexes in three separate tectonic settings were investigated in the current study. They cover three different orogenic systems (Caledonian, Tethyan and Pan-African), associated with the closure of different oceans in separate regions of the globe. They were also formed and emplaced at different times (750 – 600 Ma, 600 – 500 Ma, 100 – 85 Ma). Samples were collected from the Shetland Islands ophiolite complex on the island of Unst (Sample Site 2) and from the Berit ophiolite complex in Turkey (Sample Site 3) whereas samples from the Al'Ays ophiolite complex (Sample Site 1) were taken from an archived collection assembled in the 1970s by Dr Chris Neary.

1.7.1 Sample Site 1: Al'Ays Ophiolite Complex, Saudi Arabia

The Arabian shield (Figure 1.9) represents accreted terranes of juvenile Neoproterozoic continental crust. These formed during the break up of Rodinia (~800-900 Ma) and accreted during the closure of the Mozambique ocean, forming various composite terranes and sutures (Stern *et al.*, 2004). Numerous allochthonous ophiolite 'slivers' are incorporated within these sutures ranging from ~890 Ma to 690 Ma and reaching up to ~150km^2 in size (Stern *et al.*, 2004).

The Al'Ays complex forms part of the largest mafic-ultramafic crystalline ophiolite complex within the Saudi Arabian shield; the Jabal al Wask complex. It is located to the north-west of the Arabian shield on the Yanbu suture, which lies between the Midyan terrane to the north and the Hijaz terrane to the south (Johnson *et al.*, 2004) (Figure 1.9).

Dating of the Jabal al Wask ophiolite by (Pallister *et al.*, 1988) has reported ages ranging from 695 to 770 Ma based on zircons derived from gabbros (772 ± 16 Ma, 751 ± 11 Ma), plagiogranites (740 ± 11 Ma) and tonalites (four zircons each giving a model age of 696 ± 5 Ma). Dating of the ophiolite using Sm-Nd mineral and whole-rock techniques put the age at 743 Ma (Claesson *et al.*, 1984). Emplacement of the ophiolite likely occurred after the last of the tonalites (Salajah tonalite), which puts emplacement between 600 and 700 Ma.

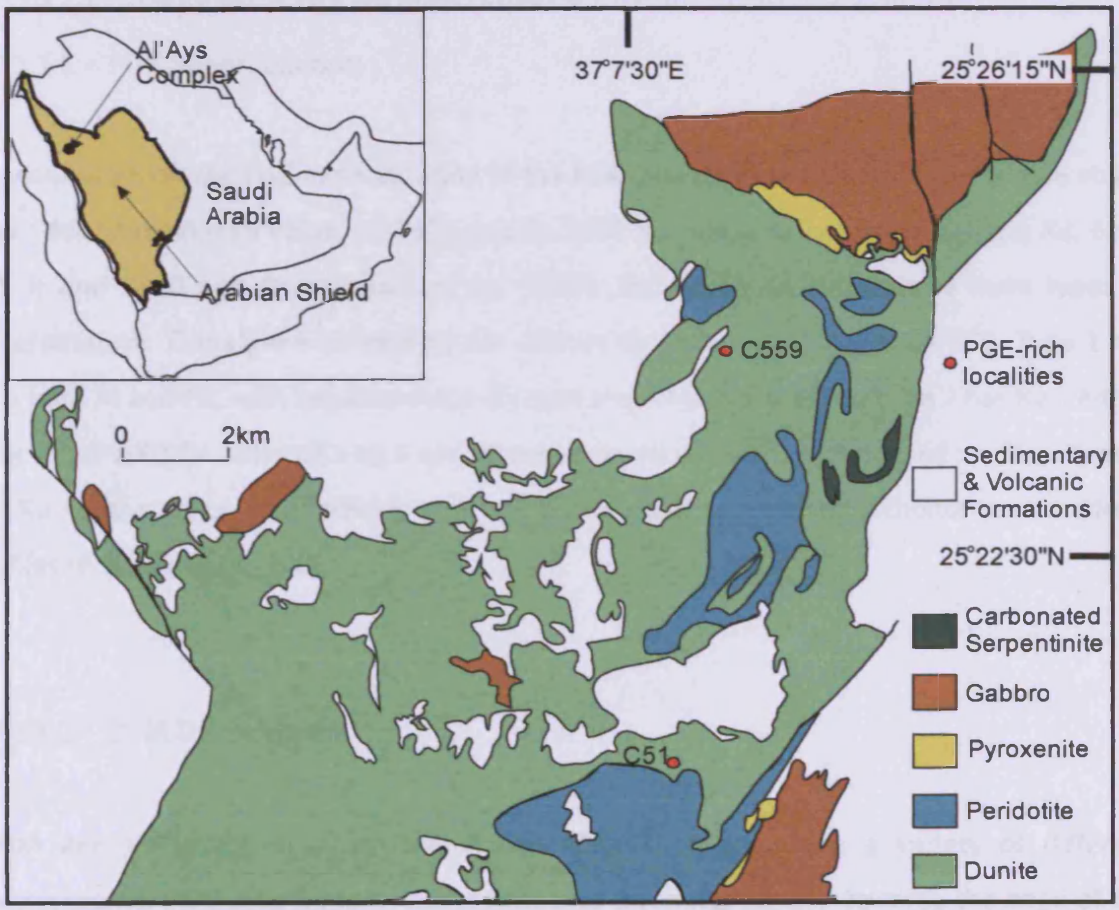

Figure 1.13: *Geological map of the Al'Ays Complex, Saudi Arabia, showing the locations of the two richest sample sites (C51 & C559). Adapted from Prichard et al. (2008).*

It was speculated during that 1970s that the The Al'Ays ophiolite formed in a supra-subduction zone setting (Neary, 1974; Bakor *et al.*, 1976), indeed Bakor *et al.* (1976) postulated that it originated in a back-arc setting. More recently it has been argued that, on the basis of the Cr#-Mg# values of residual chromite within harzburgite, that the ophiolite actually formed within a fore-arc setting (Stern *et al.*, 2004). The ophiolite contains several features diagnostic of a supra-subduction zone ophiolite. These include; a thick ultra-mafic sequence associated with podiform chromitites (Neary, 1974) and the presence of adakites, a rock type thought to be specifically associated with island-arc formation (Ahmed, 2003). Furthermore, these adakites carry the direct genetic implication of being formed from magma generated by partial melting of a descending hydrated basaltic slab (Ahmed, 2003).

1.7.1.1 Previous work on PGE mineralization within the Al'Ays ophiolite

1.7.1.1.1 PGE Mineralization

Previous work on the PGE mineralization of the Al'Ays complex has been limited to one study, which found maximum values of 2570 ppb Pt, 6870 ppb Pd, 840 ppb Rh, 5800 ppb Ru, 6200 ppb Ir and 3300 ppb Os (Prichard *et al.*, 2008). This study recorded three main types of mineralization. These were defined by the relative abundances of individual PGE. Type 1 has Ru > both Pt and Pd, with negative slope chondrite-normalized profiles. Type 2 has Ru < either Pt or Pd, (Pt+Pd)/Ir ratios of 1 to 5 and convex upward chondrite normalized profiles. Type 3 has Ru < either Pt or Pd, (Pt+Pd)/Ir ratios of 5 to 60 and positive slope chondrite normalized profiles (Prichard *et al.*, 2008).

1.7.1.1.2 PGM Development

PPGM and IPGM are observed within the Al'Ays ophiolite, with a variety of different developments. PGM may be fully enclosed within chromite, located towards the edge of the chromite grain or within the interstitial silicate matrix. Os-Ir-Ru-bearing PGM predominate within the enclosed part of the chromite, whilst PGM within the spongey rim of chromite or the interstitial silicate are far more diverse and may contain all 6 PGE as major components.

PGM from Al'Ays are very diverse. IPGM include Os-Ir-Ru alloys, Os- and Ir- bearing laurites, irarsite, Ir-Ni-Fe alloys, ruthenian cobaltite and ruthenian pentlandite. PPGM include hollingworthite, Rh antimonides, Rh arsenides, Pt-Pd-base metal alloys, geversite, sperrylite, Pd arsenide and Pd telluride. In addition pervasively altered PGM were PGE oxides, with all the PGE except Os, being found as oxides. The PGM enclosed in chromite are often euhedral whereas those in the interstitial matrix are irregular, mottled and inhomogeneous (Prichard *et al.*, 2008).

1.7.2 Sample Site 2: The Shetland Ophiolite

The Shetland Islands are situated north-northeast of Scotland (Figure 1.10) and consist of Caledonian and pre-Caledonian rocks surrounded by Devonian and younger sediments. In its continental pre-drift position the ophiolite lay midway between Scotland, Greenland and Norway (Flinn and Oglethorpe, 2005). The islands are transected by a major sinistral transcurrent fault which has been postulated to be the extension of the Great Glen fault/ Walls Boundary fault (Flinn, 1992). The Shetland ophiolite complex lies on the north-eastern most islands of Unst and Fetlar and consists of a basal thrust, overlain by harzburgite, cumulate dunite and gabbros (Figure 1.10). It is thought to have formed, in its original setting, around 600 Ma during the opening of the Iapetus ocean (Flinn and Oglethorpe, 2005). It is therefore an early Paleozoic ophiolite associated with the Appalachian-Hercynian-Caledonian-Uralian ophiolite groups.

Spray (1988) postulated that the Shetland ophiolite complex was derived from a marginal basin on the western edge of the Iapetus ocean. However, the ophiolite contains features unrelated to marginal basin settings, in particular there is clear evidence of subduction zone fluid input (in the form of pervasive hydration and podiform chromitite formation). Flinn and Oglethorpe, (2005) instead suggested that the ophiolite formed in an intra-continental ocean floored basin on the eastern edge of Laurentia. Around 500 Ma obduction initiated and overrode the highly metamorphosed Shetland-dalradian schists. This resulted in the exposure of ophiolitic pseudo-stratigraphy from the upper mantle through lower crustal ultramafics upwards to the base of the sheeted dykes (Figure 1.10) (Flinn and Oglethorpe, 2005).

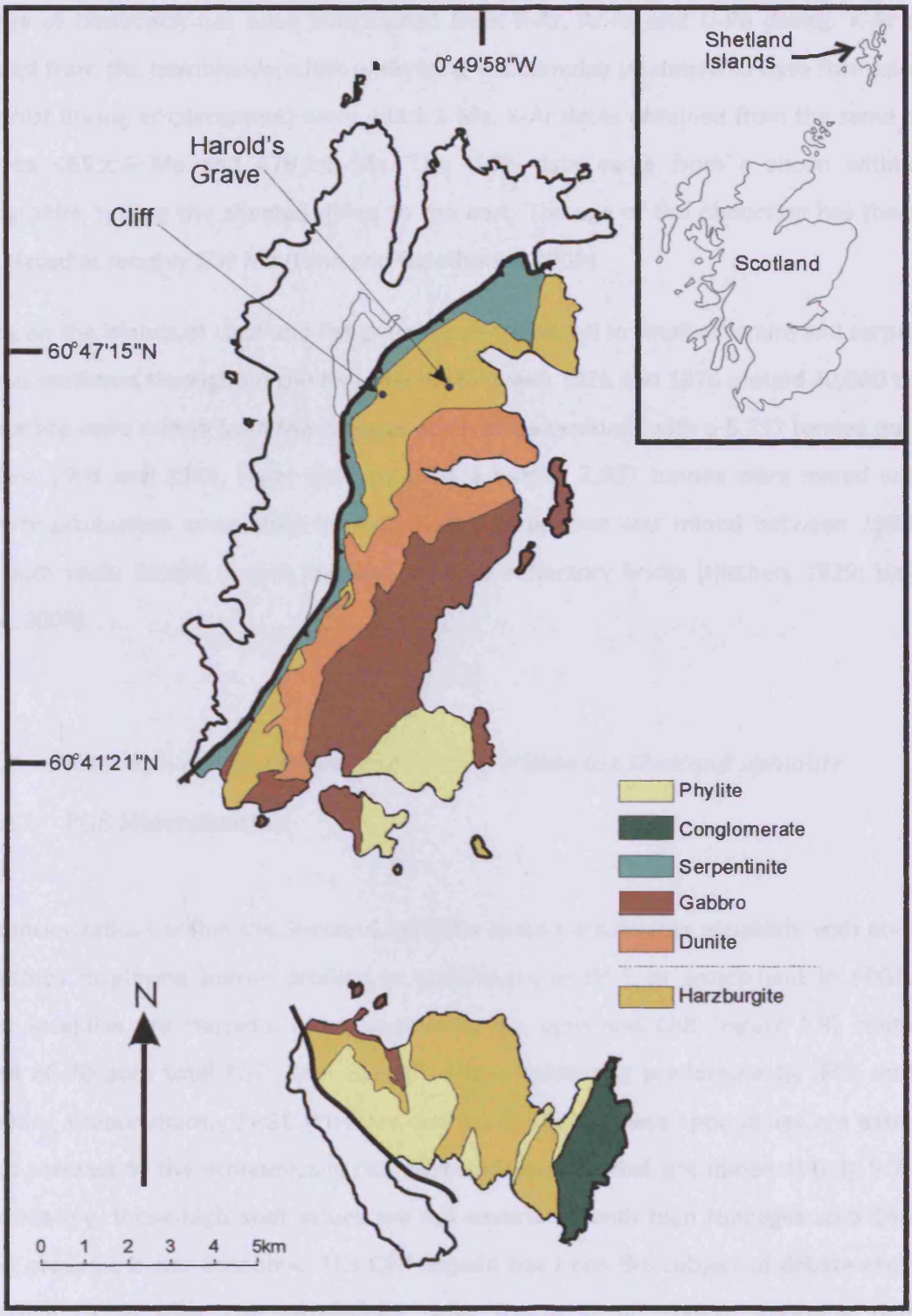

Figure 1.14: *Geological map of the Shetland ophiolite complex, developed on the islands of Unst and Fetlar. The petrological moho lies between the harzburgite and the dunite (BGS, 2002), and is marked by the dotted line in the key. The inset shows the position of the Shetland islands relative to Scotland. Also shown are the locations of the two chromitite deposits with the highest PGE concentrations (Cliff and Harold's Grave).*

The age of obduction has been constrained from K-Ar, Ar-Ar and U-Pb dating. K-Ar dates obtained from the hornblende schist underlying the complex (assumed to have formed along the thrust during emplacement) were 498 ± 2 Ma. K-Ar dates obtained from the same schist came to 465 ± 6 Ma and 479 ± 6 Ma. The U-Pb date came from a zircon within the plagiogranite cutting the sheeted dykes to the east. The age of the obduction has therefore been placed at roughly 500 Ma (Flinn and Oglethorpe, 2005).

Mining on the islands of Unst and Fetlar has been restricted to small chromite and serpentine quarries scattered throughout the two islands. Between 1823 and 1876 around 40,000 tonnes of chromite were mined from the hillsides north of baltasound, with a 5,757 tonnes quarried between 1908 and 1927. From 1936 to 1944 a further 3,907 tonnes were mined with no chromite production since 1944 (HMSO, 1949). Serpentine was mined between 1938 and 1969 with some 55,000 tonnes quarried to make refractory bricks (Hitchen, 1929; Hall and Fraser, 2004).

1.7.2.1 Previous work on PGE mineralization within the Shetland ophiolite

1.7.2.1.1 PGE Mineralization

PGE concentrations within the Shetland ophiolite show considerable variability with podiform chromitites displaying barren profiles or enrichment in IPGE or enrichment in PPGE. The richest localities are Harold's Grave containing 4-5 ppm and Cliff (Figure 1.9) containing around 60-70 ppm total PGE, with Harold's Grave containing predominantly IPGE and Cliff containing predominantly PPGE (Prichard and Lord, 1993). These spot values are extremely high in contrast to the economically rich Bushveld deposits that are mined at only 5-7 ppm. Unfortunately, these high spot values are not associated with high tonnages so a Shetland mining prospect is not economic. The Cliff deposit has been the subject of debate regarding the origin of its high PGE enrichment, with (Gunn *et al.*, 1985) proposing that the mineralization was essentially hydrothermal in origin, whilst (Prichard *et al.*, 1986) argued for a magmatic origin. (Lord *et al.*, 1994) postulated that a magmatic origin with local hydrothermal upgrading was the best explanation, as this fit the clear association of PGE with both magmatic sulphides and hydrothermal As and Sb.

Sulphur isotope analysis of the whole ophiolite has revealed a magmatic signature throughout the sequence with the exception of the lowermost talc-carbonate rocks (which includes samples from the basal thrust near the Cliff locality) and the uppermost gabbros. $\delta^{34}S$ values within the S-bearing crustal dunites of the igneous stratigraphy range from +2.5‰ to +4.3‰ indicating that primary sulphides derived from a magmatic source slightly enriched in $\delta^{34}S$, a source compatible with a supra-subduction zone origin for the ophiolite (Maynard *et al.*, 1997).

In addition to the PGE enrichment present at Cliff and Harold's Grave, there is also a considerable stratigraphically controlled enrichment of PGE within the ultramafic cumulates (Prichard and Lord, 1993; Lord and Prichard, 1997). The Shetland cumulate sequence is marked at the base by a thick (1-2 km) dunite unit in which sulphide mineralization is present, but only sparsely. S-bearing dunites are only found in close proximity to the chromitites which are also present within this thick crustal dunite. Significant PGE enrichment (1-4 ppm) is occasionally found within these sulphide-bearing dunites (Lord and Prichard, 1997).

1.7.2.1.2 PGM Development

As with the Al'Ays ophiolite both PPGM and IPGM are found. Harold's Grave contains IPGM (i.e. Os-, Ir- & Ru-bearing PGM), as well as minor PPGM (i.e. Pt-, Pd- and Rh-bearing PGM) where as Cliff contains common PPGM (e.g. sperrylite) as well as minor IPGM (e.g. irarsite) (Tarkian and Prichard, 1987; Prichard and Tarkian, 1988; Prichard *et al.*, 1989).

There have been several studies of the PGE and PGM development within the Shetland ophiolite, in particular, from Cliff and Harold's Grave. Assuming the prior crystallization of chromite grains before the igneous interstitial matrix, constraints on the order of PGM formation for the Shetland ophiolite can be established. Initial PGM are osmium-rich laurites located within chromite grains. These form the only PGM enclosed within chromites and indicate the early availability of osmium within the igneous system. Within chromite rims, iridium, palladium and ruthenium-rich PGM (e.g. irarsite, mertieite and Ru-rich laurite) become abundant suggesting their increased availability after initial chromite crystallization.

Laurite grains switch from being osmium-rich to osmium-poor implying either formation in an osmium-poor environment or re-equilibration of existing laurite with the surrounding silicate crystal mush. Laurite within the interstitial silicate becomes altered to expel Os and Ir, which forms native Os associated with irarsite (IrAsS) and pure laurite (RuS_2) (Prichard *et al.*, 1986). Outside of the chromite rims the last PGM to form contain rhodium and platinum (e.g. hollingworthite ((Rh,Pt,Pd)AsS) and sperrylite ($PtAs_2$)). During serpentinisation and weathering As, Te, Bi and S are lost producing first, PGE-alloys, and then PGE-oxides (Prichard and Tarkian, 1988; Prichard *et al.*, 1994).

1.7.3 Sample Site 3: Berit, Turkey

Ophiolites within the eastern Mediterranean lie in two main belts, namely the N-S trending Jurassic Dinarides-Hellenides within the Balkan peninsula and the E-W trending Cretaceous Taurides in southern Turkey (Uysal *et al.*, 2007; Kozlu *et al.*, 2010). The Taurides contain numerous ophiolite slivers which have been of economic importance for chromitite mining for many years. Indeed there are over 2000 chromitite deposits within Turkey (Uysal, 2008), split into six geographic regions (Kozlu *et al.*, 2010) (Figure 1.15).

Berit, which is located just north of the East Anatolian Fault, is one such chromitite-bearing ophiolite complex located within the Tauride thrust belt (Dilek *et al.*, 1999). It formed as an oceanic island arc within the southern Neotethys and was accreted on to the northward edge of the active margin over Miocene sediments around 85 Ma (Robertson *et al.*, 2006). It therefore represents a typical Mediterranean-type ophiolite formed in a SSZ setting. This ophiolite was intruded by granites 70-85 Ma (Robertson *et al.*, 2006), and is now dismembered (Yigitbas, 1989). The chromitites are predominantly located within the mantle/ crust boundary but also to a lesser extent within mantle tectonites (Figure 1.16). The Cr# of the pods range from high aluminium chromitites (0.29-0.37) to high-Cr chromitites (0.60-0.70) (Kozlu *et al.*, 2010).

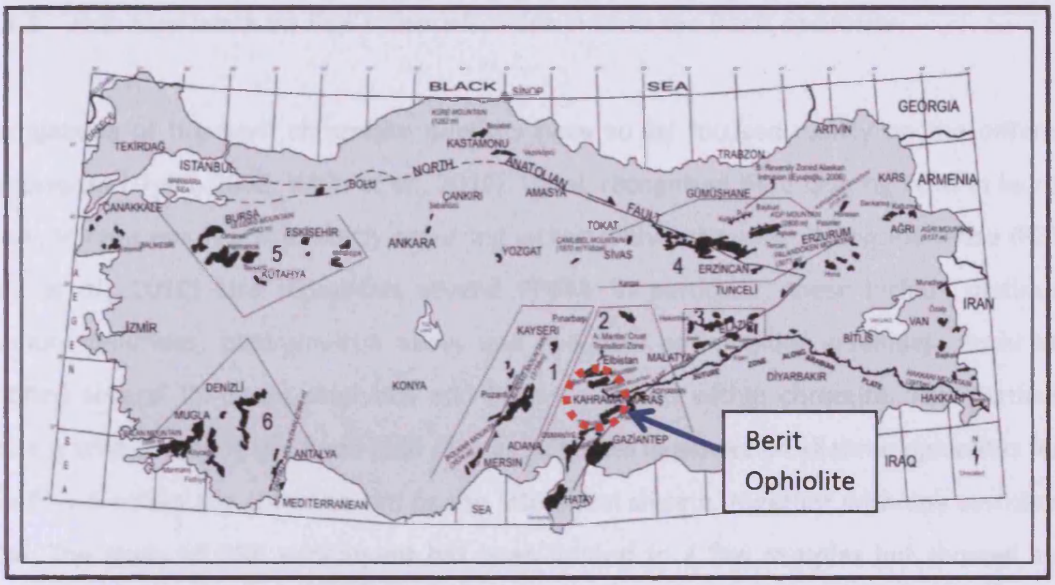

Figure 1.15: *Chromitite-bearing ophiolites within Turkey. 1-Mersin-Adana (Pozantı, Karsantı chromitites)-Kayseri (Pınarbaşı cromitites); 2-Kahramanmaraş (Elbistan-Türkoğlu chromitites), Hatay (İskenderun, Kızıldağ chromitites); 3-Elazığ (Guleman chromitites); 4-Sivas-Erzincan-Erzurum-Bayburt (Palandöken-Kop mountains chromitites); 5-Bursa-Kütahya-Eskişehir (Harmancık, Orhaneli, Karaburhan, Kavak chromitites) and 6-Muğla –Denizli (Fethiye, Köyceğiz chromitites). The chromite deposits are ordered according to their ore reserves (from the highest (number 1) to the lowest tonnage (number 6); Taken from (Kozlu et al., 2010).*

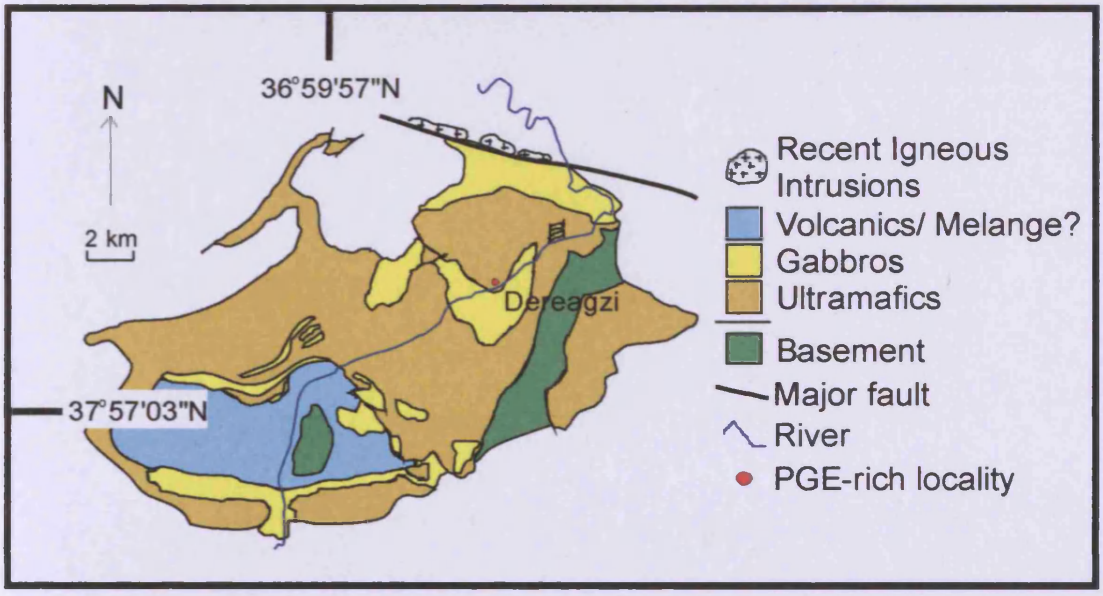

Figure 1.16: *The Berit ophiolite, showing the chromitite samples localities. The Berit ophiolite is located within the 2nd region (Kahramanmaraş) highlighted in Figure 1.15. The map is adapted from field mapping by Aydin Golakoğlu.*

1.7.3.1 Previous work on PGE mineralization within the Berit ophiolite

Investigations of the Berit chromitite deposits have so far focused mainly on the different PGM present (Uysal, 2008; Kozlu *et al.*, 2010). Uysal, recognised IPGE bearing PGM in laurite, iridium, irarsite and ruarsite mostly occurring locked within chromite. Alongside these IPGM, (Kozlu *et al.*, 2010) also recognises several PPGM, in particular, these include platinum-palladium tellurides, platinum-iron alloys and palladian antimonide/ arsenides. Kozlu also identified several Cu-based sulphides and PPGM enclosed within chromite. This particular texture is unique among the three field sites as sulphides in general in all three ophiolites tend to be found within the chromite rim or the interstitial silicate, together with any associated PPGM. The study of PGE enrichment has been limited to a few samples but showed spot values up to 5169 ppb Pt + Pd and 1561 ppb Ir + Ru (Kozlu *et al.*, 2010). These values, together with the unusual Cu-based sulphide inclusions in chromite and PPGM made the Berit ophiolite a good prospect for further investigation.

Chapter 2

Methodology

An overview of the data collection tools employed within this PhD thesis

2 Methodology

2.1 Sample collection

2.1.1 Al'Ays chromitite samples

The chromitites of Saudi Arabia were extensively sampled in the 1970s by Chris Neary, and are now housed in Leeds University and Cardiff University as a series of rock slices, small grab samples, polished blocks and polished thin sections. Aside from the polished samples already available within Cardiff, three excursions were made up to Leeds University to catalogue and then collect samples. Dr Robert Finch and Gary Keech provided access to the samples and permission to remove sections for analysis.

2.1.2 Unst chromitite and silicate samples

The chromitites of the Shetlands ophiolite were extensively mined during the latter part of the 19th, and early part of the 20th century. Initial samples were of chromitites and so sampling was restricted to spoil tips, and careful attention was paid to how isolated each quarry was and whether or not any of the spoil tips were likely to have been on the 'donkey trail' down towards the port. The 'donkey trail' was the main transport route of the chromitite samples from their in-situ locality to the exit port, and was located exclusively within the cumulate sequence just north of Baltasound (Figure 4.1). All research was performed on chromitite localities which were isolated from the 'donkey trail'. Dunite and harzburgite samples were collected from samples housed in Cardiff by Dr Hazel Prichard, and these were of similarly constrained spoil tip samples previously collected from Unst .

2.1.3 Berit chromitite and silicate samples

The chromitite deposits have been partially mined, and so presented the opportunity of collecting *in situ* samples with spatial relationships recorded between the individual samples. Three chromitite pods were sampled in detail, one of which had been previously sampled and was known the carry some high spot grades, and the other two of which were new deposits. Both chromitite and silicate samples were collected from these three pods.

2.2 Sample preparation

Once samples were back in Cardiff they were prepared into either polished blocks, polished thin sections (PTS) or crushed to be sent off for PGE analyses. For large grab samples this meant using a large mechanical saw to remove the weathered surfaces and reduce the size of the sample to several smaller samples. These smaller samples were either crushed using a jaw crusher and TEMA mill to produce a powder, or alternatively, cut by a small mechanical saw to the size required for a polished block or polished thin section. The polished blocks were then prepared by either Lawrence Badham (Cardiff University) or Peter Greatbatch (Keele University), depending on how many batches needed to be simultaneously processed. Powders were sent for PGE analyses to Genalysis Laboratories, W.Australia, where they were analysed using Ni-sulphide fire assay.

2.3 Scanning electron microscope (SEM) analysis

Major and minor elements were analysed using the Cambridge Instruments (ZEISS SMT) S360 scanning electron microscope (SEM), coupled to an Oxford Instruments INCA energy plus which included both an energy dispersive (ED) and a wave dispersive (WD) X-ray analysis system. Chromites were analysed with a 20kV accelerating volatage, 20 nA beam current and fixed beam size (approximately 10-15 nm) with a live-time of 50 s for EDX. Ti, V, Mn and Ni were analysed by WDX with count times of 20 s with 5 s on the background. A cobalt standard and separate chromite standard were used to monitor for instrumental drift. Throughout the course of the thesis three internal standards were used (C51, MBD-7 and MBD-8) to monitor for instrument drift. C51 was the initial sample. Although nothing was wrong with this sample it was decided to switch to MBD-8 early on as the degree of alteration was noticeably less. MBD-8 then broke, so the standard was switiched to MBD-7.

Each chromitite sample was analysed to maximise areal coverage, with 4-5 grains selected and the unaltered cores of the grains analysed twice. For the silicate samples 3-4 co-existing chromite and olivine grains were selected and the unaltered cores of the grains analysed twice. For each trace element in question a limit of detection (LOD) and a limit of quantification (LOQ) were first calculated (Table 2.1).

Table 2.1: *Calculated LOD and LOQ values for the trace elements analysed on the SEM.*

Element	LOD (*wt.%*)	LOQ (*wt.%*)
Mn	0.020	0.067
V	0.022	0.075
Ni	0.024	0.080
Ti	0.011	0.036

Three different chromitite samples were used to determine the LODs and the LOQs; C10 (Al'Ays, podiform, Saudi Arabia), 185A (stratiform, Madagascar) and SD159b (podiform, Oman). These values were determined by taking the difference between the peak and the background counts per second and then plotting this against the calculated concentration. The gradient of the resultant graph was then recorded. The standard deviation of the background values was then calculated. Multiplying this value by the gradient of the graph and then by 3 gives the LOD. The same procedure is followed for the LOQ just with a multiplication factor of 10 instead of 3.

2.3.1 Data Reliability – chromite analysis from chromitite samples

When handling such large quantities of data it is important that the data is both *reliable* and *valid*. A *reliable* measure is one where you are measuring values consistently, whereas a *valid* measurement is one where you are measuring the correct parameter. As such reliability is necessary but not sufficient for validity. Within these experiments it was relatively easy to ensure the correct measurement of mineral species, that is, through the use of the SEM imaging facility it was easy to pinpoint the mineral grains of choice and restrict the analyses to these. It was therefore easy to ensure *validity* providing that *reliability* could be shown. Two assumptions underlie the collection of quantitative data from chromite grains within a sample.

1. The first is that the composition of an individual chromite grain is homogenous.
2. The second is that all the other chromite grains within the sample contain the same composition, (i.e. the sample is homogenous).

In all, the range of CV values for each of the analyzed elements within the standards provides a measure of the reliability expected within a sample as a whole and allows the assessment of the second assumption – namely that chromite grains within a sample all contain the same geochemical signature.

A comparison of the CV's obtained within the individual standards with the average CV's obtained from the samples within the different fieldwork sites reveals a strong similarity (Table 2.3), showing that, on average, samples may be considered as being at least as geochemically homogenous as the individual grains within the internal standards. However, as this CV is an average there will be some samples with elemental analyses containing CV's greater than the mean CV. Some of these values may be too high meaning the sample concerned should be considered as geochemically heterogeneous.

Table 2.3: *Table comparing the coefficient of variance values obtained from the standards with the mean coefficient of variance values obtained from chromite samples from the different fieldwork sites.*

		MBD-7	MBD-8	C51	Al'Ays	Shetland	Berit
		CV	CV	CV	Mean CV	Mean CV	Mean CV
	N	*284*	*34*	*80*	*43*	*59*	*87*
Major Elements	MgO	1.99	1.49	1.88	1.70	2.64	1.56
	Al_2O_3	1.34	1.28	1.49	2.93	1.91	1.69
	Cr_2O_3	2.20	0.99	1.04	1.02	1.01	1.03
	FeO^{tot}	1.25	1.67	4.03	2.06	3.03	2.04
Trace Elements	TiO_2	5.15	10.79	9.74	10.36	7.56	8.95
	V_2O_5	8.26	13.25	14.43	14.83	11.73	8.97
	MnO	6.74	8.78	7.79	6.24	7.78	5.13
	NiO	13.07	12.16	11.51	16.36	16.34	11.72
Ratios	Cr#	1.65	0.88	0.70	0.86	0.83	1.10
	Mg#	1.78	1.20	1.63	1.42	2.27	1.31
	Cr/Fe^{2+}	3.04	2.47	3.42	2.14	3.80	2.29

Although one or two samples may be geochemically heterogeneous, the effective comparison of data between chromite samples depends on the CV within a field site being greater than the CV in a thin section. This is readily shown for the major elements (Al_2O_3, Cr_2O_3, MgO and FeO^{tot}) (Figure 2.1), where average CV values for the individual samples are far smaller than the CV values for each site.

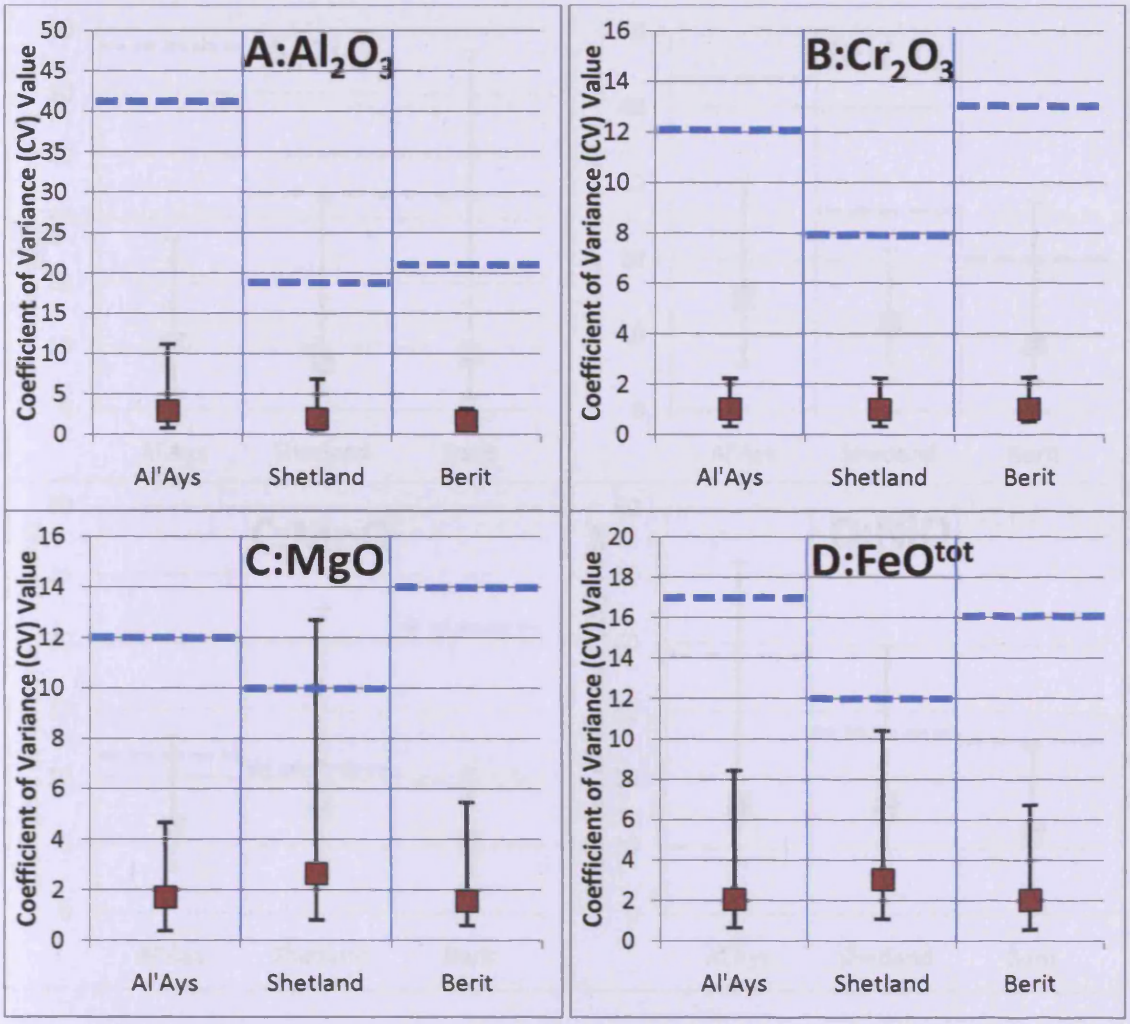

Figure 2.1: *Graphs of the mean, minimum and maximum CV value for major elements for chromitite samples from each field site. This is compared with the CV of that particular field site. Mean values are shown by red squares and the blue dashed line refers to the CV value for the whole field site for that particular element. A: Al_2O_3, B: Cr_2O_3, C: MgO, D: FeO^{tot}.*

Within the major elements there is one sample which shows greater heterogeneity than the field site which is Q3b for MgO within Shetland. After Q3b the next highest CV value is Q2 with 8.27, which is comfortably below the CV value of the field site (10.48).

Within the trace elements the average CV values are similarly comfortably below the CV value for each field site (Figure 2.2). There are a few individual exceptions. For TiO_2 there is one sample within Shetland (CF11) and one sample within Berit (MBD-8A) that approaches or exceeds the CV values of the field site. For V_2O_5 there is one sample within Berit (MBK-2), with a CV value that is too high.

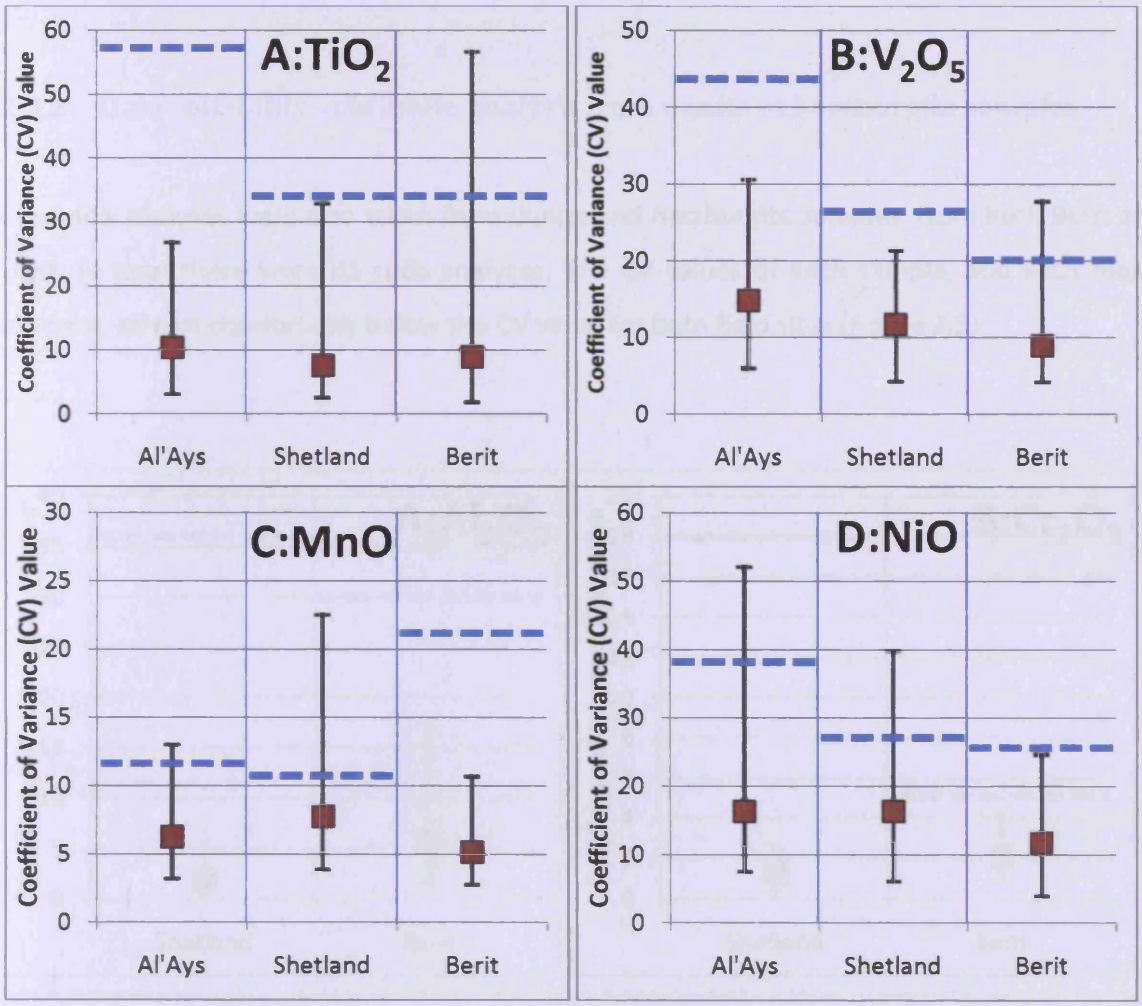

Figure 2.2: *Graphs of the mean, minimum and maximum CV value for trace elements for chromitite samples from each field site. This is compared with the CV of that particular field site. Mean values are shown by red squares and the blue dashed line refers to the CV value for the whole field site for that particular element. A: TiO_2, B: V_2O_5, C: MnO, D: NiO.*

For MnO there are several samples which exceed or approach the average CV value of the individual field site – particularly within Shetland. This may be down to two main factors. Firstly, the MnO values of the Shetland chromitites (and the Al'Ays chromitites) are very constant, leading to low CV values for the field sites. Secondly, during data collection on the SEM there is interference between the Cr-β peak and the Mn-α peak. As Cr is such a major element within chromite it is possible that the Cr-β peak artificially inflates the Mn values making it difficult to distinguish the lower Mn values. For NiO there are a few samples which contain particularly high CV values. Within Al'Ays, these are C311, C580, C54 and C60. For Shetland, these are HG5, Q3PX, Q3b, Q3a, CF14, CF6 and CF3. Within Berit, these are MBT-15, MBK-14 and MBK-2. Samples with major and trace elements with high CV values (exceeding or approaching the CV value of the field site) were considered heterogeneous.

2.3.2 Data reliability - chromite analysis from dunite of harzburgite samples

Chromite analyses were also taken from dunite and harzburgite samples, from both Berit and Unst. In total there were 33 such analyses. The CV values of each sample, and each major element, all plot comfortably below the CV value for both field sites (Figure 2.3).

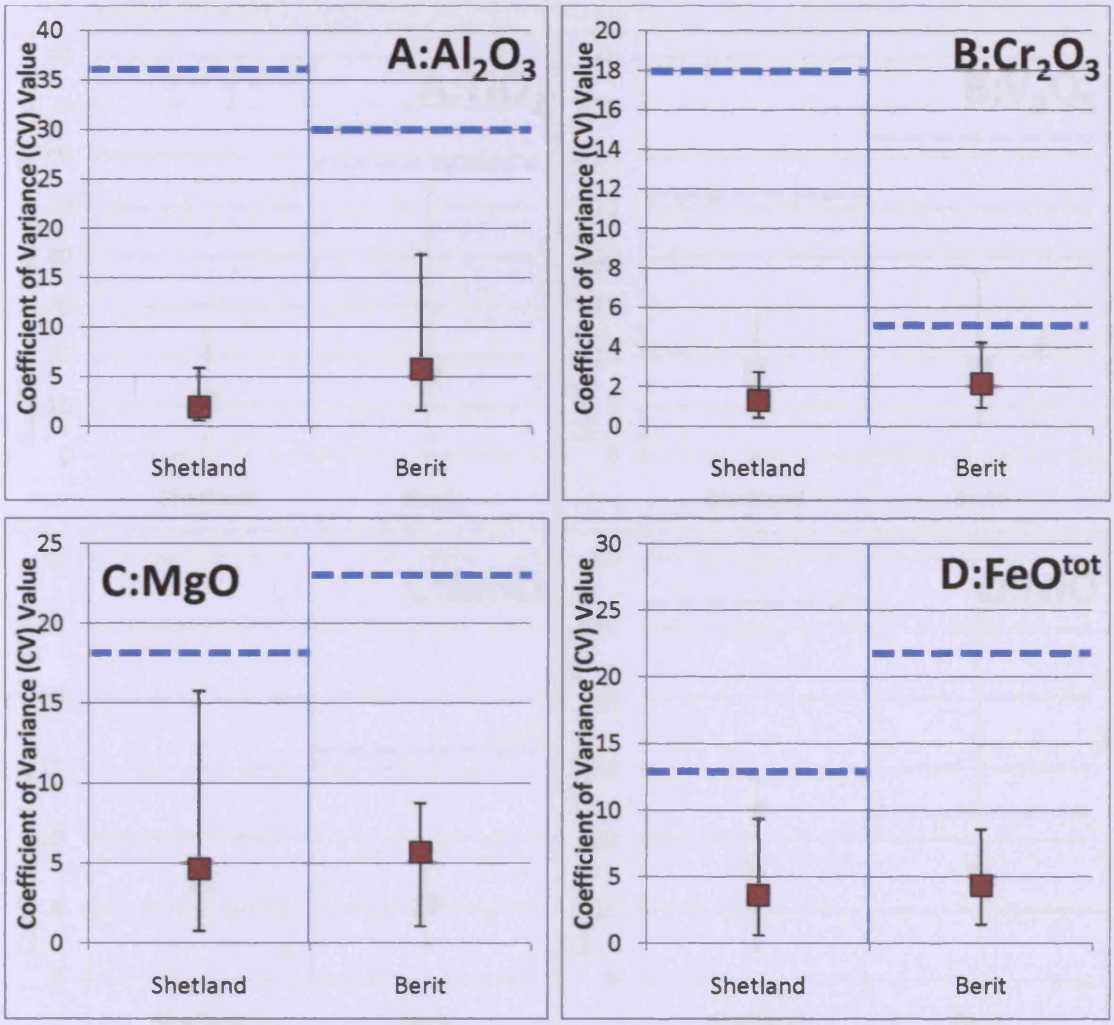

Figure 2.3: *Graphs of the mean, minimum and maximum CV value for major elements from silicate samples from each field site. This is compared with the CV of that particular field site. Mean values are shown by red squares and the blue dashed line refers to the CV value for the whole field site for that particular element. A: Al_2O_3, B: Cr_2O_3, C: MgO, D: FeO^{tot}.*

2.3.3 Data reliability – olivine analysis

Olivine grains were analysed from 45 different samples. They were analysed for SiO_2, MgO, FeO^{tot} and the four trace elements (TiO_2, V_2O_5, MnO & NiO). TiO_2 and V_2O_5 were invariably below detection limit, meaning MnO and NiO were the only detectable trace elements within the olivine grains. SiO_2 is roughly constant, as the amount of silica within olivine, regardless of its forsterite content, does not vary. This is reflected within the CV values, with no value greater than 1.23 from the two field sites. For the remaining major elements CV values are comfortably below the CV for each field site (Figure 2.5).

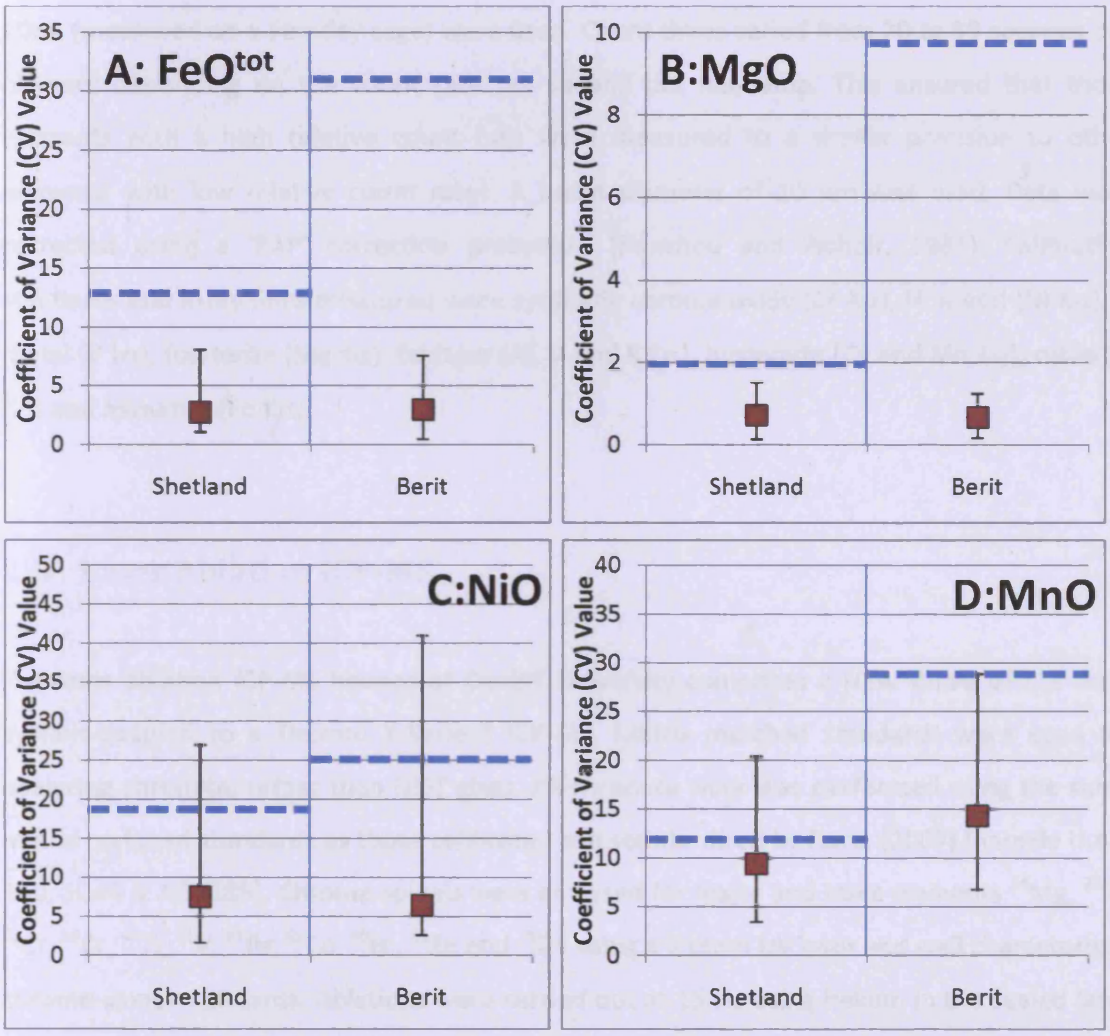

Figure 2.5: *Graphs of the mean, minimum and maximum CV values for olivine grains from from each field site. This is compared with the CV of that particular field site. Key is as for previous figures. A: FeO^{tot}, B: MgO, C: NiO, D: MnO.*

For the trace elements there are a few samples with high CV values. For NiO, these include MR12, from Shetland, and MBD-11 from Berit. For MnO, these include RLM026, MR267 and RL016 from Shetland, and MBD-11 and DMK-9 from Berit.

2.4 Electron Probe Micro-Analyzer (EPMA)

Further investigations into the homogeneity of a chromitite sample were carried out on an Electron Probe Micro-Analyzer (EPMA) housed at the Open Unviersity in Milton Keynes. This is a Cameca SX100 microprobe operating in wavelength-dispersive mode and equipped with five wavelength dispersive spectrometers. An operating voltage of 20kV and probe current of 20nA (measured on a Faraday cage) were used. Count times varied from 20 to 80 seconds per element depending on the count rate per second per nanoamp. This ensured that those elements with a high relative count rate were measured to a similar precision to other elements with low relative count rates. A beam diameter of 10 μm was used. Data were corrected using a 'PAP' correction procedure (Pouchou and Pichoir, 1985). Calibration standards and X-ray lines measured were synthetic chrome oxide (Cr Kα), Ni metal (Ni Kα), V metal (V Lα), forsterite (Mg Kα), feldspar (Al, Si and K Kα), bustamite (Ca and Mn Kα), rutile (Ti Kα) and hematite (Fe Kα).

2.5 Laser Ablation ICP-MS

The laser ablation ICP-MS housed at Cardiff University comprises a New Wave UP213 laser system coupled to a Thermo X-Series2 ICP-MS. Matrix matched standards were used for analyzing chromite, rather than NIST glass. All chromite work was performed using the same matrix matched standards as those calibrated and standardised by Dare, (2007) (namely U.A.E 140, SD44 & ADK185). Chrome-spinels were analysed for major and trace elements ^{24}Mg, ^{27}Al, ^{52}Cr, ^{53}Cr, ^{47}Ti, ^{51}V, ^{57}Fe, ^{59}Co, ^{60}Ni, ^{66}Zn and ^{71}Ga using a 213nm UV laser and well characterised chrome-spinel standards. Ablations were carried out at 15 Hz using helium in the sealed laser cell, and the resulting vapour was combined with argon before delivery into the ICP-MS. Ablations were acquired in time-resolved analysis (TRA) mode and consisted of a trace approximately 250 μm long, 40 μm wide and 10 μm deep. Typical acquisitions lasted 80 seconds.

The laser ICP-MS was tuned at the start of the day using NIST 612 to reduce low mass sensitivity while maintaining or enhancing mid to high mass sensitivity. Analytical runs consisted of a calibration block involving two measurements of three chrome-spinel standards (UAE 140, SD44 and ADK185) followed by NIST612 standards and the chromite grain analysis. Around 40-60 laser traces could be gathered in a day, which emphasizes the speed of acquisition that is possible when using the laser ICP-MS. After background correction of the data, the signals were normalized against the Mg analysed from each chromite grain on the SEM. This corrected for differences in the absolute amount of material ablated and transported during any individual analysis. This corrected signal was then converted into elemental concentrations by calibration against chromite standards (UAE 140, SD44 and ADK185). Data comparison between laser ablation and scanning electron microscope data reveals significant 1:1 relationships for Al, Cr, Fe, Ti, V, Fe and Ni (Figure 2.6). Al, Ti and Ni have particularly strong correlations ($r^2 > 0.9$). The deviations observed within the 1:1 relationship for Cr are due to two main factors. Firstly, the dynamic range for the linear calibration is exceeded at high Cr# (Figure 2.6) and secondly spikes in the TRA are caused by interferences of $^{40}Ar^{12}C$ on ^{52}Cr. This is most likely due to tiny remnants of carbon coat which may remain on the surface of the sample, possibly within fine cracks, even after careful cleaning.

2.5.1 Fe, Co and Zn values

The lower r^2 value for Fe (Figure 2.6) is due to the semi-quantitative analysis of Fe on the laser ablation system. The difficulty arises because Fe is present within the chromite lattice as both Fe^{2+} and Fe^{3+} cations, whilst the ICP-MS system only analyses for the ^{57}Fe isotope. Co and Zn are also semi-quantitative. This means that relative differences between samples should be accurately recorded (i.e. that sample A contains twice as much Co as sample B), but that the absolute values of Co in each sample are not known (i.e. does sample A contain 40 ppm to sample B's 20 ppm, or 80 ppm to 40 ppm). An unexpected inconsistency occurred with the Co and Zn analyses in that runs carried out on different days, on the same sample, often had differing values – varying by 100-150%. In order to mitigate against this effect 11 samples were re-run (incorporating samples collected on each of the previous 6 days). The difference in Co and Zn values between this day and each of the previous days was used to create an adjustment factor. Data from each of these days were then calibrated against this last day's

run and all the Co and Zn data adjusted accordingly. The effect of this adjustment was to reduce differences between days to no more than 30%.

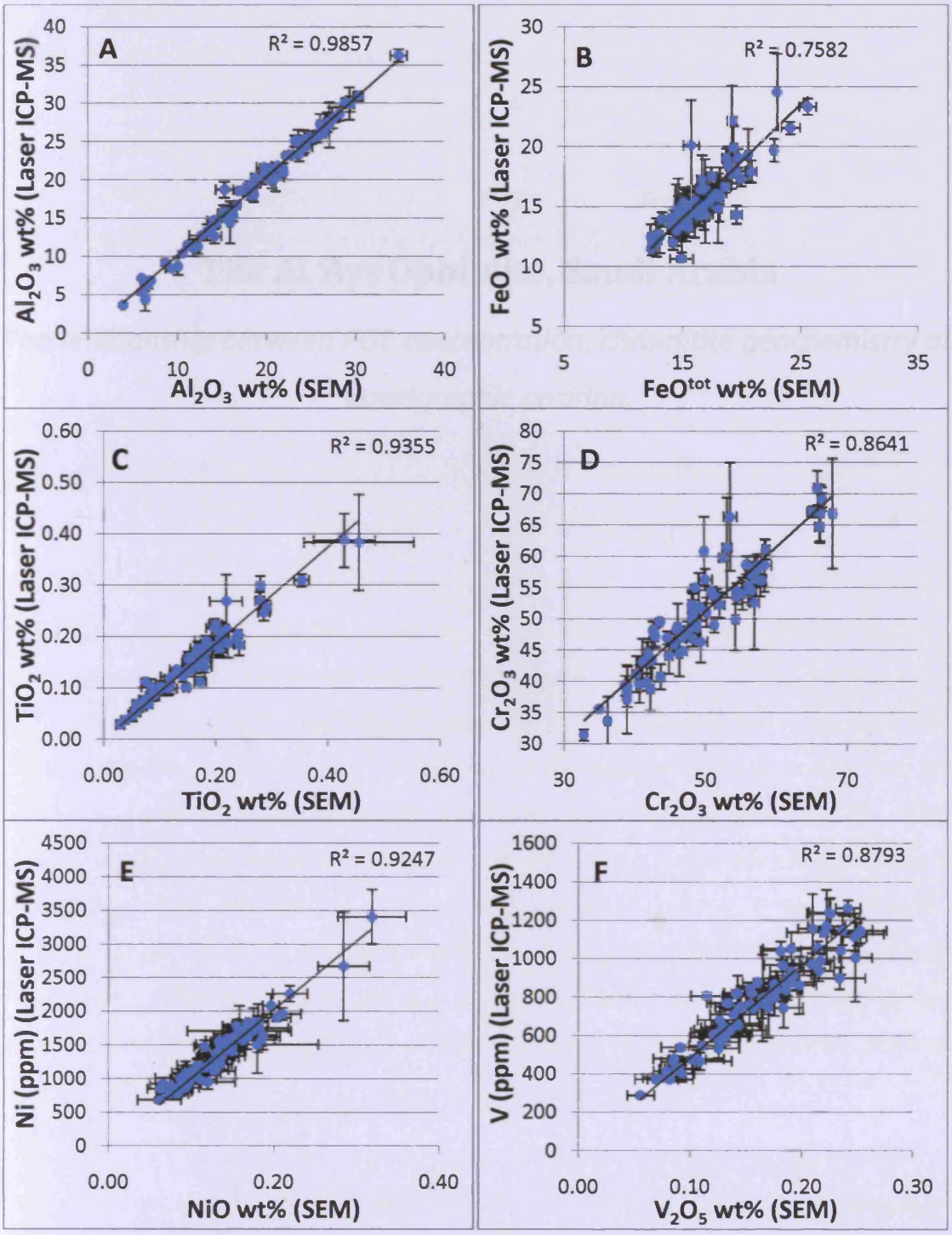

Figure 2.6: *Comparison of Laser-ablation ICP-MS and Scanning electron microprobe values for A:Al_2O_3, B: FeO^{tot}, C: TiO_2, D: Cr_2O_3, E: NiO and F: V_2O_5. Error bars are plus and minus one standard deviation.*

Chapter 3

The Al 'Ays Ophiolite, Saudi Arabia

The relationship between PGE concentration, chromitite geochemistry and stratigraphic position.

3 The Al 'Ays Ophiolite

3.1 Chromitite samples

The Al 'Ays mafic and ultramafic complex is one of a number of similar allochthonous slivers cropping out in the Arabian-Nubian Shield within Saudi Arabia (Johnson *et al.*, 2004, Stern *et al.*, 2004; Figure 3.1). The complex is a SSZ ophiolite, which has been interpreted as either a back-arc ophiolite (Bakor *et al.*, 1976) or a fore-arc ophiolite (Stern *et al.*, 2004). It consists of a series of ultramafic and mafic lithologies cropping out over roughly 100 km^2. These lithologies include peridotite, dunite, pyroxenite and gabbro that collectively are thought to be the mantle and mantle-lower crust transition zone of the partially dismembered ophiolite. The crustal units include gabbro and pyroxenite that are located to the north-east and south-east of the ophiolite. The mantle units are serpentinised peridotite (harzburgite) and dunite seen in the south-west to the north-east of the ophiolite. Some of the dunite may be crustal. Chromitite occurrences are ubiquitous throughout the serpentinised peridotite and dunite lithologies.

The present investigations are on chromitite samples collected in the early 1970s, which were taken from within the serpentinised dunite and peridotite units of the ophiolite (Figure 3.1; see Appendix 6 for chromitite pod sizes). Previous work on the Al 'Ays ophiolite suggested that the overall structure of the ophiolite closely resembles a dome anticline (Neary and Brown, 1979), which may partially explain the way the outcrop patterns of the pyroxenite unit wraps around the mantle dunite. Within this study 43 chromitite samples from 35 separate chromitite pods were analysed in detail and consigned to six different stratigraphic groups depending on their distance from outcrops of pyroxenite and gabbro to the north-east and south-east (Figure 3.2). This boundary was chosen as the most easily identifiable stratigraphic marker and a reasonable proxy for the bottom of the crustal cumulates. Owing to the alteration and deformation of the ophiolite the boundary between crustal dunite and mantle dunite is unclear.

The stratigraphic groupings were selected geographically, and with the exception of group 1, each represents a collection of separate chromitite pods located within a similar geographical region that is sub-parallel to the cumulate boundary (Figure 3.2). Stratigraphic group 1 consists of multiple samples collected from one large chromitite pod to the south of the ophiolite (Figure 3.2, Section 3.2 & Appendix 6 for sample location relative to geological map - location taken from Henry & Lefevre, 1966).

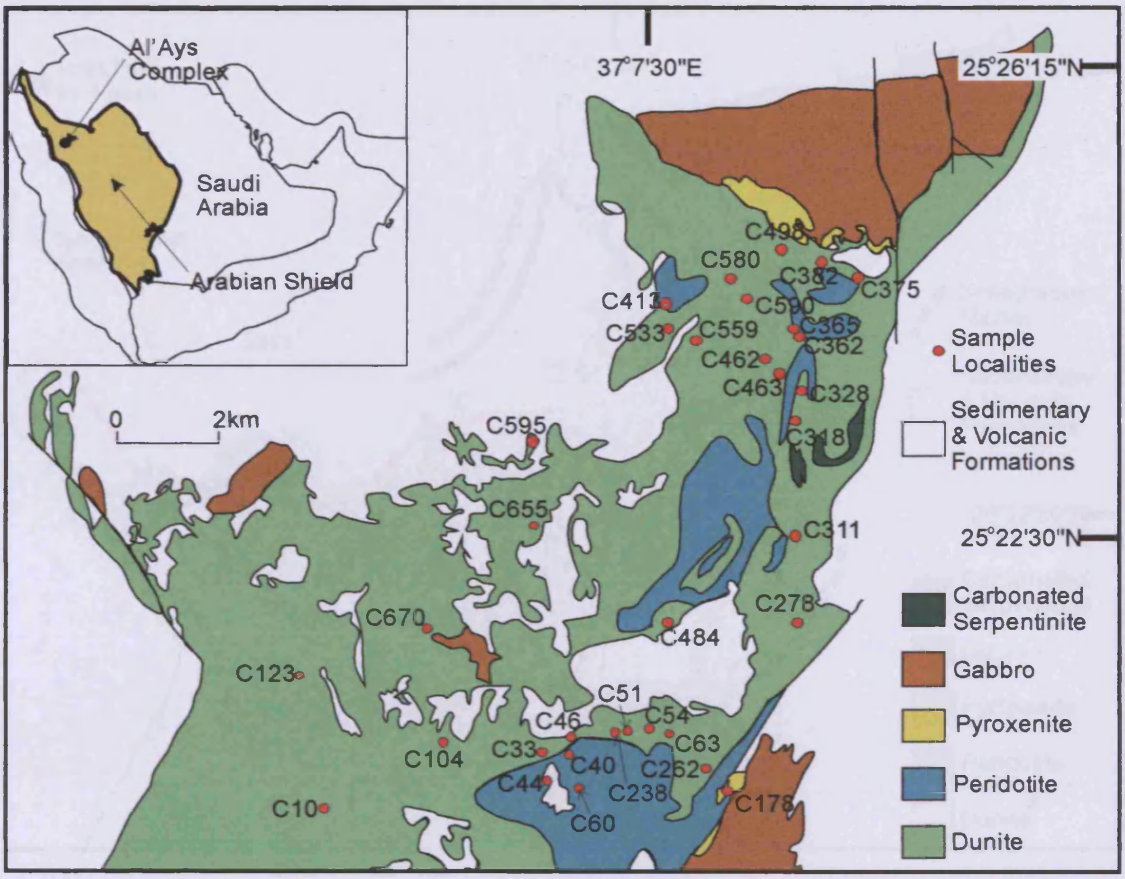

Figure 3.1: *Geological Map of the Al 'Ays ophiolite, showing the locations of the main sample localities. Chromitites C204-215 were collected from one large pod located to the south of this map. Map adapted from Prichard et al. (2008), with an amendment for the location of C655 pers. comm. Chris Neary.*

These different stratigraphic groups were delimited in order to test the proposition that the geochemistry of the chromitites is related to their distance from the pyroxenite/dunite boundary. This idea that had been suggested by Neary (1974) who observed that the Cr/Fe^{2+} ratio and Cr_2O_3 content of chromite grains show a decrease from the south-west to the north-east of the ophiolite. Except for group 1, these 35 chromitite samples had previously been analysed by Prichard *et al.* (2008) for their PGE and major element content. As part of the present study was to examine differences between the major and trace element chromite geochemistry of the defined stratigraphic groups, these 35 samples were supplemented by the analysis of single chromite grains from other chromitite samples within the ophiolite. These supplementary samples have not been analysed for PGE but were analysed for their major and trace element content to strengthen or refute the suspected relationship between chromite composition and the inferred stratigraphy. Single grains from a further 35 chromitite samples were analysed, which equated to a further 7 samples within stratigraphic group 2 through to 6 (Figure 3.2, Table 3.3).

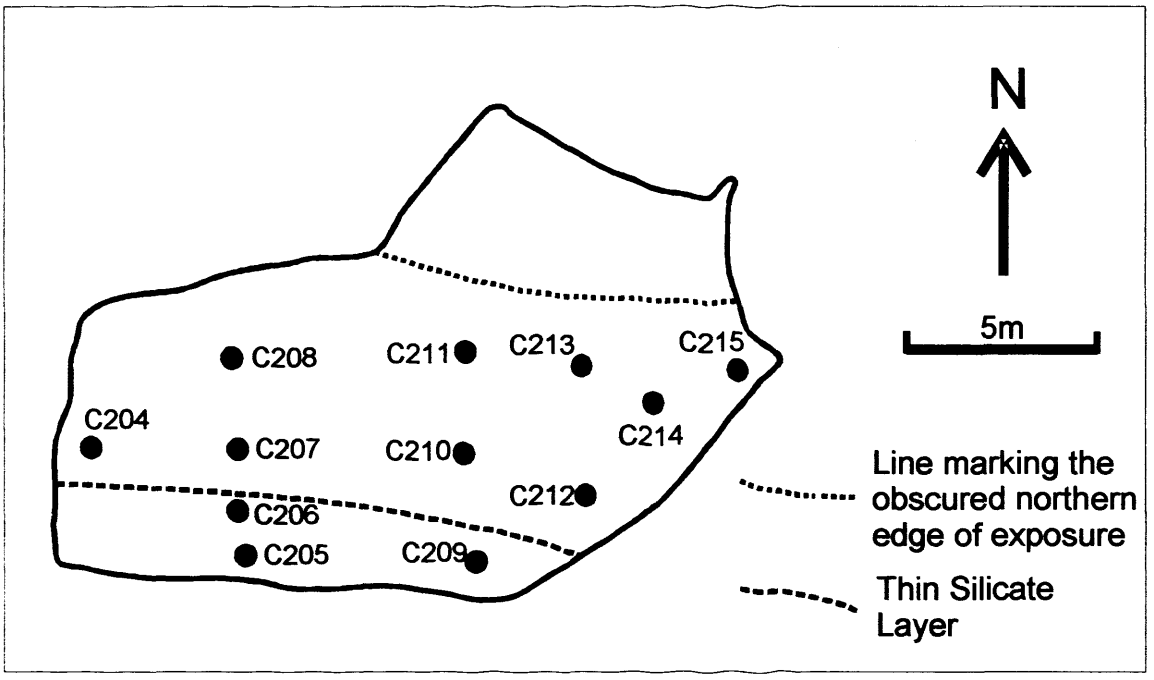

Figure 3.3: *Sample numbers within the largest pod in the Al 'Ays complex. Figure is adapted from a similar figure appearing in (Neary and Brown, 1979).*

The range in concentration of major and trace element oxides in *wt.%* for these 11 samples are Cr_2O_3; 65.00 - 66.35, Al_2O_3; 5.91 - 6.93, FeO^{tot}; 10.15 – 11.40, MgO; 13.93 – 14.93, TiO_2; 0.05 – 0.08, V_2O_5; 0.08 – 0.09, NiO; 0.12 – 0.16, MnO; 0.24 – 0.27. These ranges are very small compared to the differences in chromite compositions between pods (e.g. Cr_2O_3 ranges from 39.93 – 67.86 *wt.%*; see also - Tables 3.2, 3.3 & 3.4). The major and trace elements show complementary variations with one another (Figure 3.4). Of these, the paired variation of Cr_2O_3 with Al_2O_3 and MgO with FeO are expected because of unit cell constraints. Within the trace oxides TiO_2 and V_2O_5 are observed to vary antithetically to each other. However MnO and NiO show non-complimentary variation. Occasionally they both increase in concentration within the chromite lattice, yet at other times they vary antithetically. This is also true for the element pairs Cr-Mg, and Al-Fe^{2+} (Figure 3.4).

These results show that this chromitite pod is sufficiently homogeneous for differences between pods to be considered a true reflection of variation of composition rather than the result of random variations within chromitite pods (See also Section 2.3.1.1). Given the constraints on sample acquisition and the homogeneity of this chromitite pod, chromitites within the Al 'Ays ophiolite are hereafter assumed to have about the same degree of variation, with the geochemistry of each sampled chromitite taken to be indicative of the whole pod.

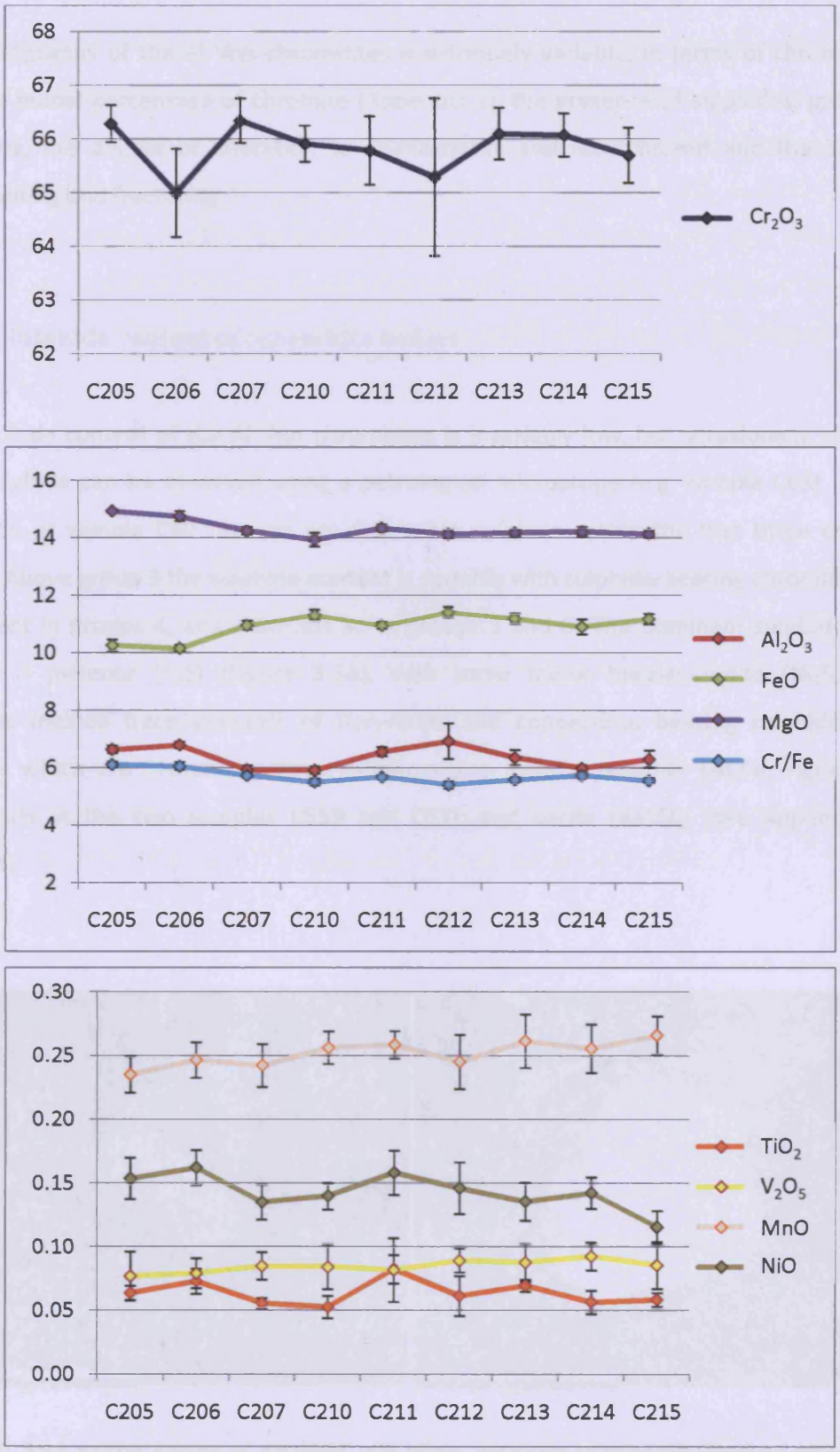

Figure 3.4: *Variation in major and trace elements throughout the largest chromitite pod within Al 'Ays. Error bars represent a range of 2 standard deviations. (Samples C208 & C209 were not analysed as the amount of remaining material was too small to be made into polished sections).*

3.3 Chromitite petrography

The petrography of the Al 'Ays chromitites is extremely variable, in terms of chromite grain size, the modal percentage of chromite (Appendix 1), the presence of sulphides, presence of inclusions, the degree of alteration to Cr-magnetite and ferritchromit and the degree of microfaulting and fracturing.

3.3.1 Sulphide content of chromitite bodies

The sulphide content of the Al 'Ays chromitites is invariably low, but occasionally up to ~1-2 *wt.%* sulphide can be observed using a petrological microscope (e.g. sample C63). With the exception of sample C10 there is no observable sulphide within the first three chromitite groups. Above group 3 the sulphide content is variable with sulphide-bearing chromitites most prominent in groups 4, and then less so in groups 5 and 6. The dominant sulphide-bearing mineral is millerite (NiS) (Figure 3.5A), with some minor heazlewoodite (Ni_3S_2). Other sulphides include trace amounts of iron-nickel and copper-iron bearing sulphides. Other minerals which are present in minor amounts also include awaruite (Ni_3Fe; Figure 3.5B – particularly in the two samples C559 and C51), and barite ($BaSO_4$) (see Appendix 7 for analyses).

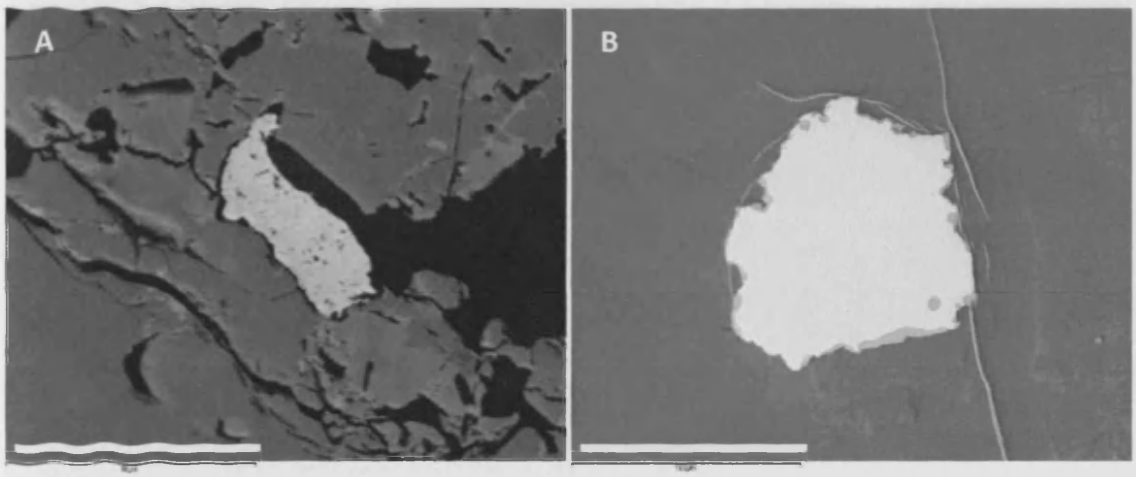

Figure 3.5: *Back scatter images of sulphides and alloys: examples of minerals observed within Al 'Ays chromitites.* ***A:*** *Millerite grain hosted at the junction of a chromite and silicate grain, scale bar represents 80 μm* ***B:*** *An awaruite grain (white), with partially oxidised rims (light grey) hosted within serpentine (mid-grey), scale bar represents 100 μm.*

3.3.2 Inclusion patterns

The presence of unusual silicate inclusion patterns is a noticeable feature of the Al 'Ays chromitites. These inclusion patterns can be split into two main subgroups; clustered inclusions located within the centre of a chromite grain (Figure 3.6A & B), and linear trails of inclusions cutting through a chromite grain (Figure 3.7A & B) (Table 3.1). In both cases their presence is anomalous with most other chromite grains within the same slide containing no such inclusion patterns. There are two exceptions to this, which are in samples C559 and C54, where these unusual inclusion patterns are abundant, occurring in the majority of the chromite grains.

3.3.2.1 Clustered inclusion patterns

This type of inclusion pattern has been noted from other ophiolite localities (e.g. Semail, (Roberts, 1986); Kempirsai, (Melcher *et al.*, 1997)). Mineralogically, the Al 'Ays inclusion clusters are filled with amphibole, which were generally edenite (richterite, potassicrichterite and sodicgedrite were also present), chlorite, minor amounts of diopside and *'ugrandite'* (predominantly Cr-grossular – see Appendix 7 for all analyses). Occasionally the inclusions are filled by base-metal sulphides. The inclusions are often euhedral to subhedral.

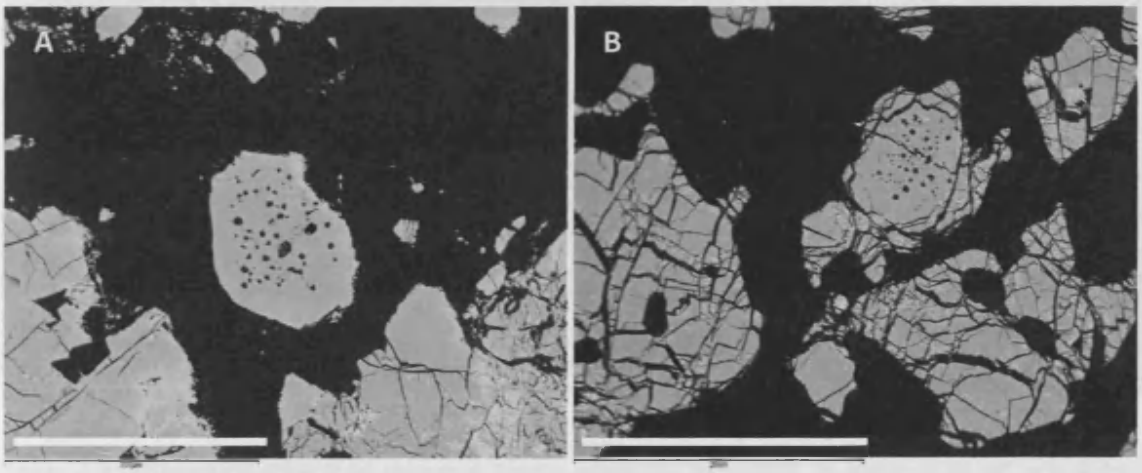

Figure 3.6: *Clustered inclusion patterns.* ***A:*** *Chromite grain containing clustered inclusions compared with the surrounding inclusion free chromite grains (sample C498), scale bar represents 700 μm.* ***B:*** *Chromite grain containing clustered inclusions (sample C262), scale bar represents 2 mm.*

3.3.2.2 *Linear trails of inclusions*

In contrast to the clustered inclusions, these linear trails of inclusions are 95% empty. The empty inclusions often display negative cubic crystal structures (Figure 3.7A), with each inclusion roughly 20-40 μm across. The linear trails occasionally form parallel aligned rows (Figure 3.7B). Empty inclusions may be the product of two main processes, (1) the removal during polishing or (2) the original containment of volatiles which escaped during the cracking of the chromite grain. When minerals are found contained within the 'cavity' at Al 'Ays, they are almost always found to be base-metal sulphides, with one instance of a PGM (Figure 3.7C & D).

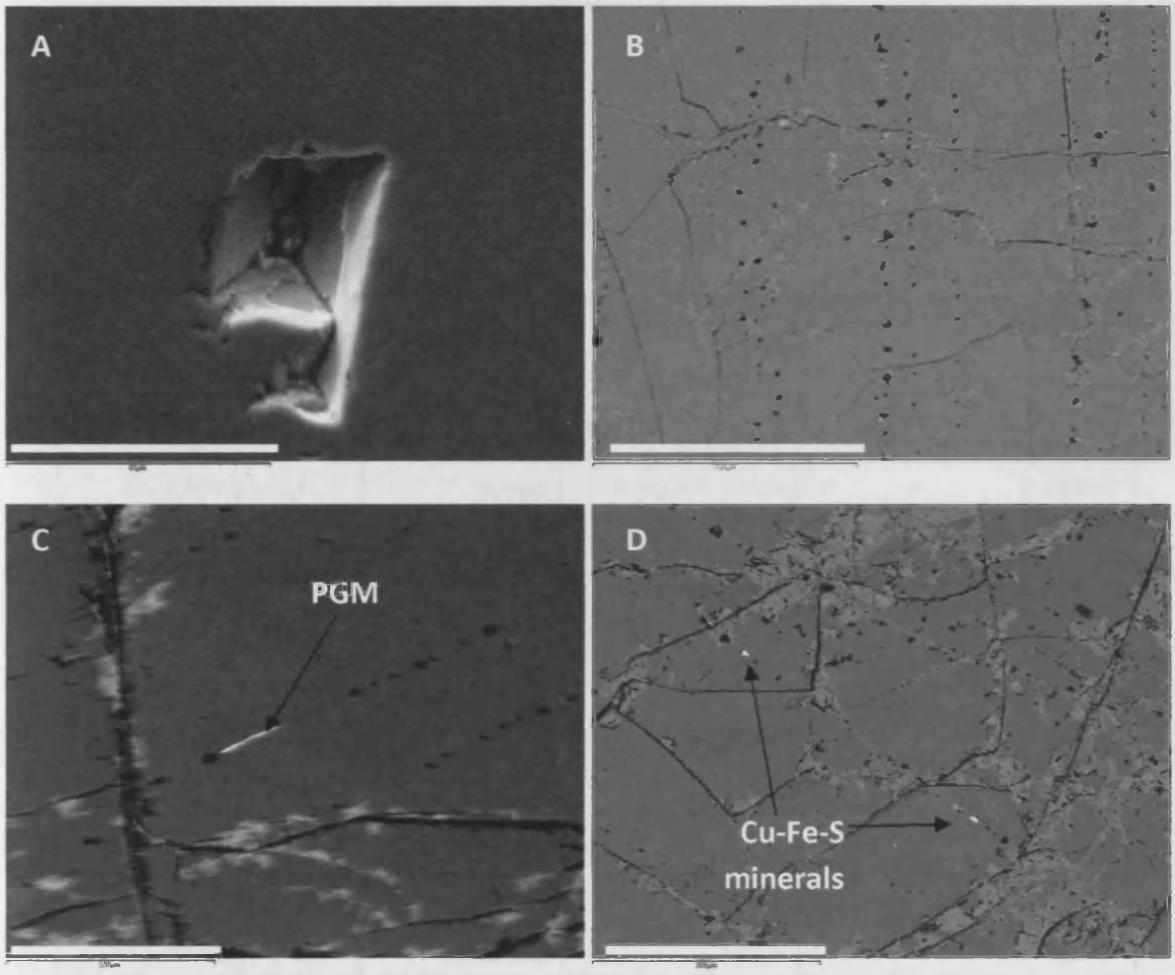

Figure 3.7: *Photomicrographs of chromite grains unusually abundant in linear trails of inclusions.* ***A:*** *Empty inclusion from an inclusion trail (sample C54) showing a negative cubic crystal structure, scale bar represents 40 μm.* ***B:*** *Several linear inclusion trails cutting through grains within sample C54, scale bar represents 700 μm.* ***C:*** *Small elongate PGM (Ir-Rh-Pt-alloy) within linear inclusion trail (sample C51), scale bar represents 200 μm.* ***D.*** *Two white Cu-Fe-S minerals in a linear inclusion trail within chromite (sample C238), scale bar represents 200 μm.*

Table 3.1: *Summary table of the variation in sulphide content, ferritchromit alteration, and type of inclusion pattern observed within the Al 'Ays chromitites. For sulphide/ BMA a 'moderate' content = ~1-2 wt.%, 'minor' = <0.5 wt.% and 'negligible' means sulphides were either unobserved or barely present. For ferritchromit alteration, 'pervasive' = >90% alteration, 'major' = > 70-90% alteration, 'moderate' = 30-70%, 'minor' = 10-30%, and negligible = <10% alteration. The abundance of each inclusion pattern is 'moderate' unless otherwise stated. For the inclusion patterns, a 'major' content refers to the presence of inclusion patterns throughout >50% of the grains, 'moderate' equals inclusion patterns in 20 – 50% of the slide, 'minor' equal inclusion patterns within <10% of the slide and 'negligible' refers to the absence of definitive inclusion patterns.*

Sample #	Group	Sulphides	Ferritchromit	Inclusion Patterns
C204-C215	1	Negligible	Negligible	Linear (minor)
C595	2	Negligible	Negligible	None
C104	2	Negligible	Minor	Linear (minor)
C670	2	Negligible	Negligible	None
C659	2	Negligible	Negligible	Linear (minor)
C10	2	Minor	Moderate	Linear (minor)
C655	2	Negligible	Negligible	None
C123	2	Negligible	Negligible	Linear (minor)
C46	3	Negligible	Major	None
C40	3	Negligible	Negligible	Linear
C60	3	Negligible	Moderate	None
C33	3	Negligible	Minor	None
C44	3	Negligible	Moderate	Linear (minor)
C318	3	Negligible	Negligible	Linear
C484	4	Negligible	Moderate	Cluster (minor)
C54	4	Negligible	Minor	**Linear (major)**
C63	4	**Moderate**	Major	Linear & Cluster
C61	4	Minor	Minor	Cluster
C51	4	**Moderate**	Moderate	Linear & Cluster
C238	4	Minor	Moderate	Linear
C413	4	Minor	Negligible	Cluster
C533	4	Minor	Moderate/ Major	Cluster
C429	4	Minor	Moderate	None
C559	4	**Moderate**	Moderate	**Cluster (major)**
C462	4	Minor	Moderate	Linear (minor)
C463	4	Minor	Moderate/ Major	None
C328	4	Negligible	Minor	Cluster
C580	5	Negligible	Moderate	Linear (minor)
C590	5	Negligible	Negligible	Linear (minor)
C311	5	Minor	Moderate	Linear & Cluster
C581	5	**Moderate**	**Pervasive**	None
C278	5	Negligible	Moderate	None
C365	5	Negligible	**Pervasive**	None
C362	5	Negligible	Moderate	Linear
C262	5	**Moderate**	Minor	Cluster
C375	6	Negligible	Major	Cluster
C382	6	Negligible	Minor	None
C385	6	Negligible	**Pervasive**	None
C498	6	Negligible	Moderate	Cluster
C178	6	Negligible	**Pervasive**	None

3.3.3 Alteration

Alteration within the chromitite samples can be considered as uniformly pervasive for the interstitial silicates but highly variable for the chromite grains (Table 3.1; Figure 3.8). Interstitial silicates, which were probably former olivine grains, are now predominantly serpentine, with occasional talc veins, chlorite (usually as overgrowths around chromite grains) and calcite.

Secondary Cr-magnetite and ferritchromit are common throughout the Al 'Ays chromitites and their collective presence within a chromitite can range from negligible (e.g. Figure 3.8A) to pervasive (e.g. Figure 3.8B). No measurement was made of the relative proportion of Cr-magnetite to ferritchromit but there is a general increase in the total degree of chromite alteration in samples closer to the pyroxenite outcrops, (i.e. within the higher group numbers ostensibly at a higher level in the upper mantle ; Table 3.1). However, unaltered chromite occurrences are spread throughout the ophiolite. Even when the alteration of chromite is pervasive there are still analysable chromite cores from which geochemical data related to the crystallisation event could be recovered.

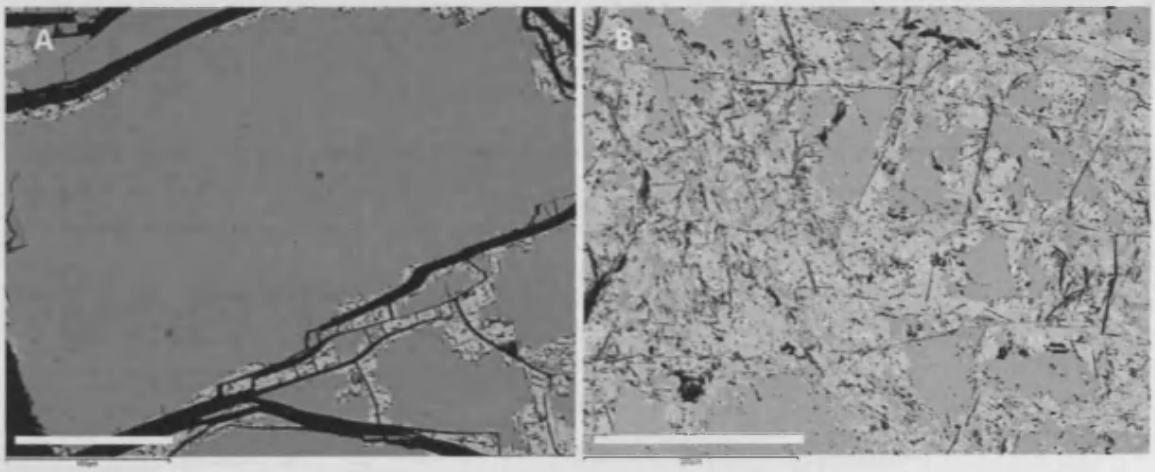

Figure 3.8: *Photomicrographs of chromite alteration observed within the Al 'Ays ophiolite. A: Very minor alteration along a fracture in a chromite grain with chromite altering to Cr-magnetite and/or ferritchromit only at the very edges and along fractures (sample C429), scale bar represents 100 μm. B: Major to pervasive chromite alteration (sample C533), scale bar represents 200 μm.*

3.3.4 Chromitite: brittle deformation

Internal micro-faulting displays a wide variety of features, including brecciation (Figure 3.9A), minor pull-apart features (Figure 3.9B) and 'hairline' mylonisation. Pull-apart features are common throughout all the chromitites but are particularly well developed in the more disseminated chromitites where the softer interstitial silicates take the brunt of the deformation. Brecciation is also common and displayed to varying degrees throughout all the chromitite deposits (e.g. Figure 3.9A). Occasionally, the chromitites display parallel to sub-parallel microfaults or even 'hairline' mylonisation which is the localisation of intense deformation along thin zones traversing the chromitite.

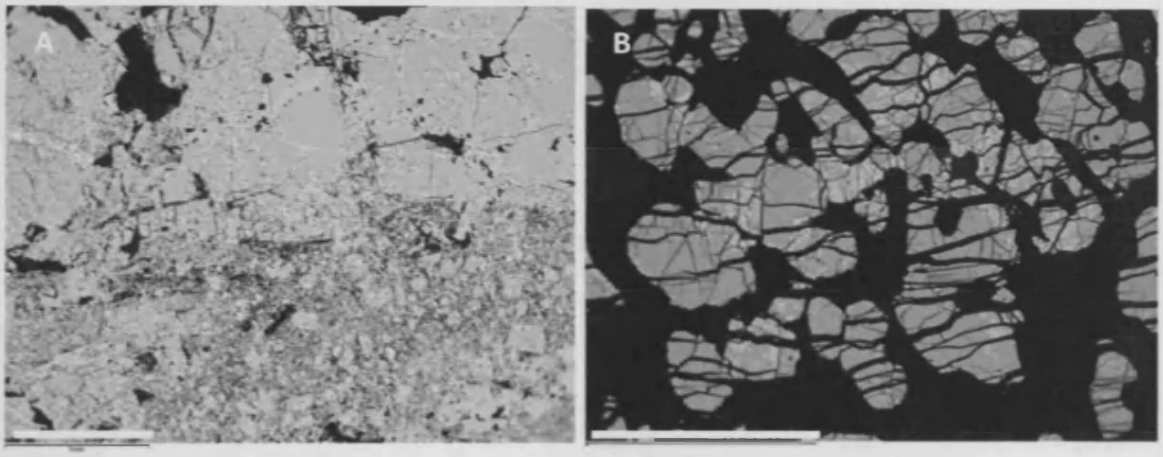

Figure 3.9: *Photomicrographs of microfaulting observed within the Al 'Ays chromitite. A: Intense and variable microbrecciation (sample C533), scale bar represents 1 mm. B: Pull-apart (sample C429), scale bar represents 2mm.*

3.4 Chromitite geochemistry

3.4.1 Intrasample geochemistry – Cr#-Mg# variations

Intrapod geochemistry for all the major and trace elements for all the ophiolites has been described in Chapter 2, and the variation within an Al 'Ays chromitite pod has been described in section 3.2. Nevertheless, it was observed that there was a slight inverse correlation, for most of the Al 'Ays chromitite samples, between Cr# and Mg# (Figure 3.10). The greater range of Mg# compared with Cr# (e.g. C580) for each sample reflects the higher degree of precision possible on the Cr_2O_3 analysis (See Section 2.3.1.1).

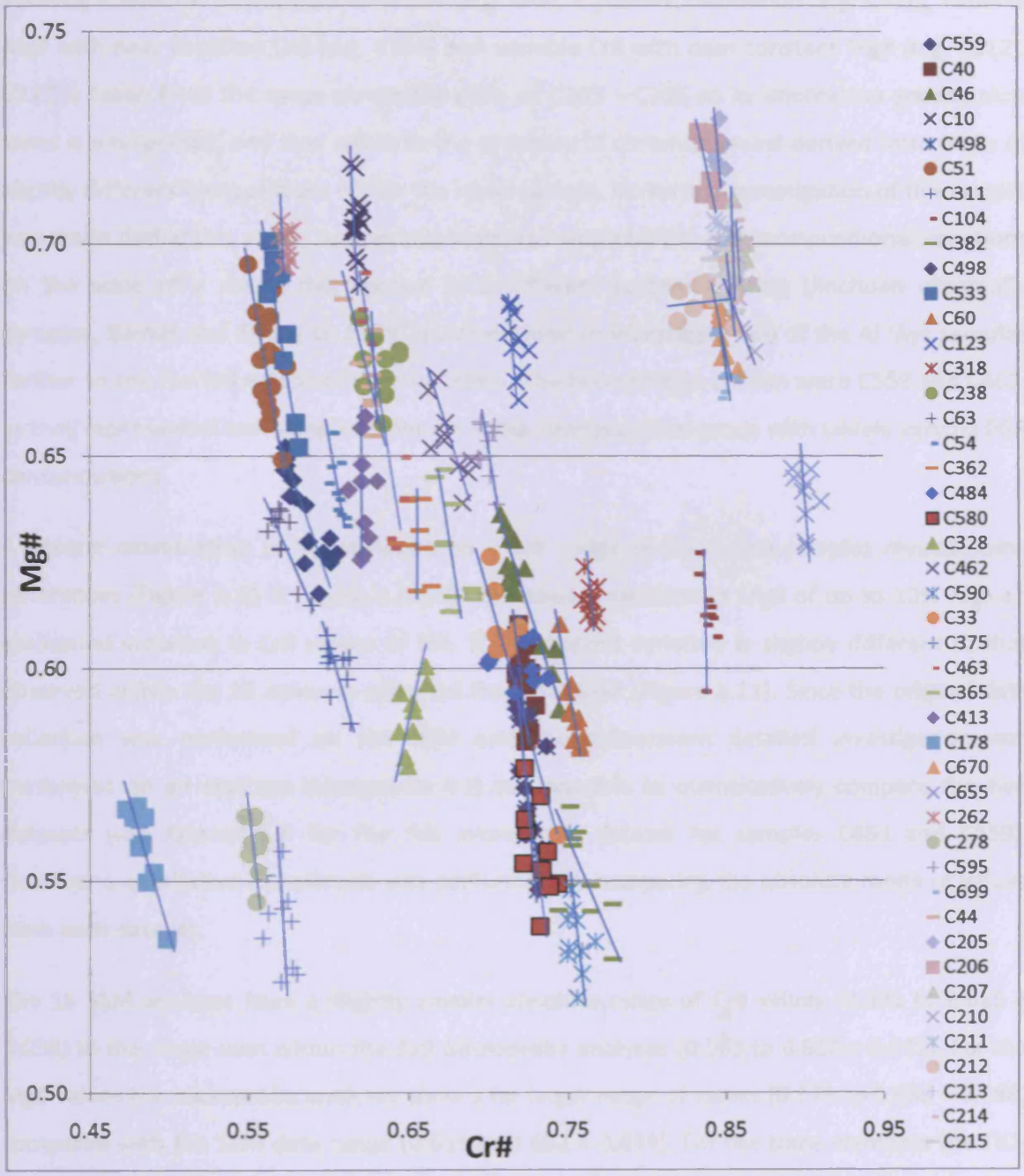

Figure 3.10; *Cr# vs Mg# values for all the grains analysed from all the samples within Al 'Ays. Each sample contains analyses from multiple (~5) grains, with each grain analysed twice. Also shown are trendlines for each sample, with the majority displaying a general elongation in the direction of inverse correlation. Trendlines were drawn by eye. Note the scale difference in X and Y axes.*

Aside from generally inverse trends (e.g. C178, C559, C63), there were also some samples showing a bimodal distribution of values (e.g. C46), a positive correlation (e.g. C328), variable Mg# with near constant Cr# (e.g. C104) and variable Cr# with near constant Mg# (e.g. C212). C212 is taken from the same chromitite pods as C205 – C215 so its anomalous geochemical trend is unexpected, and may relate to the presence of chromite grains derived from melts of slightly different compositions within the same sample. No further investigation of this sample was made during this study. As previous workers had identified wide compositional variations on the scale of a single thin section in a different tectonic setting (Jinchuan ultramafic complex, Barnes and Zhong Li, 1999) it was decided to investigate two of the Al 'Ays samples further to see the full extent of their variation. The two samples chosen were C559 and C462, as they represented two samples from the same stratigraphical group with widely varying PGE concentrations.

A general examination of the variation on a Cr# - Mg# of these two samples reveals some differences (Figure 3.11 & Figure 3.12). C559 shows a variation in Mg# of up to 10% with an associated variation in Cr# values of 5%. This observed variation is slightly different to that observed within the 16 analyses obtained from the SEM (Figure 3.11). Since the original data collection was performed on the SEM and the subsequent detailed investigation was performed on an electron microprobe it is not possible to quantitatively compare the two datasets (see Appendix 8 for the full microprobe dataset for samples C462 and C559). However a qualitative comparison was performed by comparing the absolute range of values from each dataset.

The 16 SEM analyses have a slightly smaller absolute range of Cr# values (0.591 to 0.625 = 0.034) to the range seen within the 329 Microprobe analyses (0.563 to 0.610 = 0.047). For the Mg# values the microprobe analyses show a far larger range of values (0.578 to 0.666 = 0.088) compared with the SEM data range (0.618 to 0.652 = 0.034). For the trace elements the TiO_2 range is far greater for the microprobe analyses (0.070 to 0.152 = 0.082) than for the SEM analyses (0.124 to 0.152 = 0.028) (Figure 3.11B). In contrast the V_2O_5, MnO and NiO values display a similar total range across both data sets, with the microprobe data range slightly larger (Figure 3.11B & C). V_2O_5 values are systematically higher for both C559 and C462 on the SEM as compared with the microprobe.

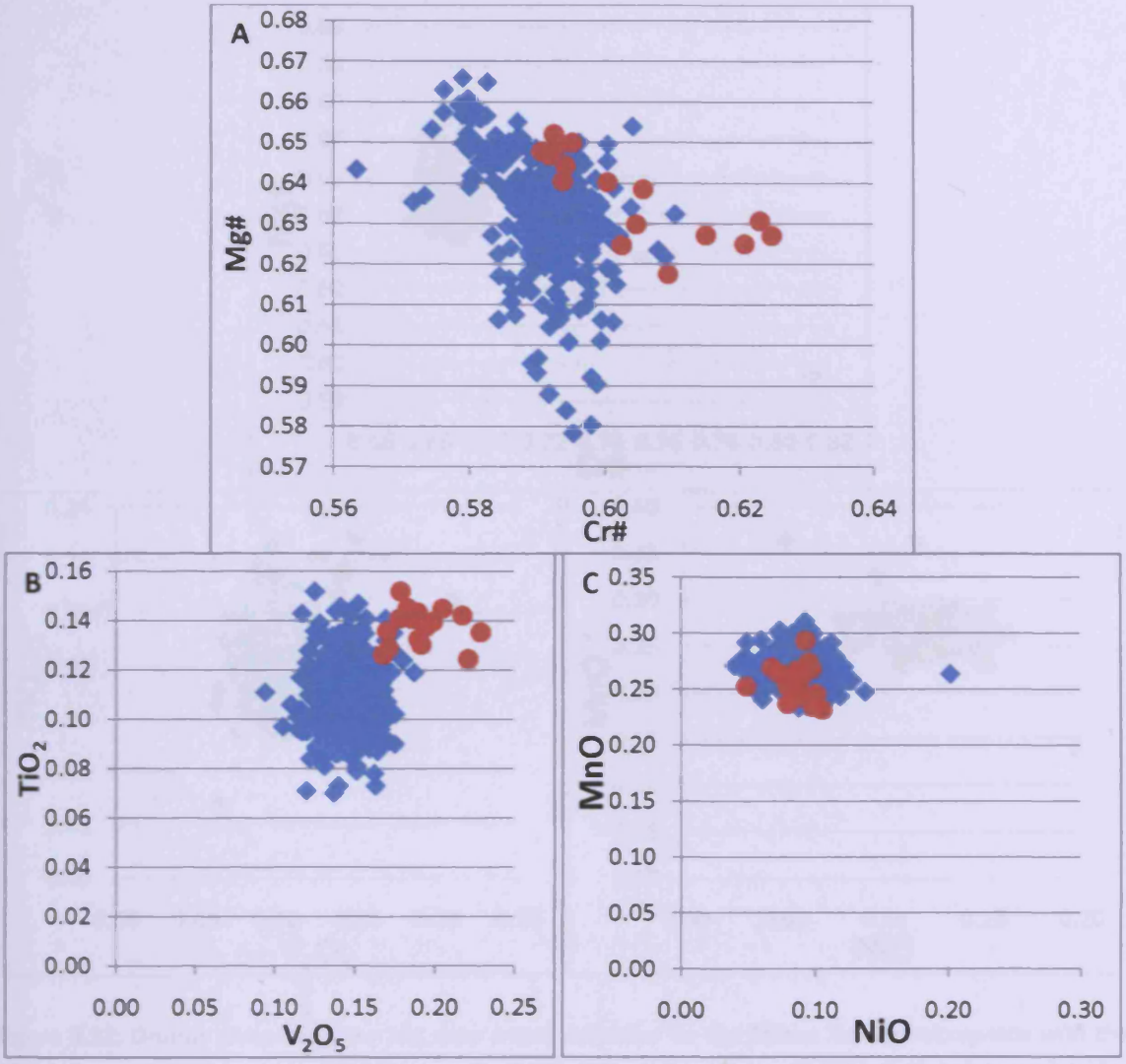

Figure 3.11: *Graphs comparing the 329 data points collected on the Open University microprobe at Milton Keynes with the 16 analyses collected on the SEM for sample C559. Red circles represent SEM data points whilst blue diamonds represent microprobe data points A: Cr# vs Mg#, B: TiO_2 vs V_2O_5, C: MnO vs NiO.*

A comparison of C462 with C559 shows that there is a much larger Cr# variation in C462, with a similar total range of Mg# values (Figure 3.12A). The analysis of C462 contains two points of interest. The first is the general grouping of the majority of analyses within a restricted Cr# - Mg# range (Fig 3.12A). This grouping covers a smaller relative range of values than that observed within C559, and shows that the majority of this sample has a tightly controlled major element composition. Similarly, the trace element data ranges show very similar behaviours to that observed within C559 (Figure 3.12B & C, compared with Figure 3.11B & C).

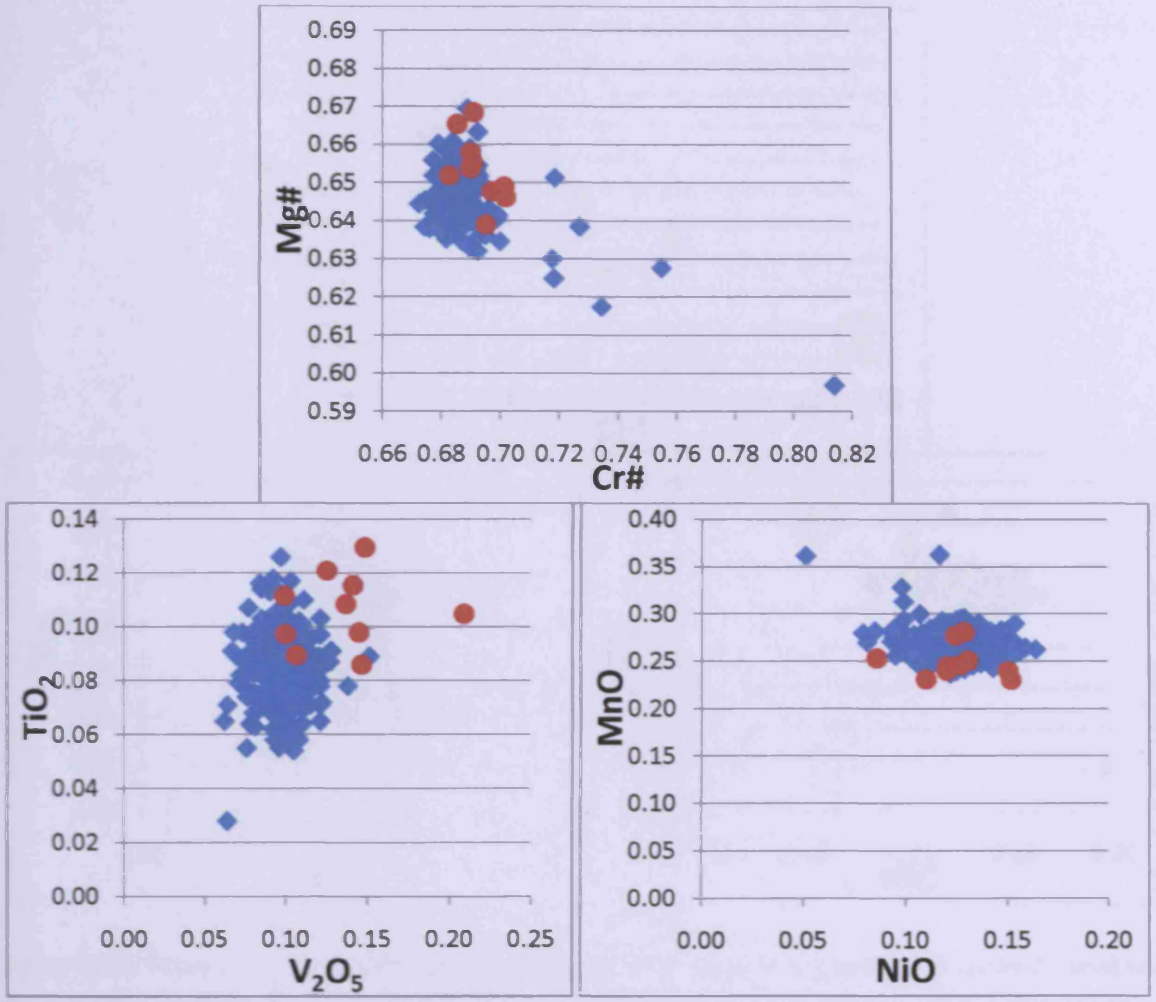

Figure 3.12: *Graphs comparing the 241 data points collected on the Milton Keynes microprobe with the 16 analyses collected on the SEM for sample C462. Red circles represent SEM data points whilst blue diamonds represent microprobe data points A: Cr# vs Mg#, B: TiO_2 vs V_2O_5, C: MnO vs NiO.*

The second point of interest is the presence of 7 analyses with higher Cr# (Figure 3.12A). These 7 analyses, together with the major grouping of microprobe analyses, form an inverse relationship where Mg# decreases with increasing Cr# (Figure 3.12A). This is the same relationship suggested by the trendlines in the majority of the Al 'Ays samples (Figure 3.10). When these 7 analyses are compared against the bulk of the microprobe dataset for their trace element content it is apparent that their trace element content does not form a similar unique data range (Figure 3.13B & C). Nevertheless, the TiO_2 content of these 7 samples is towards the lower end of the data range, with the highest Cr# chromitite also containing the lowest TiO_2 value (Figure 3.13B). The NiO range is also towards the lower end of the data range with the highest Cr# chromitite also containing the lowest NiO value (Figure 3.13C).

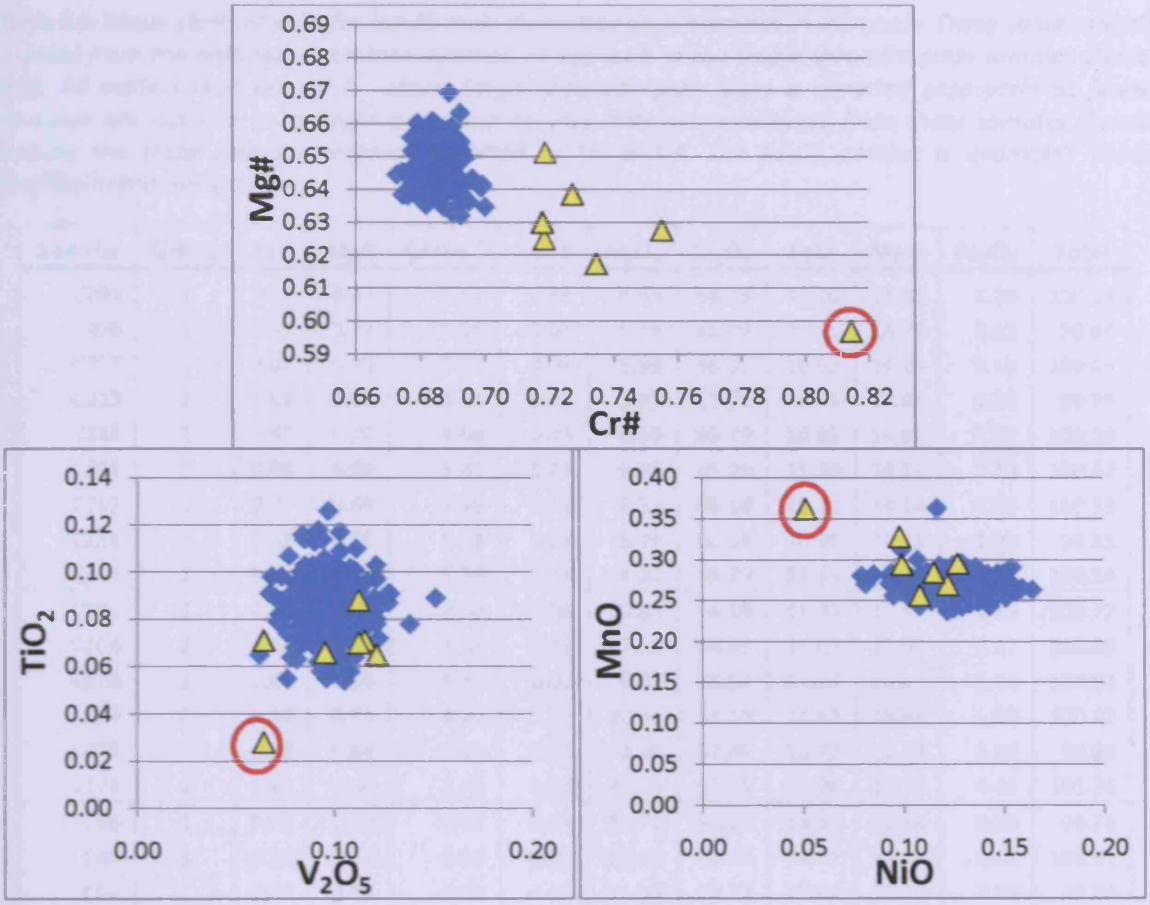

Figure 3.13: *Graphs comparing the high Cr# chromite analyses against the low Cr# chromite analyses from the 241 data points collected on the Milton Keynes microprobe for sample C462. Yellow triangles are the high Cr# chromite analyses whilst blue diamonds are the low Cr# analyses. A: Cr# vs. Mg#, B: TiO_2 vs. V_2O_5, C: MnO vs. NiO. The analysis circled in red on Figure 3.13B and C coincides with the highest Cr# analysis in Figure 3.13A.*

3.4.2 Interpod geochemistry

3.4.2.1 Major element geochemistry

The major element geochemistry of the Al 'Ays chromitites analysed during this study, lies in the fields that define ophiolitic chromitite (Figure 3.14A-D). The Cr# [Cr^{3+}/ (Cr^{3+} + Al^{3+})] varies from 0.52 to 0.92, with an associated variation in Fe^{2+}# [Fe^{2+}/(Mg^{2+} + Fe^{2+})] of 0.28 to 0.62 (Figure 3.13A & D). There are two samples which contain Fe^{2+}# values outside the defined ophiolite field range, though this is very unlikely to be significant as the fields represent 90% confidence limits on the expected range of compositions. The TiO_2 *wt.%* content ranges from 0.03 up to 0.51 (Figure 3.13B) and the Fe^{3+}# [Fe^{3+}/(Cr^{3+} + Al^{3+} + Fe^{3+})] ranges from 0.004 to 0.083 (Figure 3.13B & D) (Table 3.2 & 3.3). This range of Fe^{3+}# values lies in the lower half of the defined ophiolite field.

Table 3.2: *Major element data for the 35 main chromitite pods analysed in this study. These values are all derived from the polished chromitite sections, as opposed to the single chromite grain samples (Table 3.3). All oxide values are wt.% values. Single chromite grain data is reported separately as fewer analyses are possible on a single grain and no PGE data were collected from these samples. Totals include the trace element contents reported in Table 3.4. The Fe_2O_3 content is estimated using stoichiometric constraints.*

Site No	Group	Cr#	Mg#	Cr/Fe^{2+}	Fe^{3+}#	Al_2O_3	Cr_2O_3	FeO	MgO	Fe_2O_3	Total
C205	1	0.87	0.72	6.11	0.15	6.63	66.29	10.26	14.93	2.26	100.89
C206	1	0.87	0.72	6.05	0.03	6.79	65.00	10.15	14.75	2.42	99.67
C207	1	0.88	0.70	5.73	0.03	5.93	66.35	10.95	14.24	2.10	100.09
C210	1	0.88	0.69	5.51	0.03	5.91	65.91	11.31	13.93	2.20	99.79
C211	1	0.87	0.70	5.68	0.03	6.56	65.79	10.95	14.34	2.07	100.28
C212	1	0.86	0.69	5.41	0.03	6.93	65.29	11.40	14.12	2.19	100.47
C213	1	0.87	0.69	5.59	0.12	6.35	66.10	11.19	14.18	1.96	100.33
C214	1	0.88	0.70	5.73	0.13	5.99	66.08	10.90	14.21	2.09	99.81
C215	1	0.87	0.69	5.56	0.14	6.30	65.70	11.18	14.14	2.30	100.14
C595	2	0.71	0.65	4.00	0.08	15.33	56.19	13.27	13.95	1.35	100.77
C104	2	0.86	0.61	4.33	0.11	7.11	64.43	14.07	12.50	2.17	100.80
C670	2	0.86	0.68	5.31	0.09	6.97	65.93	11.74	13.93	1.44	100.53
C10	2	0.62	0.71	4.20	0.07	20.61	51.19	11.52	15.46	1.00	100.42
C655	2	0.92	0.64	5.02	0.10	3.90	67.86	12.77	12.73	1.80	99.53
C123	2	0.76	0.68	4.41	0.21	12.25	57.15	12.24	14.36	4.45	101.26
C46	3	0.75	0.62	3.77	0.14	12.71	56.29	14.10	12.84	3.09	99.71
C40	3	0.74	0.60	3.58	0.10	13.29	56.77	14.97	12.44	2.16	100.31
C60	3	0.78	0.59	3.67	0.13	11.09	58.37	15.04	12.13	2.78	99.99
C33	3	0.73	0.61	3.61	0.10	14.10	56.38	14.76	12.70	1.90	100.48
C44	3	0.65	0.67	3.79	0.16	18.61	50.54	12.59	14.47	3.09	100.03
C318	4	0.81	0.62	3.98	0.18	9.68	59.70	14.19	12.78	4.20	101.23
C413	4	0.64	0.64	3.46	0.15	18.54	50.07	13.69	13.73	3.02	99.73
C533	4	0.59	0.68	3.60	0.17	21.84	47.44	12.45	15.01	3.37	100.74
C559	4	0.60	0.64	3.21	0.13	21.20	48.14	14.16	13.95	2.74	100.87
C462	4	0.69	0.65	3.90	0.11	16.17	54.31	13.17	13.95	2.12	100.33
C463	4	0.65	0.66	3.72	0.13	18.57	51.54	13.11	14.33	2.60	100.81
C328	4	0.68	0.59	3.16	0.16	16.09	51.91	15.52	12.48	3.98	100.68
C63	4	0.60	0.63	3.10	0.17	21.02	46.81	14.29	13.68	3.96	100.62
C54	4	0.64	0.64	3.37	0.21	18.28	48.69	13.67	13.75	4.96	100.09
C51	4	0.58	0.67	3.44	0.12	22.90	46.70	12.85	14.81	2.32	100.23
C238	4	0.66	0.67	3.85	0.16	18.17	51.49	12.65	14.50	3.05	100.48
C484	4	0.75	0.60	3.62	0.14	12.84	56.59	14.79	12.58	3.10	100.57
C580	5	0.76	0.56	3.29	0.15	11.73	56.68	16.27	11.50	3.62	100.43
C590	5	0.79	0.54	3.25	0.16	10.02	57.85	16.80	10.99	4.12	100.50
C311	5	0.64	0.60	3.01	0.20	18.24	48.96	15.39	12.97	5.06	101.36
C278	5	0.57	0.56	2.50	0.13	22.12	44.55	16.86	11.96	3.12	99.33
C365	5	0.70	0.63	3.62	0.11	15.95	54.23	14.16	13.30	2.08	100.36
C362	5	0.69	0.63	3.54	0.18	15.89	52.15	13.93	13.35	4.08	100.04
C262	5	0.60	0.70	3.82	0.17	21.90	48.07	11.91	15.57	3.20	101.23
C375	6	0.62	0.54	2.46	0.22	18.66	45.46	17.49	11.52	6.70	100.66
C382	6	0.81	0.55	3.37	0.19	9.26	58.22	16.32	11.22	4.97	100.63
C498	6	0.74	0.57	3.41	0.07	13.78	57.16	15.84	12.02	1.34	100.75
C178	6	0.52	0.56	2.18	0.20	24.75	39.93	17.34	12.28	5.99	101.12

Table 3.3: *Major element data for all the single chromite grain samples analysed. All oxide values are wt.% values. Totals include the trace element contents reported in Table 3.5.*

Site No	Group	Cr#	Mg#	Cr/Fe^{2+}	Fe^{3+}#	Al_2O_3	Cr_2O_3	FeO	MgO	Fe_2O_3	Total
650	2	0.78	0.70	5.04	0.04	11.10	59.40	11.13	14.91	3.52	100.81
645	2	0.80	0.61	3.97	0.02	10.20	61.39	14.61	12.59	1.91	101.29
640	2	0.57	0.71	3.75	0.05	22.69	45.60	11.50	15.69	4.01	100.09
636	2	0.72	0.68	4.43	0.01	14.57	56.32	12.03	14.39	1.09	99.11
573	2	0.80	0.64	4.31	0.03	10.30	60.34	13.23	13.22	2.29	100.01
133	2	0.89	0.58	4.19	0.03	5.28	64.94	14.65	11.55	2.09	99.08
132	2	0.70	0.63	3.64	0.03	15.17	54.03	14.05	13.27	2.59	99.83
598	3	0.82	0.64	4.38	0.02	9.43	62.32	13.45	13.18	1.60	100.61
597	3	0.61	0.69	3.75	0.03	20.68	48.54	12.25	15.07	2.69	100.08
596	3	0.61	0.68	3.59	0.03	20.69	48.83	12.87	15.07	2.96	101.50
527	3	0.67	0.60	3.17	0.05	16.86	51.21	15.28	12.79	4.08	100.92
89	3	0.85	0.68	5.10	0.04	7.69	63.56	11.77	14.11	3.19	101.10
45	3	0.59	0.64	3.29	0.00	22.56	48.06	13.81	14.05	0.38	99.63
42	3	0.82	0.58	3.77	0.05	8.49	59.63	14.95	11.81	3.83	99.41
557	4	0.60	0.66	3.35	0.04	21.04	46.32	13.08	14.32	3.76	99.16
536	4	0.76	0.57	3.36	0.04	11.98	55.95	15.75	11.71	3.36	99.47
504	4	0.87	0.59	4.15	0.03	6.53	64.60	14.71	11.98	2.19	100.64
483	4	0.72	0.61	3.42	0.06	14.11	53.50	14.77	12.72	4.63	100.43
461	4	0.76	0.56	3.30	0.04	11.74	56.32	16.15	11.48	3.40	99.83
321	4	0.72	0.65	3.92	0.05	14.16	55.03	13.27	13.81	3.96	100.91
271	4	0.91	0.57	4.07	0.05	4.39	65.27	15.18	11.44	3.71	100.56
591	5	0.64	0.71	4.24	0.04	19.23	50.10	11.18	15.51	3.19	99.96
469	5	0.68	0.68	4.03	0.04	16.80	52.49	12.32	14.73	3.57	100.69
340	5	0.71	0.55	2.94	0.06	14.20	52.65	16.93	11.41	4.95	100.98
302	5	0.56	0.67	3.21	0.04	23.41	44.79	13.20	14.73	3.70	100.49
280	5	0.79	0.38	2.28	0.08	9.52	52.81	21.91	7.48	6.39	99.28
255	5	0.84	0.55	3.54	0.05	7.69	60.17	16.09	11.01	3.85	99.52
218	5	0.83	0.48	3.00	0.06	7.78	58.26	18.36	9.51	4.32	99.16
514	6	0.81	0.41	2.51	0.08	8.52	55.59	20.97	8.20	6.44	100.71
494	6	0.81	0.57	3.69	0.03	9.30	60.18	15.42	11.67	2.43	99.65
489	6	0.73	0.59	3.41	0.05	13.46	55.39	15.34	12.51	4.03	101.47
477	6	0.67	0.57	2.84	0.07	16.28	49.47	16.46	12.00	5.98	101.08
459	6	0.69	0.62	3.47	0.05	15.80	52.72	14.34	13.20	3.92	100.67
161	6	0.57	0.51	2.15	0.07	21.27	42.60	18.71	11.03	6.33	100.80
159	6	0.74	0.68	4.36	0.04	13.19	55.81	12.10	14.12	3.39	99.29

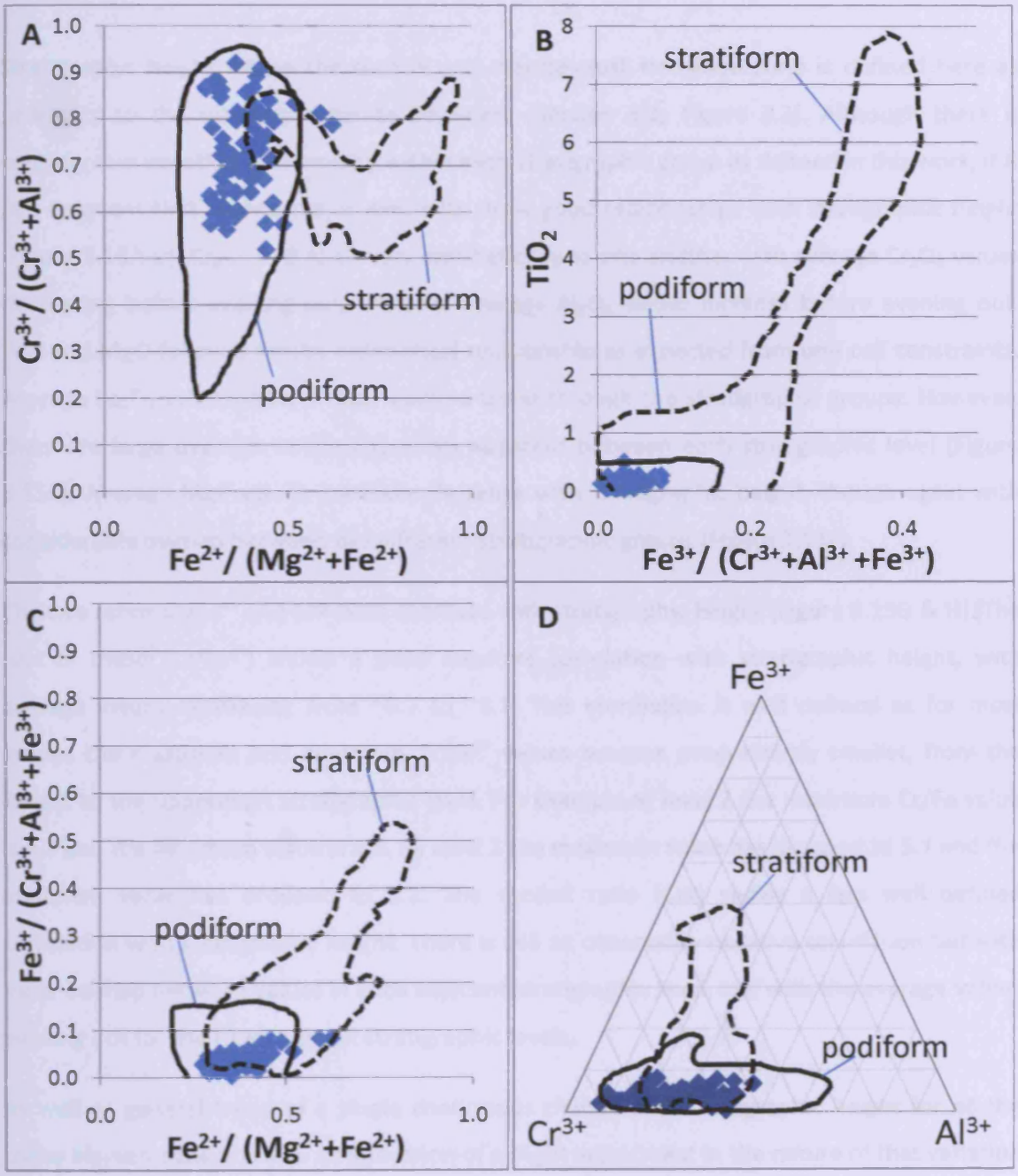

Figure 3.14: *Discrimination diagrams for ophiolitic versus stratiform chromitites (After Roeder and Barnes, 2001). The defined fields represent 90% of their analysed chromite compositions. Chromitites from Al 'Ays are plotted on 4 major elements plots and clearly fall in the ophiolite fields. A: Cr# vs Fe^{2+}#. B: TiO_2 vs Fe^{3+}#, C: Fe^{3+}# vs Fe^{2+}#, D: Ternary plot of Cr^{3+}-Al^{3+}-Fe^{3+}.*

3.4.2.1.1 The relationship of major element geochemistry to stratigraphic height

Stratigraphic height within the mantle and mantle-crust transition zone is defined here as proximity to the dunite/pyroxenite boundary (Section 3.1, Figure 3.2). Although there is considerable variation in chemistry within each stratigraphic group as defined in this work, it is still apparent that several major elements show good relationships with stratigraphic height (Figure 3.15A-D). Cr_2O_3 and Al_2O_3 vary antithetically to one another with average Cr_2O_3 values decreasing before evening out, whereas average Al_2O_3 values increase before evening out. FeO and MgO follow a similar antithetical relationship as expected from unit cell constraints. Average Fe_2O_3 values show a clear upward trend through the stratigraphic groups. However, there are large overlaps in the chemistry apparent between each stratigraphic level (Figure 3.15E). Average Mg# values gradually decrease with stratigraphic height, though again with considerable overlap between the different stratigraphic groups (Figure 3.14F).

The two ratios Cr/Fe^{2+} and Cr# both decrease with stratigraphic height (Figure 3.15G & H). The first of these (Cr/Fe^{2+}) shows a good negative correlation with stratigraphic height, with average values decreasing from ~5.7 to ~3.1. This correlation is well defined as for most groups the maximum and minimum Cr/Fe^{2+} values become progressively smaller, from the lowest to the uppermost stratigraphic level. For example at level 2 the maximum Cr/Fe value is 5.3 and the minimum value is 3.6. By level 3 the maximum value has dropped to 5.1 and the minimum value has dropped to 3.2. The second ratio (Cr#) shows a less well defined correlation with stratigraphic height. There is still an observable negative correlation but with more overlap between values in each adjacent stratigraphic level, and with the average values evening out for the three highest stratigraphic levels.

As well as general trend of a single continuous change with stratigraphic height for all the major elements there is also an indication of a slight adjustment in the nature of that variation at group 4. For example, Cr_2O_3, Al_2O_3 and Cr# all have values that level off after group 4, whilst MgO and FeO both show a slightly greater rate of change. A similar feature is observed in some of the trace elements (see Figure 3.17).

When considering the co-variation of Cr# and Mg# there is a general trend between the deep mantle chromitites (group 1) and the shallow mantle chromitites (group 6) (Figure 3.16). As can be observed group 1 chromitites have the highest Cr# and Mg# - i.e. located to the top right of the compositional range (Figure 3.16), whilst group 6 chromitites tend to contain the lowest Cr# and Mg# (Figure 3.16).

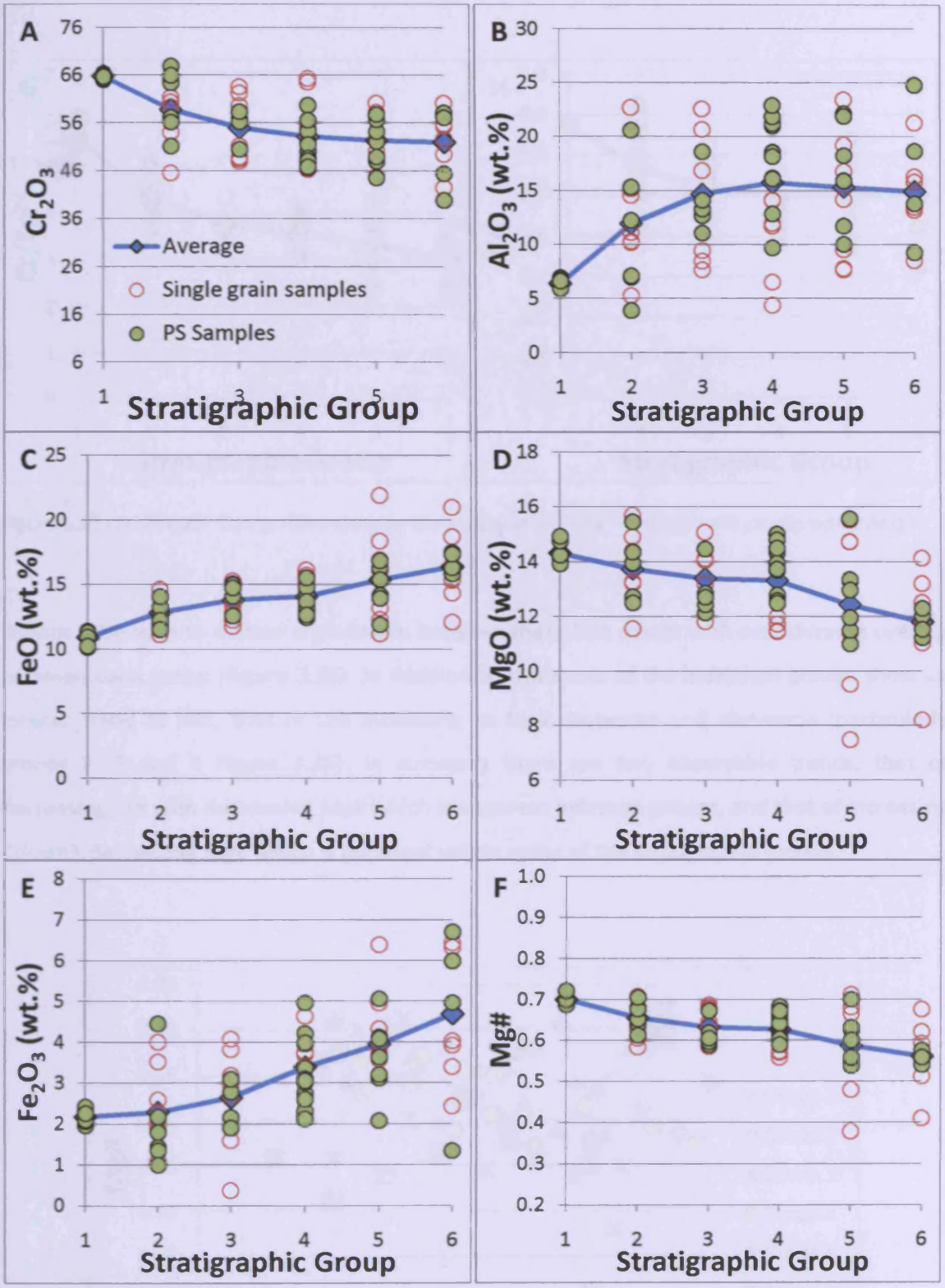

Figure 3.15: *Eight graphs (continued overleaf) showing the variation in major element geochemistry with stratigraphic height. A: Cr_2O_3, B: Al_2O_3, C: FeO, D: MgO, E: Fe_2O_3, F: Mg#, G: Cr/Fe^{2+}, H: Cr# (=Cr/(Cr+Al)). The blue line marks the average value at each stratigraphic group, the green circles mark polished section samples, whereas the clear circles mark single chromite grain samples (Legend in Figure 3.15A).*

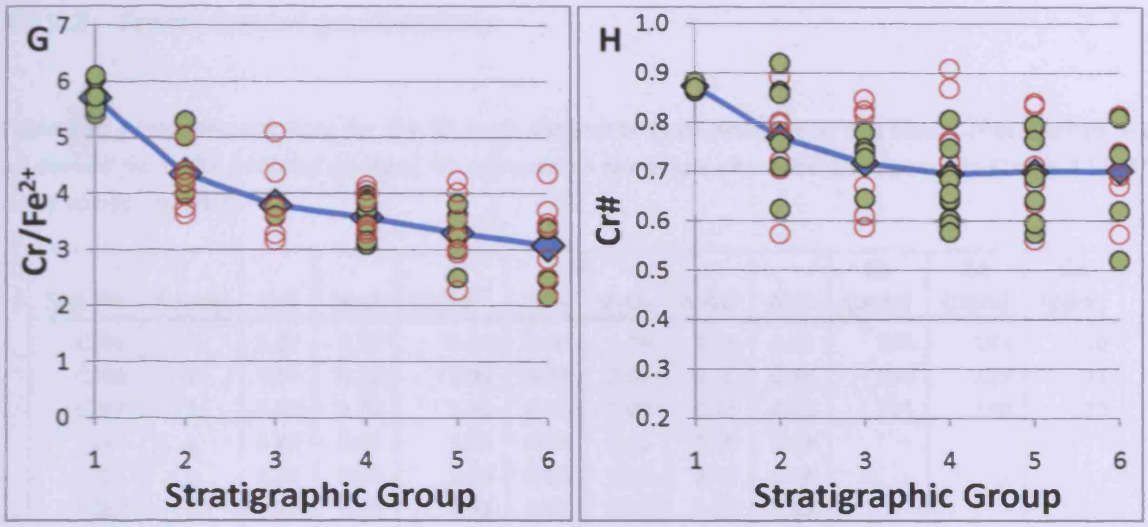

Figure 3.15 continued: *Two graphs showing the variation of Cr/Fe^{2+} and Cr# with stratigraphic height.*

Groups 2 through to 6 show a gradation between these two points with considerable overlap between each group (Figure 3.16). In addition to this some of the individual groups show an inverse trend to this, that of Cr# increasing as Mg# decreases and vica-versa (particularly groups 2, 3 and 4 Figure 3.16). In summary there are two observable trends, that of decreasing Cr# with decreasing Mg# which is apparent between groups, and that of increasing Cr# with decreasing Mg# which is apparent within some of the stratigraphic groups.

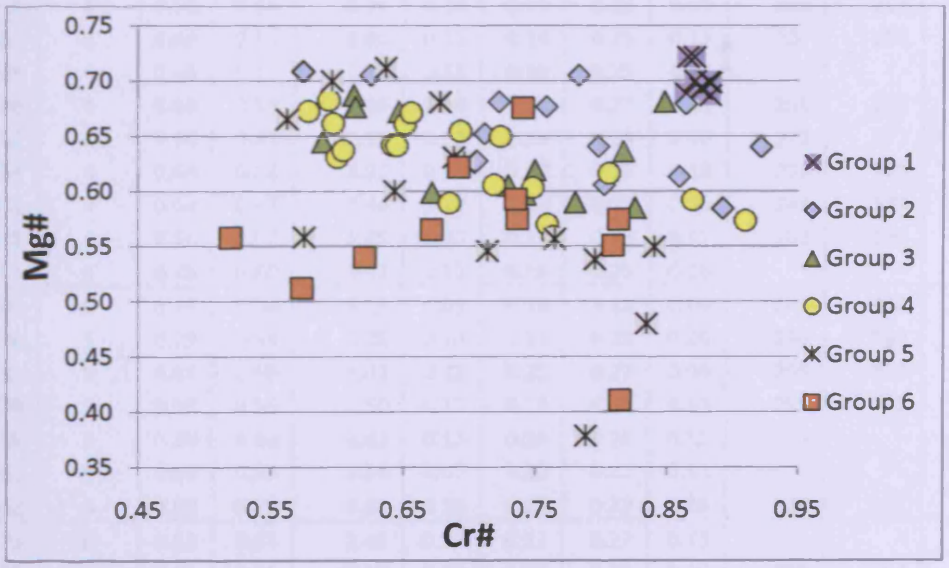

Figure 3.16: *Plot of Cr# - Mg# showing the range of values recorded at Al 'Ays. The different stratigraphical groups are defined by different colours.*

3.4.2.2 *Trace element geochemistry*

Table 3.4: *Trace element data for the 35 main chromitite pods analysed in this study. These values are all derived from the polished sections, as opposed to the single chromite grain samples (Table 3.5). All oxide values are wt.%.*

Site No	Group	Cr#	Mg#	Cr/Fe^{2+}	TiO_2	V_2O_5	MnO	NiO	Co (ppm)	Zn (ppm)	Ga (ppm)
C205	1	0.87	0.72	6.11	0.06	0.08	0.24	0.15	195	163	10
C206	1	0.87	0.72	6.05	0.07	0.08	0.25	0.16	192	123	11
C207	1	0.88	0.70	5.73	0.06	0.08	0.24	0.13	204	139	10
C210	1	0.88	0.69	5.51	0.05	0.08	0.26	0.14	-	-	-
C211	1	0.87	0.70	5.68	0.08	0.08	0.26	0.16	-	-	-
C212	1	0.86	0.69	5.41	0.06	0.09	0.25	0.15	-	-	-
C213	1	0.87	0.69	5.59	0.07	0.09	0.26	0.14	195	160	11
C214	1	0.88	0.70	5.73	0.06	0.09	0.26	0.14	191	168	10
C215	1	0.87	0.69	5.56	0.06	0.09	0.27	0.12	209	141	11
C595	2	0.71	0.65	4.00	0.12	0.21	0.25	0.10	-	-	-
C104	2	0.86	0.61	4.33	0.10	0.06	0.28	0.07	-	-	-
C670	2	0.86	0.68	5.31	0.08	0.06	0.25	0.13	196	154	11
C10	2	0.62	0.71	4.20	0.04	0.22	0.22	0.18	192	172	33
C655	2	0.92	0.64	5.02	0.03	0.09	0.28	0.07	301	259	7
C123	2	0.76	0.68	4.41	0.28	0.08	0.22	0.22	183	161	22
C46	3	0.75	0.62	3.77	0.18	0.11	0.24	0.15	225	176	29
C40	3	0.74	0.60	3.58	0.05	0.25	0.29	0.09	242	259	16
C60	3	0.78	0.59	3.67	0.03	0.21	0.28	0.06	273	234	21
C33	3	0.73	0.61	3.61	0.11	0.11	0.27	0.13	211	228	23
C44	3	0.65	0.67	3.79	0.13	0.14	0.24	0.22	-	-	-
C318	4	0.81	0.62	3.98	0.14	0.12	0.28	0.12	-	-	-
C413	4	0.64	0.64	3.46	0.16	0.12	0.23	0.15	207	255	30
C533	4	0.59	0.68	3.60	0.07	0.11	0.15	0.28	212	233	29
C559	4	0.60	0.64	3.21	0.14	0.19	0.26	0.09	246	217	38
C462	4	0.69	0.65	3.90	0.11	0.14	0.25	0.12	207	231	24
C463	4	0.65	0.66	3.72	0.11	0.16	0.25	0.14	-	-	-
C328	4	0.68	0.59	3.16	0.10	0.22	0.27	0.11	256	362	32
C63	4	0.60	0.63	3.10	0.13	0.19	0.24	0.32	272	277	31
C54	4	0.64	0.64	3.37	0.13	0.17	0.25	0.18	236	226	29
C51	4	0.58	0.67	3.44	0.12	0.16	0.23	0.15	244	189	34
C238	4	0.66	0.67	3.85	0.10	0.13	0.23	0.17	202	199	25
C484	4	0.75	0.60	3.62	0.12	0.15	0.25	0.16	-	-	-
C580	5	0.76	0.56	3.29	0.09	0.19	0.26	0.09	244	328	25
C590	5	0.79	0.54	3.25	0.10	0.24	0.28	0.09	246	333	21
C311	5	0.64	0.60	3.01	0.13	0.25	0.27	0.09	265	328	36
C278	5	0.57	0.56	2.50	0.15	0.18	0.26	0.13	295	425	42
C365	5	0.70	0.63	3.62	0.13	0.14	0.25	0.12	-	-	-
C362	5	0.69	0.63	3.54	0.07	0.20	0.25	0.11	-	-	-
C262	5	0.60	0.70	3.82	0.10	0.15	0.23	0.10	220	231	29
C375	6	0.62	0.54	2.46	0.24	0.22	0.27	0.11	-	-	-
C382	6	0.81	0.55	3.37	0.09	0.18	0.29	0.08	258	364	20
C498	6	0.74	0.57	3.41	0.07	0.19	0.28	0.08	268	261	39
C178	6	0.52	0.56	2.18	0.20	0.20	0.28	0.14	-	-	-

Table 3.5: *Trace element data and major element ratios for all the single chromite grain samples. All oxide values are wt.% values.*

Site No	Group	Cr#	Mg#	Cr/Fe^{2+}	TiO_2	V_2O_5	MnO	NiO
650	2	0.78	0.70	5.04	0.26	0.10	0.24	0.15
645	2	0.80	0.61	3.97	0.06	0.18	0.26	0.10
640	2	0.57	0.71	3.75	0.13	0.16	0.23	0.10
636	2	0.72	0.68	4.43	0.26	0.11	0.24	0.10
573	2	0.80	0.64	4.31	0.12	0.12	0.25	0.14
133	2	0.89	0.58	4.19	0.07	0.11	0.33	0.07
132	2	0.70	0.63	3.64	0.21	0.18	0.26	0.07
598	3	0.82	0.64	4.38	0.13	0.16	0.27	0.07
597	3	0.61	0.69	3.75	0.29	0.18	0.24	0.15
596	3	0.61	0.68	3.59	0.51	0.17	0.26	0.15
527	3	0.67	0.60	3.17	0.11	0.23	0.26	0.10
89	3	0.85	0.68	5.10	0.24	0.05	0.23	0.25
45	3	0.59	0.64	3.29	0.13	0.19	0.18	0.28
42	3	0.82	0.58	3.77	0.10	0.22	0.29	0.09
557	4	0.60	0.66	3.35	0.16	0.17	0.24	0.08
536	4	0.76	0.57	3.36	0.24	0.12	0.27	0.10
504	4	0.87	0.59	4.15	0.12	0.09	0.29	0.12
483	4	0.72	0.61	3.42	0.15	0.16	0.24	0.13
461	4	0.76	0.56	3.30	0.23	0.12	0.30	0.10
321	4	0.72	0.65	3.92	0.20	0.08	0.23	0.16
271	4	0.91	0.57	4.07	0.04	0.17	0.32	0.04
591	5	0.64	0.71	4.24	0.16	0.18	0.22	0.17
469	5	0.68	0.68	4.03	0.24	0.17	0.23	0.13
340	5	0.71	0.55	2.94	0.15	0.24	0.29	0.16
302	5	0.56	0.67	3.21	0.12	0.23	0.22	0.10
280	5	0.79	0.38	2.28	0.27	0.46	0.35	0.08
255	5	0.84	0.55	3.54	0.11	0.22	0.30	0.08
218	5	0.83	0.48	3.00	0.14	0.37	0.31	0.10
514	6	0.81	0.41	2.51	0.17	0.39	0.31	0.13
494	6	0.81	0.57	3.69	0.15	0.15	0.29	0.07
489	6	0.73	0.59	3.41	0.17	0.18	0.27	0.12
477	6	0.67	0.57	2.84	0.24	0.21	0.28	0.15
459	6	0.69	0.62	3.47	0.11	0.18	0.25	0.15
161	6	0.57	0.51	2.15	0.26	0.22	0.27	0.11
159	6	0.74	0.68	4.36	0.15	0.13	0.24	0.16

3.4.2.2.1 The relationship of trace element geochemistry to stratigraphic height

In addition to further investigating the relationship of major element chromite geochemistry and stratigraphy this research has also investigated the relationship of trace element (Ti, V, Mn Ni, Co, Zn and Ga) chromite geochemistry with stratigraphy.

Titanium (TiO_2) shows no particular pattern in values across the different stratigraphic groups, though there is a slight increase from group 1 to group 3 in the average values (Figure 3.17A). Overall, average V_2O_5 values show an increase with stratigraphic height from group 1 to group 6, although there are downturns in groups 4 and 6 (Figure 3.17B). Manganese (Figure 3.17C) is broadly constant throughout all the stratigraphic levels, and is therefore independent of stratigraphic height. Nickel shows a similar relationship to MnO with stratigraphic height, although punctuated by higher values within groups 2, 3 and 4. Chromitites with higher NiO values correlate to chromitites with higher proportions of nickel-sulphide minerals. Within levels 5 and 6 the NiO values reduce slightly (Figure 3.17D).

Zinc (Zn), Co and Ga were analysed using a Laser ICP-MS. Analyses of Co and Zn are "semi-quantitative" (see Section 2.5.1) but all values have been standardised relative to analyses collected on the last day, ensuring that relative differences between data points are accurate (cf. Section 2.6). A sub-set of 27 chromitite samples were analysed. These included samples from each stratigraphic height and the full range of PGE concentrations. It is apparent that both Zn and Co show weak positive correlations with stratigraphic height, with a general trend of increasing value in each successive stratigraphic group (Figure 3.17E & F). Ga shows a similar weak positive correlation with stratigraphic height, but with the average values evening out in groups 5 and 6 (Figure 3.17G). This trend is expected as the outer electronic structure of Ga is similar to that of Al (i.e. $3s^2 3p^1$ and $4s^2 4p^1$). As such it may be expected that Ga contents would follow an almost identical pattern to Al.

As with the major elements, there is also an indication of a slight adjustment in the nature of the trace element variation in group 4. For example, MnO values are constant up to group 4 before rising slightly and V_2O_5, Co and Zn show a low point in the curve at group 4. Also, NiO values show a slight decrease after group 4, with none of the high values, which had been previously observed in groups 2, 3 and 4.

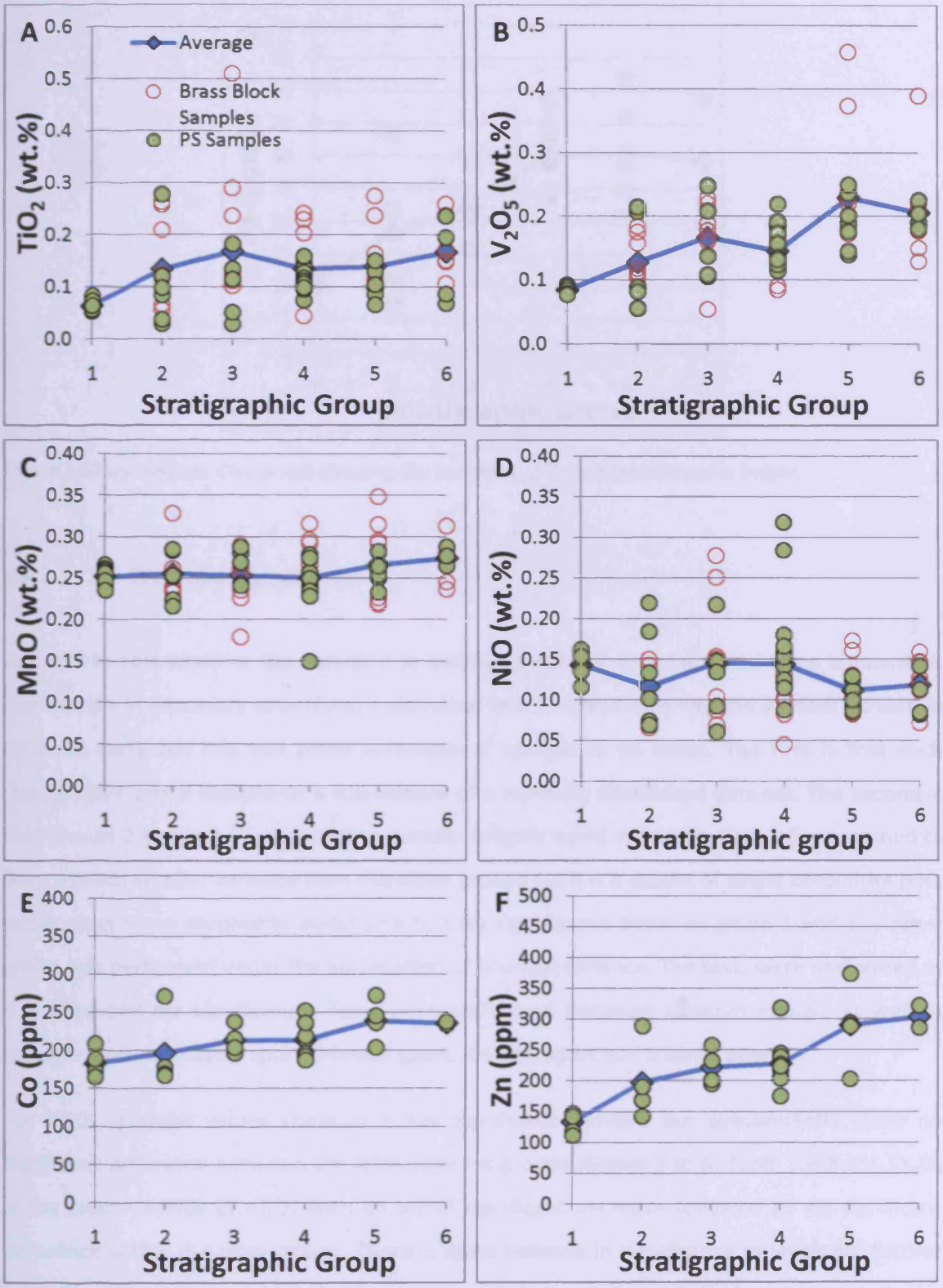

Figure 3.17: *Seven charts (continued overleaf) showing the variation in trace element geochemistry with stratigraphic height. A: TiO_2, B: V_2O_5, C: MnO, D: NiO, E: Zn, F: Co and G: Ga. The blue line marks the average value at each stratigraphic group, the green circles mark polished section samples, whilst the clear circles mark brass block samples (Legend in Figure 3.17A).*

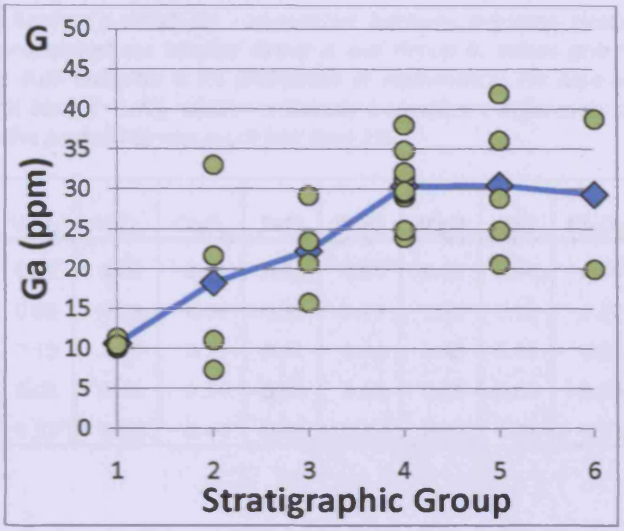

Figure 3.17 continued: *One graph showing the variation of Ga with stratigraphic height.*

3.4.2.2.1.1 Statistical significance

In order to test whether the variation in average values of the major and trace elements is significant it is necessary to perform a statistical test. The test used was the student's t-test. In order to carry out this test some assumptions needed to be made. The first is that each stratigraphic group represents a sub-sample of a normally distributed data set. The second is that groups 2 to 6 can be expected to contain roughly equal variances. Group 1 is assumed to have a much smaller variance than the other groups (as it is a subset of single chromitite pod, rather than many chromitite pods) so a test for significance between group 1 and any other group was performed under the assumption of unequal variance. The tests were performed as a 1-tailed test for significance. Tests were performed between adjacent groups, as well as between groups 2-levels apart, 3-levels apart, 4-levels apart and 5 levels apart.

For Al_2O_3, average values show an initial significant increase but subsequently show no significant difference between the later adjacent groups (Group 3 to 6, Table 3.6-3.10). Cr_2O_3 is the exact reverse of Al_2O_3 with an initial significant decrease followed by no significant difference within the later groups. There is some increase in significance as levels get further apart (e.g. for Cr_2O_3 and Al_2O_3 between groups 2 & 4). MgO and FeO should have a similar antithetical relationship due to unit cell constraints, but the variations are more significant for FeO, which increases gradually through the sequence than for MgO which decreases gradually (Table 3.6-3.10). This may be due to less precision within the MgO analyses compared with the FeO analyses.

Table 3.6: *Results of the student's t-test for comparisons between adjacent stratigraphic groups. The two stratigraphic groups being compared are labelled Group A and Group B. Values give the probability of the two groups being identical (e.g. 0.05 indicates a 5% probability of equivalence) For ease of observation, statistically significant differences are in black (<0.05), whilst statistically insignificant differences are in green. If '0.01' is in italics then it indicates that the probability was much less than 1%.*

Group A	Group B	TiO_2	V_2O_5	Al_2O_3	Cr_2O_3	FeO	MnO	MgO	NiO	Fe_2O_3	Cr#	Mg#	Cr/Fe^{2+}
1	2	0.01	0.01	*0.01*	*0.01*	*0.01*	0.35	0.06	0.04	0.36	*0.01*	*0.01*	*0.01*
2	3	0.28	0.05	0.11	0.06	0.03	0.43	0.24	0.12	0.20	0.10	0.08	0.08
3	4	0.16	0.10	0.29	0.19	0.27	0.31	0.43	0.48	0.02	0.27	0.35	0.35
4	5	0.42	*0.01*	0.41	0.34	0.04	0.11	0.08	0.05	0.05	0.45	0.05	0.05
5	6	0.13	0.23	0.43	0.44	0.18	0.27	0.22	0.28	0.11	0.49	0.22	0.19

Table 3.7: *Results of the student's t-test for comparisons between groups two levels apart.*

Group A	Group B	TiO_2	V_2O_5	Al_2O_3	Cr_2O_3	FeO	MnO	MgO	NiO	Fe_2O_3	Cr#	Mg#	Cr/Fe^{2+}
1	3	0.01	*0.01*	*0.01*	*0.01*	*0.01*	0.45	0.01	0.46	0.07	*0.01*	*0.01*	*0.01*
2	4	0.48	0.13	0.03	0.01	*0.01*	0.34	0.17	0.10	*0.01*	0.02	0.03	0.03
3	5	0.23	0.02	0.38	0.10	0.05	0.18	0.10	0.06	*0.01*	0.32	0.06	0.06
4	6	0.07	*0.01*	0.34	0.31	*0.01*	0.02	*0.01*	0.11	0.01	0.44	*0.01*	*0.01*

Table 3.8: *Results of the student's t-test for comparisons between groups three levels apart.*

Group A	Group B	TiO_2	V_2O_5	Al_2O_3	Cr_2O_3	FeO	MnO	MgO	NiO	Fe_2O_3	Cr#	Mg#	Cr/Fe^{2+}
1	4	*0.01*	*0.01*	*0.01*	*0.01*	*0.01*	0.43	*0.01*	0.48	*0.01*	*0.01*	*0.01*	*0.01*
2	5	0.43	*0.01*	0.06	*0.01*	*0.01*	0.21	0.04	0.37	*0.01*	0.04	0.01	*0.01*
3	6	0.49	0.08	0.45	0.13	*0.01*	0.04	*0.01*	0.13	*0.01*	0.34	*0.01*	*0.01*

Table 3.9: *Results of the student's t-test for comparisons between groups four levels apart.*

Group A	Group B	TiO_2	V_2O_5	Al_2O_3	Cr_2O_3	FeO	MnO	MgO	NiO	Fe_2O_3	Cr#	Mg#	Cr/Fe^{2+}
1	5	*0.01*	*0.01*	*0.01*	*0.01*	*0.01*	0.10	0.01	*0.01*	*0.01*	*0.01*	*0.01*	*0.01*
2	6	0.16	*0.01*	0.10	0.01	*0.01*	0.05	*0.01*	0.45	*0.01*	0.06	*0.01*	*0.01*

Table 3.10: *Results of the student's t-test for comparisons between groups five levels apart.*

Group A	Group B	TiO_2	V_2O_5	Al_2O_3	Cr_2O_3	FeO	MnO	MgO	NiO	Fe_2O_3	Cr#	Mg#	Cr/Fe^{2+}
1	6	0.03	*0.01*	*0.01*	*0.01*	*0.01*	0.05	0.01	0.17	*0.01*	*0.01*	*0.01*	*0.01*

Average Fe_2O_3 values show a significant increase between groups at least two levels apart, and also between adjacent groups 3, 4 and 5 (table 3.6-3.10). It is noteworthy that several elements show significant differences between adjacent groups 1 & 2, as well as adjacent groups 4 & 5 (Table 3.6).

Within the trace elements average TiO_2 values only show a significant increase when comparing group 1 values with those in any other group (Table 3.6-3.10). Average V_2O_5 values do show significant rises at adjacent stratigraphic groups, as well as between groups further apart. There are a few decreases in average value (from group 3 to 4 and group 5 to 6) but these are not significant (Table 3.6-3.10). Average MnO values show no significant variation between groups, except for between group 6 and groups 1-4. For NiO, there is significant variation between group 4 and 5 (and 1 to 5) where NiO shows a decrease in value. Co, Zn and Ga were not tested for significance as the groups were not large enough for statistical significance.

The clearest discriminant ratio is Cr/ Fe^{2+}, which shows significant variations between adjacent groups as well as groups several levels apart. The only exception to this is between groups 4 and 5, and groups 5 and 6. It is noteworthy that there are no statistically significant variables between groups 5 and 6. This strongly suggests that based on the number of pods (sites) analysed in this study that these two groups are geochemically indistinguishable.

3.4.3 MORB normalised multi element plots

MORB normalised multi element plots of the Al 'Ays chromitites reveal a strong similarity to similar plots from the Thetford chromitites in Canada (Figure 3.18), which are postulated to be supra-subduction ophiolites. The Al 'Ays ophiolite has previously been proposed to be from a supra-subduction zone setting (Bakor *et al.*, 1976; Stern *et al.*, 2004), so this similarity with the Thetford chromitites is expected. The key similarities between Thetford and Al 'Ays are in the value of Mg, FeO^{tot}, Mn and Cr_2O_3. The Al_2O_3, TiO_2, NiO and Ga values are also similar but with much larger ranges. The similar Cr_2O_3 and Al_2O_3 values in the Al 'Ays ophiolite imply that the degree of partial melting experienced within the Thetford ophiolite was similar to that in the Al 'Ays ophiolite.

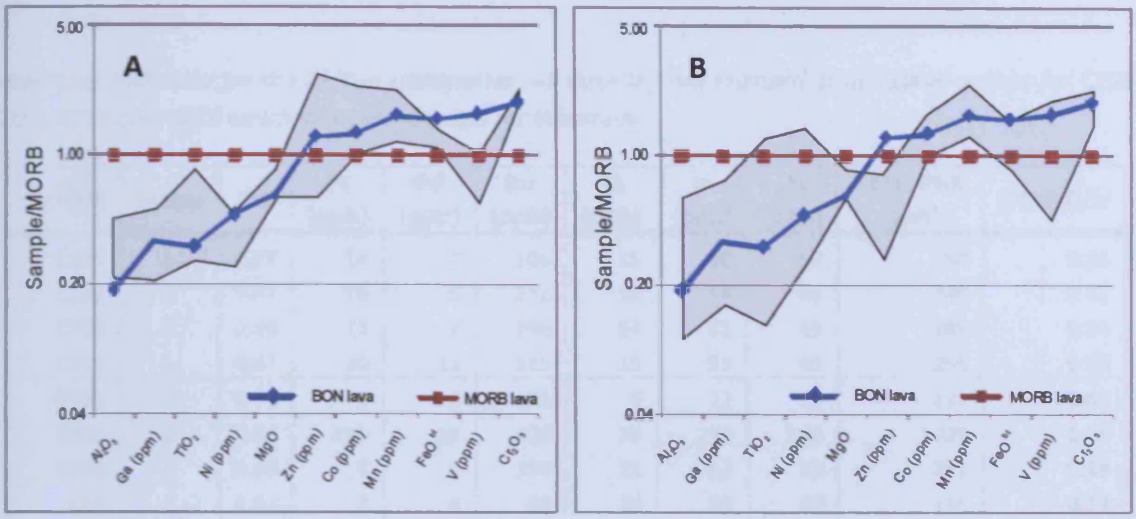

Figure 3.18: *MORB normalised multi-element plots for* ***A:*** *Thetford Chromitites (Page and Barnes, 2009) and* ***B:*** *Al 'Ays Chromitites. Regions shaded in grey show the compositional range for each ophiolite. The blue indicates the chromite composition from chromite grains within boninitic lava. MORB and boninite sources taken from Page and Barnes (2009). For Al 'Ays the Co and Zn are semi-quantitative so their absolute position relative to the y-axis is only approximate.*

3.5 The platinum-group elements (PGE)

Platinum-group element analyses from the Al 'Ays chromitites were obtained by Prichard *et al.* (2008) who described three types of PGE mineralization based on chondrite normalised plots, and the relationship of total PGE concentration to Cr_2O_3 values. 35 PGE analyses are taken from that study. This study has analysed a further 4 chromitite samples from the large chromitite pod in the south of the ophiolite. The total PGE data set is used here to compare the PGE content of the chromitites with proximity to the pyroxenite/dunite boundary and to examine the relationship between PGE content and chromite trace element geochemistry.

3.5.1 The relationship of PGE concentrations to stratigraphic height

For the individual PPGE the average values (Figure 3.19A - C) show systematic increases up to group 4. Pd is particularly well defined, with minimum and maximum values increasing from group 2 to 4. From group 4 to 5 and into group 6 the values of Pt, Pd and Rh are similar, or decrease slightly. For the individual IPGE there is no particular relationship with stratigraphic height, although the highest Os, Ir and Ru values are all located in group 4 (Figure 3.19D - F).

Table 3.11: *PGE data for the Al 'Ays chromitites. All data is from Prichard et al. (2008) except for C205, C213, C214 and C215 which were undertaken for this study.*

Sample	Group	Cr#	Pt (ppb)	Pd (ppb)	Ru (ppb)	Rh (ppb)	Ir (ppb)	Os (ppb)	Total PGE (ppb)	(Pt+Pd)/Ir
C205	1	0.87	14	7	108	15	60	50	254	0.35
C213	1	0.87	16	6	118	16	54	36	246	0.41
C214	1	0.88	14	7	100	14	61	49	245	0.34
C215	1	0.87	20	11	115	13	59	40	258	0.53
C595	2	0.71	9	6	76	6	22	12	131	0.68
C104	2	0.86	210	10	420	75	210	100	1025	1.05
C670	2	0.86	5	6	130	21	57	32	251	0.19
C10	2	0.62	8	4	96	16	63	60	246	0.17
C655	2	0.92	23	5	65	20	18	8	139	1.56
C123	2	0.76	9	2	159	26	99	35	330	0.11
C46	3	0.75	3	4	18	3	11	8	46	0.59
C40	3	0.74	62	7	218	37	138	102	564	0.50
C60	3	0.78	191	5	1050	71	722	624	2663	0.27
C33	3	0.73	336	31	373	76	279	87	1182	1.32
C44	3	0.65	47	45	82	23	82	14	293	1.12
C318	4	0.81	470	83	220	150	130	42	1095	4.25
C63	4	0.60	310	1200	130	58	50	24	1772	30.20
C54	4	0.64	200	940	150	130	52	6	1478	21.92
C51	4	0.58	970	97	5800	840	6200	3300	17207	0.17
C238	4	0.66	157	85	351	52	357	268	1270	0.68
C484	4	0.75	420	42	460	140	310	240	1612	1.49
C413	4	0.64	15	11	240	47	120	68	501	0.22
C533	4	0.59	150	1000	68	46	20	6	1290	57.50
C559	4	0.60	2570	6870	500	225	198	100	10463	47.68
C462	4	0.69	38	16	254	33	156	112	609	0.35
C463	4	0.65	46	17	200	21	147	102	533	0.43
C328	4	0.68	86	14	218	21	313	174	826	0.32
C580	5	0.76	494	165	333	111	173	142	1418	3.81
C590	5	0.79	300	28	640	230	410	290	1898	0.80
C311	5	0.64	720	340	430	147	152	41	1830	6.97
C278	5	0.57	200	36	180	80	75	30	601	3.15
C365	5	0.70	9	7	180	30	110	170	506	0.15
C362	5	0.69	65	17	540	110	160	160	1052	0.51
C262	5	0.60	69	220	73	26	55	54	497	5.25
C375	6	0.62	170	85	180	72	91	62	660	2.80
C382	6	0.81	697	36	436	155	248	200	1772	2.96
C498	6	0.74	990	100	670	210	610	320	2900	1.79
C178	6	0.52	81	100	41	45	22	14	303	8.23

When considering the two PGE subsets (PPGE and IPGE), it is apparent that they follow the same pattern as the individual components of each subset (Figure 3.20). The PPGE show a general increase in content from group 1 through to group 4. After which the maximum values decrease slightly, but still remain relatively high through to group 6. The IPGE show neither a general increase nor general decrease with stratigraphic height, though as noted with the individual IPGE, the maximum values are observed in group 4.

3.5.2 The relationship of PGE ratios to stratigraphic height

When considering the behaviour of the PGE it is often helpful to examine the ratio of the non-refractory PGE (the PPGE) to the refractory PGE (the IPGE) (e.g. (Barnes *et al.*, 1985)). Chromitites with high PGE ratios (that is high PPGE contents relative to IPGE contents) are shown to be concentrated in stratigraphic groups 4 and 5 (Figure 3.21A). Average PGE ratios are approximately constant from group 1 up to group 3 before a significant increase to group 4 and finally a decrease into group 5 and 6. The average values within groups 5 and 6 are higher than within groups 1 to 3. This pattern is the same regardless of whether the ratios of [(Pt+Pd+Rh)/(Os+Ir+Ru)], or the simplified [(Pt+Pd)/Ir] are considered (Figure 3.21B).

3.5.3 The relationship of PGE concentrations to chromite geochemistry

The observed relationship of both chromite geochemistry and PGE concentrations to stratigraphy suggests the two could be inter-related. There are several chromite major and trace elements which show either significant or visual correlations with stratigraphic height (e.g. Cr/ Fe^{2+}, Fe_2O_3, V_2O_5, and Zn). In contrast, PGE concentrations show a peak in values at stratigraphic level 4. This coincides with a dip in values for Fe, Co and Zn (Figure 3.15 & Figure 3.17) which may indicate the co-precipitation of a sulphide phase slightly reducing the availability of these elements to the oxide (e.g. chromite) phase.

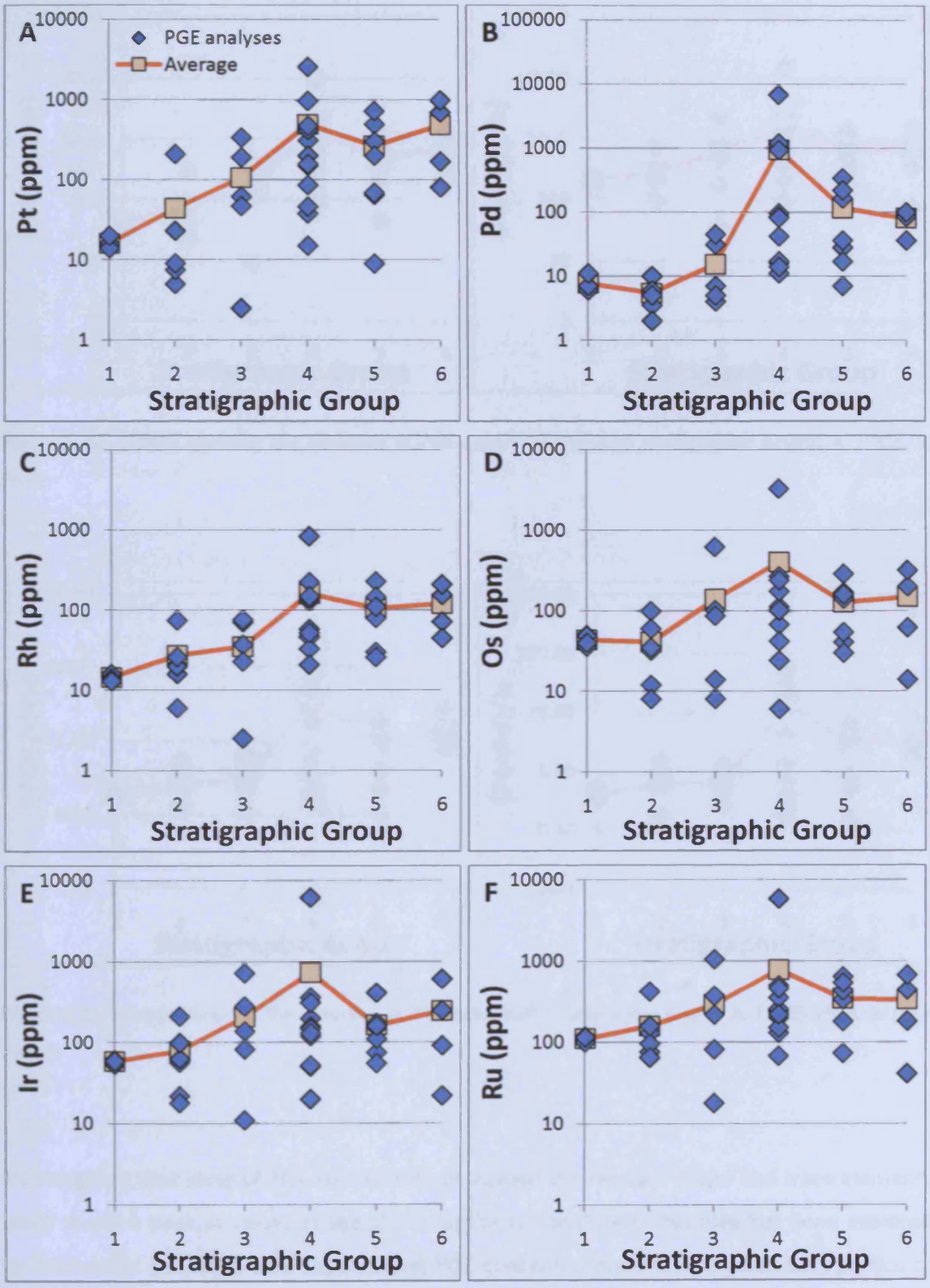

Figure 3.19: *Six charts showing the variation in platinum group element concentration with stratigraphic height. A: Pd, B: Pt, C: Rh, D: Os, E: Ir, F: Ru. The solid orange line marks the change in average value with each stratigraphic group.*

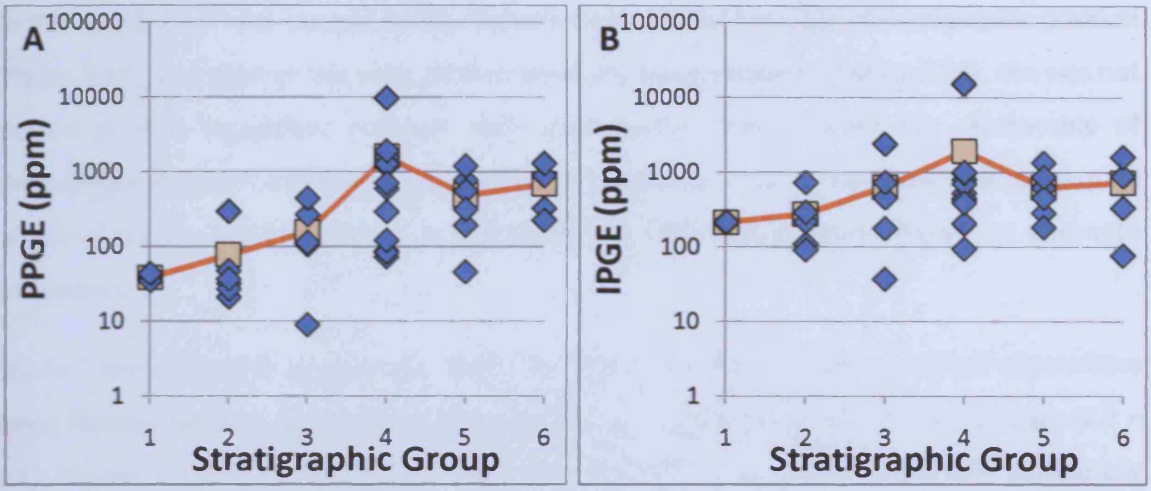

Figure 3.20: *Graphs showing the variation in PGE concentration with stratigraphic height. A: PPGE, B: IPGE.*

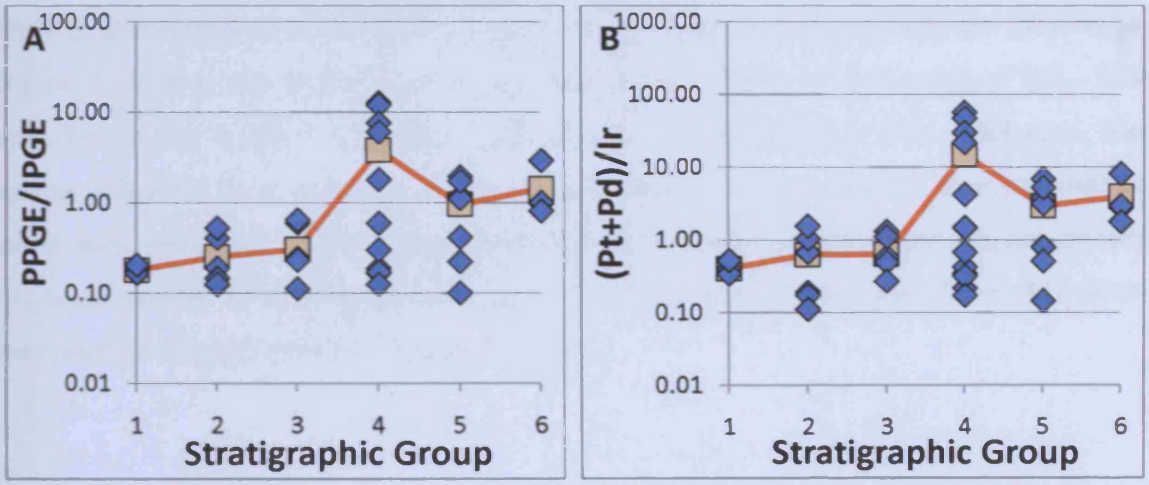

Figure 3.21: *Graphs showing the variation in PGE ratio with stratigraphic height. A: PPGE/ IPGE, B: (Pt + Pd)/ Ir.*

This suggests that plots of PGE concentrations against the relevant major and trace elements could reveal a peak in values at specific chromite compositions. This idea has been explored by Prichard *et al.* (2008) who showed that PGE concentrations are associated with particular Cr# (Cr/(Cr + Al)) values, such that a plot of (Pt+Pd)/Ir against Cr# showed peaks in PGE ratio at a Cr# of ~0.60. Taking this idea further, it is possible to plot trace and major element markers of stratigraphic height against each other to see if high PGE concentrations are associated with particular chromite compositions (Figure 3.22).

To this end Cr/ Fe^{2+} was chosen as the clearest major element marker of stratigraphic position (Figure 3.15), and against this were plotted six of the trace elements (Figure 3.22). Mn was not plotted as it is essentially constant with stratigraphic height. Given the relationship of chromite composition and PGE concentration to stratigraphy it was expected that some or all of these graphs should produce a pathfinder for PGE concentration based on chromite composition.

Cr/ Fe^{2+} values provide a good constraint for PGE concentration with enriched chromitites being located within a narrow band of values (3.0 – 3.7) compared with the total range (2.2 – 6.1) (Figure 3.22A - F). Within the trace elements TiO_2, Ga and NiO are not particularly discriminatory as the range of values for PGE-rich samples is very similar to the range of values for PGE-poor samples (Figure 3.22A, E & F). V_2O_5 values provide some constraint on high PGE concentrations with all PGE-rich chromitites having V_2O_5 values greater than 0.15 compared with the full range (0.06 – 0.25) (Figure 3.22B). Co and Zn show very distinctive patterns with PGE-rich chromitites associated with a specific range of values compared with the total range (Figure 3.22D & E). For Zn this is 213 – 322 ppm compared with the total range of 141 – 374 ppm. For Co this is 226 – 273 ppm compared with the total range of 175 – 343 ppm. The narrow range for Co is nearly exclusive with only two comparatively PGE-poor chromitites within the same range. It should be pointed out that Co and Zn (and Ga) graphs do not contain the same number of analyses as other major and trace element analyses (27 vs. 43) which may produce an apparently better discrimination.

3.5.4 The relationship of PGE ratios to chromite geochemistry

When investigating the relationship of PGE ratios ((Pt+Pd)/Ir) to chromite geochemistry a slightly different pattern to PGE concentration emerges (Figure 3.23). From all six figures it can be seen that the trace elements are not good indicators of high PGE ratio, though for V_2O_5 (Figure 3.23B), Co (Figure 3.23D), Zn (Figure 3.23E) and Ga (Figure 3.23F) there is a general tendency for high PGE ratios to be concentrated at the slightly higher values of the compositional range. What is apparent from Figure 3.23 is that the Cr/ Fe^{2+} ratio is a good indicator of higher PGE ratios with there being a definite grouping of higher PGE ratios towards the lower end of the Cr/ Fe^{2+} range.

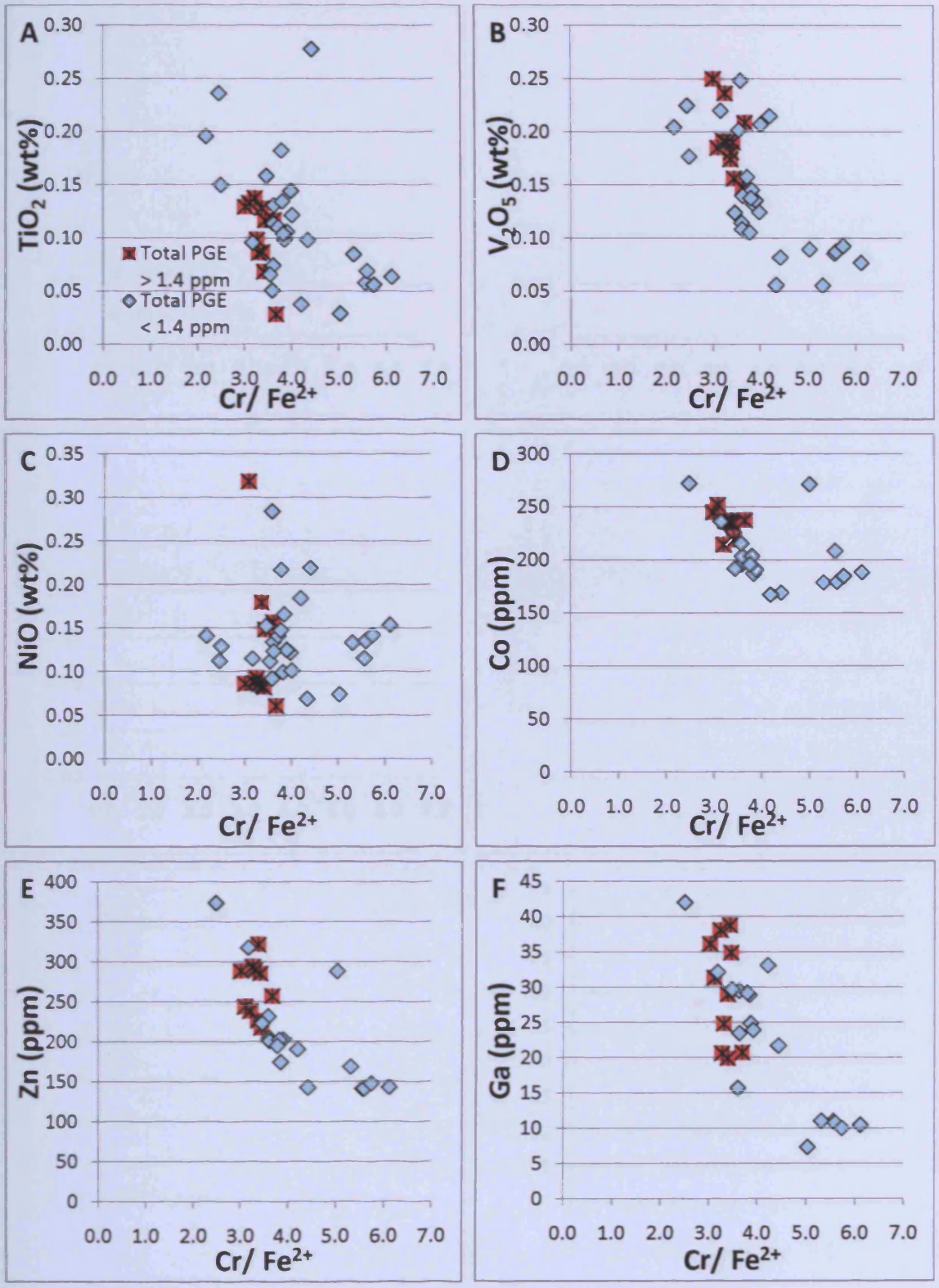

Figure 3.22: *Graphs of Cr/ Fe^{2+} against selected trace elements, A: TiO_2 (wt.%) B: V_2O_5 (wt.%) C: NiO (wt.%) D: Co (ppm), E: Zn (ppm) and F: Ga (ppm). Markers shaded in red indicate chromitites enriched in PGE (> 1.4 ppm), whereas markers shaded in blue represent chromitites with < 1.4 ppm total PGE.*

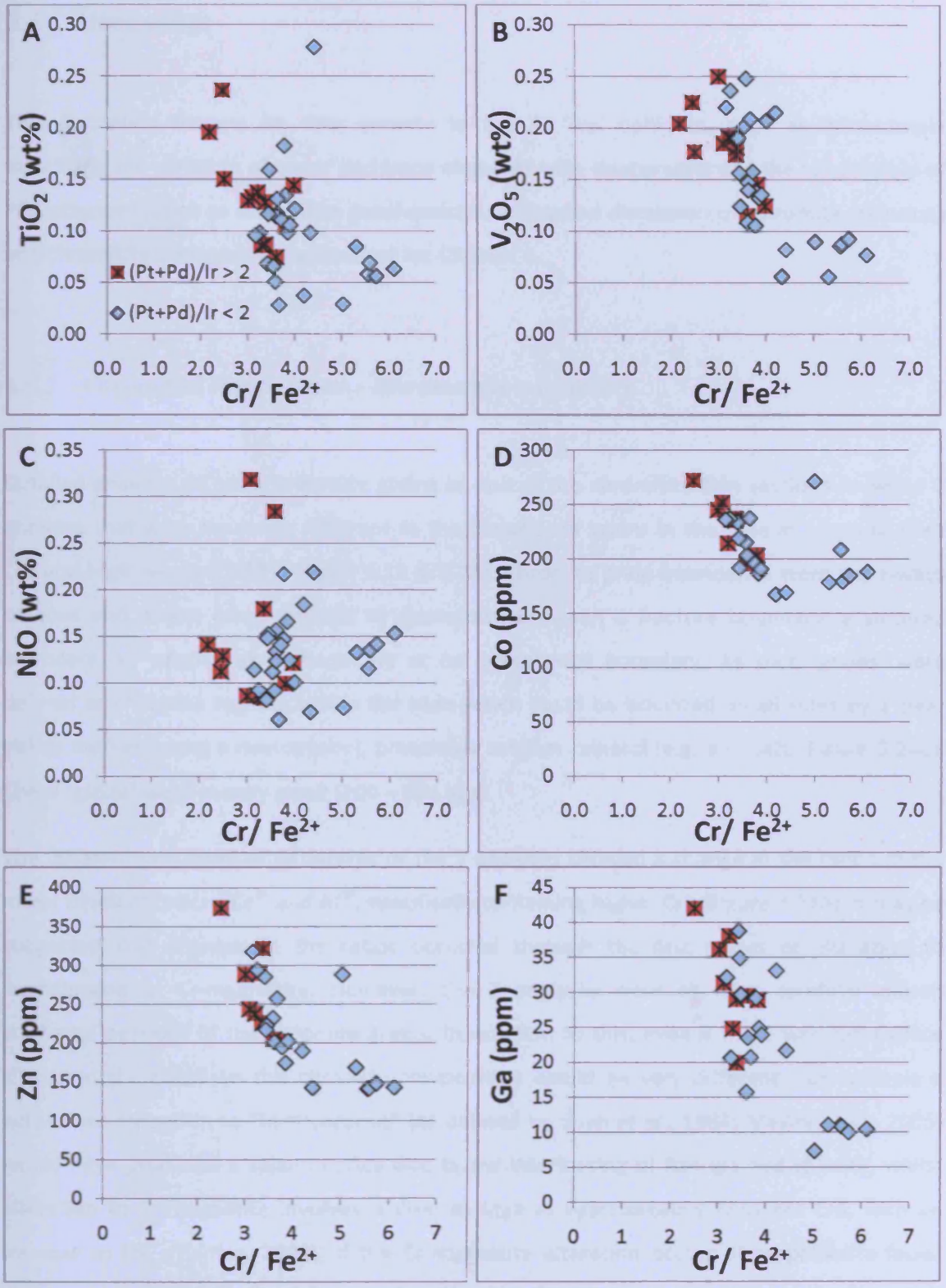

Figure 3.23: *Graphs of Cr/ Fe^{2+} against selected trace elements, A: TiO_2 (wt.%), B: V_2O_5 (wt.%), C: NiO (wt.%), D: Co (ppm), E: Zn (ppm) and F: Ga (ppm) Markers shaded in red indicate chromitites with PGE ratios >2, whereas markers shaded in blue represent chromitites with PGE ratios <2. The four PGE-poor analyses with the highest Cr/ Fe^{2+} values are all taken from the same chromitite pod.*

3.6 Discussion

This discussion focuses on data specific to the Al 'Ays ophiolite, such as intra-sample variability, the variation of major and trace elements with stratigraphy and the relationship of PGE concentrations to chromitite geochemistry. A detailed discussion on chromite inclusions and chromitite petrogenesis is reserved for Chapter 6.

3.6.1 Chromitite composition – intrasample variability

Detailed analyses of many chromite grains in one of the chromitite thin sections revealed 7 analyses that were markedly different to the majority of grains in the slide in terms of their Cr# and Mg# values (C462 – Figure 3.12 & 3.24). Chromite grain boundaries were not always obvious and it was often difficult to distinguish between a fracture boundary, a sintered boundary, an original grain boundary or an overgrowth boundary. As such 'grains' were defined as chromite regions within the slide which could be bounded on all sides by a clear visible marker (using a microprobe), preferably another mineral (e.g. a silicate, Figure 3.24C). These 'grains' were usually small (200 – 500 μm).

The different geochemical signatures of the 7 analyses showed a change in the ratios of the major trivalent cations Cr^{3+} and Al^{3+}, specifically containing higher Cr# (Figure 3.24A). It may be suggested that changes in the ratios occurred through the first stages of alteration to ferritchromit or Cr-magnetite. However, the 7 analyses were all from carefully chosen unaltered portions of the chromite grains. In addition to this, even if there was sub-surface alteration the effect on the chromite composition would be very different. For example a subsurface alteration to "ferritchromit" (as defined by Shen *et al.*, 1988; Mellini *et al.*, 2005) would have produced a spike in silica due to the interleaving of fine-grained chlorite, whilst alteration to Cr-magnetite involves a drop in Mg# at approximately constant Cr#, with an increase in Fe^{3+} (Barnes, 2000). If the Cr-magnetite alteration occurs at amphibolite facies metamorphism then higher Cr# may occur through the selective replacement of Al^{3+} by Fe^{3+} (Barnes, 2000). However, the difficulty of explaining why 7 analyses out of 239 were selectively subject to amphibolite metamorphism and the absence of any increase in the Fe^{3+} content of the 7 analyses makes it very unlikely that metamorphic overprinting is the cause.

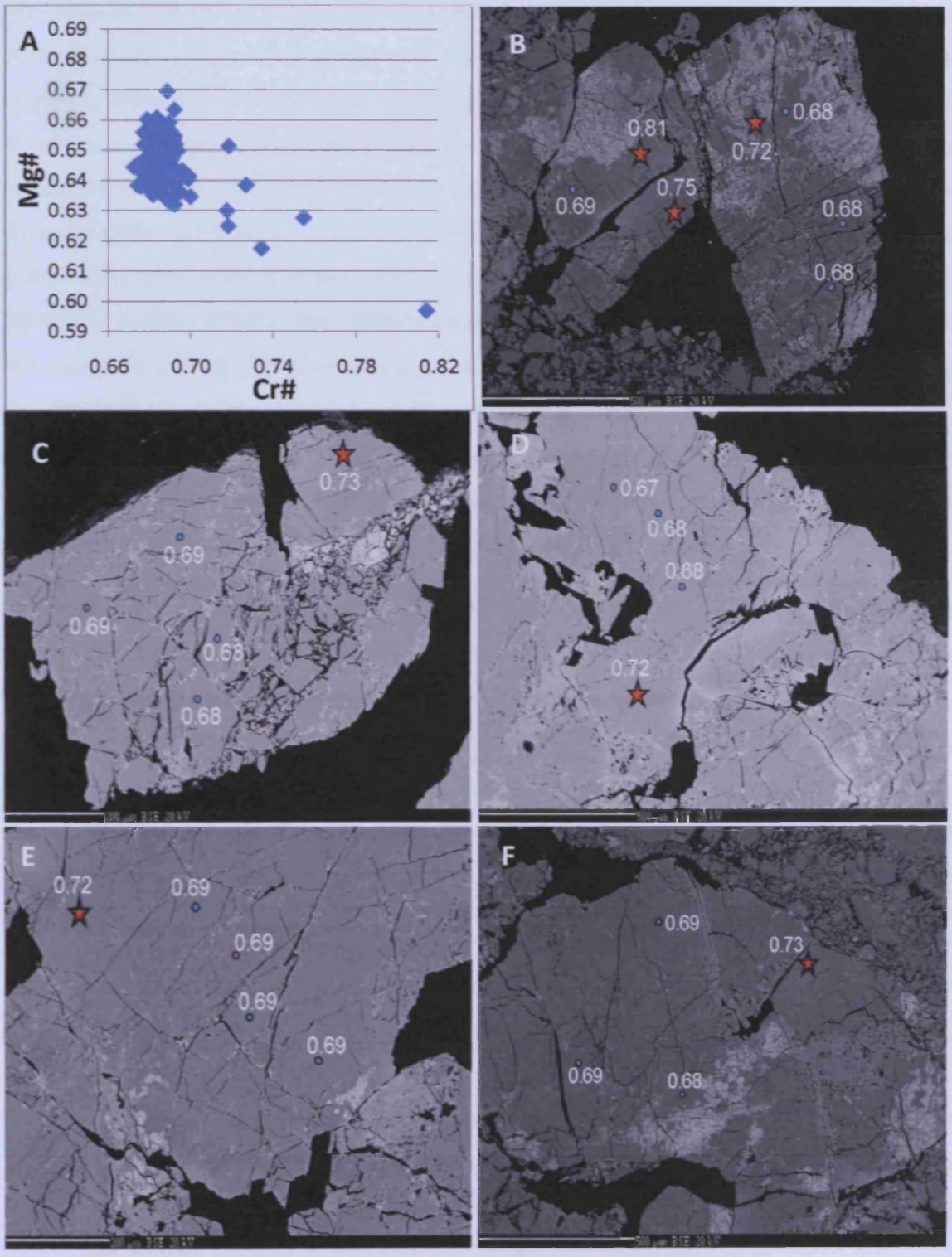

Figure 3.24: *Back Scatter Electron Images of chromite grains containing anomalous chromite compositions. The numbers refer to the Cr# collected for that particular point, with red stars referring to one of the seven anomalous analyses, whilst blue points refer to other analyses collected close by which show Cr# typical of the 232 remaining analyses. A: Cr# - Mg# plot for sample C462 showing the 7 analyses with higher Cr#. B: Grain 2&3, C: Grain 10, D: Grain 20, E: Grain 35, F: Grain 37.*

Alternatively, sub-solidus unmixing may produce large changes in trivalent proportions within chromite grains due to the separation of two spinel phases (e.g. Tamura and Arai, 2005). However, there is no visual evidence under microprobe magnification of unmixing. The remaining explanation is that these 7 analyses contain higher Cr# and lower Mg# because they crystallized from a melt of different composition to that which crystallized the bulk of the chromite grains in the polished section. As the main control on the Cr# content of chromite grains is the Al_2O_3 content of the melt (e.g. Roeder and Reynolds, 1991; Kamenetsky *et al.*, 2001), this increase in Cr# is most likely to be due to the melt containing lower Al_2O_3 contents. The associated drop in Mg# is because any changes to the Cr/Al ratio of a melt (essentially any changes to the Al_2O_3 content of the melt (Maurel and Maurel, 1982; Roeder and Reynolds, 1991; Kamenetsky *et al.*, 2001) will, in addition to any associated changes in the Mg# of the melt, cause changes in the Mg# of crystallizing chromite due to changes in the Fe-Mg exchange partition coefficient (e.g. Allan *et al.*, 1988; Naldrett *et al.*, 2009).

A second curious feature of the locations of the 7 anomalous analyses in this sample, is that they appear to occur within larger chromite grains (Figure 3.24B-F). The other analyses from these grains are typical of chromite from the rest of the slide. These 7 analyses are scattered throughout the sample and occur in grains analysed on different days indicating that these anomalous data are not associated with a particular spatial zone or chronological process caused by instrumental drift. The different Cr# of the 7 analyses may therefore reflect chromite grains which initially crystallized from a different melt. Their location 'buried' within larger chromite grains suggests that;

1. An already 'charged' magma carrying earlier xenocrysts of chromite crystallises further chromite and the dual population is subsequently sintered (or overgrown) to remove crystal boundaries, or;
2. A previous melt batch deposited higher Cr# chromite. The thin section taken parallel to the cryptic layering picked up isolated analyses from the chromitite layer below (e.g. micro-cryptic layering at Voskhod, pers comm. C. Johnson). Sintering (or overgrowth) has also removed original growth-grain boundaries.

These explanations carry the added implication that chromite grains within ophiolitic settings may either be amalgams of several much smaller grains, or enlarged through later overgrowth and that podiform chromitites as a whole may have undergone 'densification' producing an artificially low porosity (e.g. stratiform chromitites (Hulbert and Von Gruenewaldt, 1985)).

The low proportion of interstitial space within chromitites (~5%) is likely to be partly a product of overgrowth or sintering for two reasons. Firstly, if the chromite grains were modelled as spherical objects their rhombohedral packing (the most space efficient packing) would produce ~26% interstitial space. Chromite grains are not spherical and so interstitial space would probably be slightly less than 26% under ideal packing scenarios but highly unlikely to be as low as ~5%. Secondly, the presence of interlocking grains with no interstitial space strongly suggests overgrowth or sintering has occurred, squeezing out the interstitial space. Regardless of the exact mechanism the observation that the majority of the analyses lie within a fixed Cr# range suggests that during the build up of a chromitite deposit the composition of the melt remains largely constant, and that a chromitite deposit may be built up over considerable time through the repeated flux of melts of the same composition – each depositing a small amount of chromite.

From the data acquired it is difficult to definitively say which of the two explanations is most likely. However the magnitude of the difference between the Cr# of the 7 analyses and the remaining analyses leads the present author to prefer the first explanation - that of a magma already charged with chromite xenocrysts which are subsequently sintered (or possibly overgrown) to remove grain boundaries. If the higher analyses represented a partially exposed sublayer then that sublayer could be expected to contain a similar geochemical homogeneity to the layer it underlies – this is not the case. Magma charged with chromite crystals is geologically reasonable (e.g. numerous examples of phenocryst-bearing lavas and hypabyssal rocks) and has already been postulated for some stratiform chromitite deposits (e.g. Eales, 2000; Mondal and Mathez, 2007). An additional implication of these findings is that chromite geochemistry at the core of a grain can survive the processes of sintering or overgrowth at the edge of a grain. That is to say that the overgrowth or sintering process does not result in wholescale chemical homogenisation. Indeed, without amphibolite metamorphism (Barnes, 2000), alteration to Cr-magnetite or chromite unmixing (e.g. Loferski and Lipin, 1983; Tamura and Arai, 2005), the ratios between trivalent cations within unaltered chromite is essentially fixed after crystallization.

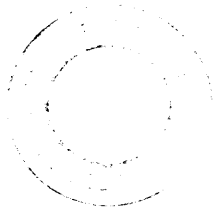

3.6.2 Chromitite compositional variation with stratigraphic height

The chromitite geochemistry of Al 'Ays displays a strong relationship to stratigraphic height with both major and trace elements showing clear patterns of change between group 1 and group 6. In addition there is a strong inverse correlation between Cr# and Mg# within groups (see groups 2, 3 and 4 in particular, Figure 3.25). This is the same as the pattern observed with sample C462 (see section 3.6.1) and is thought to result of the changing Mg-Fe exchange partition coefficient between spinel and melt caused by a change in the Cr/Al ratio of the spinel (Allan *et al.* 1988). Geologically speaking this is most likely to be caused by changing the composition of the primitive upwelling melt, in terms of its Al_2O_3 content, and indicates that the lowermost stratigraphic groups (2, 3 & 4) most likely had a changing melt composition.

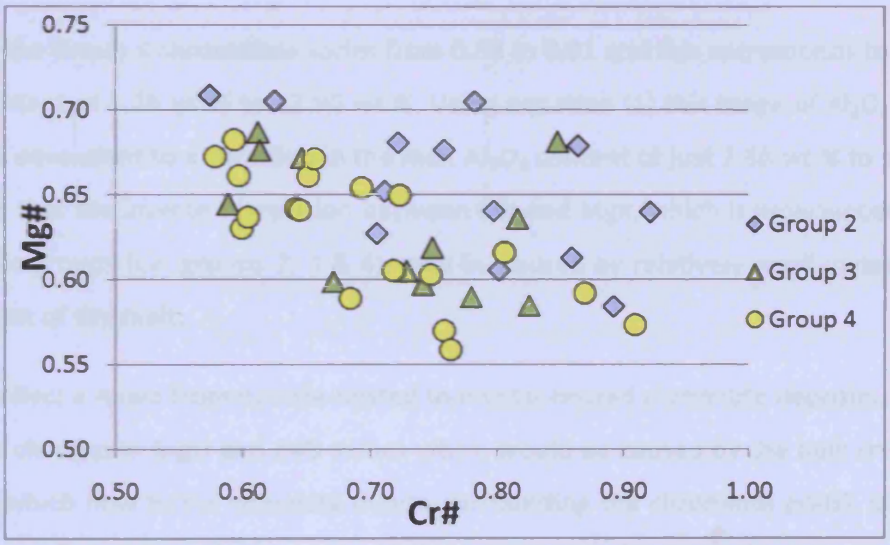

Figure 3.25: *Plot of Cr# - Mg# showing the range of values recorded within stratigraphic groups 2, 3 and 4 at Al 'Ays.*

Stratigraphic group 1 is a single chromitite pod and doesn't display this inverse correlation, though many of the samples display an inverse trend elongated along the Mg# direction (see Section 3.4.1 and Figure 3.10). Groups 5 and 6 do not display this trend so strongly and on a couple of markers are slightly different from the previous groups. For example their average Cr_2O_3, Al_2O_3 and Ga values have stopped changing relative to the previous groups, NiO values have slightly decreased, MnO values have slightly increased, MgO values are decreasing more sharply and FeO values are increasing more sharply (Figure 3.15 and 3.17).

These changes are reflected in the statistical differences beween groups 4 and 5 (Table 3.6) as well as the changes in the average Cr# and Mg# of each individual group (Figure 3.26). The groups show a trend of decreasing average Cr# and Mg# before changing slightly in the uppermost two groups to decreasing Mg# at constant Cr# (Figure 3.26).

Previous workers have suggested an empirical link between the Al_2O_3 content of the chromite and that of the parental melt (Maurel and Maurel, 1982; Kamenetsky *et al.*, 2001), Equation 1). Using Group 4 as an example it is possible to investigate how changing the Al_2O_3 content of the melt affects the Al_2O_3 content of the chromite grains.

$$ln(wt.\%\ Al_2O_3 \text{ in melt}) = 0.41322 \times ln(wt.\%\ Al_2O_3 \text{ in chromite}) + 1.38529 \quad (1)$$

The Cr# of the Group 4 chromitites varies from 0.58 to 0.91 and this corresponds to a variation in Al_2O_3 content of 4.39 *wt.%* to 22.90 *wt.%*. Using equation (1) this range of Al_2O_3 content in chromite is equivalent to a variation in the melt Al_2O_3 content of just 7.36 *wt.%* to 14.57 *wt.%*. This means that the inverse correlation between Cr# and Mg#, which is pronounced in several stratigraphic groups (i.e. groups 2, 3 & 4), may be caused by relatively small variations in the Al_2O_3 content of the melt.

This may reflect a move from mantle-hosted to crustal-hosted chromitite deposits. This would explain the changes in MgO and FeO values which would be caused by the bulk crystallization of olivine (which now forms cumulate dunite surrounding the chromitite pods), lowering the Mg# of the melt and the subsequent crystallizing chromite. However the changing Cr_2O_3 and Al_2O_3 behaviour is not predicted by this change, indeed precipitation of olivine from the melt would slightly raise the Al_2O_3 content of the melt and presumably that of the crystallizing chromite (Maurel and Maurel, 1982; Roeder and Reynolds, 1991; Kamenetsky *et al.*, 2001) (See also Figure 6.7B, Chapter 6). However, one change in physical parameters that occurs when crossing from mantle hosted to crustal hosted chromitites is a decrease in pressure. Decreasing the pressure would slightly raise the Cr# of crystallizing chromite (Roeder and Reynolds, 1991). This increase is only slight, being roughly <0.1 Cr# for a change in pressure of 10 kbars (Roeder and Reynolds, 1991). The change in pressure when transitioning from the mantle to the crust would not be this great, but may be sufficient to raise the Cr# of chromitite (at least initially) to offset the decrease expected from fractionation processes.

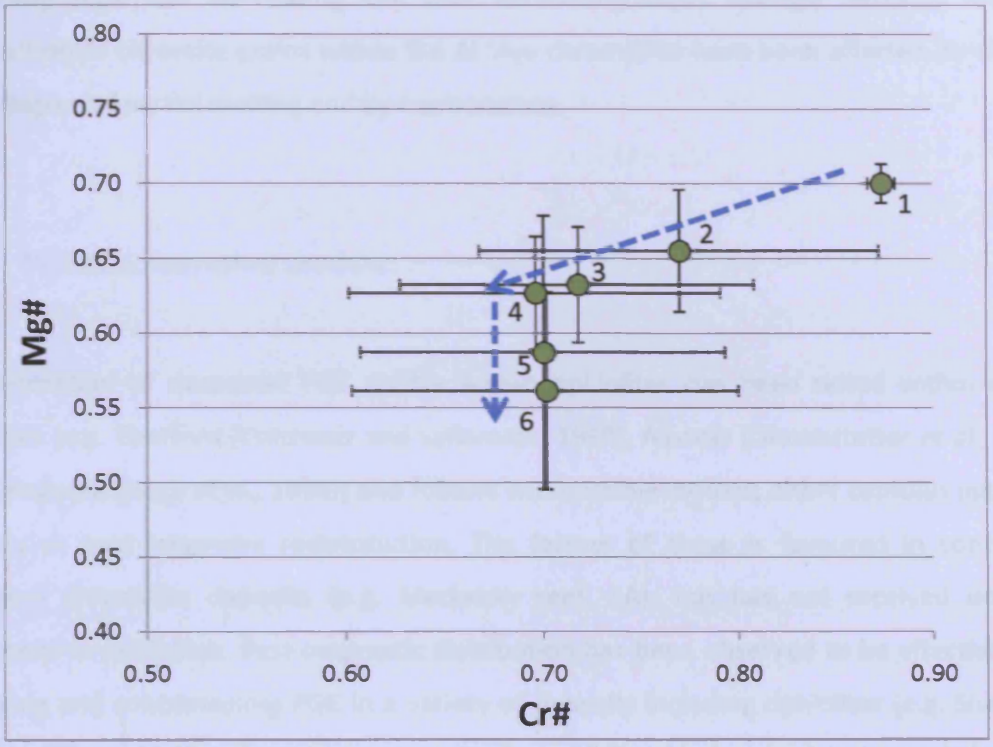

Figure 3.26: *Plot of Cr# - Mg# showing the average values for each stratigraphic group within Al 'Ays. The numbers beside the points refers to the corresponding stratigraphic group. The error bars represent plus and minus one standard deviation of the analysed values for that group (cf. Figure 3.16). The dashed blue lines mark the changing pattern of chromitite geochemistry with stratigraphic height (see text for details).*

Although, there is considerable compositional overlap between separate groups, which is reflected in the large error bars, the stepwise decrease in both Mg# and Cr# when moving from group 1 to group 4 is the cumulative product of fractionation (e.g. (Naldrett *et al.*, 2009)) and, to a lesser extent, melt/rock reaction (see Chapter 6). That this trend is observed within the Al 'Ays ophiolites is not that surprising as a reduction in both Cr# and Mg# is logically very similar to a reduction in Cr/ Fe^{2+} (Figure 3.15). The presence of this clear fractionation trend (Figure 3.26), together with the general gradual change in chromite geochemistry with proximity to the dunite/pyroxenite boundary (e.g. Cr/ Fe^{2+}, Fe_2O_3, Co, Zn) strongly suggests that the chromite is fractionating within the mantle of this ophiolite, with more fractionated chromitites being found closer to the dunite/pyroxenite boundary. That TiO_2 does not show the expected fractionation trend (Figure 3.17) most likely reflects the effect of melt-rock reaction on the TiO_2 content of the melt (see Chapter 6, Figure 6.10).

The presence of these two trends within the Al 'Ays chromitites (increasing Cr# with decreasing Mg# and decreasing Cr# with decreasing Mg#) strongly suggests that the composition of chromite grains within the Al 'Ays chromitites have been affected by changes in the degree of partial melting and by fractionation.

3.6.3 PGE concentration models

The generation of economic PGE grades within ophiolites has been noted within several ophiolites (e.g. Thetford (Corrivaux and Laflamme, 1990), Albania (Ohnenstetter *et al.*, 1999); New Caledonia (Auge *et al.*, 1998)) and follows two possible models; either cumulus magmatic sulphide or post-magmatic redistribution. The former of these is favoured in continental stratiform chromitite deposits (e.g. Merensky reef, SA), but has not received universal acceptance in ophiolites. Post-magmatic distribution has been observed to be effective in re-mobilising and concentrating PGE in a variety of deposits including ophiolites (e.g. Shetland), though within ophiolitic chromitite the scale of re-mobilisation is postulated to only be a few metres (Prichard *et al.*, 1994).

3.6.3.1 Cumulus magmatic sulphide

In order for cumulus PGE-rich magmatic sulphide to form it is necessary to extract a sulphide saturated (or near saturated) melt from the mantle during fractional partial melting. Once the sulphide component of the source region is exhausted any further melting is simply a dilution of S and PGE. Insufficient melting may leave PGE-rich sulphides in the source region. It is possible that critical batch melting may produce a PGE-rich melt which is close to sulphur saturation (Prichard *et al.*, 1996; O'Hara *et al.*, 2001; Prichard *et al.*, 2008).

In order for bulk sulphide liquid to separate from the ascending melt, sulphide saturation must occur within the melt. In a recent review of sulphide saturation within an ascending melt (Li and Ripley, 2005) recorded 3 factors that affect sulphur saturation in a silicate magma. These were; an increase in pressure, a fall in temperature and a change in magma composition (specifically a drop in Fe, or an increase in SiO_2, $Na_2O + K_2O$, or MgO) (O'Neill and Mavrogenes, 2002; Li *et al*, 2005; see Section 1.6.4).

In practice this means that in order to attain sulphur saturation the composition of the magma must change sufficiently to overcome the decrease in pressure that is increasing the sulphur solubility within the ascending melt. If chromite crystallization occurs through melt/ rock reaction then two changes in composition occur which may induce sulphur saturation, firstly there is an increase in SiO_2 due to dissolution of orthopyroxene and the precipitation of olivine (Figure 6.7A & 6.8A) and secondly the crystallization of chromite pulls Fe out of the melt. If the melt is 'chromite-fractionating' then the repetition of this process may eventually lead to sulphur saturation. Chromite crystallization may also produce a localized redox gradient facilitiating highly localized S-saturation and the precipitation of S-bearing PGM within chromite (Finnigan *et al.*, 2008).

The cumulus magmatic model is closely linked to magmatic differentiation and two predictions follow from it. Firstly, chromite geochemistry and PGE concentrations should be linked. Secondly, since chromite geochemistry is linked to stratigraphic height, so too should the timing of sulphide saturation and associated PGE concentrations. The first prediction concerns the proposed relationship between chromite geochemistry and PGE concentrations. If both chromite composition and the timing of sulphide saturation are controlled by fractionation processes during the ascent of melt through the mantle, then it is plausible that the geochemistry of the chromite grains may be linked to the timing of sulphide crystallization (and hence PGM concentration). Within Al 'Ays the PGE-rich chromitites have specific Cr/ Fe^{2+}, Co and Zn compositional ranges (Figure 3.21), which provides further support for the effect of fractionation on the chromite composition within the mantle sequence of an ophiolite.

It is interesting to note the very specific range occupied by PGE-rich chromitites on the Cr# - Mg# diagram, together with the distribution of the PGE-rich chromitite deposits (Figure 3.27). As PGE-rich chromitites contain a narrow range of Cr/Fe^{2+} values, the PGE-rich chromitites occur across a region with a reciprocal relationship between Cr# and Mg#. However, that this reciprocal relationship spans most of the Cr# range strongly suggests PGE-rich chromitites may be derived from a variety of batch melts, of varying partial melting degrees, rather than a single critical PGE-rich batch melt.

The spread of PGE ratios of the PGE-rich chromitites across the Cr# range suggests that high PGE ratios (i.e. PGE ratios > 4.00) are primarily located towards the low end of the Cr# range (Cr# < 0.7), whilst the low PGE ratio chromitites are located towards the high end of the Cr# range (Cr# > 0.7). The one clear exception to this is C51 which is a low PGE-ratio chromitite located towards the low end of the Cr# range (Figure 3.27).

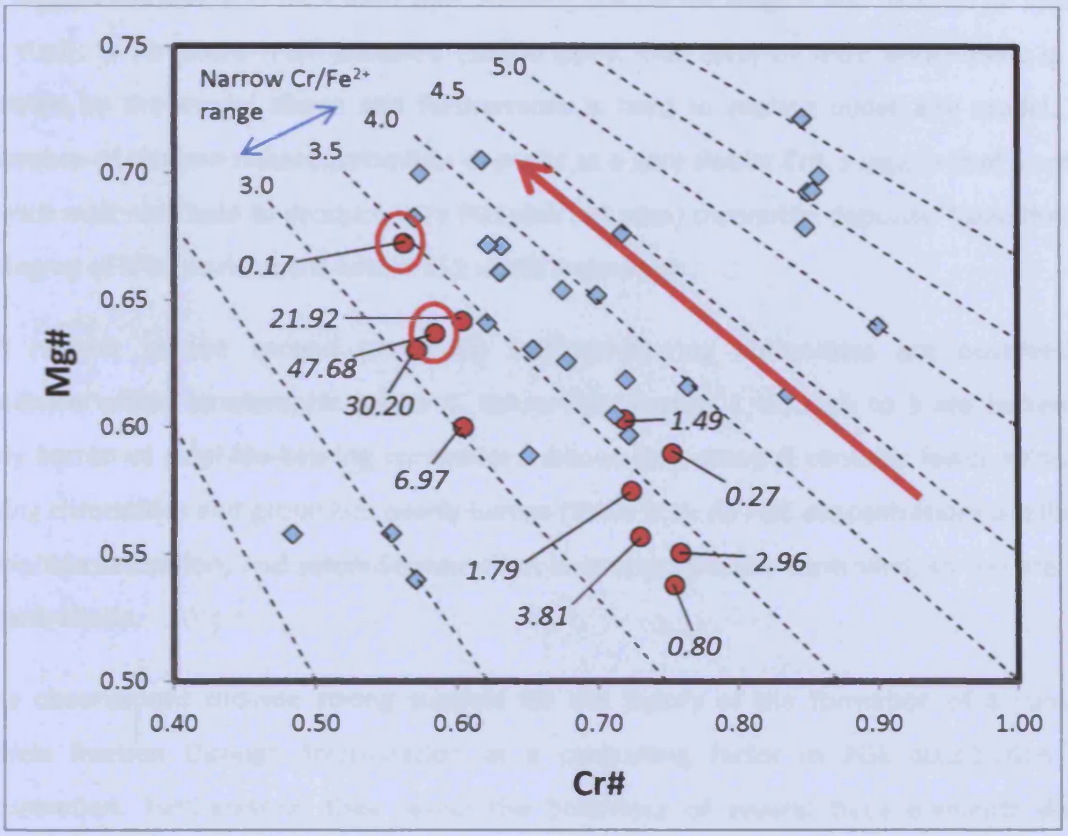

Figure 3.27: *Cr# vs. Mg# showing the PGE-rich chromitites (red circles) and the PGE-poor (blue diamonds) chromitites. The x-axis is plotted as $Cr/(Cr^{3+}+Al^{3+}+Fe^{3+})$ to facilitate the plotting of accurate isolines for Cr/Fe^{2+} values. Note that the PGE-rich chromitites occur within a specific Cr/Fe^{2+} range. The two richest chromitite deposits are circled on red. Also marked are the PGE-ratios ((Pt + Pd)/Ir) of the PGE-rich chromitites. The PGE ratio increases in the direction of the red arrow with one notable exception (samples C51).*

Using the Cr/Fe^{2+} ratio of the chromitites as a proxy for degree of fractionation it is clear that the different PGE ratios of the PGE-rich chromitites are occurring within a narrow Cr/Fe^{2+} range (i.e. are equally fractionated), suggesting that the differences in PGE concentration and ratio are not caused by fractionation. The Cr# range of the PGE-rich chromitites may therefore be used as a proxy for the degree of partial melting required to produce the chromitite in question. PGE-rich chromitites with high (Pt+Pd)/Ir are associated with low Cr# suggesting their association with lower degrees of partial melting producing PPGE-rich sulphide saturated parent magmas. On the other hand PGE-rich chromitites with low PGE-ratios are associated with high Cr# suggesting their association with higher degrees of partial melting producing IPGE-rich sulphide undersaturated parent magmas.

The one exception to this is C51, which although PPGE enriched (after C559 it contains the next highest amount of PPGE – 1907 ppb, showing the parent magma was likely to be sulphur saturated), is far more IPGE enriched (15300 ppb). This level of IPGE enrichment is not predicted by the model above and furthermore is hard to explain under any model. The occurrence of the two richest chromitite deposits at a very similar Cr#, suggests that a critical PGE-rich melt may help to produce very PGE-rich (>4 ppm) chromitite deposits. Nevertheless, the degree of IPGE enrichment within C51 is still anomalous.

With respect to the second prediction sulphide-bearing chromitites are observed in abundance within stratigraphic group 4. Below this, groups 1 through to 3 are barren, or nearly barren of sulphide-bearing chromitites. Above this, group 5 contains fewer sulphide-bearing chromitites and group 6 is nearly barren (Table 3.1). As PGE concentrations are linked to sulphide saturation, and sulphide saturation is stratigraphically controlled, so too are PGE concentrations.

These observations provide strong support for the theory of the formation of a cumulus sulphide fraction through fractionation as a controlling factor in PGE distribution and concentration. Furthermore, they reveal the behaviour of several trace elements during sulphide saturation within an ophiolite sequence. Mn remains predominantly constant throughout the stratigraphic range in this ophiolite indicating it is neither affected by chromite crystallization, nor by sulphide saturation. There is a slight rise in average Mn values following sulphide saturation in group 4, though this is only statistically significant between group 4 and group 6. Ti values are scattered showing no correlation with stratigraphic height, indicating either an independence from chromite fractionation and sulphide crystallization or a tendency for values to be changed through reaction with trapped liquid during solidification (e.g. Roeder and Campbell, 1985). A further possibility is the effect of melt/rock reaction on the TiO_2 content of the melt (see Chapter 6, Figure 6.12). Ni values show peaks in sulphide-bearing chromitites, but are otherwise fairly stable. This suggests that Ni may be equilibrating locally between chromite, sulphide and melt. In contrast V, Co and Zn all show fractionation trends, even after sulphide saturation, suggesting that all three were fractionating with chromite and were unaffected by sulphide crystallization.

3.6.3.2 PGE redistribution

An alternative model for PGE concentration focuses on the capability of post magmatic volatile fluids to remobilise PGE and potentially re-distribute them in locally higher concentrations. This has been shown to be prevalent within the Cliff chromitite in the Shetland ophiolite, where magmatic PGE grades of roughly 2-3 ppm total PGE have been re-mobilised into concentrations of roughly 60 ppm total PGE, though only on a scale of a few micrometres (e.g. Prichard *et al.* 1994).

The observations cited above fit very well with the cumulus magmatic sulphide model. However, there are two incongruous observations which need explaining. The first is that there are several sulphide-bearing chromitites which are not rich in PGE. This is readily explained by the nature of PGE extraction during sulphide saturation – namely that initial sulphide saturation will extract all the PGE from the melt, meaning any subsequent sulphide saturation events with be PGE-barren. Alternatively, the particular batch melt from the source region was not sufficient to extract the PGE and later sulphide saturation occurred in a melt that was effectively barren of PGE.

The second is that several of the PGE-rich chromitites do not contain high sulphide percentages (Table 3.1). This is especially true of the two richest chromitites, C559 and C51 (10 ppm and 17 ppm of PGE respectively). C559 contains a comparable amount of sulphides to several other chromitites but C51 is almost barren. Apart from these two chromitites the highest concentrations observed are ~3 ppm total PGE (C498).

Low sulphide, PGE-rich chromitites could be explained by the mobility of sulphur during alteration. Investigation of the sulphide and base-metal alloy inventory of the Al 'Ays chromitites reveal that C559 and C51 are unusual in containing abundant proportions of the mineral awaruite ($FeNi_3$), which is only present in very minor concentration elsewhere, if at all, within the ophiolitic chromitite. The formation of awaruite is intimately linked to serpentinising reactions involving highly reducing fluids (Eckstrand, 1975; Filippidis, 1985). Although awaruite has been found to contain PGE in other tectonic settings (Auge *et al.*, 1999) it is highly unlikely that the formation of awaruite was linked to the re-mobilisation of PGE into the chromitite deposit as one would need highly oxidised acid fluids for PGE re-mobilisation (e.g. Farrow and Watkinson, 1992) and serpentinising fluids are the exact converse of that.

Indeed analysis for the awaruite revealed no PGE concentrations above that of the gas-blank concentration (Iain Mcdonald, pers. comm.). It is possible that the formation of awaruite has stripped the chromitite deposit of PGE concentrations but since these two samples are the richest in terms of their PGE inventory (10 & 17 ppm), this would seem very unlikely. It thus appears probable that PGE redistribution did not play a part in the formation of the very PGE-rich chromitites within Al 'Ays.

3.7 Summary

The data set presented in this chapter provides evidence for the proposal of a petrogenetic model for the formation of chromitites with high PGE concentrations. Chromite composition is effected by two main processes, namely, varying the degree of partial melting of the source region and orthomagmatic fractionation processes (the effect of melt/rock reaction is discussed further in Chapter 6).

Several upwelling batch melts, with varying degrees of partial melting of the source region, ascend (at different times) through the upper mantle depositing chromite as early segregations from the magma. Within a single upwelling batch melt, initiation of chromite crystallization may occur through melt/ rock reaction (see Chapter 6 for full discussion). After chromite crystallization the melt continues to ascend through the upper mantle, possibly crystallizing more fractionated chromite higher up in the sequence, producing the observed fractionation of chromite composition with stratigraphic height. The repeated flux of batch melts through the same initial crystallization sites eventually crystallises enough chromite to produce a chromitite deposit. The variations in major and trace elements (Cr/ Fe^{2+}, Cr#, Fe_2O_3, Co and Zn) provide strong support for the fractionation of chromite within the mantle, as all show fractionation patterns with changes in stratigraphic height.

PGE-rich chromitites may be derived from melts with different partial melting percentages but require sulphur saturation to occur through the repeated addition of SiO_2 to, and removal of Fe from, the melt. This is achieved through melt/rock reaction and chromite crystallization and produces a stratigraphic control on the timing of sulphur saturation and PGE concentration. Very PGE-rich chromitite deposits occur if batch melting occurs at the critical stage of partial melting (Cr# ~ 0.60). This study has provided evidence that high-PGE concentrations may be linked to a particular chromite composition within an ophiolite.

Chapter 4

The Shetland Ophiolite, Shetlands

Implications for PGE concentration and chromite petrogenesis from chromitite pod heterogeneity

4 The Shetland Ophiolite

4.1 Chromitite samples

The Shetland ophiolite is located on the two most north-eastern islands of the Shetland islands (Unst and Fetlar). From bottom to top, the ophiolite consists of the mantle sequence, composed of harzburgite within which are dunite pods and dykes. This is overlain by crustal dunites, wehrlites, pyroxenites and gabbros. The uppermost units consist of the base of the sheeted dyke complex (Prichard, 1985). The mantle harzburgite and crustal dunites host numerous small podiform chromitite deposits, which have since been mined-out leaving spoil tips and empty quarry sites (Prichard and Neary, 1981, 1982), now mostly filled with water.

The first PGE to be discovered in Shetland were in a chromite concentrate taken from a crushing mill (Hitchen, 1929). Subsequently, IPGE-bearing PGM were located in chromitite samples (Prichard *et al.*, 1981) and Pt- and Pd-bearing PGM were later found to occur in a number of chromitite samples from the mantle and lower crustal sequence (Prichard *et al.*, 1986; Prichard and Tarkian, 1988). Prior to mining, two localities within the mantle sequence contained extremely anomalous concentrations of PGE with PPGE dominant at Cliff and IPGE enriched relative to PPGE at Harold's Grave (Prichard and Tarkian, 1988).

The distribution of the PGE in the Shetland ophiolite on Shetland has been studied extensively (Neary *et al.*, 1984; Leake and Gunn, 1985; Prichard and Tarkian, 1988; Lord *et al.*, 1994; Lord and Prichard, 1997). However, the distribution of PGE and variation of chromite composition within each chromitite pod has not been evaluated. Sampling was undertaken to determine the variation of chromite chemistry within a pod, if any, and to try to establish a link between IPGE and PPGE concentrations and chromite composition.

Within the mantle sequence, the two PGE-rich localities (Cliff and Harold's Grave) along with PGE-poor localities of Quoys, Nikkavord East and Nikkavord South were investigated (Figure 4.1). For the crustal sequence it seems likely that there may have been significant cross-contamination since during the mining phase the 'donkey trail' used to transport the chromitite ore to the crushing mill ran through this sequence (Figure 4.1). The 'donkey trail' ran to the mill site which was located next to the Hagdale chromitite deposit. Hagdale was the largest chromitite deposit on Shetland reaching up to 50 m in length. Keen of Hamar and Long Quarry spoil tips were both chosen as being relatively isolated from the 'donkey trail' and not likely to be contaminated with chromitites from another pod.

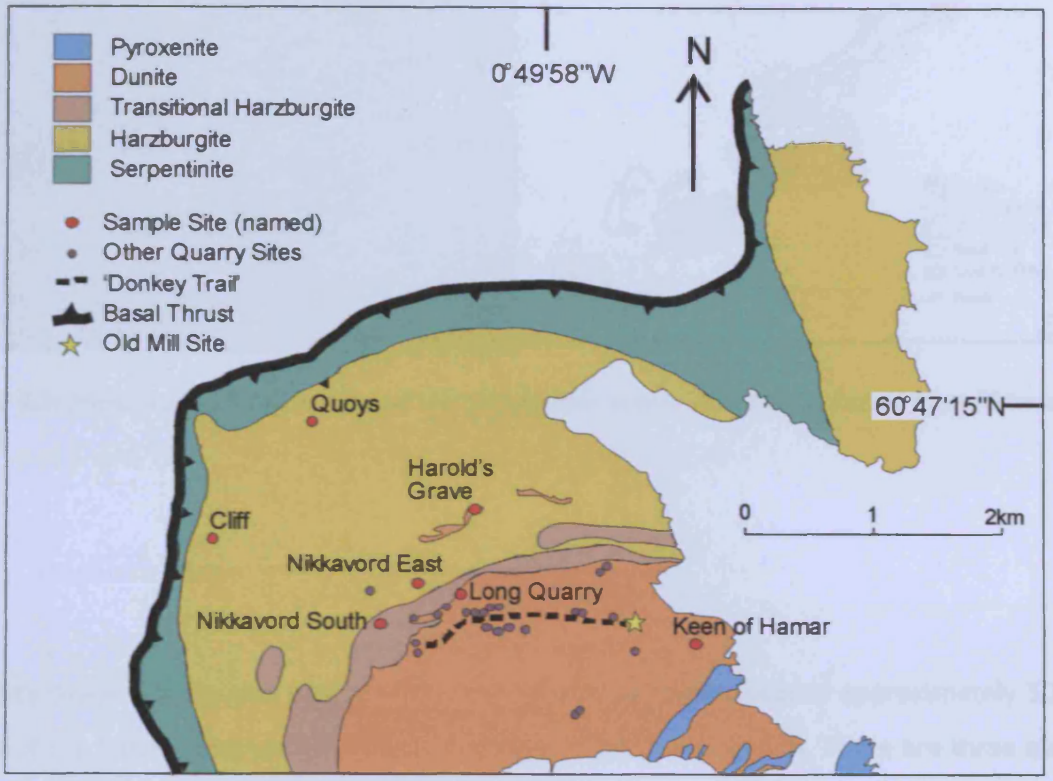

Figure 4.1: *The region of Baltasound, around the northern edge of the ophiolite outcrop, showing the studied chromitite pods (red), along with the old 'donkey trail' and other chromitite quarries (grey). Map adapted from (Gass et al. 1982; Lord, 1991).*

4.1.1 Cliff

The Cliff locality consists of a group of disused and excavated chromite quarries located just to the east of the basal thrust (Figure 4.1) within the mantle sequence. Analyses of chromitites from the spoil tips surrounding these disused quarries were found to contain high concentrations of PGE (Prichard and Tarkian, 1988). Five separate chromitite outcrops, arranged in an *en-echelon* pattern, are oriented in a NE-SW direction (Figure 4.2). Each pod is roughly 5-10 m long and encapsulated within a dunite envelope. The proximity to the basal thrust has resulted in significant fault disruption and hydrothermal infiltration probably causing the re-distribution of PGE into concentrated zones around the edges of the chromitite pods. This redistribution has likely caused the exceptionally high PGE concentrations observed at this locality (Prichard and Lord, 1993; Lord *et al.*, 1994).

Figure 4.2: *Photograph and plan view of the Cliff disused quarry site. Map adapted from (Gass et al. 1982).*

4.1.2 Harold's Grave

Harold's Grave is a disused quarry within the mantle sequence located approximately 500 m north of the harzburgite/crustal dunite boundary (Moho) (Figure 4.3). There are three quarry pools. Two are about 2 m long and the third is up to 20 m long. Analyses of chromitite taken from around these pools revealed unusually high concentrations of IPGE (Os, Ir & Ru) (Prichard *et al.*, 1986). The chromitite pod itself lies within an unusually large ENE trending dunite envelope, which is continuous over roughly 200m (Lord, 1991). There is no fault disruption of the chromitite pods, though the dunite envelope is truncated 40m to the east by a NNW trending vertical shear zone (Lord, 1991).

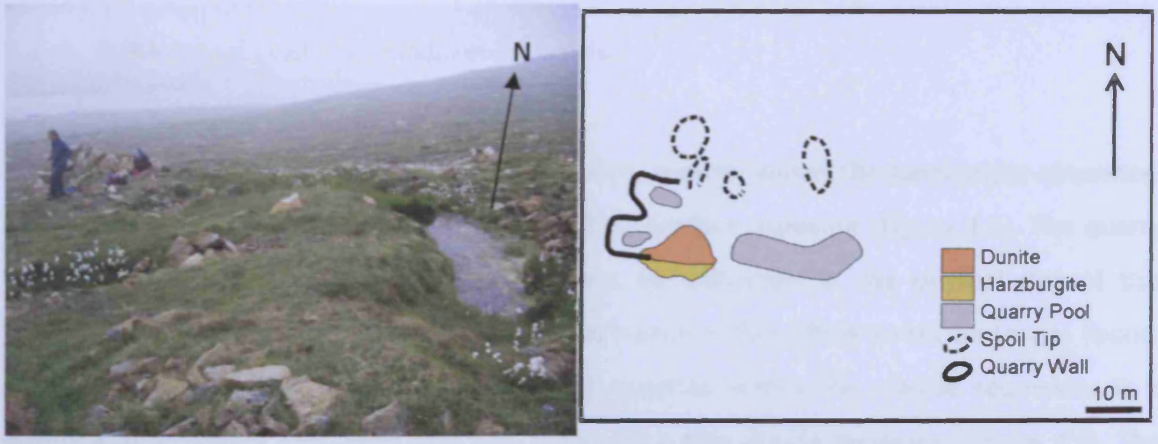

Figure 4.3: *Photograph and plan view of the Harold's Grave disused quarry site. Map adapted from (Gass et al. 1982)*

4.1.3 Quoys

Quoys is the northernmost chromite quarry and one of the largest (quarry pool = ~800m^2, Figure 4.4) after the Hagdale deposit (quarry pool = ~2500 m^2). Approximately 500 metres to the north-west of the Quoys quarry there is also a large disused talc quarry indicating fault disruption and hydrothermal transformation occurred locally. This transformation is likely to be related to the close proximity of the basal thrust which runs approximately 200m to the north-west of the Talc Quarry. Quoys chromitite pod is oriented in an ENE-WSW direction, and has either a very thin (~<1 m), fragmentary or non-existent dunite envelope.

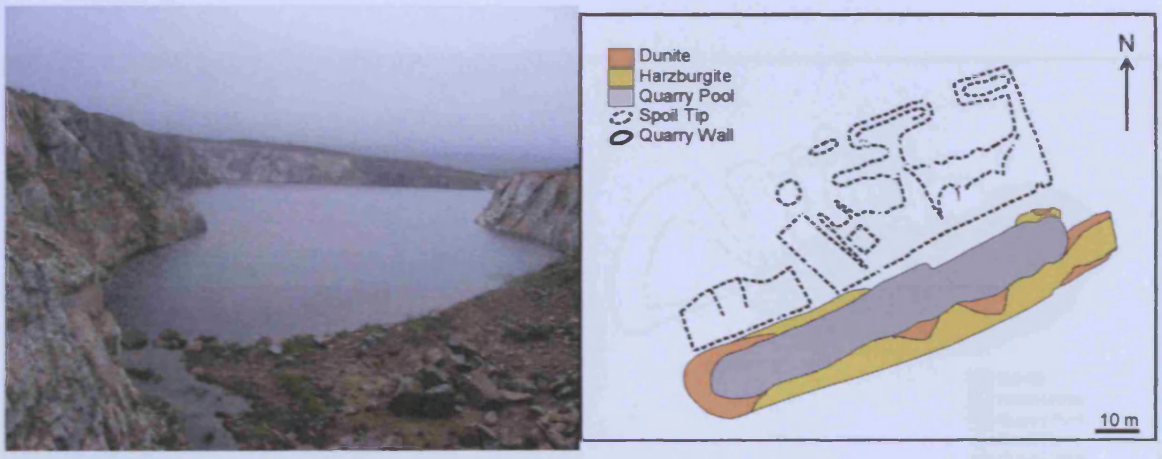

Figure 4.4: *Photograph of the talc quarry and plan overview of the Quoys chromite quarry. Map adapted from (Gass et al. 1982)*

4.1.4 Nikkavord East and Nikkavord South

Nikkavord East is a small disused chromitite quarry located within the harzburgite sequence. Aside from the quarry pool, there is no immediate surface exposure (Figure 4.5). The quarry pool is roughly 10 m in diameter, which gives an indication of the original size of this chromitite pod. There is also a small exploration trench within which no chromite was found. Nikkavord South is one of the larger disused quarries within the mantle sequence. It is elongate in a roughly east-west direction with only a thin dunite envelope (Figure 4.6). The present surface expression of the quarry consists of two separate pools, one approximately 20 m in diameter and one approximately 30 m in diameter.

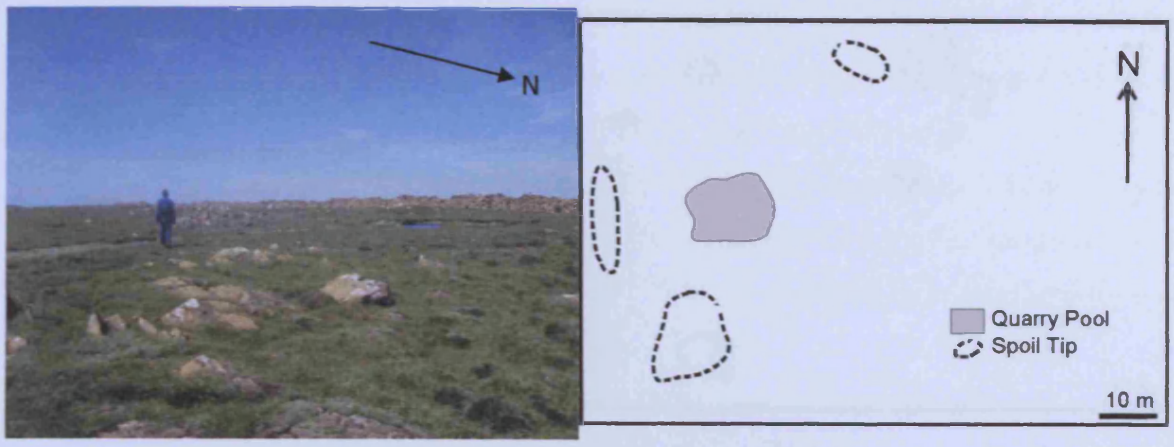

Figure 4.5: *Photograph and plan overview of the Nikkavord East quarry. Map adapted from (Gass et al. 1982).*

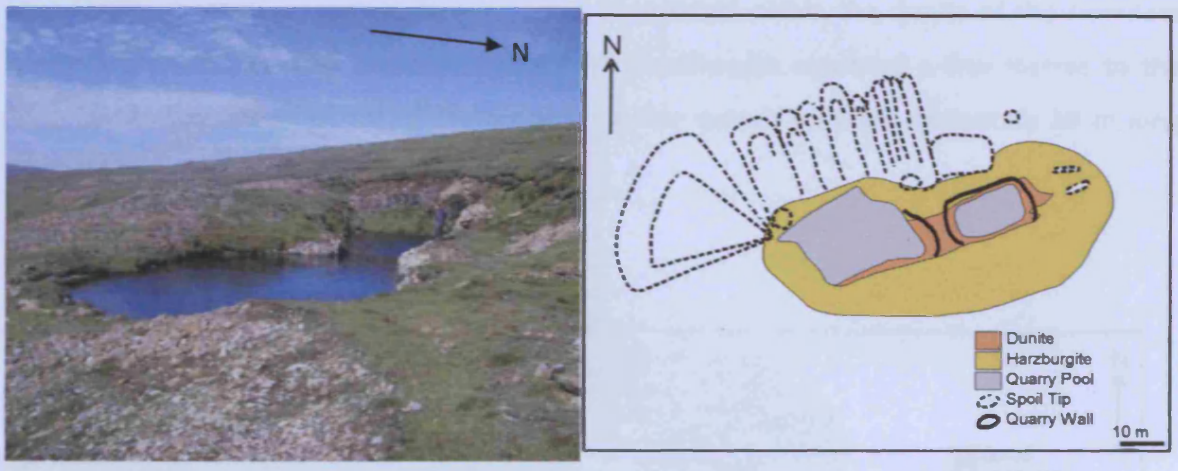

Figure 4.6: *Photograph and plan overview of the Nikkavord South quarry. Map adapted from (Gass et al. 1982).*

4.1.5 Keen of Hamar and Long Quarry

Keen of Hamar and Long Quarry are two chromitite outcrops which are found within the crustal sequence of the ophiolite (Figure 4.1). Keen of Hamar is located to the east of the original milling site, whilst Long quarry is located adjacent to the Moho, slightly north (~250 m) of the old 'donkey trail'. Keen of Hamar was a small deposit located exclusively within dunite. It is now represented by three separate pools, approximately 5 m in diameter with no discernible elongation (Figure 4.7).

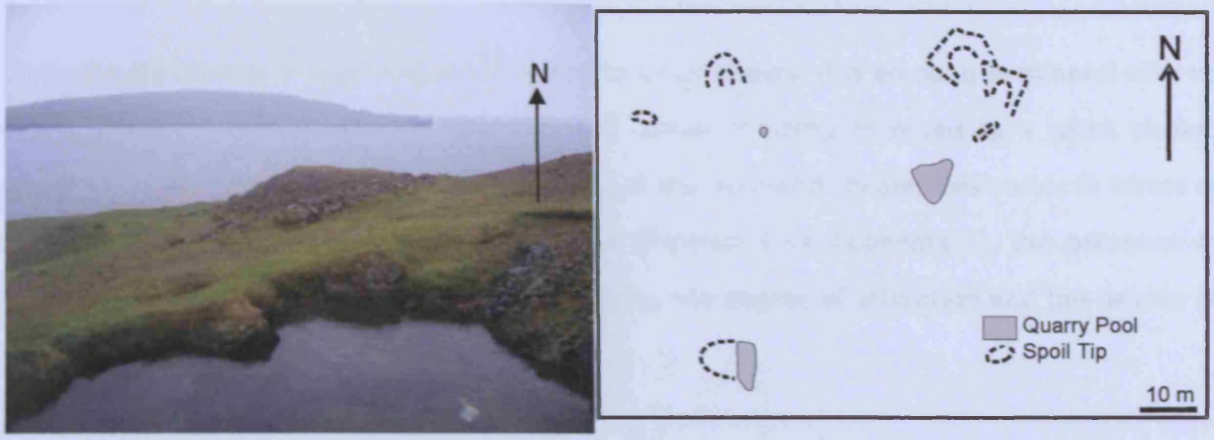

Figure 4.7: *Photograph and plan view of the Keen of Hamar deposit. Map adapted from (Gass et al. 1982).*

Long Quarry is located adjacent to the Moho. It's located within the dunite of the cumulate crustal sequence but with the extensive mantle harzburgite occurring a few metres to the north west. The pod is oriented east-west, with the quarry pool approximately 30 m long (Figure 4.8).

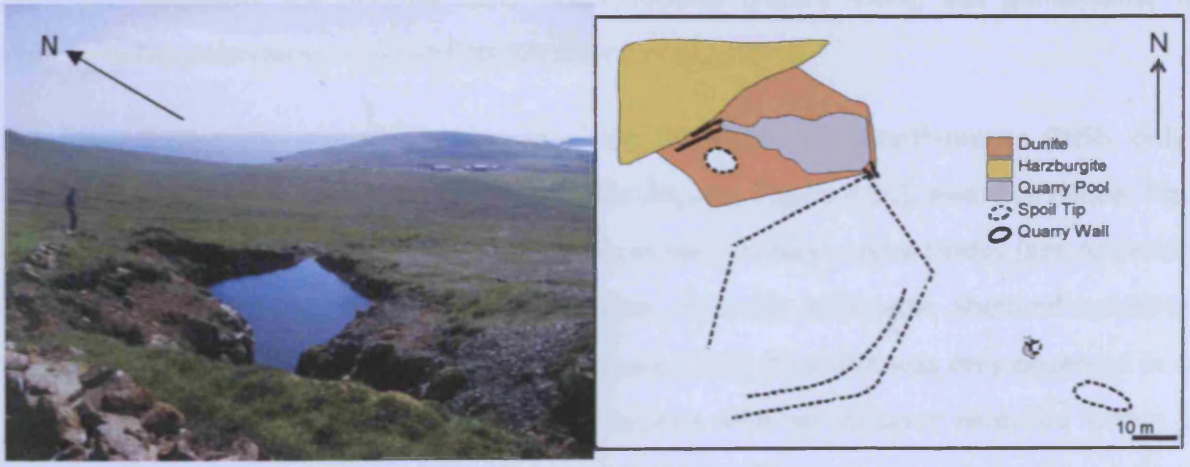

Figure 4.8: *Photograph and plan view of the Long Quarry deposit. Map adapted from (Gass et al. 1982).*

4.2 Chromitite Petrography

Chromite grains vary in size from a millimetre to a centimetre. It is an opaque mineral with no visible zonation, appearing as a dark ruby-red colour in plane-polarised light when viewed under an optical microscope. The petrography of the Shetland chromitites varies in terms of chromite grain size, the modal percentage of chromite (see Appendix 1), the presence of sulphides, the type and development of inclusions, the degree of alteration and the degree of fracturing.

4.2.1 Sulphide content of chromitite bodies

The sulphide content of the Shetland chromitites is generally low, but occasionally up to 1-2 wt% sulphide can be observed using a microscope (e.g. within samples from Cliff). Base-metal sulphides are found within chromitites throughout the mantle and crustal sequence, with large variability being observed both within, and between chromitite deposits. Although there is variability in sulphide content within a chromitite pod (Table 4.1), the chromitites at Cliff still contain the highest concentrations of those chromitites investigated during this study. The dominant sulphides are millerite and heazlewoodite (Figure 4.9A), but pentlandite, and chalcocite have also been observed (cf. (Prichard *et al.*, 1994)).

The other base-metal minerals observed within this study are, breithauptite (NiSb, only at Cliff), orcelite ($Ni_{5-x}As_2$; Figure 4.9B), maucherite ($Ni_{11}As_8$; Figure 4.9C), awaruite (Ni_3Fe: Figure 4.9D), and native base metal copper, as well as numerous base-metal oxides (see Appendix 7 for analyses). In contrast to the Al'Ays ophiolite, awaruite within the Shetland ophiolite is found in close association with pentlandite (Figure 4.9D). Awaruite was only observed in one sample (NB2b) from within the cumulate sequence with no instance recorded within the mantle chromitites, whether PGE-rich or PGE-poor. There is no relationship between chromitite sulphide content and the degree of alteration or inclusion content (Table 4.1A - C).

Table 4.1a: *Summary Table showing the variation of sulphide content, degree of alteration, and type of inclusion pattern observed within the PGE-rich chromitite deposits of the Shetland mantle sequence. 'Linear' inclusion patterns refer to linear inclusion trails through the chromite grains, whilst 'cluster' inclusion patters refer to the presence of occasional chromite grains with an unusual abundance of randomly oriented inclusions. For sulphide/ base-metal alloys (BMS) a 'moderate' content refers to ~1 wt%, 'minor' refers to <0.5 wt% and 'negligible' means sulphides were either unobserved, or only a few very small grains were seen. For alteration, 'pervasive' is >90% alteration, 'major' > 70-90% alteration, 'moderate' 30-70%, 'minor' 10-30%, and negligible is <10% alteration. Where present, the abundance of each inclusion pattern is 'moderate' unless otherwise stated. For the inclusion patterns, a 'major' content refers to the presence of inclusion patterns throughout >50% of the grains, 'moderate' - the presence of inclusion patterns in 20 – 50% of the slide, 'minor' - inclusion patterns within <10% of the slide and 'negligible' refers to the absence of definitive inclusion patterns.*

Sample #	Pod	Sulph./ BMA	Alteration	Inclusion Patterns
CF1	Cliff	Negligible	Moderate	Linear
CF10	Cliff	**Moderate**	Minor	Linear
CF11	Cliff	Negligible	Major	Linear (Minor)
CF12	Cliff	Minor	Moderate	Negligible
CF13	Cliff	Negligible	Major	Linear
CF14	Cliff	Negligible	Minor	Negligible
CF15	Cliff	**Moderate**	Major	Linear (Minor)
CF16	Cliff	Negligible	Minor	Negligible
CF17	Cliff	Negligible	Negligible	Negligible
CF18	Cliff	Negligible	Minor	Negligible
CF2	Cliff	**Moderate**	Moderate	Linear
CF3	Cliff	**Moderate**	Moderate	Linear
CF4	Cliff	Negligible	Moderate	Linear
CF5	Cliff	Minor	Moderate	Linear
CF6	Cliff	**Moderate**	Major	Negligible
CF8	Cliff	Minor	Major	Linear (Minor)
CF9	Cliff	**Moderate**	Minor	Linear
Q1 pod	H. Grave	Negligible	Minor	Negligible
Q2 pod	H. Grave	Negligible	Moderate	Negligible
Q3 pod 1	H. Grave	Negligible	Minor	Negligible
QX13 pod	H. Grave	Negligible	Moderate	Negligible
Q3PX pod	H. Grave	Minor	Major	*Inclusion rich*
HG11	H. Grave	Minor	Major	*Inclusion rich*
HG5	H. Grave	Negligible	Minor	Negligible
HG7	H. Grave	Minor	Major	Linear (Minor)
HG1	H. Grave	Minor	Moderate	Negligible
HG8	H. Grave	Minor	Moderate	Linear (Minor)
HG9	H. Grave	Negligible	Major	Linear (Minor)
HG4	H. Grave	Minor	Minor	Negligible
HG6	H. Grave	Minor	Minor	Linear (negligible)

Table 4.1b: *Summary Table of the variation of sulphide content, degree of ferritchromit alteration, and type of inclusion pattern observed within the PGE-poor chromitite deposits of the Shetland mantle sequence. Key is as for Table 4.1a.*

Sample #	Pod	Sulph./ BMA	Ferritchromit	Inclusion Patterns
QY1	Quoys	Minor	Major	Linear (Minor)
QY2	Quoys	Negligible	Moderate	Negligible
QY5	Quoys	Minor	Moderate	Linear (Minor)
QY6	Quoys	Negligible	Moderate	Linear (Minor)
QY8	Quoys	Negligible	Major	Negligible
QY9	Quoys	Negligible	Moderate	Negligible
QY10	Quoys	Minor	Minor	Linear (Minor)
NKE-1	Nkrd. East	Minor	Moderate	Negligible
NKE-2	Nkrd. East	Negligible	Moderate	Linear (Minor)
NKE-3	Nkrd. East	Negligible	Moderate	Linear (Minor)
NKE-4	Nkrd. East	**Moderate**	Major	Linear (Minor)
NKE-5	Nkrd. East	Negligible	Moderate	Linear
NKE-6	Nkrd. East	Negligible	Minor	Linear (Minor)
NKE-7	Nkrd. East	Negligible	Moderate	Negligible
NKS-1	Nkrd. South	**Moderate**	Minor	Linear
NKS-2	Nkrd. South	Negligible	Moderate	Negligible
NKS-3	Nkrd. South	Minor	Moderate	Linear
NKS-4	Nkrd. South	Minor	Moderate	Negligible
NKS-5	Nkrd. South	Negligible	**Pervasive**	Negligible
NKS-6	Nkrd. South	Minor	Major	Linear (Minor)

Table 4.1c: *Summary Table of the variation of sulphide content, degree of ferritchromit alteration, and type of inclusion pattern observed within the PGE-poor chromitite deposits of the Shetland crustal sequence. Key is as for Table 4.1a.*

Sample #	Pod	Sulph./ BMA	Ferritchromit	Inclusion Patterns
KH1	K. of Hamar	Negligible	Major	Negligible
KH2	K. of Hamar	Minor	Major	Negligible
RLM051	K. of Hamar	Minor	Minor	Linear
RLM053	K. of Hamar	Minor	Moderate	**Linear (Major)**
RLM058	K. of Hamar	Minor	**Pervasive**	Linear
LQ1	Long Quarry	**Moderate**	Moderate	Linear
LQ2	Long Quarry	**Moderate**	Minor	Linear
LQ3	Long Quarry	**Moderate**	Moderate	Negligible

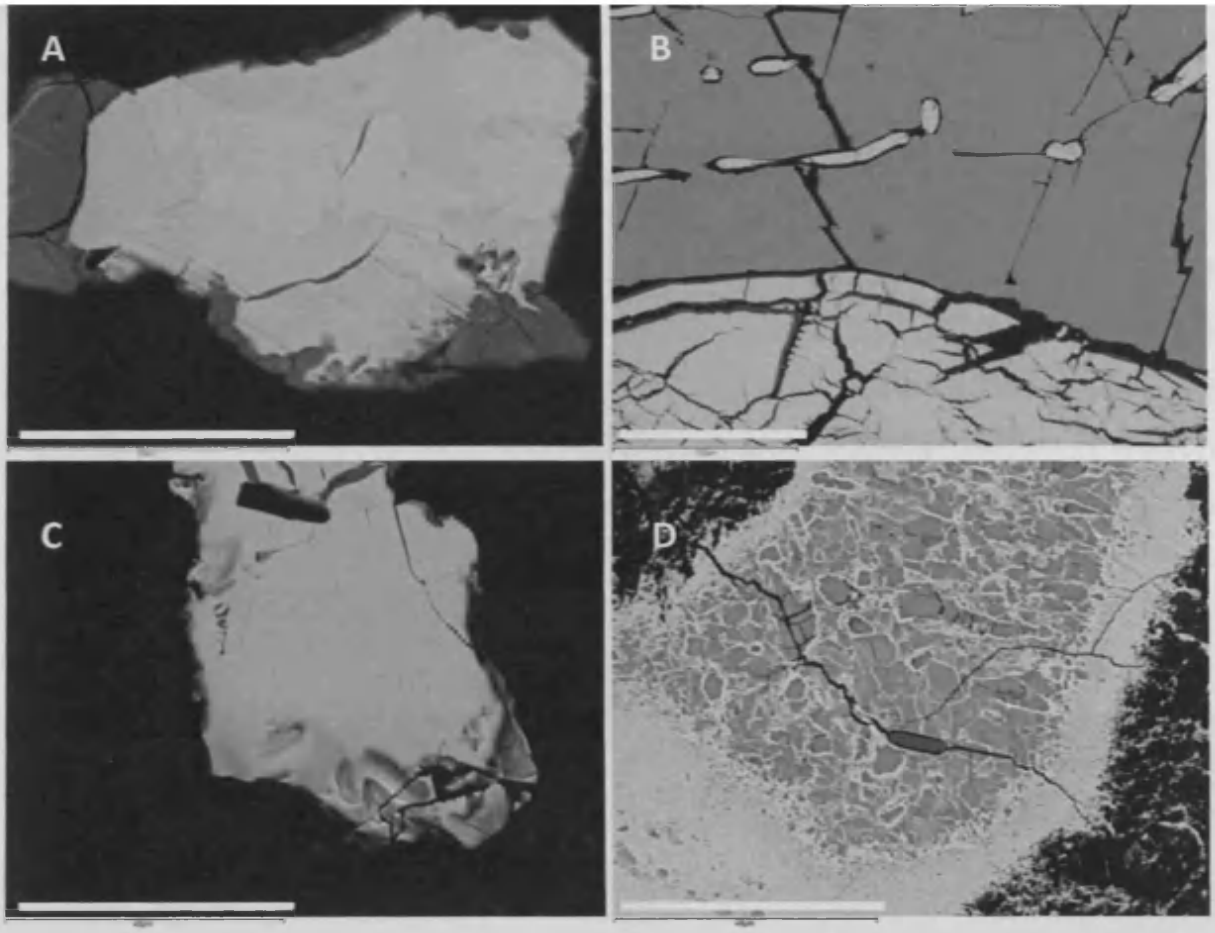

Figure 4.9: *Back scatter images of base-metal sulphides observed within Shetland chromitites. A: Millerite (lighter) and heazlewoodite (darker) in solid solution (sample LQ3), scale bar represents 50 μm. B: Orcelite (brighter) and heazlewoodite (darker) in close association (sample CF3), scale bar represents 100 μm. C: Maucherite grain (sample QY1), scale bar represents 40 μm. D: Pentlandite grain (darker), altering to awaruite (lighter) (sample NB2b), scale bar represents 40 μm.*

4.2.2 Inclusion patterns

Silicate inclusions in chromite grains within the chromitites are a common feature. Generally they are filled with low temperature silicates (e.g. chlorite) and randomly oriented with no particular clustering or spatial pattern (Figure 4.10A). Occasionally inclusions are arranged in patterns which themselves can be split into two sub-groups; clusters and linear trails. Inclusion clusters are located in the centre of a grain. A grain with an inclusion cluster is commonly juxtaposed with relatively inclusion free grains. Trails of linear inclusions cut through a chromite grain (Figure 4.10B) (Table 4.1). Grains containing either inclusion type in a thin section are anomalous in the sense that other chromite grains within the same slide don't contain similar inclusion patterns.

4.2.2.1 *Inclusion clusters*

There are a few chromitite samples which are unusually rich in inclusions (e.g. Q3PX and HG11). In these the majority of the chromite grains contain abundant inclusions (Figure 4.10A) but these are generally interconnected and merging into one another suggesting that they represent interstitial space between partially sintered grains or that the chromite grains have begun to partially dissolve during later magmatic processes. Inclusion clusters of the form observed within Al'Ays (see Section 3.3.2.1) have not been observed within the Shetland chromitites.

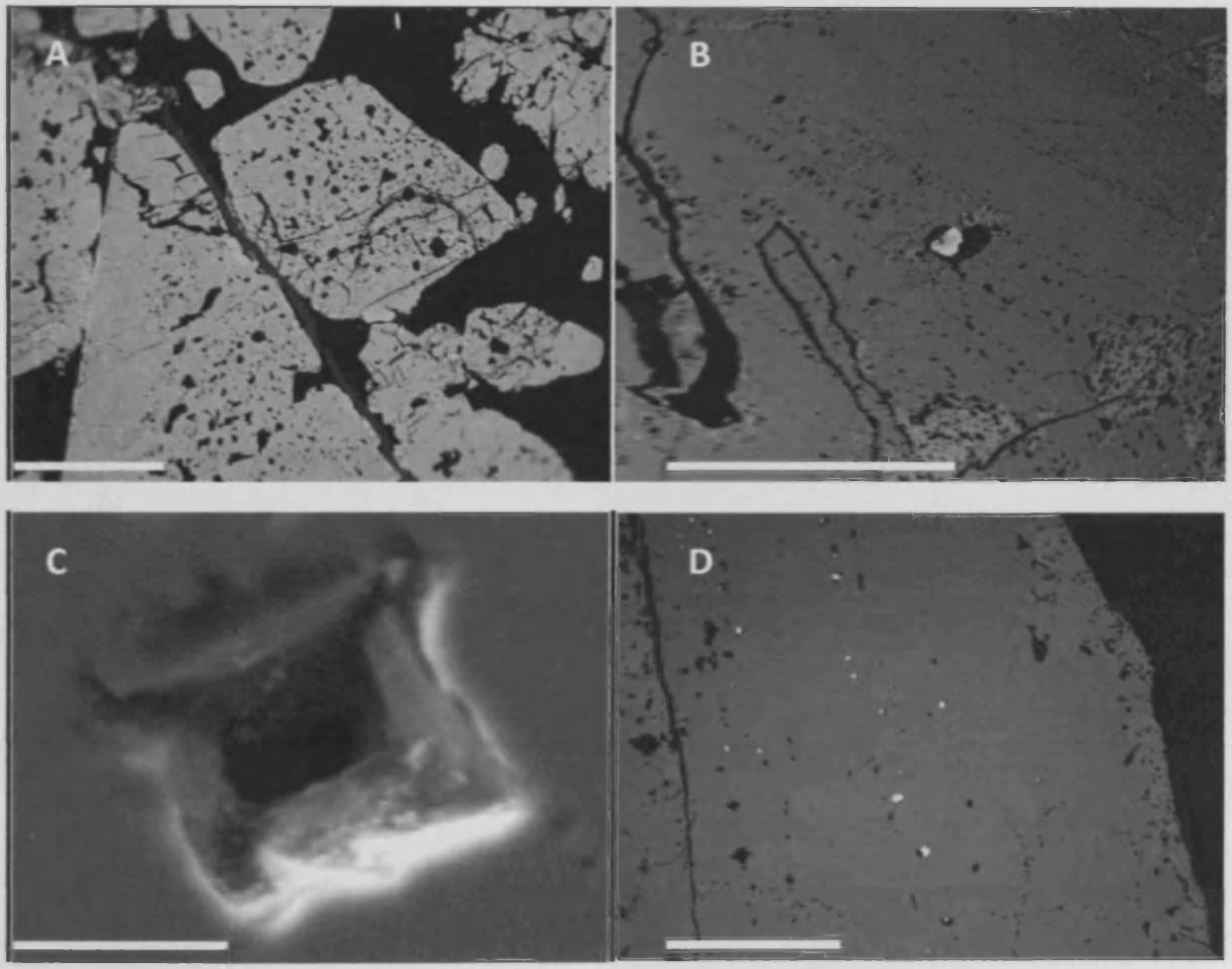

Figure 4.10: *Distribution of inclusions within the chromite grains, images A, B and D are reflected light images whilst image C is a back scatter image.* ***A:*** *Clustered inclusions within chromite grain, all filled with chromian chlorite (Q3PX). Scale bar represents 2 mm.* ***B:*** *Several parallel linear inclusion trails, all empty with poorly defined shapes and outlines. Scale bar represents 1 mm.* ***C:*** *An empty inclusion from within an empty linear inclusion trail (RLM053). Scale bar represents 10 μm.* ***D:*** *Several base-metal sulphide filled linear inclusions within a chromite grain (CF3). Scale bar represents 2 mm.*

4.2.2.2 Linear trails of inclusions

For the linear trails of inclusions, the inclusions are usually equidimensional but arranged along a linear trail. They are usually empty (Figure 4.10C) or occasionally filled with base metal sulphides (Figure 4.10D). Empty inclusion patterns occasionally show a well developed internal cubic structure (Figure 4.10C), but are often irregular in shape and outline. The predominance of empty inclusions may be due to plucking during the polishing procedure, although no remnants of a mineral fill have been observed. Alternatively they may have been filled with volatiles that subsequently escaped. Base metal sulphides included within the chromite grain may be iron, iron-nickel, copper or copper-iron bearing. In comparison to the Al'Ays ophiolite, sulphide-filled linear inclusion trails are far more prevalent but well formed cubic shaped empty inclusions are rarer in Shetland.

4.2.3 Ferritchromit alteration

In a similar manner to the Al'Ays chromitites, alteration within the Shetland chromitite samples can be considered uniformly pervasive for the interstitial silicates but highly variable for the chromite grains (Table 4.1; Figure 4.8). Interstitial silicates, which were probably olivine grains, are now predominantly serpentine, with occasional talc (or possibly brucite) veins and Cr-chlorite (usually as overgrowths around chromite grains). Cross-cutting quartz veins have been observed, and carbonate replacement of the interstitial silicates is occasionally pervasive.

Cr-magnetite and ferritchromit are common throughout the Shetland chromitites and their collective presence within a chromitite can range from negligible (e.g. Figure 4.11A) to pervasive (e.g. Figure 4.11B). The degree of chromite alteration varies both within a chromitite deposit (e.g. Cliff and Harold's Grave – Table 4.1), and between chromitite deposits. No obvious spatial pattern was observed to the chromite alteration between the analysed chromitite pods (Table 4.1). Even when the alteration of chromite is pervasive there are still analysable chromite cores from which geochemical data can be recorded.

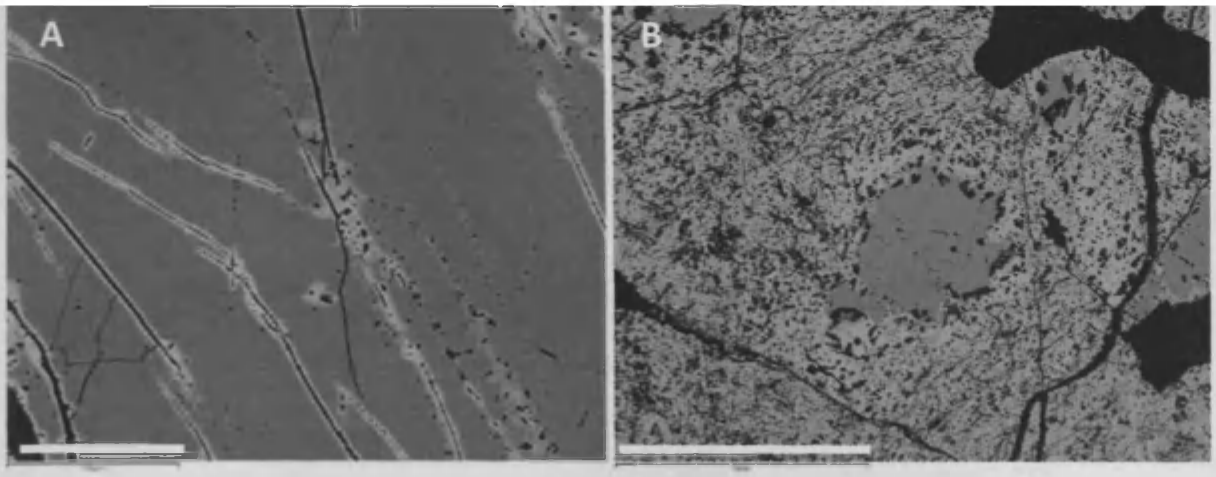

Figure 4.11: *Back scatter images of chromite alteration within the Shetland ophiolite.* ***A:*** *Minor chromite alteration associated with veins and cracks (sample CF4), scale bar represents 100 μm.* ***B:*** *Major to pervasive chromite alteration with a relatively fresh core in the centre of the FOV (sample RLM053). The alteration in RLM053 is likely to be a fine inter-leaving of Cr-magnetite and chlorite as the back scatter brightness varies from black (probably chlorite) to light grey (probably Cr-magnetite), scale bar represents 1 mm.*

4.2.4 Exsolution lamellae

An interesting feature of one of the Shetland chromitites is the presence of what appears to be exsolution lamellae within a few of the chromite grains (Figure 4.12). All the observed exsolution lamellae in the Shetland chromitites appear to contain Cr-chlorite, a low temperature alteration silicate. This is an uncommon feature of the Shetland chromitites, being observed only within one sample, and only a few grains within that sample. In contrast, it is prominent within the Berit chromitites so a full discussion of the textures, associated compositions, and possible mechanisms is reserved for the following chapter (see Section 5.2.2.2 and 5.6.2).

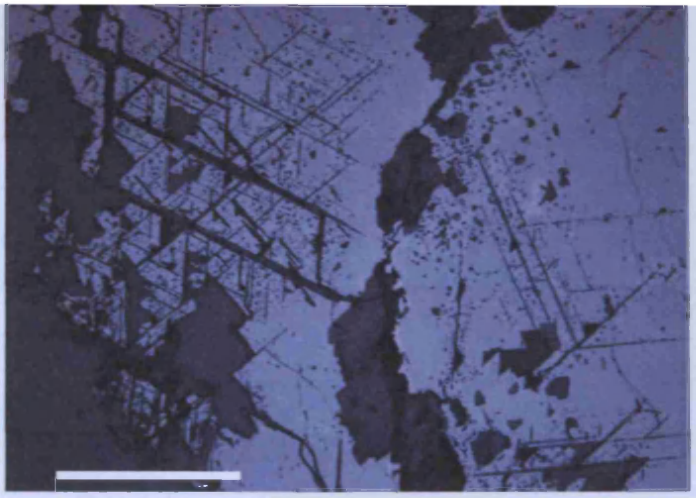

Figure 4.12: *Photomicrograph of exsolution lamellae within chromite grains (CF6). Scale bar represents 2 mm.*

4.2.5 Chromitite: brittle deformation

Internal micro-faulting within the Shetland chromitite deposits causes a similar variety of features to the Al'Ays ophiolite. Fracturing varies from minor pull-apart features through to mylonisation. Pull-apart features are common throughout all the chromitites (Figure 4.13A) but are particularly well developed in the more disseminated chromitites where the softer interstitial silicates appear to take the brunt of the deformation. Randomly oriented microfracturing (brecciation) is also common and displayed to varying degrees throughout all the chromitite deposits (e.g. Figure 4.13B). Occasionally, the chromitites display parallel microfaults or even 'hairline' mylonisation which is the localisation of intense deformation along thin zones through the chromitite. In contrast to the Al'Ays ophiolite there is much less mylonisation, or 'hairline' mylonisation present within these Shetland chromitites.

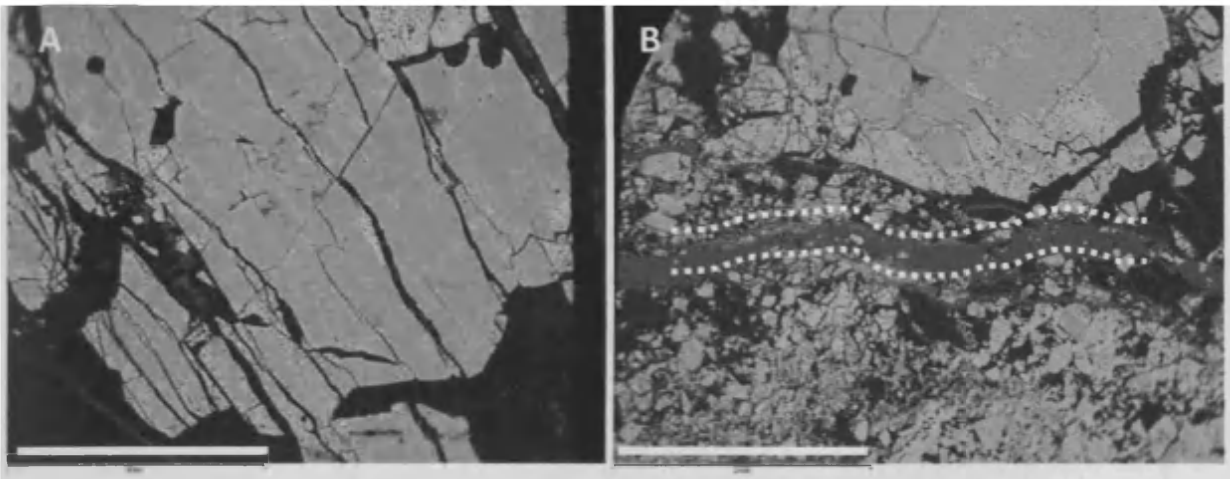

Figure 4.13: *Back Scatter Images of brittle deformation within the Shetland chromitites.* ***A:*** *Pull-apart features within chromite grains (sample CF2). Scale bar represents 3 mm.* ***B:*** *Brecciation increasing in intensity from the top to the bottom of the FOV (HG11). Scale bar represents 2 mm. The resultant brecciated vein is partially filled with calcite (between the dashed white lines).*

4.3 Silicate petrography

As well as looking at the podiform chromitite deposits, an investigation was undertaken into the surrounding dunite sheaths of Cliff, Quoys and Harold's Grave, as well as dunite samples from the cumulate sequence and harzburgite samples gathered from locations spread around the ophiolite (Figure 4.14). Silicate samples were sourced from collections housed in Cardiff University.

4.3.1 Samples

In total, 19 dunite samples were studied from the dunite sheaths surrounding Cliff, Harold's Grave and Quoys chromitite deposits in the mantle sequence, and from North of Baltasound, Long Quarry and Keen of Hamar chromitite deposits in the crustal sequence. Petrographically they are all very altered with most of the olivine replaced by serpentine, chlorite, and probably talc (Figure 4.15). Nevertheless there were 15 samples with analysable olivine and chromite grains. In total, 10 harzburgite samples were studied from various localities including Cliff, Quoys, Nikkavord South, Clibberswick North, Clibberswick South, Mid Fetlar, Vord Hill Fetlar, South of Crussa Field and Taing NU (Figure 4.14). Of the 10 samples only 6 contained analysable olivine and chromite.

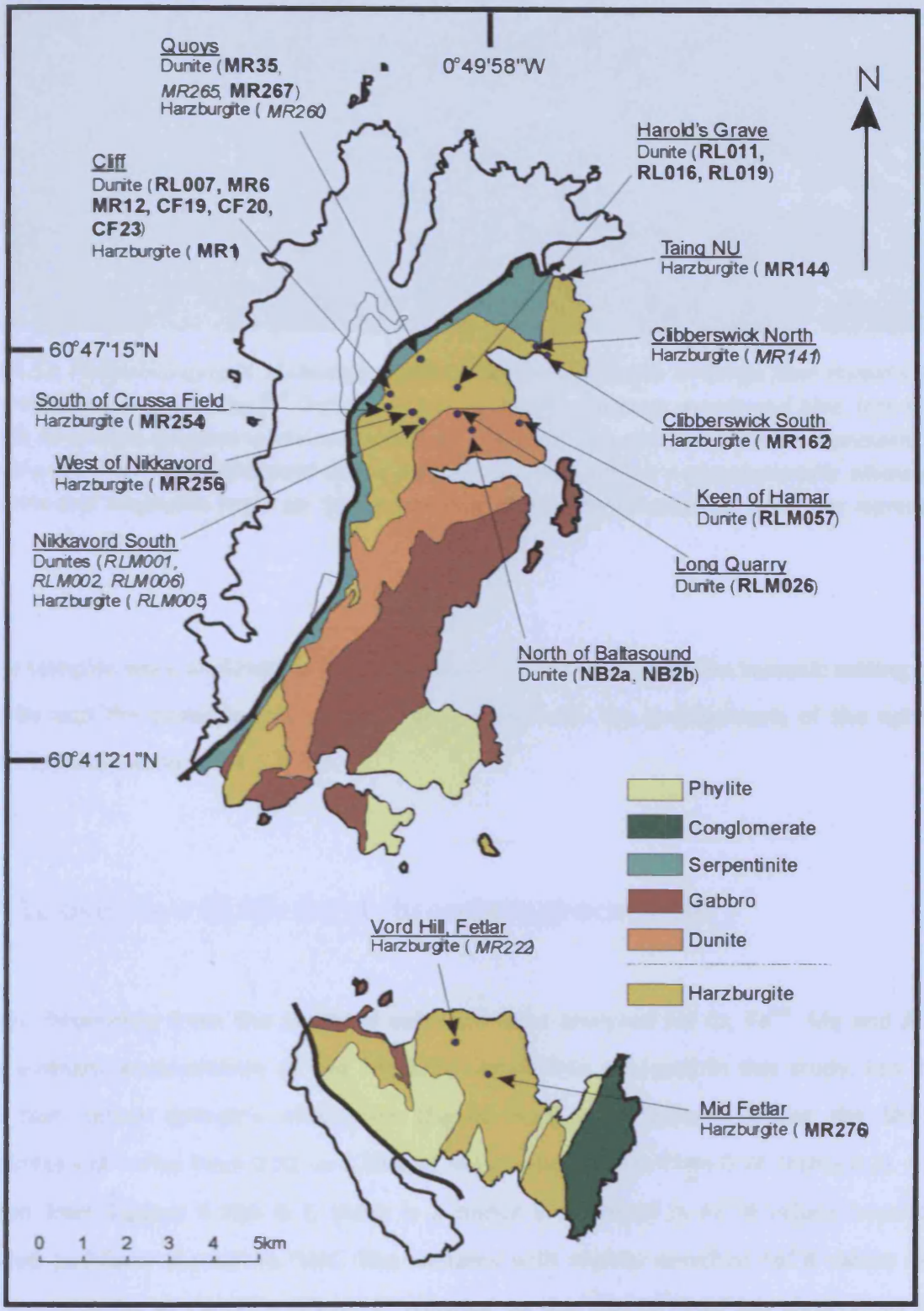

Figure 4.14: *Geological map of the Shetland ophiolite as it outcrops over the islands of Unst and Fetlar (BGS, 2002), showing the main dunite and harzburgite samples which were analysed. The localities are underlined with the sample numbers detailed within the brackets. Emboldened samples contained analysable chromite and olivine, whilst italicized samples contained no analysable chromite and olivine.*

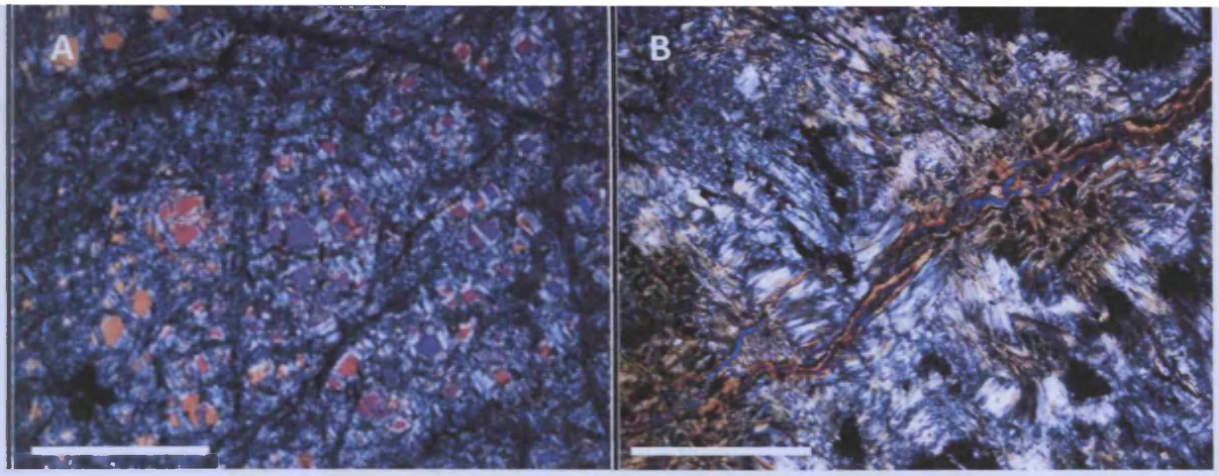

Figure 4.15: *Photomicrographs of silicates within the Shetland ophiolite. A: Dunite from Harold's Grave. Unaltered olivine is displaying 2nd Order interference colours in orange, purple and blue. Interspersed between these olivine fragments the mineralogy is predominantly serpentine. Scale bar represents 2 mm B: Harzburgite from near Nikkavord with a probable talc vein cutting a pseudomorphic olivine grain. Serpentine and magnetite make up the remainder of the interstitial minerals. Scale bar represents 2 mm.*

Silicate samples were analysed to provide additional information on the tectonic setting of the ophiolite and the possible role of melt-rock reaction on the petrogenesis of the ophiolitic chromitite (see Sections 4.4.5 & 4.4.6).

4.4 An overview of Shetland chromitite geochemistry

Fifty six chromitites from the Shetland ophiolite were analysed for Cr, Fe^{tot}, Mg and Al. The major element geochemistry of the Shetland chromitites analysed in this study, lies in the fields that define ophiolitic chromitite (Figure 4.16 A-D; Table 4.2). For the Shetland chromitites Cr# varies from 0.52 to 0.78 and Mg# varies from 0.47 to 0.74 (Table 4.2). As can be seen from Figures 4.16A & C there is a minor enrichment in Fe^{2+}# values beyond the expected podiform chromitite field. The samples with slightly enriched Fe^{2+}# values are all from the spoil tip at Harold's Grave. In contrast to this the Fe^{3+}# of the chromitites all lie within the lower half of the ophiolite field (Figure 4.16B).

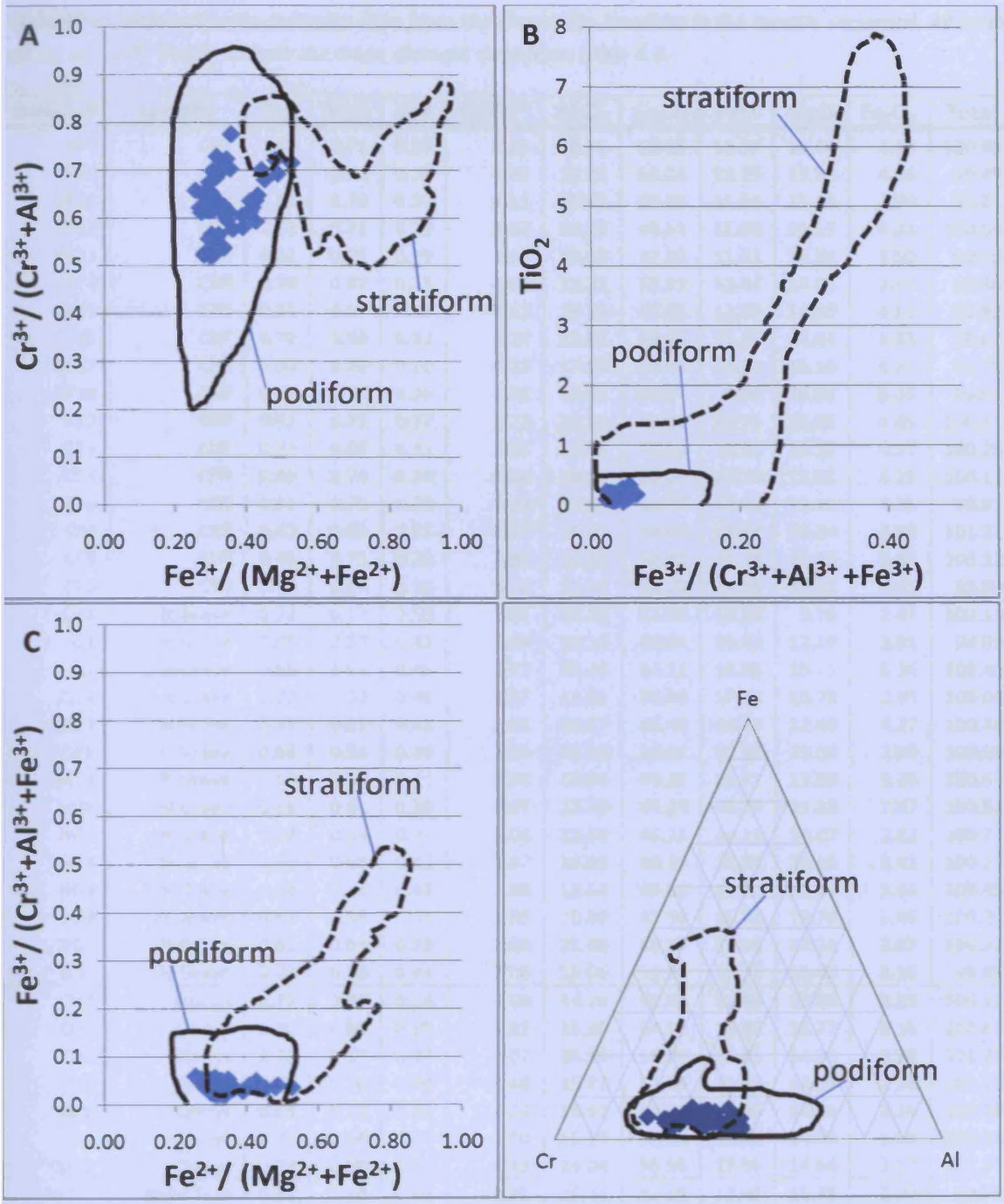

Figure 4.16: *Discrimination diagrams for ophiolitic versus stratiform chromitites (After Roeder and Barnes, 2001). The defined fields represent 90% of their analysed chromite compositions. Chromitites from Shetland are plotted on 4 major elements plots and clearly fall in the ophiolite fields. A: Cr# vs. Fe^{2+}#. B: TiO_2 vs. Fe^{3+}#, C: Fe^{3+}# vs. Fe^{2+}#, D: Ternary plot of Cr^{3+}-Al^{3+}-Fe^{3+}.*

Table 4.2a: *Major element chromite data from the chromitite localities in the mantle sequence. All oxide values are wt%. Totals include the trace element data from table 4.3.*

Sample#	Locality	Cr#	Mg#	Fe#	Cr/Fe^{2+}	Al_2O_3	Cr_2O_3	FeO	MgO	Fe_2O_3	Total
CF1	Cliff	0.65	0.71	0.29	4.25	18.11	51.13	11.37	15.44	4.10	100.83
CF10	Cliff	0.65	0.72	0.28	4.42	18.22	50.28	10.75	15.54	4.06	99.45
CF11	Cliff	0.63	0.70	0.30	4.11	19.47	50.26	11.56	15.18	2.70	99.81
CF12	Cliff	0.62	0.71	0.29	3.97	20.22	48.31	11.50	15.53	4.34	100.54
CF13	Cliff	0.62	0.71	0.29	3.98	19.69	47.99	11.41	15.31	4.50	99.55
CF14	Cliff	0.70	0.67	0.33	4.06	15.21	53.39	12.44	14.08	3.63	99.36
CF15	Cliff	0.63	0.67	0.33	3.62	19.15	48.63	12.68	14.50	4.31	99.92
CF16	Cliff	0.70	0.68	0.32	4.20	15.85	53.96	12.15	14.44	2.63	99.61
CF17	Cliff	0.65	0.70	0.30	4.13	17.84	50.38	11.52	15.10	4.26	99.75
CF18	Cliff	0.66	0.74	0.26	4.81	17.53	50.37	9.90	16.06	5.06	99.62
CF2	Cliff	0.61	0.73	0.27	4.22	20.36	48.00	10.76	16.03	4.66	100.42
CF3	Cliff	0.62	0.69	0.31	3.81	19.96	48.01	11.91	15.15	4.57	100.29
CF4	Cliff	0.65	0.70	0.30	4.04	18.18	50.24	11.76	15.05	4.21	100.11
CF5	Cliff	0.66	0.71	0.29	4.36	17.68	50.75	11.00	15.46	4.35	99.91
CF6	Cliff	0.62	0.65	0.35	3.36	20.09	48.00	13.51	14.24	4.58	101.21
CF8	Cliff	0.65	0.71	0.29	4.32	18.10	50.91	11.14	15.46	3.84	100.12
CF9	Cliff	0.78	0.64	0.36	4.18	11.26	58.20	13.15	13.32	3.41	99.99
Q3a	H.Grave	0.72	0.47	0.53	2.61	14.22	53.60	19.24	9.76	2.47	100.19
Q1	H.Grave	0.65	0.57	0.43	2.89	18.10	49.91	16.32	12.10	2.81	99.99
Q2	H.Grave	0.69	0.51	0.49	2.72	15.46	52.11	18.09	10.71	3.26	100.45
Q3b	H.Grave	0.72	0.52	0.48	2.87	13.91	53.86	17.73	10.78	2.95	100.06
QX13	H.Grave	0.59	0.57	0.43	2.61	20.87	45.46	16.47	12.46	4.27	100.48
Q3PX	H.Grave	0.68	0.55	0.45	2.90	16.30	52.01	16.97	11.59	2.86	100.50
HG11	H.Grave	0.64	0.59	0.41	2.96	18.84	49.25	15.71	12.69	3.20	100.54
HG5	H.Grave	0.58	0.61	0.39	2.87	22.38	46.24	15.24	13.38	2.47	100.52
HG7	H.Grave	0.58	0.64	0.36	3.08	22.68	46.21	14.19	14.07	2.82	100.71
HG1	H.Grave	0.62	0.58	0.42	2.87	19.53	48.15	15.86	12.46	3.41	100.22
HG8	H.Grave	0.64	0.57	0.43	2.86	18.64	49.09	16.23	12.29	3.41	100.45
HG9	H.Grave	0.61	0.59	0.41	2.85	20.00	47.39	15.71	12.78	3.46	100.20
HG4	H.Grave	0.61	0.61	0.39	3.03	21.00	48.17	15.05	13.28	2.67	100.92
HG6	H.Grave	0.70	0.56	0.44	3.06	15.06	52.92	16.33	11.62	3.16	99.85
QY1	Quoys	0.72	0.66	0.34	4.08	14.29	55.91	12.95	13.88	2.53	100.14
QY2	Quoys	0.70	0.65	0.35	3.82	15.35	54.31	13.43	13.77	3.16	100.67
QY5	Quoys	0.70	0.67	0.33	4.07	15.59	55.09	12.81	14.30	2.90	101.29
QY6	Quoys	0.70	0.70	0.30	4.48	15.87	55.06	11.61	14.94	2.18	100.21
QY8	Quoys	0.69	0.69	0.31	4.24	16.62	54.12	12.05	14.74	2.36	100.43
QY9	Quoys	0.71	0.66	0.34	4.10	15.14	55.68	12.83	14.03	1.99	100.18
QY10	Quoys	0.73	0.68	0.32	4.43	14.04	56.56	12.06	14.64	3.17	101.10
NKE-1	Nkvd East	0.52	0.70	0.30	3.35	26.44	42.65	12.02	15.71	2.20	99.75
NKE-2	Nkvd East	0.53	0.70	0.30	3.41	25.08	42.79	11.88	15.49	3.39	99.29
NKE-3	Nkvd East	0.53	0.69	0.31	3.26	25.76	42.56	12.33	15.42	3.25	100.00
NKE-4	Nkvd East	0.57	0.68	0.32	3.41	23.67	46.04	12.78	15.12	2.48	100.80
NKE-5	Nkvd East	0.52	0.70	0.30	3.36	26.45	42.81	12.05	15.83	2.77	100.63
NKE-6	Nkvd East	0.53	0.72	0.28	3.55	25.58	42.58	11.34	16.04	3.66	99.90
NKE-7	Nkvd East	0.52	0.72	0.28	3.56	26.02	42.52	11.28	16.21	3.39	100.17
NKS-1	Nkvd South	0.57	0.70	0.30	3.65	23.51	45.85	11.89	15.38	2.37	99.70
NKS-2	Nkvd South	0.55	0.69	0.31	3.45	24.71	44.77	12.28	15.44	2.46	100.39
NKS-3	Nkvd South	0.56	0.71	0.29	3.67	24.22	45.50	11.73	15.75	2.77	100.63
NKS-4	Nkvd South	0.61	0.67	0.33	3.59	20.59	48.59	12.78	14.46	2.40	99.48
NKS-5	Nkvd South	0.56	0.68	0.32	3.48	24.45	46.19	12.55	15.31	1.66	100.78
NKS-6	Nkvd South	0.60	0.65	0.35	3.34	21.52	47.51	13.45	14.23	2.49	99.82

Table 4.2b: *Major element chromite data from the chromitite localities in the crustal sequence.*

Sample#	Locality	Cr#	Mg#	Fe#	Cr/Fe^{2+}	Al_2O_3	Cr_2O_3	FeO	MgO	Fe_2O_3	Total
KH1	K. Hamar	0.56	0.69	0.31	3.35	23.10	43.43	12.26	15.11	4.85	99.44
KH2	K. Hamar	0.56	0.69	0.31	3.40	23.26	43.54	12.12	15.27	4.86	99.74
RLM053	K. Hamar	0.62	0.66	0.34	3.59	20.10	49.90	13.15	14.45	2.30	100.61
RLM058	K. Hamar	0.54	0.66	0.34	3.12	25.28	43.92	13.30	14.73	1.64	99.65
LQ1	L. Quarry	0.62	0.73	0.27	4.39	19.71	48.40	10.42	15.92	4.25	99.37
LQ2	L. Quarry	0.68	0.70	0.30	4.35	16.83	52.38	11.37	15.25	4.06	100.63
LQ3	L. Quarry	0.63	0.72	0.28	4.26	19.67	49.88	11.08	15.83	3.94	101.10

For the trace element analyses of chromitites from Shetland the total variations are as follows: TiO_2 0.05 - 0.34 wt%, V_2O_5 0.09 - 0.25 wt%, MnO 0.20 - 0.35 wt%, NiO 0.07 - 0.22 wt%, Co 174 - 295 ppm, Zn 157 - 441 ppm and Ga 20 to 53 ppm.

4.4.1 Major element variation *within* chromitite pods

Most of the chromitite pods show internal variations when plotted on a Cr# - Mg# diagram, yet there are still distinctive geochemical signatures for different pods (Figure 4.17A). Harold's Grave shows the largest variation in Cr# (0.58-0.72) and Mg# (0.47-0.64). The two ratios are inversely correlated with Cr# increasing as Mg# decreases. Cliff shows a similarly large range of Cr# values (0.61 – 0.78) with higher Mg# values (0.64 – 0.74). Despite the similar range of Cr# values to Harold's Grave, most of these are grouped towards the lower end of the Cr# with only three values over 0.67. Within the remaining chromitite deposits there is not much clear or significant covariation within the Cr# and Mg# values

Collectively the chromitite pods show a slight inverse relationship between TiO_2 and Cr# with TiO_2 values increasing as Cr# decreases (Figure 4.17B). Within the individual chromitite pods this relationship is more prevalent in Cliff, Harold's Grave and Keen of Hamar, less prevalent in Quoys, Nikkavord East and Nikkavord South and reversed as in Long Quarry which shows a positive covariation (Figure 4.16B). However, there are only three analyses within Long Quarry so this positive co-variation is not significant. Harold's Grave contains the highest TiO_2 values ranging from 0.14 to 0.34, whilst the remaining six chromitite pods contain lower TiO_2 values, ranging between 0.07 and 0.23.

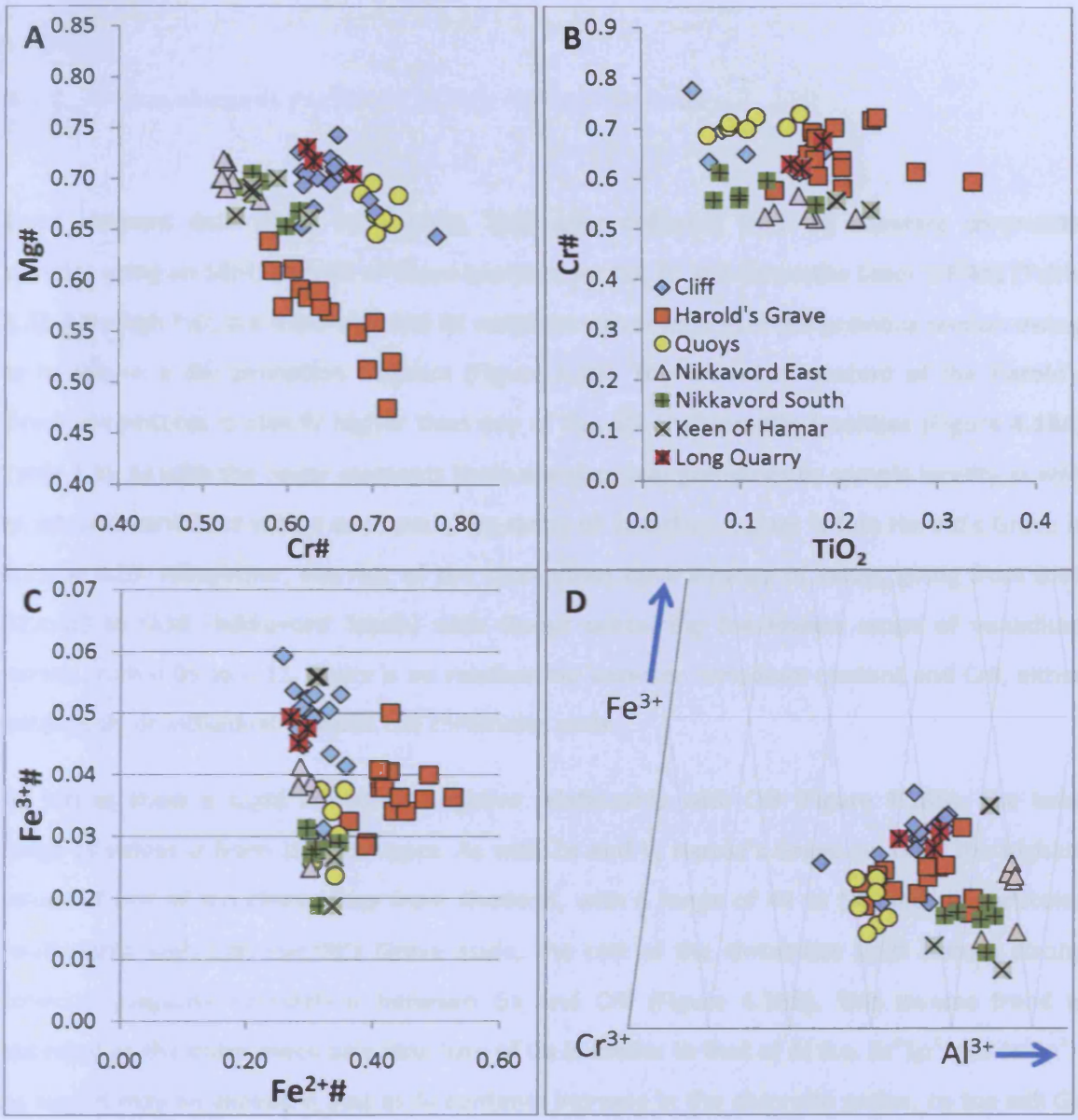

Figure 4.17: *Four graphs with major element plots for the chromitites of Shetland. Note that the axes scale has been altered from Figure 4.16 to best show the variation between chromitite pods. Figure 4.17A is expressed as Cr# - Mg# to facilitate comparisons with other published literature. A: Cr# vs. Mg#, B: Cr# vs. TiO_2, C: Fe^{3+}# vs. Fe^{2+}#, D: Ternary plot of Cr^{3+}, Al^{3+} and Fe^{3+} focussed on the lower left quadrant. Each tick represent a change in content of 10%. The legend within Figure 4.17B applies to Figures 4.17A, 4.17C and 4.17D.*

Most of the chromitite pods show large variations on a Fe^{3+}# - Fe^{2+}# diagram, but yet remain distinctive from each other (Figure 4.17C). As observed, Harold's Grave contains the highest Fe^{2+}# values with a sizeable Fe^{3+}# range. Cliff contains higher Fe^{3+}# values at lower Fe^{2+}# values. Nikkavord South, Nikkavord East, Long Quarry and Keen of Hamar all contain similar Fe^{2+}# values but with increasing Fe^{3+}# values. Quoys contains the lowest Fe^{3+}# values rising to the average value.

4.4.2 Trace element variation *within* chromitite pods

Trace element data (TiO_2, V_2O_5, MnO, NiO) were collected from 56 separate chromitite samples using an SEM, with 33 of these analysed for Co, Zn and Ga on the Laser ICP-MS (Table 4.3). Although TiO_2 is a trace element its variation was described in the previous section owing to its use in a discrimination diagram (Figure 4.16). The vanadium content of the Harold's Grave chromitites is clearly higher than any of the other chromitite localities (Figure 4.18A; Table 4.3). As with the major elements there are also clear groupings by sample locality as well as internal variations within each pod. The range of vanadium values within Harold's Grave is 0.21 to 0.25. Altogether, the rest of the chromitites have a range of values going from 0.09 (Quoys) to 0.18 (Nikkavord South) with Quoys containing the lowest range of vanadium values, from 0.09 to 0.13. There is no relationship between vanadium content and Cr#, either collectively or individually within the chromitite pods.

Ga values show a slight collective negative relationship with Cr# (Figure 4.18B). The total range of values is from 19 to 54 ppm. As with Zn and V, Harold's Grave contains the highest values of any of the chromitites from Shetland, with a range of 44 to 54, and no particular relationship with Cr#. Harold's Grave aside, the rest of the chromitite pods form a strong collective negative correlation between Ga and Cr# (Figure 4.18B). This inverse trend is expected as the outer electronic structure of Ga is similar to that of Al (i.e. $3s^2 3p^1$ and $4s^2 4p^1$). As such it may be expected that as Al contents increase in the chromite grains, so too will Ga contents.

There is no relationship either collectively or individually between the nickel content of the chromitites and the Fe^{2+}#, with the possible exception of Harold's Grave (Figure 4.18C). However, in a similar manner to vanadium each of the chromitite pods show distinctive element ranges. With respect to Ni, Harold's Grave once again appears unique, though due in this case to the higher Fe^{2+}# values as mentioned in the major element summary. Harold's Grave NiO values range from 0.07 to 0.15 with an approximate negative correlation with Fe^{2+}#. Cliff's NiO values range from 0.07 to 0.22 which is the full range encountered in the Shetland ophiolites. The remaining chromitites range in value from 0.07 (Quoys) to 0.21 (Nikkavord South).

Table 4.3a: *Trace element chromite data from the chromitite localities in the mantle sequence.*

Sample#	Locality	Cr#	Mg#	Cr/Fe^{2+}	TiO_2	V_2O_5	MnO	NiO	Co (ppm)	Zn (ppm)	Ga (ppm)
CF1	Cliff	0.65	0.71	4.25	0.17	0.13	0.24	0.14	-	-	-
CF10	Cliff	0.65	0.72	4.42	0.11	0.13	0.23	0.13	-	-	-
CF11	Cliff	0.63	0.70	4.11	0.07	0.15	0.22	0.20	-	-	-
CF12	Cliff	0.62	0.71	3.97	0.16	0.14	0.23	0.12	-	-	-
CF13	Cliff	0.62	0.71	3.98	0.16	0.13	0.22	0.14	198	181	31
CF14	Cliff	0.70	0.67	4.06	0.08	0.14	0.26	0.12	267	216	27
CF15	Cliff	0.63	0.67	3.62	0.17	0.13	0.24	0.11	-	-	-
CF16	Cliff	0.70	0.68	4.20	0.08	0.15	0.25	0.09	-	-	-
CF17	Cliff	0.65	0.70	4.13	0.17	0.12	0.25	0.11	-	-	-
CF18	Cliff	0.66	0.74	4.81	0.18	0.12	0.23	0.17	-	-	-
CF2	Cliff	0.61	0.73	4.22	0.16	0.14	0.23	0.07	197	188	36
CF3	Cliff	0.62	0.69	3.81	0.17	0.13	0.23	0.16	256	188	32
CF4	Cliff	0.65	0.70	4.04	0.18	0.13	0.25	0.13	-	-	-
CF5	Cliff	0.66	0.71	4.36	0.18	0.13	0.23	0.13	194	167	33
CF6	Cliff	0.62	0.65	3.36	0.16	0.13	0.27	0.22	-	-	-
CF8	Cliff	0.65	0.71	4.32	0.19	0.12	0.23	0.13	196	185	34
CF9	Cliff	0.78	0.64	4.18	0.05	0.17	0.30	0.13	-	-	-
Q3a	H.Grave	0.72	0.47	2.61	0.23	0.23	0.35	0.07	-	-	-
Q1	H.Grave	0.65	0.57	2.89	0.17	0.23	0.25	0.10	-	-	-
Q2	H.Grave	0.69	0.51	2.72	0.17	0.22	0.32	0.11	-	-	-
Q3b	H.Grave	0.72	0.52	2.87	0.24	0.21	0.30	0.07	-	-	-
QX13	H.Grave	0.59	0.57	2.61	0.34	0.23	0.22	0.16	-	-	-
Q3PX	H.Grave	0.68	0.55	2.90	0.18	0.22	0.27	0.10	-	-	-
HG11	H.Grave	0.64	0.59	2.96	0.20	0.25	0.24	0.15	213	361	45
HG5	H.Grave	0.58	0.61	2.87	0.20	0.25	0.25	0.11	243	383	50
HG7	H.Grave	0.58	0.64	3.08	0.14	0.22	0.23	0.14	-	-	-
HG1	H.Grave	0.62	0.58	2.87	0.20	0.24	0.24	0.13	239	345	48
HG8	H.Grave	0.64	0.57	2.86	0.18	0.22	0.26	0.12	264	375	46
HG9	H.Grave	0.61	0.59	2.85	0.28	0.21	0.24	0.13	236	340	53
HG4	H.Grave	0.61	0.61	3.03	0.18	0.23	0.25	0.10	262	391	46
HG6	H.Grave	0.70	0.56	3.06	0.20	0.21	0.26	0.10	295	441	39
QY1	Quoys	0.72	0.66	4.08	0.12	0.13	0.26	0.08	202	192	20
QY2	Quoys	0.70	0.65	3.82	0.15	0.12	0.27	0.11	200	196	23
QY5	Quoys	0.70	0.67	4.07	0.09	0.13	0.28	0.10	203	202	23
QY6	Quoys	0.70	0.70	4.48	0.11	0.11	0.23	0.09	-	-	-
QY8	Quoys	0.69	0.69	4.24	0.07	0.13	0.23	0.11	174	170	24
QY9	Quoys	0.71	0.66	4.10	0.09	0.09	0.26	0.07	250	164	20
QY10	Quoys	0.73	0.68	4.43	0.16	0.11	0.24	0.12	186	157	23
NKE-1	Nkvd East	0.52	0.70	3.35	0.22	0.15	0.20	0.17	242	221	45
NKE-2	Nkvd East	0.53	0.70	3.41	0.13	0.14	0.22	0.17	202	203	43
NKE-3	Nkvd East	0.53	0.69	3.26	0.13	0.16	0.22	0.16	215	214	47
NKE-4	Nkvd East	0.57	0.68	3.41	0.16	0.19	0.23	0.15	217	189	34
NKE-5	Nkvd East	0.52	0.70	3.36	0.18	0.15	0.22	0.17	230	216	42
NKE-6	Nkvd East	0.53	0.72	3.55	0.17	0.15	0.22	0.17	-	-	-
NKE-7	Nkvd East	0.52	0.72	3.56	0.22	0.15	0.21	0.18	-	-	-
NKS-1	Nkvd South	0.57	0.70	3.65	0.10	0.17	0.23	0.21	195	168	34
NKS-2	Nkvd South	0.55	0.69	3.45	0.18	0.14	0.22	0.19	178	188	37
NKS-3	Nkvd South	0.56	0.71	3.67	0.07	0.17	0.20	0.20	184	197	36
NKS-4	Nkvd South	0.61	0.67	3.59	0.08	0.18	0.22	0.18	210	218	39
NKS-5	Nkvd South	0.56	0.68	3.48	0.10	0.15	0.22	0.15	-	-	-
NKS-6	Nkvd South	0.60	0.65	3.34	0.13	0.14	0.23	0.13	-	-	-

Table 4.3b: *Trace element chromite data from the chromitite localities in the crustal sequence.*

Sample#	Locality	Cr#	Mg#	Cr/Fe^{2+}	TiO_2	V_2O_5	MnO	NiO	Co (ppm)	Zn (ppm)	Ga (ppm)
KH1	K. Hamar	0.56	0.69	3.35	0.20	0.13	0.22	0.13	247	225	38
KH2	K. Hamar	0.56	0.69	3.40	0.20	0.13	0.23	0.14	247	225	38
RLM053	K. Hamar	0.62	0.66	3.59	0.16	0.16	0.24	0.16	-	-	-
RLM058	K. Hamar	0.54	0.66	3.12	0.23	0.15	0.22	0.18	-	-	-
LQ1	L. Quarry	0.62	0.73	4.39	0.16	0.14	0.22	0.15	191	175	33
LQ2	L. Quarry	0.68	0.70	4.35	0.19	0.13	0.24	0.18	212	158	30
LQ3	L. Quarry	0.63	0.72	4.26	0.15	0.14	0.24	0.17	193	186	34

MnO values show an excellent positive correlation with Fe^{2+}#, both collectively and for all the individual chromitites (Figure 4.18D). Harold's Grave contains the highest values and is displaced to higher Fe^{2+}#. The full range of MnO values at Harold's Grave ranges from 0.22 to 0.36. Cliff's MnO values range from 0.22 to 0.30. The composition of the remaining chromitite pods lie between 0.20 (Nikkavord South) and 0.28 (Quoys).

Co values show a slight positive correlation with Fe^{2+}#, both collectively and for the individual chromitites (Figure 4.18E). Harold's Grave contains the highest value (295) followed by Cliff with 267 ppm. The remaining chromitite pods vary between 174 (Quoys) and 250 (Also Quoys).

Collectively Zn values show a positive correlation with Fe^{2+}#, as do all the individual chromitites except Cliff (Figure 4.18F). Harold's Grave contains all the highest Zn values with a range going from 340 to 441 ppm. The remaining chromitite deposits, including Cliff, all lie within a fairly restricted range of 157 ppm (Quoys) to 225 ppm (Keen of Hamar).

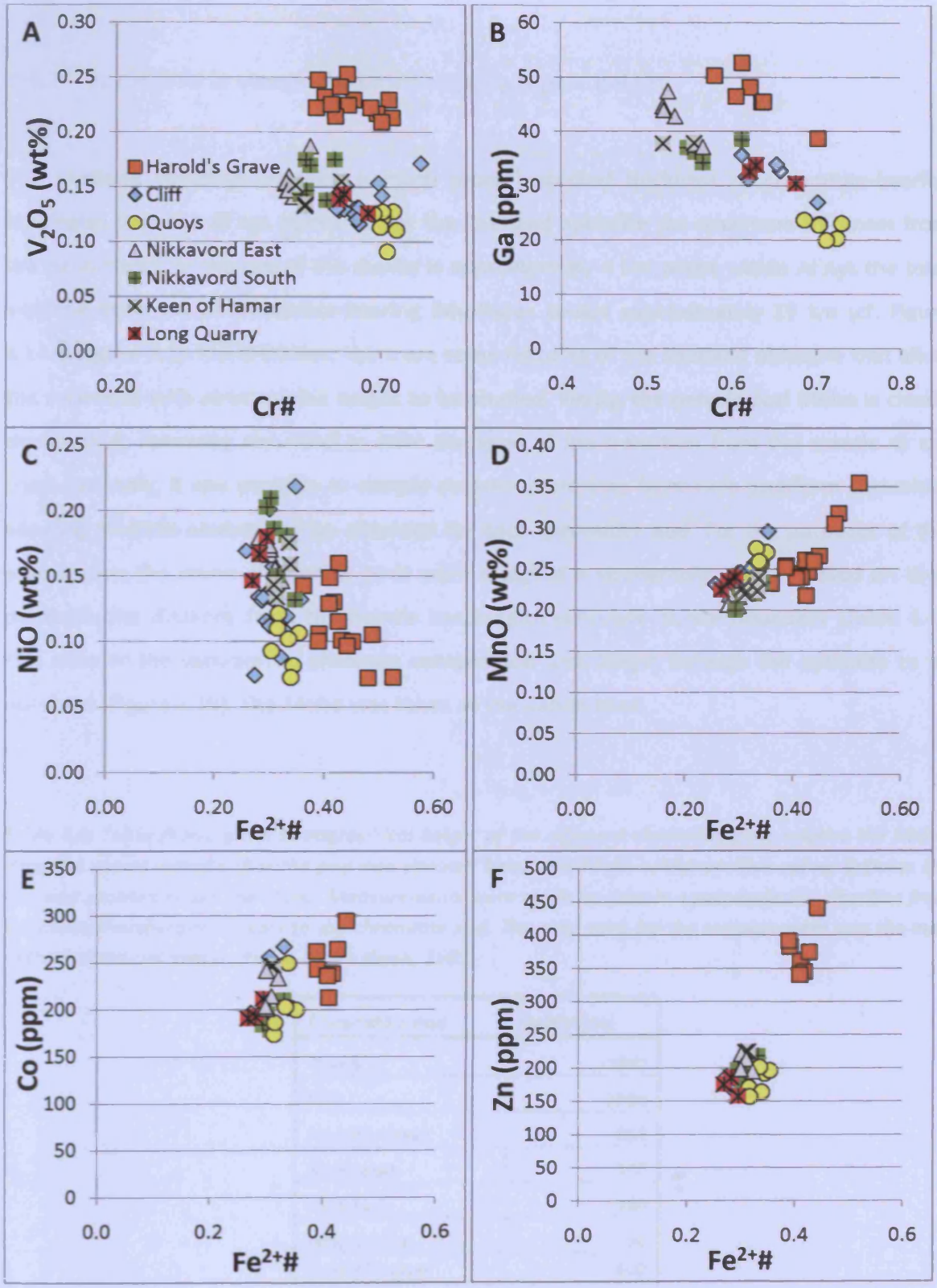

Figure 4.18: *Six trace element plots for the Shetland chromitites. The legend within Figure 4.18A applies to Figures 4.18B-F. Figures 4.18A and 4.18B are plots of V_2O_5 and Ga versus Cr#. A relationship between these elements would be expected as these trace elements would fill the same trivalent cation space within the chromite grain as Cr^{3+} and Al^{3+}. Figures 4.18C-F are plots of NiO, MnO, Co and Zn against Fe^{2+}# as these trace elements fill the same divalent cation space as Fe^{2+} and Mg^{2+}.*

4.4.3 Variations in composition with stratigraphic height

The Shetland ophiolite contains a much more restricted thickness of chromitite-bearing lithologies than the Al'Ays ophiolite. For the Shetland ophiolite the maximum thickness from the basal thrust to the top of the dunite is approximately 4 km whilst within Al'Ays the total exposed thickness of chromitite-bearing lithologies covers approximately 19 km (cf. Figure 4.14 & Figure 3.1). Nevertheless, there are some features of the Shetland ophiolite that allow the variations with stratigraphic height to be studied. Firstly, the petrological Moho is clearly demarcated, removing the need to infer the level of the transition from the mantle to the crust. Secondly, it was possible to sample several chromitites from each podiform chromitite allowing multiple analyses to be obtained for each chromitite pod. For the purposes of this examination the seven chromitite pods were assigned a stratigraphic height based on their perpendicular distance from the mantle harzburgite/cumulate dunite boundary (Table 4.4). This allowed the variation of chromite composition with height through the ophiolite to be observed (Figure 4.19). The Moho was taken as the datum level.

Table 4.4: *Table showing the stratigraphical height of the different chromitite pods relative the Moho. Negative values indicate that the pod was situated below the Moho whilst positive values indicate the pod was situated above the Moho. Measurements were made by ruler in a perpendicular direction from the dunite/harzburgite contact to the chromitite pod. The map used for the measurement was the map of the Baltasound area from R.A.Lord's thesis, 1991.*

Chromitite Pod	Height (m)
Quoys	-1600
Cliff	-1500
Harold's Grave	-650
Nkrd South	-340
Nkrd East	-280
Long Quarry	50
Keen of Hamar	600

Cr/ Fe^{2+} values initially decrease with stratigraphic height producing the lowest values in chromitite at Harold's Grave. Cr/Fe^{2+} values then rise from Harold's Grave to Long Quarry which is situated just above the Moho before decreasing again within the cumulate sequence (Figure 4.19A).

Cr# values within chromitite appear to show a small decrease when switching from the deepest mantle sequence deposit (Quoys) to the shallowest crustal sequence deposit. This trend is not significant (R^2 = 0.377), (Figure 4.19B). As with the Cr/Fe^{2+}, there appears to be another reset to slightly higher Cr# values at Long Quarry (i.e. at the base of the cumulate sequence) before values decrease again. The Cr/Fe^{2+} and Cr# patterns will be discussed again in Section 4.6.

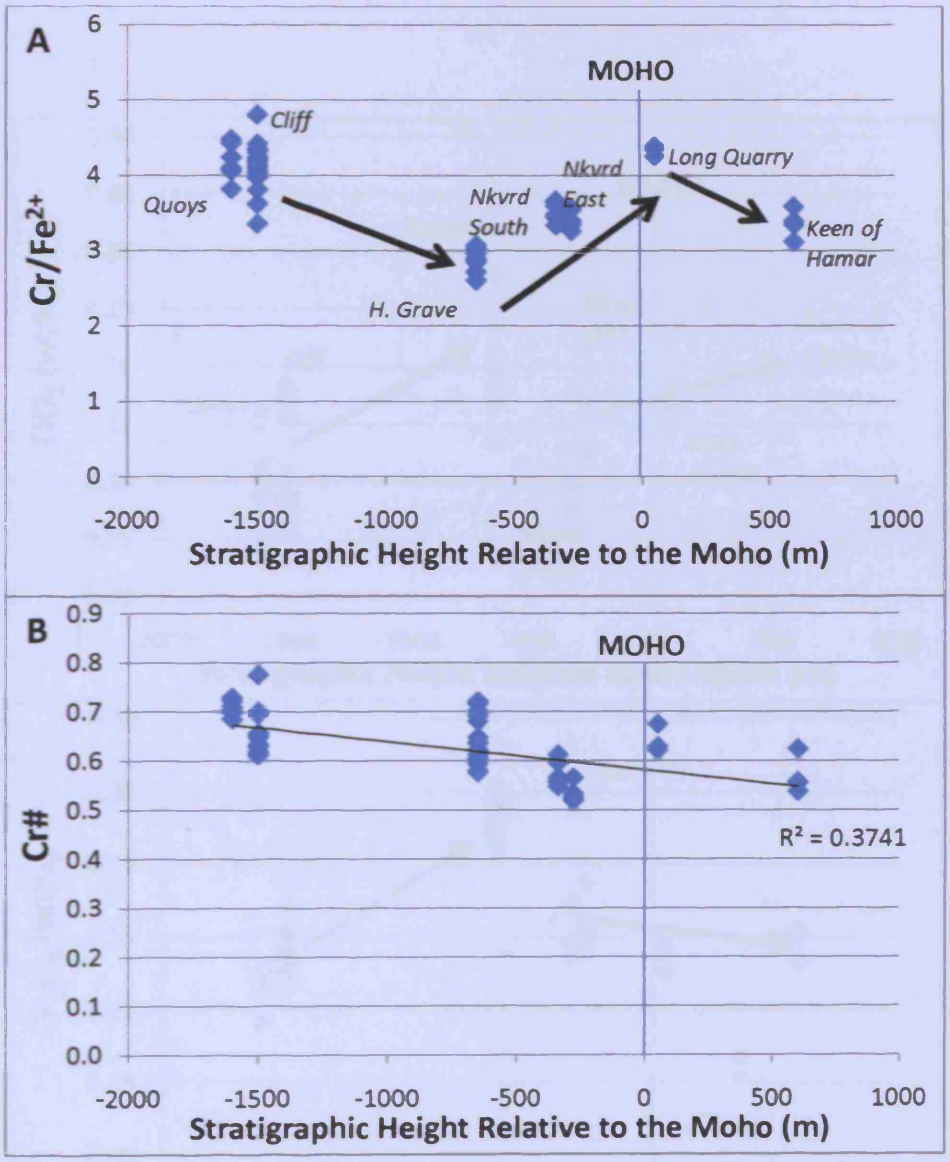

Figure 4.19: *Two graphs showing variations in major element geochemical ratios with stratigraphic height. The Moho is demarcated in each. The chromitite pods are labelled in 4.19A. A: Cr/ Fe^{2+} - arrows show the changing trends of chromite geochemical composition within the mantle and crustal sequence. B: Cr# - trendline with R^2 value also shown.*

Concentrations of trace elements within chromite grains show no definitive pattern within the mantle and cumulate sequence of the Shetland ophiolite. Nevertheless there are some points of interest. Firstly, if you include Harold's Grave as part of the mantle sequence and Nikkavord South and East as part of the transitional/cumulate sequence (e.g. as within (Lord, 1991)), then there appears to be one trend with height within the mantle sequence and a different trend with height in the transitional/cumulate sequence (Figure 4.20, 4.21 & 4.22). This is observed for TiO_2, V_2O_5, NiO, Co, Zn, Ga and possibly MnO. A discussion on these trends is reserved for Section 4.6.

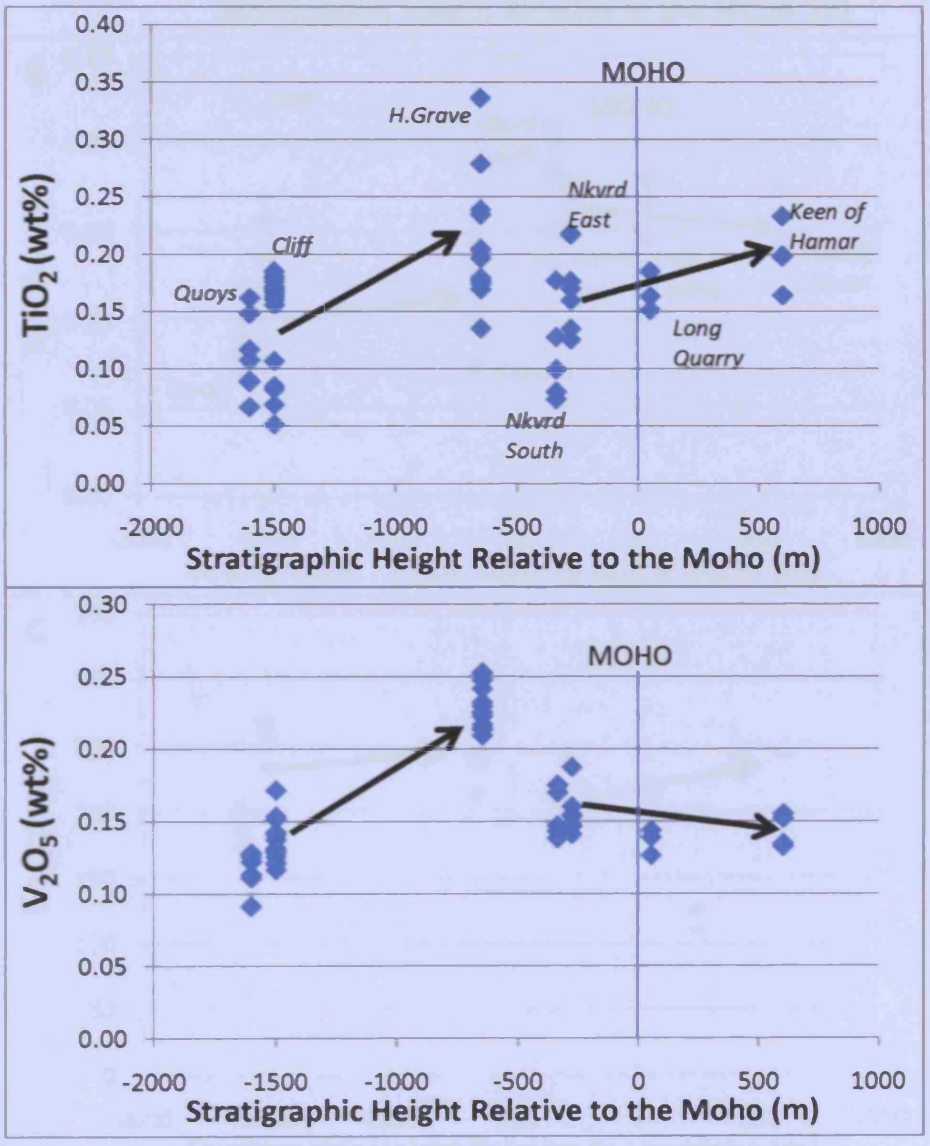

Figure 4.20: *Two graphs showing variations in trace element contents with stratigraphic height. The Moho is demarcated in each, as are arrows showing possible trends within the mantle sequence and the transitional/cumulate sequence. The chromitite pods are labelled in 4.20A. A: TiO_2, B: V_2O_5.*

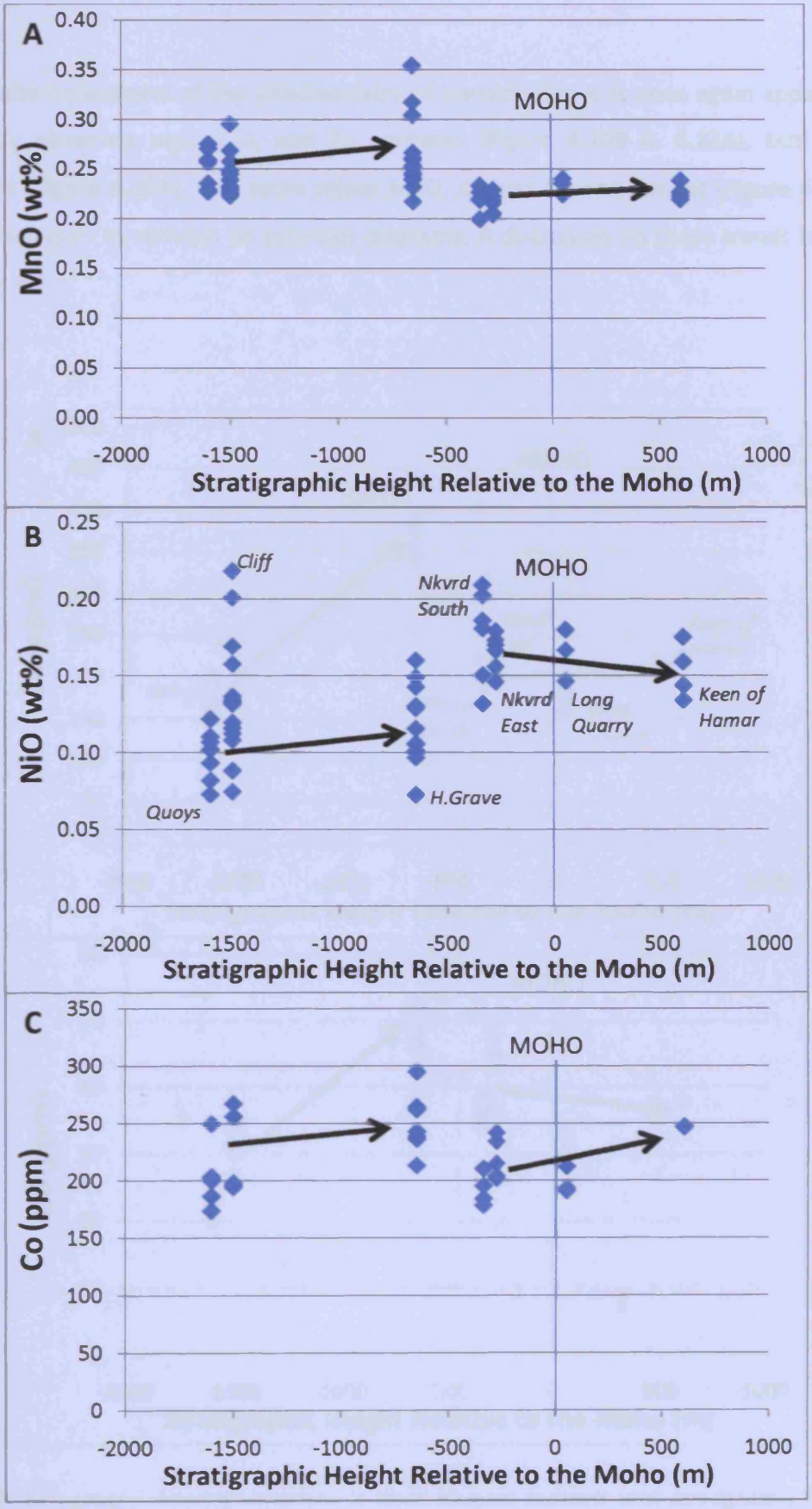

Figure 4.21: *Three graphs showing variations in trace element contents with stratigraphic height. The Moho is demarcated in each, as are arrows showing possible trends within the mantle sequence and the transitional/cumulate sequence. The chromitite pods are labelled in 4.21B. A: MnO, B: NiO, C: Co.*

Secondly, the uniqueness of the geochemistry of Harold's Grave is once again apparent with the already observed high V_2O_5 and Zn contents (Figure 4.20B & 4.22A), but also TiO_2 enrichment (Figure 4.20A), and some minor MnO, Co and Ga enrichment (Figure 4.21A, C & 4.22B), which isn't as obvious on previous diagrams. A discussion on these trends is reserved for Section 4.6.

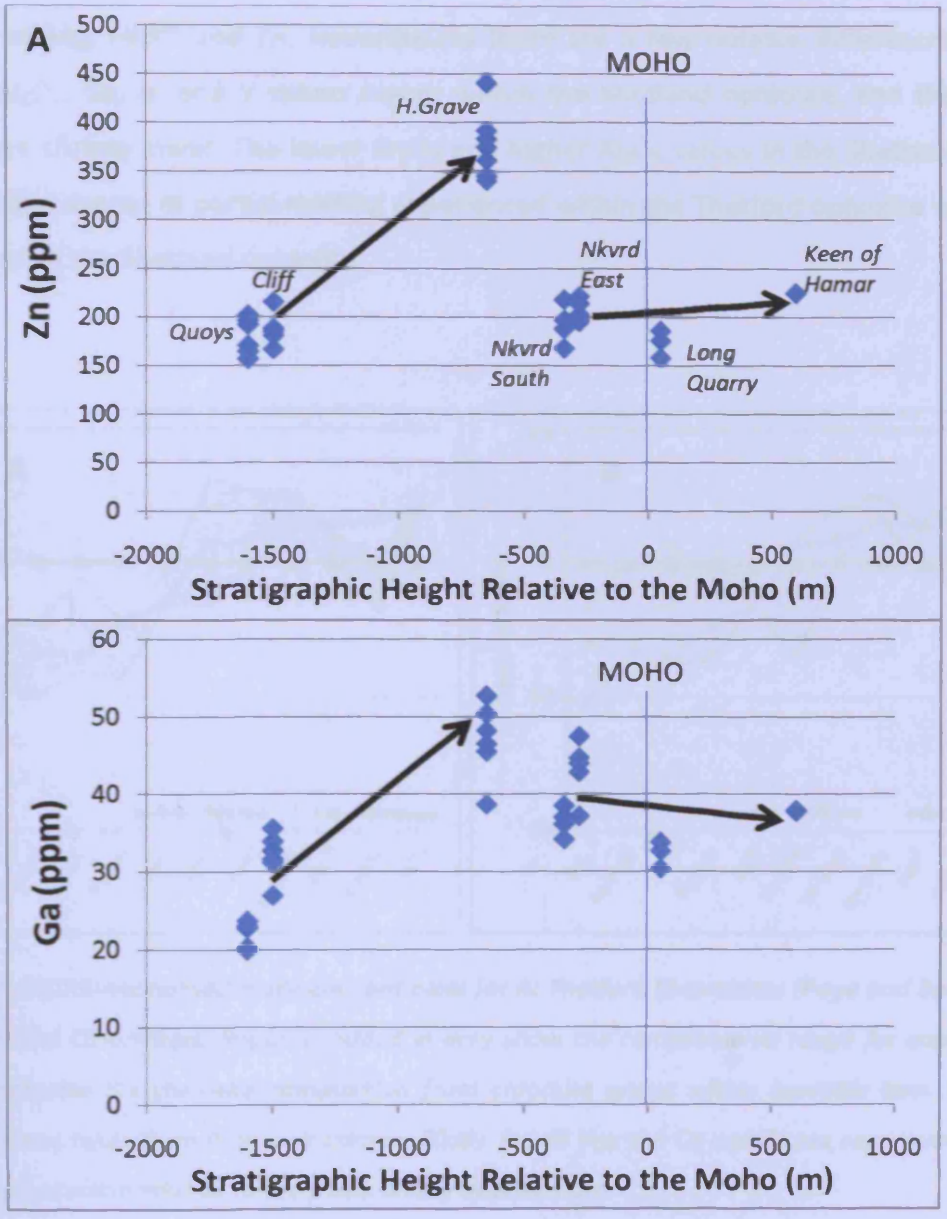

Figure 4.22: *Two graphs showing variations in trace element contents with stratigraphic height. The Moho is demarcated in each, as are arrows showing possible trends within the mantle sequence and the transitional/cumulate sequence. The chromitite pods are labelled in 4.22A. A: Zn, B: Ga*

4.4.4 MORB normalised multi-element plots

MORB normalised multi element plots of the Shetland chromitites reveal a strong affinity to similar plots from the Thetford chromitites in Canada (Figure 4.23), which are proposed to be supra-subduction ophiolites. The Shetland ophiolite has previously been postulated to be from a supra-subduction zone setting (Prichard and Tarkian, 1988), so this similarity with the Thetford chromitites is expected. The key similarities between Thetford and Shetland are in the value of Mg, FeO^{tot} and Zn. Nevertheless there are a few notable differences with the range of Al_2O_3, Ga, Ni and V values higher within the Shetland ophiolite, and the range of Cr_2O_3 values slightly lower. The lower Cr_2O_3 and higher Al_2O_3 values in the Shetland ophiolite imply that the degree of partial melting experienced within the Thetford ophiolite was slightly greater than in the Shetland ophiolite.

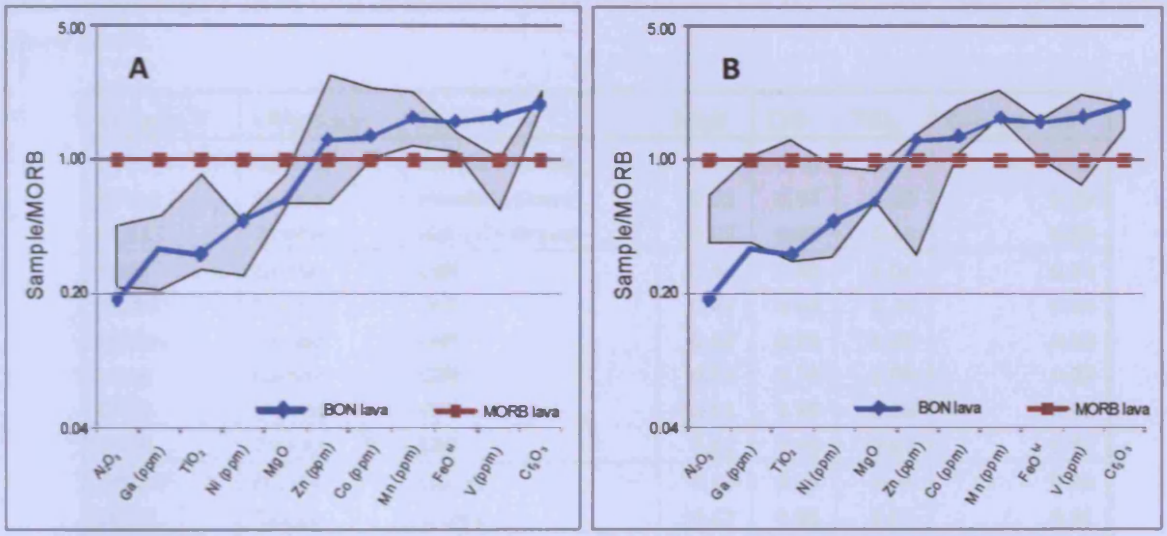

Figure 4.23: *MORB normalised multi-element plots for* ***A:*** *Thetford Chromitites (Page and Barnes, 2009) and* ***B:*** *Shetland Chromitites. Regions shaded in grey show the compositional range for each ophiolite. The blue indicates the chromite composition from chromite grains within boninitic lava. MORB and boninite sources taken from Page and Barnes (2009). For Al 'Ays the Co and Zn are semi-quantitative so their absolute position relative to the y-axis is only approximate.*

4.4.5 Olivine-Spinel Mantle Array (OSMA)

For co-existing olivine and chromite grains all (previously) mantle-hosted samples should plot within the OSMA (see Section 1.5.6 for more detail), barring any samples within podiform chromitites which plot to higher Fo# owing to re-equilibration within the 2+ cations. Dunites plotting within the OSMA may be the products of replacement (defined as dissolution of pyroxene with concomitant precipitation of olivine (Kelemen, 1995)) or products of fractional crystallization (Arai, 1994), with any samples plotting to the right of the OSMA being interpreted as the product of fractional crystallization (e.g. Pearce *et al.*, 2000) or metasomatic reaction (e.g. Arai, 1994).

Table 4.5: *Table showing the Cr#, Mg# and TiO_2 contents of chromite grains within all the dunite and harzburgite samples containing analysable olivine. Also shown are the forsterite values of the analysed olivine grains.*

Sample #	Lithology	Locality	Mg#	Cr#	TiO_2	Olivine Fo#
RLO11	Dunite	Harold's Grave	0.56	0.48	0.25	0.89
RL016	Dunite	Harold's Grave	0.61	0.37	0.10	0.89
RLO19	Dunite	Harold's Grave	0.57	0.48	0.16	0.89
MR6	Dunite	Cliff	0.46	0.80	0.04	0.92
RL007	Dunite	Cliff	0.47	0.64	0.14	0.89
MR12	Dunite	Cliff	0.44	0.73	0.06	0.92
CF19	Dunite	Cliff	0.51	0.70	0.08	0.92
CF20	Dunite	Cliff	0.51	0.70	0.08	0.92
CF23	Dunite	Cliff	0.52	0.70	0.07	0.92
MR267	Dunite	Quoys	0.49	0.65	0.04	0.89
MR35	Dunite	Quoys	0.47	0.68	0.07	0.91
MR144	Harzburgite	Taing NU	0.52	0.67	0.00	0.91
MR162	Harzburgite	Clibberswick South	0.45	0.77	0.09	0.91
MR256	Harzburgite	West of Nikkavord	0.60	0.54	0.02	0.91
MR1	Harzburgite	Cliff	0.46	0.68	0.03	0.91
MR254	Harzburgite	S. Of Crussa Field	0.57	0.55	0.02	0.91
MR276	Harzburgite	Mid Fetlar	0.71	0.30	0.04	0.91
NB2a	Dunite	Crustal	0.58	0.53	0.22	0.91
NB2b	Dunite	Crustal	0.59	0.53	0.21	0.90
RLM026	Dunite	Crustal	0.55	0.66	0.21	0.92
RLM057	Dunite	Crustal	0.62	0.52	0.22	0.91

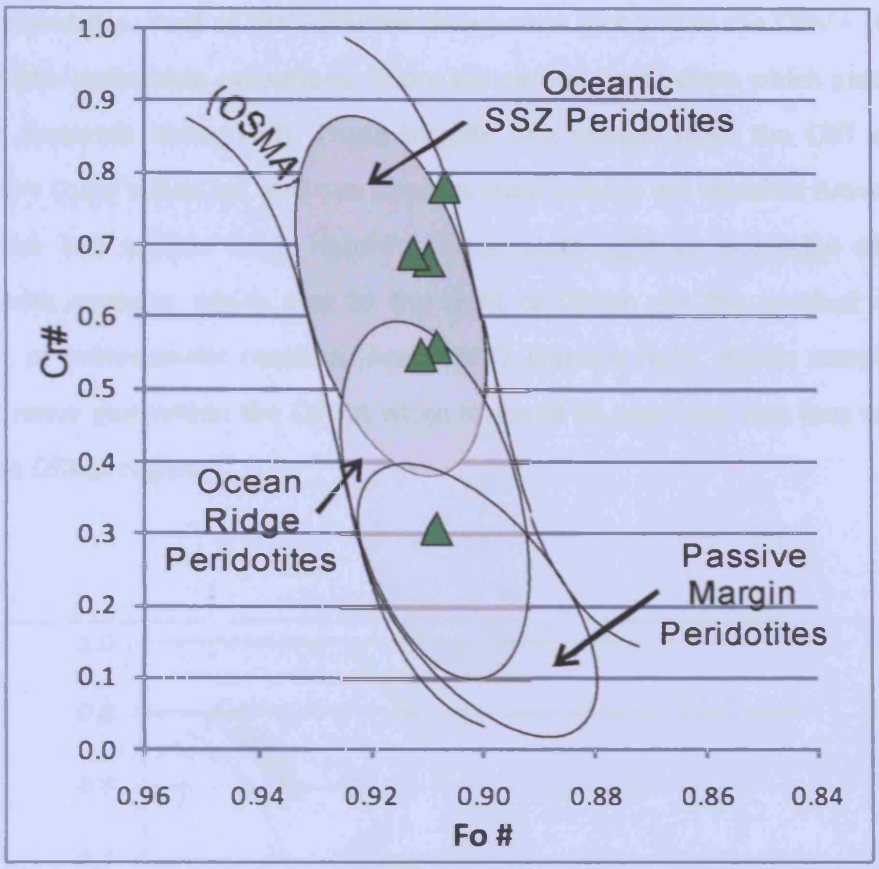

Figure 4.24: *Olivine Spinel Mantle Array (OSMA) plot showing Cr# - Fo# for the Shetland mantle harzburgites. Cr# are derived from chromite within harzburgite, whilst Fo# is derived from olivine grains within the same polished section as the chromite grains. Peridotite regions are taken from Pearce et al. (2000).*

All the harzburgite samples analysed plot within the OSMA (Figure 4.24), but at varying Cr# implying that they have been subjected to varying degrees of partial melting. The lower Cr# imply more fertile harzburgitic mantle associated with passive margins or ocean ridges whilst the higher Cr# imply more depleted harzburgitic mantle typical of SSZ peridotites. Harzburgite represents the residuum after melt extraction, into which later melts deposit chromitites. The wide variety of Cr# highlights how spatially heterogeneous melt extraction can be, as undepleted fertile peridotites contain chromite grains with low Cr# (e.g. passive margin peridotites (Table 4.5, Figure 4.24)), whereas depleted peridotites contain chromite grains with high Cr# (e.g. oceanic SSZ peridotites (Figure 4.24)).

For the dunite samples most of the collected data points plot within the OSMA (Figure 4.25), though with some noticeable exceptions. There are several data points which plot to the right of the OSMA (towards lower Fo#). These include one sample from the Cliff dunites, one sample from the Quoy's dunites, and two samples from around the Harold's Grave chromitite. In addition, the last sample from Harold's Grave plots right on the edge of the OSMA envelope. Dunite analyses which plot to the right of OSMA are the product of fractional crystallization, or metasomatic reaction (Arai, 1994). Unexpectedly, dunite samples from the cumulate sequence plot within the OSMA when it would be expected that they would plot to the right of the OSMA region.

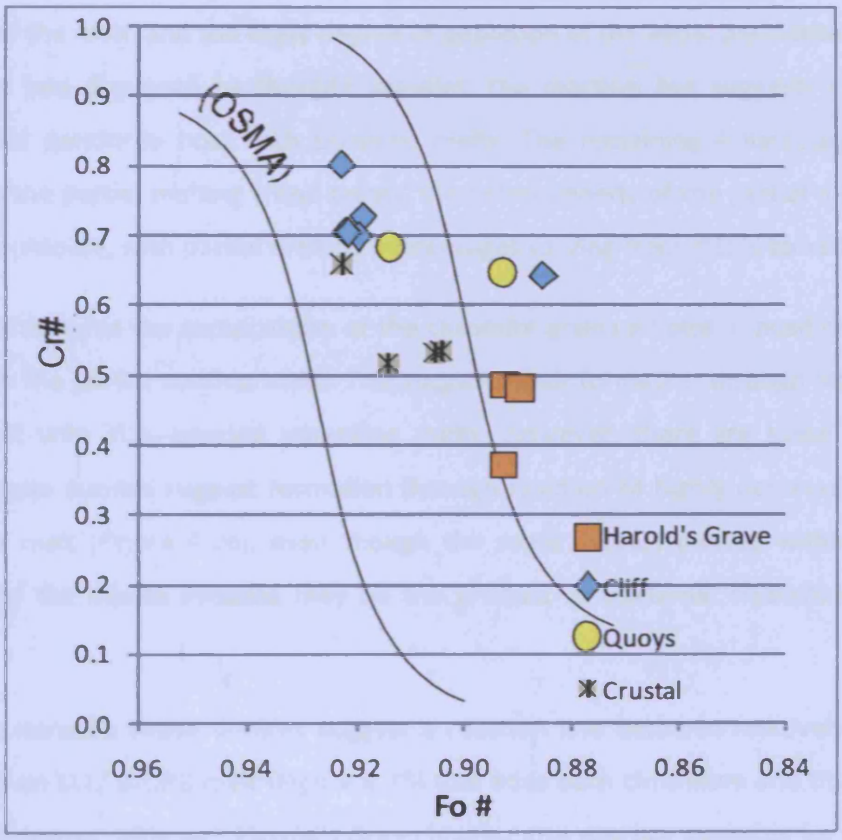

Figure 4.25: *Olivine Spinel Mantle Array (OSMA) plot showing Cr# - Fo# for the Shetland dunites (from both the mantle and crustal sequences). Cr# are taken from chromite grains within the dunite, whereas Fo# are taken from olivine grains associated with the chromite in the same section.*

4.4.6 Cr#-TiO_2 diagram (Pearce *et al.*, 2000)

The Cr# - TiO_2 diagram was developed to distinguish between the effects of partial melting and melt/rock reaction within mantle peridotites (Arai, 1992; Zhou *et al.*, 1996; Pearce *et al.*, 2000). The partial melting trend defines an expected evolution of chrome-spinel compositions during increasing degrees of partial melting (Figure 4.25). This melting model shows that the Ti content of a chromite grain rapidly decreases as the Cr# of the chromite grain and the degree of mantle melting increases. Four of the six harzburgite samples plot along this partial melting trend, with two displaced significantly from the curve (Figure 4.25). This displacement could be caused by reaction of the peridotite host with upwelling melts which re-introduce TiO_2 (e.g. (Kelemen, 1995)) and in this case produces a trend which points towards the likely composition of the melt, and the likely degree of depletion of the initial peridotite host (Figure 4.25). For the two displaced harzburgite samples, the reaction line suggests reaction of a highly depleted peridotite host with boninitic melts. The remaining 4 harzburgite samples which plot on the partial melting trend record the heterogeneity of the partial melting within the Shetland ophiolite, with partial melting percentages varying from ~15% to >30%.

For the dunite samples the composition of the chromite grains all plot in positions which are displaced from the partial melting trend. This suggests their formation through reaction of the peridotite host with TiO_2–bearing upwelling melts. However, there are some ambiguities. Firstly, the Quoys dunites suggest formation through reaction of highly depleted harzburgite with boninitic melt (Figure 4.26), even though the same dunites plotted within the OSMA suggest one of the dunite samples may be the product of fractional crystallization (Figure 4.25).

Secondly, the Harold's Grave dunites suggest a reaction line between relatively fertile host peridotite and an IAT/ MORB melt (Figure 4.25) that adds both chromium and titanium to the harzburgite. However, although Harold's Grave harzburgite was not available for analysis, the analyses from all the other harzburgite samples within the vicinity suggest extremely depleted harzburgite is more likely (the relatively fertile harzburgite sample, with a Cr# of ~0.3, was taken from the island of Fetlar 10 km to the South). Additionally, olivine compositions from Harold's Grave dunites plot to the right of the OSMA (Figure 4.24) which suggests a fractional crystallization petrogenesis; this should lead to spinel compositions with increasing Ti contents and decreasing Cr#, which clearly isn't observed (Figure 4.25).

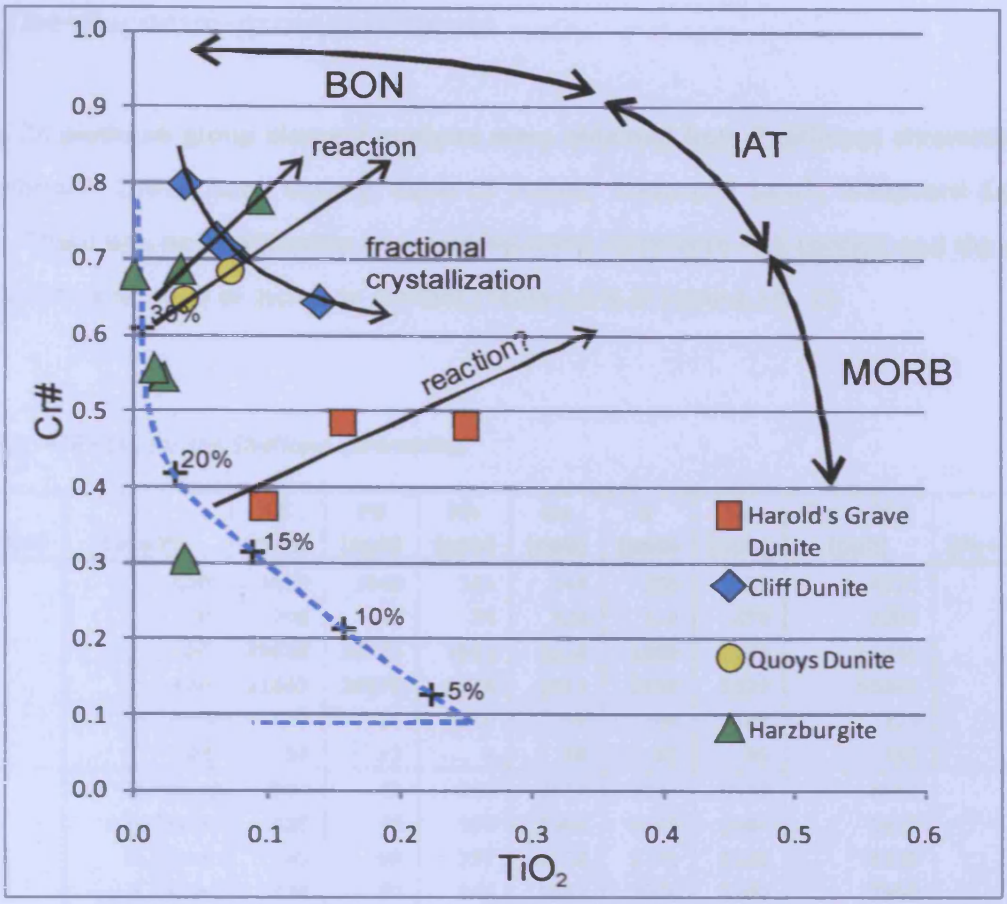

Figure 4.26: *Cr# - TiO_2 plot for chrome-spinel from mantle harzburgites and dunites from the Shetland ophiolite. The blue dashed line represents the predicted chrome-spinel composition at different degrees of partial melting (adapted from (Pearce et al. 2000)). Reaction lines for dunites produce a tie-line between expected peridotite host rock composition and the melt which has reacted with the host rock. The expected melt-composition domains are taken from Pearce et al. (2000). The fractional crystallization path for Cliff is also shown.*

Thirdly, the Cliff dunites display a trend of increasing Ti with decreasing Cr# which is exactly what is predicted by fractional crystallization processes, rather than reaction processes (Figure 4.25). However, only one of the five dunite samples plots outside the OSMA (and is therefore probably a product of fractional crystallization), with the rest plotting within the OSMA (Figure 4.24). For the dunite surrounding both Cliff and Harold's Grave chromitite pods there are mixed messages from these two generalised interpretative diagrams. This will be discussed further in Section 4.6.

4.5 The platinum-group elements

In total 34 platinum group element analyses were obtained from 7 different chromitite pods (Cliff, Harold's Grave, Long Quarry, Keen of Hamar, Nikkavord South, Nikkavord East and Quoys). There was no relationship observed between chromitite PGE content and the degree of chromitite alteration or inclusion content (Table 4.6 & cf Table 4.1A - C)

Table 4.6: *PGE data for the Shetland chromitites.*

Sample #	Locality	Pt (ppb)	Pd (ppb)	Rh (ppb)	Os (ppb)	Ir (ppb)	Ru (ppb)	Total PGE (ppb)	(Pt + Pd)/Ir
CF13	Cliff	1650	1849	141	144	208	333	4325	16.82
CF14	Cliff	708	443	74	124	174	478	2001	6.61
CF2	Cliff	19028	23733	1561	1228	1969	2927	50446	21.72
CF3	Cliff	21443	28475	1678	2013	2113	3122	58844	23.62
CF5	Cliff	19	15	10	37	44	149	274	0.77
CF8	Cliff	14	11	9	16	35	95	180	0.71
HG11	H. Grave	504	41	345	2012	2127	3533	8562	0.26
HG5	H. Grave	428	38	306	1067	2073	2964	6876	0.22
HG7	H. Grave	785	69	397	1324	2270	3483	8328	0.38
HG1	H. Grave	474	40	349	1647	2040	3400	7950	0.25
HG8	H. Grave	685	36	344	1479	2088	3183	7815	0.35
HG9	H. Grave	480	53	257	650	1159	2172	4771	0.46
HG4	H. Grave	463	54	336	1325	1974	3069	7221	0.26
HG6	H. Grave	566	40	422	2968	2861	7311	14168	0.21
QY1	Quoys	0	5	8	29	26	79	147	0.19
QY2	Quoys	0	9	16	29	48	110	212	0.19
QY5	Quoys	49	68	19	41	52	147	376	2.25
QY6	Quoys	0	6	9	40	52	118	225	0.12
QY8	Quoys	37	3	14	23	40	88	205	1.00
QY9	Quoys	0	6	10	24	44	108	192	0.14
QY10	Quoys	3	6	10	20	21	64	124	0.43
NKE 2	Nkvd East	5	8	4	4	8	26	55	1.63
NKE 3	Nkvd East	0	22	3	6	8	25	64	2.75
NKE 6	Nkvd East	0	4	2	3	7	17	33	0.57
NKE 7	Nkvd East	5	2	5	5	17	32	66	0.41
NKS 1	Nkvd South	47	88	15	35	47	85	317	2.87
NKS 2	Nkvd South	0	4	4	16	20	34	78	0.20
NKS 3	Nkvd South	10	23	5	27	23	53	141	1.43
NKS 4	Nkvd South	9	10	7	18	33	72	149	0.58
LQ1	Long Quarry	21	8	11	46	38	76	200	0.76
LQ2	Long Quarry	59	71	18	35	48	109	340	2.71
LQ3	Long Quarry	16	7	12	57	45	130	267	0.51
KH1	K. of Hamar	18	10	5	24	32	73	162	0.88
KH2	K. of Hamar	19	13	5	21	33	75	166	0.97

4.5.1 The PGE-rich localities – Cliff & Harold's Grave

The findings from this research support the observation that barring occasional mineralization within the cumulate dunites - up to several 100s ppb Pt & Pd (Lord and Prichard, 1997), and one instance of up to 1 ppm at Jimmies Quarry (Lord, 1991) - the only PGE-rich localities are Cliff and Harold's Grave. The PGE inventories from these two localities are very different. As has been pointed out in previous work (Prichard *et al.*, 1986) the mineralisation at Cliff is dominated by Pt and Pd, is heavily linked to sulphide mineralization and is variable. Mineralisation at Harold's Grave is dominated by IPGE and appears more consistent in both grade and PPGE/IPGE ratio.

The current study has shown that the total PGE content in chromitites from Cliff is highly variable. Comparing CF3 with CF8 there are over two orders of magnitude difference between the total PGE contents, with CF3 containing 58,000 ppb total PGE and CF8 containing just 180 ppb total PGE. For the individual Pt and Pd values the differences are even greater, reaching up to three orders of magnitude. The total range of Pt values is 14 to 21443 ppb, whilst for Pd the values range from 11 to 28475 ppb. The differences are also reflected in changing PGE ratios with the ((Pt+Pd)/Ir) ratio varying from 0.71 to 23.62. Cliff also shows variation within the chondrite normalised curves with positive sloped (CF2, CF3 and CF13), jagged (CF14) and flat to negatively sloped (CF5 and CF8) profiles (Figure 4.27). The jagged and flat to negatively sloped chondrite normalised profiles are all marked by peaks in Ru chondrite normalised values.

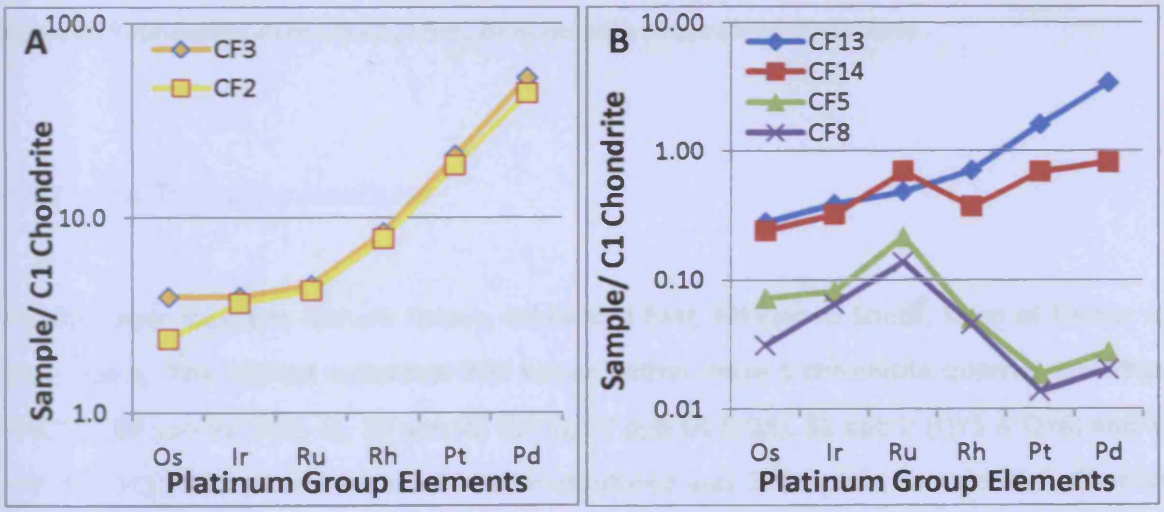

Figure 4.27: *Chondrite normalised graphs from Cliff chromitite samples.* ***A:*** *The two richest samples showing positive sloped profiles.* ***B:*** *The rest of the Cliff samples showing a variety of profiles. Note: The scales on the vertical axes differ from A to B. Chondrite values taken from Naldrett and Duke (1980).*

The PGE mineralisation at Harold's Grave is very different from that encountered at Cliff. Firstly, it is dominated by the IPGE, rather than Pt and Pd, with concentrations of Ir and Ru over 1 ppm in every sample analysed. Secondly, it is far more consistent, with total PGE grades varying between 4,771 and 14,168 ppb. This variation, although large, is less than an order of magnitude. Thirdly, PGE ratios ((Pt+Pd)/Ir) are remarkably consistent with the range going from 0.21 to 0.46. The consistency is also marked by the similar chondrite normalised curves, which are all negatively sloped, and can all be plotted on the same axes (Figure 4.27). Every analysed sample is marked by a peak in Ru chondrite normalised values.

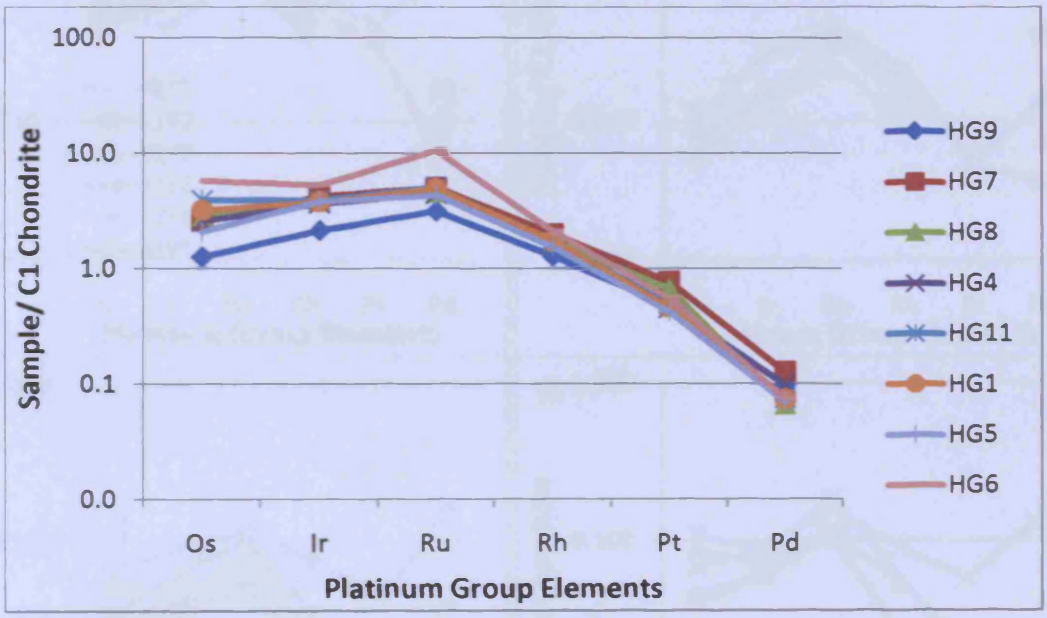

Figure 4.28: *Chondrite normalised graphs from Harold's Grave chromitite quarry*

4.5.2 The PGE-poor localities

The PGE-poor localities include Quoys, Nikkavord East, Nikkavord South, Keen of Hamar and Long Quarry. The highest individual PGE values within these 5 chromitite quarries are 59 ppb Pt (LQ2), 88 ppb Pd (NKS-1), 19 ppb Rh (QY5), 57 ppb Os (LQ3), 52 ppb Ir (QY5 & QY6) and 147 ppb Ru (QY5). The maximum total PGE encountered was 376 ppb in sample QY5. Chondrite normalised plots of the 5 chromitite pods reveal remarkable similarities between them, and also with the general profile shape observed at Harold's Grave.

That is, the profiles are broadly negatively sloping, but with a pronounced Ru peak (Figure 4.28). Another difference from Harold's Grave, aside from the absolute chondrite normalised values, is that the Pt/Pd ratio tends to be lower within the PGE-poor localities (0 – 12.33) than within Harold's Grave (8.57 – 19.03). There is also considerable variability between Pt and Pd, which is likely to be a reflection of the higher mobility of Pd as documented in numerous cases ((Fuchs and Rose, 1974; Lord, 1994; Seabrook *et al.*, 2004)).

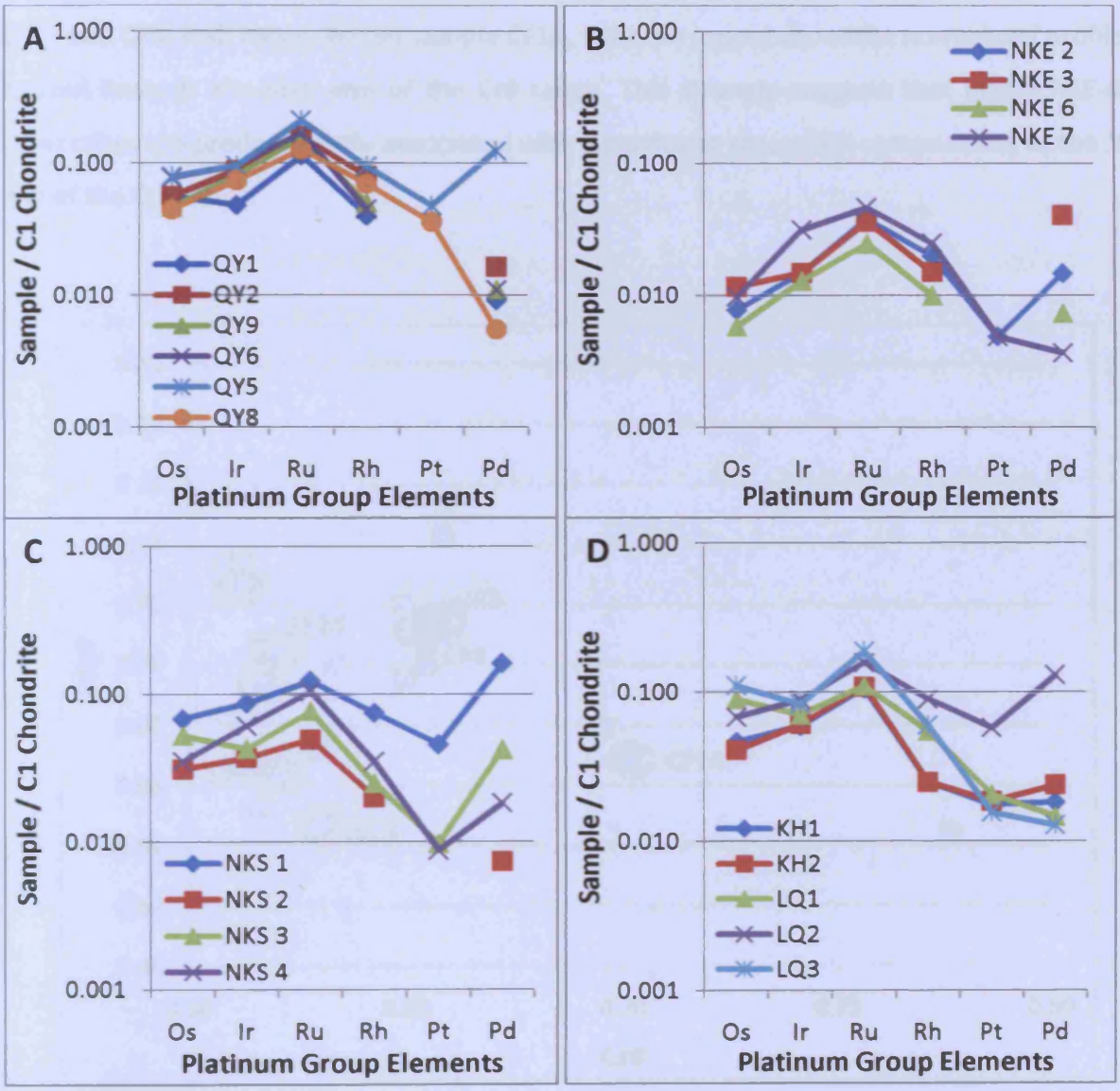

Figure 4.29: *Chondrite normalised graphs from the PGE-poor chromitite localities. A:Quoys, B: Nikkavord East, C: Nikkavord South, D: Keen of Hamar and Long Quarry. Some Pt values within Quoys, Nikkavord East and Nikkavord South contain zero values (values below detection limit), and therefore do not plot on a logarithmic scale.*

4.5.2.1 *The relationship of PGE concentration to chromite geochemistry - Cliff*

The Cliff chromitite samples are not geochemically unique, overlapping with samples from Long Quarry and Quoys (Figure 4.16 & 4.17). However, within the range of Cliff chromitite compositions the PGE-rich samples with pronounced positive sloped chondrite normalised curves (CF2, CF3, CF13, CL3, CL7 & 1349) are located towards the lowest end of the Cr# range (Figure 4.28). The two PGE-poor chromitite samples (CF5 and CF8) are both located towards the centre of the Cr# range (Figure 4.29), whilst the relatively intermediate (relative to CF2, CF13 and CF3) PGE concentrated sample CF14, with the jagged chondrite normalised profile is located towards the high end of the Cr# range. This strongly suggests that highly PGE-rich chromitites are predominantly associated with a particular chromitite composition, at the low end of the Cr# range.

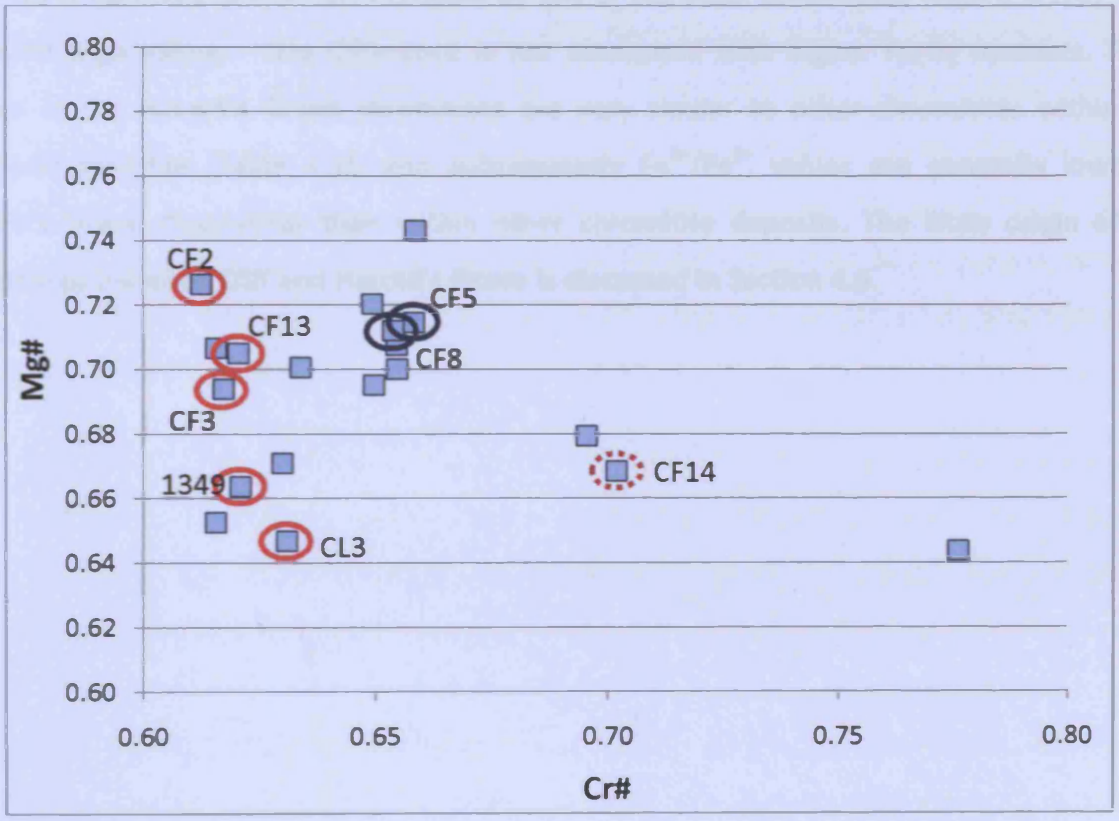

Figure 4.30: *Plot of Cr# - Mg# for the Cliff chromitite samples. Circled data points refer to samples with associated PGE analyses. Red circles indicate highly PGE-enriched samples with strong positively sloped chondrite normalised plots. Samples 1349 and CL3 are also circled in red as previous mineralogical studies had indicated the presence of numerous PGM (Prichard et al. 1989). The dashed red circle indicates a moderately enriched sample with a jagged chondrite normalised plot. Blue circles represent PGE-poor samples.*

4.5.2.2 The relationship of PGE concentration to chromite geochemistry – Harold's Grave

In contrast to the Cliff chromitite samples, the Harold's Grave samples are uniformly PGE-enriched, and also geochemically distinct from the rest of the analysed Shetland chromitites. This geochemical distinctiveness is observable with two main criteria. Firstly, the chromite grains within the chromitite samples are all enriched in V, Zn and Ga (Figure 4.18 to such an extent that the lowest concentrations within Harold's Grave are still higher than all the other values recorded within the Shetland chromitites). Furthermore, the highest Mn, Ti, and Co values within the Shetland chromitites are all contained within Harold's Grave, though with some overlap with other chromitite pods at the lower values (Figure 4.18). The second main difference is observed in the Mg# - Cr# plots, where the region occupied by the Harold's Grave samples is distinctly below that occupied by any of the other chromitites (Figure 4.17a) – i.e. at lower Mg# values. This difference is not associated with higher Fe_2O_3 contents. Fe_2O_3 values of the Harold's Grave chromitites are very similar to other chromitites within the Shetland ophiolite (Table 4.2), and subsequently Fe^{3+}/Fe^{2+} values are generally lower in Harold's Grave chromitites than within other chromitite deposits. The likely origin of the differences between Cliff and Harold's Grave is discussed in Section 4.6.

4.6 Discussion

This discussion focuses on data specific to the Shetland ophiolite, such as tectonic setting, the variation of major and trace elements with stratigraphy and the relationship of PGE concentrations to chromitite geochemistry. A detailed discussion on chromite inclusions and chromitite petrogenesis is reserved for Chapter 6.

4.6.1 Tectonic Setting

Initial theories surrounding the tectonic setting of the Shetland ophiolite argued, on the basis of a metamorphosed MORB sequence beneath the Shetland ophiolite, that it represents obducted passive margin formerly located on the junction between Laurentia and the Iapetus ocean (Spray, 1988). More recently it has been proposed that, based on the presence of the Cliff Hills Group to the south, that the ophiolite formed within an intra-continental setting (Flinn and Oglethorpe, 2005) (Figure 4.31). Flinn and Oglethorpe (2005) argue that the sedimentary and volcanic infill of the Cliff Hills group, characterized by greywackes, turbidites, volcaniclastics and basic magmatic rocks (including basalts and possibly komatiites (Flinn and Moffat, 1985) is typical of an extensional basin. Eastward subduction of the intra-continental crust beneath this basin was followed by westwards obduction of the subducting slab (Flinn and Oglethorpe, 2005) (Figure 4.31).

From this study and the literature, it is apparent that there are two problems with this later model. Firstly, Stern, (2004) suggests that it is extremely difficult to obduct the subducting slab. Secondly the highly depleted nature of the mantle sequence, characterized by harzburgite rather than lherzolite suggests significant partial melting has already occurred within the ophiolite – this is confirmed by the Cr#-TiO_2 values of chromite grains within the harzburgite (Figure 4.26). Flinn and Ogelthorpe (2005) argue that the subducting slab became hydrated during subduction, along with the mantle wedge, presumably leading to the partial melting of the downgoing slab and the formation of the depleted harzburgite residue. However, they provide no mechanism for hydrating the downgoing slab, and there is no reason subduction would lead to anything other than hydration of the mantle wedge as water gets driven off the subducting slab. An amendment is therefore proposed to the tectonic history of the Shetland ophiolite in light of these two points (Figure 4.32).

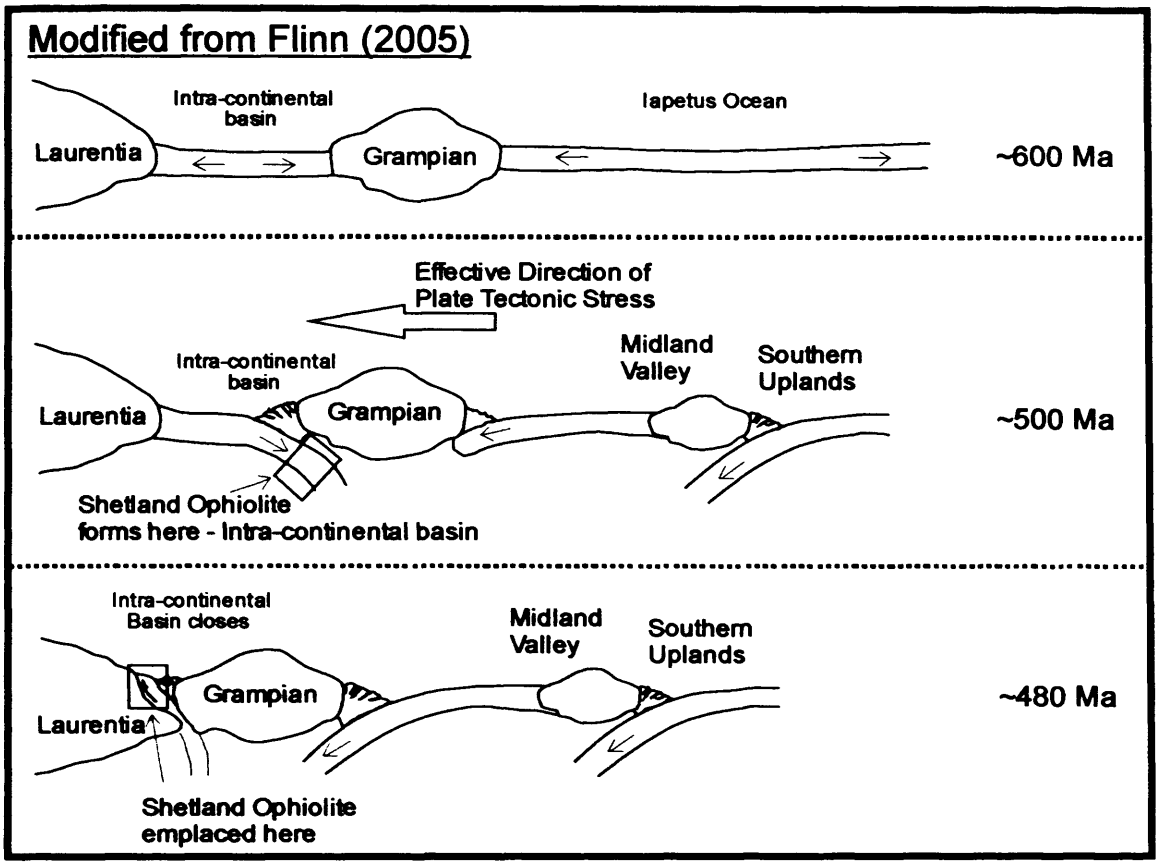

Figure 4.31: *Tectonic history of the Shetland ophiolite. Adapted from Flinn and Oglethorpe, 2005.*

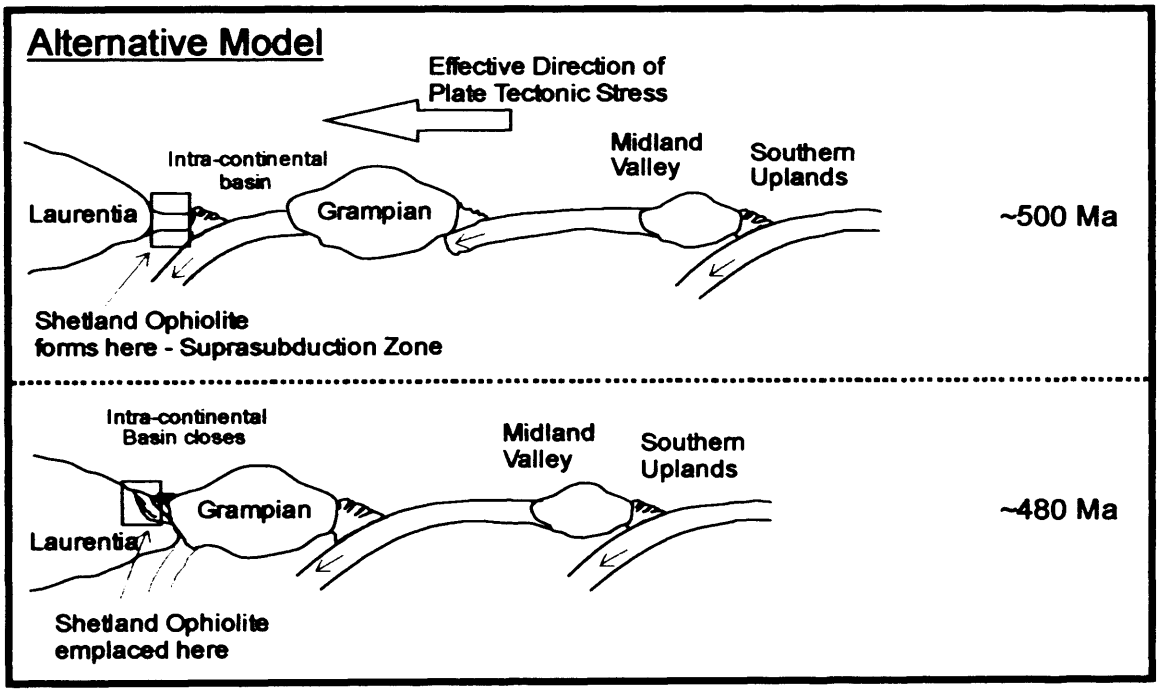

Figure 4.32: *Revised tectonic history of the Shetland ophiolite, showing the last two stages in the evolution of the Shetland ophiolite. The position at ~600 Ma is as for Figure 4.31.*

It is proposed that the Shetland ophiolite must lie in a supra-subduction zone (SSZ) setting, above the mantle wedge of a westward dipping subduction zone (Figure 4.32). The SSZ nature of the ophiolite is supported by analyses of harzburgite from the Shetland ophiolite which unambiguously suggest a SSZ setting (Figure 4.26). That this SSZ setting was most likely situated above a westward dipping subduction zone, rather than an eastward dipping subduction zone, is based on the geophysical data reported in the Flinn and Oglethorpe paper. They show that the suture zone associated with the ophiolite lies to the east, and furthermore that the basal thrust dips eastwards. If the ophiolite formed above a SSZ then this suggests that the subducting slab dipped down from the east to the west – i.e. was westward dipping.

4.6.2 Chromitite composition

4.6.2.1 Interpod variation

Within the Al'Ays ophiolite the study of 35 separate chromitite bodies enabled an investigation into the variation in chromitite geochemistry with stratigraphical height. With the limited thickness of the Shetland ophiolite (particularly of the mantle sequence) and the focus on intra-chromitite variation within 7 chromitite localities there could not be the same resolution at the Al'Ays ophiolite on stratigraphical variations. Nevertheless, there are some interesting observations to be drawn from the stratigraphical relationships.

4.6.2.1.1 Interpod variation (i) Cr# vs. Mg# plot

The first observation is that the chromitite geochemistry of chromitites within Shetland displays two main trends on a Cr# - Mg# plot (see Section 3.6.2 for similar trends in the Al'Ays stratigraphic groups and Section 6.2.3 for further discussion). The first trend (equivalent to trend A in Section 3.6.2 & 6.2.3) is a strong inverse relationship between Cr# and Mg# which is apparent within chromitite pods (see Section 4.6.2.2.1 for further discussion). The second trend is a direct relationship between Cr# and Mg# (i.e. Mg# values decrease as Cr# values decrease, this is equivalent to trend B in Section 3.6.2 & 6.2.3). This is displayed to some extent within the Cliff chromitite pod (see Section 4.6.2.2.2 for further discussion) but is otherwise only observed between the Harold's Grave chromitite and the rest of the chromitite pods.

The second trend of decreasing Cr# with decreasing Mg# is equivalent to a fractionation trend ((Naldrett *et al.*, 2009), see also Section 3.6.2 and 6.2.3). If fractionation of olivine and chromite is occurring between chromitite samples within the Shetland ophiolite then the Mg# of both chromite and olivine grains should be lower, and this is certainly what is observed (e.g. Figure 4.25 for Fo# of olivine in dunite envelope, and Figure 4.33 for Mg# of chromite in chromitite). This suggests that the parental melt from which the Harold's Grave chromitite crystallized may have fractionated relative to the other Shetland chromitite deposits (see also 4.6.2.1.3 for discussion on trace element variations).

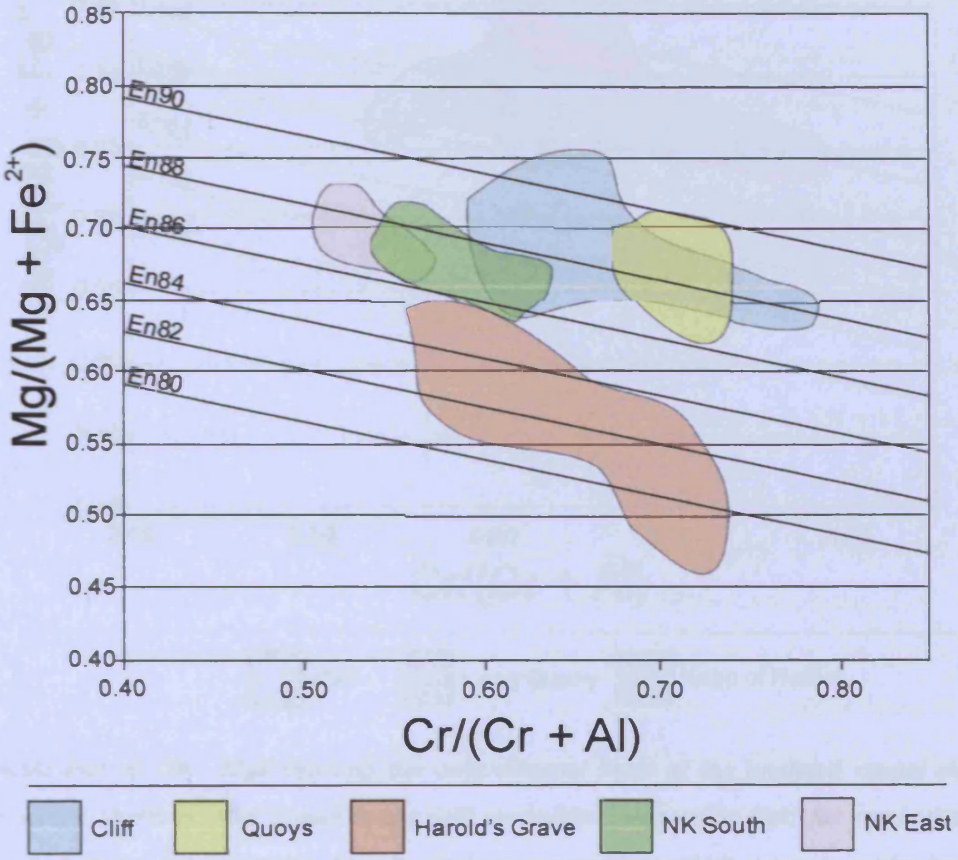

Figure 4.33: *Plot of Cr# - Mg# showing the compositional fields of the analysed mantle chromitite deposits within Shetland. The contours represent the expected variation in Mg# ratio of the spinel which would result from variation in the Cr# of the same spinel in equilibrium with a liquid of constant Mg# (it is expressed by En content of orthopyroxene which would be in equilibrium with this liquid – these lines are adapted from Naldrett et al. 2009).*

Chromitites in the crustal sequence display the same two trends that were observed within the mantle sequence (Figure 4.34), namely an inverse relationship between Cr# and Mg# observed within chromitite pods and a relationship of decreasing Cr# and Mg# observed between chromitite pods. The decrease in Cr# and Mg# from Long Quarry to Keen of Hamar is indicative of a simple fractionation process operating in the magma chamber.

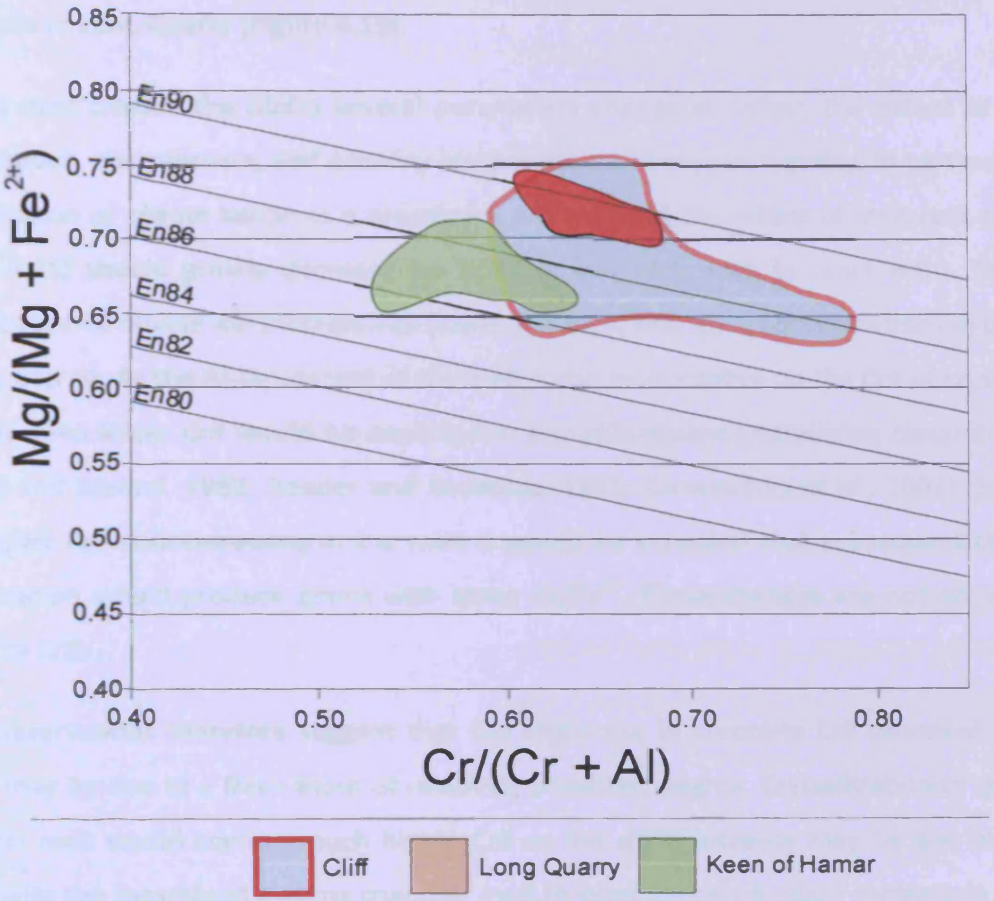

Figure 4.34: *Plot of Cr# - Mg# showing the compositional fields of the analysed crustal chromitite deposits within Shetland. Also shown is the Cliff chromitite composition field for comparison. Long Quarry, which is the deeper crustal deposit, displays compositions which are very similar to the Cliff chromitite deposit Long Quarry is the deeper crustal chromitite, with Keen of Hamar slightly shallower. The contours represent the expected variation in Mg# ratio of the spinel which would result from variation in the Cr# of the same spinel in equilibrium with a liquid of constant Mg# (it is expressed by En content of orthopyroxene which would be in equilibrium with this liquid – these lines are adapted from Naldrett et al. 2009).*

4.6.2.1.2 Interpod variation - (ii) Cr/Fe^{2+} and Cr#

The second observation is that the transition from mantle to crust does not result in a decrease in Cr/Fe^{2+} and Cr# values, which may be expected if only simple fractionation processes were operating (Figure 4.19). In fact a slight increase is observed in both these ratios in Long Quarry, compared with the Nikkavord sites (Figure 4.19). Indeed, the Cr/Fe^{2+} ratio in chromite actually rises from Harold's Grave to Nikkavord South/Nikkavord East and then again to Long Quarry (Figure 4.19).

When a melt crosses the Moho several parameters change including, the extent of olivine crystallization, the pressure, and possibly temperature and oxygen fugacity. In particular bulk crystallization of olivine becomes a prominent process, and the extent of melt-rock reaction (Figure 4.25) should greatly decrease (as there is very little rock to react with). This bulk crystallization of olivine will increase Fe# (lower the Mg#) and Al_2O_3 concentrations in the melt (see Chapter 6). As the Al_2O_3 content of the melt is the main control on the Cr# of crystallizing chromite then lower Cr# would be expected in any subsequent crystallizing chromite grains (Maurel and Maurel, 1982; Roeder and Reynolds, 1991; Kamenetsky *et al.*, 2001). Similarly, with higher Fe# concentrations in the melt it would be expected that subsequent chromite crystallization would produce grains with lower Cr/Fe^{2+}. These changes are not observed in Cr/Fe^{2+} or Cr#.

These observations therefore suggest that the slight rise in chromite Cr# observed in Long Quarry may be due to a fresh input of relatively primitive magma. Crystallization of chromite from this melt would contain much higher Cr# so the slight increase may be due to partial mixing with the incumbent magma chamber melt to produce only a minor increase in Cr#. An influx of a more primitive magma source would also be reflected in the Fo# of the crustal dunites, which should maintain a high forsterite content. This is indeed what is observed and may explain why all the analysed crustal olivine grains have Fo#'s which lie within the OSMA (Figure 4.25).

In addition, the change in physical parameters when switching from a melt conduit to an overlying melt chamber may also affect the Cr# and Cr/Fe^{2+} ratio of crystallizing chromite. A drop in pressure may raise the Cr# value (Roeder and Reynolds, 1991). This effect is only slight (see Section 3.6.2), but as noted in chapter 3 may be sufficient to initially raise the Cr#. However, lowering the temperature or adjusting the fO_2 has only negligible effects on the Cr# of the crystallizing chromite grain (Roeder and Reynolds, 1991).

A fresh influx of primitive melt might be expected to effect the trace element contents of the chromite grains as well (e.g. lower TiO_2 contents). This is not observed (Figure 4.20 & Figure 4.21), as the trace element contents of Long Quarry tend to lie at the midpoint between the Nikkavord trace element contents and the Keen of Hamar trace element contents (see next Section 4.6.2.1.3) This may be due to the mixing of a new more primitive melt with an incumbent partially evolved melt. In summary, the data suggest that the small rise in Cr/Fe^{2+} and Cr# may be caused by a fresh influx of more primitive melt into the magma chamber which may partially mix with the incumbent melt.

4.6.2.1.3 Interpod variation - (iii) Trace element variations

The third observation is that trace element concentrations within chromite grains seem to follow two patterns with stratigraphic height. The first is defined between Cliff, Quoys and Harold's Grave, and the second is defined between Nikkavord South, Nikkavord East, Long Quarry and Keen of Hamar (Figure 4.20 & Figure 4.21). A similar pattern is observed within Cr/Fe^{2+} as well (Figure 4.19 & Section 4.6.2.1.1). There are two possible explanations for this. The first is that it defines the dominance of different processes at different stratigraphic heights within the ophiolite. Within the mantle sequence orthomagmatic fractionation processes were dominant between Cliff, Quoys and Harold's Grave leading the pattern of decreasing Cr/Fe^{2+} and Cr# with increasing TiO_2, Ga, Co, V and Zn (melt-rock reaction is also expected to effect the melt composition and this is covered in more detail within Chapter 6 - in summary though, the dissolution of pyroxene into the melt partially cancels out the effect of olivine crystallization from the melt). From Nikkavord South to Keen of Hamar the interplay of processes changes with the possible effects of magma mixing and pressure changes overprinting simple fractionation changes. In order for this to be true Nikkavord South and Nikkavord East may have to be considered as part of the cumulate sequence, at least in terms of allowing magma mixing and pressure decreases to be a factor in changing the composition of crystallizing chromite. Evidence for this was found by Lord (1991) who after detailed mapping of the contact suggested that both deposits may lie in a transition zone between the mantle and the cumulate sequence. Further evidence for fractionation is found with the presence of cumulus magmatic sulphide (Table 4.1) within Harold's Grave and moderate concentrations of PPGE (~1 ppm, Table 4.5)

The second possibility relates to the relatively high trace element concentrations that are present within Harold's Grave (Figure 4.20 & Figure 4.21). The two identified patterns rely in part on these high trace element concentrations and they may be explainable by processes other than fractionation. Previous work on chromite in komatiites suggested that elevated trace elements, together with lower Mg#, were caused by the extensive reaction of chromite with 'trapped' intercumulus melt and a prolonged cooling history (Barnes, 1998). Although possible, the concept of a 'trapped' intercumulus phase seems unlikely due to the lack of large amounts of interstitial silicates (i.e. an initially trapped intercumulus melt may have escaped, or only been temporarily trapped). Nevertheless, the large dunite envelope may represent evidence for a significant volume of intercumulus melt which had time to react extensively with the wallrock, and precipitate olivine. If the large dunite envelope is evidence for an extensive body or intercumulus melt then chromite geochemistry may have been modified through reaction with this melt (Barnes, 1998). A prolonged cooling history where crystallizing chromite has time to re-equilibrate with a larger amount of melt is unlikely, as there are no processes occurring within the mantle that would sufficiently decrease the cooling rate (as opposed to the crust where hydrothermal circulation may decrease the cooling rate e.g. Coogan *et al.*, 2002). In summary, it appears plausible that both fractionation and reaction with a partially trapped intercumulus melt has produced the higher trace element concentrations and lower Mg# values observed within the Harold's Grave chromitites

4.6.2.2 Intrapod variation

Intrapod (within pod as opposed to between pod) geochemical variation has not been explored in much detail within the published literature but such investigations that have been made have recorded the homogeneity of chromitite pod compositions (Bakor *et al.*, 1976), (Johnson, pers. comm.). It is therefore particularly interesting to observe the extreme heterogeneity within individual chromitite pods in the Shetland ophiolite, especially in the two PGE-rich chromitite deposits (Cliff and Harold's Grave) (Figure 4.17 & 4.18), which have the highest range of chromite compositions.

4.6.2.2.1 Intrapod variation – (i) Cliff

Using average chromite analyses in each thin section, Cliff chromitite compositions appear to form two separate trends. The first is an inverse correlation between Cr# and Mg# (Figure 4.35, trend A). The second trend is one of decreasing Cr# and decreasing Mg# (Figure 4.35, trend B). Upon further analysis, the individual grain analyses were split into two subsets based on their TiO_2 content (Figure 4.36), with every analysed chromite grain used. As can be observed, chromite grains with a high TiO_2 content form a pronounced trend B (as well as a possible second trend, Bii – see Figure 4.36) whilst chromite grains with a low TiO_2 content form a clear trend A. High-Ti grains also have lower Al_2O_3 contents as can be inferred from their lower Cr#, and slightly different Fe contents (Figure 4.37).

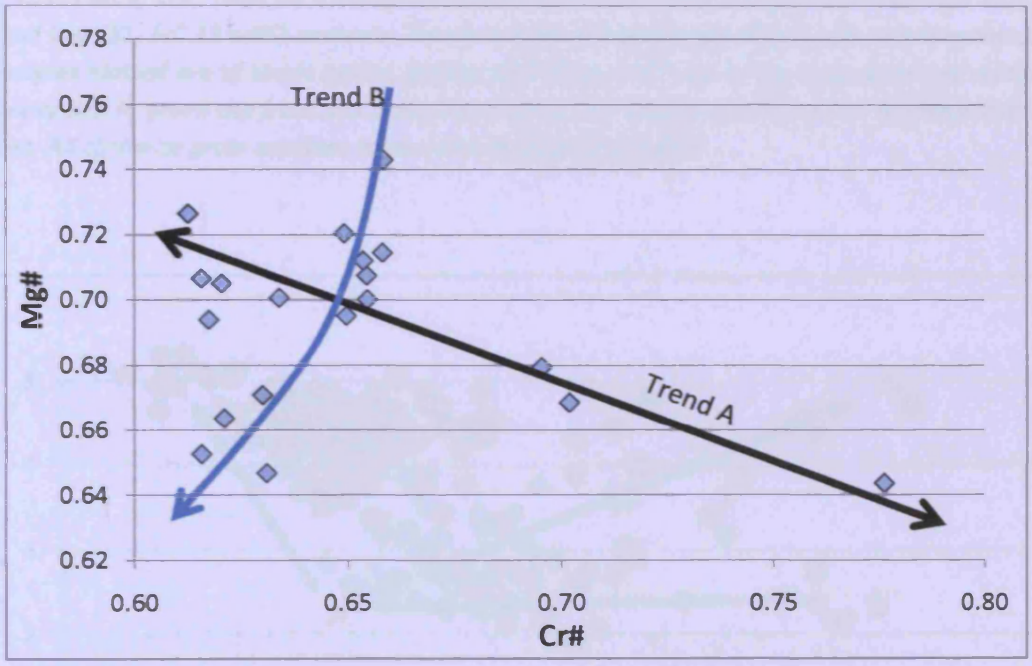

Figure 4.35: *Plot of Cr# - Mg# for the Cliff chromitite deposit. Trends A and B are highlighted on the graph. Each point is an average of 8-10 analyses in a prepared section.*

Investigating the Cr# - TiO_2 trend of the Cliff chromitites and dunites reveals two more trends, which to avoid confusion are labelled trend D and trend E (Figure 4.38). Trend D shows a pattern of decreasing Cr# with increasing TiO_2, whilst trend E shows a pattern of increasing TiO_2 with near constant or slightly increasing Cr#.

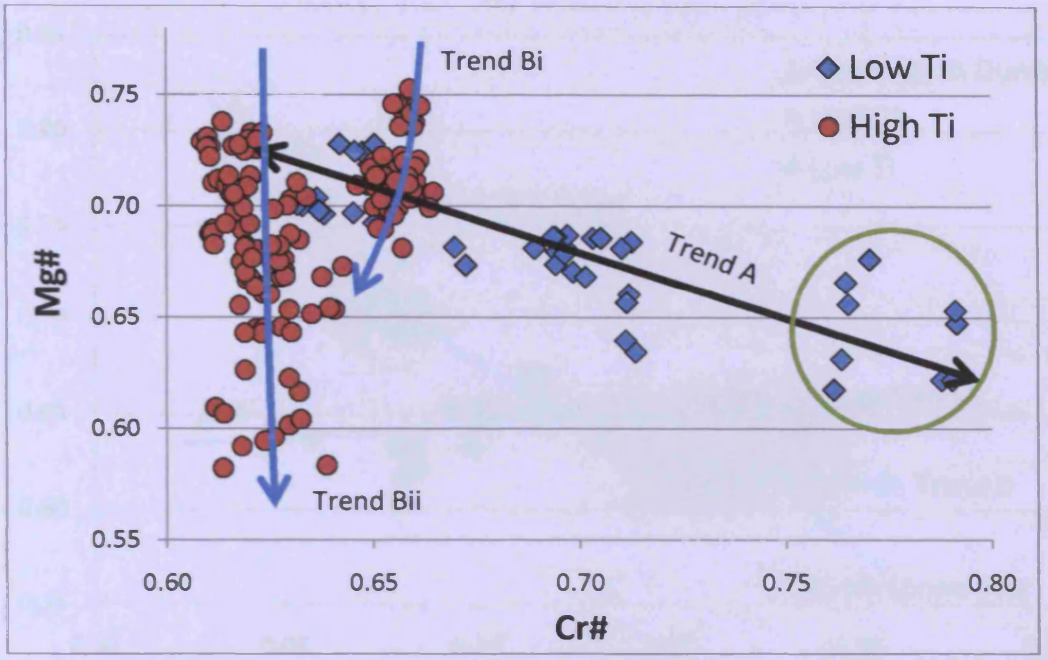

Figure 4.36: *Plot of Cr# - Mg# for the Cliff chromitite deposit, showing the split between high TiO_2 (>0.13 wt%) and low TiO_2 (<0.13 wt%) contents. Trends A & B are highlighted with B split into two trends; Bi & Bii. Analyses plotted are of single grains, groups of 8-10 of which are in the same prepared section. The analyses circled in green are from one sample and show both large variation and a bimodal distribution of values. All chromite grain analyses taken from chromitite samples.*

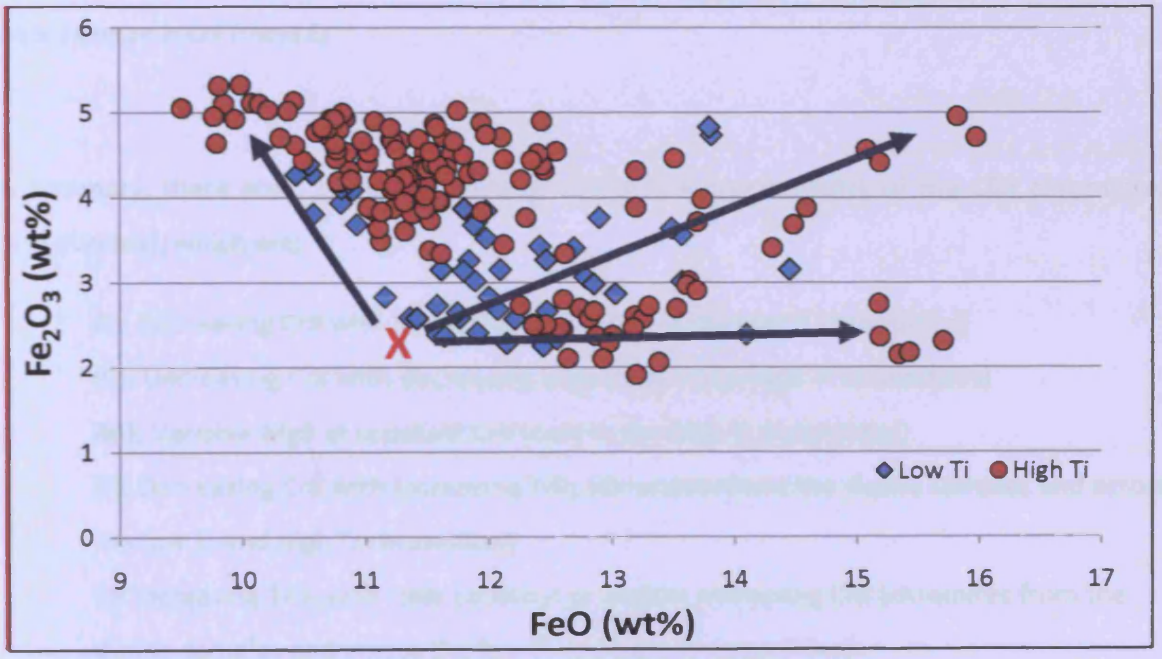

Figure 4.37: *Fe_2O_3 vs. FeO graph showing the contrast between high TiO_2 and low TiO_2 chromite grain analyses. There is a wide spread of Fe_2O_3 and FeO values across both high and low TiO_2 chromite grains though with a tendency for the high TiO_2 grains to contain higher Fe_2O_3 and FeO values. Note: starting from X both FeO and Fe_2O_3 are higher in the high Ti Group than in the low Ti Group (i.e. Fe (total) increases from low Ti to high Ti). All chromite grain analyses taken from chromitite samples.*

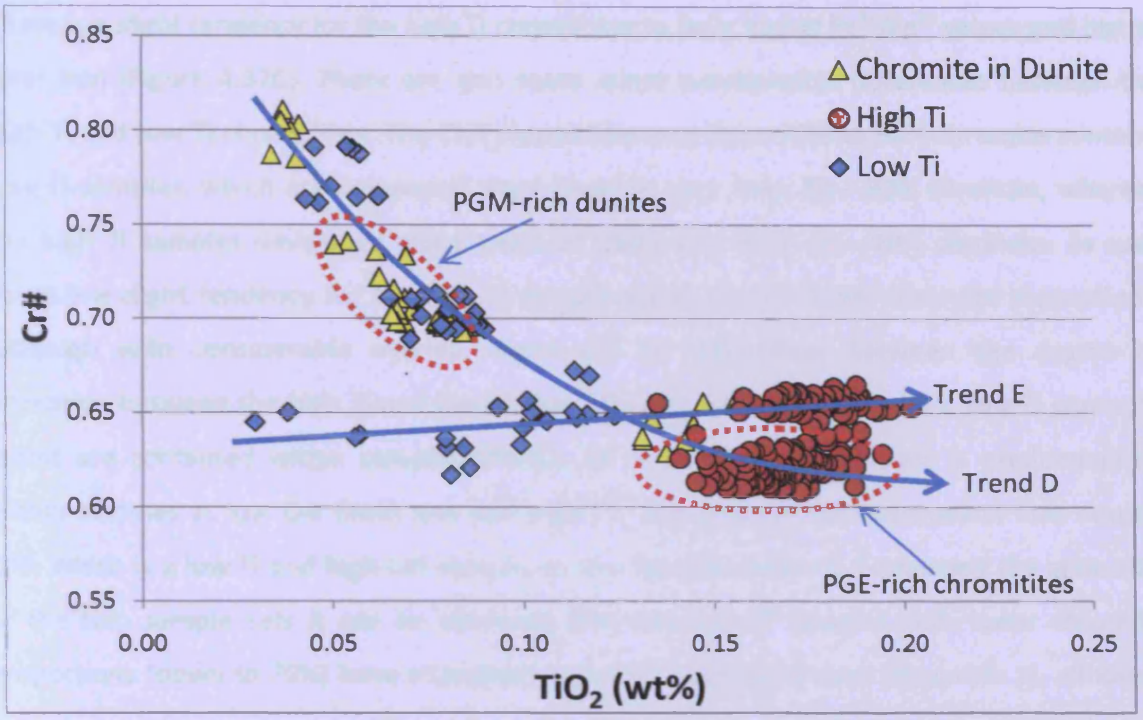

Figure 4.38: *Cr# vs. TiO_2 for the Cliff deposit showing the composition of chromite from both dunite and chromitite samples. Including the position of the PGE-rich dunite and chromitite samples there is a clear trend of increasing TiO_2 content with decreasing Cr# content (trend D). The dunites where not quantitatively analysed for PGE but were observed using scanning electron microscopy to be rich in sulfides and PGM (Appendix 1). Also shown is a trend of increasing TiO_2 content with a concomitant slight increase in Cr# (trend E).*

In summary, there are 5 identifiable trends within the geochemistry of the Cliff chromitites (and dunites), which are;

A): Decreasing Cr# with increasing Mg# (only in the low Ti chromitites)

Bi): Decreasing Cr# with decreasing Mg# (only in the high Ti chromitites)

Bii): Variable Mg# at constant Cr# (only in the high Ti chromitites)

D): Decreasing Cr# with increasing TiO_2 (chromites from the dunite samples and across the low Ti and high Ti chromitites)

E): Increasing TiO_2 with near constant or slightly increasing Cr# (chromites from the dunite samples and across the low Ti and high Ti chromitites)

There is a slight tendency for the high Ti chromitites to have higher Fe^{3+}/Fe^{2+} values and higher total iron (Figure 4.37C). There are also some minor petrographic differences between the high Ti and low Ti chromitites. The Cliff chromitites vary from 70% to 90% chromite content. Low Ti samples, which are developed along trend A, vary from 80 – 90% chromite, whereas the high Ti samples developed along trend Bi (&Bii) vary from 70 - 90% chromite. As such there is a slight tendency for the high Ti sample set to contain lower chromite proportions, although with considerable overlap. There are no differences between the degree of alteration between the high Ti and low Ti chromite samples (see Appendix 1, low Ti chromite grains are contained within samples CF9-11, 14 & 16). Sulphide content is predominantly within samples at low Cr# (both low and high Ti), though with the observation that sample CF9, which is a low Ti and high Cr# sample, is also sulphide-bearing. Comparing the grain size of the two sample sets it can be observed that the high Ti samples with lower chromite proportions (down to 70%) have a tendency towards larger grain sizes (Appendix 1), although as with overall chromite proportions there is a large overlap in chromite grain sizes between high Ti and low Ti samples. This may be a product of fracturing, in the sense that the size being measured is sometimes not 'true' grain size but influenced by 'breakage size'. As such the samples with higher proportions of chromite will take up more of the brittle deformation within the chromite grains leading to smaller apparent grain sizes.

Interpreting these trends accurately is of potential importance due to the PGE contents of the chromitites (Figure 4.38). The very high PGE concentrations are associated with the high Ti chromitites (so along trend Bi (or Bii)) but particularly within the dunites and chromitites which delimit trend D. Indeed all the analysed PGE-rich samples, both chromitites and dunites lie on this trend (though not all samples that lie on this trend are PGE-rich). There were no PGE-rich concentrations observed with the chromitites that make up trend E and the two poorest PGE values lie within this trend.

Trend A (decreasing Cr# with increasing Mg#) may be explained by a changing magma inputs, with the changing Cr/Al ratio being reflected by reciprocal changes in Mg/Fe ratio during spinel crystallization (Figure 4.35, see also Chapter 6). Trend A may be generally interpreted as changes in melt composition without the precipitation of silicate. However, these same samples also make up part of **trend D**, which is increasing TiO_2 with decreasing Cr# - see discussion on trend D, which might make an explanation of changing magma input too simplistic.

Trend Bi (decreasing Cr# with decreasing Mg#) may be explained by fractionation whereby the Mg content of the melt decreases due the crystallization of olivine (cf. Ulmer, 1989) and/or chromite, meaning that subsequent chromite grains have lower Mg# and lower Cr# (lower Cr# are due to the slight increase in Al_2O_3 concentrations due to the crystallization of olivine). In contrast to trend A, changes along trend B may be generally interpreted as a result of the co-precipitation of silicate (i.e. olivine) and chromite. It could also be explained by reaction with trapped intercumulus melt (Roeder and Campbell, 1985). Either explanation may account for the slightly higher Fe^{3+}/Fe^{2+} ratios, which may occur as the melt differentiates.

Trend Bii (near constant Cr# with variable Mg#) may be explained by post-solidus re-equilibration between olivine and chromite and may be partly due to the lower chromite proportions within some of the high Ti chromitites. These lower proportions allow for greater Fe-Mg exchange and re-equilibration between the chromite grains and the silicates leading to a potential wide range of Mg#. This is labelled trend Bii as it also involves the presence of olivine with chromite but with the trend a result of post-solidus re-equilibration rather than changes in the melt composition due to the simultaneous crystallization of chromite and olivine. However, in some instances the variation in Mg# within a section is very large (e.g. the Mg# in sample CL3 varies from 0.58 to 0.69). This variation, in a chromitite dominant section (85% chromite) may be too large for post-solidus re-equilbration and may instead reflect the presence of a bulk sulphide liquid on the liquidus at the time of chromite crystallization within these samples. During cooling (from ~1600°C to 900°C), chromite will be non-stoichiometric and contain vacant Fe^{2+} sites, which may be filled by interaction with an interstitial magmatic sulphide liquid (Naldrett and Lehmann, 1988, Naldrett *et al*, 2009). As sample CL3 is a sulphide-rich chromitite the large range in Mg# may be due to interaction of chromite with this sulphide component.

Trend D (increase in TiO_2 with decreasing Cr#) this is typical of two main processes, either fractionation or reaction with a trapped intercumulus melt (Roeder and Campbell, 1985). It suggests that the low Ti chromitites and some of the high Ti chromitites, together with the chromite from the dunite samples formed due to one of the two cited processes. During fractionation or reaction with a trapped intercumulus melt, it is expected that the Mg# of the crystallizing chromite would decrease in a direction along trend B (e.g. Barnes, 1998; Naldrett *et al.*, 2009; Figure 4.35) and this is not observed throughout the low Ti chromitites and selected high Ti chromitites (Figure 4.39). That trend D involves chromite from dunites suggests that chromite and olivine are co-precipitating and being subsequently separated.

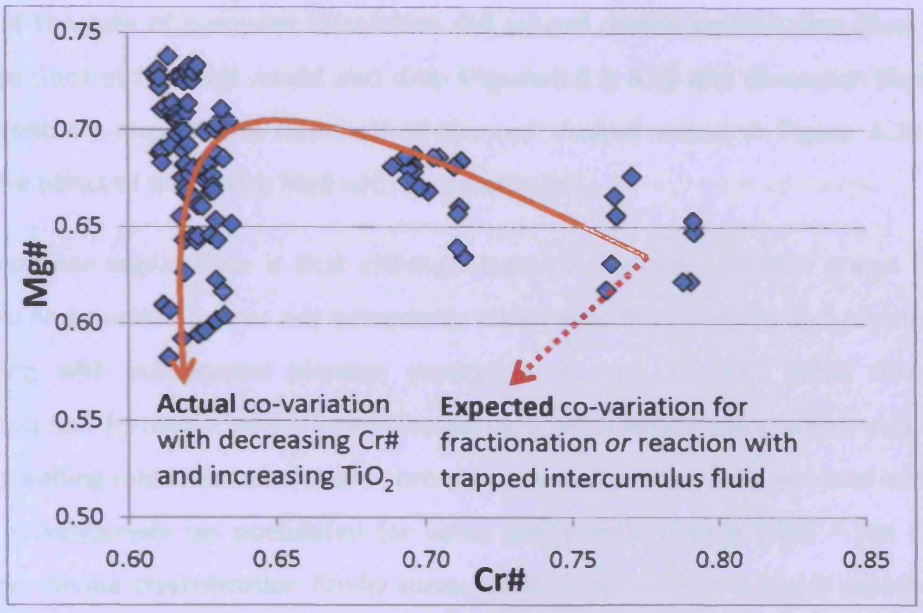

Figure 4.39: *Cr#-Mg# plot for the low Ti and high Ti chromitite samples which make up trend D in Figure 4.38. Chromite analyses from dunite samples are excluded due to the dominant effect of post-solidus re-equilibration on the Mg/Fe ratio of chromite when chromite is a minor phase. With decreasing Cr# and increasing TiO_2 – i.e. fractionation or reaction with a trapped intercumulus melt - the expected co-variation of Cr# with Mg# is marked by the red dashed arrow (Barnes, 1998; Naldrett et al. 2000). The actual co-variation follows a markedly different pattern.*

The actual change in Mg# for samples from trend D is initially an increase in values with decreasing Cr# followed by a sharp decrease at constant Cr# (trend A followed by trend Bii). This latter change of trend Bii is largely interpreted as the effect of bulk sulphide liquid interstitial to the chromite grains and the increasing uptake of Fe^{2+} by chromite as a result (Naldrett and Lehmann, 1988; Naldrett *et al*, 2009).

The initial increase in Mg# with decreasing Cr# (trend A) in a system where chromite and olivine is co-precipitating is very hard to explain. It may be related to the added complexity of melt-rock reaction within ophiolitic settings (See Figure 6.7 and associated discussion). Since melt-rock reaction involves the dissolution of orthopyroxene (or clinopyroxene) there is a re-introduction of Mg and Fe into the melt. If the rate of pyroxene dissolution greatly exceeds the volume of olivine precipitation then there will be no significant depletion of Mg and Fe from the melt (indeed there may be a slight increase in the melt - see Figure 6.7 & 6.8). The Mg# number of crystallizing chromite will only significantly decrease if olivine is crystallizing from the melt at a rate equal to, or greater than, the dissolution of pyroxene into the melt (see Figure 6.7 & discussion therein).

However, if the rate of pyroxene dissolution did exceed olivine precipitation then the Al_2O_3 and TiO_2 content of the melt would also drop (Figure 6.8 & 6.12 and discussion therein). This would essentially reverse the direction of the red dashed arrow in Figure 4.39 and not produce the effect of increasing Mg# with decreasing Cr#.

Another possible explanation is that although trend D involves chromite grains from both chromitites and dunites it does not necessarily follow that the chromite and olivine were co-precipitating with subsequent physical separation. It may be that initial chromite-only precipitation had formed a poorly consolidated chromitite segregation, which was disturbed by later upwelling melts. Some of these chromite grains may then have become included into the melt as xenocrysts (as postulated for some grains with sample C462 – see Chapter 3) before later olivine crystallization finally surrounded them. As such trend D represents a co-variation occurring in a melt which is just (initially at least) crystallizing out chromite, with the composition of the melt becoming progressively richer in TiO_2 and Al_2O_3. The progressive change in melt composition may occur through the role of water immiscibility (see Section 6.2.4). If the initial melt was boninitic then water unmixing may produce a residual, partially devolatilized melt which is more tholeiitic (e.g. as suggested by Tamura, (1994) who noted that boninites may be 'dried' during ascent to produce tholeiitic melts – except in this case the 'drying' is *in-situ*). As devolatilisation proceeds, subsequent chromite crystallization from the residual silicate melt may be of higher Mg#, higher TiO_2 and lower Cr# chromite grains. This model suggests that localized fractionation was caused by progressive devolatilisation of the melt, leading eventually to sulphur saturation and the concentration of anomalous amounts of PGE (Figure 4.38). The later crystallization of olivine which incorporates chromite xenocrysts may also gather some of the PGE-rich bulk-sulphide liquid explaining the observation of PGM-rich dunites (Figure 4.38). Within this model one point remains unclear, namely why does the first chromitite sample, with the highest Cr#, also contain moderate sulphide contents (sample CF9 – Appendix 1).

Trend E (increase in TiO_2 with near constant or slightly increasing Cr#) is analogous to the effects of melt-rock reaction on the composition of chromite grains within peridotite, although in this instant it may be the reaction of new melt with already formed chromitite. If the new melt has a similar Cr/Al ratio to the crystallized chromite grains but higher TiO_2 contents then the change in composition caused by the reaction would be to increase the TiO_2 content at near constant Cr#.

In summary it appears that the five trends observed at Cliff may be the interplay of up to five different processes (orthomagmatic fractionation, fractionation by water immiscibility, post-solidus re-equilibration, melt-rock reaction and equilibration of chromite with an unmixed bulk sulphide phase) with fractionation by water immiscibility and sulphur saturation (trend D) possibly playing a key part in the formation of the PGE-rich concentrations in both the dunites and the chromitites. Furthermore, with respect to the OSMA and Cr#-TiO_2 plots (Figure 4.25 & 4.26) it seems apparent that dunite samples which were the product of fractional crystallization may plot within the OSMA (e.g. (Arai, 1994)), as only the most fractionated dunite sample plots outside the OSMA.

4.6.2.2.2 Intrapod variation – (ii) The other chromitite pods (Harold's Grave, Quoys)

All the chromitite pods display an inverse correlation between Cr# and Mg# - that is as Cr# increases, Mg# decreases and vica versa (Figure 4.33 & Figure 4.34). This is particularly so of Harold's Grave and Quoys located within the mantle sequence. This is most likely to be caused by changing the composition of the upwelling melt, specifically in terms of its Al_2O_3 content (see also, Section 3.6.1)(Naldrett *et al.*, 2009) and may suggest that the melt composition at any one chromitite pod was evolving through time. Using the empirical formula linking the Al_2O_3 content of the chromite and that of its parental melt ((Maurel and Maurel, 1982; Kamenetsky *et al.*, 2001), Equation 1), the variation in the Al_2O_3 content of the melt required to produce the variation in Al_2O_3 content of the chromite grains was investigated.

$$ln(\text{wt\% } Al_2O_3 \text{ in melt}) = 0.41322 \times ln(\text{wt\% } Al_2O_3 \text{ in chromite}) + 1.38529 \quad (1)$$

The Cr# of the Harold's Grave chromitites varies from 0.57 to 0.72 and this corresponds to a variation in Al_2O_3 content of 13.91 wt% to 22.68 wt%. Using equation (1) this range of Al_2O_3 content in chromite is equivalent to a variation in the melt Al_2O_3 content of just 11.86 wt% to 14.51 wt%. This means that the inverse correlation between Cr# and Mg#, which is pronounced in several chromitite deposits (e.g. Harold's Grave), may be caused by relatively small variations in the Al_2O_3 content of the melt.

Alternative explanations for the Cr# - Mg# intrapod variability include changing the physical parameters under which chromite crystallizes (e.g. pressure, temperature) or for melt-rock reaction to partially cancel out the effect of simple fractionation (or reaction with intercumulus melt) on the Mg# of crystallizing chromite (see Chapter 6). The former are highly unlikely within the mantle as pressure and temperature decreases will be negligible and may indeed only play a role within cumulate chromitites, or with the transition to the cumulate sequence. Evidence from the Cliff chromitite-dunite analyses suggested that fractionation may occur without the expected change in Mg# but be recorded in the Cr#-TiO_2 of the chromitite and dunite samples. Analysis of dunite and chromitite samples from Harold's Grave and Quoys reveal no indication of fractionation processes (Figure 4.40, cf. Figure 4.38). The implication from this is that the dunite samples from Harold's Grave which plot outside the OSMA (Figure 4.25) do so because of metasomatic reaction (Arai, 1994) rather than fractional crystallization.

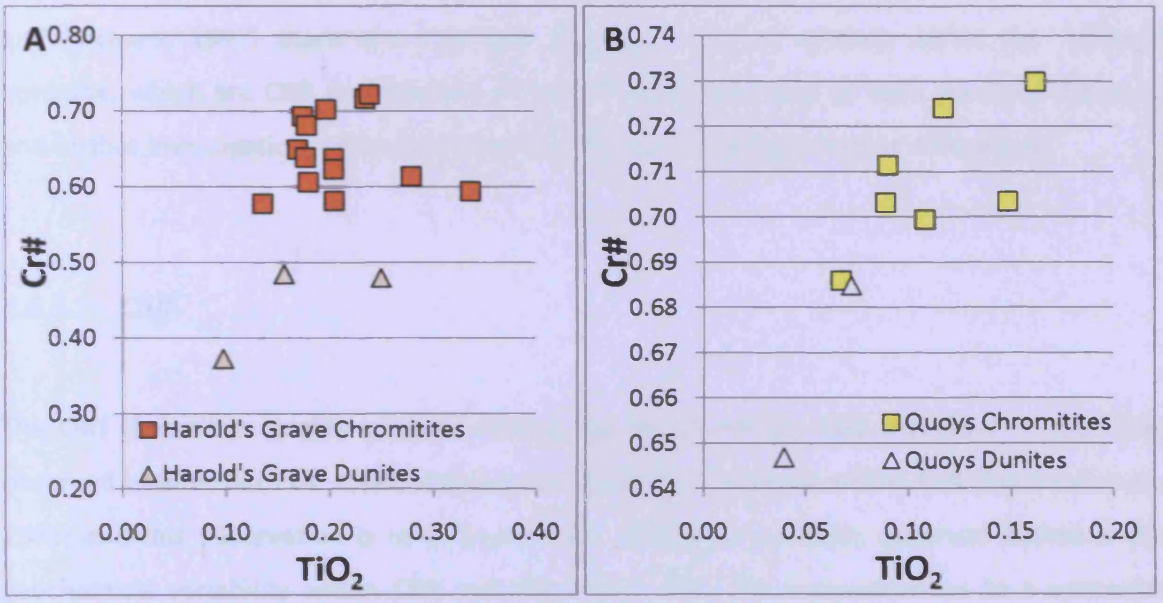

Figure 4.40: *Cr# vs. TiO_2 for the* ***A:*** *Harold's Grave deposit and* ***B:*** *Quoys deposit showing the composition of chromite from both dunite and chromitite samples. There is no trend of increasing TiO_2 content with decreasing Cr# content. Note that the axes scales are not the same on both graphs.*

In summary, the large geochemical variations identified within chromitite pods at Harold's Grave and Quoys suggest that the formation of ophiolitic chromitites may occur through the removal of chromite from numerous separate batch melts. As numerous batch melts are required the composition of the source region from which the melts are extracted may gradually evolve with time, producing melts with varying Al_2O_3 contents (Haraguchi and Ishii, 2007; Dilek and Thy, 2009). As each melt fluxes through a site of chromite crystallization there is the potential for a little more chromium to be removed from the melt, and therefore for more chromite to crystallize. The repetition of this process, with numerous batch melts may allow the eventual construction of a chromitite pod with varying Cr# ratios.

4.6.3 PGE concentration

Aside from the PGE concentrations identified from the cumulate sequence (Lord, 1991; Lord and Prichard, 1997) there are only two particular sites of interest within the Shetland ophiolite, which are Cliff and Harold's Grave. The characteristics of each are very different, and further investigation within this thesis has served to highlight further differences.

4.6.3.1 Cliff

The Cliff chromitite locality is world famous for an anomalous PGE inventory. It has been observed before that PGE concentrations are particularly variable within Cliff (Prichard *et al.*, 1986) and this observation is re-enforced here. What has not been observed before is the geochemical variability within Cliff and the link of high PGE concentrations to a particular chromite compositional range within Cliff chromitite – notably towards the lowest Cr#, and highest TiO_2 in the deposit (Figure 4.35).

One of the most recent investigations into Cliff concluded that initial PGE concentrations were by magmatic fractionation followed by a hydrothermal overprint by an As-rich serpentinising fluid which has re-mobilised and re-concentrated the PGE (Lord *et al.*, 1994). This investigation confirms this hypothesis and adds further detail.

Firstly, the association of high PGE concentrations with low Cr# and high TiO_2 values relative to the some of the other Cliff chromitite analyses (Figure 4.36), suggests high PGE concentrations occurred only after some fractionation. This fractionation presumably led to sulphide saturation and the unusual concentration of PPGE's.

Within Cliff several PGM are As-, Sb- and Te-bearing (Prichard *et al.*, 1994) and may be the product of either late magmatic or secondary alteration processes. Late-magmatic As-bearing fluids have been proposed at major PGE-bearing Ni-Cu deposits such as Sudbury and Noril'sk-Tanakh through the separation of a volatile rich fluid from the melt (e.g. Genkin and Evstigneeva, 1986; Li *et al.*, 1992) as well as within other chromitite deposits (Auge and Lerouge, 2004)). In contrast secondary alteration of sulphide-bearing PGM to arsenides, antimonides and tellurides may occur during serpentinisation (e.g. Yang and Seccombe, 1993). Previous work on the Cliff deposits argued that the introduction of As, Sb and Te to the Cliff site was hydrothermal and associated with the serpentinisation of the ophiolite (Prichard *et al.*, 1994). The main argument put forward is the very low sulphide concentrations found within ophiolites in general and Cliff in particular (rarely > 1-2 %), and that therefore associated magmatic As, Sb and Te would be negligible. The hydrothermal event responsible for the serpentinisation is thought to be coeval with that which produced the talc mineralisation along the basal thrust (Neary and Prichard, 1985; Prichard *et al.*, 1994), especially as arsenic anomalies commonly correlate with talc-rich lithologies (Prichard and Lord, 1993). The hydrothermal event was accompanied by the formation of both tourmaline-bearing quartz veins and molybdenite-bearing chlorite veins which in places cross-cut the ophiolite and adjacent metasedimentary units.

This dates the hydrothermal event as post-emplacement (Prichard *et al.*, 1994). If the presence of As-, Sb- and Te- bearing PGM at Cliff suggests the introduction of fluids during a post-emplacement hydrothermal event, then it is possible that the high PGE concentrations present within Cliff represent the effect of hydrothermal upgrading (Lord *et al.*, 1994). As such there are two possible remobilisation processes. Either the As-rich fluids scavenged PGE locally (on the scale of a few metres), and re-concentrated them within a couple of the pods, forming anomalously high concentrations, or the PGE were scavenged from further afield, possibly brought in by the As-rich fluids, and only focussed on a couple of the chromitite pods.

Distinguishing between these is not immediately obvious, though exploration studies on rocks, soils and careful examination of PGE distribution in bulk rock and PGM assemblages indicate that the mobility of PGE during moderate serpentinisation is very limited (Prichard and Lord, 1993; Garuti *et al.*, 1999). Furthermore, since Os, Ir and Ru are trapped within chromite and therefore presumably part of the original magmatic crystallization process it is apparent that these chromitites were certainly enriched before any hydrothermal re-concentration, but to an unknown extent.

These observations, coupled with the abundant presence of magmatic sulphides at Cliff (Maynard *et al.*, 1997), and the coupling of PPGE to sulphur within the melt makes the likely source of the PPGE the original sulphide crystallization, which has subsequently been partially re-mobilised. This makes the first of the re-mobilisation options, that As-rich fluids only re-mobilised PGE on metre length scale, the most likely.

4.6.3.2 Harold's Grave

In contrast to the Cliff chromitite deposit, the Harold's Grave deposit is far more uniform in its PGE concentrations. Throughout the eight chromitites investigated the variation in total PGE is less than an order of magnitude, and this is reflected across the individual PGE as well. The type of mineralisation is very different from Cliff, being dominated by Os, Ir and Ru, rather than Pt, Pd and Rh, though these elements (particularly Pt) are also present. Geochemically speaking, this mineralisation ranges across the entire compositional range of Harold's Grave, from a Cr# of 0.58 to 0.72 and there is no correlation between the magnitude of the PGE content and the Cr#.

Since the chromite geochemical variation follows an inverse trend between Cr# and Mg# (Figure 4.30), with no indication of fractionation on a Cr#-TiO_2 plot (Figure 4.33 & Figure 4.37), the variation in Cr# and Mg# represents the varying compositions of the batch melts that have combined to build up the chromitite pod. The coincidence between Harold's Grave chromite grains containing these elevated trace element compositions and its unusually high and consistent IPGE mineralisation suggests that there is a link between the two processes. The elevated trace element concentrations and lower Mg# values of the chromite grains are thought to reflect the process of fractionation and reaction with a partially trapped intercumulus melt within the mantle.

Chromite has been proposed as a collector for PGE (Finnigan *et al.*, 2008), and the observations of IPGM included within chromite grains suggest chromite is particularly effective at encouraging the crystallization of IPGM from the melt. If chromite crystallizing at Harold's Grave has had an extended chromite-melt reaction then there may have been greater opportunities for IPGM collection by crystallizing chromite. Extended reaction with a partially trapped intercumulus melt would have contributed to higher trace element values, and this may have subsequently allowed the collection of more IPGM from the melt. The composition of this trapped intercumulus melt may either be the highly differentiated remnant of the initial silicate melt from which the chromite grains crystallized or evidence for an unmixed volatile-rich phase (see Section 6.2.4). That there is minor PPGE mineralization (particularly Pt which is ~0.5 ppm) fits with the minor sulphide crystallization observed at Harold's Grave, and the already mentioned fractionation prior to the crystallization of the Harold's Grave chromitites.

4.6.3.3 PGE concentration - Summary

This study within the Shetland ophiolite has unambiguously shown a link between PGE concentrations and chromite geochemistry, though of two different types. Firstly, the concentrations within Harold's Grave show a link between the composition of chromite when chromite itself is the major collector of the IPGE. This link shows that fractionation within the mantle sequence and reaction with a partially trapped intercumulus melt were the likely causes for the final crystallization of minor PPGM and large amounts of IPGM. These processes produced a chromitite pod which is compositionally unique within the analyzed Shetland chromitite pods.

The chromite compositions at Cliff show significant overlap with other PGE-poor chromitite pods (i.e. Quoys and Long Quarry), but the internal variation within Cliff shows that initial PGE concentration was within the low Cr#, high TiO_2 chromitite groups. Furthermore, the PGM-rich dunites and PGE-rich chromitites lie on a fractionation trend of decreasing Cr# with increasing TiO_2 indicating that fractionation played a prominent role in the petrogenesis of the Cliff chromitite and PGE deposit. The role of water unmixing may explain why the Mg# of the chromite grains initially increases rather than decreases as would be expected within a fractionating system. It also appears that re-mobilization of the PGE most likely occurred through scavenging of localized PGE and re-concentration over a metre-length scale.

Chapter 5

The Berit Ophiolite, Turkey

An interpretation of bimodal chromite compositions and the unusual presence of chlorite lamellae within chromite grains

5 The Berit Ophiolite

5.1 Chromitite samples

The Berit ophiolite is located within the E-W trending Tauride belt in southern Turkey and is situated just north of the East Anatolian Fault. It formed in an oceanic island arc within the southern Neo-Tethys and was accreted to the northern edge of the active margin around 85 Ma (Robertson *et al.*, 2006). It is a typical Mediterranean-type ophiolite formed in a SSZ setting consisting of a series of sliced and fault bounded ultramafic and mafic slivers, which as yet have not been distinguished, but are thought to represent the mantle-crust transition zone of a large ophiolite (Figure 5.1, Robertson *et al.*, 2006; Aydin Golakoglu, pers. comm.).

This investigation has examined two sets of samples. Sixteen were collected by Hatice Kozlu from 7 separate chromitite pods, 7 of which came from a single pod at Dereagzi. In addition a personal visit to Berit yielded 9 *in-situ* samples from Dereagzi, together with samples from two chromitite pods that had not been investigated previously; Demerlik (10 samples) and Kabakteppe (16 samples).

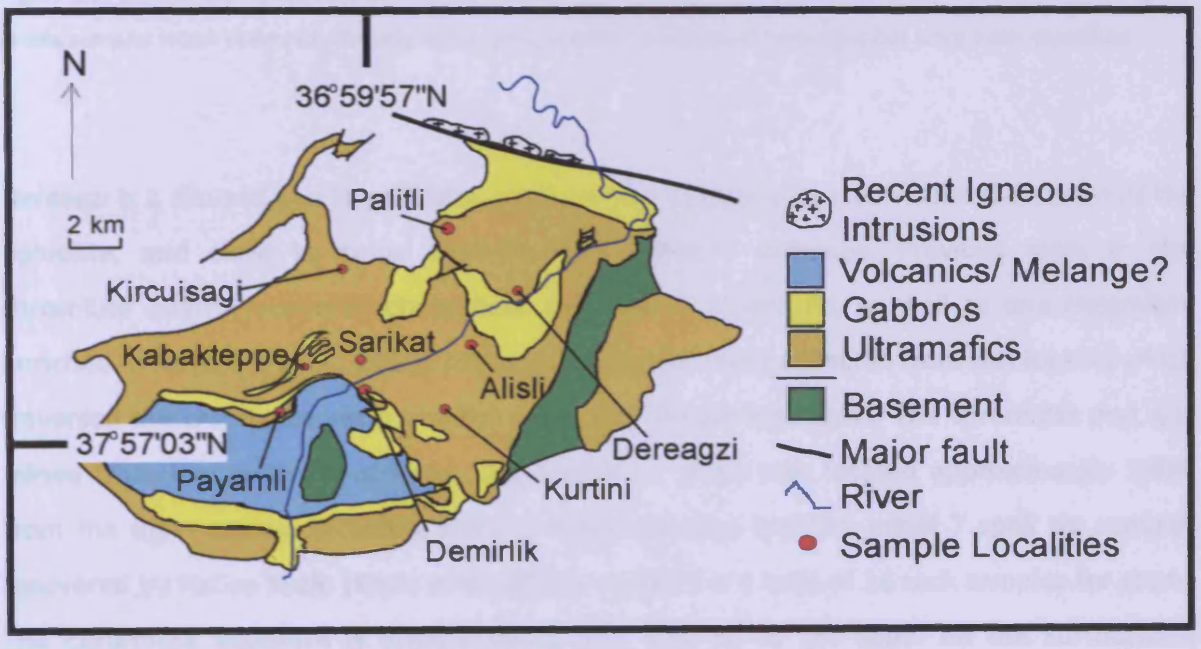

Figure 5.1: *The Berit ophiolite, showing the sampled chromitite samples localities, including the three main localities – Deragzi, Demerlik and Kabakteppe. Map adapted from work by Aydin Golakoğlu (2010).*

5.1.1 Dereagzi

Figure 5.2: *The Dereagzi outcrop, showing the remaining chromitite seam (shaded in grey) and the positions of the in-situ samples which collected. The original chromitite outcrop was much larger but has since been mined out.*

Dereagzi is a disused and largely excavated chromitite quarry located within the centre of the ophiolite, and close to some fault-bounded gabbroic outcrops. Previous work in this chromitite quarry recovered chromitites enriched in Pt and Pd, as well as one chromitite enriched in Ru (Kozlu *et al.*, 2010). Nine in-situ samples were collected from this locality which traversed the chromitite seam and the associated dunite lithologies. The chromitite pod was mined from two separate quarries, the second of which was located approximately 100m from the main quarry. Including these 9 *in-situ* samples and the initial 7 spoil tip samples recovered by Hatice Kozlu (Kozlu *et al.*, 2010), resulted in a total of 16 rock samples for study. The chromitite exposure is approximately 9m long by 50 cm wide. All the surrounding lithologies were found to be dunitic.

5.1.2 Demerlik

Demerlik is a chromitite quarry located close (~50m) to fault bounded gabbroic outcrops and what is currently considered to be the ophiolite melange (Figure 5.1, Aydin Golakoglu, pers. comm.). Even within Berit, it is an isolated and relatively untouched (only partially mined) chromitite pod from which 10 in-situ samples have been collected during this study. The chromitite exposure is approximately 9 m long by 1.5m high and is bounded by dunite. The dunite extends approximately 3 m above, and half a metre below the chromitite pod up to the point where the exposure is lost. A pyroxenite vein cross-cuts part of the outcrop (Figure 5.3).

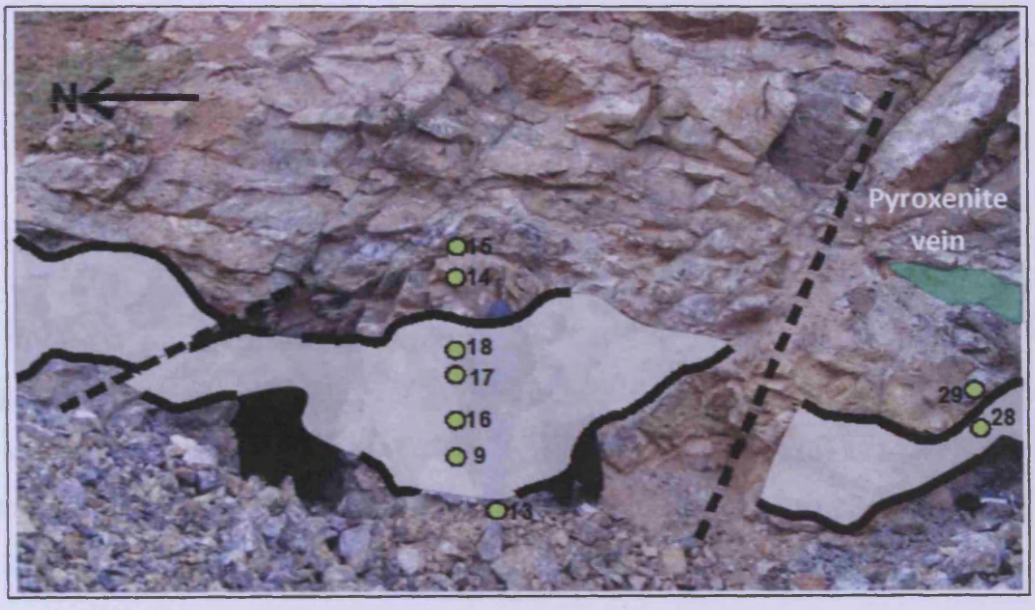

Figure 5.3: *The Demerlik outcrop, showing the main chromitite seam shaded in grey and the in-situ samples which were gathered. The position of the outcropping pyroxenite vein (with offset features either side) is also shown.*

5.1.3 Kabakteppe

Kabakteppe is a massive (>75% chromite) to disseminated (<75% chromite) chromitite pod located within the ultramafic sequence and close to several elongate gabbroic outcrops (Figure 5.1, Aydin Golakoglu pers. comm). At its thickest point the chromitite outcrop reaches ~15m thick and ~40m long with potentially more chromitite buried beneath the surface. Pyroxenite veins also cross-cut this outcrop. As at Demerlik, Kabakteppe is a partially mined deposit still containing in-situ chromitite. In total 16 in-situ samples were collected.

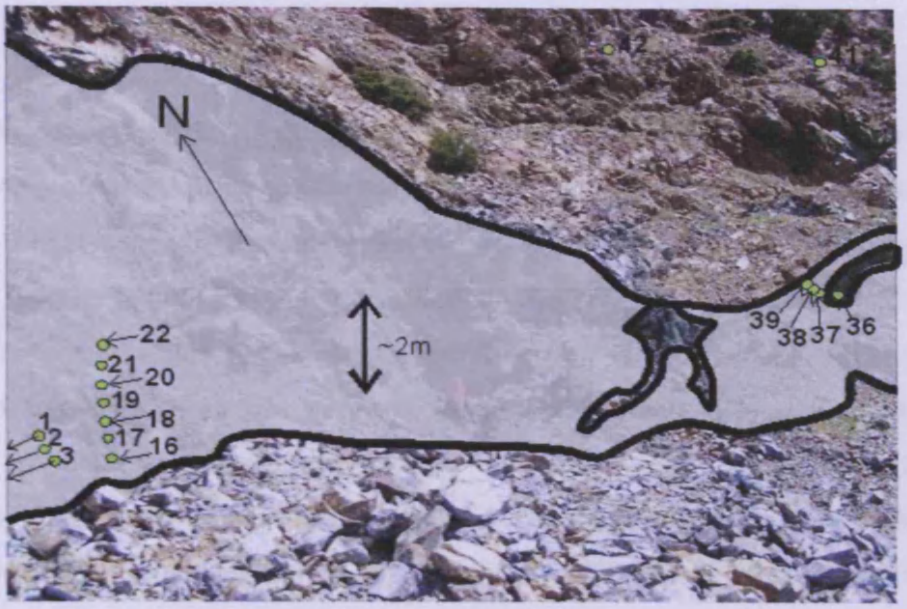

Figure 5.4: *The Kabakteppe outcrop, showing the main chromitite seam shaded in grey and the in-situ samples which were gathered. At its thickest point the chromitite seam is approximately 15 m thick.*

5.1.4 Other chromitite samples

Aside from the three chromitite localities described above and the previously collected Dereagzi samples there were 9 other chromitite samples collected from 6 other localities. These were collected by Hatice Kozlu from spoil tips at Kurtini (MBI-2, MBI-5 and MBI-9), Kirciusagi (MBK-2 and MBK-14), Sarikat (MBS-1), Alisli (MBA-6), Payamli (MBP-3) and Palitli (MBT-15).

5.2 Chromitite Petrography

Chromite grains that are present in the Berit chromitites vary in size from a millimetre to approximately half a centimetre. They are roughly equidimensional with chromite grain size generally larger in massive chromitites than in disseminated chromitites (Appendix 1). There was no observed preferred orientation of chromite grains to the general overall shape of the pod. The petrography of the Berit chromitites varies in terms of the modal percentage of chromite (see Appendix 1), the presence of sulphides, the type and development of inclusions, the degree of alteration and the degree of fracturing. The other feature of particular interest is the pervasive presence of what appears to be chlorite-filled exsolution lamellae.

5.2.1 Sulphide content of chromitite bodies

The sulphide content of the Berit chromitites is invariably low, but often around ~1 wt% sulphide can be observed using a microscope (e.g. at Dereagzi, Table 5.1). In general, sulphide abundance is higher than in chromitites from either Shetland or Al 'Ays with the exception of one or two samples (e.g. CF2 at Cliff in Shetland or C63 in stratigraphic group 4 from Al 'Ays). Sulphides are located within all the Berit chromitite pods, with variability being observed both within, and between chromitite deposits (Appendix 1; Table 5.1). Despite the greater abundance of sulphides in Berit the sulphide mineralogy within the samples is generally simpler than observed in either Al'Ays or Shetland. It is dominated by millerite, heazlewoodite (Figure 5.5A) and pentlandite (Figure 5.5B) with some minor chalcopyrite and bornite (Kozlu *et al.*, 2010). Except for these base metal sulphides no other Ni-or Cu-bearing minerals including, awaruite and orcelite have been observed within the Berit chromitites.

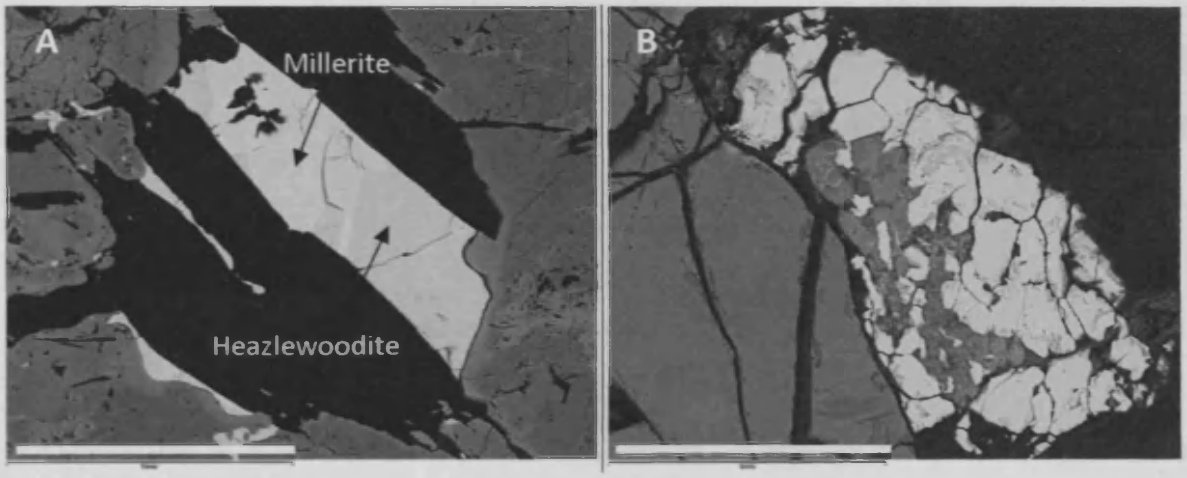

Figure 5.5: *Scanning electron images of sulphides within the Berit chromitites. A: A composite central mineral of Millerite and heazlewoodite within a silicate inclusion (black) within chromite (dark grey) (ADer-2), scale bar represents 6 mm. B: Granular pentlandite (light grey) intergrown with an iron oxide adjacent to chromite (grey) and silicate (black) (KBK-21), scale bar represents 4 mm.*

5.2.2 Inclusion Patterns

Silicate inclusions within chromite grains in the chromitites are a common feature. Generally they are randomly oriented with no particular clustering or spatial pattern. Nevertheless occasionally they are arranged in unusual patterns which can be divided into two sub-groups;

(1) inclusion clusters, located within the centre of a grain and juxtaposed with relatively inclusion free chromite grains (Figure 5.6A & B), and (ii) linear trails of inclusions cutting through a chromite grain (Figure 5.6C & D) (Table 5.1). In both cases their presence when observed in a thin section viewed under reflected light is usually anomalous with most other chromite grains in the same slide containing no such inclusion patterns.

5.2.2.1 Inclusion clusters

Inclusions in clusters are usually filled with silicates, or base metal sulphides, with only the smallest inclusions being empty. There is no particular orientation of the inclusions, but the predominant textural feature is the juxtaposition of inclusion abundant chromite grains with chromite grains completely barren of inclusions (Figure 5.5B). Within Berit, the abundance of this inclusion pattern (11 out of 38 sections) is similar to that observed within Al'Ays (11 out of 51) sections, but more than that observed within Shetland (no unequivocal inclusion clusters observed). Inclusion clusters are filled with edenite, diopside, chlorite and occasionally enstatite (Figure 5.6; see Appendix 6 for analyses). Chromite grains with inclusion clusters were observed in both massive chromitites and in chromite grains from within dunite samples.

5.2.2.2 Linear trails of inclusions

In a similar way to those inclusions observed in Unst and Al 'Ays the inclusions that form linear patterns in chromitite from Berit are observed to be empty (Figure 5.5C) or occasionally filled with base metal sulphides (Figure 5.5D). These individual empty inclusions show a well developed internal cubic structure. The predominance of empty inclusions may be due to plucking during the polishing procedure. However, plucking is unlikely as the presence of silicate inclusions in the cluster patterns and empty inclusions in the lines is strong evidence that the linear inclusions were not selectively plucked but were volatile-filled as plucking during the making of the slides would probably have plucked both textural types. Base metal sulphides included within the chromite grain are iron, iron-nickel, copper or copper-iron bearing (qualitative analyses were obtained as quantitative analyses were beyond the scope of this study – Appendix 7 contains all qualitative analyses).

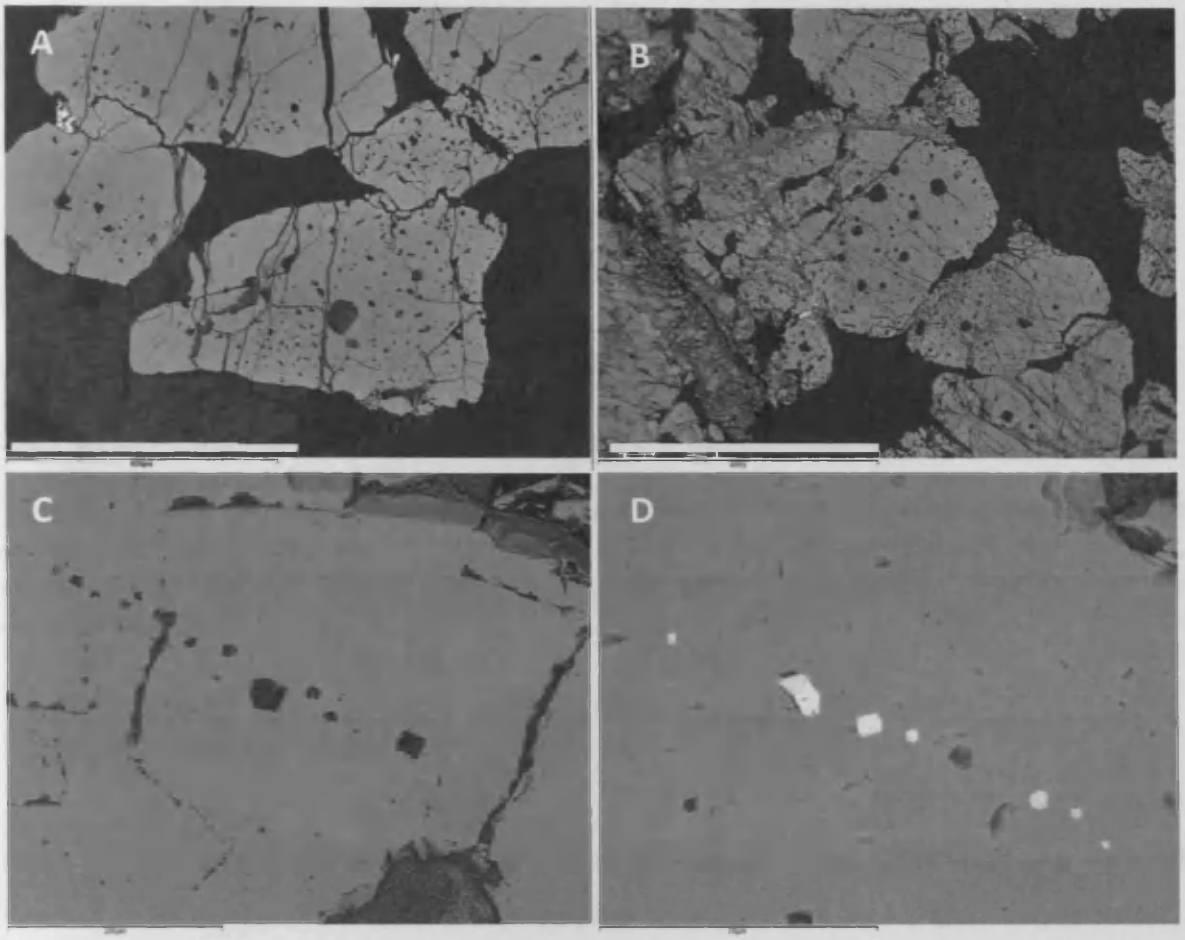

Figure 5.6: *Inclusion patterns within the chromite grains. A: Inclusion clusters within chromite from a dunite sample (ADer-12), scale bar represents 600 μm. B: Altered inclusion cluster within massive chromitite (ADer-3), scale bar represents 4 mm. C: An empty inclusion trail (MBD-7), scale bar represents 200 μm. D: Several base-metal sulphides filling a linear trail of inclusions within a chromite grain (MBD-7), scale bar represents 70 μm.*

5.2.3 Chromitite alteration

Alteration within the chromitite samples can be considered as minor to moderate for the interstitial silicates but highly variable for the chromite grains (Table 5.1; Figure 5.7). No measurement was made of the relative proportion of Cr-magnetite to ferritchromit but their collective presence within a chromitite ranges from negligible (e.g. Figure 5.7A) to pervasive (e.g. Figure 5.7B, and see Table 5.1). Although chromite alteration is common throughout the Berit chromitites, it's generally a less dominant presence (i.e. no major or pervasive alteration, Table 5.1) than in both the Al'Ays or Shetland ophiolite and unaltered chromite grains were observed in every chromitite section.

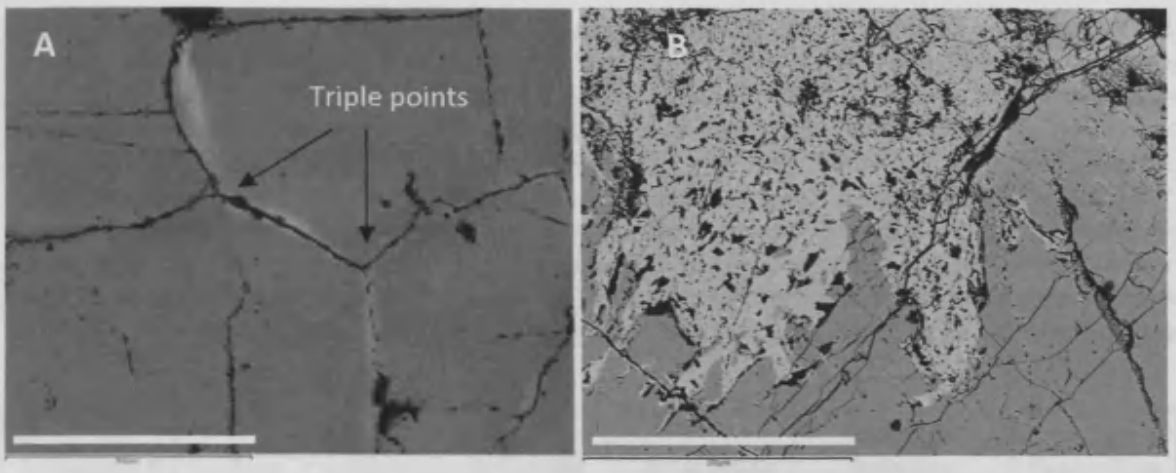

Figure 5.7: *Ferritchromit alteration within the Berit ophiolite. A: Nearly completely unaltered chromite grains (MBD-7). Also shown are two triple junctions, which are indicative of re-crystallization processes, scale bar represents 500 μm. B: Major to pervasive ferritchromit alteration (Ader-4), scale bar represents 200 μm.*

5.2.4 Exsolution lamellae

A prominent feature of some (30 samples) of the Berit samples is the presence of what appears to be exsolution lamellae within a few of the chromite grains (Figure 5.8, Table 5.2). These can either be present as large lamellae (several cm's long) (Figure 5.8A) which span whole chromite grains or small μm length exsolution, with the small μm exsolution usually only present within the altered rims of the chromite grains (Figure 5.8B). Regardless of size, all the observed exsolution lamellae contain chlorite which, within ultramafic assemblages, is normally interpreted as the alteration product of olivine, orthopyroxene, spinel and vapour (Jenkins, 1981; Jenkins and Chermovsky, 1986).

The most pervasive development of exsolution lamellae is within highly disseminated samples, such as dunites, where chromite grains are present from 1-2 modal% (e.g. Figure 5.8A). Nevertheless, the development of exsolution lamellae also occurs within chromite grains in chromitite samples (see Table 5.1). Where it does occur this development is unevenly distributed, with some grains within a slide showing extensive exsolution lamellae (Figure 5.8C), whereas others remain completely devoid of lamellae (Figure 5.8D). In the majority of cases chlorite is not just developed within the lamellae but also forms overgrowths around the chromite grains (Figure 5.8E & F). These overgrowths are not restricted to chromite grains containing exsolution lamellae but are generally more extensive around those grains that contain lamellae.

Table 5.1: *Summary table of the variation in base metal sulphide content, alteration, type of inclusion pattern observed, and the presence of absence of exsolution within the Dereagzi, Demerlik, Kabakteppe and other analysed chromitite pods. For sulphides a 'moderate' content = ~1-2 wt%, 'minor' = <0.5 wt% and 'negligible' means sulphides were either unobserved or barely present. For alteration, 'pervasive' = >90% alteration, 'major' = > 70-90% alteration, 'moderate' = 30-70%, 'minor' = 10-30%, and negligible = <10% alteration. The abundance of each inclusion pattern is 'moderate' unless otherwise stated. For the inclusion patterns, a 'major' content refers to the presence of inclusion patterns throughout >50% of the grains, 'moderate' equals inclusion patterns in 20 – 50% of the slide, 'minor' equal inclusion patterns within <10% of the slide and 'negligible' refers to the absence of definitive inclusion patterns. Exsolution lamellae within the chromite grains are recorded as either present (Yes), very occasionally present (Minor) or absent (No).*

Sample #	Pod	Type	Sulphide	Alteration	Inclusion Patterns	Exsolution
MBD-4	Dereagzi	Chr	Negligible	Moderate	Linear (minor)	No
MBD-7	Dereagzi	Chr	Minor	Negligible	Cluster & Linear	No
MBD-8	Dereagzi	Chr	Minor	Moderate	Negligible	No
MBD-8A	Dereagzi	Chr	Minor	Minor	None	No
MBD-8B	Dereagzi	Chr	Negligible	Negligible	Cluster (minor)	No
MBD-11	Dereagzi	Chr	**Moderate**	Minor	Cluster	Minor
MBD-13	Dereagzi	Chr	Minor	Negligible	Cluster	No
Ader-2	Dereagzi	Chr	**Moderate**	Minor	Linear (minor)	**Yes**
Ader-3	Dereagzi	Chr	**Moderate**	Moderate	Negligible	**Yes**
Ader-4	Dereagzi	Chr	Minor	Minor	Linear (minor)	**Yes**
Ader-5	Dereagzi	Chr	Minor	Minor	Linear (minor)	**Yes**
DMK-9	Demerlik	Chr	Negligible	Negligible	Negligible	No
DMK-12	Demerlik	Chr	Negligible	Negligible	Negligible	Minor
DMK-16	Demerlik	Chr	Minor	Minor	Cluster & Linear	Minor
DMK-17	Demerlik	Chr	Minor	Negligible	Cluster & Linear	No
DMK-18	Demerlik	Chr	Negligible	Negligible	Linear	No
DMK-28	Demerlik	Chr	Minor	Minor	Cluster (minor)	Minor
KBK-2	Kabakteppe	Chr	Minor	Minor	Linear	Minor
KBK-16	Kabakteppe	Chr	Minor	Negligible	Linear (minor)	Minor
KBK-17	Kabakteppe	D.Chr	Minor	Moderate	Cluster	Minor
KBK-18	Kabakteppe	D.Chr	Minor	Minor	Negligible	Minor
KBK-19	Kabakteppe	Chr	Negligible	Negligible	Cluster (minor)	Minor
KBK-20	Kabakteppe	Chr	Minor	Moderate	Negligible	**Yes**
KBK-21	Kabakteppe	Chr	**Moderate**	Negligible	Cluster & Linear	No
KBK-22	Kabakteppe	Chr	Minor	Negligible	Circular	No
KBK-37	Kabakteppe	Chr	Minor	Minor	Cluster & Linear	**Yes**
KBK-38	Kabakteppe	Chr	Negligible	Minor	Linear	No
KBK-39	Kabakteppe	Chr	Negligible	Minor	Cluster & Linear	Minor
MBI-2	Kurtini	Chr	Minor	Negligible	Cluster & Linear	Minor
MBI-5	Kurtini	Chr	**Moderate**	Negligible	Linear (minor)	Minor
MBI-9	Kurtini	Chr	Minor	Negligible	Linear (minor)	Minor
MBK-2	Kirciusagi	Chr	Negligible	Negligible	Cluster	No
MBK-14	Kirciusagi	Chr	Negligible	Negligible	Negligible	No
MBS-1	Sarikat	Chr	**Moderate**	Minor	Cluster & Linear	Minor
MBA-6	Alisli	Chr	Negligible	Negligible	Linear (minor)	No
MBP-3	Payamli	Chr	Negligible	Minor	Negligible	Minor
MBT-15	Palitli	Chr	Minor	Negligible	Linear (minor)	No

f exsolution were induced by deformation then this would more likely be focussed around the edges of chromite grains (as in Figure 5.8E), than throughout the grain. However, the development of these lamellae within the Berit samples is ubiquitously associated with chemical alteration of the chromite grain hosting the lamellae (Figure 5.8A, B, C & E). This was easily observed using a back-scatter electron detector where the altered portions of the grains appear brighter (e.g. Figure 5.8C) which would be the case for a Cr-magnetite alteration.

The geochemical change between chromite grains containing, and chromite grains without exsolution lamellae is marked by both major and trace elements (Table 5.2 & Figure 5.9).The chromite grains with exsolution lamellae contain higher MnO, NiO, Fe^{2+} and Fe^{3+} values together with lower MgO, Cr_2O_3, Al_2O_3, TiO_2 and V_2O_5 values (Figure 5.9 A-F and Table 5.2) than other lamellae-free chromite grains. A discussion of the origin of these exsolution textures and the geochemical variations is given in section 5.6.2

Table 5.2a: *Table showing the major element analyses from chromite grains containing exsolution lamellae and chromite grains without exsolution lamellae. The column labelled Exs refers to whether the analysed grains contained exsolution lamellae or not. The totals are calculated for total Fe and include the trace elements in Table 5.1b.*

Sample	Exs	Mg#	Cr#	Al_2O_3	Cr_2O_3	MgO	FeO	Fe_2O_3	Totals
Ader-2	Yes	0.68	0.52	25.46	40.51	15.16	12.80	5.32	99.57
Ader-4	Yes	0.69	0.55	22.44	41.46	15.14	12.37	8.24	99.64
Ader-5	Yes	0.68	0.55	23.25	41.91	15.21	12.78	7.72	100.88
Ader-2	No	0.72	0.52	25.88	41.97	16.39	11.31	4.51	100.37
Ader-4	No	0.71	0.53	24.67	41.91	15.82	11.74	5.37	99.78
Ader-5	No	0.70	0.54	24.52	42.41	15.68	12.25	5.58	100.71

Table 5.2b: *Table showing the major element analyses from chromite grains containing exsolution lamellae and chromite grains without exsolution lamellae.*

Sample	Exs	Mg#	Cr#	TiO_2	V_2O_5	MnO	NiO
Ader-2	Yes	0.68	0.52	0.22	0.23	0.28	0.11
Ader-4	Yes	0.69	0.55	0.18	0.23	0.28	0.12
Ader-5	Yes	0.68	0.55	0.18	0.21	0.27	0.12
Ader-2	No	0.72	0.52	0.22	0.23	0.22	0.09
Ader-4	No	0.71	0.53	0.20	0.23	0.27	0.11
Ader-5	No	0.70	0.54	0.23	0.23	0.26	0.10

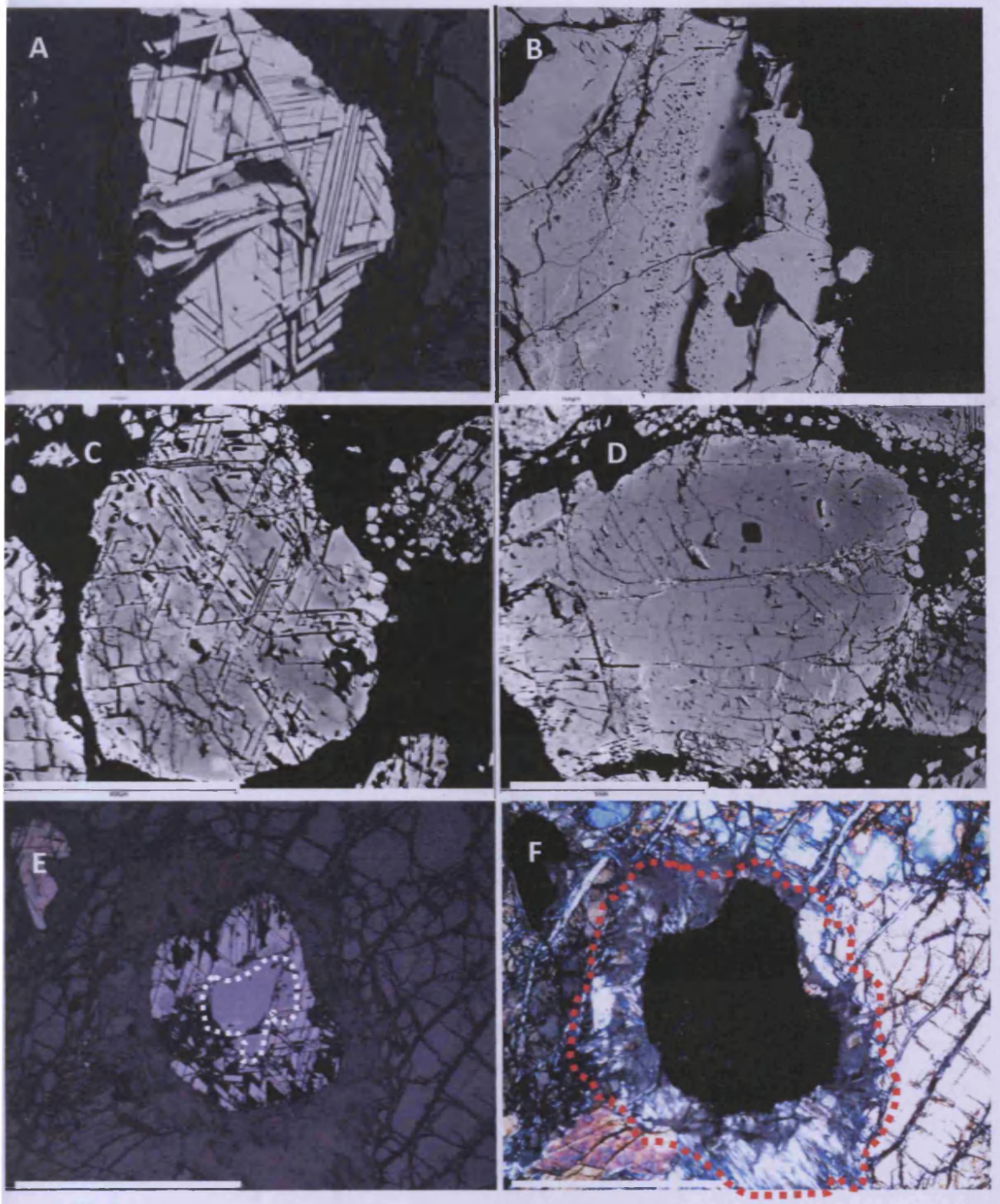

Figure 5.8: *Back scatter images (A-D) and photomicrographs (E-F) of exsolution lamellae within chromite grains.* ***A:*** *Large scale exsolution that crosses the whole chromite grain (ADer-8). Exsolution lamellae are parallel and without needle-like terminations, in a fashion analogous to Widmanstatten patterns in meteorites. scale bar represents 200 μm.* ***B:*** *Small intra-grain scale exsolution (ADer-3), scale bar represents 100 μm.* ***C:*** *Pervasive development of exsolution lamellae within a grain (Ader-4), scale bar represents 600 μm.* ***D:*** *Chromite grain from Ader-4 without any exsolution lamellae, scale bar represents 1 mm.* ***E:*** *Reflected light photomicrograph (Ader-9) showing exsolution lamellae developed only within the altered rim of a chromite grain, the unaltered core is circled by a dashed white line, scale bar represents 2 mm.* ***F:*** *Image E, but under cross-polarized transmitted light showing the chlorite overgrowth around the chromite grain (outer limit of the chlorite marked by a red dashed line), outside of which is olivine, scale bar represents 2 mm.*

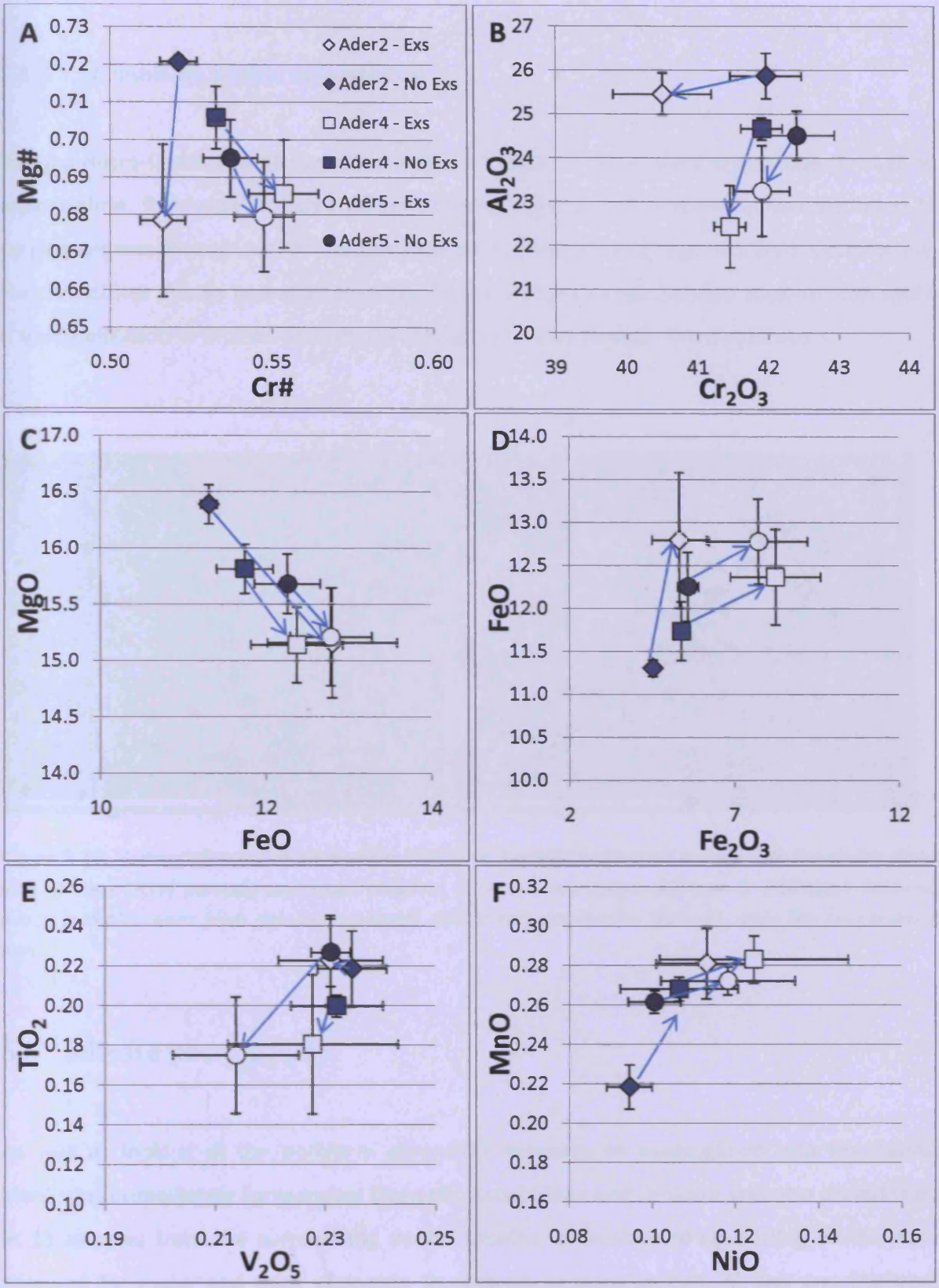

Figure 5.9: *Graphs comparing analyses from chromite grains containing exsolution lamellae (empty markers) with chromite grains free from exsolution lamellae (solid markers). A: Cr# vs. Mg#, B: Cr_2O_3 vs. Al_2O_3, C: MgO vs. FeO, D: FeO vs. Fe_2O_3, E: TiO_2 vs. V_2O_5, F: MnO vs. NiO. The key for both diagrams is displayed in Figure 5.9A. The arrows mark the change in composition that occurs within a sample by the transition from chromite grains with no exsolution to chromite grains containing exsolution. Error bars represent a range of two standard deviations.*

5.2.5 Chromitite: brittle deformation

Internal micro-faulting displays a wide variety of features, from minor brecciation through to mylonisation. Randomly oriented microfracturing (brecciation) is common and displayed to varying degrees throughout chromitites from all the deposits (e.g. Figure 5.10A). Occasionally, the chromitites display pull-apart features (Figure 5.10B) or even 'hairline' mylonisation which is the localisation of intense deformation along thin zones through the chromitite.

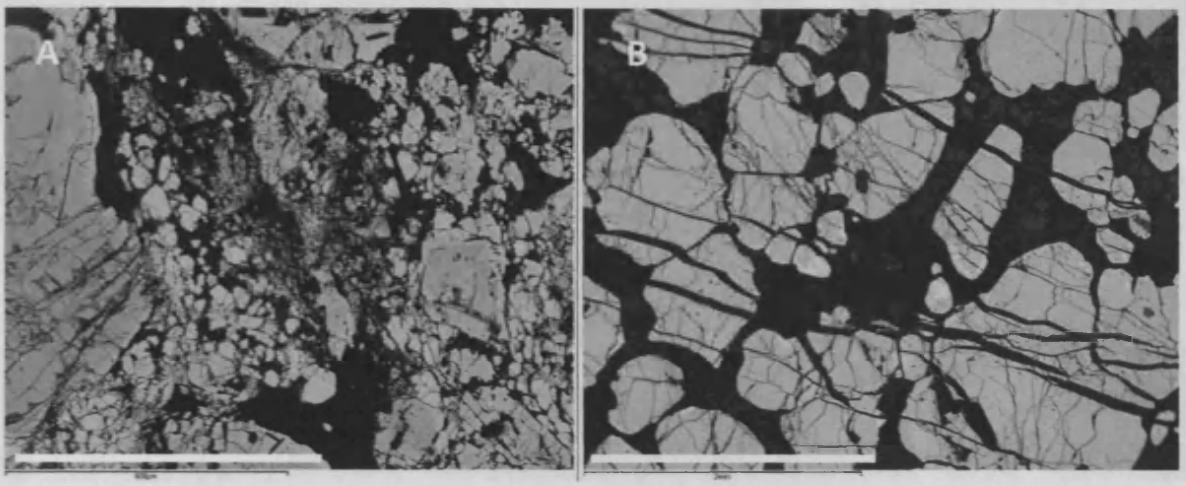

Figure 5.10: *Brittle deformation photomicrographs. A: Partially brecciated sample with the centre of the field of view (FOV) partially mylonised (Ader-4), scale bar represents 600 μm. B: Pull-apart features, which typically result from volume expansion during serpentinisation (Ader-4), scale bar represents 2 mm.*

5.3 Silicate petrography

As well as looking at the podiform chromitite deposits, an investigation into the dunitic lithologies immediately surrounding Demerlik, Kabakteppe and Dereagzi was also undertaken. In 13 samples from the surrounding dunite sheaths, chromite and co-existing olivine were analysed for major and trace elements. In contrast to samples from Al 'Ays and Shetland, olivine is often well preserved within the chromitite bodies. These dunite and chromitite samples gave a total data set of 24 samples with co-existing chromite and olivine.

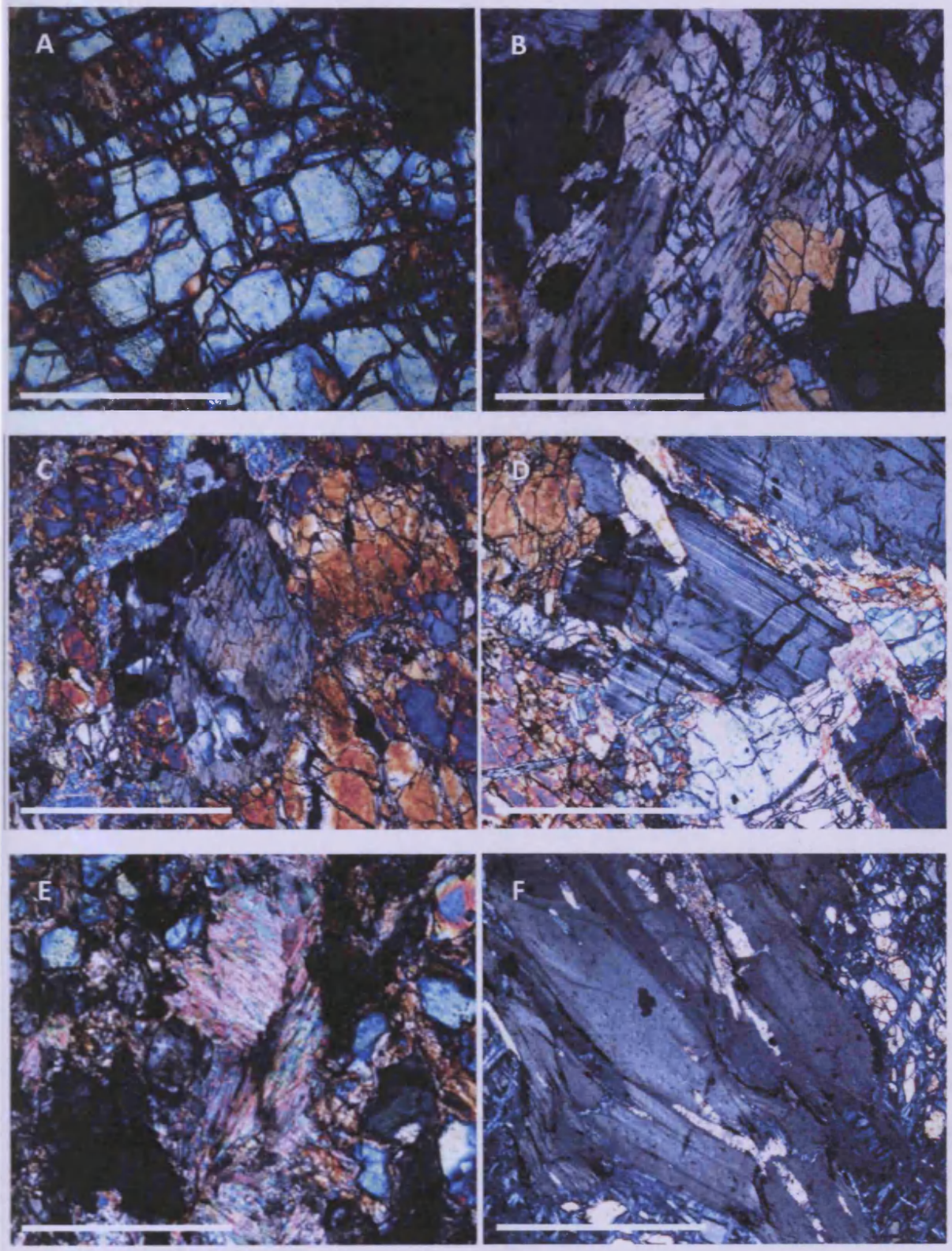

Figure 5.11: *Photomicrographs of silicates within the Berit ophiolite.* ***A:*** *Olivine grain showing minor alteration to serpentine, scale bar represents 2 mm.* ***B:*** *Amphibole grains closely associated with granular olivine. The extinction angle, as with most amphiboles observed from Berit is ~5°-10°, scale bar represents 2 mm.* ***C:*** *Basal section of an amphibole grain showing two prominent cleavages at 120°, scale bar represents 2 mm* ***D:*** *A rare observation of a plagioclase grain, scale bar represents 2 mm.* ***E:*** *A collection of talc laths, scale bar represents 2 mm.* ***F:*** *Chlorite laths, scale bar represents 2 mm.*

The silicate samples were all very well preserved with fresh olivine being the main constituent (Figure 5.11A). Accessory minerals include clinopyroxene, amphibole (Figure 5.11B & C), and chromite, with amphibole present in proportions of up to 2-3 %. The amphibole grains frequently show two cleavage planes oriented at 120° to one another. They show no pleochroism and a slightly inclined extinction in prismatic grains suggesting cummingtonite as the most likely mineral speciation. Occasional twinning within the grains is further confirmation of this identification. Occasionally the amphibole grains show well developed prismatic grains with straight extinction which may be anthophyllite, though this is rare and may just be an unusual cut of the cummingtonite grains. One plagioclase grain was also observed (Figure 5.11D).

Other minerals observed are serpentine, talc and chlorite. Serpentine is a minor constituent and usually restricted to infilling cracks within olivine. In contrast to Al'Ays and Shetland, talc (Figure 5.11E) is usually more common than serpentine. Chlorite is also present (Figure 5.11F), though at concentrations no greater than 1%. Where present it is commonly found as overgrowths around chromite grains, particularly when the chromite grain displays prominent exsolution lamellae (see Figure 5.8E & F).

5.4 Chromitite geochemistry

5.4.1 Major element geochemistry

The analyses of the major element geochemistry of the Berit chromitites predominantly falls in the fields that define ophiolitic chromitite (Figure 5.12A-D). The Cr# varies from 0.39 to 0.82, with an associated variation in Fe^{2+}# of 0.25 to 0.59 (Figure 5.12A & C). The TiO_2 wt% content ranges from 0.14 up to 0.45 (Figure 5.12B) and the Fe^{3+}# [Fe^{3+}/(Cr^{3+} + Al^{3+} + Fe^{3+})] ranges from 0.02 to 0.07 (Figure 5.12B & C) (Table 5.2). There are two groupings of values apparent in graphs A, C and D.

Table 5.3: *Major element chromite data from the chromitite localities of Demerlik, Kabakteppe, Dereagzi and other sample localities within Berit. Totals include the trace element data from Table 5.3.*

Sample#	Locality	Cr#	Mg#	Cr/Fe^{2+}	Al_2O_3	Cr_2O_3	FeO	MgO	Fe_2O_3	Total
MBD-4	Dereagzi	0.68	0.52	2.63	15.84	49.72	17.84	10.98	5.76	100.96
MBD-7	Dereagzi	0.44	0.68	2.47	30.20	34.91	13.35	15.59	5.90	100.92
MBD-8	Dereagzi	0.45	0.68	2.63	29.41	36.15	12.99	15.70	5.57	100.88
MBD-8A	Dereagzi	0.39	0.71	2.58	35.52	33.41	12.24	16.71	1.99	100.55
MBD-8B	Dereagzi	0.45	0.71	2.88	30.46	36.72	12.05	16.44	4.52	101.20
MBD-11	Dereagzi	0.44	0.66	2.40	30.30	34.95	13.75	15.29	5.50	100.79
MBD-13	Dereagzi	0.39	0.72	2.61	34.85	32.81	11.88	16.75	3.34	100.20
Ader-2	Dereagzi	0.53	0.71	3.45	25.64	42.38	11.62	16.04	3.86	100.28
Ader-3	Dereagzi	0.54	0.70	3.40	24.33	42.90	11.92	15.84	5.19	100.99
Ader-4	Dereagzi	0.55	0.69	3.32	24.05	43.63	12.41	15.50	4.87	101.24
Ader-5	Dereagzi	0.54	0.68	3.13	24.52	42.41	12.25	15.68	5.58	101.26
DMK-9	Demerlik	0.49	0.68	2.83	27.52	38.87	13.00	15.17	4.80	100.11
DMK-12	Demerlik	0.54	0.66	2.99	24.25	42.19	13.33	14.82	5.35	100.77
DMK-16	Demerlik	0.49	0.67	2.76	27.73	39.03	13.36	15.05	4.32	100.25
DMK-17	Demerlik	0.50	0.70	3.13	27.34	40.40	12.20	15.67	3.62	99.90
DMK-18	Demerlik	0.50	0.69	3.08	27.08	40.63	12.47	15.56	3.96	100.41
DMK-28	Demerlik	0.50	0.71	3.27	27.44	40.17	11.60	16.06	3.89	99.86
KBK-2	Kabakteppe	0.53	0.66	2.91	24.42	41.83	13.59	14.54	4.52	99.91
KBK-16	Kabakteppe	0.50	0.71	3.25	26.79	39.46	11.46	16.02	5.16	99.65
KBK-17	Kabakteppe	0.50	0.64	2.55	26.87	39.28	14.54	14.29	5.20	100.92
KBK-18	Kabakteppe	0.50	0.65	2.66	26.35	39.64	14.07	14.42	4.93	100.20
KBK-19	Kabakteppe	0.50	0.69	3.09	26.92	40.55	12.39	15.60	3.87	100.11
KBK-20	Kabakteppe	0.50	0.69	3.04	27.05	40.18	12.50	15.42	3.71	99.65
KBK-21	Kabakteppe	0.51	0.69	3.15	26.86	41.03	12.29	15.69	3.34	100.03
KBK-22	Kabakteppe	0.52	0.70	3.23	26.05	41.64	12.20	15.71	3.86	100.29
KBK-37	Kabakteppe	0.47	0.72	3.23	29.33	38.84	11.38	16.65	3.91	100.87
KBK-38	Kabakteppe	0.47	0.73	3.25	28.90	38.62	11.23	16.65	4.45	100.65
KBK-39	Kabakteppe	0.48	0.72	3.22	28.23	38.90	11.43	16.32	4.29	99.96
MBI-2	Kurtini	0.48	0.70	3.04	28.11	38.87	12.09	15.84	4.06	99.74
MBI-5	Kurtini	0.50	0.75	3.81	27.54	40.79	10.13	17.32	4.57	101.13
MBI-9	Kurtini	0.47	0.71	3.13	28.61	38.46	11.62	16.24	4.39	100.11
MBK-2	Kirciusagi	0.64	0.41	2.05	17.71	46.58	21.43	8.42	4.63	99.43
MBK-14	Kirciusagi	0.82	0.45	2.80	8.58	57.62	19.44	9.00	5.20	100.60
MBS-1	Sarikat	0.52	0.70	3.23	25.63	40.94	11.97	15.71	5.16	100.22
MBA-6	Alisli	0.54	0.64	2.72	24.22	41.66	14.46	14.25	5.66	101.10
MBP-3	Payamli	0.54	0.68	3.15	24.34	43.24	12.98	15.17	4.06	100.67
MBT-15	Palitli	0.78	0.48	2.87	10.53	57.06	18.77	9.90	4.42	101.41

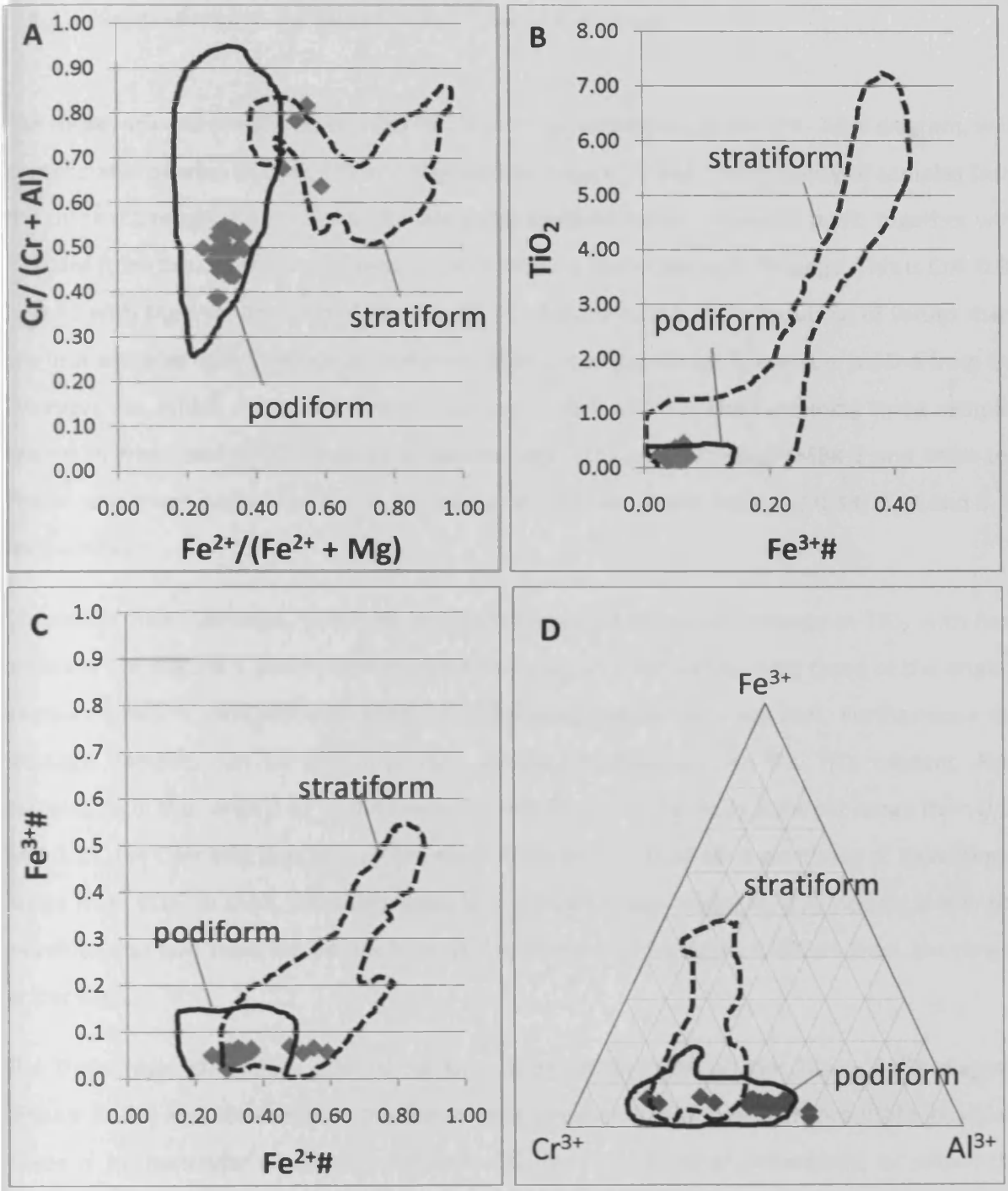

Figure 5.12: *Four graphs of major element plots for the chromitites of Berit. On each graph are two delimited fields, one for 'podiform' chromitites, and the other for 'stratiform' chromitites. These fields are taken from Roeder & Barnes, 2001, and represent 90% of studied chromite compositions.*

5.4.2 Major element variation within chromitite pods

The three main chromitite pods show minor internal variations on the Cr# - Mg# diagram, with considerable overlap in their Cr# and Mg# values (Figure 5.13A). The majority of samples from the three (Dereagzi, Demerlik and Kabakteppe) multi-sampled chromitite pods, together with samples from the other chromitite pods, plot within a restricted high-Al range. This is Cr#: 0.39 to 0.55 with Mg# varying from 0.64 to 0.75. In addition to this main grouping of values there are four samples with significantly different high-Cr compositions. The first is MBD-4 from the Dereagzi site, which contains a Cr# of 0.68 and a Mg# of 0.52. The remaining three samples are taken from two different pods at Sarikat (MBT-15) and Kirciusagi (MBK-2 and MBK-14). These have much higher Cr#'s of 0.78, 0.64 and 0.82, and lower Mg#'s of 0.48, 0.41 and 0.45 respectively.

Chromitite from Dereagzi, Demerlik and Kabakteppe all show an increase in TiO_2 with near constant Cr# (Figure 5.13B). Dereagzi shows a little more variability, with three of the original samples (MBD-4, MBD-8A and MBD-13) containing higher or lower Cr#. Furthermore the Dereagzi samples can be split into two subgroups depending on the TiO_2 content. Four samples lie in the range 0.37 to 0.45 with the rest lying in a distinctly different range from 0.14 and 0.23. For Demerlik the TiO_2 values range from 0.15 to 0.24 whereas those at Kabakteppe range from 0.16 to 0.35. Although there is a similarly large range in TiO_2 values, this is not developed as two separate populations at Kabakteppe and therefore differs from the ranges at Dereagzi.

The three main chromitite pods show large internal variation on the TiO_2 – Fe^{3+}# diagram (Figure 5.13C) and considerable overlap in their geochemistries between chromitite localities. There is no particular correlation between TiO_2 and Fe^{3+}# either collectively, or within the individual chromitite pods.

The three main chromitite pods show large internal variation on the Fe^{2+}# – Fe^{3+}# diagram (Figure 5.13D), with considerable overlap in their chemistries between chromitite localities. The three main chromitite pods and most of the other chromitite samples form a clear overlapping positive relationship between Fe^{2+}# and Fe^{3+}# with Fe^{3+}# values varying by a greater relative percent than Fe^{2+}# values. Four samples including one sample from Dereagzi (MBD-4) and three others (MBK-2, MBK-14, MBT-15) plot to higher Fe^{2+}# values without any increase in Fe^{3+}#.

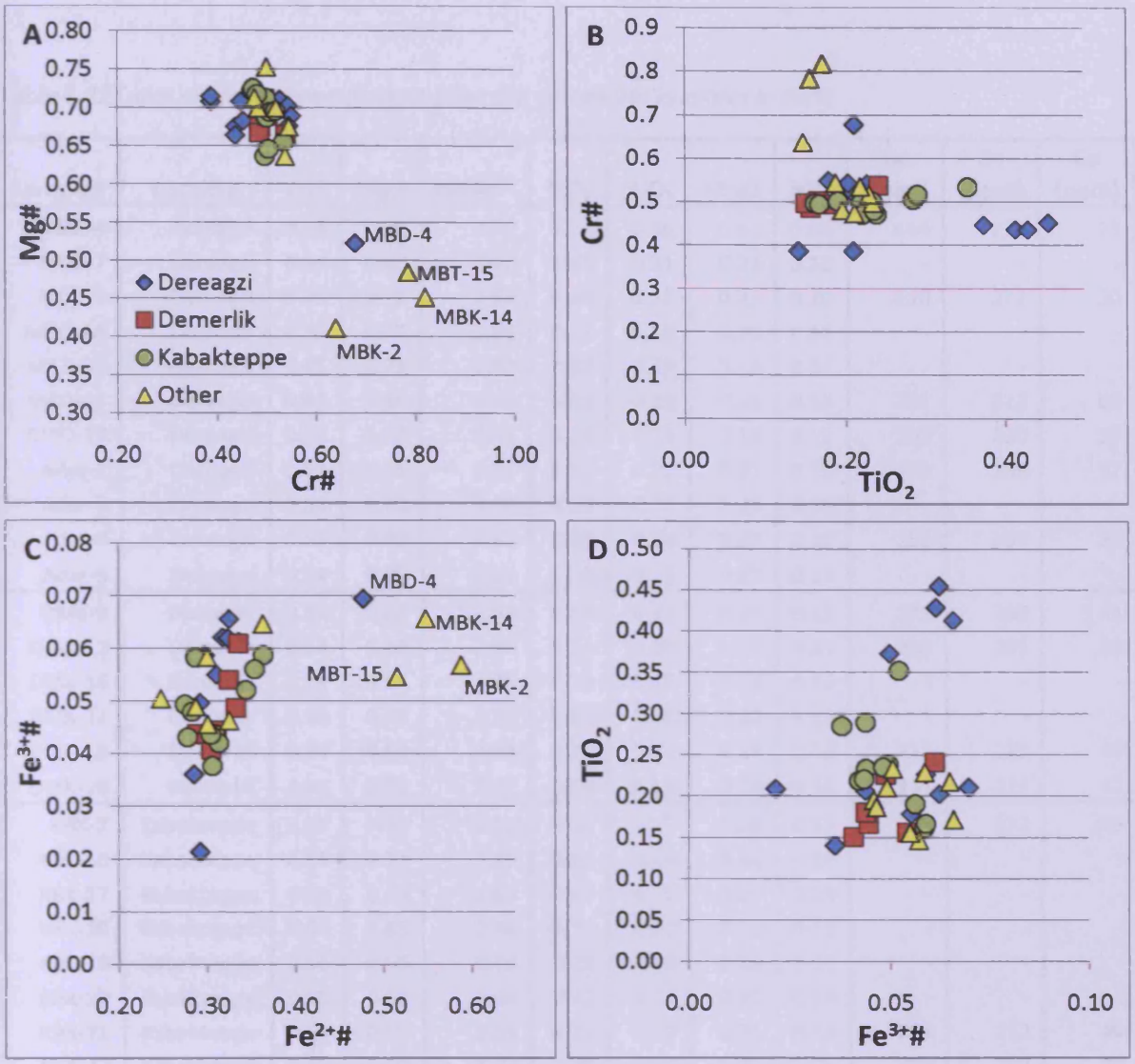

Figure 5.13: *Four graphs with major element plots for the chromitites of Berit. Note that the axes scale has been altered from Figure 5.12 to best show the variation between chromitite pods. Figure 5.13A is expressed as Cr# - Mg# to facilitate comparisons with other published literature. The legend within Figure 5.13A applies to Figure 5.13B, 5.13C and 5.13D. The four samples with distinctive Cr# and Mg# values are distinguished on Figure A & C.*

5.4.3 Trace element variation within chromitite pods

Trace element data for TiO_2, V_2O_5, MnO and NiO were collected from the three chromitite pods together with the other chromitites from Berit. Cobalt, Zn and Ga data were collected from 14 chromitites, from the three localities Kabakteppe, Demerlik and Dereagzi. The TiO_2 data has been described within the major element geochemistry section (Section 5.4.2), due to its use within the discrimination diagrams of Roeder and Barnes, (2001).

Table 5.4: *Trace element chromite data from the chromitite localities in Berit.*

Sample#	Locality	Cr#	Mg#	Cr/Fe^{2+}	TiO_2	V_2O_5	MnO	NiO	Co (ppm)	Zn (ppm)	Ga (ppm)
MBD-4	Dereagzi	0.68	0.52	2.63	0.21	0.16	0.36	0.09	444	772	23
MBD-7	Dereagzi	0.44	0.68	2.47	0.41	0.21	0.23	0.12	-	-	-
MBD-8	Dereagzi	0.45	0.68	2.63	0.45	0.18	0.23	0.20	210	271	50
MBD-8A	Dereagzi	0.39	0.71	2.58	0.21	0.16	0.20	0.11	-	-	-
MBD-8B	Dereagzi	0.45	0.71	2.88	0.37	0.19	0.24	0.21	-	-	-
MBD-11	Dereagzi	0.44	0.66	2.40	0.43	0.19	0.25	0.13	231	322	65
MBD-13	Dereagzi	0.39	0.72	2.61	0.14	0.14	0.18	0.11	202	290	37
Ader-2	Dereagzi	0.53	0.71	3.45	0.21	0.22	0.21	0.10	232	355	37
Ader-3	Dereagzi	0.54	0.70	3.40	0.23	0.23	0.25	0.10	-	-	-
Ader-4	Dereagzi	0.55	0.69	3.32	0.18	0.24	0.27	0.10	252	387	34
Ader-5	Dereagzi	0.54	0.68	3.13	0.20	0.23	0.27	0.11	-	-	-
DMK-9	Demerlik	0.49	0.68	2.83	0.16	0.17	0.26	0.15	272	289	41
DMK-12	Demerlik	0.54	0.66	2.99	0.24	0.20	0.25	0.15	256	281	36
DMK-16	Demerlik	0.49	0.67	2.76	0.23	0.15	0.22	0.16	-	-	-
DMK-17	Demerlik	0.50	0.70	3.13	0.15	0.16	0.22	0.15	-	-	-
DMK-18	Demerlik	0.50	0.69	3.08	0.17	0.15	0.23	0.16	217	223	40
DMK-28	Demerlik	0.50	0.71	3.27	0.18	0.15	0.22	0.16	197	224	42
KBK-2	Kabakteppe	0.53	0.66	2.91	0.35	0.22	0.26	0.17	235	372	45
KBK-16	Kabakteppe	0.50	0.71	3.25	0.16	0.19	0.24	0.15	-	-	-
KBK-17	Kabakteppe	0.50	0.64	2.55	0.17	0.18	0.27	0.14	-	-	-
KBK-18	Kabakteppe	0.50	0.65	2.66	0.19	0.20	0.27	0.12	-	-	-
KBK-19	Kabakteppe	0.50	0.69	3.09	0.23	0.18	0.23	0.14	-	-	-
KBK-20	Kabakteppe	0.50	0.69	3.04	0.22	0.18	0.25	0.14	-	-	-
KBK-21	Kabakteppe	0.51	0.69	3.15	0.28	0.19	0.21	0.15	209	212	40
KBK-22	Kabakteppe	0.52	0.70	3.23	0.29	0.19	0.22	0.15	209	242	39
KBK-37	Kabakteppe	0.47	0.72	3.23	0.22	0.17	0.22	0.15	206	237	42
KBK-38	Kabakteppe	0.47	0.73	3.25	0.24	0.16	0.22	0.18	220	245	43
KBK-39	Kabakteppe	0.48	0.72	3.22	0.24	0.18	0.22	0.15	215	251	41
MBI-2	Kurtini	0.48	0.70	3.04	0.20	0.17	0.22	0.19	-	-	-
MBI-5	Kurtini	0.50	0.75	3.81	0.23	0.18	0.21	0.14	-	-	-
MBI-9	Kurtini	0.47	0.71	3.13	0.21	0.16	0.22	0.20	-	-	-
MBK-2	Kirciusagi	0.64	0.41	2.05	0.15	0.07	0.37	0.08	398	2077	57
MBK-14	Kirciusagi	0.82	0.45	2.80	0.17	0.10	0.43	0.07	431	1034	15
MBS-1	Sarikat	0.52	0.70	3.23	0.23	0.22	0.22	0.14	-	-	-
MBA-6	Alisli	0.54	0.64	2.72	0.22	0.23	0.26	0.14	213	291	37
MBP-3	Payamli	0.54	0.68	3.15	0.19	0.25	0.25	0.19	-	-	-
MBT-15	Palitli	0.78	0.48	2.87	0.16	0.13	0.38	0.06	427	772	16

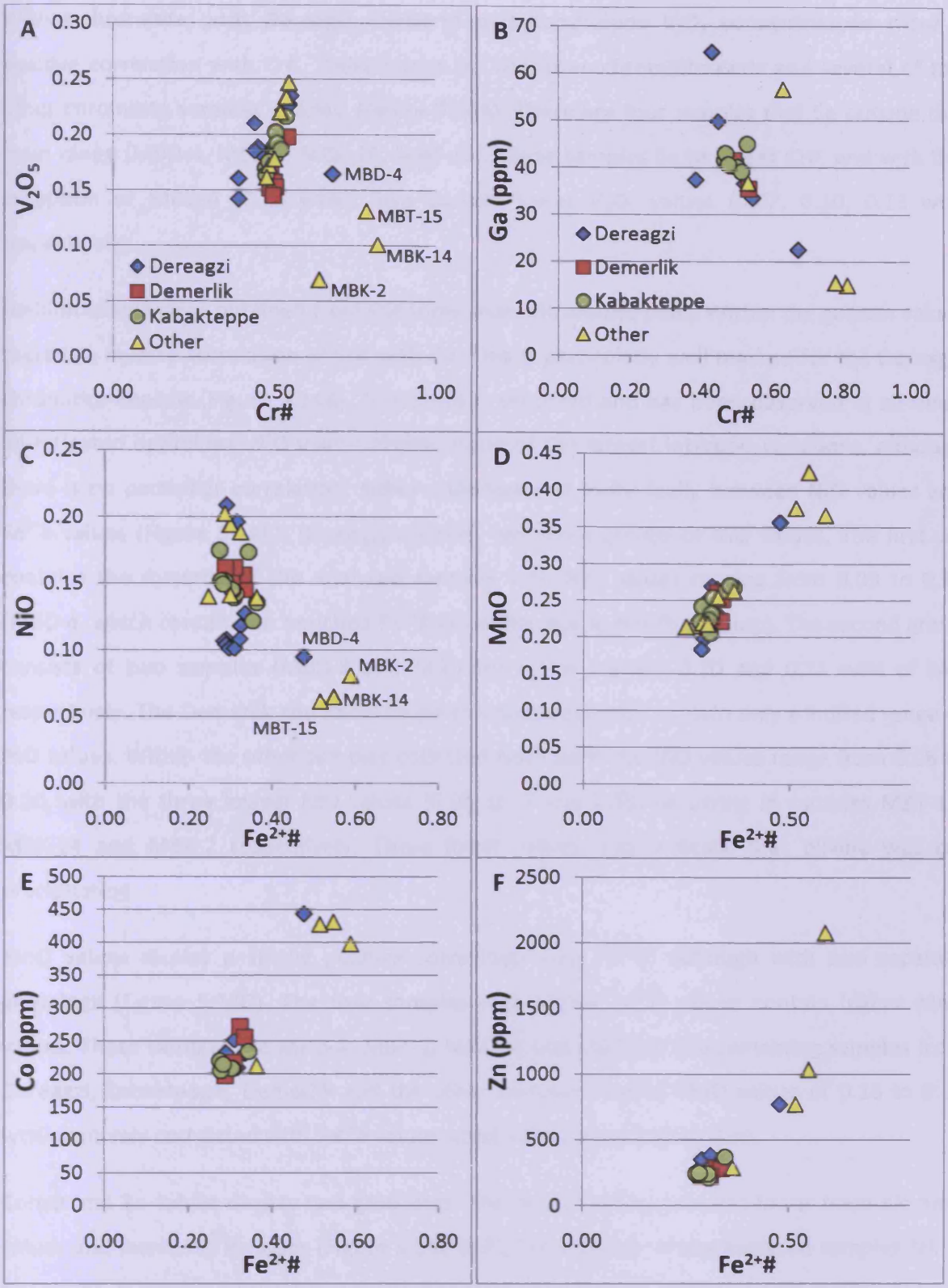

Figure 5.14: *Six trace elements plots for the Berit chromitites. The legend within Figure 5.14A applies to Figures 5.14B-F. Figures 5.14A and 5.14B are plots of V_2O_5 and Ga against Cr#, as these trace elements fill the same trivalent cation space within the chromite grain as Cr^{3+} and Al^{3+}. Figures 5.14C-F are plots of NiO, MnO, Co and Zn against Fe^{2+}# as these trace elements fill the same divalent cation space as Fe^{2+} and Mg^{2+}. The four samples with distinctive Cr# and Mg# values are distinguished on Figure A & B.*

Within chromitite pods Dereagzi, Demerlik and Kabakteppe V_2O_5 concentrations show a positive correlation with Cr#. These values for the three chromitite pods and several of the other chromitite samples overlap (Figure 5.14A). There are four samples that lie outside this main range (MBD-4, MBK-2, MBK-14, MBT-15). These samples lie to higher Cr#, and with the exception of MBD-4 (0.16 wt%), also contain lower V_2O_5 values (0.07, 0.10, 0.13 wt% respectively).

Gallium values were obtained from the three main chromitite pods. Within the gallium values there is a inverse correlation of Cr# with Ga. This is particularly well marked for the Dereagzi chromitite deposit (Figure 5.14B). This trend is expected and has been observed in all three investigated ophiolites. NiO values display some of the largest interpod variations, although there is no particular correlation, either collectively or individually between NiO values and Fe^{2+}# values (Figure 5.14C). Dereagzi contains two main groups of NiO values. The first set contains the majority of the analysed samples with NiO values ranging from 0.09 to 0.13 (MBD-4, which contains an enriched Fe^{2+}# value, fits in into this first group). The second group consists of two samples (MBD-8 and MBD-8B) which contain 0.20 and 0.21 wt% of NiO respectively. The Demerlik and Kabakteppe chromitite samples contain only a limited range of NiO values. Within the other samples collected from Berit the NiO values range from 0.06 to 0.20, with the three lowest NiO values (0.06, 0.07 and 0.08) occurring in samples MBT-15, MBK-14 and MBK-2 respectively. These lower values may indicate that olivine was co-precipitating.

MnO values display a strong positive correlation with Fe^{2+}#, although with two separate groupings (Figure 5.14D). The four samples with higher Fe^{2+}# values contain higher MnO values. These samples are MBD-4, MBK-2, MBK-14 and MBT-15. The remaining samples from Dereagzi, Kabakteppe, Demerlik and the other samples contain MnO values of 0.18 to 0.27 wt% positively correlated with Fe^{2+}# values which range from 0.25 to 0.36.

Cobalt and Zn values display two groupings. The first grouping contains lower trace element values and lower Fe^{2+}# values (Figure 5.14E & F). The majority of the analysed samples fall in this range, including all the Kabakteppe and Demerlik samples, together with the majority of the Dereagzi samples and MBA-6. The second grouping contains higher trace element values and higher Fe^{2+}# values and consists of the four previously mentioned anomalous chromitite samples (MBT-15, MBD-4, MBK-2 and MBK-14).

5.4.4 MORB normalised multi-element plots

MORB normalised multi-element plots of a set of elements for the Berit chromitites reveal some differences to similar plots of chromitites from the Thetford ophiolite in Canada (Figure 5.15; Page and Barnes, 2009), which are postulated to be fore-arc type supra subduction ophiolites. In particular the bulk of the chromitite data from the Berit ophiolite has an array with a closer resemblance to the MORB-type lava, than the Boninite-type lava (Figure 5.15B).

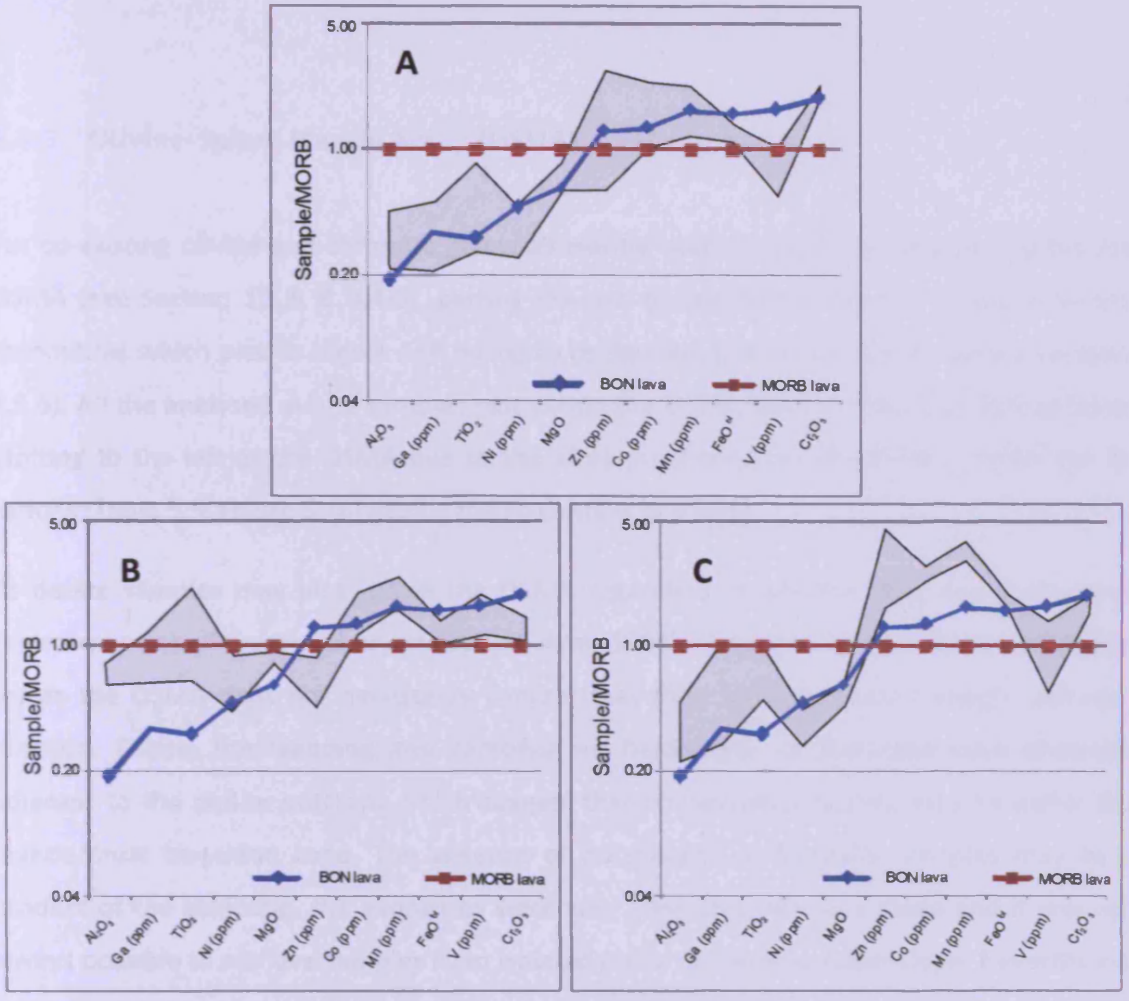

Figure 5.15: *MORB normalised multi-element plots for the Thetford Chromitites (**A**) (Page and Barnes, 2009) and the Berit Chromitites (**B** & **C**). B: shows the compositional range of the majority of the Berit chromitites. C shows the compositional range of the 4 samples which carry a distinctive geochemistry from the rest (MBT-15, MBD-4, MBT-15, MBK-2). The blue line indicates the chromite composition from a chromite grain within a boninitic lava. MORB and boninite sources taken from Page and Barnes (2009). Note: the Co and Zn values for B & C are semi-quantitative.*

The key differences are in Al_2O_3, Ga, Ni, MgO and Cr_2O_3. The lower Cr_2O_3 and higher Al_2O_3 imply that lower degrees of partial melting occurred to produce the parent liquid of the Berit chromitites, than the degree of melting required to eventually result in the formation of the Thetford chromitites. However there are 4 samples which contain noticeably different geochemistry from the majority of the Berit chromitites (MBT-15, MBD-4, MBK-2, MBK-14). These show greater similarity to both the Thetford chromitites and boninitic lava (Figure 5.15C), as well as the Al'Ays and Shetland chromitites (Section 3.4.3 & 4.4.4), than to the bulk of the Berit chromitites.

5.4.5 Olivine-Spinel Mantle Array (OSMA)

For co-existing olivine and chromite grains all mantle hosted samples should plot within the OSMA (see Section 1.5.6 & 4.4.5), barring the use of any olivine samples within podiform chromitites which plot to higher Fo# owing to re-equilibration within the 2+ cations (Section 1.5.6). All the analysed dunite samples plot within the OSMA, with all the chromitite samples plotting to the left of the OSMA due to the afore-mentioned re-equilibration within the 2+ cations (Table 5.5, Figure 5.16) raising the Fo content of olivine.

As dunite samples may plot within the OSMA regardless of whether they are products of replacement or of fractional crystallization (Arai, 1994), the presence of dunites exclusively within the OSMA does not necessarily confirm that their formation was through melt-rock reaction. During the mapping and sampling no harzburgite or lherzolite were observed adjacent to the dunite outcrops which suggest that stratigraphically they may lie within the mantle/crust transition zone. The absence of harzburgite or lherzolite samples may be a product of the sampling, the exposures were very good, but also very steep and it was not always possible to retrieve samples from isolated areas up-slope or down-slope. Nevertheless reconnaissance mapping of the area has so far only observed mafic-ultramafic cumulates associated with the chromitite deposits (Aydin Golakoglu, pers. comm). It is interesting to note that two of the dunite samples contain chromite grains which plot with elevated Cr# compared with the rest of the analysed dunites (Figure 5.16). This may suggest their formation from more primitive magmas (see Section 1.5.6). These two samples are discussed further in Section 5.6.1.

Table 5.5: *Table showing the Cr#, Mg# and TiO_2 contents of chromite grains within all the dunite samples and any chromitite samples containing analysable olivine. Also shown are the forsterite values of the analysable olivine grains.*

Sample	Lithology	Locality	Mg#	Cr#	TiO_2	Olivine Fo#
Ader-1	Dunite	Dereagzi	0.28	0.80	0.39	0.92
Ader-9	Dunite	Dereagzi	0.46	0.52	0.12	0.90
Ader-12	Dunite	Dereagzi	0.54	0.57	0.05	0.92
Ader-13	Dunite	Dereagzi	0.24	0.84	0.46	0.91
MBD-11	Chromitite	Dereagzi	0.66	0.44	0.43	0.93
DMK-9	Chromitite	Demerlik	0.68	0.49	0.16	0.94
DMK-12	Chromitite	Demerlik	0.66	0.54	0.24	0.95
DMK-13	Dunite	Demerlik	0.52	0.53	0.24	0.92
DMK-14	Dunite	Demerlik	0.49	0.51	0.33	0.91
DMK-15	Dunite	Demerlik	0.37	0.64	0.20	0.91
DMK-18	Chromitite	Demerlik	0.69	0.50	0.17	0.95
DMK-28	Chromitite	Demerlik	0.71	0.50	0.18	0.96
DMK-29	Dunite	Demerlik	0.44	0.57	0.45	0.91
KBK-1	Dunite	Kabakteppe	0.47	0.57	0.35	0.92
KBK-3	Dunite	Kabakteppe	0.49	0.55	0.22	0.91
KBK-41	Dunite	Kabakteppe	0.49	0.52	0.06	0.91
KBK-42	Dunite	Kabakteppe	0.41	0.56	0.05	0.91
KBK-16	Chromitite	Kabakteppe	0.71	0.50	0.16	0.95
KBK-17	Chromitite	Kabakteppe	0.64	0.50	0.17	0.93
KBK-18	Chromitite	Kabakteppe	0.65	0.50	0.19	0.94
KBK-21	Chromitite	Kabakteppe	0.69	0.51	0.28	0.95
KBK-22	Chromitite	Kabakteppe	0.70	0.52	0.29	0.95
KBK-36	Dunite	Kabakteppe	0.48	0.55	0.34	0.91
KBK-37	Chromitite	Kabakteppe	0.72	0.47	0.22	0.96
KBK-38	Chromitite	Kabakteppe	0.73	0.47	0.24	0.96
KBK-39	Chromitite	Kabakteppe	0.72	0.48	0.24	0.95

5.4.6 Cr#-TiO_2 diagram (Pearce *et al.*, 2000)

The Cr# - TiO_2 diagram for chromite grains in mantle peridotite samples was developed to distinguish between the effects of partial melting and melt/rock reaction (Arai, 1992; Zhou *et al.*, 1996; Pearce *et al.*, 2000) (see section 1.5.6 for more details). For the Berit dunite samples the majority of those analysed plot along a reaction trend between highly depleted peridotite and a MORB-type melt (Table 5.5, Figure 5.17). There are two chromite grains from within the dunite samples which suggest they have been produced through a reaction between highly depleted peridotite and island-arc tholeiite magma rather than highly depleted peridotite and MORB magma. These were the same two samples with high Cr# within the OSMA array (Figure 5.16), and are discussed further in Section 5.6.1.

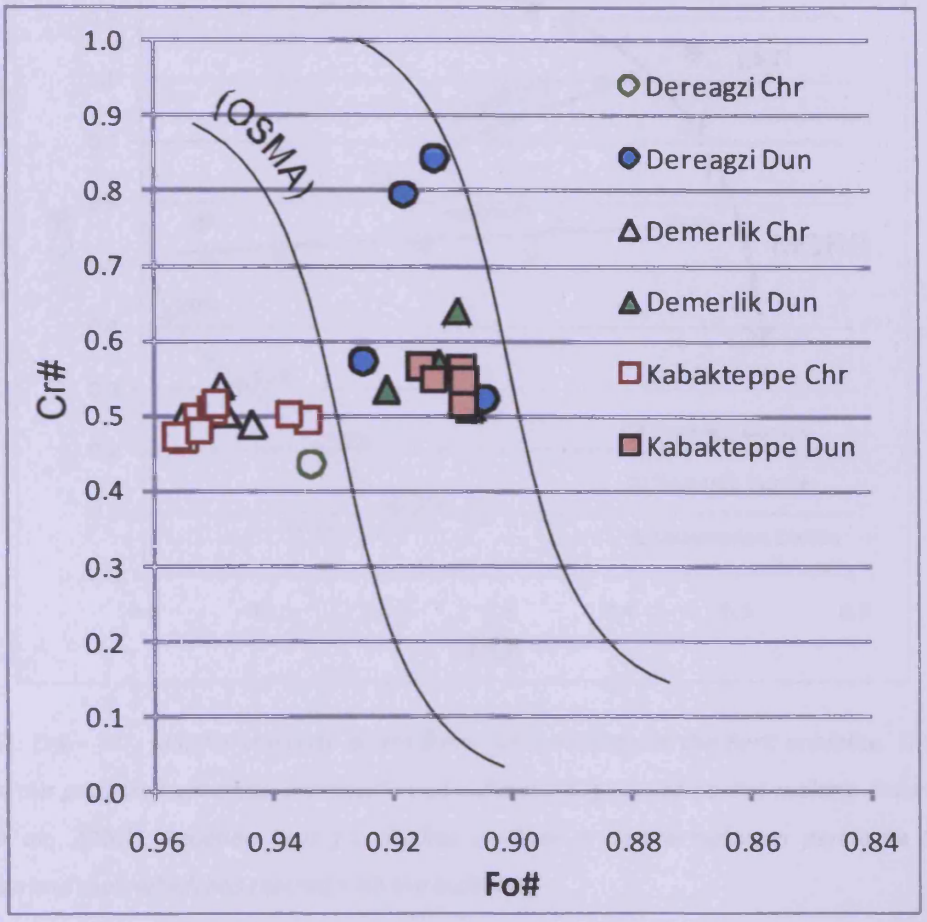

Figure 5.16: *Olivine Spinel Mantle Array (OSMA) (e.g. (Arai, 1994)) plot showing Cr# - Fo# for the Berit chromitites and dunites.*

It is not clear how diagnostic the Cr# - TiO_2 diagram would be within the mantle/crust transition zone of an ophiolite, particularly if there is no hostrock (i.e. harzburgite or lherzolite) for the upwelling melt to react with – and none was unambiguously observed. Analogous high-Al chromitites within the Chinese ophiolites (Zhou *et al.*, 1998), which are postulated to be of back-arc origin and the presence of hydrous silicate inclusions within the chromitites indicates that the melt was hydrous and therefore makes reaction with a MORB-type melt unlikely. Further research on this ophiolite requires the identification and analysis of mantle hostrock (whether lherzolite or harzburgite) to use this diagram more effectively.

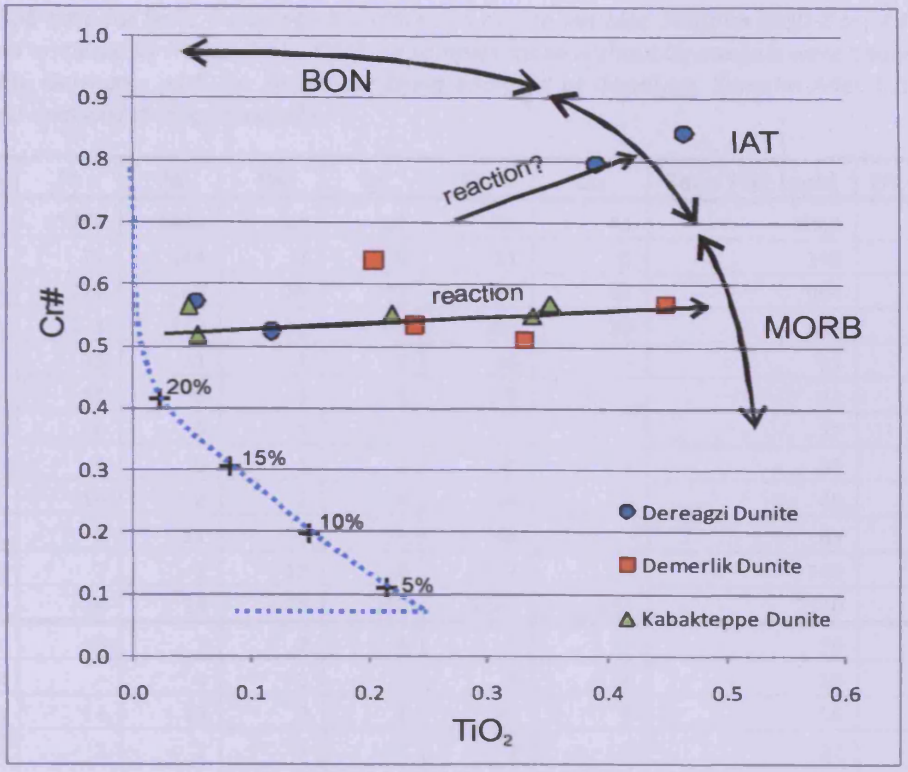

Figure 5.17: *Cr# - TiO_2 plot for chromite grains from the dunites from the Berit ophiolite. The blueline represents the predicted chromite composition at different degrees of partial melting (adapted from (Pearce et al., 2000)). Reaction lines for dunites produce a tie-line between peridotite host rock composition and melt which has reacted with the host rock.*

5.5 The platinum-group elements

Previous analyses of PGE's from chromitites within the Berit ophiolite revealed some high PGE values in individual samples, including some anomalous Pt and Pd concentrations (e.g. MBD-8 from Dereagzi; Table 5.6; Kozlu *et al.*, 2010). This provided the rationale for a field trip to Berit in order to collect more detailed *in-situ* samples from three chromitite pods at Dereagzi, Demerlik and Kabakteppe. Sulphide-bearing chromitites and dunites from Dereagzi were analysed and uniformly returned extremely low PGE values (ADer-1 to ADer-13 – Table 5.6), suggesting that the mechanism concentrating PGE can produce extremely variable PGE values within a single chromitite pod (similar to the observation at the Cliff chromitite quarry). The very low PGM content of the samples with only the occasional very small Os-Ir-Ru grain observed was also replicated in chromitite samples from Demerlik and Kabakteppe so PGE analyses were not performed from these sites.

Table 5.6: *PGE data for Berit, including chromitite and dunite samples. Samples MBD-8 to MBT-15 were collected and analysed by Hatice Kozlu. Of these samples those without Os analysis were analysed at the Karlsruhe lab, Germany, with the remainder being analysed at Genalysis. Samples Ader-1 to 13 were collected and analysed during this study.*

Sample#	Pt	Pd	Rh	Ir	Ru	Os	Total PGE (ppb)	(Pt + Pd)/Ir
MBD-8	1700	4469	31	25	35	41	6301	246.8
MBD-7	74	144	6	6	11	5	246	36.3
MBD-13	321	509	18	32	51	33	964	25.9
MBK-2	271	143	23	62	108	28	635	6.7
MBD-11	25	31	2	7	16	-	81	8.1
MBA-6	11	6	1	2	12	-	32	6.9
MBP-3	10	3	1	3	9	-	27	4.1
MBI-5	9	5	2	8	25	-	50	1.8
MBS-1	10	2	2	8	19	-	40	1.5
MBK-14	5	11	5	17	45	-	83	1.0
MBD-4	7	1	13	110	617	-	749	0.1
MBT-15	14	14	28	286	1275	523	2140	0.1
ADer-1	6	7	2	6	6	3	30	2.2
ADer-2	-	4	1	-	8	3	16	-
ADer-3	14	10	2	4	19	7	56	6.0
ADer-4	2	7	1	2	7	3	22	4.5
ADer-5	5	7	-	-	8	3	23	-
ADer-8	9	14	2	5	7	7	44	4.6
ADer-9	7	12	2	5	8	5	39	3.8
ADer-13	15	14	2	4	7	3	45	7.3

Chondrite normalised graphs of the Dereagzi dunites and chromitites show a jagged, but otherwise fairly or relatively flat profile (Figure 5.18). However, many of the PGE's are present in concentrations that are so low as to be just below their detection limit.

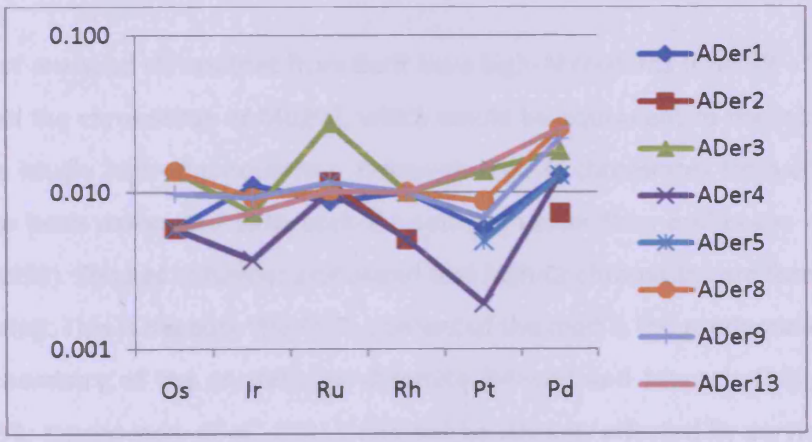

Figure 5.18: *Chondrite normalised graph for the dunites and chromitites from the Dereagzi outcrop. Sample Ader2 to Ader5 are the chromitite samples.*

5.6 Discussion

5.6.1 Tectonic setting

The presence within the Berit ophiolite of two distinct chromitite groups (high- Al chromitites with a Cr# < 0.55 and high Cr chromitites with a Cr# > 0.64) based on differences in their geochemistry without any chromitites of intermediate composition (Figure 5.13, 5.14 & 5.15; Uysal, 2008; Kozlu *et al.*, 2010) suggests that two different magma types have infiltrated the ophiolite. Petrographically the four high-Cr# samples are marked by a generally poor preservation of interstitial silicates, a lack of silicate inclusions and extensive fracturing (Appendix 1). This is typical of chromitites that have been 'squeezed' and 'tectonized' during mantle flow prior to obduction (see Figure 1.7; Nicolas, 1989). In contrast many (though not all) of the high-Al chromitites are well preserved with obvious silicate inclusions and well preserved interstitial silicates. These petrographic differences, together with the obvious geochemical differences suggest that the four anomalous chromitite samples may have formed within a different tectonic setting.

This has been previously observed within another Turkish ophiolite (Muğla: (Uysal, 2009)), where a tectonic switch was proposed to explain a difference in chromitite geochemistry. Uysal proposed that the high-Al (Cr#: 49 - 54) chromitites formed at a fast-spreading mid-ocean ridge setting. As the extensional regime finished, subduction was initiated, presumably below the previous site of high-Al chromitite deposition – leading to boninitic melts and high-Cr chromitites.

The majority of analysed chromitites from Berit have high-Al contents (Cr#: 39 – 55, some with lower Cr# than the chromitites of Muğla), which would be equivalent to the mid-ocean ridge setting of the Muğla high-Al chromitites. However, high-Al chromitites from other ophiolite localities have been associated with back-arc settings rather than mid-ocean ridge settings (Zhou *et al.*, 1998). Zhou *et al* further postulated that high-Cr chromitites are formed within an island-arc setting. This is because the Al_2O_3 content of the melt is the predominant control on the Cr# geochemistry of the crystallizing chromite (Maurel and Maurel, 1982; Roeder and Reynolds, 1991; Kamenetsky *et al.*, 2001), and will be strongly affected by varying the degree of partial melting in the source region. As such, higher degrees of partial melting within the island arc or possibly the fore-arc setting will produce higher Cr# chromitites.

In addition the Berit high-Al chromitites also contain hydrous inclusions (e.g. edenite), along with their anhydrous inclusions (e.g. diopside) suggesting that the magma from which the chromites crystallized was hydrous. This is significant because the water content of MORB magmas is much lower and hydrous inclusions within chromite grains formed within the mantle or the deep crust are therefore highly unlikely. This suggests a possible switch in tectonic setting from island arc to back-arc (as the high-Cr chromitites are more deformed they may have formed earlier) as a cause of the variation in chromitite geochemistry within the Berit ophiolite. The predominance of high-Al chromitites within Berit suggests that back-arc ophiolite magmatism dominated over island-arc magmatism within this ophiolite.

The grab and in-situ samples taken from the Dereagzi outcrop show some wide ranging chromite compositions which could be construed as evidence for both melts within a very close spatial association. For the grab samples MBD-4 contains a unique chromite geochemistry compared with other chromitite samples from the same location (e.g. MBD-7, MBD-8, MBD-13: Table 5.3 & (Kozlu *et al.*, 2010)).

Investigation of the exact location of grab sample MBD-4 revealed that it came from a spoil tip associated with a smaller pod slightly separated from the main outcrop (Kozlu, pers.comm, Figure 5.19). One possible explanation is that this smaller pod may have been faulted into proximity, rather than unequivocal evidence of compositionally very different melts sharing the same melt pathways.

The in-situ dunite samples contain chromite grains which show large variations in composition over very small scales (a few cm's) (Figure 5.16, 5.17 & 5.20). In particular Ader-12, which lies between Ader-1 and Ader-13 contains chromite with a Cr# of 0.57 whilst the latter samples contain Cr#'s of 0.80 and 0.84. Ader-9 which is from the same locality contains a Cr# of 0.52 (Figure 5.20, Table 5.7).

However, the large geochemical variations within the dunite samples, over such a small scale, need not be explained by large changes in the composition of the crystallizing melts. The main reason to suppose otherwise is a detailed look at the composition of the high Cr# chromite grains. Relative to the low Cr# chromite grains the high Cr# chromite grains also contain enriched FeO, TiO_2, MnO, NiO, highly enriched Fe_2O_3, depleted Al_2O_3 and depleted MgO. In contrast, V_2O_5 and Cr_2O_3 are roughly constant across the four samples (Table 5.7).

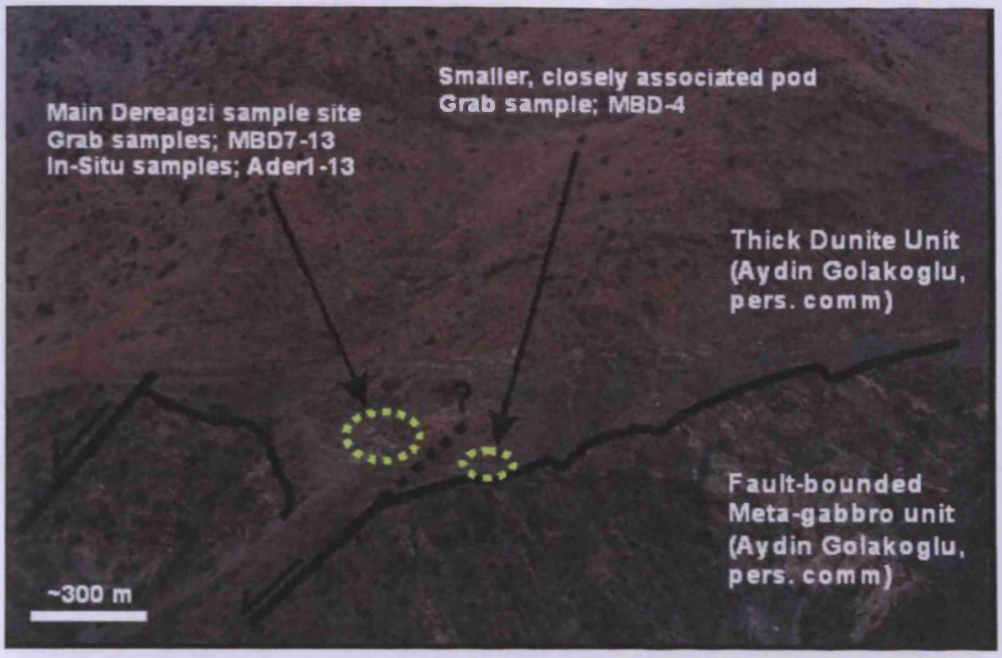

Figure 5.19: *Overview map of the Dereagzi quarry showing the main chromitite quarry from which the bulk of the samples were taken and the smaller chromitite pod from which grab sample MBD-4 was taken.*

Table 5.7: *Table comparing major and trace element concentrations of chromite grains within dunites from the Dereagzi outcrop. Ader-1 and Ader-13 contain high Cr# compared with Ader-9 and Ader-12 which contain lower Cr#.*

	Ader-1	Ader-13	Ader-9	Ader-12
Cr#	0.80	0.84	0.52	0.57
Al_2O_3	6.89	4.86	23.00	21.05
Cr_2O_3	40.05	39.20	37.67	41.96
FeO	24.94	25.97	20.81	17.58
Fe_2O_3	23.55	25.95	9.29	8.49
MgO	5.49	4.58	9.90	11.71
TiO_2	0.39	0.46	0.12	0.05
V_2O_5	0.27	0.34	0.42	0.23
MnO	0.50	0.52	0.36	0.34
NiO	0.23	0.27	0.17	0.12

The approximate constancy of the Cr_2O_3 values across both high and low Cr# chromitites shows that the variation in Cr# is caused by the preferential replacement of Al_2O_3 by Fe_2O_3 within the high Cr# chromite grains. This may occur during amphibolite facies metamorphism due to the metamorphic exchange of Al and Fe^{3+} between chromite and chlorite (Barnes, 2000; Makeyev, 2006). These authors also observed a similar enrichment in MnO, TiO_2 and FeO together with the depletion of MgO.

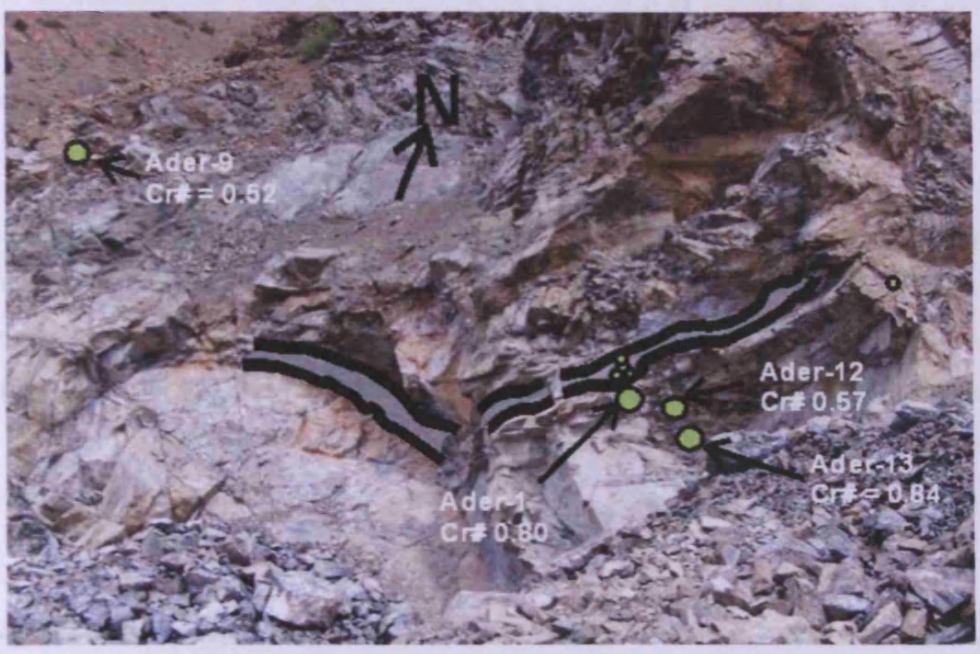

Figure 5.20: *Map of the Dereagzi outcrop showing the analysed dunite samples and their associated chrome-spinel compositions.*

However both authors reported a decrease in NiO in the metamorphosed chromite grains (Barnes, 2000; Makeyev, 2006). The most likely explanation for the observed enrichment within the metamorphosed Berit chromite grains may be the high Fe^{3+} values attained during chemical alteration (Table 5.5). This is because Fe^{3+} rich spinels tend towards the inverse spinel structure, where divalent ions are in octahedral co-ordination (Barnes, 1998). As nickel has a strong octahedral site preference the partition coefficient between Ni and chromite will increase if the Fe^{3+} content of the chromite increases sufficiently to allow for prevalent octahedral site co-ordination (Barnes, 1998).

The study of Al-Fe^{3+} exchange in komatiitic chromite grains also observed that the effect was occasionally restricted to only a few grains within each locality. The explanation given for the high degree of variability was the variation in fluid-rock ratios (Barnes, 2000), and the supposition that low fluid contents may cause elemental transport restrictions. If this is the case then large variations may occur with the fluid-rock ratio over very small distances (Figure 5.20).

As such it is only the variations in the chromite geochemistry within the chromitites which provide an indication of a change in melt composition, and as argued above, they point to a switch between island arc and back-arc magmatism with the latter being the more dominant of the two. This may be achieved shortly after subduction initiation due to slab roll-back (Wortel and Spakman, 2000 & references therein) (Figure 5.21).

If the rate of roll-back exceeded the rate at which the subduction zone was travelling over the mantle (at least initially), then the locus of island arc magmatism will move towards the ocean. This means that a supra-subduction site that was on the island arc axis will be left behind and fall into the back-arc region (Figure 5.21). Back-arc magmatism must be sufficiently 'wet' to allow for hydrous silicates to form as inclusions within the chromite. If this is not the case, then adjustments in this model are required.

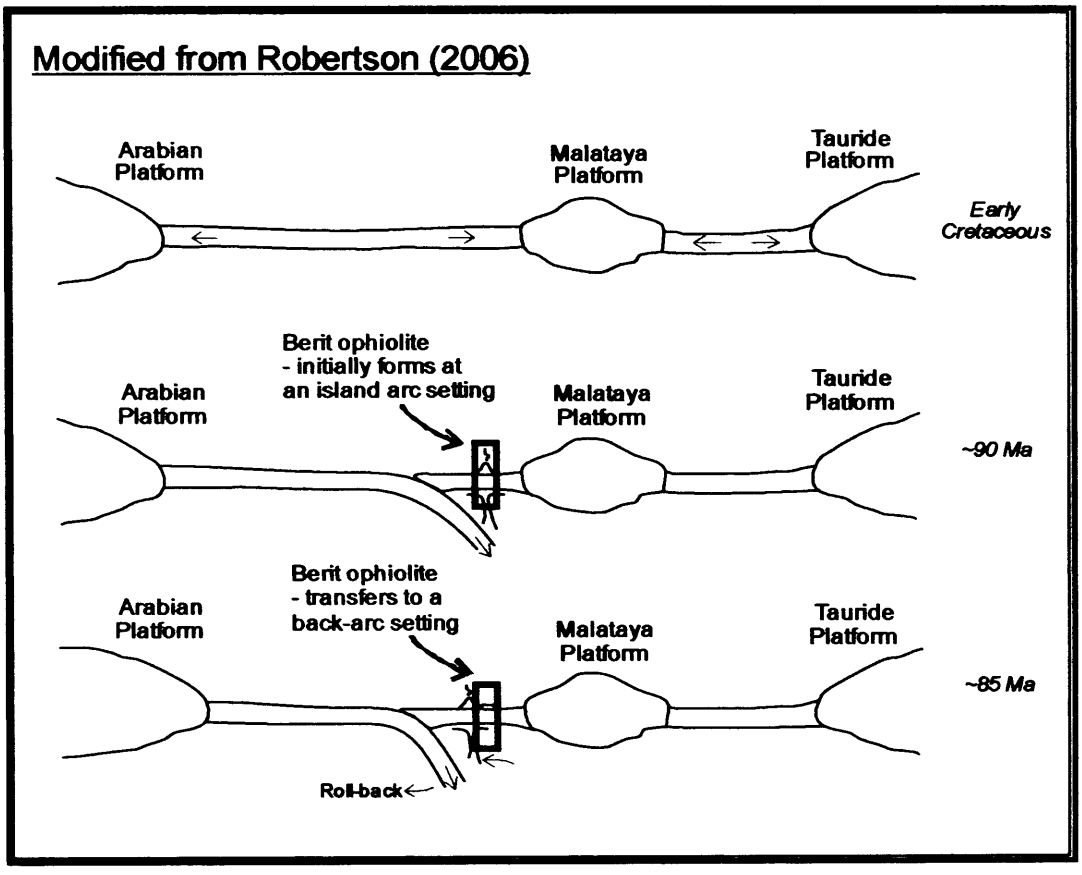

Figure 5.21: *Tectonic history of the Berit ophiolite showing a switch in tectonic setting from island arc to back-arc shortly after subduction initiation.*

5.6.2 The formation of chlorite-filled exsolution lamellae

5.6.2.1 Are the textures representative of exsolution lamellae?

There are three possible explanations for the formation of chlorite filled lamellae showing crystallographic orientation, namely controlled by cleavage, intergrowth or exsolution textures. Chromite has poorly developed cleavage along {111}, which could produce partings oriented at 60° to one another. However these are nearly always overprinted by intense cracking (Ramdohr, 1980; Christiansen, 1986). Whilst some of the features observed within Berit could be attributed to a poorly developed cleavage, the repeated occurrence of fine-grained chlorite inclusions oriented at 60° to one another make cleavage a somewhat unsatisfactory explanation.

Chlorite filled lamellae (oriented parallel to the {111} plane) have been reported from chromite within the Pedra Branca Mafic-Ultramafic complex, Brazil (Fleet *et al.*, 1993). They interpreted the feature as representing the product of intergrown chlorite-chromite grains, and crucially did not equate the texture as having formed through exsolution. Since there was considerable misfit in the strain-free equivalent lattices of chromite and chlorite, Fleet *et al.* (1993) postulated a possible interlayer of brucite. Whilst Fleet *et al.* (1993) go to some lengths to show that the interface between the chromite and the chlorite is not optimal the discussion on the formation of the intergrowths itself is limited. In short they propose that these chlorite filled lamellae form through the diffusion of constituents through the chromite lattice with lamellae finally nucleating within the core of the grain. Whilst lattice diffusion is conceivable, no explanation is given of why oriented chlorite lamellae should nucleate in such a manner, especially along a non-optimal interface, or if such a mechanism is possible why it is not a far more widespread occurrence. Given the mechanism proposed by Fleet *et al.* the present author does not have any explanation as to why this texture is not more widely observed.

A further possible explanation is that the textures represent the product of exsolution whereby a pre-chlorite phase exsolves out of the chromite grain before being altered to chlorite. In a review in 1942, Schwarz outlined 11 criteria necessary for exsolution. Some of these criteria are meaningless if the exsolved phase then undergoes alteration (e.g. 'the inclusions are often single crystal units'), or if the exsolution is the product of metamorphism/ alteration (e.g. 'even distribution of inclusions throughout the grain'). Of those criteria that remain the clearest indicators of exsolution are:

(1) Exsolution inclusions show crystallographic control and are widely distributed.

(2) Inclusions may be lamellar and characterized by sharp yet smooth boundaries,

(3) There is no enlargement is present where exsolution blades cross or join,

(4) If the included mineral is present outside the intergrowth then the manner of occurrence becomes an indication either for or against exsolution. If the occurrence is as veinlets then exsolution is unlikely. If the occurrence is as contemporaneous grains then exsolution is favoured. Chlorite occurrences within the analysed Berit samples were always as contemporaneous grains.

(5) Orientation of blades differs for each grain, dependent on the relation of the polished plane to crystal orientation.

The chlorite-filled lamellae within the Berit chromitites and dunites fulfill all these criteria. These tests along with the arguments against the intergrowth mechanism proposed by Fleet *et al.* (1993) lead the present author to prefer the formation of these lamellae by exsolution of a pre-chlorite phase followed by alteration.

5.6.2.2 Examples of exsolution within chromite grains

Although unusual, exsolution in chromite has been predicted theoretically (Sack and Ghiorso, 1991), and observed repeatedly in several different tectonic settings (e.g. Loferski and Lipin, 1983; Eales *et al.*, 1988; Zakrzewski, 1989; Barnes and Tang, 1999; Tamura and Arai, 2005). Exsolution in chromite appears to follow two main patterns, either crystallographically oriented exsolution lamellae (e.g. Deb and Chakraborty, 1961; Loferski and Lipin, 1983; Yamamoto *et al.*, 2008) or blocky irregular exsolution (e.g. Eales *et al.*, 1988; Proenza *et al.*, 2008). Occasionally the blocky irregular exsolution form complex symplectic textures (Tamura and Arai, 2005). For oriented exsolution lamellae within a chromite host, the lamellae may be filled with ilmenite (Deb and Chakraborty, 1961; Eales *et al.*, 1988), ulvospinel (Barnes and Tang, 1999) or clinopyroxene and coesite (Yamamoto *et al.*, 2008). Alternatively, in chromium-free spinels, oriented exsolution has produced Fe^{3+}-rich spinel hosted within Al-rich spinel (Ahmed *et al.*, 2008). One worker has produced research into the presence of Al-rich oriented exsolution lamellae hosted within chromite grains (Loferski and Lipin, 1983).

Loferski and Lipin, (1983) discovered exsolution lamellae in chromite within ultramafic rocks metamorphosed to amphibolites facies, from the Red Lodge District, Montana. They reported three textures. The first is irregular blocky exsolution of a Fe-rich spinel guest within an Al-rich chrome-spinel host (type A), and the second is composed of elongated oriented exsolution of predominantly an Al-rich chrome-spinel guest within a Fe-rich host (type B). Type C exsolution consists of extremely fine lamellae of an Al-rich mineral within Fe-rich chromite. Analysis of the spinel pairs within both type A and type B exsolution reveals a miscibility gap in the Cr-Al-Fe^{3+} plane of the spinel prism, which accords well with that predicted by thermodynamic considerations (Sack and Ghiorso, 1991) very similar to those reported by Tamura and Arai in 2005. The fine size of the type C exsolution meant separate analysis of the host and the guest were not possible, though the bulk composition did lie within the miscibility gap defined by type A and type B exsolution, suggesting that the guest in this instance was also Al-rich spinel (Figure 5.22).

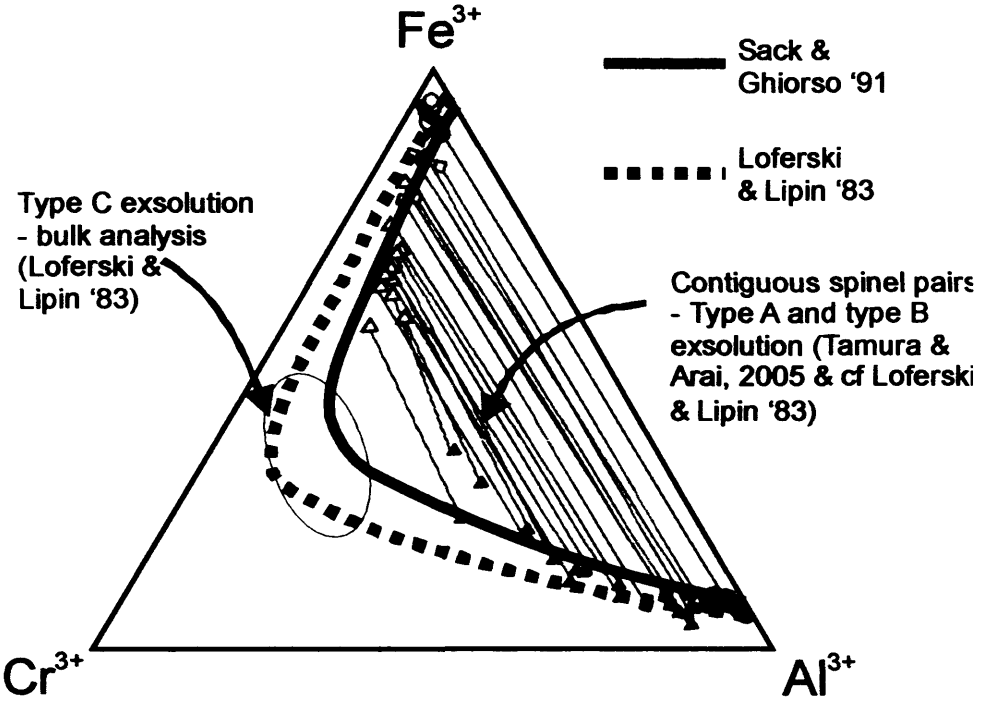

Figure 5.22: *Compositional plot through the Cr-Al-Fe^{3+} plane of the spinel prism. The dashed line represents the solvus estimated by Loferski and Lipin, (1983) from contiguous pairs within the Red Lodge District, Montana. The solid line represents the solvus calculated from thermodynamic considerations by Sack and Ghiorso (1991) for spinels co-existing with Fo_{95} olivine at 600 °C. Also shown are contiguous pairs reported by Tamura and Arai (2005) in the Iwanai-Dake peridotite complex, which are equivalent to the contiguous pairs reported by Loferski & Lipin (1983). The bulk composition of type C exsolution from Loferski & Lipin (1983) is also shown.*

The observation of exsolved clinopyroxene and coesite within chromite was made from podiform chromitites from the Luobusa ophiolite in southern Tibet (Yamamoto *et al.*, 2008). They postulated an ultra-high pressure origin (100 to >380 km) for the chromite grains exsolving clinopyroxene (which they identified as diopside). Yamamoto *et al.*, (2008) referred to other published literature on the Luobusa ophiolite to support their inference, including the observation of micro-diamonds, coesite and highly reduced metal phases and their likely origin within the deep mantle (e.g. Bai *et al.*, 1993; Robinson *et al.*, 2004; Yang *et al.*, 2007) .

However, there are several reasons to suppose that the chlorite filled lamellae have not formed by alteration from clinopyroxene. Firstly, the clinopyroxene inclusions observed in the Luobusa chromite grains were very small, extending no larger than half a mm in length. This contrasts to the cm-scale chlorite lamellae in Berit. Secondly, the observed clinopyroxene lamellae within Luobusa were associated with coesite. This suggests a similar association would be observable within Berit, and coesite would survive the effects of alteration. However, no coesite or quartz was observed. Thirdly, no UHP minerals of any kind have been observed within Berit either by previous workers or during this study. Finally, although diopside may alter to chlorite there would be an expected accessory Ca-bearing phase (e.g. calcite, epidote) none of which were observed.

5.6.2.3 Why is there exsolution within the Berit chromitites?

Geochemically, the chromite grains which host chlorite filled exsolution lamallae within the Pedra Blanca Mafic-Ultramafic complex (Fleet *et al.*, 1993) are very similar to those within the Berit ophiolite, and both lie noticeably outside the miscibility gap defined by previous workers (e.g. the miscibility gap defined by (Loferski and Lipin, 1983; Barnes and Roeder, 2001) for reported spinel-spinel associations (Figure 5.23). Nevertheless, the compositions of the chromite host do lie within an immiscibility field defined by Sack and Ghiorso '91 for chrome-spinels co-existing with Fo_{90} olivine. In Berit the forsterite number of olivine within chromitites usually lies around Fo_{94-96}. However, this is mainly due to the re-equilibration of minor olivine with the bulk quantities of chromite which surround it. The likely crystallization composition of the olivine will be closer to Fo_{90} as shown by the olivine within the dunites surrounding the chromitite pods (cf. Figure 5.16). This means that after crystallization and cooling these chromite grains would have resided within a miscibility field.

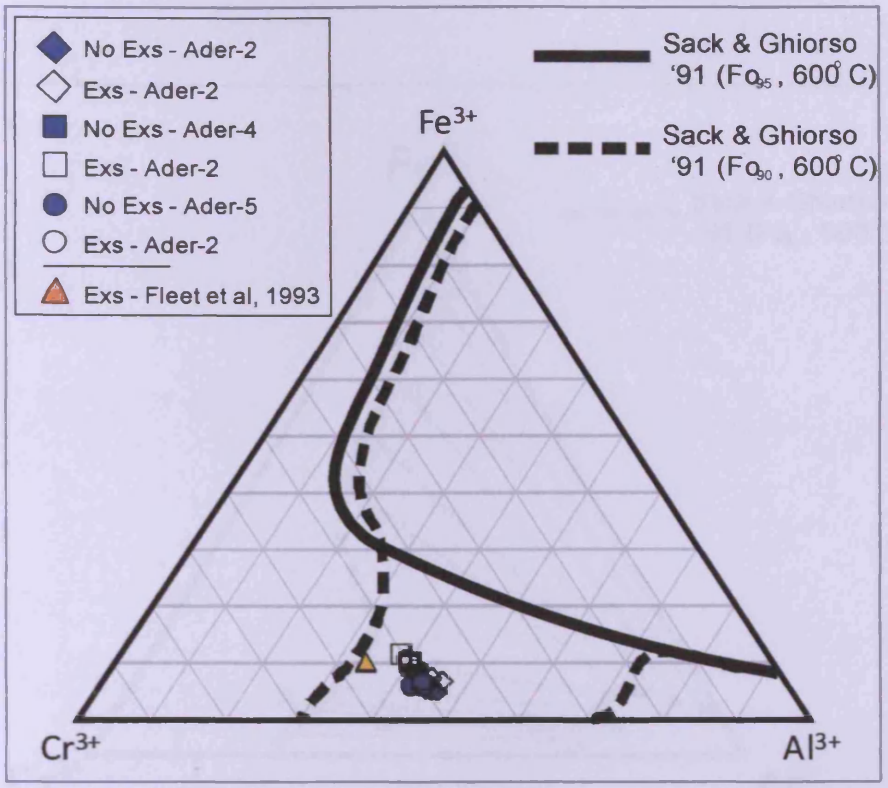

Figure 5.23: *Compositional plot through the Cr-Al-Fe^{3+} plane of the spinel prism. The dashed line represents the solvus calculated from thermodynamic considerations by Sack & Ghiorso, 1991 for spinels co-existing with Fo_{90} olivine at 600°C. Also shown are the compositions of chrome-spinels from Berit which host exsolution (empty markers), chrome-spinels which are free of exsolution (solid blue markers), and a comparison to the chrome-spinels observed in the Pedra Blanca mafic-ultramafic complex which also apparently host chlorite exsolution.*

During exsolution of these chromite grains two phases would be expected to form - namely a relatively Cr-rich, Al-poor chrome-spinel (composition A; Figure 5.24) and a relatively Al-rich, Cr-poor spinel (composition B; Figure 5.24). As it is, the chromite hosting the exsolving phase retains a composition within the miscibility fields (open markers, Figure 5.23). This may be explained by the kinetics of exsolution and the exact location of the dashed solvus line at slightly higher temperatures. With the solvus as calculated by Sack and Ghiorso, (1991) a cross-section through 'A', 'B' and 'C' will show a solvus curve with composition 'C' lying within, or near, the metastable field (Figure 5.25). At slightly higher temperatures it is reasonable to assume that the two-phase region gets smaller. Using the lever rule it is apparent that the formation of phase A would be limited in this scenario and the formation of phase B could be extensive. The hotter temperature might have the further effect of increasing the rate of reaction producing coarse lamellae, observable under a microscope.

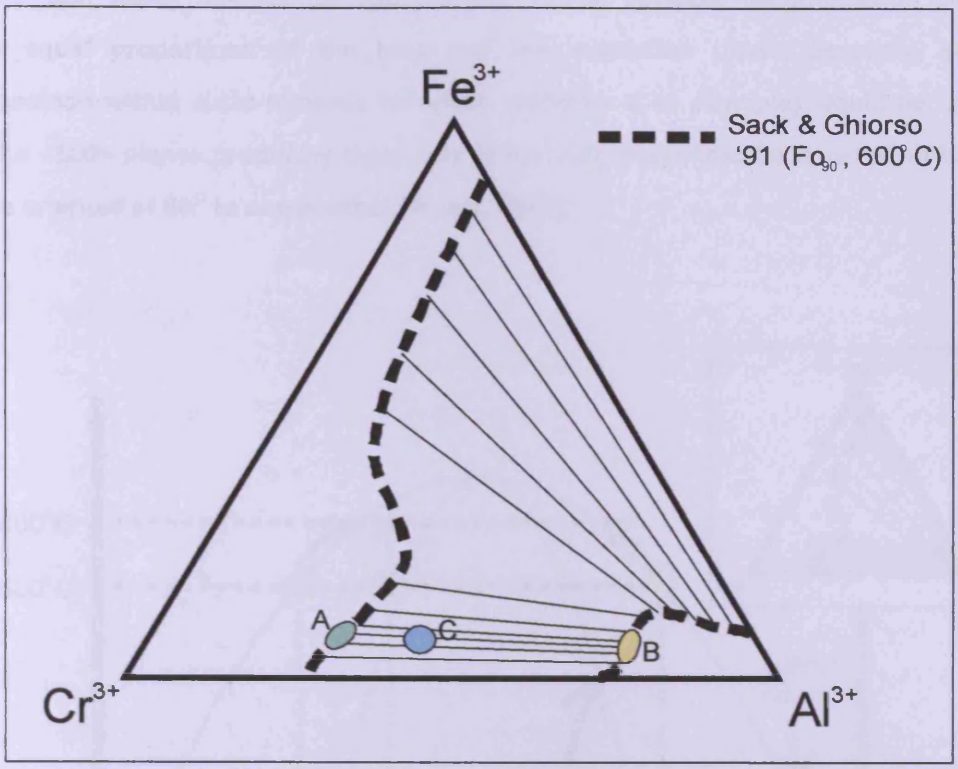

Figure 5.24: *Compositional plot through the Cr-Al-Fe^{3+} plane of the spinel prism. The dashed line represents the solvus calculated by Sack & Ghiorso (1991) for spinels co-existing with Fo_{90} olivine at 600°C. Solid lines denote tie lines between co-existing spinels. 'C' denotes the compositional area formed by the Berit chromitites. 'A' and 'B' denote the expected products of complete exsolution during unmixing of the chromite grains during metamorphism.*

A further implication of the location of composition 'C' with respect to the solvus is the likely exsolution mechanism. If 'C' lies between the solvus and spinodal curves (Figure 5.25) the chromite grain concerned will be metastable, rather than unstable. Minerals lying below the spinodal (i.e. unstable) are more likely to exsolve phases by spinodal decomposition and contain a roughly equal proportion of each phase. The exact proportions would still be subject to the lever rule, but as the spinodal curve lies centrally below the solvus curve the approximate proportions of phases 'A' and 'B' will be similar. In contrast metastable minerals will exsolve by a process of 'nucleation and growth' which usually requires a perturbation in the system to overcome the energy barrier associated with nucleation (Putnis, 1992).

The textures observed within the Berit chromitites of exsolution lamellae make spinodal decomposition highly unlikely for two reasons. Firstly, spinodal decomposition produces roughly equal proportions of the host and the exsolution phase. Secondly, spinodal decomposition within cubic minerals (of which chromite is an example) would be favoured along the <100> planes producing three sets of mutually perpendicular lamellae rather than lamellae oriented at 60° to one another (Putnis, 1992).

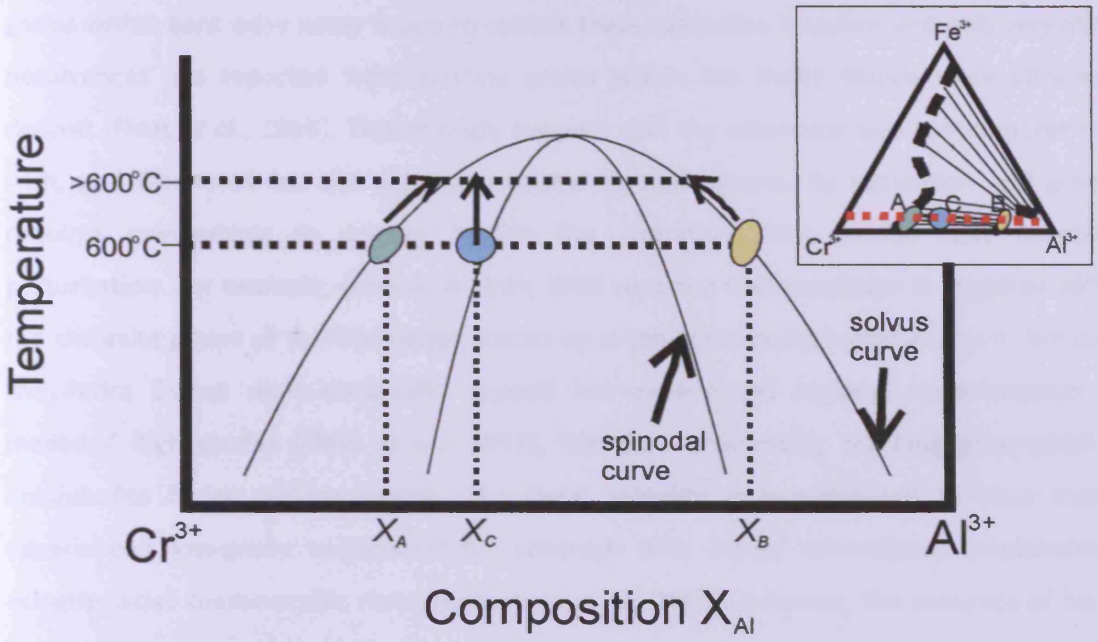

Figure 5.25: *The solvus curve as a function of temperature and composition. Composition is taken parallel to the red-dashed line (inset), which is approximately parallel to the Cr^{3+}-Al^{3+} base of the ternary system Cr^{3+}-Al^{3+}-Fe^{3+}. Also marked are the expected products of exsolution (composition X_A and X_B) after exsolution of chromite have composition X_C. If the temperature of exsolution occurs slightly higher than 600°C, then the product X_A has a very similar composition to X_C and the proportion of X_B formed is higher (by the lever rule). Furthermore at higher temperature the rate of reaction is higher producing coarse exsolution products and observable lamellae.*

Aside from the observation of lamellae at 60° to one another no measurement was made of the precise orientation of these lamellae relative to the chromite lattice. Nevertheless identical patterns of exsolution (i.e. lamellae at 60° to one another) within chromite have previously been shown to be parallel to the {111} plane of the chromite lattice (Fleet *et al.*, 1993). It therefore seems probable that these exsolution lamellae are oriented parallel to the {111} plane of the chromite lattice.

5.6.2.4 What caused the 'nucleation and growth'?

A key similarity of the Berit chromitites to the Pedra Blanca chromitites analysed by Fleet *et al.* (1993) is the association of chlorite lamellae with alteration of the chromite grains. The alteration is defined by an increase in Fe content (both Fe^{2+} and Fe^{3+}), MnO, NiO and a decrease in Al_2O_3 and a minor decrease in Cr_2O_3 (Table 5.2). These trends, although minor, are equivalent to the gradual alteration of chromite to Cr-magnetite (e.g. (Barnes, 2000)). The restriction of exsolution to altered chromite grains is so prevalent that 'pristine' chromite grains within Berit were never found to contain these exsolution lamellae, and only very minor occurrences are reported from pristine grains within the Pedra Blanca mafic-ultramafic deposit (Fleet *et al.*, 1993). This strongly suggests that the exsolution was contemporaneous with, and facilitated by, the alteration of the chromite grains. As nucleation and growth requires overcoming an energy barrier the alteration may provide that necessary perturbation. For example, Loferski & Lipin, 1983 reported that exsolution is triggered within the chromite grains of the Red Lodge district by amphibolite facies metamorphism. Similarly, the Pedra Blanca mafic-ultramafic deposit has experienced regional metamorphism to medium/ high grades (Fleet *et al.*, 1993), therefore presumably reaching greenschist to amphibolite facies metamorphism. The Berit ophiolite is hypothesized to have mainly experienced low-grade metamorphism although with locally intercalated amphibolite - eclogite facies metamorphic rocks (Robertson *et al.*, 2006). However, the presence of highly altered chromite grains within the Dereagzi deposit, as well as amphibole minerals (cummingtonite, anthophyllite and/or tremolite) observed at all localities suggests that the degree of metamorphism within the Berit ophiolite has been undereported with at least amphibolite grades affecting parts of the ophiolite, previously reported as only having undergone greenschist metamorphism.

At the temperature of exsolution the expected exsolved phase would be close to spinel *sensu strictu* ($MgAl_2O_4$) and based on other crystallographically oriented exsolution within chromite grains would grow parallel to the {111} plane (equivalent to growth in three directions at 60° to one another) (e.g. for ilmenite (Deb and Chakraborty, 1961), for spinel (Loferski and Lipin, 1983)). The one exception to this is the growth of clinopyroxene along {011} and {010} within the chromite grain. As the clinopyroxene exsolution within chromite formed under a unique set of conditions it seems reasonable to presume that spinel exsolution within chromite forming under conditions of nucleation and growth would form along the {111} plane.

5.6.2.5 Why are the exsolution lamellae filled with chlorite?

The expected composition of the exsolution 'guest' is close to spinel *sensu strictu* ($MgAl_2O_4$). During metamorphism, spinel may revert to chlorite under the following reaction (Kimball, 1990; Merlini *et al.*, 2009), with the SiO_2, H_2O and MgO provided by the fluid phase. The presence of minor Cr, means the product is more likely to be Cr-chlorite (formerly kammererite).

$$MgAl_2O_4 + 4MgO + 3SiO_2 + 4H_2O \rightarrow Mg_5Al[(OH)_8AlSi_3O_{10}]$$

Indeed in ultramafic systems chlorite is the stable Al-bearing phase during amphibolite facies metamorphism (Jenkins and Chermovsky, 1986; Spear, 1993) and spinel is unstable (Jenkins and Chermovsky, 1986). It follows that the conditions necessary to facilitate exsolution of spinel from chromite coincided with the conditions necessary to alter spinel to chlorite. Where chlorite is present as entirely encapsulated inclusions (e.g. Figure 5.8B) it is hypothesized that lattice diffusion of SiO_2 and H_2O through the chromite lattice has occurred (in a manner suggested by Fleet *et al.* 1994) with chlorite nucleating where spinel is exsolving.

It therefore seems likely that the exsolution observed in the chromitites at Berit is due to immiscibility within the chromite grain which unmixed following amphibolite metamorphism. This was followed by immediate alteration to chlorite. Exsolution required the chromite grains in question to be exposed to fluids at a sufficiently high temperature. This may explain why the most well developed exsolution lamellae were restricted to chromite grains within disseminated dunites as olivine grains would provide less resistance to metamorphosing fluids than the chromite grains within a chromitite.

The exsolution must have occurred during metamorphism (rather than cooling) as exsolution is only present within altered sections of the chromite grains, and furthermore not present throughout chromite grains within the Berit ophiolite. Metamorphism within the chromite grains of Berit, led to crystallographically controlled exsolution of spinel *sensu strictu* into an environment saturated with MgO, SiO_2 and H_2O resulting in the simultaneous alteration to chlorite.

5.6.2.6 Why were exsolution lamellae observed within one sample from Shetland?

Given the explanation for chlorite-filled exsolution lamellae proposed above it is surprising that any exsolution lamellae were observed within chromite grains from the Shetland ophiolite. It is just a few grains, in one sample, but nevertheless is clearly present (Section 4.2.4). The Shetland ophiolite has not undergone amphibolite metamorphism and compositionally the chromite grains lie outside (towards higher Cr#) the solvus proposed by Sack and Ghiorso, (1991) for chromite grains associated with Fo_{90} olivine grains. It is conceivable that the solvus expands at lower temperatures to reach the higher Cr# compositions but then the energy barrier that needs to be overcome for spinel nucleation becomes much higher.

If the texture formed by the same mechanism (i.e. exsolution of a pre-chlorite phase, followed by alteration) then the only possible mechanism is;

1. The solvus expands at lower temperatures (e.g. 500°C) to incorporate higher Cr# chromite grains
2. The temperature to be held steady once the solvus crosses the compositional range of the chromite grain (i.e. very slow-cooling). This allows any nucleating phase the chance to grow. Alternatively, any mechanism which raises the temperature (e.g. regional metamorphism) must not push the composition of the chromite grain outside of the solvus.
3. Possible facilitation of exsolution by metamorphism once again – though in this case fluids associated with upper greenschist facies and not amphibolite facies.

The kinetics of the above scenario are not favourable, especially as exsolution must occur at lower temperatures. This may be the reason why this texture is so infrequently observed.

5.6.3 Why are there some PGE-rich samples at Berit?

This investigation has unfortunately been unable to find any further PGE concentrations greater than that detailed in Kozlu *et al.*, 2010. The sliced and diced nature of the ophiolite outcrop meant no stratigraphic relationships could be tested and as mentioned the chromite geochemistry was largely split into two subsets (High-Cr and high-Al). Nevertheless, high PGE concentrations have been reported from this ophiolite and linked to a general sulphide saturation model through fractionation or possibly to a critical PGE-rich melt fraction sourced from the mantle (Kozlu *et al.*, 2010).

One salient observation from this study may be the nature of the sulphides within the PPGE-poor samples of Dereagzi and PPGM-barren samples of Demerlik and Kabakteppe. These base-metal sulphides are invariably Fe-Ni-rich being exclusively pentlandite, millerite or heazlewoodite with no Cu-rich sulphides observed. In contrast the relatively PPGE-rich samples reported by Kozlu *et al.*, (2010) contains Cu-rich sulphides, chalcopyrite and bornite. This may reflect a correlation between PPGE concentration and fractionation of the base-metal sulphides. During cooling immiscible sulphide liquids fractionate into Ni-, Fe-rich mono-sulfide solid solution (MSS) and a Cu-rich intermediate solid solution (ISS), with Pt and Pd being incorporated into the Cu-rich liquid (e.g. Prichard *et al.*, 2004b). If during this fractionation the ISS becomes separated from the MSS then PPGE mineralization will be associated with the ISS-rich liquids and any subsequent Cu-rich sulphides which crystallize from them. The remaining MSS liquid (from which pentlandite will form) will be PPGE-poor and thus chromitite containing just pentlandite, millerite and heazlewoodite will not contain any PPGM. Separation of Cu-bearing sulphides from Fe-Ni-bearing sulphides is geologically possible and has been previously described in some major PGE-Ni-Cu deposits (e.g. Sudbury Li *et al.*, 1992). Furthermore, this feature of PPGE and PPGM only associated with samples containing Cu-bearing sulphides is also found within the Shetland ophiolite (Prichard *et al.*, 1994). Whole-rock analysis for PGE and Cu has been performed at Al 'Ays and Shetland. For Al 'Ays there is a weakly positive correlation between Pd and Cu (Prichard *et al.*, 2008). At Shetland Cu is concentrated in the same lithologies (i.e. the chromitites) as Pt and Pd within the ultramafic lithologies (Prichard and Lord, 1990). However, Cu concentrations are higher in the PGE-barren gabbros that overlie the ultramafic mantle and lower crust (Prichard and Lord, 1990), suggesting further exploration into any possible links takes account of the respective location within the ophiolite.

Chapter 6

Discussion

A discussion on the formation of inclusion patterns and the petrogenesis of podiform chromitite.

6 Discussion

6.1 Chromitite petrography – inclusion patterns

Inclusions within chromite grains are of particular interest as they carry information on other phases present on the liquidus or suspended in the silicate melt at the time of chromite crystallization. This discussion focuses on two types of inclusion pattern; clustered inclusions and linear trails of inclusions.

6.1.1 Clustered inclusions

Clustered inclusions within chromite grains consist of three main types.

A. Anhydrous silicates such as clinopyroxene.
B. Hydrous silicates such as edenite and phlogopite
C. Hydrous low-temperature silicates such as chlorite, serpentine and *'ugrandite.'* This third type is assumed to be the alteration product of either of the first two due to post-magmatic processes (e.g. serpentinisation) which may occur within an ophiolite.

The presence of type A silicates within chromite grains either represents their co-precipitation with chromite or their prior crystallization within a fluid phase and subsequent encapsulation within a crystallizing chromite grain. Type-B silicates may represent the reaction of type-A silicates with an interstitial or unmixed volatile-rich fluid phase (H_2O and CO_2-bearing; e.g. (Kamenetsky and Kamenetsky, 2010)) or the direct crystallization from that unmixed volatile-rich silicate-bearing fluid phase. The formation of clustered inclusion patterns may be explained by three main processes depending on the time of formation of the chromite grain hosting the inclusions and the surrounding chromite grains which are inclusion empty.

1. Formation of inclusion-rich chromite grains within the silicate melt prior to the majority of chromite crystallization (Figure 6.1A)
2. Formation of inclusion-rich chromite grains within the silicate melt simultaneously to the formation of inclusion-poor chromite grains within the silicate melt (Figure 6.1B).
3. Formation of inclusion-rich chromite grains after the formation of the most of the chromite grains within the chromitite deposit (Figure 6.1C).

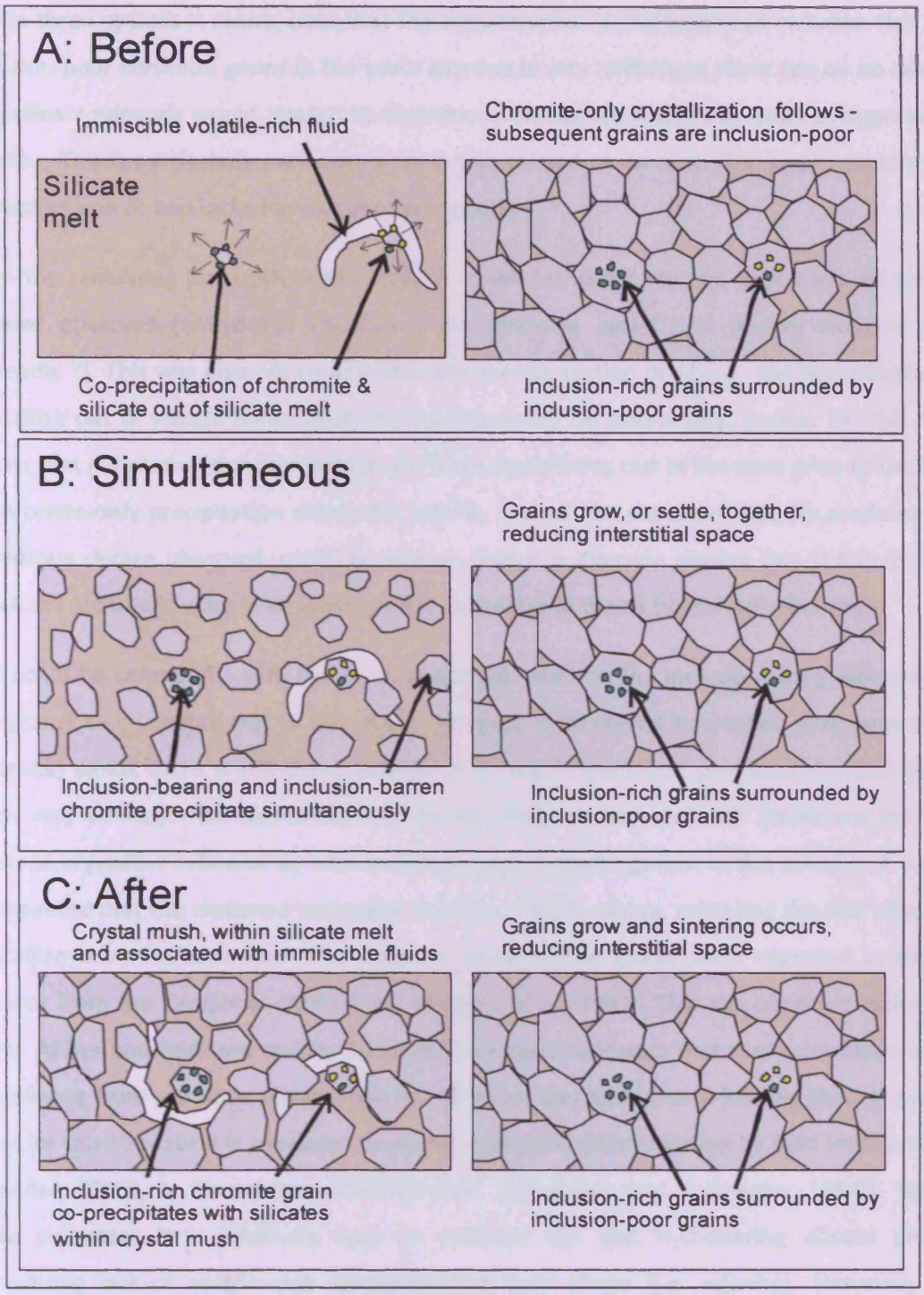

Figure 6.1: *Schematic diagrams on possible formation timings of chromite grains containing clustered inclusions within chromitite sections largely free of inclusions. Green inclusions represent anhydrous silicates, whilst yellow inclusions represent hydrous inclusions probably formed by reaction of anhydrous silicates with non-silicate immiscible liquid.* ***A:*** *Formation of inclusion-rich chromite grain prior to the formation of the chromitite deposit.* ***B:*** *Formation of inclusion-rich chromite grains simultaneously to inclusion-poor chromite grains.* ***C:*** *Formation of inclusion-rich chromite grains after the formation of the rest of the chromite grains within the chromitite.*

Of the three options it seems clear that the simultaneous crystallization of inclusion-rich and inclusion-poor chromite grains in the same location is very unlikely as there can be no reason why silicate minerals would 'prefer' to nucleate in abundance within one grain as opposed to another. This is particularly pertinent when a thin section containing >100 grains contains no more than one or two inclusion-rich chromite grains.

From the remaining two options the content of the inclusions may be important. All type-A silicates observed (anhydrous silicates) were pyroxene based and usually diopside (see Appendix 7). This was also observed within the mantle section of Al'Ays. The first silicates to crystallize out of silicate melt within the mantle would be olivine (e.g. (Irvine, 1977b)). This means that if inclusion-rich chromite grains were crystallizing out of the melt prior to the bulk of chromite-only precipitation within the mantle, it would be expected that the predominant anhydrous silicate observed would be olivine. That it is diopside implies that the fluid from which the inclusions were precipitating was more evolved than a typical primitive melt.

This could be compatible with the third theory, namely that the inclusion-rich grains are the last grains to crystallize out of the melt. However, new crystal nucleation and growth (of chromite) whilst there is still the possibility of Ostwald ripening of previously formed grains seem very unlikely. This leaves the first theory, that the inclusion-rich grains are the first grains to crystallize followed by later inclusion-poor chromite grains. In this scenario it would be expected that the clustered inclusions would be mainly olivine, reflecting the first phase to crystallize out of silicate melt (for example some olivine grains were reported in similar textures from the Kempirsai chromitites, Melcher *et al.*, 1997). That the observed inclusions within Al'Ays and Berit are mainly diopside and edenite suggests that the inclusions are not crystallizing from primitive silicate melt but from an unmixed silicate-bearing fluid phase. In order for this to occur it is necessary to evoke 'magmatic differentiation by fluid immiscibility' (Roedder, 1992), or 'emanation differentiation' (Kovalenko and Kovalenko, 1984)). Within these processes it is relatively easy to envisage Na- and H_2O-bearing silicate phases crystallizing out of volatile-rich silicate-bearing fluid phase (i.e. edenite). However, the crystallization of anhydrous diopside is less obvious and it remains to be shown that fluid or volatile unmixing can produce seemingly well differentiated anhydrous silicates early in the crystallization sequence.

6.1.2 Linear trails of inclusions

As well as explaining the presence of these linear trails of inclusions, it is necessary to explain how they may cut through several grains, occasionally cross-cut one another (Figure 6.2), are often continuous for several mms (Figure 6.3) and most of which are >95% empty in polished thin sections. The observation that the majority of inclusions are empty strongly suggests that they originally contained volatiles which 'escaped' either shortly after formation, during brittle faulting of the chromite grains, or during the preparation of the polished section. Volatiles would most likely be sourced from an immiscible non-silicate liquid which would be associated with the silicate melt. These immiscible non-silicate liquids may form within silicate melts through decompression, cooling and even crystallization (e.g. (Roedder, 1992; Kamenetsky and Kamenetsky, 2010)).

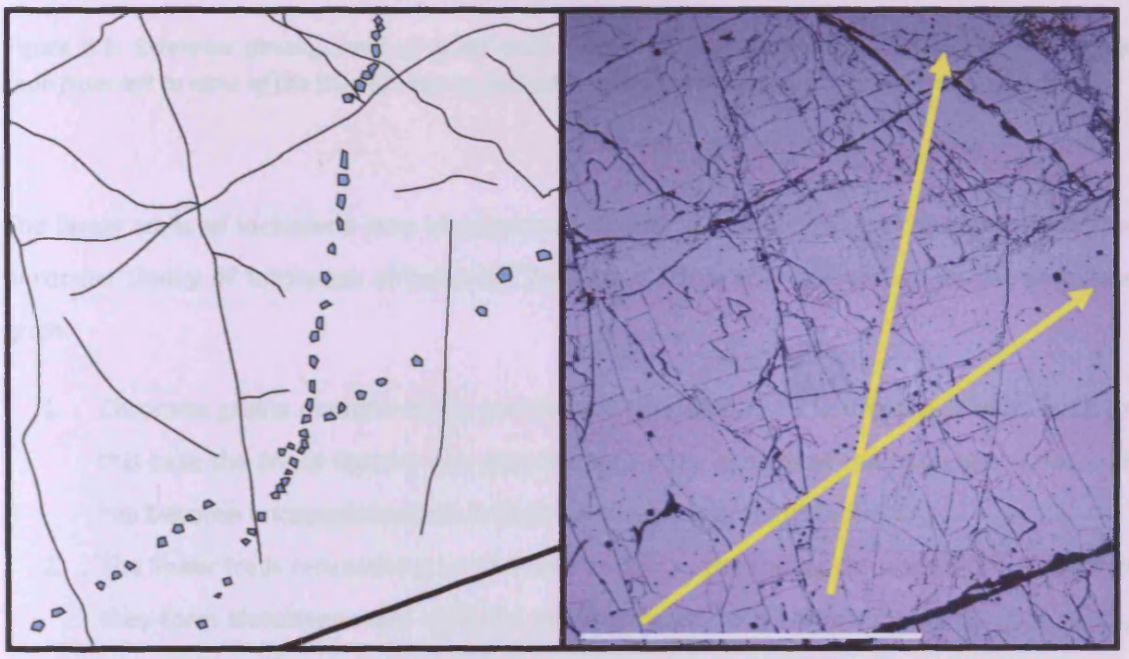

Figure 6.2: *Map of two cross-cutting linear trails of inclusions. The inclusions are marked in blue on the left hand side and by yellow lines of the right hand side. Although grain boundaries are not certain due to the high degree of sintering it is possible that the inclusion trails are also cutting across former grain boundaries. Scale bar represents 2 mm. Photo taken from sample C210, Al'Ays.*

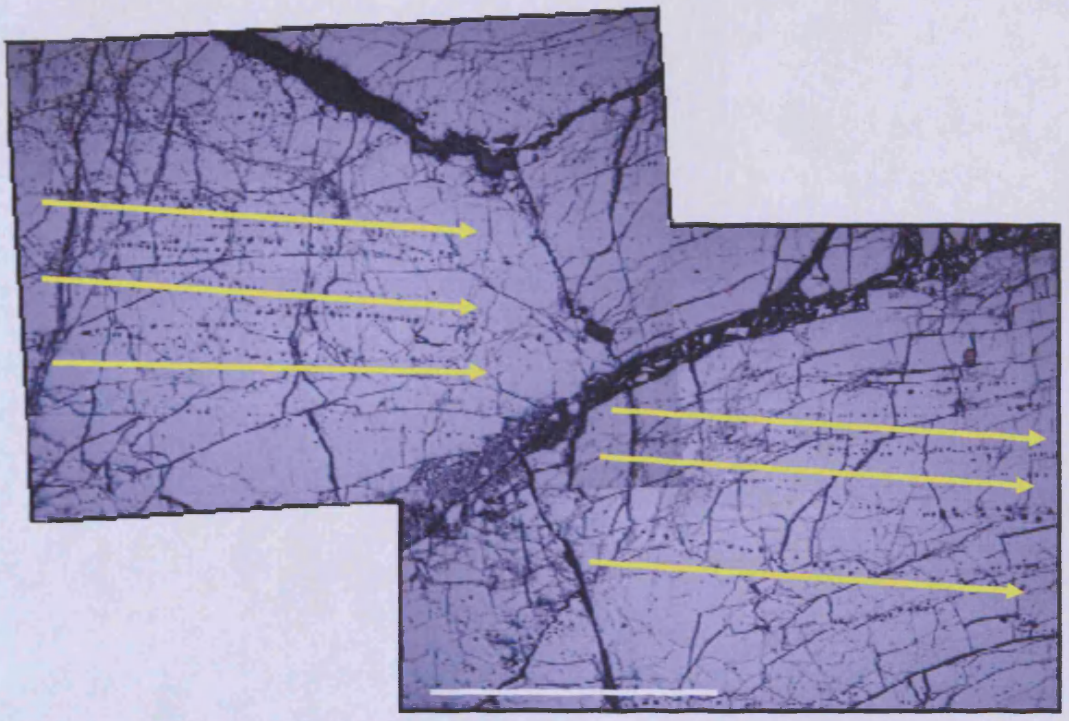

Figure 6.3: *Extensive development of linear trails of inclusions within sample C54.The inclusion trails span from left to right of the field of view as indicated by the yellow arrows. Scale bar represents 2 mm.*

The linear trails of inclusions may be produced by one of three processes depending on the particular timing of formation of the linear feature which is now present within the chromite grain.

1. Chromite grains overgrowing a volatile rich stratified layer within the silicate melt. In this case the linear feature was present before the growth of the chromite grains and has become encapsulated within the final chromite grain (Figure 6.4A).
2. The linear trails represent growth fronts within an expanding chromite crystal. As such they form simultaneously with the chromite grain, and represent volatile rich fluids, within the silicate melt, which were associated with, or trapped against, the crystallizing chromite (Figure 6.4B).
3. The linear trails form after chromite crystallization. As such they would represent volatile-rich fluids which fracture the partially consolidated chromitite mush along the weakest points (i.e. fractures in grains or grain boundaries). Recrystallization of the chromite grain encapsulates some of these volatiles leaving a linear trail (Figure 6.4C). These trails are analogous to the pseudosecondary inclusions defined by Roedder (1979).

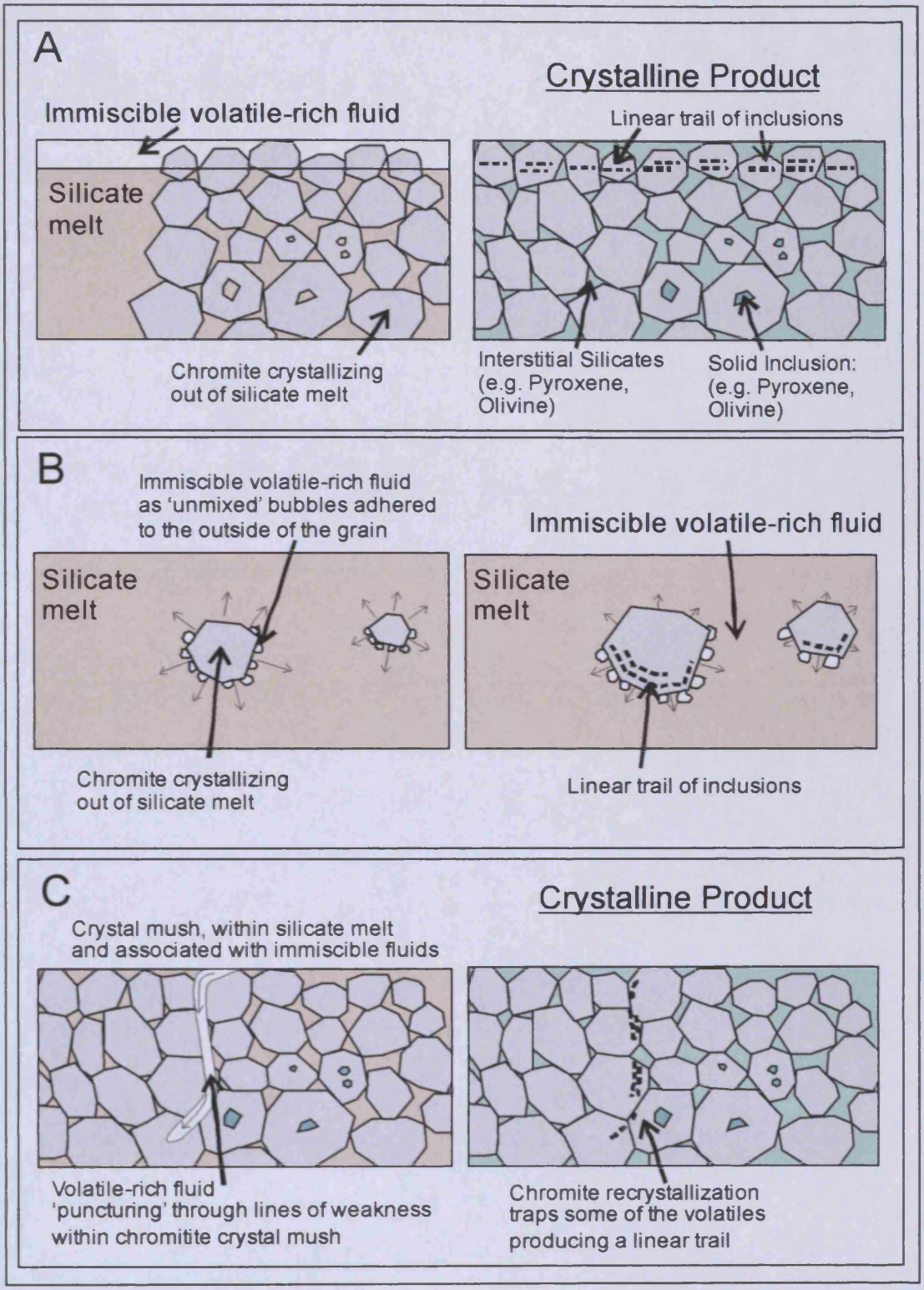

Figure 6.4: *Schematic diagrams on possible timings for the formation of linear trails of inclusions.* ***A:*** *Formation of linear trails by overgrowth through a previously present stratified immiscible volatile layer within the silicate melt.* ***B:*** *Formation of linear trails as growth fronts within an intimately associated chromite grain and immiscible non-silicate liquid.* ***C:*** *Formation of linear trails as immiscible volatile-rich fluids 'puncture' along existing lines of weakness (pre-existing fracture planes or sintered boundaries) within the crystal mush. Recrystallization of chromite grains encapsulates some of the volatiles.*

The fact that these linear trails may cross-cut one another would seem to rule out the first theory - that the chromite grains were crystallizing over a stratified layer within the melt. In addition to this it seems unlikely that an unmixed volatile rich layer would remain in a stable stratiform habit as the chromite grains grew.

Due to the high degree of sintering and fracturing that has occurred it is difficult to definitively tell whether the trails cut through grain boundaries, though the observation of extensive trails within samples such as C210 (e.g. Figure 6.2) and C54 (e.g. Figure 6.3) would strongly suggest that likelihood. The observation that linear trails are often quite extensive (several mm's, and up to cm's in length), may cut grain boundaries, and are observed to cut one another, makes it extremely unlikely that they represent the remnants of growth fronts within growing chromite grains. Furthermore, in such a scenario it would be expected that silicate melt would also become trapped, producing silicate inclusions, and the inclusions would wrap around the crystal faces formed non-linear trails (Figure 6.5). Neither of these are observed. Therefore, of the three possible timings for the formation of the linear trails of inclusions, the third theory is favoured – that is, formation by volatile-rich inclusions which 'puncture' along lines of weakness followed by recrystallization and trapping.

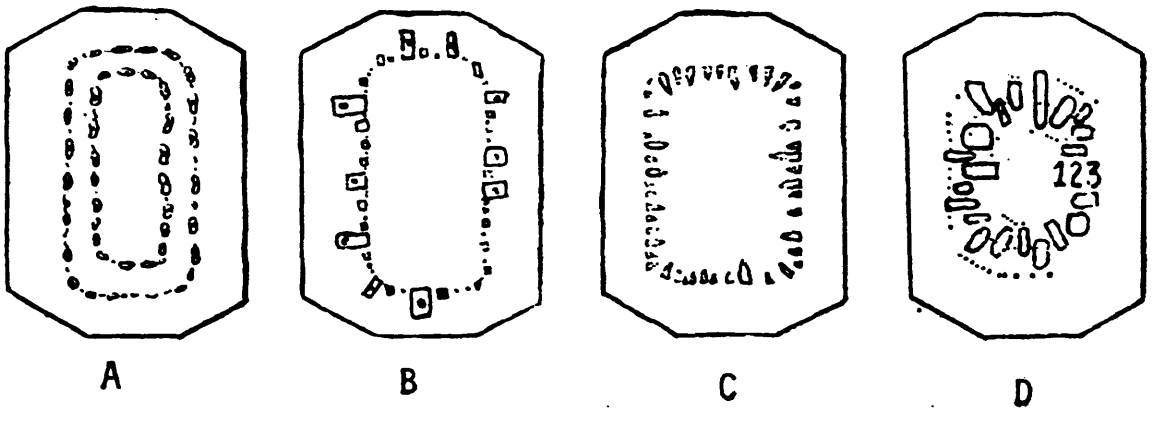

Figure 6.5: *Trails of inclusions formed at growth fronts within the growing crystal lattice. Although linear for a time they are observed to kink round or wrap around the crystal. The figure is taken from Roedder (1979).*

6.2 Chromitite petrogenesis

In order to consider the factors effecting podiform chromitite formation it is useful to break it down into three constituent parts.

1. Why does chromite begin to precipitate?
2. Why does chromite continue to precipitate?
3. Why does chromite concentrate to form podiform chromitite deposits?

6.2.1 Why does chromite begin to precipitate?

This first question is relatively straightforward as a primitive melt of composition *'a'* ascending through the mantle will lie on the olivine-chromite cotectic (Figure 6.6A). This means that olivine and chromite will be the first minerals to precipitate out of the melt, in the approximate proportion of 99% olivine and 1% chromite (Irvine, 1977b). With no mechanical sorting the resultant rock type produced from these crystallization proportions would be a dunite with disseminated chromite.

Chromite-only crystallization may occur through changes in the physical parameters of the system (e.g. changing pressure, temperature or fO_2; (Murck and Campbell, 1986; Lipin, 1993)), or through changes occurring in the composition of the melt (e.g. melt-rock reaction, or unmixing of water from the melt). A change in the physical parameters of the system could move the phase boundary such that melt *'a'* now lies within the chromite-only crystallization field (Figure 6.6B). This is particularly true for loss of water due to pressure reduction since water is not shown in the 'condensed' phase diagram. A change in the composition of the melt, such as silica enrichment, through melt-rock reaction could move melt 'a' into the chromite crystallization field (Zhou *et al.*, 1994) (Figure 6.6C).

Once chromite-only crystallization has begun the composition of the melt quickly returns back to the olivine-chromite cotectic (Figure 6.6D) and crystallization proportions return to 99% olivine and 1% chromite. The degree of chromite-only crystallization will depend upon the extent of the change in either the melt composition (Figure 6.6C) or the phase boundary perturbation (Figure 6.6C) and the supply of chromium.

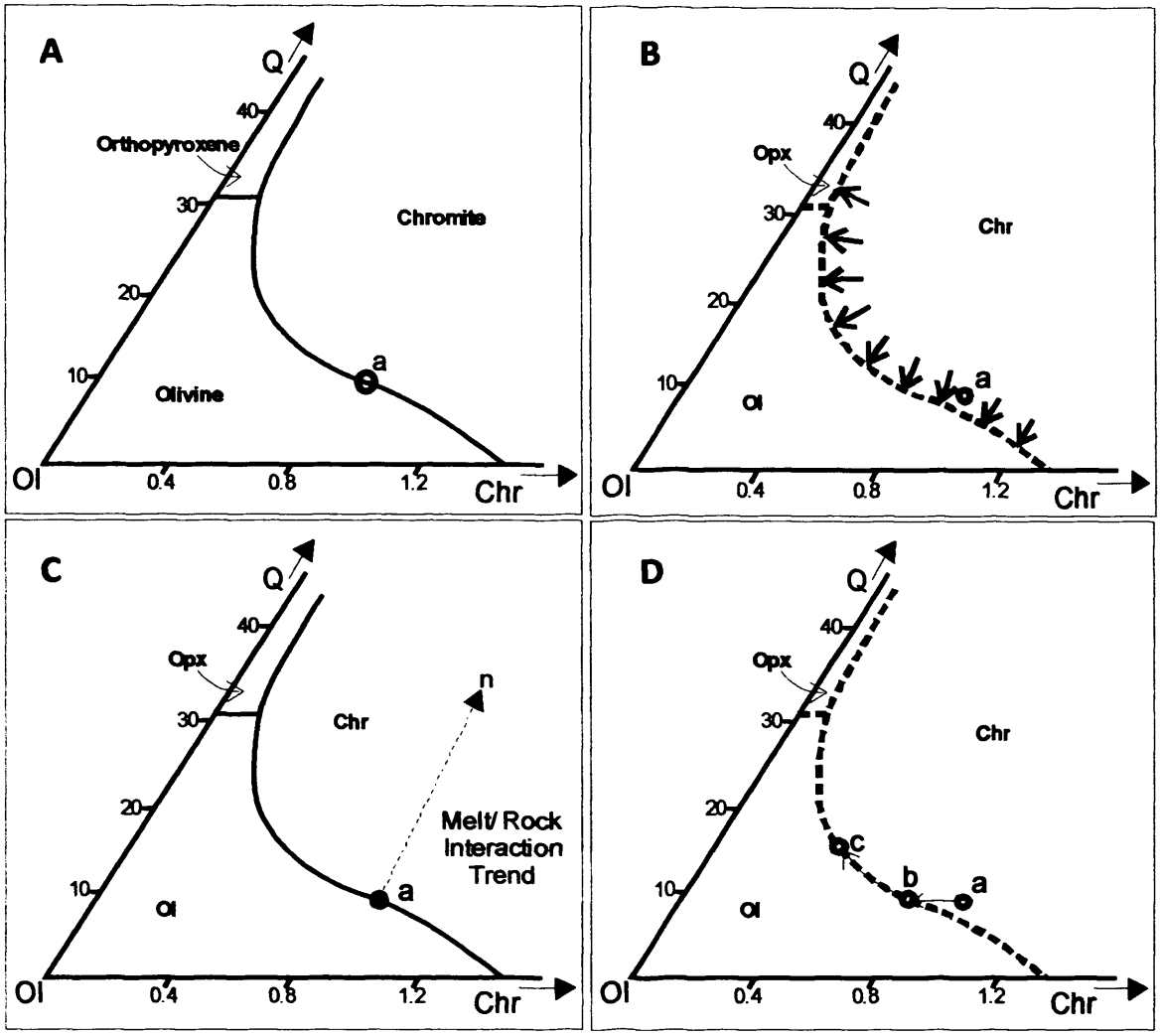

Figure 6.6: ***Phase diagrams, A: Primitive melt of composition 'a' lying on the olivine-chromite cotectic. B: Perturbation in the physical parameters of the system (e.g. temperature) or resulting changes to the melt in elements not depicted e.g. volatiles may move the phase boundaries resulting in melt 'a' lying in the chromite-only crystallization field. C: Melt-rock reaction trend showing the change on composition of melt 'a' which would result D: Chromite-only crystallization which brings the composition of melt 'a' back to the olivine-chromite cotectic at point 'b'. The crystallization path may follow the olivine-chromite cotectic from 'b' to 'c' precipitating out olivine and chromite (Diagram adapted from Irvine, 1977a). It is important to note that the chromite-olivine cotectic as calculated by Irvine, (1977b) is complexly curved towards Cr being variously convex or concave depending on the starting composition. Irvine, (1977b) defined six compositions with only the first four corresponding to natural olivine-controlled magmas. Of these remaining four compositions boninite-type magmas are most likely to correspond to type 3 (or possibly 4) and result in cotectics which are originally convex, and then concave towards chromite (as in the above diagrams). This is because liquid paths 1&2 follow a crystallization sequence of olivine (&chromite) to plagioclase and then pyroxene, which doesn't correspond to supra-subduction zone magmas which tend towards the ultramafic pyroxenite sequences crystallizing before plagioclase appears on the liquidus.***

6.2.2 Why does chromite continue to precipitate?

The second question is more complicated as chromium concentrations within primitive melts are very low (~1200 ppm for a boninite, (Malpas *et al.*, 1997)). This means that the amount of chromite that could precipitate out of a primitive melt in a closed system would be very small. Therefore, in order for chromite crystallization to continue some replenishment of the chromium content of the melt is required.

The continuous replenishment of chromium into the melt may be considered as either 'from the sides' (i.e. dissolution of host rock) or from beneath (i.e. continuously upwelling melt). The classical model for chromite-only crystallization with continuous chromium replenishment from the source region is that of magmatic differentiation. Magmatic differentiation considers the chromitites to be the products of fractional crystallization and crystal settling within an upwelling primitive melt (Thayer, 1964, Neary and Brown, 1979; Brown, 1980; Lago *et al.*, 1982; Leblanc and Ceuleneer, 1991; Roberts and Neary, 1993) which may in turn fractionate and deposit lower Cr# chromitites higher up in the sequence. Chromium replenishment 'from the sides' is one aspect of the melt-rock reaction model and is based on the observation that dissolution of pyroxene grains into the melt will add some chromium (Figure 6.7D & 6.8D; Buchl *et al.*, 2004; Rollinson, 2005).

Melt-rock reaction considers the chromitites to form through the reaction of boninitic (or tholeiitic) magmas with depleted peridotite. This reaction involves the dissolution of orthopyroxene with or without the concomitant precipitation of olivine. This dissolution occurs because the peridotite host is out of equilibrium with the boninitic melt coming from greater depth and charged with water (Quick, 1981; Kelemen, 1995). The dissolution–precipitation reaction adds silica to the melt, pushing the melt into chromite saturation (Zhou *et al.*, 1994; Edwards *et al.*, 2000) (Figure 6.6C).

It is noteworthy that the compositions of melt that fluxes through the mantle sequence may evolve with time as the degree of partial melting of the source region changes (e.g. (Haraguchi and Ishii, 2007; Dilek and Thy, 2009)). A varying degree of partial melting may be compatible with either model as melts of differing composition may both fractionate, and/or react with the hostrock. This discussion only considers these two models; magmatic differentiation and melt-rock reaction, and how they affect the interpretation of key elements of the collected data.

6.2.2.1 Melt-rock reaction

The melt-rock reaction model was initially developed to explain the formation of chromitite pods within an ophiolite, and their close association with dunite envelopes (e.g. Zhou *et al.*, 1996). It has since developed to describe the variation in chromite compositions across a whole ophiolite. For example, Zhou and Robinson, (1997) argue that different Cr# chromitites represent formation from melts of different compositions in different tectonic settings. Alternatively, Rollinson, (2005) argues that differing Cr# chromitites may be explained by melts of different compositions, but that the variation in composition is caused by melt-rock reaction, where increasing melt-rock ratios produces higher Cr# chromitites.

Within an exclusively melt-rock reaction model, each chromitite pod represents the reaction of a batch melt with the host peridotite at that particular location in the mantle sequence. Within the model proposed by Zhou and Robinson, (1997) chromite composition within a chromitite pod is taken to be diagnostic of the degree of partial melting in the source region, and the geodynamic setting of the ophiolite (e.g. fore-arc, arc or back-arc). Ophiolites containing predominantly high Cr# chromitites are thought to be derived from fore-arc to island-arc settings and ophiolites with predominantly low Cr# chromitites are thought to be derived from back-arc settings (Malpas *et al.*, 1997; Zhou *et al.*, 1998). Chromitites with a large range of Cr# values are usually interpreted as having undergone a switch in tectonic settings (e.g. Oman, Ahmed & Arai, 2002).

Within this melt-rock reaction model there are two possible mechanisms for producing the wide array of Cr# values displayed at Al'Ays (0.50 to 0.92). Firstly, there could be a transition from tholeiitic to boninitic magmas occurring within the same tectonic setting. This would change the Al_2O_3 content of the melt, which is the dominant control on the Cr# of crystallizing chromite (Maurel and Maurel, 1982; Roeder and Reynolds, 1991; Kamenetsky *et al.*, 2001), thereby producing the wide range of chromite Cr# compositions. This scenario could occur beneath an extended fore-arc environment where rapid slab roll-back induces mantle return flow and asthenospheric diapirism. This in turn provides more fertile melt triggering greater degrees of shallow melting within the highly depleted hydrous fore-arc mantle, finally producing boninitic magmas (Haraguchi and Ishii, 2007; Dilek and Thy, 2009).

Table 6.1: *Compositions used to model the effect of pyroxene dissolution on the composition of upwelling boninitic melts. Boninite (BON[1]) is taken from Falloon & Danyushevsky (2000). The olivine[2] composition is taken from the present study (sample MR1). The orthopyroxene and clinopyroxene (Opx[3] & Cpx[3]) compositions are taken from mantle harzburgites from the Othrys ophiolite, Greece, Barth et al. (2003). The Cr_2O_3 content of the boninite is taken from (Malpas et al., 1997).*

	BON[1]	Olivine[2]	Opx[3]	Cpx[3]
SiO_2	51.88	41.6	55.2	52.2
TiO_2	0.70	0.00	0.02	0.08
Al_2O_3	8.71	0.00	3.38	3.02
FeO	8.94	8.54	6.18	2.19
MnO	0.12	0.14	0.13	0.07
MgO	20.69	49.81	33.31	16.97
CaO	7.10	0.00	0.62	23.56
Na_2O	1.70	0.00	0.00	0.07
K_2O	0.16	0.00	0.00	0.00
Cr_2O_3*	0.0018	0.00	0.62	0.70
H_2O	2.40	0.00	0.00	0.00

If only dissolution of pyroxene into the melt is occurring (i.e. there is no olivine or chromite crystallization) then the melt could become further depleted in Al_2O_3 (Figure 6.7B). Experimental studies have shown an empirical link between the Al_2O_3 content of the melt and the Al_2O_3 content of the crystallizing chromite ((Maurel and Maurel, 1982; Kamenetsky *et al.*, 2001)). This means that the Al_2O_3 content of the melt will be inversely proportional to the Cr# of crystallizing chromite and that progressive dissolution of pyroxene into a melt will lead to an increase in the Cr# of subsequent chromite crystallization, not a decrease.

Dissolution of pyroxene into the melt also leads to higher Mg# within the melt (Figure 6.7C). If the Mg# of melt is proportional to the Mg# of crystallizing chromite then increased dissolution would lead to higher Mg# as well as higher Cr#. This trend is the reverse of that observed within the Al'Ays ophiolite and the reverse of what would be expected from a melt which is crystallizing out chromite (e.g. (Naldrett *et al.*, 2009)).

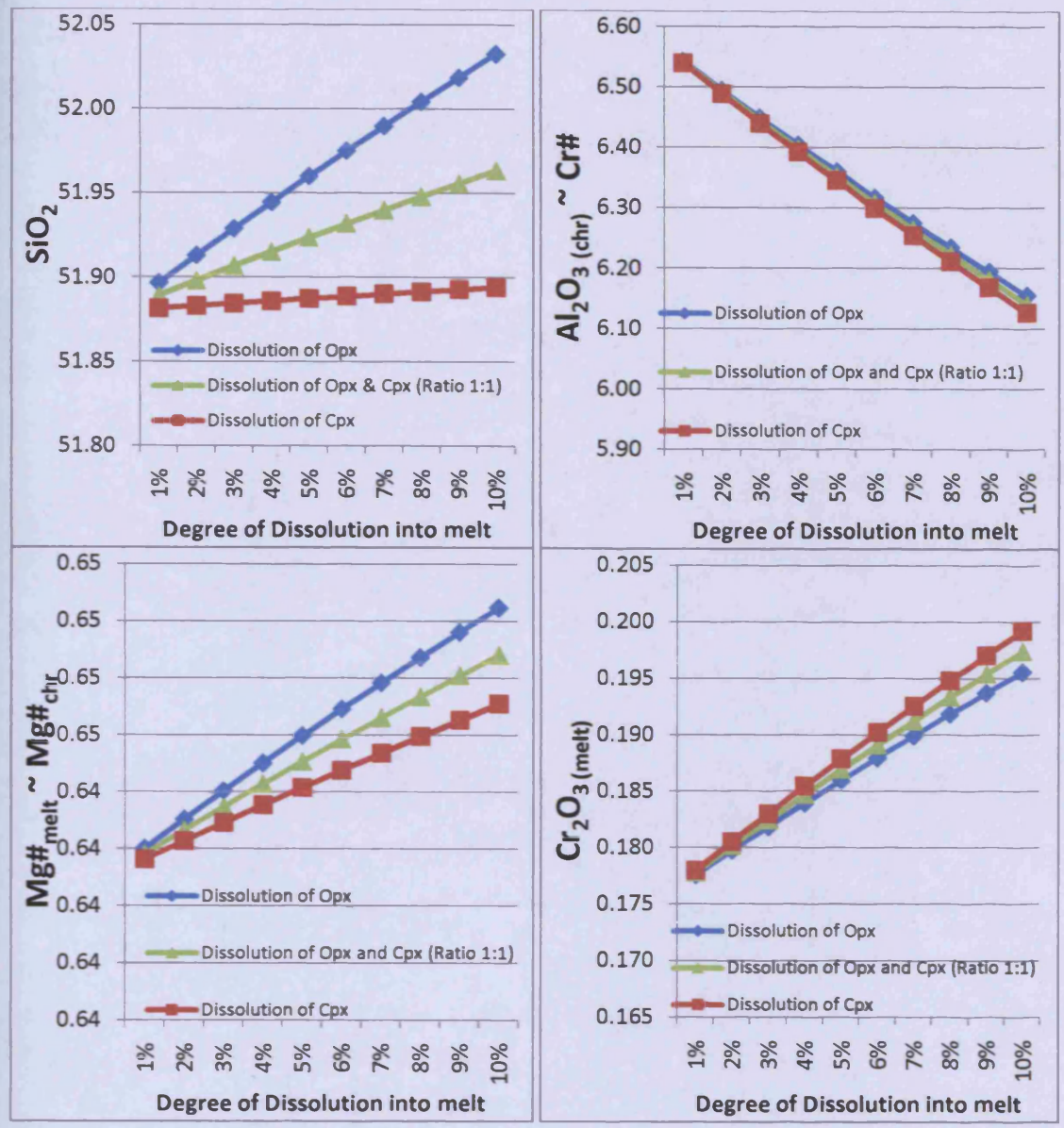

Figure 6.7: *Graphs showing the effect of progressive dissolution of pyroxene grains into upwelling boninitic melts. A: The SiO_2 content of the melt.* ***B:*** *The Al_2O_3 content of chromite which would crystallize out of the melt. The Al_2O_3 content is calculated using the equation of Maurel & Maurel, 1982 linking the Al_2O_3 content of chromite and the Al_2O_3 content of its parental melt [$ln(wt\%Al_2O_3$ in melt) = $0.41322*(ln(wt\%Al_2O_3$ in chromite)) + 1.38529].* ***C:*** *The Mg# ($Mg^{2+}/(Mg^{2+}+Fe^{2+})$)of the melt, which is assumed to be proportional to the Mg# of any chromite which crystallizes out. For convenience the valency of the iron within the melt is assumed to be 2+.* ***D****: The Cr_2O_3 content of the melt. For 10% dissolution into the melt the Cr content rises from approximately 1200 ppm to 1400 ppm. This is very likely to be below the solubility limit of chromium within boninite melts (Crawford, 1989 and references therein; Edwards et al., 2000)*

It is noteworthy that the dissolution of pyroxene into melt raises the chromium content of the melt, even at relatively low percentages of dissolution (Figure 6.7D). Pyroxene dissolution may therefore be an effective means of replenishing the chromium content of a melt, at least partially. When this model is adapted to allow for olivine precipitation along with pyroxene dissolution (i.e. the dissolution-precipitation reaction thought to be the origin of the dunite envelope) the effect on the Al_2O_3, Mg#, Cr_2O_3 and SiO_2 content of the melt all change (Figure 6.8).

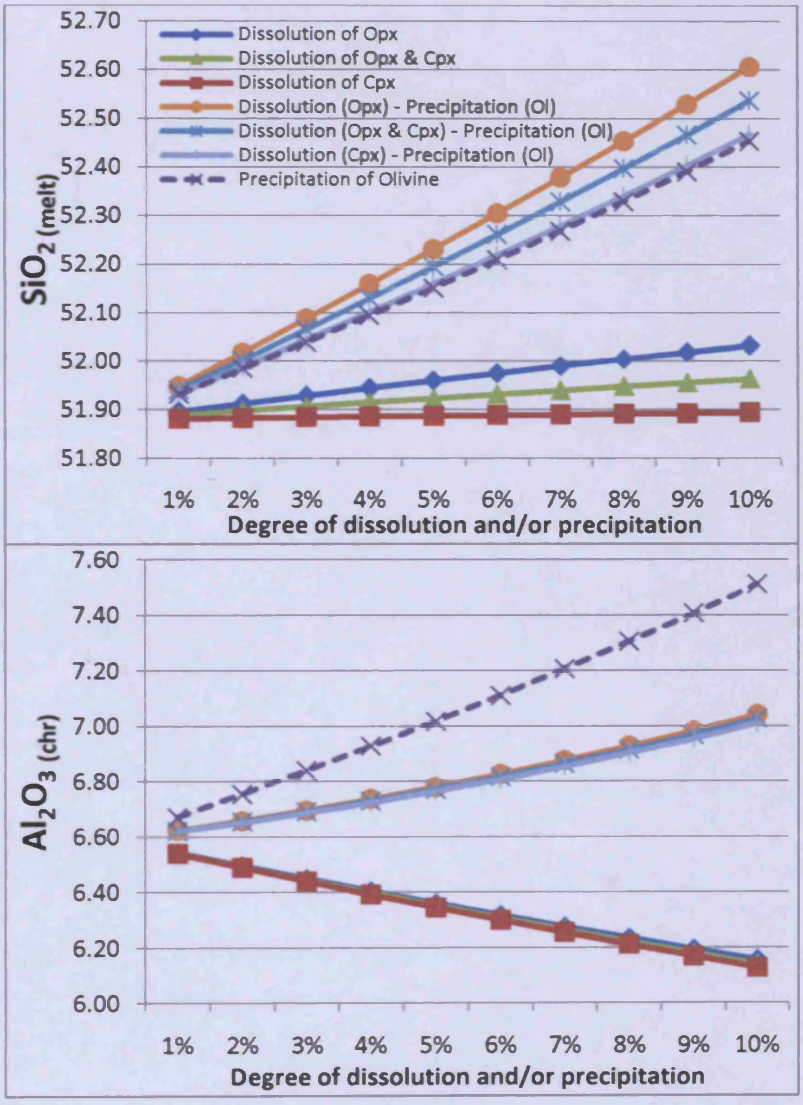

Figure 6.8: *Graphs showing the effect of the progressive dissolution of pyroxene grains into, and precipitation of olivine grains out of, upwelling boninitic melts.* ***A:*** *The SiO_2 content of the melt.* ***B:*** *The Al_2O_3 content of chromite which would crystallize out of the melt. The Al_2O_3 content of chromite is calculated using the equation of Maurel & Maurel, 1982 linking the Al_2O_3 content of chromite and the Al_2O_3 content of its parental melt [$ln(wt\%Al_2O_3$ in melt) = 0.41322*($ln(wt\%Al_2O_3$ in chromite)) + 1.38529]. The key for B: is as in A.*

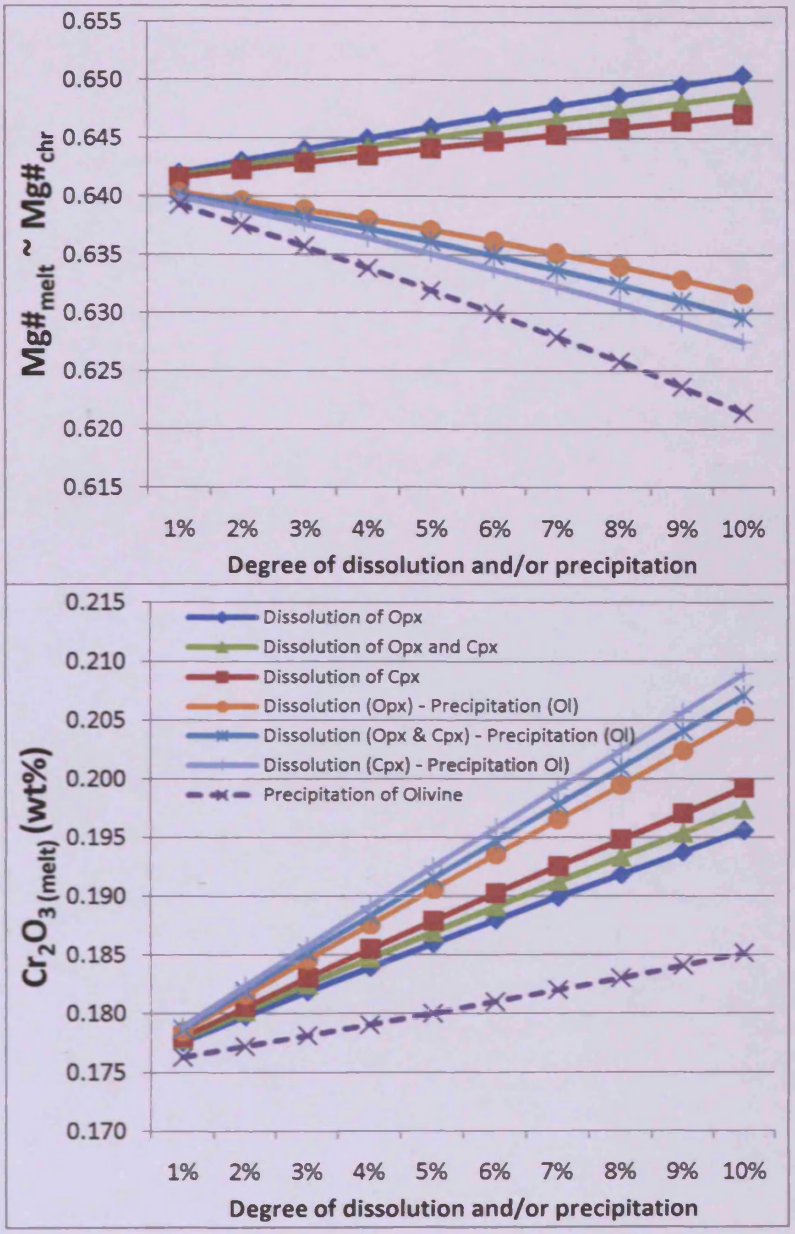

Figure 6.8 continued: C: *The Mg# ($Mg^{2+}/(Mg^{2+}+Fe^{2+})$) of the melt, which is assumed to be proportional to the Mg# of any chromite which crystallizes out. For convenience the valency of the iron within the melt is assumed to be 2+.* ***D:*** *The Cr_2O_3 content of the melt. Although the Cr_2O_3 content increases more rapidly than by dissolution alone, the solubility limit of chromium is not thought to be met (e.g. Crawford, 1989 and references therein). The key for C is as in D.*

The SiO_2 content of the melt increases more rapidly as a result of simultaneous pyroxene dissolution and olivine precipitation (Figure 6.8A). The behaviour of Al_2O_3 in the melt reverses, with the Al_2O_3 content of the melt (and therefore of crystallizing chromite grains) now increasing rather than decreasing (Figure 6.8B). The Mg# of the melt also shows a reversal

with the Mg# of the melt decreasing rather than increasing (Figure 6.8C). The Cr_2O_3 content increases more rapidly when olivine precipitation incorporates pyroxene dissolution. This is expected as the dissolving mineral (pyroxene) contains minor Cr whilst the precipitating mineral (olivine) is barren of any Cr content (Table 6.1). This would mean that as the degree of dissolution-precipitation is increased (i.e. as the melt traverses an increasing thickness of mantle) the resultant Cr# of crystallizing chromite grains would be lower. The degree of this reduction in Cr# would be minor as even with a 10% (by volume relative to the total melt volume) degree of dissolution and precipitation the increase in the Al_2O_3 content of the chromite that would crystallize is just 0.4 wt% (Figure 6.7B). In order to change the Al_2O_3 content of the crystallizing chromite by the degree observed within the Al'Ays ophiolite (3.9 – 24.75 wt%), the degree of dissolution and precipitation would have to >60% by volume of the original melt. The associated changes in the melt make this geologically impossible as the MgO content would decrease to <0 wt% of the melt by this stage. It is not therefore possible to account for changes in the Cr# of crystallizing chromite within the Al'Ays ophiolite simply by changing the degree of simultaneous pyroxene dissolution and olivine precipitation that has occurred within the melt.

Previous authors have noted that increasing the silica content of the melt may increase the Cr# content of the chromite which subsequently crystallizes out independently of any other change in the melt (Irvine, 1977a; Schwessinger and Muan, 1992). Schwessinger & Muan, 1992 showed that varying the Si/Al ratio from 2 to 14 produced changes in the Cr# content of the spinels of 0.3 to 0.9. Although melt-rock reaction would add silica to the melt, the change in the Si/Al ratio produced in the melt as a result, even after a 10% by volume reaction, was just 0.07. This would have no significant effect on the Cr# of crystallizing chromite (Schwessinger and Muan, 1992).

A second challenge with maintaining chromite crystallization through melt-rock reaction is the size of the dunite sheath produced. As the dissolution-precipitation reaction is considered to be the main genetic cause of the dunite envelope surrounding chromitite pods it should then be expected that the size of the envelope is proportional to the size of the chromitite pod. This is empirically not the case (e.g. dunites around the Luobosa chromitites, (Zhou *et al.*, 1996)). Furthermore, the initial formation of a dunite envelope will act as a barrier to subsequent upwelling melts preventing further dissolution-precipitation reactions and inhibiting the formation of more chromite.

6.2.2.2 Magmatic differentiation

The second model considers the composition of chromitite pods within the ophiolite mantle as being the product of a melt rising through the mantle that fractionates as it rises. Within this model any change in chromite composition with stratigraphic height will be due to fractionation processes as the melt rises. Within upwelling melts a perturbation within the physical or chemical constraints of the system may move the melt into the 'chromite only' crystallization field, thereby inducing initial chromite crystallization (Figure 6.6D). This perturbation may be through melt-rock reaction thereby affecting the composition of the melt, or through a change in the physical or chemical parameters (e.g. volatile unmixing and loss) which would move the phase boundary. Importantly the resultant melt composition could lie within the chromite crystallization field.

The composition of the first chromite grains will reflect the extent of partial melting of the source region. After initial chromite crystallization the melt will not be fully depleted in chromium as the melt returns to the chromite-olivine liquidus before chromium is completely removed from the system (e.g. Figure 6.6D). This melt will continue to ascend through the mantle possibly crystallising olivine and chromite as it rises (in the approximate proportion of 99% olivine and 1% chromite). As this melt continues to ascend a second perturbation in the physical or chemical conditions of the system may lead to a second site of chromite crystallization stratigraphically higher in the sequence (closer to the geophysical Moho). This second site could have a modified chromite composition (lower Cr# and Cr/ Fe^{2+} ratio) and hence the chromite composition fractionates.

As the chromium content of the melt is low it will need to be constantly replenished for any chromitite deposit to form. This could be achieved by the repeated flux of new batch melts from below the site of chromite deposition (i.e. from the source region). In this way a chromitite pod represents the product of numerous batch melts which deposit a little chromite along the way, before ascending to higher levels in the mantle and depositing a little more chromite. Podiform chromitite sites may therefore represent areas of the mantle where upwelling primitive melts have been repeatedly focussed, paused or slowed down for a while and where chromite has been repeatedly precipitated. Within this model the dunite envelope which invariably surrounds the chromitite pod may represent olivine that crystallized simultaneously with the chromite but which was subsequently separated from the chromite (e.g. by mechanical sorting (Lago *et al.*, 1982), Figure 6.10).

Olivine precipitation without pyroxene dissolution produces a similar increase in the SiO_2 content of the melt as the dissolution-precipitation reaction (Figure 6.8A). The increase in Al_2O_3 and decrease in Mg# content of the melt is more pronounced for olivine precipitation than for the dissolution-precipitation reaction. This means that a melt which has experienced more olivine crystallization will eventually crystallize chromite of lower Cr#. Interestingly the Cr_2O_3 content of the melt is slightly increased by olivine crystallization (Figure 6.8B).

Chromite composition controlled by fractionation suggests two main observations. Firstly, there should be a continuous spectrum between the highest and lowest Cr# (and Cr/Fe^{2+} values) values, and secondly there should be a stratigraphic control of chromite composition, as low Cr# or Cr/ Fe^{2+} chromitites crystallize higher in the stratigraphic sequence.

However, there are some difficulties with this model. The first is the strong control on chromite composition, particularly Cr#, which is exerted by the Al_2O_3 content of the melt (Maurel and Maurel, 1982; Roeder and Reynolds, 1991; Kamenetsky *et al.*, 2001). The Al_2O_3 content of the melt may be altered through changes in the degree of partial melting, changes in the degree of depletion of the source region – both of which are likely geological controls that may affect melts within an ophiolitic setting (e.g. (Haraguchi and Ishii, 2007)) and melt-rock reaction (Figure 6.7A). A second difficulty is the strong evidence for a replacive origin of much of the ophiolitic mantle dunite, and the evidence that upwelling primitive melts will react with harzburgite to form dunite (Quick, 1981; Fisk, 1986; Kelemen, 1990, 1995; Zhou *et al.*, 1996). This evidence was well summarized by Kelemen (1990) who provided three major arguments for the presence of replacive dunite within peridotite sections.

1. Dunite bodies usually cross-cut modal banding and/or pyroxenite bands without offsetting these features.
2. Peridotite inclusions within discordant dunite bodies have clearly decreased in size such that if intervening dunite was removed the included peridotite would not 'fit' any of the surrounding walls.
3. Compositionally, an origin through *in situ* partial melting of the peridotite host requires very high degrees of partial fusion (>40%, Kelemen, 1995). Conversely a predominantly cumulate origin (i.e. dunite dykes) should produce olivine grains which are more Fe-enriched than the peridotite host. In individual cases this may be the case but in general the range of dunite compositions is identical for the dunite as well as the host peridotite.

6.2.3 Why does chromite concentrate to form podiform chromitite deposits?

6.2.3.1 Melt-rock reaction and magmatic differentiation

It seems likely that explaining the formation of podiform chromitite as well as the pattern of chromite composition variation across an ophiolite requires a composite cumulative-reaction model (Arai and Yurimoto, 1994; Matveev and Ballhaus, 2002; Rollinson, 2008; Page and Barnes, 2009). In this model the crystallization of chromite (and olivine) takes place within an intramantle magma channel with dynamic mechanical sorting of chromite from olivine ((Lago *et al.*, 1982; Leblanc and Ceuleneer, 1991)). Chromite concentration occurs due to a combination of chromite-only crystallization and chromite separation from olivine during mechanical sorting.

Chromite-only crystallization initiates due to either melt-rock reaction and/or the mixing of a primitive melt with a previously reacted melt ('a hybridized melt', Figure 6.9; Arai and Yurimoto, 1994; Zhou *et al.*, 1994; Zhou *et al.*, 1996; Morishita *et al.*, 2006) or the unmixing of water from the melt forming a two-phase system (e.g. Matveev and Ballhaus, 2002, see Section 6.2.4). Chromite-only segregation may continue beyond chromite-only crystallization by the removal of olivine during mechanical sorting. This may bring relatively fresh peridotite into contact with primitive melt allowing for repeated melt-rock reaction and chromite-only crystallization (Figure 6.10).

Chromium may be replenished by a combination of dissolution of pyroxene from the host rock and a continuously supplied primitive melt. Within this model the composition of the chromite reflects the composition of the melt from which it crystallizes. The melt composition will depend upon the degree of partial melting of the source region, the degree of fractionation prior to this particular chromite crystallization and, in the case of crystallization from a hybridized melt, the degree of reaction between primitive melts and mantle peridotite. Chromite composition will evolve with stratigraphic height through these fractionation and melt-rock reaction processes forming lower Cr# and lower Cr/Fe^{2+} ratio chromitites closer to the geophysical Moho.

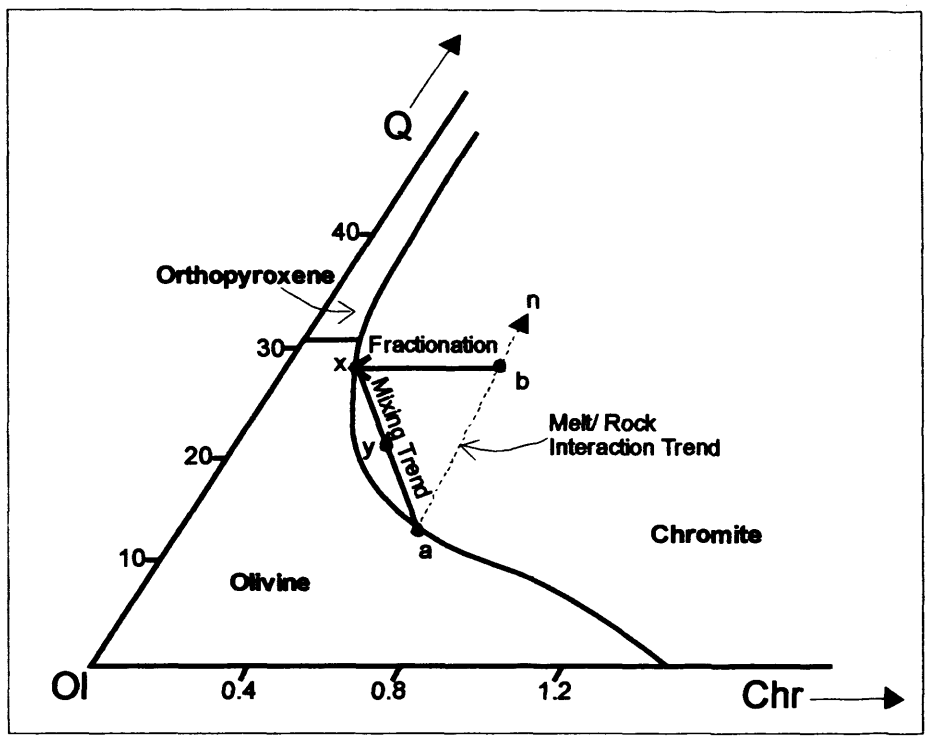

Figure 6.9: *Phase diagram showing chromite-only crystallization through melt-rock reaction and the mixing of an evolved secondary melt with a replenished primary melt. Primitive melt 'a' reacts with the host peridotite producing a melt with composition along the tie-line 'a-n'. This composition lies in the chromite only field and following chromite-only crystallization moves to 'x'. Mixing of this fractionated magma with new batches of primitive magma produces a hybridized melt 'y' which also lies within the chromite field.*

Evidence for the role of partial melting and fractionation in the composition of crystallizing chromite has been found in both the Al'Ays and the Shetland ophiolites and follows the recent work by Naldrett *et al.* (2009). Although working on stratiform chromitites Naldrett *et al.*, (2009) highlighted the variation in chromite composition with stratigraphic height within the stratiform Bushveld chromitites and described two trends. The variations in chromite geochemistry (in terms of Cr# - Mg#) within the Bushveld chromitites are unambiguously thought to be the product of two main processes, namely the influx of new magma (trend A) and the fractionation of orthopyroxene and olivine (trend B) (Figure 6.11). Within ophiolitic complexes such as Al 'Ays and Shetland the same two trends have been found. Trend A, which is present in both ophiolites, represents the variation that may occur due to changes in the composition of the upwelling melts. Changes in the Cr/Al ratio of a spinel will cause coupled changes in the Mg/Fe^{2+} ratio of that same spinel regardless of whether the liquid from which the spinel crystallizes has experienced any change in the Mg/Fe^{2+} ratio.

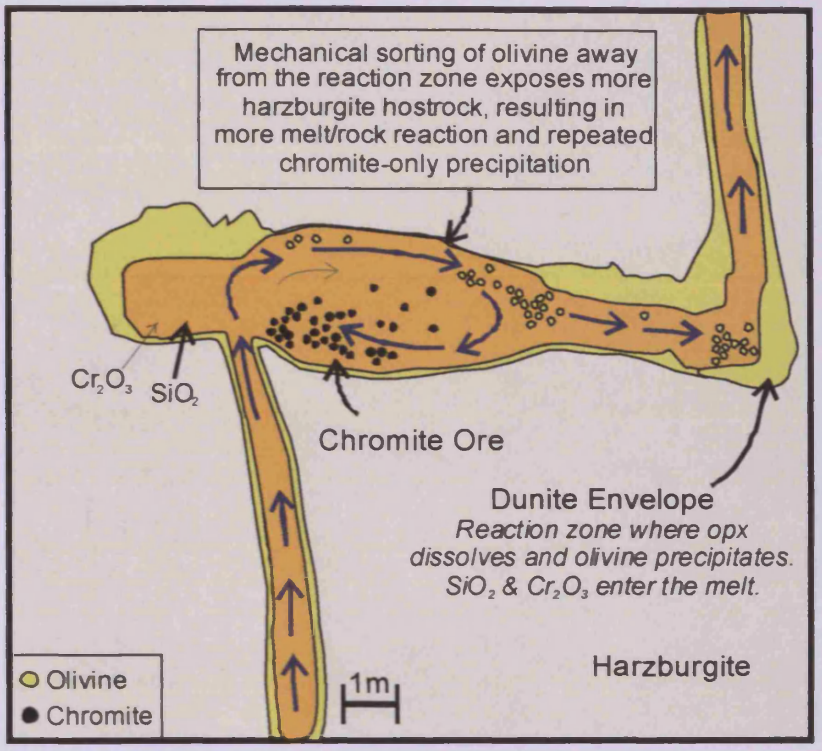

Figure 6.10: *Schematic diagram showing a proposed mechanical sorting mechanism for repeatedly bringing melt into contact with peridotite hostrock, resulting in repeated melt-rock reaction and chromite-only precipitation. Diagram is adapted from Lago et al., 1982. The pod is taken as pseudo-horizontal as any sorting which occurred within a vertical melt pool would be repeatedly disrupted by subsequent melt pulses.*

An evolving melt source within the same tectonic and geographical setting has been observed within the Kizildag ophiolite (Diley & Thy, 2009) and the Izu Bonin forearc region (Haraguchi and Ishii, 2007) where an evolution between island-arc tholeiite (IAT) and boninite magma was observed. Diley and Thy, (2009) postulated that the evolution occurred as the proto-arc developed into a forearc setting. Within the proto-arc setting the melting of subduction-modified mantle initially produces IAT magmas. Slab roll-back, arc-wedge corner flow and asthenospheric diapiric upwelling of fertile mantle raise the temperature in the melting column producing eventual boninite melts (Figure 6.11 for transition direction). Alternatively, the zoned diapir model (originally Tamura, 1994, but also favoured by Haraguchi and Ishii, 2007) details how tholeiite magmas may be derived from boninite magmas. They argue that during the ascent of a wet mantle diapir (the source to a boninite melt) through the mantle

wedge it may interact with hot fertile mantle which has upwelled into the mantle wedge. This interaction may dehydrate the outer edge of the rising diapir. When the diapir finally reaches the upper mantle the hotter, drier outer edge generates tholeiite melts and the cooler, wetter core generates boninite melts (Figure 6.11 for transition direction). The greatest control on the Cr# content of the chromite is the Al_2O_3 content of the melt at the time of crystallization (e.g. (Maurel and Maurel, 1982; Roeder and Reynolds, 1991; Kamenetsky *et al.*, 2001);). Practically, this means that if melts were to evolve, for example from tholeiitic to boninitic, (Haraguchi and Ishii, 2007; Dilek and Thy, 2009), the change in composition of the associated chrome-spinels would follow trend A (see Figure 6.11).

The presence of trend A in several of the individual stratigraphic groups (groups 2, 3 and 4) of Al'Ays, the single chromitite sample (C462) from Al'Ays and the individual chromitite pods of Shetland strongly suggests that the composition of batch melts being derived from the mantle was changing with time. Trend A further implies that individual chromitite pods are the composite result of numerous batch melts precipitating small amounts of chromite on their way through the mantle. Trend A may be interpreted as changes in melt composition that occur without the precipitation of silicate. Trend A as identified in the ophiolite chromitites shows similarities to both the 'Cr-Al' and 'Rum' trends discussed by Barnes and Roeder, (2001)(Figure 1.8). This is because the variation on Fe^{3+} contents of the chromitites is very minor so a ternary plot of Cr^{3+}-Al^{3+}-Fe^{3+} will produce the 'Cr-Al' trend. However the rate of change of Mg# (which is 1 – Fe#) relative to Cr# in the chromitites is far greater than expected for the 'Cr-Al' trend and therefore on a Cr#-Mg# plot the trend produced is equivalent to the 'Rum' trend.

Trend B represents the variations that may occur through the crystallization of olivine and/ or chromite (i.e. by fractionation processes – the general case being change in melt composition that occur due to co-precipitation of silicate and chromite), to a lesser extent by the dissolution-precipitation reaction (Figure 6.7), and also by reactions with trapped intercumulus melt (Roeder and Campbell, 1985; Barnes, 1998). The lack of a significant volume of trapped interstitial silicates within podiform chromitites makes the last explanation less likely, except as a possible factor in the Harold's Grave chromitite deposit where exceptionally high trace element concentrations (relative to other Shetland chromitites), and the large associated dunite envelope make it a plausible factor. Melt-rock reaction and olivine crystallization will increase the concentrations of Al_2O_3 within the magma, in turn leading to a reduction in the Cr# values of crystallizing chromite grains. Similarly the crystallization of

olivine will reduce the Mg# content of the magma resulting in a reduction in the Mg# of crystallizing chromite grains. Of these two effects, olivine crystallization is more dominant, producing approximately double the change in the Al_2O_3 and Mg# content of the melt to that resulting from the dissolution-precipitation reaction (Figure 6.7B & C).

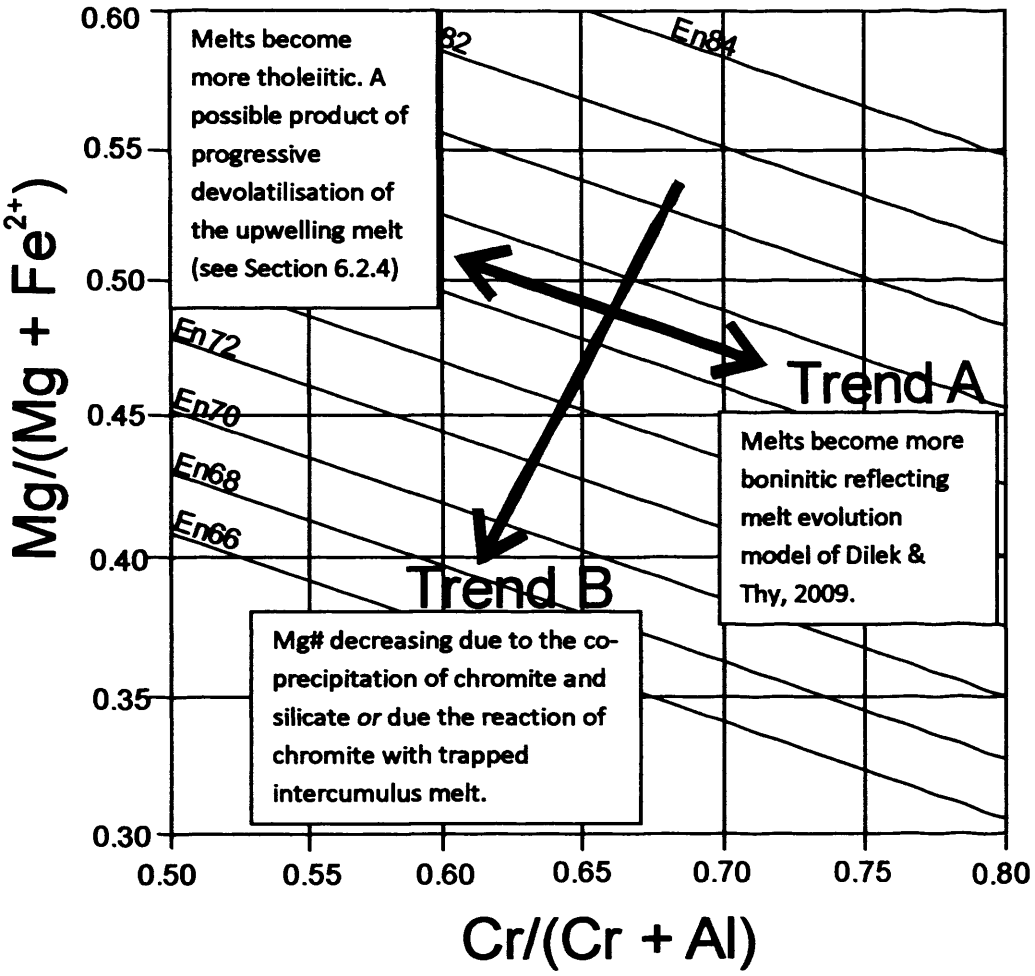

Figure 6.11: *Plot of Cr# - Mg# showing the described trends within the Bushveld chromitites. The contours represent the expected variation in Mg# ratio of the spinel which would result from variation in the Cr# of the same spinel in equilibrium with a liquid of constant Mg# (it is expressed by En content of orthopyroxene which would be in equilibrium with this liquid, the En contents and gradients are derived from (Naldrett et al., 2009). Also marked are the interpretations for the changing compositions of trends A & B. For trend A, increasing Cr# (with decreasing Mg#) would reflect the melt evolution model of Dilek and Thy, 2009, whereas decreasing Cr# (with increasing Mg#) may be the product of a melt which devolatilises as it rises. This may occur during ascent (e.g. Tamura, 1994) or in-situ through water unmixing (see Section 6.2.4).*

The effect of olivine crystallization on the melt process is analogous to the effect of the progressive crystallization of orthopyroxene within the Bushveld Complex (Naldrett *et al.*, 2009). Practically, this means that if fractionation and melt-rock reaction processes are occurring within the mantle the change in composition of chrome-spinels would follow trend B.

Within Al'Ays trend B is displayed by the stepwise transition along to lower Cr# and Mg# that is apparent from stratigraphic group 1 to stratigraphic group 4 (see Figure 3.24). This is interpreted as being the cumulative product of fractionation and some melt-rock reaction within the upwelling primitive melts. Trend B is also present within Shetland, though to a far lesser extent, with Harold's grave containing chromite compositions with much lower Mg# (see Figure 4.33) than the rest of the analysed chromitite pods from Shetland. The lack of distinctive fractionation trends within the TiO_2 values, either in Al'Ays or in Shetland (with the exception of within the Cliff chromitite deposit), may reflect the effect of melt-rock reaction on the TiO_2 content of the melt (Figure 6.12). Dissolution of opx and cpx into the melt has the effect of diluting TiO_2, which would otherwise increase in concentration during the precipitation of olivine (Figure 6.12).

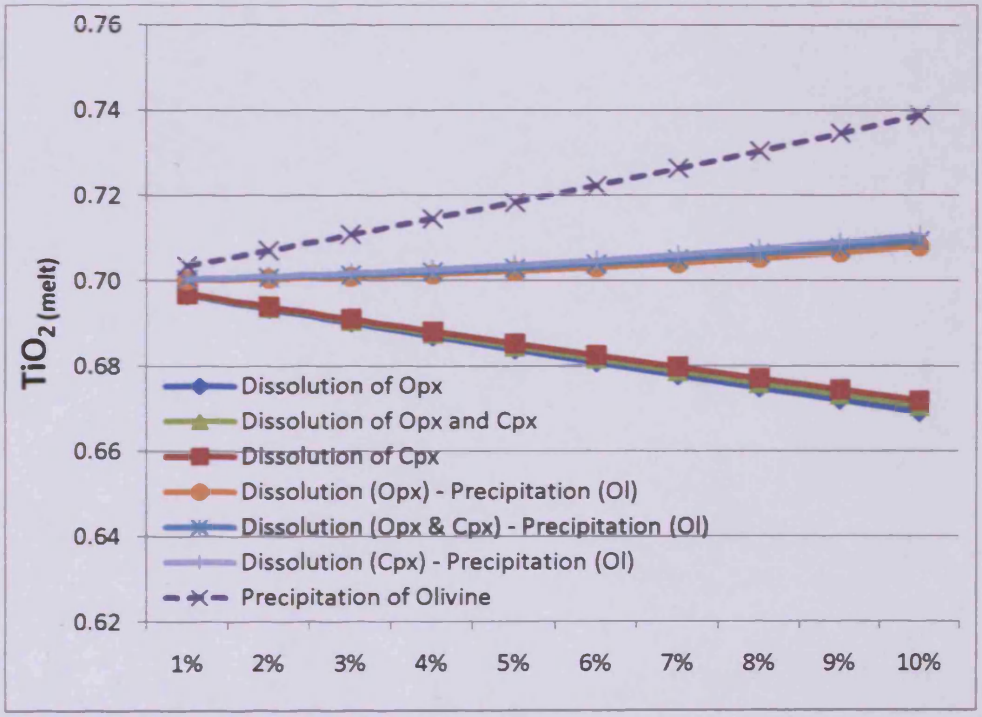

Figure 6.12: *Graph showing the effect of the progressive dissolution of pyroxene grains into, and precipitation of olivine grains out of, upwelling boninitic melts on the TiO_2 content of the melt.*

The difference between the Shetland and Al'Ays ophiolites in terms of the prominence of trend B within Al'Ays and the relative lack of trend B within Shetland (aside from Harold's Grave) may be expected from the way melts travel from the source region to the crust. As melts travel up vertical channelways, there may be considerable 'horizontal' heterogeneity *between* different melt pathways (Figure 6.13); that is, variations in the degree of source region melting, how much different melts fractionate on route, and the degree of melt-rock reaction. In addition, all melts are expected to fractionate out minerals (olivine and chromite), as well as react with the host-rock during ascent, producing 'vertical' heterogeneity *within* a melt (Figure 6.13). Al'Ays contains large stratigraphical range of upper mantle allowing 'vertical' heterogeneity to be observed, whilst the limited mantle stratigraphical range within Shetlands, meant 'vertical' heterogeneity was limited and it was only possible to study 'horizontal' heterogeneity.

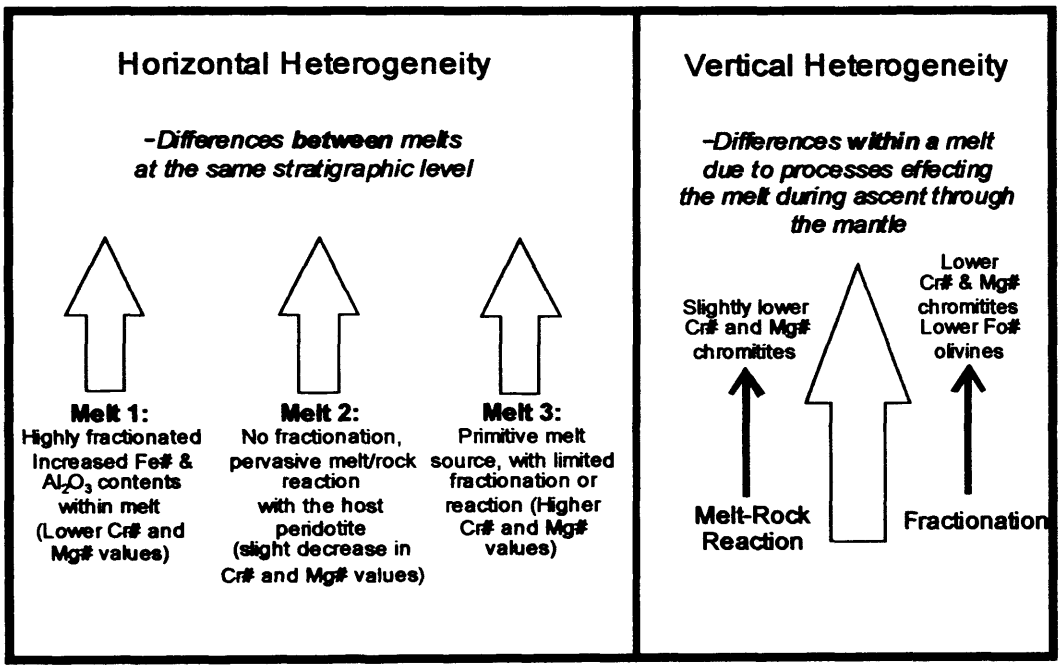

Figure 6.13: *Caption explaining 'horizontal' and 'vertical' heterogeneity within ophiolitic chromitite. Melts at the same stratigraphic level may contain different Cr# compositions as a result of differing degrees of melt-rock reaction and fractionation. This results in horizontal heterogeneity. During the ascent of melt through the mantle section melts will experience varying degrees of melt-rock reaction and fractionation. The product of these effects will be to reduce the Cr# and Mg# of precipitating chromite grains during the approach to the Moho.*

6.2.4 Postscript: The role of water in chromitite petrogenesis

6.2.4.1 The unmixing of a water-rich phase

The model outlined above includes continued melt-rock reaction. This requires the repeated transfer of olivine away from the hostrock to bring fresh peridotite into contact with primitive melt and therefore repeat melt-rock reaction and chromite-only crystallization (Figure 6.10). Although this is plausible, the potential role of water/volatile unmixing may provide a more simple option.

Aside from the observation of hydrous silicate inclusions and linear inclusion trails no other data specific to the role of water in chromitite petrogenesis were obtained. Nevertheless, water within boninitic melt may play an important role in the petrogenesis of the chromitite deposits, both as a dissolved constituent and during unmixing of a separate water/volatile-rich fluid phase. Chromium is present in the melt as Cr^{2+}, Cr^{3+} and Cr^{6+}, with the concentration of Cr^{3+} controlling the stability of chromian spinel (Roeder and Reynolds, 1991). As Cr^{3+} has a strong octahedral site preference (Burns, 1973; Murck and Campbell, 1986) it will be most soluble in melts with a low degree of polymerization of the Si network (Edwards *et al.*, 2000). When water is present as a dissolved constituent of basaltic melt, it will decrease melt polymerisation and viscosity, which therefore increases the Cr solubility in the melt (Edwards *et al*, 2000).

The presence of dissolved water in melts derived from the mantle in supra-subduction zone settings will thererfore greatly increase the amount of Cr that can be transported from the melting zone to the site of chromitite crystallization (e.g. estimates given in Malpas, 1997 for the Cr content of tholeiite – 600 ppm vs. boninite – 1200 ppm melts).

As the melt ascends through from the source region it will unmix a vapour phase in response to the decreasing pressure. The depth of unmixing will depend upon the dissolved water content, the temperature and the pressure. At the likely depth of chromitite formation (~6 – 8 km) the expected pressure is approximately 0.2 Gpa (Edwards *et al.*, 2000; Matveev & Ballhaus, 2002) and the temperature is approximately 1100°C. For these conditions, and with a dissolved water content of ~2wt% (e.g. Sobolev and Chaussidon, 1996; Falloon and Danyushevsky, 2000) it was argued that water would remain dissolved in the melt, and not unmix until much later – i.e. after the crystallization of the crustal pyroxenites (Edwards *et al.*, 2000).

However, several authors have suggested that the water content of mafic arc magmas may be significantly higher than this, lying in the region of 4-6 wt% (e.g. Sisson and Groove, 1993; Matveev & Ballhaus, 2002; Brophy, 2009; and Elburg 2010). Brophy (2009) argued that water unmixing (termed H_2O exsolution in the paper) would occur at depths between 4 km and 11 km depending on the water content (in the range 4 – 6 wt%). This means that at the depth of chromitite formation the unmixing of a vapour phase is possible, and could be repeated or semi-continuous as magma rises.

The unmixing of a vapour phase (to form an H_2O-, CO_2-, volatile-rich fluid phase) may lead to chromite crystallization and concentration through the following principal mechanism.

1. Chromite may crystallise from the denser, devolatilised silicate melt as the loss of water increases the polymerization of Si network and lowers the Cr solubility (e.g. Edwards *et al.*, 2000). This may therefore induce Cr super-saturation and crystallization. The exact nature of the separated water-rich, volatile-rich phase is unclear with some authors describing it as an H-rich reducing phase (Johan *et al.*, 1983, 1986), whilst other suggest it is a water-rich oxidising phase (Matveev and Ballhaus, 2002). In either case Cr super-saturation would occur in the resulting devolatilised silicate melt.
2. In immiscible basalt-water melt systems (magma, water, oxide and silicate particles) chromite and olivine microphenocrysts will be separated from each other by their differential wetting properties. With the onset of chromite crystallization within the devolatilised silicate melt, further vapour unmixing will nucleate on chromite microphenocrysts. The volatile-rich fluid containing chromite microphenocrysts will then rise through the devolatilised silicate melt (see Figure 1.6). In this process the volatile bubble collects oxide crystals from the magma in the manner analogous of froth flotation (Matveev and Ballhaus) where air bubbles collect particles from the water in a system of water, air, ore and gangue particles.

A further implication of this model is the formation of the dunite envelope which surrounds podiform chromitites. This is generally assumed to be a product of melt-rock reaction (e.g. Zhou, 1994, 1996), where a single-phase silicate melt interacts with the hostrock peridotite. However, in a two-phase system where there is an unmixed water/volatile-rich phase associated with devolatilised silicate melt, it may be the unmixed water/volatile-rich phase which reacts with the hostrock.

The volatile phase may be more pervasive, migrating more easily through, and reacting with, pyroxene-bearing peridotite than the de-volatilised silicate melt (e.g. Edwards *et al.*, 2000). The water/volatile-rich phase may freely migrate along these boundaries, dissolving orthopyroxene. However, since this is a two-phase system where unmixing has already occurred it is unlikely that constituents dissolved into the water/volatile-rich phase will mix back into the devolatilised silicate melt.

This therefore means that chromite crystallization may not be facilitated by an increase in the Si content of the melt, but by the rapid reduction in Cr-solubility within the de-volatilised silicate melt due to water unmixing. The relative volume of any exsolved water-rich phase, and the degree of possible pyroxene dissolution that this phase would be capable of is unclear. It seems unlikely that a water-rich phase would precipitate olivine following any pyroxene dissolution, unless by a process of metasomatic transformation (equation 1; Johan, 1986).

$$\text{opx} + \text{volatile liquid} = \text{ol} + (\text{volatile liquid containing elements leached out}) \quad (1)$$

How viable this transformation is, is also unclear, but may account for the apparent competence of previously analysed dunite envelopes. For example, Zhou *et al.* (1996) measured the change in geochemistry of chromite and silicate grains across a dunite envelope and into harzburgite. They observed that the modification in chromite and silicate geochemistry was gradual and systematic across the envelope suggesting that during the formation of the dunite from harzburgite the hostrock retained a rigid competence. Zhou *et al.* (1996) suggested that the peridotite hostrock acted like a 'chromatographic column' to the upwelling melt, which may also mean that the hostrock retains its competence during reaction with a single phase (i.e. exsolved water-rich fluid) silicate melt. Without disputing this possibility, one potential difficulty with applying this to chromite precipitation is the likely location of chromite crystallization. As the silicate melt leaches through the hostrock (which retains its competence) it will become chemically modified (e.g. Figure 6.7 & 6.8). The modified melt may then crystallize chromite, as its composition lies on the chromite-only crystallization field (e.g. Zhou *et al.*, 1994), but the resultant chromite grains will be situated within the dunite envelope. It appears geometrically difficult for the hostrock to both act as 'chromatographic column' and for modifications of the reacting melt composition to occur within the melt conduit.

It could be argued that exsolution of a water-rich phase may occur after melt-rock reaction, possibly triggered by, the dissolution-precipitation reaction. This two-stage process would allow the dunite envelope to form through melt-rock reaction before water unmixing and chromite crystallization occurred in the devolatilised silicate melt due to reduced Cr-solubility.

Water unmixing facilitated by melt-rock reaction would occur if during the ascent through the mantle a single-phase (i.e. no exsolved water-rich fluid) silicate melt lies very close to water saturation. As this single-phase melts reacts with the hostrock, progressive melt-rock reaction and separate olivine precipitation (as olivine lies on the liquidus) may additionally increase the water concentration of the melt (Figure 6.14). However, applying this to chromite precipitation may struggle with the same geometrical problems as highlighted previously (i.e. it appears difficult for modifications of the reacting melt composition to occur within the melt conduit, when the melt is leaching into the hostrock).

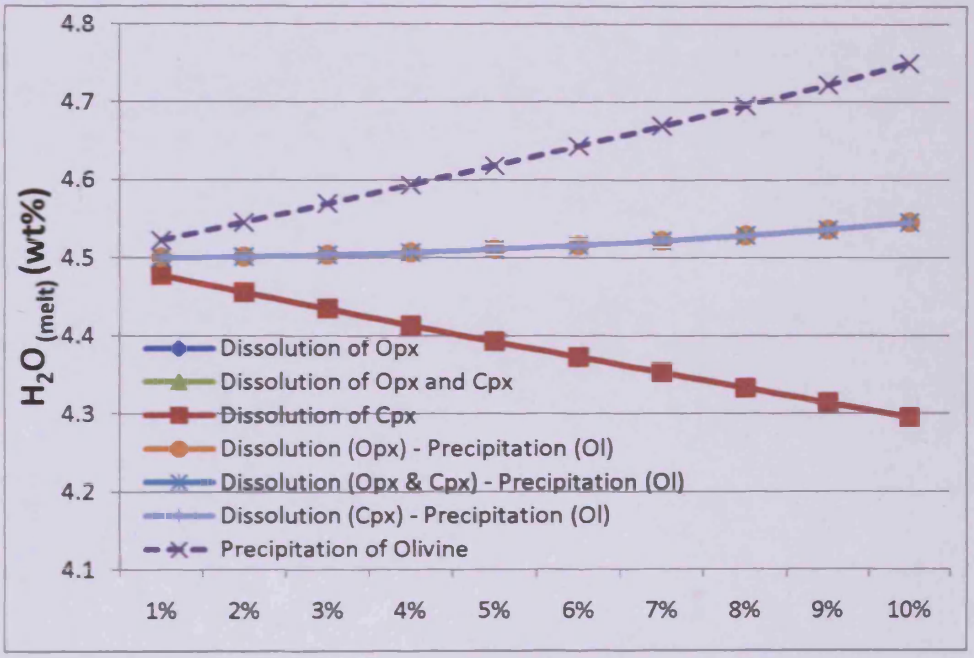

Figure 6.14: *Graph showing the effect of the progressive dissolution of pyroxene grains into, and precipitation of olivine grains out of, upwelling boninitic melts on the H_2O content of the melt. The initial starting content of the melt is taken as 4.5 wt% (e.g. the lower end of Brophy's, 2009 estimate for the H_2O content of mafic arc magmas). Dissolution of pyroxene into the melt, lowers the water content. Melt-rock reaction raises it slightly, whilst olivine precipitation raises the water content substantially.*

It is therefore apparent that within a water unmixing model the formation of the dunite envelope will be through reaction of the water-rich exsolved fluid with the hostrock producing an *in-situ* metasomatic transformation. Chromitite precipitation occurs in the devolatilised melt due to a reduction in Cr-solubility with possible further segregations (from olivine) due to the differential wetting properties of the chromite crystal surfaces (Matveev and Ballhaus, 2002).

The volume of chromite segregated from the upwelling melts will rely on two factors. The first is the degree of initial volatile loss, which produces chromite-only crystallization in the devolatilised melt. The greater the degree of volatile loss the more chromite will crystallize before the melt returns to the olivine-chromite liquidus. It is possible that chromite-only crystallization would be continuous if the rate of melt ascent and replenishment is constant, and devolatilisation was occurring at the same location. If chromite-only crystallization was not continuous the second factor is the relative volume of volatile-rich fluid produced and the efficacy with which this fluid can separate chromite from olivine in melts which continue to flux through the system and which may be crystallizing along the olivine-chromite liquidus.

The possible effect of volatile unmixing on the composition of chromite grains crystallizing out of the residual devolatilised melt is shown in Figure 6.11. An initially boninitic melt with very minor devolatilisation may produce relatively high Cr# and low Mg# chromite grains. With progressive devolatilisation the composition of the melt may become more 'tholeiitic'. This is analogous to the zoned diapir model where boninites may become progressively dried during ascent through the mantle (Tamura, 1994), except that the 'drying' is occurring *in-situ*. As a result, with progressive devolatilisation, the composition of the chromite grains follows trend A towards lower Cr# and higher Mg# (and possibly higher TiO_2 - Section 4.6.2.2.1).

6.2.5 Chromitite petrogenesis summary and implications for PGE enrichment

The discussion has suggested two general models for chromitite petrogenesis with some mutual areas of overlap. Within both models melt composition is expected to evolve with ascent through the mantle through the processes of melt-rock reaction and fractionation. Fractionation covers changes in the composition of the melt due to chromite and olivine crystallization and changes that occur due to volatile loss. Melt composition may be affected by both the effects of crystallization and of volatile loss.

1. The upwelling of a single phase silicate melt interacts with peridotite hostrock with which it is out of equilibrium. This results in the dissolution of pyroxene and precipitation of olivine. The remaining silicate melt becomes enriched in SiO_2 and Cr_2O_3 pushing the melt into the chromite-only crystallization field. Further chromite-only crystallization and separation of chromite from olivine is facilitated by mechanical sorting which repeatedly exposed fresh peridotite to upwelling melts repeating melt-rock reaction.
2. An upwelling single-phase silicate melt lies close to water super-saturation. With increasing ascent and decompression (and/or olivine crystallization – Figure 6.14) water super-saturation occurs and there is unmixing of a second water- and volatile- rich phase. The unmixing of this water-rich phase significantly decreases the Cr solubility in the remaining devolatilised silicate melt leading to chromite-only precipitation. When chromite and olivine co-crystallise their segregation is aided by the differential wetting properties of chromite and olivine, with chromite being 'collected' by the unmixed water-rich phase.

If both models of chromitite formation occur in natural environments then this may answer the question of why some dunites contain podiform chromitites, why some dunites are barren of podiform chromitites and why the size of the dunite envelope is independent of the size of the chromitite pod. For example chromitite barren dunites may occur if melt-rock reaction occurs with the hostrock maintaining its competence (i.e. no mechanical sorting, or fresh exposure of peridotite to primitive melt). In this scenario chromitite crystallization may never occur in bulk within the melt conduit and a predominantly olivine-bearing pod is produced. If mechanical sorting is pervasive and there is no competence to the hostrock during leaching and reaction then chromite-only crystallization may occur within the melt conduit with additional physical separation of chromite from olivine (e.g. Figure 6.10). Alternatively the dunite may form through metasomatic transformation by an unmixed volatile-rich phase. The thickness of the dunite envelope would then depend upon the degree of devolatilisation (i.e. the water content at super-saturation) which may vary with stratigraphic height, or with melt composition. Crucially the thickness of dunite formed may be very different (though it is unclear to what extent) to that expected from interaction between a single phase silicate melt and hostrock.

The different textural associations of IPGE (generally included in chromite) and PPGE (generally included within the interstitial silicates) suggests there possible concentration by different mechanisms. Within the first model, PGE concentration may be driven by a redox gradient at the boundary of crystallizing chromite. This may preferentially incorporate IPGE (Finnigan *et al.*, 2008). If the formation of chromitites is primarily controlled by water immiscibilty within upwelling melts (2nd model) then the predominance of IPGM within chromite may be explained by the ability of a water/volatile-rich phase to collect both chromite and IPGM (Matveev and Ballhaus, 2002).

PPGE concentration within both models may be driven by the onset of sulphur saturation through the gradual decrease of temperature, and change in melt composition with the ascent of melts through the mantle. The possible dependence of PPGE enrichment on the Cu-rich portion of the sulphide fractionates requires more investigation.

In either model, IPGE enrichment processes are largely independent of PPGE enrichment processes. Furthermore, this may explain the general predominance of IPGE enrichment over PPGE enrichment within ophiolites as sulphur saturation events are only rarely observed in association with podiform chromitites.

Chapter 7

Conclusions and Recommendations

7 Conclusions and Recommendations

7.1 Recap of main aims

This thesis investigated the chromite geochemistry and PGE concentrations in podiform chromitites from three ophiolites (Al 'Ays, Shetland and Berit) with the aim of testing whether; (1) there was any link between the two, (2) what the presence, or absence of a link reveals about the mechanism of PGE concentration and (3) why some chromitite pods are highly PGE-enriched. In addition to partially answering these questions, further insights were obtained into podiform chromitite petrogenesis and the formation of particular chromitite textures. The conclusions are detailed below focussing in turn on the main conclusions from each ophiolite before general conclusions and recommendations for future work.

7.1.1 Chapter 3: The Al 'Ays ophiolite

Chromite composition between Al 'Ays chromitites shows a continuous gradual change with stratigraphic height for all major and most trace elements. In particular two trends are apparent on a Cr#-Mg# plot; trend A, which is an inverse correlation between Cr# and Mg#, is apparent ***within*** stratigraphic groups; trend B, which is a positive correlation between Cr# and Mg#, is apparent ***between*** stratigraphic groups. Trend A is interpreted as being primarily due to the changing composition of melts being produced from the source region, whereas Trend B is interpreted as primarily a function of orthomagmatic fractionation (and melt-rock reaction) within the thick mantle sequence. On a smaller scale it was observed that single chromitite thin sections may contain major element heterogeneity. This observation within one thin section from Al 'Ays is interpreted as a product of an already 'charged' magma carrying chromite xenocrysts. Further chromite crystallization and sintering/overgrowth removes previous crystal boundaries, yet preserves the variable chemistry within.

PGE concentration is initially interpreted as the result of the separation of a sulphide liquid from the melt, caused by the effects of melt-rock reaction and fractionation on the composition of upwelling melts. Sulphide melt separation has led to the simultaneous concentration of PGE. Both sulphide saturation and chromite composition are effected by fractionation and it is confirmed that PGE-rich chromitites are associated with a particular chromite chemistry. In particular Cr/Fe^{2+} vs. Co, Cr/Fe^{2+} vs. Zn and Cr#-Mg# provide good

discrimination diagrams for PGE-rich chromitites in the Al 'Ays ophiolite. However, the different textural associations of the IPGM and PPGM (as detailed by numerous previous workers) together with results from Chapter 4 suggest that IPGE and PPGE enrichment may result from processes capable of being decoupled. It is suggested that, for this ophiolite, PPGE-rich, low Cr# chromitites formed form PPGE-rich sulphide saturated parent magmas, whereas IPGE-rich, high Cr# chromitites form from IPGE-rich sulphide under-saturated magmas. The IPGE enrichment encountered in sample C51 remains enigmatic within this model as it is a low Cr# deposit.

7.1.2 Chapter 4: The Shetland ophiolite

Formerly, the Shetland ophiolite was thought to have formed within an intra-continental basin. This basin underwent eastward-dipping subduction before closure of the basin led to westward obduction of the subducting slab (Flinn & Oglethorpe, 2005). This study prefers a different model that takes account of the extreme difficulty of obducting a subducting slab (Stern, 2004). It is proposed that the intra-continental basin underwent westward dipping subduction, with final obduction of mantle and crust from the supra-subduction zone (and not the subducting slab) westward onto the Laurentian continent.

Analysis of several (7) chromitite deposits within the mantle and crustal sequence reveals that the majority of deposits have a similar chromite chemistry aside from Harold's Grave which is unique in terms of its major and trace element inventory. These Shetland chromitite compositions show the same two trends as the Al 'Ays ophiolite with trend A (negative correlation between Cr# and Mg#) predominant ***within*** all of the chromitite deposits. Trend B (positive correlation between Cr# and Mg#) is apparent ***between*** the Harold's Grave deposit and the rest of the chromitite deposits and to a lesser extent ***within*** one deposit (Cliff).

The Cliff chromitite deposit carries several geochemical co-variations in addition to trends A & B. In particular there is a clear division between samples using TiO_2 contents with low TiO_2 chromite grains forming trend A and high TiO_2 chromite grains forming trend B (with sub-trends, Bi & Bii). Two other co-variation patterns are evident on a Cr#-TiO_2 (in spinel) plot involving chromite and chromitiferous dunite. The first is a negative correlation between Cr# and TiO_2 (labelled trend D). The second is a weakly positive correlation between Cr# and TiO_2 (labelled trend E). Of particular interest is the location of the PGM-rich dunite samples and PGE-rich chromitite samples solely within trend D. Interpreting the processes producing this

trend is very difficult but may be partially explained by fractionation due to the progressive unmixing of a water-rich phase, followed by sulphur saturation.

Within Harold's Grave the high IPGE concentrations are associated with a unique chromite geochemistry. Trace element concentrations are higher than, and the Mg# lower than, any of the other chromitite deposits embraced by this study. This is interpreted as a product of fractionation and reaction with a trapped intercumulus melt. The extended reaction of chromite with trapped intercumulus melt has facilitated the collection of high concentrations of IPGM by the precipitating chromite grains (Finnigan *et al.*, 2008). There are three indications that IPGE and PPGE enrichment processes may be decoupled, these include (1) the different textural locations of PGM (as noted by previous workers), (2) the presence of IPGE enrichment in Harold's Grave associated with a unique chromite geochemistry, and (3) PPGE enrichment at Cliff itself associated with localized fractionation patterns.

Chapters 3 & 4 have provided evidence that high-PGE concentrations may be linked to a particular chromite composition within an ophiolite, as well as requiring other processes to concentrate IPGE and PPGE.

7.1.3 Chapter 5: The Berit ophiolite

No further anomalous PGE concentrations were found within this ophiolite, despite sampling deposits which were previously found to be highly enriched. This suggests that PGE concentrations can display extreme variation over very short distances. Investigation of the chromite geochemistry suggests that a switch in tectonic setting has occurred within this ophiolite in a manner analogous to that observed in other Turkish ophiolites (e.g. Uysal, 2009). This switch is tentatively interpreted as a switch between back-arc and island-arc magmatism.

The formation of chlorite filled lamellae, oriented along the {111} plane of the chromite lattice is interpreted as the product of amphibolite facies metamorphism within the Berit ophiolite. This metamorphism has led to the nucleation and growth of spinel (*sensu strictu*) within chromite in an environment where spinel itself is thermodynamically unstable. This in turn has led to the simultaneous alteration of this unmixed spinel to chlorite (Cr-clinochlore).

As with Al 'Ays and Shetland the observed IPGM in Berit are concentrated within chromite grains and are not associated with sulphur saturation (i.e. the PGM, although occasionally sulphide-bearing are not associated with sulphides). In contrast, the association of the PPGE

mineralization with Cu-bearing sulphides is of interest, and similar to that observed in previous studies on the Shetland and Al 'Ays ophiolite. It may be that the precipitation of Cu-bearing sulphides is essential to the concentration of PPGE within ophiolitic chromitite. This observation may further confirm the essential decoupling of IPGE enrichment processes from PPGE enrichment processes within ophiolites.

7.1.4 Chapter 6: Discussion of inclusions and chromitite petrogenesis

The two predominantly observed inclusion patterns are clustered inclusions and linear trails of inclusions. The former is interpreted as a **primary** feature where early formed chromite grains co-precipitate with anhydrous and hydrous silicates. Later crystallization of chromite grains produces the final texture of inclusion-rich chromite grains within an inclusion-empty chromitite. The second inclusion pattern is interpreted as a **pseudo-secondary** feature in a manner analogous to that proposed by Roedder (1979). These inclusions are interpreted as products of late-stage volatile-rich fluids which 'puncture' along fractures or grain boundaries due to volatile overpressure, before re-healing of the chromite grains traps some of the volatiles.

Two general models for chromitite petrogenesis are proposed, which are based on models of melt-rock reaction suggested by Zhou *et al.* (1994) and water unmixing suggested by Matveev and Ballhaus (2002). The two models are;

Model 1: Chromite-only crystallization is facilitated by melt-rock reaction which adds SiO_2 and Cr_2O_3 into the single phase silicate melt, pushing the melt into the chromite-only crystallization field. Further chromite-only crystallization, and separation of chromite from olivine, is facilitated by mechanical sorting. This repeatedly exposes fresh peridotite to upwelling melts, thus repeating melt-rock reaction. This mechanical sorting is analogous to that proposed by Lago *et al.* (1982), though this author prefers a horizontal melt pool to prevent repeated disruption of any chromite segregation.

Model 2: Upwelling single phase silicate melts lie close to water super-saturation. With further decompression (and possibly facilitated by olivine precipitation) water super-saturation occurs and there is unmixing of a second water and volatile rich phase. The unmixing of a water-rich phase significantly decreases the chromium solubility in the remaining devolatilised silicate melt thus leading to chromite-only precipitation. Segregation

of chromite from olivine is aided by the differential wetting properties of chromite and olivine, with chromite being 'collected' by the unmixed water-rich phase. This second model carries a further implication for PGE enrichment, namely that unusual Os-Ir-Ru enrichment (e.g. sample C51 in Al 'Ays) may be explained by concentration of the IPGM by the immiscible water-rich phase.

There are three mutual areas of overlap between these two models. Firstly, melt composition is expected to evolve with ascent through the mantle by melt-rock reaction and orthomagmatic fractionation. Secondly, chromium solubility within the melt is very limited so an open-system is required to produce any sizeable chromitite deposit (e.g. Edwards *et al.*, 2000). Thirdly, chromitite deposits represent the cumulative product of numerous batch melts depositing a little chromite before continuing their ascent through the mantle/crust.

7.1.5 PGE-enrichment processes in ophiolites

This author's view is that IPGE and PPPE enrichment processes in ophiolitic chromitite are likely to be decoupled. IPGE-enrichment may be driven by two principal processes, both of which occur as IPGE-saturation events; these are:

(1) A redox gradient forming at the boundary of crystallizing chromite which causes the precipitation of IPGM that are then preferentially incorporated (Finnigan *et al.*, 2008); This process may be particularly well facilitated when chromite is able to react with large amounts of trapped intercumulus melt (as hypothesized for Harold's Grave), as more IPGE may be incorporated into the IPGE-saturation events. As Harold's Grave also contains elevated trace element values (relative to the other analysed chromitite deposits), then deposits in other ophiolites with relatively elevated trace elements may also be enriched in IPGM. The absence of elevated trace element concentrations in sample C51 from Al 'Ays, shows that this mechanism is not sufficient to explain all unusual IPGE enrichment.

(2) Water unmixing within upwelling melts leading to the formation of a water/volatile-rich phase with collects chromite and micronuggets of IPGM (Matveev and Ballhaus, 2002). The presence of IPGM micronuggets in the melt may be caused by the process of water unmixing as IPGE solubility will be greatly reduced in the devolatilised melt (e.g. Borinsov and Palme, 2000), potentially causing an IPGE-saturation event.

In either of the above scenarios, IPGE-saturation events may 'pull' a little sulphur out of the melt resulting in the final texture of sulphide-bearing IPGM enclosed within chromite. In contrast to IPGE concentration, PPGE concentration may be driven by the onset of sulphur saturation, through the gradual decrease of temperature and change in melt composition with the ascent of melts through the mantle. Sulphur saturation events occur later in the crystallization sequence 'pulling' the remaining PPGE out of the melt producing the final texture of sulphide-bearing PPGM associated with base-metal sulphides and included interstitial to the chromite grains.

This decoupled process may explain the general predominance of IPGE enrichment over PPGE enrichment within ophiolites, as sulphur saturation events are only rarely observed in association with podiform chromitites.

7.2 Recommendations - Future Work

Further work on the Shetland and Berit ophiolites is required to more accurately determine their tectonic history. For the Shetland ophiolite this should start with the harzburgite and sheeted dyke sections, as the apparent presence of passive margin harzburgite on the island of Fetlar (which contains no appreciable chromitite deposits) together with the presence of MORB and island arc-type dykes (Prichard, pers. comm.) suggests there is more detail to be gathered leading to a complex tectonic history. For the Berit ophiolite detailed mapping of the ophiolite is required, particularly the unequivocal identification of mantle host rock (whether lherzolite or harzburgite) as the chromitite setting is unclear.

The forsterite contents of olivine within the Shetland crustal dunites were surprisingly high. Further investigation may clarify whether these compositions are typical of the dunite sequence as a whole, or whether they show a gradual decrease from the bottom (near the petrological Moho) to the top (near the gabbro) as would be expected from a fractionally crystallizing sequence. Further analysis of the dunite compositions within Cliff and Harold's Grave may help distinguish between processes controlling chromite chemistry, particularly if gathered as *in-situ* samples to preserve spatial relationships. This is necessary as the key co-variation in the Cliff deposit (trend D, which contains all the PGE-enriched samples) is currently only tentatively attributed to a process.

Further investigation of the linear trails of inclusions is required to test their proposed origin. If they did form as pseudo-secondary features through the action of an unmixed volatile-rich phase, then volatile-bearing residues would be expected along the surfaces of the empty inclusions.

The link between PPGE-rich chromitites and the presence of Cu-bearing sulphides would provide an important control for PPGE concentration. Such an investigation would need to take into account the possible effects of the post-magmatic redistribution of base-metals through hydrothermal fluids. More work is required on the separation of IPGM from PPGM in ophiolitic chromitites. Although their different textural relationships are well documented, the precise reason for their decoupling is not. If it depends on the exsolution of an immiscible volatile-rich phase, then what is the likely composition of this unmixed phase (e.g. is it oxidising or reducing) and does it collect IPGE, or micronuggets of already crystallized IPGM?

References

Acharyya, S.K., 2007, Collisional emplacement history of the Naga-Andaman ophiolites and the position of the eastern Indian suture: Journal of Asian Earth Sciences, v. 29, p. 229-242.

Ahmed, A.H., and Arai, S., 2002, Unexpectedly high-PGE chromitite from the deeper mantle section of the northern Oman ophiolite and its tectonic implications: Contributions to Mineralogy and Petrology, v. 143, p. 263-278.

Ahmed, A.H., and Arai, S., 2003, Platinum-group minerals in podiform chromitites of the Oman ophiolite: Canadian Mineralogist, v. 41, p. 597-616.

Ahmed, A.H., Arai, S., Abdel-Aziz, Y.M., and Rahimi, A., 2005, Spinel composition as a petrogenetic indicator of the mantle section in the Neoproterozoic Bou Azzer ophiolite, Anti-Atlas, Morocco: Precambrian Research, v. 138, p. 225-234.

Ahmed, A.H., Arai, S., and Attia, A.K., 2001, Petrological Characteristics of podiform chromitites and associated peridotites of the Pan African Proterozoic ophiolite complexes of Egypt: Mineralium Deposita, v. 36, p. 72-84.

Ahmed, A.H., Helmy, H.M., Arai, S., and Yoshikawa, M., 2008, Magmatic Unmixing in spinel from late Precambrian concentrically-zoned mafic-ultramafic intrusions, Eastern Desert, Egypt.: Lithos, v. 104, p. 85-98.

Ahmed, Z., 1984, Stratigraphic and Textural Variations in the Chromite Composition of the Ophiolitic Sakhakot-Qila Complex, Pakistan: Economic Geology, v. 79, p. 1334-1359.

Ahmed, Z., 2003, Geochemical and Genetic Implications of Adakites Associated with the Suprasubduction-Type Al-Ays Ophiolite, Northwestern Arabian Shield: International Geology Review, v. 45, p. 176-190.

Ahmed, Z., and Hariri, M.M., 2008, Neoproterozoic Ophiolites as developed in Saudi Arabia and their Oceanic and Pericontinental Domains: Arabian Journal for Science and Engineering, v. 33, p. 17-54.

Al-Shanti, A.M., and El-Mahdy, O.R., 1988, Geological Studies and Assessment of Chromite Occurrences in Saudi Arabia KACST Project No. AT-6-094.

Alard, O., Griffin, W.L., Lorand, J.P., Jackson, S.E., and O'Reilly, S.Y., 2000, Non-chondritic distribution of the highly siderophile elements in mantle sulphides: Nature, v. 407, p. 891-894.

Allan, J.F., Sack, R.O., and Batiza, R., 1988, Cr-rich spinels as petrogenetic indicators: MORB-type lavas from the Lamont seamount chain, eastern Pacific: American Mineralogist, v. 73, p. 741-753.

Amstutz, G.C., 1979, The early history of the term Ophiolites and its evolution until 1945 *in* Panayiotou, A., ed., International Ophiolite Symposium: Cyprus, p. 149-152.

Anonymous, 1972, Penrose field conference on ophiolites: Geotimes, v.17, p. 24-25

Arai, S., 1987, An estimation of the least depleted spinel peridotite on the basis of olivine-spinel mantle array: Neues Jahrbuch Fur Mineralogie-Monatshefte, p. 347-354.

Arai, S., 1990, What kind of magmas could be equilibrated with ophiolitc peridotites?, *in* Malpas, J., Moores, E., Panayiotou, A., and Xenophontus, C., eds., Ophiolites, Oceanic Crustal Analogue, Proceedings Symposium "Troodos 1987" p. 557-565.

Arai, S., 1992, Chemistry of Chromian Spinel in Volcanic-Rocks as a Potential Guide to Magma Chemistry: Mineralogical Magazine, v. 56, p. 173-184.

Arai, S., 1994, Characterization of Spinel Peridotites by Olivine Spinel Compositional Relationships - Review and Interpretation: Chemical Geology, v. 113, p. 191-204.

Arai, S., 1999, Platinum-group minerals in podiform chromitite from the Kamuikotan zone, Hokkaido, Northern Japan: Resource Geology, v. 49, p. 39-47.

Arai, S., and Matsukage, K., 1998, Petrology of a chromitite micropod from Hess Deep, equatorial Pacific: a comparison between abyssal and Alpine-type podiform chromitites: Lithos, v. 43, p. 1-14.

Arai, S., Uesugi, J., and Ahmed, A.H., 2004, Upper crustal podiform chromitite from the northern Oman ophiolite as the stratigraphically shallowest chromitite in ophiolite and its implication for Cr concentration: Contributions to Mineralogy and Petrology, v. 147, p. 145-154.

Arai, S., and Yurimoto, H., 1994, Podiform chromitites of the Tari-Misaka ultramafic complex, southwestern Japan, as mantle-melt interaction products: Economic Geology, v. 89, p. 1279-1288.

Augé, T., 1985, Platinum-group-mineral inclusions in ophiolitic chromitite from the Vourinos complex, Greece: Canadian Mineralogist, v. 23, p. 163-171.

Augé, T., 1988, Platinum-group minerals in the Tiebaghi and Vourinos Ophiolitic complexes: Genetic Implications: Canadian Mineralogist, v. 26, p. 177-192.

Augé, T., Cabri, L.J., Legendre, O., McMahon, G., and Cocherie, A., 1999, PGE distribution in base-metal alloys and sulphides of the New Caledonia ophiolite Canadian Mineralogist, v. 37, p. 1147-1161.

Augé, T., Legendre, O., and Maurizot, P., 1998, The distribution of Pt and Ru-Os-Ir minerals in the New Caledonia ophiolite, *in* Laverov, N.P., and Distler, V.V., eds., International Platinum: Athens, Theophrastus publications p. 141-154.

Augé, T., and Lerouge, C., 2004, Mineral-chemistry and stable-isotope constraints on the magmatism, hydrothermal alteration, and related PGE-(base metal sulphide) mineralisation of the Mesoarchaean Baula-Nuasahi Complex, India.: Mineralium Deposita, v. 39, p. 583-607.

Bacuta, G.C.J., Lipin, B.R., Gibbs, A.K., and Kay, R.W., 1988, Platinum-group element abundance in chromite deposits of the Acoje ophiolite block, Zambales ophiolite complex, Philippines, *in* Prichard, H.M., Potts, P.J., Bowles, J.F., and Cribb, S.J., eds., Geo-Platinum Symposium Volume, Elsevier, p. 381-382.

Bai, W.-J., Zhou, M.F., and Robinson, P.T., 1993, Possibly diamond-bearing mantle peridotites and podiform chromitites in the Luobusa and Donqiao ophiolites, Tibet: Canadian Journal of Earth Sciences, v. 30, p. 1650 - 1659.

Bakor, A.R., Gass, I.G., and Neary, C.R., 1976, Jabal Al Wask, Northwest Saudi Arabia: An Eocambiran Back-Arc Ophiolite: Earth and Planetary Science Letters, v. 30, p. 1-9.

Ballhaus, C., 1998, Origin of podiform chromite deposits by magma mingling: Earth and Planetary Science Letters, v. 156, p. 185-193.

Barnes, S.J., 1998, Chromite in Komatiites, 1. Magmatic Controls on Crystallization and Composition: Journal of Petrology, v. 39, p. 1689 - 1720.

Barnes, S.J., 2000, Chromite in komatiites, II. Modification during greenschist to mid-amphibolite facies metamorphism: Journal of Petrology, v. 41, p. 387-409.

Barnes, S.J., Naldrett, A.J., and Gorton, M.P., 1985, The origin of the fractionation of platinum-group elements in terrestrial magmas: Chemical Geology, v. 53, p. 303-323.

Barnes, S.J., and Picard, C.P., 1993, The Behavior of Platinum-Group Elements during Partial Melting, Crystal Fractionation, and Sulfide Segregation - an Example from the Cape-Smith Fold Belt, Northern Quebec: Geochimica Et Cosmochimica Acta, v. 57, p. 79-87.

Barnes, S.J., and Roeder, P.L., 2001, The range of spinel compositions in terrestrial mafic and ultramafic rocks: Journal of Petrology, v. 42, p. 2279-2302.

Barnes, S.J., and Tang, Z.-L., 1999, Chrome-spinels from the Jinchuan Ni-Cu Sulfide Deposit, Gansu Province, People's Republic of China.: Economic Geology, v. 94, p. 343-356.

Barth, M.G., Mason, P.R.D., Davies, G.R., Dijkstra, A.H., and Drury, M.R., 2003, Geochemistry of the Othris Ophiolite, Greece: Evidence for refertilization: Journal of Petrology, v. 44, p. 1759 - 1785.

Bedini, R.M., and Bodinier, J.L., 1999, Distribution of incompatible trace elements between the constituents of spinel peridotite xenoliths: ICP-MS data from the East African Rift: Geochimica Et Cosmochimica Acta, v. 63, p. 3883-3900.

Bédard, E., Hébert, R., Guilmette, C., and Dostal, J., 2008, The supra-ophiolitic sedimentary cover of the Asbestos ophiolite, Québec, Canada: First geochemical evidence of transition from oceanic to continental sediment flux: Lithos, v. 105, p. 239-252.

BGS, 2002, BRITISH GEOLOGICAL SURVEY. Unst and Fetlar. Scotland Sheet 131. Solid and Drift geology. 1:50000: Nottingham, British Geological Survey.

Bockrath, C., Ballhaus, C., and Holzheid, A., 2004, Fractionation of the Platinum-Group Elements During Mantle Melting: Science, v. 305, p. 1951-1953.

Bortolotti, V., and Principi, G., 2005, Tethyan ophiolites and Pangea break-up: Island Arc, v. 14, p. 442-470.

Borisov, A., and Palme, H., 2000. Solubilities of noble metals in Fe-containing silicate melts as derived from experiments in Fe-free systems: American Mineralogist. v.85, p. 1665-1673.

Brophy, J.G., 2009, Decompression and H_2O exsolution driven crystallization and fractionation: development of a new model for low-pressure fractional crystallization in calc-alkaline magmatic systems: Contributions to Mineralogy and Petrology, v. 157, p. 797-811.

Brown, M., 1980, Textural and geochemical evidence for the origin of some chromite deposits in the Oman ophiolite, Proceedings of the International Ophiolite Symposium: Cyprus, p. 714-721.

Buchl, A., Brugmann, G., and Batanova, V.G., 2004, Formation of podiform chromitite deposits: implications from PGE abundances and Os isotopic compositions of chromites from the Troodos complex, Cyprus: Chemical Geology, v. 208, p. 217-232.

Burgath, K.P., 1988, Platinum-group minerals in ophiolitic chromitites and alluvial placer deposits, Meratus-Bobaris area, southeast Kalimantan., Proceedings of the Geo-Platinum 1987: Milton Keynes, p. 383-403.

Burns, R.G., 1973, The partitioning of trace transition elements in crystal structures: a provocative review with applications to mantle geochemistry: Geochimica et Cosmochimica Acta, v. 37, p. 2395-2403.

Canil, D., 1999, Vanadium partitioning between orthopyroxene, spinel and silicate melt and the redox states of mantle source regions for primary magmas: Geochimica et Cosmochimica Acta, v. 63, p. 557-572.

Canil, D., 2002, Vanadium in peridotites, mantle redox and tectonic environments: Archean to present: Earth and Planetary Science Letters, v. 195, p. 75-90.

Castillo, P.R., 2006, An overview of adakite petrogenesis: Chinese Science Bulletin, v. 51, p. 258-268.

Cawthorn, R.G., 2002, The role of magma mixing in the genesis of PGE mineralization in the Bushveld Complex: Thermodynamic calculations and new interpretations - a discussion: Economic Geology, v. 97, p. 663-666.

Cawthorn, R.G., 2005, Pressure fluctuations and the formation of the PGE-rich Merensky and chromitite reefs, Bushveld Complex: Mineralium Deposita, v. 40, p. 231-235.

Christiansen, F.G., 1985, Deformation fabric and microstructures in ophiolitic chromitites and host ultramafics, Sultanate of Oman: Geologische Rundschau, v. 74, p. 61-76.

Christiansen, F.G., 1986, Deformation of chromite: S.E.M. investigations: Tectonophysics, v. 121, p. 175-196.

Claesson, S., Pallister, J.S., and Tatsumoto, M., 1984, Samarium-Neodymium data on two late Proterozoic ophiolites of Saudi Arabia and implications for crustal and mantle evolution.: Contributions to Mineralogy and Petrology, v. 85, p. 244-252.

Constantinides, C.C., Kingston, G.A., and Fisher, P.C., 1980, The occurrence of platinum-group minerals in the chromitites of the Kokkinorotsos chrome mine, Cyprus., *in* Panayiotou, A., ed., Ophiolites Proceedings International Ophiolite Symposium Cyprus: Nicosia, Ministry of Agriculture and Natural Resources, Geological Survey Report, p. 93-101.

Coogan, L.A., Jenkin, G.R.T., and Wilson, R.N., 2002, Constraining the cooling rate of the lower oceanic crust: a new approach applied to the Oman ophiolite: Earth and Planetary Science Letters, v. 199, p. 127-146.

Corrivaux, L., and Laflamme, J.H.G., 1990, Mineralogie des elements du grouped u platine dans les chromitites de l'ophiolite de Thetford mines, Quebec: Canadian Mineralogist, v. 28.

Crawford, A.J., 1989, Boninites and related rocks: London, Unwin Hyman.

Dare, S., 2007, Chrome-Spinel geochemistry of the northern Oman-United Arab Emirates Ophiolite: Cardiff, Cardiff University.

Deb, S.F.N.I., and Chakraborty, K.L., 1961, Origin of chromite deposits associated with the ultrabasic rocks of the eastern part of the indian peninsula: Proceedings of the National Institute for Science in India, v. 27, p. 508-519.

Dick, H.J.B., and Bullen, T., 1984, Chromian Spinel as a petrogenetic indicator in abyssal and alpine-type peridotites and spatially associated lavas: Contributions to Mineralogy and Petrology, v. 86, p. 54-76.

Dickey Jr, J.S., 1975, A hypothesis of origin for podiform chromite deposits: Geochimica et Cosmochimica Acta, v. 39, p. 1061-1062,IN17-IN18,1063-1074.

Dilek, Y., 2003a, Ophiolite concept and it evolution, *in* Dilek, Y., and Newcomb, S., eds., Ophiolite Concept and the Evolution of Geological Thought, Geological Society of America, p. 1-16.

Dilek, Y., 2003b, Ophiolite pulses, mantle plumes and orogeny *in* Dilek, Y., and Robinson, P.T., eds., Ophiolites in Earth History: Bath, The Geological Society Publishing House.

Dilek, Y., and Thy, P., 2009, Island arc tholeiite to boninitic melt evolution of the Cretaceous Kizildag (Turkey) ophiolite: Model for multi-stage early arc-forearc magmatism in Tethyan subduction factories: Lithos, v. 113, p. 68-87.

Dilek, Y., Thy, P., Hacker, B., and Grunvig, S., 1999, Structure and petrology of the Tauride ophiolites and mafic dike intrusions (Turkey): Implications for the Neotethyan ocean.: Geological Society of America, v. 111, p. 1192-1216.

Distler, V.V., Kryachko, V.V., and Yudovskaya, M.A., 2003, Formation conditions of platinum-group metals in chromite ores of the Kempirsai ore field: Geology of Ore Deposits, v. 45, p. 37-65.

Distler, V.V., Kryachko, V.V., and Yudovskaya, M.A., 2008, Ore petrology of chromite-PGE mineralization in the Kempirsai ophiolite complex: Mineralogy and Petrology, v. 92, p. 31-58.

Eales, H.V., 2000, Implications for the chromium budget of the Western Limb of the Bushveld Complex South African Journal of Geology, v. 103, p. 141-150.

Eales, H.V., Wilson, A., and Reynolds, I., 1988, Complex unmixed spinels in layered intrusions within an obducted ophiolite in the Natal-Namaqua mobile belt: Mineralium Deposita, v. 23, p. 150-157.

Eckstrand, O.R., 1975, The Dumont serpentinite; a model for control of nickeliferous opaque mineral assemblages by alteration reactions in ultramafic rocks: Economic Geology, v. 70, p. 183-201.

Economou-Eliopoulos, M., 1996, Platinum-group element distribution in chromite ores from ophiolite complexes: Implications for their exploration: Ore Geology Reviews, v. 11, p. 363-381.

Economou-Eliopoulos, M., Tarkian, M., and Sambanis, G., 1999, On the geochemistry of chromitites from the Pindos ophiolite complex, Greece: Chemie Der Erde-Geochemistry, v. 59, p. 19-31.

Edwards, S.J., Pearce, J.A., and Freeman, J., 2000, New Insights concerning the influence of water during the formation of podiform chromitite Geological Society of America p. 139-147.

Elburg, M.A., 2010, Sources and processes in arc magmatism: the crucial role of water: Geologica Belgica, v. 13, p. 121-136.

El Ghorfi, M., Melcher, F., Oberthur, T., Boukhari, A.E., Maacha, L., Maddi, A., and Mhaili, M., 2008, Platinum group minerals in podiform chromitites of the Bou Azzer ophiolite, Anti Atlas, Central Morocco: Mineralogy and Petrology, v. 92, p. 59 - 80.

Evans, B.W., and Frost, B.R., 1975, Chrome-spinel in progressive metamorphism - a preliminary analysis: Geochimica et Cosmochimica Acta, v. 39, p. 959 - 972.

Falloon, T.J., and Danyushevsky, L.V., 2000, Melting of Refractory Mantle at 1.5, 2 and 2.5 GPa under Anhydrous and H_2O-undersaturated Conditions: Implications for the Petrogenesis of High-Ca Boninites and the Influence of Subduction Components on Mantle Melting: Journal of Petrology, v. 41, p. 257-283.

Farrow, C.E.G., and Watkinson, D.H., 1992, Alteration and the role of fluids in Ni, Cu and Platinum-Group Element Deposition, Sudbury Igneous Complex Contact, Onaping-Levack area, Ontario: Mineralogy and Petrology, v. 46, p. 67-83.

Filippidis, A., 1985, Formation of awaruite in the system Ni-Fe-Mg-Si-O-H-S and olivine hydration with NaOH solution, an experimental study: Economic Geology, v. 80, p. 1974-1980.

Finnigan, C.S., Brenan, J.M., Mungall, J.E., and McDonough, W.F., 2008, Experiments and models bearing on the role of chromite as a collector of platinum group minerals by local reduction: Journal of Petrology, v. 49, p. 1647-1665.

Fisk, M.R., 1986, Basalt magma interaction with harzburgite and the formation of high-magnesium andesites: Geophysical Research Letters, v. 13, p. 467-470.

Fleet, M.E., Nelson, A., and Pan, Y., 1993, Oriented chlorite lamellae in chromite from the Pedra Branca Mafic-Ultramafic Complex, Ceara, Brazil.: American Mineralogist, v. 78, p. 68-74.

Flinn, D., 1985, The Caledonides of Shetland, *in* Gee., D.G.a.S., B. A., ed., The Caledonide Orogeny - Scandinavia and related Areas, John Wiley & Sons Ltd., p. 1159-1172.

Flinn, D., 1992, The history of the Walls Boundary fault, Shetland: the northward continuation of the Great Glen fault from Scotland: Journal of the Geological Society, v. 149, p. 721-726.

Flinn, D., and Moffat, D.T., 1985, A peridotitic komatiite from the Dalradian of Shetland: Geological Journal, v. 20, p. 287-292.

Flinn, D., and Oglethorpe, J.D., 2005, A history of the Shetland Ophiolite Complex: Scottish Journal of Geology, v. 41, p. 141-148.

Frisch, T., 1971, Alteration of Chrome-spinel in a dunite nodule from Lanzarote, Canary Islands: Lithos, v. 4, p. 83-91.

Fuchs, W.A., and Rose, A.W., 1974, The geochemical behaviour of platinum and palladium in the weathering cycle in the stillwater complex, Montana: Economic Geology, v. 69, p. 332-346.

Gahlan, H.A., and Arai, S., 2007, Genesis of peculiarly zoned Co, Zn and Mn-rich chomian spinel in serpentinite of Bou-Azzer ophiolite, Anti-Atlas, Morocco: Journal of Mineralogical and Petrological Sciences, v. 102, p. 69-85.

Garuti, G., Gazzotti, M., and Torresruiz, J., 1995, Iridium, Rhodium, and Platinum Sulfides in Chromitites from the Ultramafic Massifs of Finero, Italy, and Ojen, Spain: Canadian Mineralogist, v. 33, p. 509-520.

Garuti, G., Pushkarev, E., Zaccarini, F., Cabella, R., and Anikina, E., 2003, Chromite composition and platinum-group mineral assemblage in the Uktus Uralian-Alaskan-type complex (Central Urals, Russia): Mineralium Deposita, v. 38, p. 312-326.

Garuti, G., Zaccarini, F., and Economou-Eliopoulos, M., 1999, Paragenesis and composition of laurite from chromitites of Othrys (Greece): implication for Os-Ru fractionation in ophiolitic upper mantle of the Balkan Peninsula: Mineralium Deposita, v. 34, p. 312-319.

Gass, I.G., Neary, C.R., Prichard, H., and Bartholomew, I.D., 1982, The Chromite of the Shetland Ophiolite: A Re-Appraisal in the Light of New Theory and Techniques, Open University, p. 264.

Genkin, A.D., and Evstigneeva, T.L., 1986, Associations of platinum-group minerals of the Noril'sk copper-nickel sulfide ores: Economic Geology, v. 81, p. 1203-1212.

GeoMapApp, 2009, Marine Geoscience Data System, Volume www.marine-geo.org.

Ghazi, A.M., 2004, Geochemical characteristics, ^{40}Ar-^{39}Ar ages and original tectonic setting of the Bandi-e-Zeyerat/Dar Ana ophiolite, Makran accretionary prism, S E Iran: Tectonophysics, v. 393, p. 175-196.

Godard, M., Bosch, D., and Einaudi, F., 2006, A MORB source for low-Ti magmatism in the Semail ophiolite: Chemical Geology, v. 234, p. 58-78.

Greenbaum, D., 1977, Chromiteferous rocks of the Troodos ophiolite Complex, Cyprus: Economic Geology, v. 72, p. 1175-1194.

Gunn, A.G., C., L.R., Styles, M.T., and Bateson, J.H., 1985, Platinum-group element mineralisation in the Unst ophiolite, Shetland, Mineral Reconnaissance Programme, Volume 73, British Geological Survey, p. 115.

Hall, A., and Fraser, A., 2004, Shetland Landscapes, Edinburgh, Scotland. *Web page.*

Hall, R., 2002, Cenozoic geological and plate tectonic evolution of SE Asia and the SW Pacific: Computer-based reconstructions, model and animations: Journal of Asian Earth Sciences, v. 20, p. 353-431.

Hamlyn, P.R., and Keays, R.R., 1986, Sulfur saturation and second-stage melts: application to the Bushveld platinum metal deposits: Economic Geology, v. 81, p. 1431-1445.

Hamlyn, P.R., Keays, R.R., Cameron, W.E., Crawford, A.J., and Waldron, H.M., 1985, Precious Metals in Magnesian Low-Ti Lavas - Implications for Metallogenesis and Sulfur Saturation in Primary Magmas: Geochimica Et Cosmochimica Acta, v. 49, p. 1797-1811.

Haraguchi, S., and Ishii, T., 2007, Simultaneous boninitic and arc-tholeiitic volcanism in the Izu forearc region during early arc volcanism, based on ODP leg 125 site 786: Contributions to Mineralogy and Petrology, v. 153, p. 509-531.

Henderson, P., 1975, Reaction trends shown by chrome-spinels of the Rhum layered intrusion: Geochimica et Cosmochimica Acta, v. 39.

Henderson, P., and Wood, R.J., 1981, Reaction relationships of chrome-spinels in igenous rocks - further evidence from the layered intrusions of Rhum and Mull, Inner Hebrides, Scotland: Contributions to Mineralogy and Petrology, v. 78, p. 225-229.

Henry, B., and Lefevre, J.C., 1966, Preliminary report on the mineral resources and geology of the area north of Al 'Ays, *in* BRGM, ed., Volume S. G. JED. 66A20: Kingdom of Saudi Arabia, Ministry of Petroleum and Mineral Resources, p. 88.

Hitchen, C.S., 1929, Unst and its chromite deposits: Mining Magazine, v. 40, p. 18-24.

HMSO Command Paper, 1949, Chromite - Shetlands, Mineral Exploration in Britain, Mineral Development Committee.

Hulbert, L.J., and Von Gruenewaldt, G., 1985, Textural and compositional features of chromite in the Lower and Critical Zones of the Bushveld Complex South of Potgietersrus: Economic Geology, v. 80, p. 872-895.

Hutchinson, D., Prichard, H., and Macleod, C.J., 1999, Evidence for partial melting and melt impregnation of mantle peridotites leading to PGM depostion: A comparison of samples from the Lizard and Troodos ophiolites and the Tonga trench., *in* Stanley, C., ed., Mineral Deposits: Processes to Processing, Volume 1: Rotterdam, The Netherlands, p. 729-732.

Irvine, T.N., 1977a, Chromite crystallization in the join Mg_2SiO_4-$CaMgSi_2O_6$-$CaAl_2Si_2O_6$-$MgCr_2O_4$-SiO_2: Yearbook - Carnegie Institute of Washington, v. 76, p. 465-472.

Irvine, T.N., 1977b, Origin of chromitite layers in the Muskox intrusion and other stratiform intrusions: A new interpretation Geology, v. 5.

Ishiwatari, A., and Tsujimori, T., 2003, Paleozoic ophiolites and blueschists in Japan and Russian Primorye in the tectonic framework of East Asia: A synthesis: Island Arc, v. 12, p. 190-206.

Jenkins, D.M., 1981, Experimental Phase Relations of Hydrous Peridotites Modelled in the System H_2O-CaO-MgO-Al_2O_3-SiO_2: Contributions to Mineralogy and Petrology, v. 77, p. 166-176.

Jenkins, D.M., and Chermovsky, J.V., 1986, Phase equilibria and crystallographic properties of Mg-chlorite: American Mineralogist, v. 71, p. 924-936.

Johan, Z., 1986, Chromite deposits in the Massif du Sud ophiolite, New Caledonia: Genetic considerations, Chromites, UNESCO's IGCP-197 Project on Metallogeny of Ophiolites: Athens, Theophrastus Publications, p. 311-339.

Johan, Z., Dunlop, H., Le Bel, L., Robert, J.-L., and Volfinger, M., 1983, Origin of chromite deposits from ophiolitic complexes: Evidence for a volatile- and sodium-rich reducing fluid phase: Fortschritte der Mineralogie, v. 61, p. 105-107.

Johnson, P.R., and Kattan, F.H., 2001, Oblique sinistral transpression in the Arabian shield: the timing and kinematics of the Neoproterozoic suture zone: Precambrian Research, v. 107, p. 117-138.

Johnson, P.R., Kattan, F.H., and Al-Saleh, A.M., 2004, Neoproterozoic Ophiolites in the Arabian Shield: Field Relations and Structure, *in* Kusky, T.M., ed., Precambrian Ophiolites and Related Rocks, Volume 13: Developments in Precambrian Geology: Amsterdam, Elsevier, p. 129-162.

Jugo, P.J., 2009, Sulfur content at sulfide saturation in oxidized magmas: Geology, v. 37, p. 415-418.

Kamenetsky, V.S., Crawford, A.J., and Meffre, S., 2001, Factors controlling chemistry of magmatic spinel: an empirical study of associated olivine, Cr-spinel and melt inclusions from primitive rocks: Journal of Petrology, v. 42, p. 655-671.

Kamenetsky, V.S., and Kamenetsky, M.B., 2010, Magmatic fluids immiscible with silicate melts: examples from inclusions in phenocrysts and glasses, and implications for magma evolution and metal transport: Geofluids, v. 10, p. 293-311.

Kapsiotis, A., Tsikouras, B., Grammatikopoulos, T., Karipi, S., and Hatzipanagiotou, K., 2007, On the metamorphic modification of Cr-spinel compositions from the ultrabasic rocks of the Pindos ophiolite complex (NW Greece). Bulletin of the Geological Society of Greece, v. Proceedings of the 11th International Congress, p. 781-793.

Kelemen, P.B., 1990, Reaction between ultramafic rock and fractionating basaltic magma I. Phase relations, the origin of calc-alkaline magma series, and the formation of discordant dunite: Journal of Petrology, v. 31, p. 51-98.

Kelemen, P.B., 1995, Extraction of mid-ocean ridge basalt from the upwelling mantle by focused flow of melt in dunite channels: Nature, v. 375, p. 747-753.

Kelemen, P.B., Dick, H.J.B., and Quick, J.E., 1992, Formation of Harzburgite by Pervasive Melt Rock Reaction in the Upper Mantle: Nature, v. 358, p. 635-641.

Kepezhinskas, P., and Defant, M.J., 2001, Nonchondritic Pt/Pd ratios in arc mantle xenoliths: Evidence for platinum enrichment in depleted island-arc mantle sources: Geology, v. 29, p. 851-854.

Khalil, I., 2007, Chromite mineralization in ultramafic rocks of the Wadi Ghadir area, Eastern Desert, Egypt: mineralogical, microchemical and genetic studies,: N. Jb. Miner. Abh., v. 183, p. 283-296.

Kimball, K.L., 1990, Effects of hydrothermal alteration on the composition of chromian spinels: Contributions to Mineralogy and Petrology, v. 105, p. 337-346.

Konstantopoulou, G., and Economou-Eliopoulos, M., 1991, Distribution of Platinum-Group Elements and Gold within the Vourinos Chromitite Ores, Greece: Economic Geology, v. 86, p. 1672-1682.

Kovalenko, V.I., and Kovalenko, N.I., 1984, Problems of the origin, ore-bearing and evolution of rare-metal granitoids: Physics of the Earth and Planetary Interiors, v. 35, p. 51-62.

Kozlu, H., Prichard, H.M., Melcher, F., Fisher, P., Brough, C.P., and Stueben, D., 2010, Relationships between platinum-group elements and minerals and the geochemistry of the chromitite in the Berit ophiolite (Kahranmaras), SE Turkey: Turkish Journal of Earth Sciences (in press).

Kruger, F.J., Kinnaird, J.A., Nex, A.M., and Cawthorn, R.G., 2002, Chromite is the Key to PGE, 9th International Platinum Symposium: Montana.

Kusky, T.M., 2004, Epilogue: What if anything have we learned about Precambrian ophiolites and early Earth processes, *in* Kusky, T.M., ed., Precambrian Ophiolites and Related Rocks, Volume 13: Developments in Precambrian Geology: Amsterdam, Elsevier, p. 727-737.

Kusky, T.M., Li, J.H., and Tucker, R.T., 2001, The Archean Dongwanzi ophiolite complex, North China Craton: 2.505 Billion Year Old Oceanic Crust and Mantle Science, v. 292, p. 1142-1145.

Lago, B.L., Rabinowicz, M., and Nicolas, A., 1982, Podiform Chromite Ore Bodies: A Genetic Model: Journal of Petrology, v. 23, p. 103-125.

Leake, R.C., and Gunn, A.G., 1985, Exploration for PGE mineralization in the Unst ophiolite, Shetland: Geology in the Real World, v. The Kingsley Dunham Volume, p. 253-266.

Leblanc, M., and Ceuleneer, G., 1991, Chromite crystallization in a multicellular magma flow: Evidence from a chromitite dike in the Oman ophiolite: Lithos, v. 27, p. 231-257.

Lehmann, J., 1983, Diffusion between Olivine and Spinel - Application to Geothermometry: Earth and Planetary Science Letters, v. 64, p. 123-138.

Li, C., Naldrett, A.J., Coats, C.J.A., and Johnnessen, P., 1992, Platinum, palladium, gold and copper-rich stringers at the Strathcona mine, Sudbury: their enrichment by fractionation of a sulfide liquid: Economic Geology, v. 87, p. 1584-1598.

Li, C., and Ripley, E.M., 2005, Empirical equations to predict the sulfur content of mafic magmas at sulfide saturation and applications to magmatic sulfide deposits: Mineralium Deposita, v. 40, p. 218 - 230.

Lipin, B.R., 1993, Pressure increases, the formation of chromite seams, and the development of the ultramafic series in the Stillwater Complex, Montana: Journal of Petrology, v. 34, p. 955-976.

Loferski, P.J., and Lipin, B.R., 1983, Exsolution in metamorphosed chromite from the Red Lodge district, Montana: American Mineralogist, v. 68, p. 777-789.

Lorand, J.P., and Alard, O., 2001, Platinum-group element abundances in the upper mantle: New constraints from in situ and whole-rock analyses of massif central xenoliths (France): Geochimica et Cosmochimica Acta, v. 65, p. 2789-2806.

Lorand, J.P., Luguet, A., and Alard, O., 2008, Platinum-group elements: A new set of key tracers for the Earth's interior: Elements, v. 4, p. 247-252.

Lorand, J.P., Pattou, L., and Gros, M., 1999, Fractionation of Platinum-group elements and gold in the upper mantle: A detailed study in Pyrenean orogenic lherzolites: Journal of Petrology, v. 40, p. 957-981.

Lord, R.A., 1991, Platinum Group Element Mineralisation in the Shetland Ophiolite Complex: Cardiff, Cardiff University.

Lord, R.A., 1994, Evidence for the mobility of PGE in the secondary environment in the Shetland ophiolite complex: Transactions: Institution of Mining and Metallurgy, v. 103, p. 79-86.

Lord, R.A., and Prichard, H.M., 1997, Exploration and origin of stratigraphically controlled platinum-group element mineralization in crustal-sequence ultramafics, Shetland ophiolite complex: Transactions: Institution of Mining and Metallurgy, p. B179-B193.

Lord, R.A., Prichard, H.M., and Neary, C.R., 1994, Magmatic platinum-group element concentrations and hydrothermal upgrading in Shetland ophiolite complex: Transactions: Institution of Mining and Metallurgy, v. 103, p. B87-B193.

Luguet, A., Alard, O., Lorand, J.P., Pearson, N.J., Ryan, C., and O'Reilly, S.Y., 2001, Laser-ablation microprobe (LAM)-ICPMS unravels the highly siderophile element geochemistry of the oceanic mantle: Earth and Planetary Science Letters, v. 189, p. 285-294.

Luguet, A., Lorand, J.P., and Seyler, M., 2003, Sulfide petrology and highly siderophile element geochemistry of abyssal peridotites: A coupled study of samples from the Kane Fracture Zone (45Â°W 23Â°20N, MARK area, Atlantic Ocean): Geochimica et Cosmochimica Acta, v. 67, p. 1553-1570.

Luguet, A., Shirey, S.B., Lorand, J.P., Horan, M.F., and Carlson, R.W., 2007, Residual platinum-group minerals from highly depleted harzburgites of the Lherz massif (France) and their role in HSE fractionation of the mantle>: Geochimica et Cosmochimica Acta, v. 71, p. 3082-3097.

Makeyev, A.B., 2006, Typomorphic features of chrome-spinel and mineralogical prospecting guides for Cr ore mineralization: Russian Journal of Earth Sciences, v. 8.

Malpas, J., Robinson, P.T., and Zhou, M.F., 1997, Chromite and ultramafic rock compositional zoning through a paleotransform fault, Poum, New Caledonia: Discussion: Economic Geology, v. 92, p. 502-503.

Matveev, S., and Ballhaus, C., 2002, Role of water in the origin of podiform chromitite deposits: Earth and Planetary Science Letters, v. 203, p. 235-243.

Maurel, C., and Maurel, P., 1982, Etude experimentale de la distribution de l'aluminium entre bain silicate basique et spinelle chromifere. Implications petrogenetiques: teneur en chrome des spinelles: Bulletin de Mineralogie., v. 105, p. 197-202.

Mavrogenes, J.A., and O'Neill, H.S.C., 1999, The relative effects of pressure, temperature and oxygen fugacity on the solubility of sulfide in mafic magmas: Geochimica Et Cosmochimica Acta, v. 63, p. 1173-1180.

Maynard, J., Prichard, H.M., Ixer, R.A., Lord, R.A., Wright, I.P., Pillinger, C.T., McConville, P., Boyce, A.J., and Fallick., A.E., 1997, Sulphur isotope study of Ni-Fe-Cu mineralization in the Shetland Ophiolite: Transactions: Institution of Mining and Metallurgy, v. 106, p. 12.

McDonald, I., and Viljoen, K.S., 2006, Platinum-group element geochemistry of mantle eclogites: a reconnaissance study of xenoliths from the Orapa kimberlite, Botswana: Applied Earth Science (Trans. Inst. Min. Metall. B), v. 115, p. 81-93.

Mcdonough, W.F., and Sun, S.S., 1995, The Composition of the Earth: Chemical Geology, v. 120, p. 223-253.

Melcher, F., Grum, W., Simon, G., Thalhammer, T.V., and Stumpfl, E.F., 1997, Petrogenesis of the Ophiolitic Giant Chromite Dposits of Kempirsai, Kazakhstan: a Study of Solid and Fluid Inclusions in Chromite: Journal of Petrology, v. 38, p. 1419-1458.

Mellini, M., Rumori, C., and Viti, C., 2005, Hydrothermally reset magmatic spinels in retrograde serpentinites: Formation of "ferritchromit" rims and chlorite aureoles: Contributions to Mineralogy and Petrology, v. 149, p. 266-275.

Merlini, A., Grieco, G., and Diella, V., 2009, Ferritchromite and chromian-chlorite formation in melange-hosted Kalkan chromitite (Southern Urals, Russia): American Mineralogist, v. 94, p. 1459-1467.

Mernagh, T.P., Heinrich, C.A., Leckie, J.F., Carville, D.P., Gilbert, D.J., Valenta, R.K., and Wyborn, L.A.I., 1994, Chemistry of low-temperature hydrothermal gold, platinum, and palladium (±uranium) mineralization at Coronation Hill, Northern Territory, Australia: Economic Geology, v. 89, p. 1053-1073.

Mitchell, R.H., and Keays, R.R., 1981, Abundance and distribution of gold, palladium and iridium in some spinel and garnet lherzolites: implications for the nature and origin of precious metal-rich intergranular components in the upper mantle: Geochimica et Cosmochimica Acta, v. 45, p. 2425-2433,2435-2442.

Mondal, S.K., and Mathez, E.A., 2007, Origin of the UG2 chromitite layer, Bushveld Complex: Journal of Petrology, v. 48, p. 495-510.

Monnier, C., Girardeau, J., Maury, R.C., and Cotten, J., 1995, Back-arc basin origin for the East Sulawesi ophiolite (eastern Indonesia): Geology, v. 23, p. 851-854.

Moreno, T., Prichard, H.M., Lunar, R., Monterrubio, S., and Fisher, P., 1999, Formation of a secondary platinum-group mineral assemblage in chromitites from the Harbeira ultramafic massif in Cabo Ortegal, NW Spain: Eur. J. Mineral., v. 11, p. 363-378.

Morishita, T., Andal, E.S., Arai, S., and Ishida, Y., 2006, Podiform chromitites in the lherzolite-dominant mantle section of the Isabela ophiolite, the Philippines: Island Arc, v. 15, p. 84-101.

Moutte, J., 1982, Chromite deposits of the Tiebaghi ultramafic massif, New Caledonia: Economic Geology, v. 77, , p. 576-591.

Mukherjee, R., Mondal, S.K., and Rosing, M.T., 2010, Compositional variations in the Mesoarchean chromites of the Nuggihalli schist belt, Western Dharwar Craton (India): potential parental melts and implications for tectonic setting: Contributions to Mineralogy and Petrology, v. 160, p. 868-885.

Mungall, J.E., 2002, Roasting the mantle: Slab melting and the genesis of major Au and Au-rich Cu deposits:: Geology, v. 30, p. 915-918.

Mungall, J.E., 2005, Magmatic geochemistry of the platinum-group elements, *in* Mungall, J.E., ed., Exploration for platinum-group element deposits, Volume 35, Mineralogical Association of Canada: Short Course Series p. 1-34.

Mungall, J.E., and Naldrett, A.J., 2008, Ore Deposits of the Platinum-Group Elements: Elements, v. 4, p. 253-258.

Murck, B.W., and Campbell, I.H., 1986, The effects of temperature, oxygen fugacity and melt composition on the behaviour of chromium in basic and ultrabasic melts: Geochimica et Cosmochimica Acta, v. 50, p. 1871-1887.

Naldrett, A.J., 1999, World-class Ni-Cu-PGE deposits: key factors in their genesis: Mineralium Deposita, v. 34, p. 227-240.

Naldrett, A.J., 2004, Magmatic Sulfide Deposits New York, Springer-Verlag Berlin Heidelberg

Naldrett, A. J., and Duke, J. M., 1980, Platinum metals in magmatic sulfide ores: Science, v. 208, p. 1417-1428

Naldrett, A.J., Kinnaird, J.A., Wilson, A., Yudovskaya, M.A., McQuade, S., Chunnett, G., and Stanley, C., 2009, Chromite composition and PGE content of Bushveld chromitites: Part 1 - the Lower and Middle Groups: Transactions: Institution of Mining and Metallurgy, v. 118, p. 131-161.

Naldrett, A.J., and Lehmann, J., 1988, Spinel non-stoichiometry as the explanation for Ni- Cu- and PGE-enriched sulphides in chromitites, *in* Prichard, H.M., Potts, P.J., Bowles, J.F., and Cribb, S.J., eds., Geoplatinum '87: London, Elsevier, p. 93-110.

Neary, C.R., 1974, Chromitiferous Ultrabasic Rocks in the Northern Hijaz on Saudi Arabia [PhD thesis]: Leeds, University of Leeds.

Neary, C.R., and Brown, M.A., 1979, Chromites from the Al'Ays Complex, Saudi Arabia, and the Semail Complex, Oman: Contributions to Mineralogy and Petrology, v. 69, p. 329-336.

Neary, C.R., and Prichard, H., 1985, Molybdenum mineralization on Unst, Shetland Isles: Scottish Journal of Geology, v. 21, p. 197-204.

Neary, C.R., Prichard, H.M., and Potts, P.J., 1984, Chromite, platinoids, gold and moly in the Shetlands. : Mining Magazine, p. 559-560.

Nicolas, A., 1989, Structures of ophiolites and dynamics of oceanic lithosphere: Dordrecht, Amsterdam, Kulwer Academic Publishers 367 p.

O'Hara, M.J., Fry, N., and Prichard, H.M., 2001, Minor Phases as Carriers of Trace Elements in Non-Modal Crystal-Liquid Separation Processes I: Basic Relationships: Journal of Petrology, v. 42, p. 17.

O'Neill, H.S.C., and Mavrogenes, J.A., 2002, The sulfide capacity and the sulfur content at sulfide saturation of silicate melts at 1400oC and 1 bar: Journal of Petrology, v. 43, p. 1049-1087.

Ogasawara, M., Nakagawa, M., Al-Azri, H., and Al-Araimi, M., 2002, PGE Abundance in Chromitites of the Northern Samail Ophiolite, Oman, 9th International Platinum Symposium: Montana.

Ohnenstetter, M., Johan, Z., Coherie, A., Fouillac, A., Guerrot, C., Ohnenstetter, D., Chaussidon, M., Rouer, O., Makovicky, E., Makovicky, M., Rose-Hansen, J., Karup-Moller, S., Vaughan, D., Tumer, G., Pattrick, R.A.D., Gize, A.P., Lyon, I., and McDonald, I., 1999, New exploration methods for platinum and rhodium deposits poor in base-metal sulfides: Transactions: Institution of Mining and Metallurgy, Section B, v. 108, p. 119-150.

Ohnenstetter, M., Karaj, N., Neziraj, A., Johan, Z., and Cina, A., 1991, Le potentiel platinifere des ophiolites: mineralisations en elements du groupe du platine (PGE) dans les massifs de Tropoja et Bulquiza, Albanie: Compus Rendus de l'Acadamie des Sciences, Paris, v. 13, p. 201-208.

Onyeagocha, A.C., 1974, Alteration of Chromite from the twin sisters Dunite, Washington: American Mineralogist, v. 59, p. 608-612.

Orberger, B., Fredrich, G., and Woermann, E., 1988, Platinum-group element mineralisation in the ultramafic sequence of the Acoje ophiolite block, Zambales, Philippines. , *in* Prichard, H.M., Potts, P.J., Bowles, J.F.W., and Cribb, S.J., eds., Geo-platinum symposium volume, Elsevier, p. 361-380.

Page, N.J., Engin, T., Singer, D.A., and Haffty, J., 1984, Distribution of platinum-group elements in the Bati Kef chromite deposit, Guleman-Elazig area, eastern Turkey: Economic Geology, v. 79, p. 177-184.

Page, P., and Barnes, S.J., 2009, Using Trace Elements in Chromites to Constrain the Origin of Podiform Chromitites in the Thetford Mines Ophiolite, Quebec, Canada: Economic Geology, v. 104, p. 997-1018.

Paktunc, A.D., 1990, Origin of podiform chromitite deposits by multistage melting, melt segregation and magma mixing in the upper mantle: Ore Geology Reviews, v. 5, p. 211-222.

Pallister, J.S., Stacey, J.S., Fisher, L.B., and Premo, W.R., 1987, Arabian Shield ophiolites and Late Proterozoic microplate accretion: Geology, v. 15, p. 320-323.

Pallister, J.S., Stacey, J.S., Fisher, L.B., and Premo, W.R., 1988, Precambrian ophiolites of Arabia: Geologic settings, U-Pb geochronology, Pb-Isotope characteristics, and implications for continental accretion: Precambrian Research, v. 38, p. 1-54.

Parkinson, I.J., and Arculus, R.J., 1999, The redox state of subduction zones: insights from arc-peridotites: Chemical Geology, v. 160, p. 409-423.

Pearce, J.A., 2003, Supra-subduction zone ophiolites: The search for modern analogues, *in* Dilek, Y.a.N., S., ed., Ophiolite Concept and the Evolution of Geological Thought, The Geological Society of America, p. 269-294.

Pearce, J.A., Barker, P.F., Edwards, S.J., Parkinson, I.J., and Leat, P.T., 2000, Geochemistry and tectonic significance of peridotites from the South Sandwich arc-basin system, South Atlantic: Contributions to Mineralogy and Petrology, v. 139, p. 36-53.

Pedersen, R.B., Johannesen, G.M., and Boyd, R., 1993, Stratiform PGE mineralisations in the ultramafic cumulates of the Leka ophiolite complex, central Norway: Economic Geology, v. 88, p. 782-803.

Peltonen, P., 1995, Crystallization and re-equilibration of zoned chromite in ultramafic cumulates, Vammala Ni-belt, Southwestern Finland: Canadian Mineralogist, v. 33, p. 521-535.

Peregoedova, A., Barnes, S.J., and Baker, D.R., 2004, The formation of Pt-Ir alloys and Cu-Pd-rich sulfide melts by partial desulfurization of Fe-Ni-Cu sulfides: Results of experiments and implications for natural systems: Chemical Geology, v. 208, p. 247-264.

Pouchou, J.L., and Pichoir, F., 1985, "PAP" procedure for improved quantitative analysis: Microbeam Analysis, v. 20, p. 104-105.

Prendergast, M.D., 2008, Archean Komatiitic Sill-hosted Chromite Deposits in the Zimbabwe Craton: Economic Geology, v. 103, p. 981-1004.

Prichard, H., 1985, The Shetland Ophiolite, *in* Gee, D.G., and Sturt, B.A., eds., The Caledonide Orogen: Scandinavia and related areas., Volume 2, Wiley and Sons Ltd. , p. 1173-1184.

Prichard, H., and Lord, R.A., 1988, The Shetland ophiolite: Evidence for a supra-subduction origin and implications for PGE mineralization. , *in* Boissonnas, J., and Omenetto, P., eds., Mineral Deposits in the European Community, Springer Verlag, p. 289-302.

Prichard, H., and Lord, R.A., 1993, An overview of the PGE concentrations in the Shetland ophiolite complex., *in* Prichard, H., Alabaster, T., Harris, N.B., and Neary, C.R., eds., Magmatic Processes and Plate Tectonics, Volume 76, Geological Society of London, p. 273-294.

Prichard, H., and Neary, C.R., 1981, Chromite in the Shetlands Ophiolite Complex In. An International Symposium on metallogeny of mafic and ultramafic complexes, UNESCO Volume 3: Athens, UNESCO Project 169, p. 343-360.

Prichard, H., Sa, J.H.S., and Fisher, P.C., 2001, Platinum-group mineral assemblages and chromite composition in the altered and deformed Bacuri Complex, Amapa, Northeastern Brazil.: Canadian Mineralogist, v. 39, p. 377-396.

Prichard, H.M., 2007, Natural and Artificial Platinum and Palladium Occurrences World-Wide, *in* Sammonds, P.R., and Thompson, J.M.T., eds., Advances in Earth Science: From Earthquakes to Global Warming, Volume 2: London, Imperial College Press.

Prichard, H.M., Barnes, S.-J., Maier, W.D., and Fisher, P., 2004a, Variations in the nature of the platinum-group minerals in a cross-section through the Merensky reef at Impala platinum: Implications for the mode of formation of the reef: The Canadian Mineralogist, v. 42, p. 423-437.

Prichard, H. M. and Brough, C. (2009) Potential of ophiolite complexes to host PGE deposits. In New developments in magmatic Ni-Cu and PGE deposits; LI, C. and RIPLEY E. M. (Eds.) Geological publishing house Beijing, 277-290

Prichard, H.M., Hutchinson, D., and Fisher, P.C., 2004b, Petrology and Crystallization History of Multiphase Sulfide Droplets in a Mafic Dike from Uruguay: Implications for the Origin of Cu-Ni-PGE Sulfide Deposits: Economic Geology, v. 99, p. 365-376.

Prichard, H.M., Ixer, R.A., Lord, R.A., Maynard, J., and Williams, N., 1994, Assemblages of Platinum-Group Minerals and Sulfides in Silicate Lithologies and Chromite-Rich Rocks within the Shetland Ophiolite: Canadian Mineralogist, v. 32, p. 271-294.

Prichard, H.M., and Lord, R.A., 1990, Platinum and Palladium in the Troodos Ophiolite Complex, Cyprus: Canadian Mineralogist, v. 28, p. 607-617.

Prichard, H.M., and Lord, R.A., 1990, Platinum mineralisation in the Shetland ophiolite: MIRO research programme, contract no. RC 48, Sponsored by Riofinex North and Consolidated Gold Fields.

Prichard, H.M., Lord, R.A., and Neary, C.R., 1996, A Model to Explain the Occurrence of Platinum- and Palladium-Rich Ophiolite Complexes: Journal of the Geological Society, London, v. 153, p. 323-328.

Prichard, H.M., and Neary, C.R., 1982, Some observations of Chromite in Shetland Ophiolite Complex: Ofioliti, p. 455-466.

Prichard, H.M., Neary, C.R., Fisher, P.C., and O'Hara, M.J., 2008, PGE-rich Podiform Chromitites in the Al'Ays Ophiolite Complex, Saudi Arabia: An example of Critical Mantle Melting to Extract and Concentrate PGE.: Economic Geology, v. 103, p. 1507-1529.

Prichard, H.M., Neary, C.R., and Potts, P.J., 1986, Platinum group minerals in the Shetland Ophiolite, *in* Gallagher, M.J., Ixer, R.A., Neary, C.R., and Prichard, H.M., eds., Metallogeny of the Basic and Ultrabasic Rocks.

Prichard, H.M., Potts, P.J., and Neary, C.R., 1981, Platinum-group minerals in the Shetland ophiolite complex: Transactions: Institution of Mining and Metallurgy B, v. 90, p. 186-188.

Prichard, H.M., Potts, P.J., Neary, C.R., Lord, R.A., and Ward, G.R., 1989, Development of techniques for the determination of the platinum-group elements in ultramafic rock complexes of potential economic significance: mineralogical studies Luxembourg, Commission of the European Communities.

Prichard, H.M., and Tarkian, M., 1988, Platinum and Palladium Minerals from two PGE-Rich Localities in the Shetland Ophiolite Complex: Canadian Mineralogist, v. 26, p. 979-990.

Proenza, J.A., Gervilla, F., Melgarejo, J.C., and Bodinier, J.L., 1999, Al- and Cr- rich chromitites from the Mayari-Baracoa Ophiolitic Belt (Eastern Cuba): Consequence of Interaction between Volatile-Rich melts and peridotites in Suprasubduction Mantle: Economic Geology, v. 94, p. 547 - 566.

Proenza, J.A., Ortega-Gutiérrez, F., Camprubí, A., Tritlla, J., Elías-Herrera, M., and Reyes-Salas, M., 2004, Paleozoic serpentinite-enclosed chromitites from Tehuitzingo (Acatlán Complex, southern Mexico): A petrological and mineralogical study: Journal of South American Earth Sciences, v. 16, p. 649-666.

Proenza, J.A., Zaccarini, F., Escayola, M., Cabana, C., Schalamuk, A., and Garuti, G., 2008, Composition and textures of chromite and platinum-group minerals in chromitites of the western ophiolitic belt from Pampean Ranges of Cordoba, Argentina.: Ore Geology Reviews, v. 33, p. 32-48.

Pubellier, M., Monnier, C., Maury, R., and Tamayo, R., 2004, Plate kinematics, origin and tectonic emplacement of supra-subduction ophiolites in SE Asia: Tectonophysics, v. 392, p. 9-36.

Putnis, A., 1992, Introduction to Mineral Sciences, Cambridge University Press.

Quick, J.E., 1981, The origin and significance of large, tabular dunite bodies in the Trinity peridotite, northern California.: Contributions to Mineralogy and Petrology, v. 78, p. 413-422.

Ramdohr, P., 1980, The ore minerals and their intergrowths: Oxford, Pergamon.

Rehkämper, M., Halliday, A.N., Fitton, J.G., Lee, D.C., Wieneke, M., and Arndt, N.T., 1999, Ir, Ru, Pt, and Pd in basalts and komatiites: New constraints for the geochemical behavior of the platinum-group elements in the mantle: Geochimica et Cosmochimica Acta, v. 63, p. 3915-3934.

Roberts, S., 1986, The role of igneous processes in the formation of ophiolitic chromitite, Earth Sciences: Milton Keynes, Open University.

Roberts, S., Rassios, A., Wright, L., Vacondoios, I., Grivas, E., Nesbitt, R.W., Neary, C.R., Moat, T., and Konstantopoulou, L., 1988, Structural Controls on the location and form of the Vourinos chromite deposits, *in* Boissonnas, J., and Omenetto, P., eds., Mineral Deposits within the European Community Volume 6, Geological Society of Applied Mineralogy Special Publication, p. 249-266.

Roberts, S., and Neary, C.R., 1993, Petrogenesis of ophiolitic chromitite, *in* Prichard, H., Alabaster, T., Harris, N.B., and Neary, C.R., eds., Magmatic Processe sand Plate Tectonics, Volume 76, Geological Society Special Publication p. 257-272.

Robertson, A.H.F., Ustaömer, T., Parlak, O., Ünlügenc, U.C., Taşli, K., and Inan, N., 2006, The Berit transect of the Tauride thrust belt, S Turkey: Late Cretaceous-Early Cenozoic accretionary/collisional processes related to closure of the Southern Neotethys: Journal of Asian Earth Sciences, v. 27, p. 108-145.

Robinson, P.T., Bai, W.-J., Malpas, J., Yang, J.S., Zhou, M.F., Fang, Q.-S., Hu, X.F., Cameron, S., and Standigel, H., 2004, Ultra-high pressure minerals in the Luobusa Ophiolite, Tibet, and their tectonic implications, *in* Malpas, J., Fletcher, C.J.N., Ali, J.R., and Aitchison, J.C., eds., Aspects of the Tectonic Evolution of China, Geological Society of London, p. 247-271.

Robinson, P.T., and Zhou, M.F., 2008, The origin and tectonic setting of ophiolites in China: Journal of Asian Earth Sciences, v. 32, p. 301-307.

Robinson, P.T., Zhou, M.F., Hu, X.F., Reynolds, P., Wenji, B., and Yang, J.S., 1999, Geochemical constraints on the origin of the Hegenshan Ophiolite, Inner Mongolia, China: Journal of Asian Earth Sciences, v. 17, p. 423-442.

Roedder, E., 1979, Origin and significance of magmatic inclusions: Bulletin de Mineralogie., v. 102, p. 487-510.

Roedder, E., 1992, Fluid inclusion evidence for immiscibility in magmatic differentiation: Geochimica et Cosmochimica Acta, v. 56, p. 5-20.

Roeder, P.L., and Campbell, I.H., 1985, The effect of postcumulus reactions on composition of chrome-spinels from the Jimberlana Intrusion: Journal of Petrology, v. 26, p. 763-786.

Roeder, P.L., and Reynolds, I., 1991, Crystallization of Chromite and Chromium Solubility in Basaltic Melts: Journal of Petrology, v. 32, p. 909-934.

Rollinson, H., 2005, Chromite in the mantle section of the Oman ophiolite: A new genetic model: The Island Arc, v. 14, p. 542-550.

Rollinson, H., 2008, The geochemistry of mantle chromitites from the northern part of the Oman ophiolite: Inferred parental melt compositions Contributions to Mineralogy and Petrology, v. 156, p. 273-288.

Ross, M., and Nolan, R.P., 2003, History of Asbestos Discovery and use and Asbestos-Related Disease in Context with the Occurrence of Asbestos within Ophiolite Complexes, *in* Dilek, Y.a.N., S., ed., Ophiolite Concept and the Evolution of Geological Thought, The Geological Society of America, p. 1-16.

Sack, R.O., and Ghiorso, M.S., 1991, Chromian spinels as petrogenetic indicators: Thermodynamics and petrological applications: American Mineralogist, v. 76, p. 827-847.

Schellart, W.P., Kennett, B.L.N., Spakman, W., and Amaru, M., 2009, Plate reconstructions and tomography reveal a fossil lower mantle slab below the Tasman Sea: Earth and Planetary Science Letters.

Schwessinger, W.T., and Muan, A., 1992, Spinel-Silicate Equilibria in the System MgO-FeO-Fe_2O_3-Al_2O_3--Cr_2O_3-SiO_2: Phase Equilibria, v. 75, p. 1390-1398.

Scowen, P.A.H., Roeder, P.L., and Helz, R.T., 1991, Reequilibration of chromite within Kilauea Iki lava lake, Hawaii: Contributions to Mineralogy and Petrology, v. 107, p. 8-20.

Seabrook, C.L., Prichard, H., and Fisher, P., 2004, Platinum-group minerals in the Raglan Ni-Cu-(PGE) deposit, Cape Smith, Canada.: Canadian Mineralogist, v. 9th International Platinum Symposium, p. 485-497.

Shen, P., Hwang, S.-L., Chu, H.-T., and Jeng, R.-C., 1988, STEM study of "ferritchromit" from the Heng-Chun chromitite: American Mineralogist, v. 73, p. 383-388.

Shervais, J.W., 1982, TiV plots and the petrogenesis of modern and ophiolitic lavas: Earth and Planetary Science Letters, v. 59, p. 101-118.

Sisson, T.W., and Grove, T.L., 1993, Experimental investigations of the role of H_2O in calc-alkaline differentiation and subduction zone magmatism: Contributions to Mineralogy and Petrology, v. 113, p. 143-166.

Skobelev, S.F., Hanon, M., Klerkx, J., Govorova, N.N., Lukina, N.V., and Kazmin, V.G., 2004, Active faults in Africa: A review: Tectonophysics, v. 380, p. 131-137.

Sobolev, V.S., and Chaussidon, M., 1996, H_2O concentrations in primary melts from supra-subduction zones and mid-ocean ridges: Implications for H2O storage and recycling in the mantle: Earth and Planetary Science Letters, v. 137, p. 45-55.

Sobolev, V.S., and Kostyuk, V.P., 1975, Magmatic crystallization based on a study of melt inclusions: Novosibirsk: Fluid Inclusion Research, v. 9, p. 182-253.

Spear, F.S., 1993, Metamorphic Phase Equilibria and P-T-Time paths: Washington D. C., Mineralogical Society of America.

Spray, J.G., 1988, Thrust-related metamorphism beneath the Shetland Islands oceanic fragment, northeast Scotland: Canadian Journal of Earth Sciences v. 25, p. 1760 - 1776.

Stern, R.J., 2004, Subduction initiation: Spontaneous and induced: Earth and Planetary Science Letters, v. 226, p. 275-292.

Stern, R.J., Johnson, P.R., Kroner, A., and Yibas, B., 2004, Neoproterozoic Ophiolites of the Arabian-Nubian Shield, *in* Kusky, T.M., ed., Precambrian Ophiolites and Related Rocks, Volume 13: Developments in Precambrian Geology: Amsterdam, Elsevier, p. 95-128.

Stowe, C.W., 1987a, Distribution of Chromite Ore Fields, *in* Stowe, C.W., ed., Evolution of Chromium Ore Fields, Van Nostrand Reinhold Company Inc., p. 49-70.

Stowe, C.W., 1987b, The Mineral Chromitite, *in* Stowe, C.W., ed., Evolution of Chromium Ore Fields: New York, Van Nostrand Reinhold Company Inc., p. 1-22.

Suita, M., Pedrosa-Soares, A., Leite, C., Nilson, A., and Prichard, H., 2004, Complexos ofioliticos do Brasil e a metalogenia comparada das faixas aracuai e brasilia, *in* Pereira, E., Castroviejo, R., and Ortiz, F., eds., Complejos Ofioliticos en Iberoamerica: Madrid, p. 101-132.

Suzuki, A.M., Yasuda, A., and Ozawa, K., 2008, Cr and Al diffusion in chromite spinel: experimental determination and its implication for diffusion creep: Physics and Chemistry of Minerals, v. 35, p. 433-445.

Takazawa, E., Abe, N., Seyler, M., and Meurer, W.P., 2007, Hybridization of Dunite and Gabbroic Minerals in Hole 1271B From Mid-Atlantic Ridge 15°N: Implications for Melt Flow and Reaction in the Upper Mantle, *in* Kelemen, P.B., Kikawa, E., and Miller, D.J., eds., Proceedings of the Ocean drilling Program, Scientific Results, Volume 209.

Talkington, R.W., Watkinson, D.H., Whittaker, P.J., and Jones, P.C., 1984, Platinum-group minerals and other solid inclusions in chromite of ophiolitic complexes: Occurrence and petrological significance: TMPM Tschermaks Mineralogische und Petrographische Mitteilungen, v. 32, p. 285-301.

Tamura, A., and Arai, S., 2005, Unmixed spinel in chromitite from the Iwanai-dake peridotite complex, Hokkaido, Japan: A reaction between peridotite and highly oxidised magma in the mantle wedge.: American Mineralogist, v. 90, p. 473-480.

Tamura, A., and Arai, S., 2006, Harzburgite-dunite-orthopyroxenite suite as a record of supra-subduction zone setting for the Oman ophiolite mantle: Lithos, v. 90, p. 43-56.

Tamura, Y., 1994, Genesis if Island Arc Magmas by Mantle-Derived Bimodal Magmatism: Evidence from the Shirahama Group, Japan.: Journal of Petrology, v. 35, p. 619-645.

Tarkian, M., Economou-Eliopoulos, M., and Sambanis, G., 1996, Platinum-group minerals in chromitites from the Pindos ophiolite complex, Greece: Neues Jahrbuch Fur Mineralogie-Monatshefte, p. 145-160.

Tarkian, M., and Prichard, H.M., 1987, Irarsite-Hollingworthite Solid-Solution Series and Other Associated Ru-, Os-, Ir-, and Rh bearing PGM's from the Shetland Ophiolite Complex: Mineralium Deposita, v. 22, p. 178-184.

Thayer, T.P., 1964, Principal features and origin of podiform chromitite deposits, and some observations on the Guleman-Soridag district, Turkey: Economic Geology, v. 59, p. 1497-1524.

Tribuzio, R., Thirlwall, M.F., and Vannucci, R., 2004, Origin of the gabbro-peridotite association from the northern Apennine ophiolite: Journal of Petrology, v. 45, p. 1109-1124.

Tsoupas, G., and Economou-Eliopoulos, M., 2008, High PGE contents and extremely abundant PGE-minerals hosted in chromitites from the Veria ophiolite complex, northern Greece: Ore Geology Reviews, v. 33, p. 3-19.

Tsukanov, N.V., Kramer, W., Skolotnev, S.G., Luchitskaya, M.V., and Seifert, W., 2007, Ophiolites of the Eastern Peninsulas zone (Eastern Kamchatka): Age, composition, and geodynamic diversity: Island Arc, v. 16, p. 431-456.

Ulmer, P., 1989, The dependence of the Fe^{2+}-Mg^{2+} cation-partitioning between olivine and basaltic liquid on pressure, temperature and composition: Contributions to Mineralogy and Petrology, v. 101, p. 261-273.

Uysal, I., 2008, Platinum-group Minerals (PGM) and Other Solid Inclusions in th Elbistan-Kahramanmaras Mantle-hosted Ophiolitic Chromitites, South-eastern Turkey: Their Petrogenetic Significance.: Turkish Journal of Earth Sciences, v. 17, p. 729-740.

Uysal, I., 2009, Petrology of Al- and Cr- rich ophiolitic chromitites from the Muğla, SW Turkey: implications from composition of chromite, solid inclusions of platinum-group mineral, silicate, and base-metal mineral, and Os-isotope geochemistry: Contributions to Mineralogy and Petrology, v. 158, p. 659-674.

Uysal, I., Kaliwoda, M., Karsli, O., Tarkian, M., Sadiklar, M.B., and Ottley, C.J., 2007, Compositional variations as a result of partial melting and melt-peridotite interaction in an upper mantle section from the Ortaca area, southwestern Turkey: Canadian Mineralogist, v. 45, p. 1471-1493.

Uysal, I., Sadiklar, M.B., Tarkian, M., Karsli, O., and Aydin, F., 2005, Mineralogy and composition of the chromitites and their platinum-group minerals from Ortaca (Muğla-SW Turkey): Evidence for ophiolitic chromitite genesis: Mineralogy and Petrology, v. 83, p. 219-242.

van der Veen, A.H., and Maaskant, P., 1995, Chromian spinel mineralogy of the Stare Ransko gabbro-peridotite, Czech Republic, and its implications for sulfide mineralization: Mineralium Deposita, v. 30, p. 397-407.

Wang, W.L., Aitchison, J.C., Lo, C.H., and Zeng, Q.G., 2008, Geochemistry and geochronology of the amphibolite blocks in ophiolitic mélanges along Bangong-Nujiang suture, central Tibet: Journal of Asian Earth Sciences, v. 33, p. 122-138.

Wilson, J.T., 1968, Static or mobile earth: the current scientific revolution: Proceedings of the American Philosophical Society, v. 112, p. 309-320.

Wortel, M.J.R., and Spakman, W., 2000, Subduction and Slab Detachment in the Mediterranean-Carpathian Region: Science, v. 290, p. 1910 - 1917.

Yamamoto, S., Komiya, T., Hirose, K., and Maruyama, S., 2008, Coesite and clinopyroxene exsolution lamellae in chromites: *in-situ* ultrahigh pressure evidence from podiform chromitites in the Luobusa ophiolite, southern Tibet: Lithos, v. 109, p. 314-322.

Yang, J.S., Dobizhinetskaya, L., Bai, W.-J., Fang, Q.-S., Robinson, P.T., Zhang, J., and Green, H.W., 2007, Diamond and coesite-bearing chromitites from the Luobusa ophiolite, Tibet: Geology, v. 35, p. 875-878.

Yang, K., and Seccombe, P.K., 1993, Platinum-group minerals in the chromitites from the Great Serpentinite Belt, NSW, Australia: Mineralogy and Petrology, v. 47, p. 263-286.

Yigitbas, E., 1989, The investigation of petrology of tectonic assemblages around the Engizek (K.Maras) Mountain Istanbul University.

Yumul Jr, G.P., Dimalanta, C.B., Maglambayan, V.B., and Tamayo Jr, R.A., 2003, Mineralization controls in island arc settings: Insights from Philippine metallic deposits: Gondwana Research, v. 6, p. 767-776.

Zaccarini, F., Pushkarev, E., and Garuti, G., 2008, Platinum-group element mineralogy and geochemistry of chromitite of the Kluchevskoy ophiolite complex, central Urals (Russia): Ore Geology Reviews, v. 33, p. 20-30.

Zakrzewski, M.A., 1989, Chromian spinels from Kusa, Bergslagen, Sweden: American Mineralogist, v. 74, p. 448-455.

Zhang, Q., Wang, C.Y., Liu, D., Jian, P., Qian, Q., Zhou, G., and Robinson, P.T., 2008, A brief review of ophiolites in China: Journal of Asian Earth Sciences, v. 32, p. 308-324.

Zhao, G., Wilde, S.A., Li, S., Sun, M., Grant, M.L., and Li, X., 2007, U-Pb zircon age constraints on the Dongwanzi ultramafic-mafic body, North China, confirm it is not an Archean ophiolite: Earth and Planetary Science Letters, v. 255, p. 85-93.

Zhou, M.-F., and Robinson, P.T., 1997, Origin and tectonic environment of podiform chromite deposits: Economic Geology, v. 92, p. 259-262.

Zhou, M.-F., Robinson, P.T., and Bai, W.-J., 1994, Formation of podiform chromitites by melt/ rock interaction in the upper mantle: Mineralium Deposita, v. 29, p. 98-101.

Zhou, M.-F., Robinson, P.T., Malpas, J., Edwards, S.J., and Qi, L., 2005, REE and PGE Geochemical Constraints on the Formation of Dunites in the Luobosa Ophiolite, Southern Tibet: Journal of Petrology, v. 46, p. 615-639

Zhou, M.-F., Robinson, P.T., Malpas, J., and Li, Z., 1996, Podiform Chromitites in the Luobusa Ophiolite (Southern Tibet): Implications for Melt-Rock Interaction and Chromite Segregation in the Upper Mantle: Journal of Petrology, v. 37, p. 3-21.

Zhou, M.-F., Sun, M., Keays, R.R., and Kerrich, W., 1998, Controls on platinum-group elemental distributions of podiform chromitites: A case study of high-Cr and high-Al chromitites from Chinese orogenic belts: Geochimica et Cosmochimica Acta, v. 62, p. 677-688.

Appendix 1 – Petrological Descriptions

The petrological description of chromitite samples recorded the, mineral abundance, degree of chromite alteration, grain size, accessory sulphide content and any inclusion or fracture pattern (Table A1.1). For sulphides a 'moderate' content = ~1-2 wt%, 'minor' = <0.5 wt% and 'negligible' means sulphides were either unobserved or barely present. For alteration, 'pervasive' = >90% alteration, 'major' = > 70-90% alteration, 'moderate' = 30-70%, 'minor' = 10-30%, and negligible = <10% alteration. Alteration referred to the presence of either Cr-magnetite and/or ferritchromit. The petrological description of silicate samples recorded the mineral abundance, grain size and provided a short description of the slide (Table A1.2).

Table A1.1: *An example of a chromitite sample petrological description.*

Sample #	Pod	Minerals	Abundance (%)	Grain Size	Alteration	Sulphides	Inclusions & Other Notes
Q1	Harold's Grave	Chromite	80	Up to 2 mm	Minor	Negligible	Generally equigranular chromite grains with interstitial serpentine and Cr-chlorite (kammererite). Talc is a very minor component. There are also a couple of cross-cutting quartz veins. Fracturing is largely unoriented.
		Serp & Talc	15	Very fine			
		Other (Chl)	5	Very fine			

Table A1.2: *An example of a silicate sample petrological description.*

Sample #	Location	Rock Type	Minerals	Abundance	Grain Size	Description
DMK-15	Demerlik	Dunite/ Harzburgite?	Olivine	75	Up to 3 mm	Altered dunite, with serpentine and talc, being common replacement products. Chromite is an obvious interstitial mineral, as is minor orthopyroxene, clinopyroxene and chlorite, the latter usually being found in association with chromite. There are also some very minor concentrations of sulphide blebs. There were no exsolution patterns observed within the chromite.
			Serpentine & Talc	13	Very fine	
			Chromite	2	Up to 2 mm	
			Other (Pyr & Chl)	10	Up to 2 mm	

Al'Ays Chromitite Samples

Sample #	Group	Minerals	Abundance (%)	Grain Size	Alteration	Sulphides	Inclusions & Other Notes
C178	7	Chromite	90	Up to 4 mm	Pervasive	Negligible	Silicate inclusions are absent. Only a small section of the slide was analysable, isolated to one corner. There are minor oriented features and fracturing throughout
		Serp & Talc	10	Very fine			
		Other	-	-			
C375	7	Chromite	80	Up to 3 mm	Major	Negligible	Clustered silicate inclusions are present in some chromite grains. There is brittle fracturing throughout, with some hairline mylonisation in places.
		Serp & Talc	20	Very fine			
		Other	-	-			
C382	7	Chromite	95	Up to 3 mm	Minor	Negligible	No silicate inclusions. Considering the PGE content (~1700 ppb) the sulphide content is very low with only a few inclusions. There is brittle fracturing throughout, with some hairline mylonisation in places.
		Serp & Talc	5	Very fine			
		Other	-	-			
C498	7	Chromite	80	Up to 3 mm	Moderate	Negligible	Several chromite grains contain clustered inclusions, though the majority are barren. There is brittle fracturing throughout, with some hairline mylonisation in places.
		Serp & Talc	20	Very fine			
		Other	-	-			
C385	7	Chromite	95	Up to 3 mm	Pervasive	Negligible	Barely any chromite grains to analyse, and impossible to look for silicate inclusions. Fracturing was also pervasive with oriented and unoriented fracture patterns
		Serp & Talc	5	Very fine			
		Other	-	-			
C278	6	Chromite	80	Up to 2 mm	Moderate	Negligible	Poorly made mount. No silicate inclusions. There is brittle fracturing throughout, with some hairline mylonisation in places.
		Serp & Talc	20	Very fine			
		Other	-	-			
C311	6	Chromite	90	Up to 4 mm	Moderate	Minor	Several chromite grains contain linear inclusion trails as well as randomly oriented circular inclusions. There is brittle fracturing throughout, with some hairline mylonisation in places.
		Serp & Talc	10	Very fine			
		Other	-	-			
C362	6	Chromite	90	Up to 5 mm	Moderate	Negligible	Linear inclusions trails, often running parallel to each other.Fracturing was also pervasive with oriented and unoriented fracture patterns
		Serp & Talc	10	Very fine			
		Other	-	-			
C365	6	Chromite	95	Up to 2 mm	Pervasive	Negligible	No obvious silicate inclusions. Fracturing was alrgely unoriented, occasionally superimposed by hairline mylonisation.
		Serp & Talc	5	Very fine			
		Other	-	-			

Sample #	Group	Minerals	Abundance (%)	Grain Size	Alteration	Sulphides	Inclusions & Other Notes
C590	6	Chromite	95	Up to 5 mm	Negligible	Negligible	Only a few linear inclusion trails. There is brittle fracturing throughout, with some hairline mylonisation in places.
		Serp & Talc	5	Very fine			
		Other	-	-			
C580	6	Chromite	85	Up to 3 mm	Moderate	Negligible	Only a few linear inclusion trails. There is brittle fracturing throughout, with some hairline mylonisation in places.
		Serp & Talc	15	Very fine			
		Other	0	-			
C262	6	Chromite	80	Up to 5 mm	Minor	Moderate	A few grains contain randomly oriented circular silicate inclusions. Most chromite grains are 2-3 mm. The predominant fracture pattern is oriented features within the chromite grains
		Serp & Talc	20	Very fine			
		Other	-	-			
C581	6	Chromite	75	Up to 2 mm	Pervasive	Moderate	Almost disseminated. No unusual silicate inclusions. The predominant fracture pattern is oriented features within the chromite grains
		Serp & Talc	25	Very fine			
		Other	-	-			
C54	5	Chromite	95	Up to 5 mm	Minor	Negligible	There are spectacular and extensive linear inclusion trails running throughout the chromite grains. There is brittle fracturing throughout, with some hairline mylonisation in places.
		Serp & Talc	5	Very fine			
		Other	-	-			
C63	5	Chromite	80	Up to 5 mm	Major	Moderate	Several chromite grains contain linear inclusion trails as well as clustered inclusions. There is brittle fracturing throughout, with some hairline mylonisation in places.
		Serp & Talc	20	Very fine			
		Other	-	-			
C238	5	Chromite	95	Up to 5 mm	Moderate	Minor	There are several chromite grains containing linear inclusion trails. There is brittle fracturing throughout, with some hairline mylonisation in places.
		Serp & Talc	5	Very fine			
		Other	-	-			
C52	5	Chromite	90	Up to 2 mm	Moderate	Minor	Several linear inclusion trails, always empty and often undulating. There is brittle fracturing throughout, with some hairline mylonisation in places.
		Serp & Talc	10	Very fine			
		Other	-	-			
C61	5	Chromite	90	Up to 2 mm	Minor	Minor	Several grains contain abundant, clustered inclusions. There is little evidence of linear inclusion trails. No obvious silicate inclusions. Fracturing was largely unoriented, occasionally superimposed by hairline mylonisation.
		Serp & Talc	10	Very fine			
		Other	-	-			

Sample #	Group	Minerals	Abundance (%)	Grain Size	Alteration	Sulphides	Inclusions & Other Notes
C249	5	Chromite	95	Up to 5 mm	Moderate	Minor	No obvious silicate inclusions. Very annealed grains. Fracturing was largely unoriented, occasionally superimposed by hairline mylonisation.
		Serp & Talc	5	Very fine			
		Other	-	-			
C250	5	Chromite	80	Up to 1 mm	Moderate to Major	Moderate	1 grain contains a high concentration of clustered silicate inclusions. The predominant fracture pattern is oriented features within the chromite grains
		Serp & Talc	20	Very fine			
		Other	-	-			
C251	5	Chromite	90	Up to 2 mm	Minor to Moderate	Minor	A few small linear inclusions trails. Fracturing was largely unoriented, occasionally superimposed by hairline mylonisation.
		Serp & Talc	10	Very fine			
		Other	-	-			
C578	5	Chromite					*Polish was too bad for sample analysis*
C51	5	Chromite	80	Up to 2 mm	Moderate	Moderate	There are several chromite grains which contain obvious and extensive linear inclusions. There is brittle fracturing throughout, with some hairline mylonisation in places.
		Serp & Talc	20	Very fine			
		Other	-	-			
C429	4	Chromite	80	Up to 1 mm	Moderate	Minor	No unusual silicate inclusion patterns. The predominant fracture pattern is oriented features within the chromite grains
		Serp & Talc	20	Very fine			
		Other	-	-			
C328	4	Chromite	85	Up to 2 mm	Minor	Negligible	There are a few grains containing randomly oriented circular inclusions. Fracturing was largely unoriented, occasionally superimposed by hairline mylonisation.
		Serp & Talc	15	Very fine			
		Other	-	-			
C413	4	Chromite	90	Up to 2 mm	Negligible	Minor	There are a few grains containing randomly oriented circular inclusions. There is roughly oriented, brittle fracturing throughout, with some hairline mylonisation in places.
		Serp & Talc	10	Very fine			
		Other	-	-			
C462	4	Chromite	90	Up to 2 mm	Moderate	Minor	There are a few linear inclusion trails through the chromite grains. There is roughly oriented, brittle fracturing throughout, with some hairline mylonisation in places.
		Serp & Talc	10	Very fine			
		Other	-	-			
C463	4	Chromite	95	Up to 2 mm	Moderate to Major	Minor	No silicate inclusions - possibly due to grain destruction and expulsion. Fracturing was largely unoriented, occasionally superimposed by hairline mylonisation.
		Serp & Talc	5	Very fine			
		Other	-	-			

Sample #	Group	Minerals	Abundance (%)	Grain Size	Alteration	Sulphides	Inclusions & Other Notes
C533	4	Chromite	90	Up to 2 mm	Moderate to Major	Minor	Several grains contain clustered silicate inclusions. In this instance they are fairly amorphous in shape. Fracturing was largely unoriented, occasionally superimposed by hairline mylonisation.
		Serp & Talc	10	Very fine			
		Other	-	-			
C559	4	Chromite	90	Up to 3 mm	Moderate	Moderate	**Most** grains contain clustered silicate inclusions. Fracturing was largely unoriented, occasionally superimposed by hairline mylonisation.
		Serp & Talc	10	Very fine			
		Other	-	-			
C461	4	Chromite					*Polish was too bad for sample analysis*
C033	3	Chromite	95	Up to 4 mm	Minor	Negligible	Very few silicate inclusions and no patterns. Interstitial silicates may include some carbonates. Fracturing was largely unoriented, occasionally superimposed by hairline mylonisation.
		Serp & Talc	4 to 5	Very fine			
		Other	Up to 1	Very fine			
C040	3	Chromite	95	Up to 5 mm	Negligible	Negligible	Several unusual linear silicate inclusion trails. Chromite grains are very annealed. There is roughly oriented, brittle fracturing throughout, with some hairline mylonisation in places.
		Serp & Talc	5	Very fine			
		Other	-	-			
C044	3	Chromite	95	Up to 2 mm	Moderate	Negligible	Some unusual linear silicate inclusion trails. Not a very well polished block in places. Intensely mylonised sample.
		Serp & Talc	5	Very fine			
		Other	-	-			
C046	3	Chromite	95	Up to 2 mm	Major	Negligible	No unusual silicate inclusions. Intensely mylonised sample
		Serp & Talc	5	Very fine			
		Other	-	-			
C060	3	Chromite	90	Up to 4 mm	Moderate	Negligible	No unusual silicate inclusions. Fracturing was largely unoriented, occasionally superimposed by hairline mylonisation.
		Serp & Talc	10	Very fine			
		Other	-	-			
C318	3	Chromite	95	Up to 3 mm	Negligible	Negligible	Several linear inclusion trails, often curved occuring in different orientations. Fracturing was largely unoriented, occasionally superimposed by hairline mylonisation.
		Serp & Talc	5	Very fine			
		Other	-	-			
C484	3	Chromite	Up to 99	Fine	Moderate	Negligible	Some sections of the mount contain randomly oriented silicate inclusions. The mount is badly polished in places. Intensely mylonised sample.
		Serp & Talc	1	Very fine			
		Other	-	-			

Sample #	Group	Minerals	Abundance (%)	Grain Size	Alteration	Sulphides	Inclusions & Other Notes
C010	2	Chromite	95	Up to 1 mm	Moderate	Minor	A few linear inclusion trails. Fracturing was largely unoriented, occasionally superimposed by hairline mylonisation.
		Serp & Talc	5	Very fine			
		Other	-	-			
C104	2	Chromite	95	Up to 4 mm	Minor	Negligible	One or two small linear inclusion trails. Fracturing was largely unoriented, occasionally superimposed by hairline mylonisation.
		Serp & Talc	5	Very fine			
		Other	-	-			
C123	2	Chromite	Up to 99	Fragmented	Negligible	Negligible	A few linear inclusion trails. Intensely mylonised in places
		Serp & Talc	1	Very fine			
C595	2	Chromite	95	Up to 1 mm	Negligible	Negligible	No obvious inclusion patterns, but the polish on the block is badly finished. Intensely mylonised in places.
		Serp & Talc	5	Very fine			
C655	2	Chromite	95	Up to 4 mm	Negligible	Negligible	No obvious inclusion patterns. Fracturing was largely unoriented, occasionally superimposed by hairline mylonisation.
		Serp & Talc	5	Very fine			
		Other	-	-			
C670	2	Chromite	95	Up to 4 mm	Negligible	Negligible	No obvious inclusion patterns. Fracturing was Fracturing was largely unoriented, occasionally superimposed by hairline mylonisation. largely unoriented, occasionally superimposed by hairline mylonisation.
		Serp & Talc	5	Very fine			
		Other	-	-			
C659	2	Chromite	95	Up to 4 mm	Negligible	Negligible	One or two small linear inclusion trails. Fracturing was largely unoriented, occasionally superimposed by hairline mylonisation.
		Serp & Talc	5	Very fine			
		Other	-	-			
C204	1	Chromite	Up to 99	Fragmented	Negligible	Negligible	Possibly some linear inclusion trails, which might be crossing each other, hard to differentiate from polishing cracks
		Serp & Talc	1	Very fine			
		Other	-	-			
C205	1	Chromite	Up to 99	Fragmented	Negligible	Negligible	No obvious inclusion trails. There is roughly oriented, brittle fracturing throughout, with some hairline mylonisation in places.
		Serp & Talc	1	Very fine			
		Other	-	-			
C206	1	Chromite	Up to 99	Fragmented	Negligible	Negligible	No obvious inclusion trails. There is roughly oriented, brittle fracturing throughout, with some hairline mylonisation in places.
		Serp & Talc	1	Very fine			
		Other	-	-			

Sample #	Group	Minerals	Abundance (%)	Grain Size	Alteration	Sulphides	Inclusions & Other Notes
C207	1	Chromite	Up to 99	Fragmented	Negligible	Negligible	Possibly some linear inclusion trails, which might be crossing each other, hard to differentiate from polishing cracks. There is roughly oriented, brittle fracturing throughout, with some hairline mylonisation in places.
		Serp & Talc	1	Very fine			
		Other	-	-			
C208	1	Chromite	Up to 99	Fragmented	Negligible	Negligible	Possibly some linear inclusion trails, which might be crossing each other, hard to differentiate from polishing cracks. There is roughly oriented, brittle fracturing throughout, with some hairline mylonisation in places.
		Serp & Talc	1	Very fine			
		Other	-	-			
C209	1	Chromite	Up to 99	Fragmented	Negligible	Negligible	No obvious inclusion trails. There is roughly oriented, brittle fracturing throughout, with some hairline mylonisation in places.
		Serp & Talc	1	Very fine			
		Other	-	-			
C210	1	Chromite	Up to 99	Fragmented	Negligible	Negligible	Probably some linear inclusion trails, undulating but always empty. There is roughly oriented, brittle fracturing throughout, with some hairline mylonisation in places.
		Serp & Talc	1	Very fine			
		Other	-	-			
C211	1	Chromite	95	Fragmented	Negligible	Negligible	A patch of heavily altered silicate, Probably some linear inclusion trails, undulating but always empty. There is roughly oriented, brittle fracturing throughout, with some hairline mylonisation in places.
		Serp & Talc	5	Very fine			
		Other	-	-			
C212	1	Chromite	Up to 99	Fragmented	Negligible	Negligible	No obvious inclusion trails. There is roughly oriented, brittle fracturing throughout, with some hairline mylonisation in places.
		Serp & Talc	1	Very fine			
		Other	-	-			
C213	1	Chromite	Up to 99	Fragmented	Negligible	Negligible	No obvious inclusion trails. There is roughly oriented, brittle fracturing throughout, with some hairline mylonisation in places.
		Serp & Talc	1	Very fine			
		Other	-	-			
C214	1	Chromite	Up to 99	Fragmented	Negligible	Negligible	No obvious inclusion trails. There is roughly oriented, brittle fracturing throughout, with some hairline mylonisation in places.
		Serp & Talc	1	Very fine			
		Other	-	-			
C215	1	Chromite	Up to 99	Fragmented	Negligible	Negligible	One or two small linear inclusion trails. There is roughly oriented, brittle fracturing throughout, with some hairline mylonisation in places.
		Serp & Talc	1	Very fine			
		Other	-	-			

Shetland Chromitite Samples

Sample #	Pod	Minerals	Abundance (%)	Grain Size	Alteration	Sulphides	Inclusions & Other Notes
HG1	Harold's Grave	Chromite	90	Up to 4 mm	Moderate	Minor	Possibly a few small linear inclusion trails - always empty. Largely unoriented fractures spread throughout the mount.
		Serp & Talc	10	Very fine			
		Other	-	-			
HG4	Harold's Grave	Chromite	90	Up to 3 mm	Minor	Minor	A few grains have a higher proportion of clustered inclusions, but nothing extraordinary. Largely unoriented fractures spread throughout the mount.
		Serp & Talc	10	Very fine			
		Other	-	-			
HG5	Harold's Grave	Chromite	85	Up to 2 mm	Minor to Moderate	Negligible	No obvious silicate inlcusion patterns. There is roughly oriented, brittle fracturing throughout, with some hairline mylonisation in places.
		Serp & Talc	15	Very fine			
		Other	-	-			
HG6	Harold's Grave	Chromite	90	Up to 3 mm	Minor	Moderate	Most of the chromite grains are full of amorphous, almost dendritic randomly oriented silicate inclusions. There is roughly oriented, brittle fracturing throughout, with some hairline mylonisation in places.
		Serp & Talc	10	Very fine			
		Other	-	-			
HG7	Harold's Grave	Chromite	90	Up to 4 mm	Moderate to Major	Minor	There are some fine-scale linear inclusion trails, but the extent of the ferritchromit alteration masks more than that. There are roughly oriented fractures throughout the mount
		Serp & Talc	10	Very fine			
		Other	-	-			
HG8	Harold's Grave	Chromite	90	Up to 4 mm	Moderate	Minor	Several chromite grains are full of amorphous, randomly oriented silicate inclusions. There are also a few fine-scale linear inclusion trails. Fracturing was also pervasive with oriented and unoriented fracture patterns
		Serp & Talc	10	Very fine			
		Other	-	-			
HG9	Harold's Grave	Chromite	90	Up to 1 mm	Moderate to Major	Negligible	A few small linear inclusion trails - always empty. Largely unoriented fractures spread throughout the mount.
		Serp & Talc	10	Very fine			
		Other	-	-			
HG11	Harold's Grave	Chromite	90	Up to 2 mm	Major	Moderate	Some chromite grains are full of clustered silicate inclusions. There are a few fine-scale linear inclusion trails. Fracturing was also pervasive with oriented and unoriented fracture patterns
		Serp & Talc	10	Very fine			
		Other	-	-			
Q3a	Harold's Grave	Chromite	95	Up to 2 mm	Minor	Negligible	Most chromite alteration is concentrated along mylonised bands, and the sample is mildly brecciated. There are no obvious clustered or linear inclusion patterns. Chlorite is present in very minor concentrations.
		Serp & Talc	5	Very fine			
		Other	0	-			

Sample #	Pod	Minerals	Abundance (%)	Grain Size	Alteration	Sulphides	Inclusions & Other Notes
Q1	Harold's Grave	Chromite	80	Up to 2 mm	Minor	Negligible	Generally equigranular chromite grains with interstitial serpentine and Cr-chlorite (kammererite). Talc is a very minor component. There are also a couple of cross-cutting quartz veins. Fracturing is largely unoriented.
		Serp & Talc	15	Very fine			
		Other (Chl)	5	Very fine			
QX13	Harold's Grave	Chromite	95	Up to 3 mm	Moderate	Negligible	No obvious inclusion patterns, and fracturing is largely oriented with ferritchromit alteration often driven by the presence of fracture planes. The minor interstitial silicates are dominated by serpentine (no observed talc).
		Serp & Talc	5	Very fine			
		Other	-	-			
Q2	Harold's Grave	Chromite	95	Up to 1 mm	Moderate	Negligible	Heavily brecciated with several hairline mylonites running through the sample. There were no obvious linear or clustered inclusions running through the chromite grains.
		Serpentine	5	Very fine			
Q3PX	Harold's Grave	Chromite	75	Up to 5 mm	Major	Minor	Large grains, with **most** grains filled with clustered silicate inclusions. These are now mostly, if not completely, serpentine. Talc veins, minor chlorite and sulphides are all found within the interstitial serpentine.
		Serp & Talc	20	Very fine			
		Other	5	Up to 1 mm			
QY1	Quoys	Chromite	85	Up to 2 mm	Moderate to Major	Minor	Other silicates are probably Cr-mica related. There are a few fine-scale linear inclusion trails. Fracturing was also pervasive with oriented and unoriented fracture patterns
		Serp & Talc	10	Very fine			
		Other	5	Very fine			
QY2	Quoys	Chromite	85	Up to 2 mm	Moderate	Negligible	Other silicates are probably Cr-mica (kammererite). There are no clustered or linear inclusion patterns. Fracturing is predominantly oriented with significant unoriented patterns.
		Serp & Talc	10	Very fine			
		Other	5	Very fine			
QY5	Quoys	Chromite	85	Up to 3 mm	Moderate	Minor	Other silicates are probably Cr-mica related. There are a few fine-scale linear inclusion trails. Fracturing was also pervasive with oriented and unoriented fracture patterns
		Serp & Talc	10	Very fine			
		Other	5	Very fine			
QY6	Quoys	Chromite	90	Up to 3 mm	Moderate	Negligible	Other silicates are probably Cr-mica related. There are a few fine-scale linear inclusion trails. Fracturing was also pervasive with oriented and unoriented fracture patterns
		Serp & Talc	8	Very fine			
		Other	2	Very fine			
QY8	Quoys	Chromite	85	Up to 4 mm	Major	Negligible	Cr-mica (kammererite) is clearly present within the silicate matrix, and ferritchromit alteration of the chromite grains is a major presence. Fracture patterns are largely unoriented.
		Serp & Talc	5	Very fine			
		Other	10	Very fine			
QY9	Quoys	Chromite	85	Up to 4 mm	Moderate	Negligible	Other silicates (together with serpentine and talc) in this sample are more likely to be nickel carbonate owing to their distinct pistachio colour. Fracture patterns are largely unoriented.
		Serp & Talc	5	Very fine			
		Other	10	Very fine			

Sample #	Pod	Minerals	Abundance (%)	Grain Size	Alteration	Sulphides	Inclusions & Other Notes
QY10	Quoys	Chromite	90	Up to 6 mm	Minor	Minor	Several small linear inclusion trails. Fracturing is minor but where present is largely oriented. The other silicates are dominated by serpentine and talc.
		Serp & Talc	10	Very fine			
CF1	Cliff	Chromite	85	Up to 1 cm	Moderate	Negligible	Several linear inclusion trails, always empty. Fracturing was also pervasive with oriented and unoriented fracture patterns
		Serp & Talc	15	Very fine			
CF2	Cliff	Chromite	85	Up to 3 mm	Moderate	Moderate	Several linear inclusion trails. Some of which may be full of sulphides. Fracturing was also pervasive with oriented and unoriented fracture patterns.
		Serp & Talc	12	Very fine			
		Other	3	Very fine			
CF3	Cliff	Chromite	80	Up to 5 mm	Moderate	Moderate	Several linear inclusions trails, often filled with base-metal sulphides. Otherwise they are empty. Largely unoriented fractures spread throughout the mount.
		Serp & Talc	15	Very fine			
		Other	5	Very fine			
CF4	Cliff	Chromite	85	Up to 3 mm	Moderate	Negligible	Several linear inclusion trails, always empty. Fracturing was also pervasive with oriented and unoriented fracture patterns.
		Serp & Talc	8	Very fine			
		Other	7	Very fine			
CF5	Cliff	Chromite	75	Up to 3 mm	Moderate	Minor	Several linear inclusion trails, always empty. Largely unoriented fractures spread throughout the mount.
		Serp & Talc	25	Very fine			
CF6	Cliff	Chromite	85	Up to 3 mm	Moderate to Major	Moderate	No obvious linear inclusion trails. Fracturing was also pervasive with oriented and unoriented fracture patterns.
		Serp & Talc	10	Very fine			
		Other	5	Very fine			
CF8	Cliff	Chromite	85	Up to 3 mm	Major	Minor	A couple of linear inclusion trails. Always empty and fine. Largely unoriented fractures spread throughout the mount.
		Serp & Talc	15	Very fine			
CF9	Cliff	Chromite	85	Up to 2 mm	Minor	Moderate	Several linear inclusion trails, mostly empty but occasionally with base-metal sulphide inclusions. Fracturing was also pervasive with oriented and unoriented fracture patterns.
		Serp & Talc	10	Very fine			
		Other	5	Very fine			
CF10	Cliff	Chromite	88	Up to 4 mm	Minor	Moderate	Several linear Inclusion trails of varying sizes, but usually empty. Secondary mineral with euhedral sulphides present. Fracturing was also pervasive with oriented and unoriented fracture patterns.
		Serp & Talc	10	Very fine			
		Other	2	Very fine			

Sample #	Pod	Minerals	Abundance (%)	Grain Size	Alteration	Sulphides	Inclusions & Other Notes
CF11	Cliff	Chromite	90	Up to 3 mm	Major	Negligible	Some very small linear inclusion trails. Fracturing was also pervasive with oriented and unoriented fracture patterns.
		Serp & Talc	10	Very fine			
CF12	Cliff	Chromite	90	Up to 3 mm	Moderate	Minor	No obvious linear inclusion trails. Fracturing was also pervasive with oriented and unoriented fracture patterns.
		Serp & Talc	7	Very fine			
		Other	3	Very fine			
CF13	Cliff	Chromite	85	Up to 1 cm	Major	Negligible	Several linear inclusions trails, on a variety of scales, nearly all of which appear empty. Fracturing was also pervasive with oriented and unoriented fracture patterns.
		Serp & Talc	15	Very fine			
CF14	Cliff	Chromite	80	Up to 2 mm	Minor	Negligible	Very little evidence for unusual inclusion trails, or other inclusion patterns. Fracturing is intense throughout and largely unoriented.
		Serp & Talc	17	Very fine			
		Other	3	Very fine			
CF15	Cliff	Chromite	80	Up to 2 mm	Moderate to Major	Moderate	Only very small inclusion trails. Fracturing is intense throughout and largely unoriented, with some minor orientation in places.
		Serp & Talc	20	Very fine			
CF16	Cliff	Chromite	85	Up to 2 mm	Minor	Negligible	No clustered or linear inclusion patterns. There is some minor development of chlorite and calcite within the interstitial silicates. The chromite grains are quite brecciated.
		Serp & Talc	10	Very fine			
		Other	5	Very fine			
CF17	Cliff	Chromite	75	Up to 5 mm	Negligible	Negligible	No clustered or linear inclusion patterns. There are two veins cross-cutting the slide, which are partially filled with calcite. In addition there are minor developments of chlorite scattered throughout.
		Serp & Talc	25	Very fine			
		Other	5	Very fine			
CF18	Cliff	Chromite	75	Up to 1 cm	Minor	Negligible	No clustered or linear inclusion patterns to speak of. The chromite grains themselves are particularly large in places suggesting annealing has taken place. Fracturing is minor but largely oriented.
		Serp & Talc	25	Very fine			
		Other	0	Very fine			
1349	Cliff	Chromite	70	Up to 6 mm	Moderate	Moderate	No clustered inclusions, but some minor linear inclusion patterns. Sulphides consist of both Fe and Cu-Fe based and there is also chlorite and calcite developed within the interstitial silicates.
		Serp & Talc	25	Very fine			
		Other	5	Very fine			
CL3	Cliff	Chromite	85	Up to 1 cm	Moderate	Moderate	Some minor linear inclusion trails but no clustered inclusions. Sulphides were present both interstitially and as inclusions within the chromite. Chlorite (kammererite) is a common interstitial silicate.
		Serp & Talc	15	Very fine			
		Other	5	Very fine			

Sample #	Pod	Minerals	Abundance (%)	Grain Size	Alteration	Sulphides	Inclusions & Other Notes
NKS-1	Nikkavord South	Chromite	90	Up to 7 mm	Minor to Moderate	Moderate	Several linear inclusion trails. However, they are nearly always empty, which is surprising given the number of sulphides in the slide. Largely unoriented fractures spread throughout the mount.
		Serp & Talc	10	Very fine			
		Other	0	-			
NKS-2	Nikkavord South	Chromite	90	Up to 7 mm	Moderate	Negligible	No obvious linear inclusion trails. Largely unoriented fractures spread throughout the mount.
		Serp & Talc	10	Very fine			
NKS-3	Nikkavord South	Chromite	95	Up to 7 mm	Moderate	Minor	Several Linear inclusion trails, largely empty with none of the sulphides unambiguously present within the inclusion trail. Largely unoriented fractures spread throughout the mount.
		Serp & Talc	5	Very fine			
		Other	0	-			
NKS-4	Nikkavord South	Chromite	90	Up to 5 mm	Moderate	Minor	No obvious linear inclusion trails. Some unusually high concentrations of inclusions in some grains - possibly annealing. Largely unoriented fractures spread throughout the mount.
		Serp & Talc	10	Very fine			
		Other	0	-			
NKS-5	Nikkavord South	Chromite	90	Up to 5 mm	Pervasive	Negligible	Impossible to tell if there are unusual inclusions trails in this due to the ferritchromit alteration. Fracturing was also pervasive with oriented and unoriented fracture patterns.
		Serp & Talc	10	Very fine			
		Other	0	-			
NKS-6	Nikkavord South	Chromite	85	Up to 3 mm	Major	Minor	A few, generally fine linear inclusions trails - though always empty. Fracturing was also pervasive with oriented and unoriented fracture patterns.
		Serp & Talc	10	Very fine			
		Other	5	-			
NKE-1	Nikkavord East	Chromite	90	Up to 3 mm	Moderate	Minor	No obvious linear inclusion trails. Fracturing was also pervasive with oriented and unoriented fracture patterns.
		Serp & Talc	10	Very fine			
		Other	0	-			
NKE-2	Nikkavord East	Chromite	90	Up to 3 mm	Moderate	Negligible	Some small linear inclusion trails - always empty. Fracturing was also pervasive with oriented and unoriented fracture patterns.
		Serp & Talc	8	Very fine			
		Other	2	Very fine			
NKE-3	Nikkavord East	Chromite	85	Up tp 3 mm	Moderate	Negligible	Some very small linear inclusion trails. Fracturing was also pervasive with oriented and unoriented fracture patterns.
		Serp & Talc	15	Very fine			
NKE-4	Nikkavord East	Chromite	90	Up to 3 mm	Moderate to Major	Moderate	Only a few very small linear inclusion trails. Fracturing was also pervasive with oriented and unoriented fracture patterns.
		Serp & Talc	10	Very fine			
		Other	0	-			

Sample #	Pod	Minerals	Abundance (%)	Grain Size	Alteration	Sulphides	Inclusions & Other Notes
NKE-5	Nikkavord East	Chromite	85	Up to 4 mm	Moderate	Negligible	Several Linear inclusion trails, largely empty. Fracturing was also pervasive with oriented and unoriented fracture patterns.
		Serp & Talc	15	Very fine			
NKE-6	Nikkavord East	Chromite	90	Up to 2 mm	Minor to Moderate	Negligible	Only a few very small linear inclusion trails. Fracturing was also pervasive with oriented and unoriented fracture patterns.
		Serp & Talc	10	Very fine			
		Other	0	-			
NKE-7	Nikkavord East	Chromite	85	Up to 4 mm	Moderate	Negligible	No obvious linear inclusion trails. Fracturing was also pervasive with oriented and unoriented fracture patterns.
		Serp & Talc	15	Very fine			
KH1	Keen of Hamar	Chromite	70	Up to 1 mm	Major	Negligible	No obvious linear inclusion trails, but there are a few grains full of circular inclusion patterns. An almost disseminated chromitite with oriented features within the chromite grains
		Serp & Talc	30	Very fine			
		Other	0	-			
KH2	Keen of Hamar	Chromite	70	Up to 1 mm	Major	Minor	No obvious circular or linear inclusion patterns. An almost disseminated chromitite with oriented features within the chromite grains
		Serp & Talc	30	Very fine			
		Other	0	-			
RLM051	Keen of Hamar	Chromite	95	Up to 5 mm	Minor	Minor	A relatively fresh chromitite sample with small-scale, empty linear inclusions prominent throughout. Fracture patterns are largely unoriented with
		Serp & Talc	5	Very fine			
		Other	0	Very fine			
RLM053	Keen of Hamar	Chromite	90	Up to 3 mm	Moderate	Minor	Several, almost pervasive in extent, linear inclusion trails. There are also some possible circular inclusion patterns. Fracturing was also pervasive with oriented and unoriented fracture patterns.
		Serp & Talc	10	Very fine			
		Other	0	-			
RLM058	Keen of Hamar	Chromite	90	Up to 3 mm	Pervasive	Minor	Several linear inclusion trails, but much of the texture is masked, or covered by, the intense alteration to ferritchromit. Fracturing was also pervasive with oriented and unoriented fracture patterns.
		Serp & Talc	10	Very fine			
		Other	0	-			
LQ1	Long Quarry	Chromite	85	Up to 3 mm	Moderate	Moderate	Several linear inclusion trails, but no obvioius circular inclusion patterns. Fracturing was also pervasive with oriented and unoriented fracture patterns.
		Serp & Talc	15	Very fine			
		Other	0	-			
LQ2	Long Quarry	Chromite	80	Up to 4 mm	Minor	Moderate	Several linear inclusion trails, but no obvioius circular inclusion patterns. Fracturing was also pervasive with oriented and unoriented fracture patterns.
		Serp & Talc	20	Very fine			
		Other	0	-			

Sample #	Pod	Minerals	Abundance (%)	Grain Size	Alteration	Sulphides	Inclusions & Other Notes
LQ3	Long Quarry	Chromite	90	Up to 3 mm	Moderate	Moderate	Possibly a few fine linear inclusions trails. No obvious circular inclusion patterns. Fracturing was also pervasive with oriented and unoriented fracture patterns.
		Serp & Talc	10	Very fine			
		Other	0	-			

Shetland Silicate Samples

Sample #	Location	Rock Type	Minerals	Abundance	Grain Size	Description
MR267	Quoys	Dunite/ Serpentinite	Olivine	10-15%	<0.5 mm	A pervasively serpentinsed dunite. Olivine occurs as fragments within a serpentine and talc groundmass.There is a slight fabric to the slide, with a preferred orientation to many of the fibrous alteration minerals. There is also some iron staining and magnetite.
			Serpentine & Talc	85%	<0.5 mm	
			Chromite & Other	2%	Up to 1 mm	
MR265	Quoys	Dunite/ Serpentinite	Olivine	75%	<0.5 mm	The olivine grains are not too badly altered, with the outline of original grains still visible (1-2 mm). There are chromite grains unevenly scattered throughout the slide, as well as some magnetite
			Serpentine & Talc	20-25%	<0.5 mm	
			Chromite & Other	2%	Up to 0.5 mm	
MR35	Quoys	Dunite/ Serpentinite	Olivine	<5%	<0.5 mm	Alteration within this slide is pervasive with very little original olivine left. The primary magmatic rock was probably a dunite. The chromite also looks altered though some of the grains may be analysable. There is also some magnetite scattered throughout the slide
			Serpentine & Talc	95%	<0.5 mm	
			Chromite	<1%	Up to 0.5 mm	
			Other	1%	<0.5 mm	
MR260	Quoys	Harzburgite/ Serpentinite	Olivine	20-25%	<0.5 mm	Very altered. Possibly an original harzburgitic rock with evidence for pyroxene pseudomorphing and alteration to chlorite. There is some fresh olivine as well, but mostly this has also been altered to serpentine and talc. There is very little chromite, and the majority of the analysable oxides are in fact magnetite.
			Serp/ Talc & Chlte	70-75%	<0.5 mm	
			Chromite	<1%	Up to 0.5 mm	
			Other	1%	<0.5 mm	
RL007	Cliff	Dunite/ Serpentinite	Olivine	15-20%	<0.5 mm	A pervasively serpentinsed dunite. Olivine occurs as fragments within a serpentine and talc groundmass.There is also some iron staining and magnetite.
			Serpentine & Talc	80%	<0.5 mm	
			Chromite	1%	Up to 0.5 mm	
			Other	1%	<0.5 mm	
MR6	Cliff	Dunite/ Serpentinite	Olivine	50%	<0.5 mm	The olivine grains are moderately altered, with the outline of original grains still visible (1-2 mm). There are chromite grains unevenly scattered throughout the slide, as well as some magnetite
			Serpentine & Talc	45-50%	<0.5 mm	
			Chromite	1%	Up to 0.5 mm	
			Other	1%	<0.5 mm	
MR12	Cliff	Dunite/ Serpentinite	Olivine	40%	<0.5 mm	Moderately altered dunite. The olivine grains show obvious indications of relic grain boundaries (1-2 mm), with these boundaries interlocking and anhedral. The groundmass is dominated by serpentine and talc. Chromite and magnetite are minor constituents.
			Serpentine & Talc	55-60%	<0.5 mm	
			Chromite	1%	Up to 0.5 mm	
			Other	1%	<0.5 mm	

Sample #	Location	Rock Type	Minerals	Abundance	Grain Size	Description
CF19	Cliff	Dunite/ Serpentinite	Olivine	20	Up to 4 mm	Heavily altered dunite with some chromite and sulphide mineralisation. Olivine grains show relic grain boundaries. Serpentine is the predominant alteration silicate with very little talc. The main sulphides are millerite and heazlewoodite as well as some native copper. Sulphide mineralisation is largely vein controlled. Chromite alteration is minor. Several PGM were observed.
			Serpentine & Talc	76	Very fine	
			Chromite	2	Up to 2 mm	
			Sulphides	2	Up to 1 mm	
			Other	-	-	
CF20	Cliff	Dunite/ Serpentinite	Olivine	20	Up to 4 mm	Heavily altered dunite with some chromite and sulphide mineralisation. Olivine grains show relic grain boundaries. Serpentine is the predominant alteration silicate with very little (if any) talc. The main sulphides are millerite and heazlewoodite as well as some native copper (slightly more than previous slide). Sulphide mineralisation is largely vein controlled. Chromite alteration is moderate. Several PGM were observed.
			Serpentine & Talc	72	Very fine	
			Chromite	4	Up to 2 mm	
			Sulphides	4	Up to 1 mm	
			Other	-	-	
CF21	Cliff	Dunite/ Serpentinite	Olivine	30-35%	Up to 2 mm	Moderately altered dunite. The olivine grains show obvious indications of relic grain boundaries, with these boundaries interlocking and anhedral. The groundmass is dominated by serpentine and talc. Chromite and magnetite are minor constituents. Several PGM were observed.
			Serpentine & Talc	55-60%	<0.5 mm	
			Chromite & Other	2-3%	Up to 2 mm	
			Sulphides	2%	Up to 2 mm	
CF23	Cliff	Dunite/ Serpentinite	Olivine	40-50%	Up to 2 mm	Moderately altered dunite. The olivine grains show obvious indications of relic grain boundaries, with these boundaries interlocking and anhedral. The groundmass is dominated by serpentine and talc. Chromite and magnetite are minor constituents. The sulphides consist of pentlandite and pyrrhotite with chalcopyrite also present. Several PGM were observed.
			Serpentine & Talc	40-45%	<0.5 mm	
			Chromite	2%	Up to 2 mm	
			Sulphides	2%	Up to 2 mm	
			Other	<1%	<0.5 mm	
MR1	Cliff	Harzburgite/ Serpentinite	Olivine	5%	<0.5 mm	Very altered. Possibly an original harzburgitic rock with pseudomorphing and alteration to chlorite. There is some fresh olivine as well, but mostly this has also been altered to serpentine and talc. There is some chromite, and a large proportion of magnetite, particularly in the pseudomorphs
			Serp/ Talc & Chlte	90%	<0.5 mm	
			Chromite	1%	<0.5 mm	
			Magnetite	3-4%	<0.5 mm	
RL011	Harold's Grave	Dunite/ Serpentinite	Olivine	80%	0.5 mm	The olivine grains are fairly pristine, with the outline of original grains still visible (1-2 mm). There are chromite grains unevenly scattered throughout the slide, as well as some magnetite. There is also some iron staining along micro-veins
			Serpentine & Talc	15-20%	<0.5mm	
			Chromite	1%	Up to 1 mm	
			Other	1%	<0.5 mm	
RL016	Harold's Grave	Dunite/ Serpentinite	Olivine	45-50%	<0.5 mm	Moderately altered dunite, with serpentinisation reducing about half of the olivine grains to serpentine. There is chromite and magnetite scattered throughout the slide and some iron staining along micro-veins.
			Serpentine & Talc	50%	<0.5 mm	
			Chromite	1-2%	<0.5 mm	
			Other	1%	<0.5 mm	

Sample #	Location	Rock Type	Minerals	Abundance	Grain Size	Description
RL019	Harold's Grave	Dunite/ Serpentinite	Olivine	30-35%	<0.5 mm	Moderately altered dunite, with serpentinisation reducing about half of the olivine grains to serpentine. There is chromite and magnetite scattered throughout the slide. Iron staining is also prevelant ocurring along several parallel micro-veins
			Serpentine & Talc	65%	<0.5mm	
			Chromite	1%	<0.5 mm	
			Other	1%	<0.5 mm	
MR222	Vord Hill Fetlar	Harzburgite/ Serpentinite	Olivine	25%	Up to 2 mm	Moderately altered lherzolite/ wehrlite. Some large pervasively altered clinopyroxene (Cpx) grains, largely pseudomorphic and replaced by clays. There are occasional fresh fragments of Cpx. Olivine is moderately fresh, with some alteration to serpentine & talc. Chromite is a minor constituent but also moderately altered.
			Serp/ Talc & Chl	45-50%	<0.5 mm	
			Chromite	1%	<0.5 mm	
			Cpx/ (Opx)	25-30%	Up to 5 mm	
			Other	1%	<0.5 mm	
MR254	South of Crussa Field	Harzburgite/ Serpentinite	Olivine	35	Up to 2 mm	Heavily altered harzburgite with some relic pyroxene shaped grains. The pyroxenes have been completely replaced by talc, and some minor magnetite. The predominant alteration mineral is serpentine, with some minor talc. No chlorite was observed. The chromite grains show moderate to major alteration to ferritchromit.
			Serpentine and Talc	60	Very fine	
			Chromite	1	~0.5 mm	
			Magnetite	3	Very fine	
			Other	1	Very fine	
MR276	Mid Fetlar	Harzburgite/ Serpentinite	Olivine	15	Up to 2 mm	Heavily altered harzburgite with some relic pyroxene shaped grains. The pyroxenes have been completely replaced by talc, and some minor magnetite. The predominant alteration mineral is serpentine, with some minor talc and some very minor chlorite. The chlorite is usually associated with the altered chromite. The chromite grains are mostly completely altered to ferritchromit.
			Serp/ Talc & Chl	75	Very fine	
			Chromite	1	~0.5 mm	
			Magnetite	3	Very fine	
			Other	1	Very fine	
MR162	Clibbers-wick South	Harzburgite/ Serpentinite	Olivine	10-15%	Up to 2 mm	Heavily altered. Probably an original harzburgitic rock with some relic olivine, showing pervasive alteration to serpentine and magnetite. Pyroxene pseudomorphs are present but completely replaced by talc and magnetite. There is some minor chromite, which appear quite fresh, and some possible minor sulphide deportment.
			Serp/ Talc & Chl	80%	<0.5 mm	
			Chromite	<1%	~0.5mm	
			Magnetite	~5%	<0.5 mm	
			Other	<1%	<0.5 mm	
MR144	Taing NU	Harzburgite/ Serpentinite	Olivine	5-10%	<0.5 mm	Very altered. Probably an original harzburgitic rock with some relic orthopyroxene, usually heavily altered to chlorite. There is some fresh olivine as well, but mostly this has also been altered to serpentine and talc. There is some minor chromite, which unusually appears quite fresh.
			Serp/ Talc & Chl	85%	<0.5 mm	
			Orthopyroxene	3-4%	Up to 1 mm	
			Chromite	<1%	<0.5 mm	
			Other	<1%	<0.5 mm	

Sample #	Location	Rock Type	Minerals	Abundance	Grain Size	Description
MR256	West of Nikkavord	Harzburgite/ Serpentinite	Olivine	10-15%	Up to 2 mm	Heavily altered. Probably an original harzburgitic rock with some relic olivine, showing pervasive alteration to serpentine and magnetite. Pyroxene pseudomorphs are present but completely replaced by talc and magnetite. There is some minor chromite, showing moderate or major alteration to ferritchromit. No sulphides were observed.
			Serp/ Talc & Chl	80%	<0.5 mm	
			Chromite	<1%	Up to 1 mm	
			Magnetite	~5%	<0.5 mm	
			Other	<1%	<0.5 mm	
MR141	Clibbers-wick North	Harzburgite/ Serpentinite	Olivine	20-25%	Up to 2 mm	Altered. Probably an original harzburgitic rock with some relic (ortho)pyroxene, usually heavily altered to chlorite and amphibole. There is some fresh olivine which has also been altered to serpentine and talc. There is some minor chromite, showing moderate alteration and generally surrounded by chloritic haloes (probably kammererite). Also some minor sulphide!
			Serp/ Talc & Chl	50-55%	<0.5 mm	
			Pyroxene/ Amphibole	20%	Up to 2 mm	
			Chromite	<1%	Up to 1 mm	
			Other	<1%	<0.5 mm	
NB2a	North of Balta-sound	Dunite/ Serpentinite	Olivine	5%	<0.5 mm	An original dunitic rock which has been pervasively serpentinised leaving only a few olivine remnants. Chromite grains are scattered evenly throughout and show only minor alteration. There is also some very minor sulphide mineralisation, with what was formerly pentlandite now altered to awaruite.
			Serpentine & Talc	90-95%	<0.5 mm	
			Chromite	2%	0.2- 0.5 mm	
			Other	1%	Up to 0.5 mm	
NB2b	North of Balta-sound	Dunite/ Serpentinite	Olivine	5%	<0.5 mm	An original dunitic rock which has been pervasively serpentinised leaving only a few olivine remnants. Chromite grains are scattered evenly throughout and show only minor alteration. In contrast to the previous slide there is a little more sulphide mineralisation, including pyrrhotite, pentlandite and awaruite which is forming around the rims of the pentlandite.
			Serpentine & Talc	90-95%	<0.5 mm	
			Chromite	2%	0.2-0.5 mm	
			Sulphides	1-2%	Up to 0.5 mm	
RLM026	Long Quarry	Dunite/ Serpentinite	Olivine	20%	<0.5 mm	An original dunitic rock which has been pervasively serpentinised leaving only a few olivine remnants. Chromite grains are scattered evenly throughout and show only minor alteration. Magnetite is occasionally developed along small micro-veins and there are also one or two small sulphide grains.
			Serp/ Talc & Chl	75-80%	<0.5 mm	
			Chromite	1%	Up to 0.5 mm	
			Magnetite	<1%	<0.5 mm	
RLM057	Long Quarry	Dunite/ Serpentinite	Olivine	1	Very fine	A pervasively serpentinised rock with only a few fragments of olivine remaining. The predominant alteration mineral is serpentine with no, or very little, talc observed. Chromite grains are spread throughout, generally reaching up to 0.5 mm in diameter. They generally show moderate to minor alteration.
			Serpentine & Talc	95	Very fine	
			Chromite	3	Very fine	
			Other	-	-	

Berit Chromitite Samples

Sample #	Locality	Minerals	Abundance (%)	Grain Size	Alteration	Sulphides	Inclusions & Other Notes
KBK-2	Kabak-teppe	Chromite	90	Up to 4 mm	Minor	Minor	Inclusion rich, but with no major circular inclusion patterns. Linear inclusion patterns are present, as are some silicate exsolution. Fracturing was also pervasive with oriented and unoriented fracture patterns
		Olivine	3	Very fine			
		Serp & Talc	7	Very fine			
KBK-16	Kabak-teppe	Chromite	70	Up to 3 mm	Negligible	Minor	Some very small linear inclusion trails, usually filled with silicates. Otherwise, samples are generally inclusion rich. Largely unoriented fractures spread throughout the mount.
		Olivine	20	Up to 2 mm			
		Serp & Talc	10	Very fine			
KBK-17	Kabak-teppe	Chromite	30	Up to 1 mm	Moderate	Minor	Disseminated Chromitite, with some circular inclusion patterns, and some small linear inclusion trails. Some minor silicate exsolution. Largely unoriented fractures spread throughout the mount.
		Olivine	60	Up to 1 mm			
		Serp & Talc	10	fine			
KBK-18	Kabak-teppe	Chromite	30	Up to 2 mm	Minor	Minor	Disseminated Chromitite, with several grains containing inclusions, but no obvious patterns. There is some very minor silicate exsolution. Largely unoriented fractures spread throughout the mount.
		Olivine	60	Up to 2 mm			
		Serp & Talc	10	fine			
KBK-19	Kabak-teppe	Chromite	80	Up to 2 mm	Negligible	Negligible	There are some minor circular inclusion patterns, with no obvious linear inclusion patterns. There are some small silicate exsolution occurrences. Fracturing was also pervasive with oriented and unoriented fracture patterns
		Olivine	-	-			
		Serp & Talc	20	Very fine			
KBK-20	Kabak-teppe	Chromite	90	Up to 2 mm	Moderate	Minor	There are lots of inclusions, but no particular inclusion patterns, either ciruclar or linear. There are lots of silicate exsolution occurrences. Fracturing was also pervasive with oriented and unoriented fracture patterns
		Olivine	-	-			
		Serp & Talc	10	Very fine			
KBK-21	Kabak-teppe	Chromite	70	Up to 2 mm	Negligible	Moderate	Several circular inclusion patterns, usually filled with silicates. Similarly there are a few linear inclusion trails with silicate inclusions. Largely unoriented fractures spread throughout the mount.
		Olivine	20	Up to 2 mm			
		Serp & Talc	10	Very fine			
KBK-22	Kabak-teppe	Chromite	80	Up to 3 mm	Negligible	Minor	Circular inclusion patterns, usually filled with silicates. No obvious linear inclusion trails. Largely unoriented fractures spread throughout the mount.
		Olivine	10	Up to 2 mm			
		Serp & Talc	10	Very fine			
KBK-37	Kabak-teppe	Chromite	75	Up to 2 mm	Minor	Minor	Some circular and linear inclusion patterns, which are often filled with silicates. There are also some crystallographic lamellae. Largely unoriented fractures spread .
		Olivine	5	Up to 2 mm			
		Serp & Talc	20	Very fine			

Sample #	Group	Minerals	Abundance (%)	Grain Size	Alteration	Sulphides	Inclusions & Other Notes
KBK-38	Kabak-teppe	Chromite	75	Up to 3 mm	Minor	Minor	Linear inclusion trails are frequent, but small. No particular cluster inclusion patters. Inclusions are filled with silicates or empty. Largely unoriented fractures spread throughout the mount.
		Olivine	5	Fine			
		Serp & Talc	20	Very fine			
KBK-39	Kabak-teppe	Chromite	70	Up to 1 mm	Minor (associated with vein)	Negligible	Some circular inclusion patterns, and a few small linear inclusion trails, which are often filled with silicates. Largely unoriented fractures spread throughout the mount.
		Olivine	5	Fine			
		Serp & Talc	25	Very fine			
MBI-5	Kurtini	Chromite	90	Up to 1 mm	Negligible	Moderate	Silicate inclusions are common, very occasionally as small linear inclusions. There are no unusual circular inclusion patterns. Largely unoriented fractures spread throughout the mount.
		Olivine	5	Fine			
		Serp & Talc	5	Very fine			
MBI-9	Kurtini	Chromite	90	Up to 2 mm	Negligible	Minor	Possibly, some very minor linear inclusions - no obvious circular inclusion patterns. Largely unoriented fractures spread throughout the mount.
		Olivine	5	Up to 1 mm			
		Serp & Talc	5	Very fine			
MBA-6	Alisli	Chromite	95	< 1mm	Negligible	Negligible	Several linear inclusion trails, always empty and very fine. No obvious circular inclusion patterns. Fracturing was largely unoriented, occasionally superimposed by hairline mylonisation.
		Olivine	0	-			
		Serp & Talc	5	Very fine			
MBP-3	Payamli	Chromite	95	< 1mm	Minor	Negligible	No obvious linear or circular inclusion patterns. Fracturing was largely unoriented, occasionally superimposed by hairline mylonisation.
		Olivine	0	-			
		Serp & Talc	5	Very fine			
MBT-15	Palitli	Chromite	95	Up to 1 mm	Negligible	Minor	Possibly, some very minor linear inclusions - no obvious circular inclusion patterns. Largely unoriented fractures spread throughout the mount.
		Olivine	2	Fine			
		Serp & Talc	3	Very fine			
MBS-1	Sarikat	Chromite	90	Up to 2 mm	Minor	Moderate	Both linear and circular inclusion patterns on display. Linear inclusion patterns occur over a variety of scales. Fracturing was also pervasive with oriented and unoriented fracture patterns
		Olivine	5	Fine			
		Serp & Talc	5	Very fine			
MBI-2	Kurtini	Chromite	90	Up to 2 mm	Negligible	Minor	Some prominent circular inclusion patterns, as well as linear inclusion trails - though the latter are normally on a small scale. Fracturing was also pervasive with oriented and unoriented fracture patterns
		Olivine	5	Fine			
		Serp & Talc	5	Very fine			

Sample #	Group	Minerals	Abundance (%)	Grain Size	Alteration	Sulphides	Inclusions & Other Notes
MBK-2	Kirciusagi	Chromite	90	Up to 2 mm	Negligible	Negligible	Polish is bad, but there are some obvious circular inclusion patterns. No obvious linear inclusion trails. Fracturing is extensive, with oriented and unoriented fracture patterns as well as hairline mylonites
		Olivine	0	-			
		Serp & Talc	10	Very fine			
MBK-14	Kirciusagi	Chromite	90	Up to 1 mm	Negligible	Negligible	No obvious circular or linear inclusion patterns. Fracturing is extensive, with oriented and unoriented fracture patterns as well as hairline mylonites
		Olivine	0	-			
		Serp & Talc	10	Very fine			
DMK-9	Demerlik	Chromite	60	Up to 1 mm	Negligible	Negligible	Absent, or very minor inclusion patterns. Largely unoriented fractures spread throughout the mount.
		Olivine	10	Fine			
		Serp & Talc	30	Very fine			
DMK-12	Demerlik	Chromite	70	Up to 2 mm	Negligible	Negligible	Some minor clustered inclusion patterns, and no obvious linear inclusion patterns. Fracturing was also pervasive with oriented and unoriented fracture patterns
		Olivine	15	Fine			
		Serp & Talc	15	Very fine			
DMK-16	Demerlik	Chromite	70	Up to 1 mm	Minor	Minor	There are some minor clustered and linear inclusion patterns, as well as some very minor crystallographic exsolution. There are oriented and unoriented fracture patterns, with some oriented fractures producing extended parallel microfaults.
		Olivine	15	Fine			
		Serp & Talc	15	Very fine			
DMK-17	Demerlik	Chromite	80	Up to 2 mm	Negligible	Minor	There are some minor circular and linear inclusion patterns. No crystallographic exsolution was observed. Largely unoriented fractures spread throughout the mount.
		Olivine	10	Fine			
		Serp & Talc	10	Very fine			
DMK-18	Demerlik	Chromite	70	Up to 2 mm	Negligible	Negligible	There are some minor linear inclusions, apparently filled by silicates. No obvious crystallographic lamellae. Largely unoriented fractures spread throughout the mount.
		Olivine	10	fine			
		Serp & Talc	20	Very fine			
DMK-28	Demerlik	Chromite	85	Up to 1 mm	Minor	Minor	Some minor circular inclusion patterns, and exsolution lamellae, with very few linear inclusion trails. Fracturing was also pervasive with oriented and unoriented fracture patterns
		Olivine	5	fine			
		Serp & Talc	10	Very fine			
MBD-4	Dereagzi	Chromite	90	Up to 2 mm	Moderate	Negligible	Several fine-scale linear inclusion trails (which appear empty). No obvious circular inclusion patterns, or exsolution lamellae. Fracturing was also pervasive with oriented and unoriented fracture patterns
		Olivine	0	-			
		Serp & Talc	10	Very fine			

Sample #	Group	Minerals	Abundance (%)	Grain Size	Alteration	Sulphides	Inclusions & Other Notes
MBD-7	Dereagzi	Chromite	85	Up to 1 mm	Negligible	Minor	Clustered inclusions are a common feature, as are linear inclusions, the latter often filled with sulphides. Fracturing is largely unoriented. Sulphides were only ever found as inclusions within the chromite grains.
		Olivine	0	-			
		Serp & Talc	15	Very fine			
MBD-8	Dereagzi	Chromite	90	Up to 2 mm	Moderate	Minor	No unusual silicate inclusion patterns of any kind - though there may be some on a very fine scale. No exsolution lamellae. Fracturing is extensive, with oriented and unoriented fracture patterns as well as hairline mylonites
		Olivine	0	-			
		Serp & Talc	10	Very fine			
MBD-8A	Dereagzi	Chromite	90	Up to 1 mm	Minor	Minor	Equigranular chromite sample with minor oriented fracture patterns. Inclusions are common within the chromite grains, though not with any particular pattern. Rutile and sulphides are found within the interstitial silicates.
		Olivine	0	-			
		Serp & Talc	10	Very fine			
MBD-8B	Dereagzi	Chromite	95	Up to 3 mm	Negligible	Negligible	There are a couple of grains with clustered inclusion patterns, and no linear inclusion patterns. There are occasional developments of rutile, and a few PGM present. Fracturing is minor, and largely unoriented.
		Olivine	0	-			
		Serp & Talc	5	Very fine			
MBD-11	Dereagzi	Chromite	80	Up to 2 mm	Minor	Moderate	Plenty of circular inclusion patterns, with no obvious linear inclusion trails. There are hints of exsolution lamellae (v.minor if at all). Fracturing was also pervasive with oriented and unoriented fracture patterns
		Olivine	10	Up to 1 mm			
		Serp & Talc	10	Very fine			
MBD-13	Dereagzi	Chromite	90	Up to 1 mm	Negligible	Minor	Several circular inclusion patterns within the chromite grains. Negligible linear inclusion patterns. No exsolution lamellae. The predominant fracture pattern is oriented features within the chromite grains
		Olivine	0	-			
		Serp & Talc	10	Very fine			
Ader-2	Dereagzi	Chromite	85	Up to 2 mm	Minor	Moderate	There are some minor linear inclusion trails (empty), and some crystallographic lamellae filled with silicates (on the edge of chromite grains). Fracturing was also pervasive with oriented and unoriented fracture patterns
		Olivine	0	-			
		Serp & Talc	15	Very fine			
Ader-3	Dereagzi	Chromite	90	Up to 2 mm	Moderate	Moderate	There are some minor linear inclusion trails present throughout the slide (empty), bar some elongate silicates. No circular inclusion patterns. Fracturing was also pervasive with oriented and unoriented fracture patterns
		Olivine	0	-			
		Serp & Talc	10	Very fine			
Ader-4	Dereagzi	Chromite	85	Up to 3 mm	Minor	Minor	No obvious linear or circular inclusion patterns. There are however some crystallographic lamellae filled with silicates. Fracturing was also pervasive with oriented and unoriented fracture patterns
		Olivine	0	-			
		Serp & Talc	15	Very fine			

Sample #	Pod	Minerals	Abundance (%)	Grain Size	Alteration	Sulphides	Inclusions & Other Notes
Ader-5	Dereagzi	Chromite	85	Up to 3 mm	Minor	Minor	There are some minor linear inclusion trails (empty), and some crystallographic lamellae filled with silicates. Fracturing was also pervasive with oriented and unoriented fracture patterns
		Olivine	0	-			
		Serp & Talc	15	Very fine			

Berit Silicate Samples

Sample #	Location	Rock Type	Minerals	Abundance (%)	Grain Size	Description
Ader-1	Dereagzi	Dunite	Olivine	80	Up to 4 mm	A fresh dunite with interstitial chromite and base metal sulphides. There is no evidence for unusual inclusion patterns within the chromite, or for the development of exsolution lamellae. There are some amphibole grains (cummingtonite), occasional clinopyroxene, chlorite and talc
			Serpentine & Talc	15	Very fine	
			Chromite	1	Up to 1 mm	
			Other (Am & Chl)	4	Very fine	
Ader-8	Dereagzi	Dunite	Olivine	70	Up to 2 mm	Variably altered dunite, with some olivine grains showing pervasive replacement by talc, which is more common in this slide that serpentine. Chromite grains are small (typically <0.5 mm), but all show well developed exsolution lamallae and are associated with chlorite overgrowths. Talc and cummingtonite (~8%) were also observed.
			Serpentine & Talc	20	Very fine	
			Chromite	<1	Very fine	
			Other (Am & Chl)	10	Very fine	
Ader-9	Dereagzi	Dunite	Olivine	70	Up to 4 mm	Variably altered dunite, with some olivine grains containing serpentine veins. Talc, amphibole (cmt) and clinopyroxene were also observed with talc more common than serpentine. Chromite occasionally shows very strong exsolution lamellae development, and this is invariably associated with marked chlorite overgrowths.
			Serpentine & Talc	25	Up to 1 mm	
			Chromite	1	<1 mm	
			Other (Am & Chl)	4	Very fine	
Ader-12	Dereagzi	Dunite	Olivine	65	Up to 4 mm	Fresh olivine grains with interstitial base metal sulphides, and some minor cumulate chromite. There are some amphibole grains (cummingtonite), occasional clinopyroxene, chlorite and talc . Chromite displays several textures, including exsolution lamellae and cluster inclusion patterns.
			Serp/ Talc & Chlte	20	Very fine	
			Chromite	10	Up to 2 mm	
			Other (Am & Cpx)	5	fine	
Ader-13	Dereagzi	Dunite	Olivine	85	Up to 4 mm	A fresh dunite rock, with some minor interstitial chromite and some base-metal sulphide mineralisation. The chromite grains show some minor developments of exsolution lamellae, always in conjunction with significant chlorite overgrowths. Chlorite is also present in other parts of the slide. Talc and amphibole were also observed.
			Serpentine & Talc	10	Very fine	
			Chromite	<1	Up to 1 mm	
			Other (Chl)	5	Up to 2 mm	
DMK-13	Demerlik	Dunite	Olivine	65	Up to 4 mm	Slightly overpolished slide (lots of holes). Variably altered olivine grains with developments of serpentine and talc as the principle alteration. Sulphide minerals are also found in very minor concentrations, as was chlorite. Only a few chromite grains show any development of exsolution lamellae. Talc and amphibole were also observed.
			Serpentine & Talc	13	Very fine	
			Chromite	2	Up to 1 mm	
			Other (Chl & Holes!)	20	Up to 1 mm	

Sample #	Location	Rock Type	Minerals	Abundance	Grain Size	Description
DMK-14	Demerlik	Dunite/ Harzburgite?	Olivine	65	Up to 4 mm	A relatively fresh dunitic rock with interstitial chromite and base metal sulphides. There also appears to be some clinopyroxene, (~aegirine-augite, with low extinction angles). Roughly half of the chromite grains display very well developed silicate exsolution lamellae. Talc and amphibole were also observed.
			Serpentine & Talc	20	Very fine	
			Chromite	5	Up to 1 mm	
			Other (Cpx & Chl)	10	Up to 2 mm	
DMK-15	Demerlik	Dunite/ Harzburgite?	Olivine	75	Up to 3 mm	Altered dunite, with serpentine and particularly talc, being common replacement products. Chromite is an obvious interstitial mineral, as is minor amphibole, clinopyroxene and chlorite, the latter usually being found in association with chromite. There are also some very minor concentrations of sulphide blebs. There were no exsolution patterns observed within the chromite.
			Serpentine & Talc	13	Very fine	
			Chromite	2	Up to 2 mm	
			Other (Am, Cpx & Chl)	10	Up to 2 mm	
DMK-29	Demerlik	Dunite/ Harzburgite?	Olivine	80	Up to 2 mm	Variably altered dunite, with some interstitial chromite. The chromite grains are variably altered, with some showing well developed exsolution textures. In addition, many of these chromite grains have a pronounced chlorite overgrowth. There was some minor amphibole and talc.
			Serpentine & Talc	13	Very fine	
			Chromite	2	Up to 1 mm	
			Other (Am & Chl)	5	Up to 2 mm	
KBK-1	Kabakteppe	Dunite	Olivine	90	Up to 4 mm	A fresh dunitic rock with minor interstitial chromite. There also appears to be some minor base-metal sulphide development. The chromite grains are relatively pristine, though one or two do show the development of exsolution lamellae. There was some minor chlorite developed around the chromite grains.
			Serpentine & Talc	8	Very fine	
			Chromite	1	Up to 1 mm	
			Other (Chl)	1	Up to 1 mm	
KBK-3	Kabakteppe	Dunite	Olivine	90	Up to 4 mm	Dunite, with largely unaltered olivine grains and about 2% of associated interstitial chromite grains. There is some chlorite development around the chromite grains. There was no evidence of exsolution lamellae within the chromite grains. No amphibole was observed.
			Serpentine & Talc	7	Very fine	
			Chromite	2	Up to 1 mm	
			Other (Chl)	1	Up to 1 mm	
KBK-36	Kabakteppe	Dunite	Olivine	85	Up to 4mm	A fresh dunitic rock with interstitial chromite and some minor sulphide development. There also appears to be some clinopyroxene, (The cpx shows only slightly inclined extinction and high interference colours – possibly aegirine-augite). Most of the chromite grains show well developed exsolution lamellae, and this is associated with well developed chlorite grains surrounding the chromite grains.
			Serp/ Talc & Chlte	10	Very fine	
			Chromite	1	Up to 2 mm	
			Sulphides	<1	<0.5 mm	
			Other (Am & Chl)	3	Up to 1 mm	

Sample #	Location	Rock Type	Minerals	Abundance (%)	Grain Size	Description
KBK-41	Kabakteppe	Dunite	Olivine	85	Up to 4 mm	A fresh dunitic rock with interstitial chromite. There also appears to be some amphibole with only mildly inclined extinction (cummingtonite). Anthophyllite may also be present within this slide. The chromite grains are relatively pristine, and although chlorite is present it is not particularly well developed around the chromite grains.
			Serpentine & Talc	11	Very fine	
			Chromite	<1	Up to 1 mm	
			Other (Am & Chl)	3	Up to 2 mm	
KBK-42	Kabakteppe	Dunite	Olivine	85	Up to 2 mm	A fresh dunitic rock with interstitial chromite. There also appears to be some amphibole with only mildly inclined extinction (cummingtonite). Just over half of the chromite grains display very well developed silicate exsolution lamellae. Chlorite is also well developed as an alteration product around the chromite grains.
			Serpentine & Talc	9	Very fine	
			Chromite	1	Up to 1 mm	
			Other (Am & Chl)	5	Up to 1 mm	

Appendix 2 - Chromite analyses from Chromitite Samples

Al'Ays chromitite analysis

Sample	C375									
Analysis#	1	2	3	4	5	6	7	8	9	10
TiO_2	0.24	0.24	0.24	0.23	0.24	0.24	0.25	0.22	0.23	0.23
V_2O_5	0.24	0.28	0.23	0.21	0.22	0.24	0.21	0.19	0.21	0.23
Al_2O_3	18.47	18.83	19.00	18.95	19.24	18.73	18.91	18.87	17.69	17.86
Cr_2O_3	46.03	45.38	46.77	46.47	44.54	44.75	44.68	45.49	45.29	45.19
FeO^{tot}	23.70	23.76	23.30	23.35	23.69	23.66	23.54	22.93	23.66	23.59
MnO	0.28	0.25	0.28	0.25	0.27	0.27	0.27	0.26	0.25	0.26
MgO	11.30	11.23	11.39	11.80	11.44	11.77	11.53	11.56	11.36	11.80
NiO	0.13	0.11	0.12	0.11	0.12	0.09	0.13	0.08	0.12	0.11
Cr#	0.63	0.62	0.62	0.62	0.61	0.62	0.61	0.62	0.63	0.63
Mg#	0.53	0.53	0.53	0.55	0.54	0.55	0.54	0.54	0.54	0.56
Cr/Fe^{2+}	2.43	2.38	2.44	2.50	2.39	2.48	2.44	2.48	2.49	2.55

Sample	C382									
Analysis#	1	2	3	4	5	6	7	8	9	10
TiO_2	0.09	0.08	0.08	0.10	0.08	0.06	0.10	0.09	0.09	0.09
V_2O_5	0.14	0.18	0.17	0.19	0.21	0.19	0.19	0.18	0.17	0.18
Al_2O_3	9.57	9.62	8.80	8.94	8.18	8.24	9.75	9.85	9.84	9.80
Cr_2O_3	57.84	57.98	58.21	58.24	60.04	59.55	57.67	58.60	57.42	56.64
FeO^{tot}	20.56	20.50	20.92	20.92	21.39	21.39	20.10	20.16	20.80	21.16
MnO	0.29	0.29	0.28	0.29	0.30	0.32	0.27	0.28	0.28	0.28
MgO	11.38	11.45	11.11	11.00	11.17	10.78	11.59	11.57	11.18	10.99
NiO	0.08	0.10	0.05	0.07	0.09	0.09	0.10	0.09	0.09	0.09
Cr#	0.80	0.80	0.82	0.81	0.83	0.83	0.80	0.80	0.80	0.79
Mg#	0.56	0.56	0.55	0.54	0.54	0.53	0.57	0.56	0.55	0.54
Cr/Fe^{2+}	3.41	3.42	3.38	3.33	3.41	3.32	3.46	3.44	3.31	3.25

Sample	C498						
Analysis#	1	2	3	4	5	6	7
TiO_2	0.07	0.07	0.07	0.08	0.07	0.08	0.06
V_2O_5	0.19	0.18	0.22	0.20	0.21	0.20	0.15
Al_2O_3	13.80	13.55	13.31	14.03	13.82	13.55	14.03
Cr_2O_3	57.36	56.97	57.36	57.79	56.54	56.97	57.82
FeO^{tot}	17.75	17.37	17.36	16.47	16.91	17.26	17.11
MnO	0.32	0.30	0.29	0.26	0.27	0.29	0.28
MgO	11.76	11.29	11.57	12.46	11.87	12.62	11.80
NiO	0.08	0.08	0.11	0.08	0.07	0.07	0.07
Cr#	0.74	0.74	0.74	0.73	0.73	0.74	0.73
Mg#	0.56	0.55	0.56	0.59	0.57	0.60	0.56
Cr/Fe^{2+}	3.30	3.24	3.31	3.53	3.37	3.58	3.33

Sample	C498 continued						
Analysis#	8	9	10	11	12	13	14
TiO_2	0.07	0.07	0.07	0.07	0.06	0.06	0.06
V_2O_5	0.18	0.20	0.18	0.19	0.20	0.17	0.19
Al_2O_3	13.86	14.07	14.19	13.28	13.57	14.05	13.77
Cr_2O_3	56.82	56.15	56.31	58.36	57.18	57.44	57.11
FeO^{tot}	16.92	16.60	16.08	16.77	17.41	17.27	17.31
MnO	0.28	0.27	0.25	0.26	0.24	0.27	0.28
MgO	12.41	11.92	12.27	12.23	12.39	11.90	11.84
NiO	0.09	0.07	0.08	0.07	0.07	0.11	0.09
Cr#	0.73	0.73	0.73	0.75	0.74	0.73	0.74
Mg#	0.59	0.58	0.59	0.58	0.59	0.57	0.57
Cr/Fe^{2+}	3.53	3.39	3.51	3.52	3.49	3.34	3.35

Sample	C178									
Analysis#	1	2	3	4	5	6	7	8	9	10
TiO_2	0.20	-	0.18	0.19	0.21	0.19	0.22	0.20	0.18	0.18
V_2O_5	0.19	-	0.22	0.19	0.20	0.21	0.19	0.22	0.20	0.22
Al_2O_3	25.37	25.28	23.95	24.04	24.73	24.76	24.88	24.70	24.85	24.90
Cr_2O_3	39.66	39.33	40.78	40.48	39.65	39.34	40.14	40.10	39.79	40.08
FeO^{tot}	22.39	22.72	23.02	23.35	22.61	22.17	22.77	23.16	22.89	22.26
MnO	0.34	0.29	0.29	0.27	0.26	0.28	0.25	0.26	0.28	0.25
MgO	12.49	12.41	11.69	12.13	12.42	12.40	12.13	12.38	12.30	12.47
NiO	0.15	-	0.16	0.15	0.14	0.15	0.12	0.15	0.13	0.12
Cr#	0.51	0.51	0.53	0.53	0.52	0.52	0.52	0.52	0.52	0.52
Mg#	0.57	0.57	0.54	0.55	0.56	0.57	0.55	0.56	0.56	0.57
Cr/Fe^{2+}	2.19	2.20	2.14	2.18	2.20	2.21	2.14	2.18	2.17	2.21

Sample	C580									
Analysis#	1	2	3	4	5	6	7	8	9	10
TiO_2	0.09	0.08	0.08	0.09	0.09	0.08	0.08	0.09	0.09	0.10
V_2O_5	0.24	0.19	0.21	0.16	0.15	0.18	0.18	0.21	0.20	0.19
Al_2O_3	12.38	12.59	12.29	12.40	11.39	11.33	11.76	11.91	10.46	10.82
Cr_2O_3	56.43	56.38	56.13	55.56	56.30	56.95	57.65	57.14	57.16	57.08
FeO^{tot}	18.80	18.83	19.13	19.09	19.07	19.02	19.91	20.09	20.89	20.52
MnO	0.23	0.25	0.26	0.26	0.28	0.29	0.24	0.26	0.26	0.26
MgO	12.00	11.65	11.68	11.34	11.62	11.17	11.54	11.20	11.48	11.29
NiO	0.13	0.06	0.04	0.07	0.11	0.08	0.09	0.07	0.12	0.08
Cr#	0.75	0.75	0.75	0.75	0.77	0.77	0.77	0.76	0.79	0.78
Mg#	0.58	0.56	0.56	0.55	0.57	0.55	0.55	0.54	0.56	0.55
Cr/Fe^{2+}	3.40	3.29	3.30	3.23	3.40	3.29	3.27	3.16	3.32	3.26

Sample	C590										
Analysis#	1	2	3	4	5	6	7	8	9	10	11
TiO_2	0.11	0.11	0.11	0.10	0.09	0.10	0.10	0.08	0.11	0.09	0.10
V_2O_5	0.22	0.26	0.20	0.24	0.27	0.25	0.26	0.24	0.24	0.19	0.23
Al_2O_3	10.10	10.24	10.10	9.95	9.76	10.07	9.95	9.46	10.10	10.22	10.26
Cr_2O_3	58.02	57.05	57.46	57.80	57.45	57.62	56.92	58.13	58.28	58.68	58.95
FeO^{tot}	20.32	20.54	20.66	20.65	20.50	20.74	20.74	20.07	20.64	20.28	20.50
MnO	0.27	0.28	0.30	0.27	0.28	0.30	0.27	0.28	0.27	0.29	0.29
MgO	11.06	10.82	11.03	11.12	10.65	10.61	10.81	10.80	11.31	11.64	11.03
NiO	0.10	0.08	0.07	0.08	0.10	0.10	0.09	0.08	0.12	0.12	0.09
Cr#	0.79	0.79	0.79	0.80	0.80	0.79	0.79	0.80	0.79	0.79	0.79
Mg#	0.54	0.53	0.54	0.54	0.53	0.52	0.53	0.54	0.55	0.56	0.53
Cr/Fe^{2+}	3.27	3.19	3.25	3.28	3.20	3.15	3.20	3.29	3.31	3.42	3.24

Sample	C311									
Analysis#	1	2	3	4	5	6	7	8	9	10
TiO_2	0.13	0.12	0.15	0.14	0.15	0.13	0.13	0.11	0.12	0.12
V_2O_5	0.26	0.26	0.29	0.24	0.29	0.22	0.24	0.24	0.23	0.24
Al_2O_3	18.70	18.67	18.61	18.10	17.62	18.01	17.90	18.38	18.35	18.09
Cr_2O_3	48.92	48.61	48.78	48.76	49.24	49.51	49.67	48.20	48.19	49.77
FeO^{tot}	19.68	19.69	19.81	20.77	20.18	20.04	19.80	19.61	19.79	20.08
MnO	0.23	0.27	0.26	0.30	0.27	0.26	0.26	0.28	0.24	0.29
MgO	13.11	13.09	13.09	12.83	12.86	13.05	13.03	13.04	12.88	12.72
NiO	0.09	0.09	0.10	0.10	0.10	0.10	0.09	0.07	0.12	0.00
Cr#	0.64	0.64	0.64	0.64	0.65	0.65	0.65	0.64	0.64	0.65
Mg#	0.60	0.60	0.60	0.59	0.60	0.60	0.60	0.61	0.60	0.59
Cr/Fe^{2+}	3.01	3.01	3.00	2.94	3.01	3.04	3.06	3.04	2.99	2.95

Sample	C278									
Analysis#	1	2	3	4	5	6	7	8	9	10
TiO_2	0.16	0.15	0.15	0.15	0.14	0.15	0.16	0.14	0.15	0.15
V_2O_5	0.18	0.17	0.16	0.20	0.18	0.20	0.20	0.14	0.16	0.20
Al_2O_3	22.12	22.21	22.42	22.31	22.20	21.96	21.80	21.95	22.20	22.03
Cr_2O_3	44.95	44.72	44.35	44.13	44.16	44.58	44.87	44.47	44.68	44.62
FeO^{tot}	19.59	19.94	19.60	19.55	19.76	19.63	19.70	19.98	19.44	19.49
MnO	0.26	0.26	0.26	0.26	0.27	0.29	0.26	0.26	0.27	0.27
MgO	11.99	12.04	11.92	11.88	12.12	12.11	11.99	11.59	11.80	12.13
NiO	0.13	0.14	0.14	0.13	0.12	0.12	0.14	0.16	0.11	0.10
Cr#	0.58	0.57	0.57	0.57	0.57	0.58	0.58	0.58	0.57	0.58
Mg#	0.56	0.56	0.56	0.56	0.57	0.56	0.56	0.55	0.55	0.57
Cr/Fe^{2+}	2.51	2.50	2.47	2.47	2.51	2.54	2.52	2.44	2.48	2.54

Sample	C365										
Analysis#	1	2	3	4	5	6	7	8	9	10	11
TiO_2	0.15	0.14	0.13	0.14	0.12	0.13	0.13	0.13	0.12	0.11	0.14
V_2O_5	0.12	0.16	0.14	0.15	0.09	0.14	0.15	0.16	0.13	0.14	0.14
Al_2O_3	16.14	16.27	16.29	15.21	15.40	15.82	16.47	16.18	15.88	15.92	15.84
Cr_2O_3	54.72	53.74	54.21	54.88	54.79	53.47	53.62	54.22	53.83	53.99	55.06
FeO^{tot}	15.65	15.95	16.12	16.29	15.85	15.68	15.72	16.59	16.59	16.30	15.56
MnO	0.23	0.25	0.25	0.24	0.25	0.25	0.23	0.26	0.27	0.24	0.26
MgO	13.70	13.40	13.06	13.09	12.98	13.67	13.79	13.09	13.39	13.05	13.07
NiO	0.14	0.13	0.07	0.13	0.14	0.14	0.15	0.12	0.10	0.12	0.13
Cr#	0.69	0.69	0.69	0.71	0.70	0.69	0.69	0.69	0.69	0.69	0.70
Mg#	0.64	0.63	0.61	0.62	0.62	0.65	0.65	0.61	0.63	0.62	0.62
Cr/Fe^{2+}	3.74	3.62	3.50	3.61	3.62	3.80	3.75	3.48	3.62	3.53	3.59

Sample	C362								
Analysis#	1	2	3	4	5	6	7	8	9
TiO_2	0.07	0.08	0.08	0.06	0.06	0.05	0.06	0.06	0.07
V_2O_5	0.19	0.21	0.22	0.19	0.17	0.23	0.17	0.21	0.23
Al_2O_3	16.61	15.81	16.02	16.01	15.64	15.45	16.04	15.73	15.72
Cr_2O_3	51.30	51.37	51.79	52.09	52.58	52.64	53.58	52.46	51.56
FeO^{tot}	17.60	17.39	17.76	17.71	17.66	17.64	17.53	17.66	17.47
MnO	0.23	0.25	0.26	0.24	0.25	0.28	0.26	0.26	0.25
MgO	13.35	13.43	13.32	13.05	13.29	13.57	13.24	13.43	13.47
NiO	0.12	0.15	0.11	0.08	0.10	0.13	0.12	0.08	0.12
Cr#	0.67	0.69	0.68	0.69	0.69	0.70	0.69	0.69	0.69
Mg#	0.63	0.64	0.63	0.62	0.63	0.64	0.62	0.63	0.64
Cr/Fe^{2+}	3.46	3.60	3.50	3.43	3.55	3.66	3.49	3.57	3.61

Sample	C262									
Analysis#	1	2	3	4	5	6	7	8	9	10
TiO_2	0.11	0.11	0.10	0.11	0.10	0.11	0.11	0.10	0.10	0.11
V_2O_5	0.18	0.16	0.15	0.13	0.13	0.11	0.17	0.13	0.15	0.13
Al_2O_3	21.97	22.08	21.65	21.71	21.83	21.90	22.18	22.26	21.60	21.83
Cr_2O_3	48.15	48.19	47.62	47.82	48.19	48.30	47.70	47.98	48.56	48.19
FeO^{tot}	14.67	14.86	14.94	14.79	14.98	14.81	14.60	14.66	14.91	14.66
MnO	0.24	0.22	0.24	0.24	0.23	0.23	0.22	0.24	0.24	0.23
MgO	15.59	15.51	15.62	15.41	15.65	15.50	15.62	15.46	15.70	15.64
NiO	0.10	0.10	0.11	0.12	0.12	0.08	0.11	0.07	0.10	0.08
Cr#	0.60	0.59	0.60	0.60	0.60	0.60	0.59	0.59	0.60	0.60
Mg#	0.70	0.69	0.71	0.70	0.70	0.70	0.70	0.69	0.70	0.70
Cr/Fe^{2+}	3.81	3.75	3.87	3.80	3.84	3.79	3.81	3.74	3.89	3.86

Sample	C413									
Analysis#	1	2	3	4	5	6	7	8	9	10
TiO_2	0.17	0.16	0.15	0.15	0.16	0.16	0.15	0.15	0.17	0.16
V_2O_5	0.10	0.13	0.14	0.12	0.12	0.11	0.12	0.13	0.12	0.14
Al_2O_3	18.71	18.31	18.74	18.07	18.53	18.03	18.75	18.96	18.88	18.43
Cr_2O_3	50.01	50.94	50.36	49.82	49.94	49.94	50.06	49.85	49.92	49.84
FeO^{tot}	16.28	16.11	16.43	16.00	16.24	16.59	16.66	16.95	16.63	16.23
MnO	0.27	0.22	0.22	0.23	0.23	0.24	0.22	0.22	0.24	0.25
MgO	13.54	13.85	13.91	14.03	13.41	14.04	13.43	13.89	13.39	13.84
NiO	0.15	0.16	0.14	0.11	0.16	0.16	0.13	0.19	0.18	0.15
Cr#	0.64	0.65	0.64	0.65	0.64	0.65	0.64	0.64	0.64	0.64
Mg#	0.63	0.64	0.64	0.66	0.63	0.66	0.63	0.64	0.63	0.65
Cr/Fe^{2+}	3.40	3.53	3.48	3.65	3.38	3.61	3.32	3.42	3.31	3.52

Sample	C533									
Analysis#	1	2	3	4	5	6	7	8	9	10
TiO_2	0.07	0.07	0.07	0.07	0.07	0.08	0.07	0.08	0.08	0.08
V_2O_5	0.09	0.11	0.12	0.11	0.11	0.13	0.12	0.13	0.12	0.11
Al_2O_3	21.87	22.07	21.68	21.71	21.48	21.62	22.13	22.03	21.89	21.96
Cr_2O_3	47.72	47.46	47.59	48.17	47.09	47.39	47.46	46.85	47.76	46.95
FeO^{tot}	15.22	15.29	15.39	15.80	15.80	15.53	15.61	15.71	15.25	15.15
MnO	0.15	0.15	0.15	0.15	0.14	0.14	0.15	0.16	0.15	0.17
MgO	14.90	14.75	14.30	14.30	15.31	15.27	15.39	15.18	15.34	15.41
NiO	0.29	0.30	0.25	0.25	0.33	0.28	0.27	0.25	0.32	0.32
Cr#	0.59	0.59	0.60	0.60	0.60	0.60	0.59	0.59	0.59	0.59
Mg#	0.68	0.67	0.66	0.65	0.70	0.69	0.69	0.69	0.69	0.70
Cr/Fe^{2+}	3.59	3.51	3.39	3.35	3.74	3.71	3.68	3.61	3.73	3.78

Sample	C559							
Anl#	1	2	3	4	5	6	7	8
TiO_2	0.15	0.12	0.14	0.14	0.13	0.14	0.13	0.13
V_2O_5	0.18	0.22	0.20	0.18	0.17	0.20	0.17	0.19
Al_2O_3	21.31	21.60	21.55	21.92	21.89	22.13	21.80	20.28
Cr_2O_3	46.75	46.72	47.08	47.69	47.74	47.64	47.30	49.50
FeO^{tot}	16.26	16.19	15.91	16.46	16.46	16.17	16.19	17.13
MnO	0.25	0.27	0.24	0.27	0.24	0.25	0.25	0.26
MgO	14.09	14.02	13.97	14.36	14.10	14.34	14.31	13.68
NiO	0.09	0.10	0.09	0.10	0.08	0.10	0.08	0.09
Cr#	0.60	0.59	0.59	0.59	0.59	0.59	0.59	0.62
Mg#	0.65	0.65	0.64	0.65	0.64	0.65	0.65	0.63
Cr/Fe^{2+}	3.27	3.24	3.24	3.26	3.20	3.24	3.29	3.20

Sample	C559 Continued							
Anl#	9	10	11	12	13	14	15	16
TiO_2	0.13	0.14	0.14	0.14	0.15	0.14	0.14	0.14
V_2O_5	0.19	0.19	0.19	0.23	0.18	0.19	0.22	0.17
Al_2O_3	19.99	20.65	20.03	21.07	21.46	21.00	21.42	21.04
Cr_2O_3	49.27	49.19	49.75	48.08	48.10	48.11	48.43	48.96
FeO^{tot}	17.18	16.96	17.04	16.61	16.90	16.70	17.05	16.91
MnO	0.29	0.26	0.25	0.27	0.23	0.27	0.27	0.23
MgO	13.75	13.77	13.72	13.71	14.13	13.97	13.76	13.51
NiO	0.09	0.07	0.05	0.09	0.11	0.07	0.09	0.10
Cr#	0.62	0.61	0.62	0.60	0.60	0.61	0.60	0.61
Mg#	0.63	0.63	0.63	0.63	0.64	0.64	0.62	0.62
Cr/Fe^{2+}	3.25	3.19	3.23	3.17	3.21	3.23	3.11	3.10

Sample	C462									
Analysis#	1	2	3	4	5	6	7	8	9	10
TiO_2	0.11	0.09	0.13	0.09	0.10	0.10	0.12	0.10	0.12	0.11
V_2O_5	0.10	0.15	0.15	0.11	0.14	0.10	0.13	0.21	0.14	0.14
Al_2O_3	15.92	15.93	16.52	16.68	16.20	16.26	15.83	15.64	16.37	16.37
Cr_2O_3	54.68	54.19	53.64	53.51	53.73	53.94	55.42	54.91	54.51	54.57
FeO^{tot}	15.13	14.75	15.43	15.38	15.07	14.84	14.65	14.96	15.25	15.31
MnO	0.25	0.23	0.25	0.25	0.24	0.23	0.28	0.28	0.25	0.24
MgO	13.79	13.43	14.34	13.92	13.88	13.98	13.84	13.72	14.10	14.48
NiO	0.12	0.15	0.09	0.13	0.12	0.11	0.12	0.13	0.13	0.15
Cr#	0.70	0.70	0.69	0.68	0.69	0.69	0.70	0.70	0.69	0.69
Mg#	0.65	0.64	0.67	0.65	0.65	0.66	0.65	0.65	0.66	0.67
Cr/Fe^{2+}	3.87	3.79	3.95	3.82	3.88	3.94	3.93	3.88	3.90	4.03

Sample	C463							
Analysis#	1	2	3	4	5	6	7	8
TiO_2	0.10	0.12	0.12	0.10	0.12	0.12	0.10	0.11
V_2O_5	0.15	0.16	0.15	0.17	0.17	0.15	0.18	0.14
Al_2O_3	18.62	18.42	19.04	19.00	18.82	18.48	18.51	17.66
Cr_2O_3	51.19	51.06	51.26	50.77	51.86	52.49	51.80	51.93
FeO^{tot}	15.38	15.45	15.38	15.26	15.72	15.20	15.84	15.38
MnO	0.24	0.23	0.24	0.27	0.27	0.26	0.23	0.23
MgO	14.69	15.15	15.06	14.85	13.64	13.83	13.54	13.88
NiO	0.18	0.13	0.13	0.16	0.16	0.15	0.11	0.11
Cr#	0.65	0.65	0.64	0.64	0.65	0.66	0.65	0.66
Mg#	0.68	0.69	0.68	0.68	0.63	0.64	0.63	0.65
Cr/Fe^{2+}	3.86	4.04	3.92	3.88	3.44	3.58	3.43	3.68

Sample	C328								
Analysis#	1	2	3	4	5	6	7	8	9
TiO_2	0.10	0.10	0.09	0.08	0.09	0.09	0.11	0.10	0.10
V_2O_5	0.23	0.29	0.19	0.24	0.20	0.19	0.20	0.21	0.24
Al_2O_3	16.72	16.67	15.44	15.59	16.30	16.11	15.78	15.88	16.30
Cr_2O_3	51.20	51.58	52.70	53.09	52.27	51.79	50.80	52.02	51.77
FeO^{tot}	18.90	18.95	18.97	19.06	18.86	18.99	19.41	19.29	19.47
MnO	0.25	0.27	0.30	0.29	0.24	0.24	0.28	0.29	0.29
MgO	12.39	12.29	12.61	12.83	12.57	12.36	12.45	12.54	12.24
NiO	0.09	0.13	0.12	0.11	0.08	0.10	0.13	0.13	0.13
Cr#	0.67	0.67	0.70	0.70	0.68	0.68	0.68	0.69	0.68
Mg#	0.59	0.58	0.60	0.60	0.59	0.59	0.59	0.59	0.58
Cr/Fe^{2+}	3.09	3.06	3.28	3.30	3.18	3.14	3.17	3.19	3.06

Sample	C63										
Analysis#	1	2	3	4	5	6	7	8	9	10	11
TiO_2	0.14	0.15	0.13	0.13	0.13	0.13	0.13	0.14	0.13	0.12	0.14
V_2O_5	0.18	0.18	0.20	0.17	0.18	0.18	0.19	0.21	0.19	0.18	0.18
Al_2O_3	20.87	21.43	21.52	21.37	21.48	21.59	21.82	21.31	21.22	19.50	19.10
Cr_2O_3	46.09	46.65	46.49	47.16	46.63	46.85	46.31	46.73	46.68	47.61	47.66
FeO^{tot}	17.29	17.39	17.75	16.93	17.14	17.71	17.70	17.67	17.78	19.78	19.19
MnO	0.23	0.23	0.23	0.23	0.25	0.21	0.23	0.24	0.24	0.26	0.25
MgO	13.65	13.78	13.87	13.77	13.83	13.94	13.82	13.65	13.62	13.38	13.16
NiO	0.30	0.36	0.32	0.32	0.33	0.24	0.26	0.31	0.34	0.37	0.36
Cr#	0.60	0.59	0.59	0.60	0.59	0.59	0.59	0.60	0.60	0.62	0.63
Mg#	0.64	0.63	0.64	0.63	0.64	0.64	0.63	0.63	0.63	0.62	0.61
Cr/Fe^{2+}	3.14	3.12	3.10	3.15	3.15	3.10	3.06	3.07	3.07	3.05	3.07

Sample	C54									
Analysis#	1	2	3	4	5	6	7	8	9	10
TiO_2	0.13	0.13	0.13	0.14	0.13	0.13	0.13	0.13	0.12	0.12
V_2O_5	0.19	0.17	0.13	0.14	0.22	0.17	0.18	0.17	0.18	0.21
Al_2O_3	18.37	18.57	18.11	18.19	18.46	18.32	18.22	18.18	18.26	18.10
Cr_2O_3	49.13	49.75	48.41	48.52	48.95	49.31	48.16	48.18	48.15	48.38
FeO^{tot}	18.68	18.23	18.06	17.56	18.16	18.16	18.15	18.60	17.84	17.93
MnO	0.22	0.24	0.25	0.24	0.23	0.25	0.25	0.27	0.24	0.26
MgO	13.83	13.77	13.59	13.78	13.72	13.69	13.82	13.77	13.56	13.98
NiO	0.10	0.12	0.17	0.21	0.11	0.12	0.18	0.18	0.32	0.29
Cr#	0.64	0.64	0.64	0.64	0.64	0.64	0.64	0.64	0.64	0.64
Mg#	0.64	0.63	0.64	0.65	0.64	0.64	0.65	0.64	0.64	0.66
Cr/Fe^{2+}	3.31	3.31	3.36	3.44	3.31	3.33	3.40	3.35	3.37	3.49

Sample	C51							
Anl#	1	2	3	4	5	6	7	8
TiO_2	0.12	0.10	0.13	0.12	0.11	0.11	0.11	0.11
V_2O_5	0.16	0.15	0.14	0.17	0.15	0.15	0.18	0.15
Al_2O_3	23.06	22.88	23.26	22.24	21.97	22.82	22.62	22.96
Cr_2O_3	47.07	46.01	46.32	47.09	46.43	46.50	46.36	45.79
FeO^{tot}	14.62	14.79	15.05	14.47	15.83	15.40	15.23	14.65
MnO	0.23	0.23	0.23	0.22	0.24	0.23	0.21	0.23
MgO	14.90	14.41	14.66	14.60	14.76	14.43	14.39	14.62
NiO	0.16	0.13	0.14	0.16	0.13	0.12	0.17	0.15
Cr#	0.58	0.57	0.57	0.59	0.59	0.58	0.58	0.57
Mg#	0.67	0.66	0.67	0.67	0.67	0.66	0.66	0.67
Cr/Fe^{2+}	3.47	3.33	3.33	3.49	3.46	3.29	3.32	3.42

Sample	C51 continued ...							
Anl#	9	10	11	12	13	14	15	16
TiO_2	0.11	0.13	0.11	0.12	0.13	0.12	0.11	0.11
V_2O_5	0.18	0.13	0.20	0.15	0.13	0.15	0.16	0.15
Al_2O_3	23.84	22.91	22.45	23.18	22.74	23.31	23.40	22.81
Cr_2O_3	46.89	46.84	46.28	45.82	47.32	47.31	47.94	47.26
FeO^{tot}	14.56	14.91	14.05	14.79	15.19	15.15	14.95	15.30
MnO	0.23	0.21	0.25	0.25	0.24	0.21	0.24	0.24
MgO	15.32	14.65	14.97	15.35	15.18	15.25	14.44	14.97
NiO	0.14	0.15	0.13	0.14	0.15	0.15	0.18	0.17
Cr#	0.57	0.58	0.58	0.57	0.58	0.58	0.58	0.58
Mg#	0.68	0.67	0.69	0.70	0.68	0.68	0.65	0.67
Cr/Fe^{2+}	3.51	3.39	3.64	3.61	3.56	3.50	3.26	3.46

Sample	C238									
Analysis#	1	2	3	4	5	6	7	8	9	10
TiO_2	0.09	0.10	0.09	0.10	0.09	0.10	0.10	0.10	0.11	0.11
V_2O_5	0.13	0.12	0.14	0.13	0.16	0.11	0.14	0.15	0.11	0.14
Al_2O_3	18.00	18.47	18.16	17.99	18.02	18.14	18.65	18.44	17.87	17.98
Cr_2O_3	51.28	50.64	52.47	52.41	51.32	51.14	51.16	50.84	51.85	51.77
FeO^{tot}	15.65	15.93	14.33	14.48	15.29	15.43	15.92	15.89	15.53	15.52
MnO	0.24	0.22	0.21	0.21	0.23	0.25	0.23	0.23	0.25	0.22
MgO	14.64	14.38	14.56	14.56	14.24	14.04	14.69	14.87	14.54	14.44
NiO	0.15	0.19	0.16	0.16	0.18	0.19	0.15	0.15	0.15	0.19
Cr#	0.66	0.65	0.66	0.66	0.66	0.65	0.65	0.65	0.66	0.66
Mg#	0.68	0.67	0.67	0.67	0.66	0.66	0.67	0.68	0.67	0.67
Cr/Fe^{2+}	3.91	3.73	3.95	3.96	3.79	3.71	3.80	3.90	3.89	3.83

Sample	C484									
Analysis#	1	2	3	4	5	6	7	8	9	10
TiO_2	0.14	0.12	0.11	0.10	0.09	0.10	0.13	0.12	0.13	0.14
V_2O_5	0.12	0.14	0.13	0.14	0.11	0.17	0.20	0.16	0.16	0.14
Al_2O_3	12.70	12.72	12.54	12.29	12.33	12.14	12.61	12.93	13.99	14.16
Cr_2O_3	56.83	56.22	56.37	57.16	57.15	57.03	56.98	56.30	55.81	56.07
FeO^{tot}	17.74	17.28	16.64	16.75	17.80	17.96	17.71	18.03	18.05	17.79
MnO	0.22	0.24	0.27	0.25	0.25	0.25	0.27	0.26	0.21	0.25
MgO	12.81	12.68	12.46	12.30	12.48	12.40	12.73	12.40	12.77	12.80
NiO	0.14	0.14	0.19	0.15	0.16	0.18	0.14	0.18	0.13	0.16
Cr#	0.75	0.75	0.75	0.76	0.76	0.76	0.75	0.74	0.73	0.73
Mg#	0.61	0.61	0.61	0.60	0.60	0.60	0.61	0.59	0.60	0.60
Cr/Fe^{2+}	3.68	3.69	3.71	3.66	3.64	3.61	3.66	3.53	3.50	3.52

Sample	C46							
Anls#	1	2	3	4	5	6	7	8
TiO_2	0.14	0.15	0.16	0.15	0.19	0.20	0.18	0.19
V_2O_5	0.13	0.12	0.13	0.16	0.13	0.08	0.12	0.09
Al_2O_3	10.34	10.45	10.74	10.44	11.89	13.55	13.74	13.51
Cr_2O_3	57.33	57.67	57.02	57.46	55.23	56.25	56.54	56.37
FeO^{tot}	18.82	19.08	19.06	19.16	18.00	16.23	15.67	15.39
MnO	0.24	0.28	0.26	0.28	0.24	0.26	0.24	0.21
MgO	12.41	12.14	12.48	12.33	12.77	12.88	13.22	12.94
NiO	0.17	0.17	0.18	0.15	0.15	0.15	0.12	0.14
Cr#	0.79	0.79	0.78	0.79	0.76	0.74	0.73	0.74
Mg#	0.60	0.59	0.61	0.60	0.62	0.62	0.63	0.62
Cr/Fe^{2+}	3.75	3.63	3.72	3.69	3.76	3.74	3.87	3.83

Sample	C46 continued ...							
Anl#	9	10	11	12	13	14	15	16
TiO_2	0.20	0.19	0.20	0.19	0.20	0.20	0.19	0.19
V_2O_5	0.08	0.07	0.08	0.09	0.11	0.08	0.11	0.11
Al_2O_3	13.98	13.95	14.07	14.00	13.21	12.99	13.18	13.28
Cr_2O_3	56.31	56.05	56.00	55.86	55.91	55.48	55.56	55.62
FeO^{tot}	15.75	15.49	15.73	15.68	16.50	16.44	16.75	16.38
MnO	0.24	0.22	0.22	0.23	0.25	0.23	0.24	0.23
MgO	13.35	13.17	13.38	13.01	12.85	12.84	12.89	12.82
NiO	0.15	0.13	0.11	0.14	0.14	0.16	0.12	0.15
Cr#	0.73	0.73	0.73	0.73	0.74	0.74	0.74	0.74
Mg#	0.63	0.63	0.64	0.62	0.62	0.62	0.62	0.62
Cr/Fe^{2+}	3.87	3.85	3.88	3.78	3.74	3.80	3.74	3.76

Sample	C40							
Anl#	1	2	3	4	5	6	7	8
TiO_2	0.05	0.06	0.05	0.05	0.04	0.06	0.05	0.04
V_2O_5	0.26	0.25	0.24	0.22	0.24	0.25	0.25	0.22
Al_2O_3	12.91	12.78	12.95	12.82	12.94	13.32	13.40	13.27
Cr_2O_3	56.49	57.39	56.72	57.82	56.81	57.13	57.35	57.40
FeO^{tot}	17.86	17.86	17.77	17.53	16.85	17.21	17.12	17.39
MnO	0.30	0.27	0.29	0.29	0.29	0.30	0.30	0.28
MgO	12.50	12.54	12.11	12.41	12.57	12.21	12.25	12.28
NiO	0.10	0.09	0.07	0.10	0.10	0.06	0.08	0.07
Cr#	0.75	0.75	0.75	0.75	0.75	0.74	0.74	0.74
Mg#	0.60	0.60	0.58	0.59	0.61	0.58	0.58	0.59
Cr/Fe^{2+}	3.57	3.58	3.47	3.58	3.68	3.49	3.50	3.51

Sample	C40 continued ...							
Anl#	9	10	11	12	13	14	15	16
TiO_2	0.06	0.06	0.06	0.05	0.06	0.05	0.04	0.04
V_2O_5	0.23	0.26	0.24	0.25	0.26	0.25	0.25	0.28
Al_2O_3	13.61	13.58	13.34	13.65	13.43	13.50	13.64	13.48
Cr_2O_3	57.51	57.13	56.58	56.80	55.89	55.87	55.67	55.83
FeO^{tot}	16.35	16.52	16.77	16.56	16.33	15.97	16.23	16.35
MnO	0.28	0.27	0.28	0.29	0.30	0.27	0.29	0.29
MgO	12.57	12.59	12.58	12.58	12.54	12.59	12.26	12.38
NiO	0.11	0.07	0.11	0.10	0.11	0.12	0.09	0.10
Cr#	0.74	0.74	0.74	0.74	0.74	0.74	0.73	0.74
Mg#	0.60	0.60	0.60	0.60	0.61	0.61	0.60	0.60
Cr/Fe^{2+}	3.62	3.61	3.64	3.62	3.66	3.69	3.56	3.60

Sample	C60										
Analysis#	1	2	3	4	5	6	7	8	9	10	11
TiO_2	0.03	0.02	0.03	0.02	0.03	0.02	0.04	0.04	0.02	0.03	0.03
V_2O_5	0.21	0.20	0.19	0.22	0.21	0.21	0.25	0.22	0.22	0.19	0.20
Al_2O_3	11.01	11.10	11.21	11.48	11.10	10.98	10.85	10.78	10.97	11.27	11.21
Cr_2O_3	58.48	58.27	58.11	58.16	58.05	58.53	58.81	57.46	57.98	59.48	58.78
FeO^{tot}	17.64	17.67	17.43	17.13	17.58	17.45	17.69	17.80	17.31	17.70	17.51
MnO	0.29	0.27	0.29	0.29	0.28	0.27	0.28	0.31	0.27	0.27	0.28
MgO	12.09	12.12	12.63	11.97	12.11	12.07	12.03	12.11	11.81	12.11	12.37
NiO	0.04	0.11	0.05	0.00	0.05	0.10	0.05	0.04	0.07	0.10	0.07
Cr#	0.78	0.78	0.78	0.77	0.78	0.78	0.78	0.78	0.78	0.78	0.78
Mg#	0.59	0.59	0.61	0.58	0.59	0.59	0.58	0.59	0.58	0.58	0.60
Cr/Fe^{2+}	3.65	3.66	3.82	3.61	3.66	3.68	3.64	3.69	3.62	3.63	3.72

Sample	C33								
Analysis#	1	2	3	4	5	6	7	8	9
TiO_2	0.15	0.11	0.11	0.12	0.10	0.11	0.09	0.11	0.12
V_2O_5	0.12	0.07	0.11	0.17	0.07	0.10	0.11	0.10	0.12
Al_2O_3	12.16	14.17	13.69	14.33	14.52	14.74	14.43	14.34	14.54
Cr_2O_3	57.78	56.43	56.36	55.98	56.19	56.54	56.84	55.79	55.52
FeO^{tot}	17.88	16.42	16.05	16.47	16.66	16.13	16.13	16.38	16.15
MnO	0.36	0.25	0.26	0.26	0.26	0.27	0.25	0.25	0.26
MgO	11.55	12.68	12.68	13.06	12.75	12.84	12.83	13.22	12.71
NiO	0.12	0.16	0.12	0.16	0.14	0.13	0.13	0.12	0.12
Cr#	0.76	0.73	0.73	0.72	0.72	0.72	0.73	0.72	0.72
Mg#	0.56	0.60	0.61	0.62	0.60	0.61	0.61	0.63	0.61
Cr/Fe^{2+}	3.39	3.61	3.69	3.68	3.57	3.61	3.63	3.75	3.59

Sample	C44									
Analysis#	1	2	3	4	5	6	7	8	9	10
TiO_2	0.15	0.13	0.14	0.14	0.14	0.14	0.12	0.13	0.14	0.13
V_2O_5	0.16	0.11	0.17	0.15	0.18	0.14	0.13	0.12	0.13	0.10
Al_2O_3	18.32	18.55	18.74	18.25	18.20	18.38	18.72	18.44	19.26	19.20
Cr_2O_3	50.73	50.41	51.19	50.74	50.78	50.56	50.97	50.98	49.50	49.53
FeO^{tot}	15.68	15.88	15.59	15.72	15.59	15.48	14.80	14.85	15.17	14.99
MnO	0.24	0.23	0.25	0.27	0.26	0.24	0.21	0.24	0.22	0.24
MgO	14.34	14.50	14.16	14.22	14.36	14.15	14.50	14.63	14.99	14.80
NiO	0.23	0.22	0.24	0.25	0.28	0.29	0.20	0.17	0.13	0.16
Cr#	0.65	0.65	0.65	0.65	0.65	0.65	0.65	0.65	0.63	0.63
Mg#	0.67	0.67	0.65	0.66	0.67	0.66	0.67	0.68	0.69	0.69
Cr/Fe^{2+}	3.75	3.78	3.64	3.73	3.79	3.71	3.84	3.92	3.92	3.90

Sample	C318									
Analysis#	1	2	3	4	5	6	7	8	9	10
TiO_2	0.14	0.14	0.15	0.15	0.14	0.13	0.15	0.14	0.15	0.15
V_2O_5	0.14	0.11	0.13	0.09	0.11	0.13	0.13	0.15	0.10	0.16
Al_2O_3	9.57	9.81	9.53	9.51	9.68	9.97	9.93	9.80	9.52	9.52
Cr_2O_3	59.42	59.78	59.46	59.66	59.77	59.91	59.58	59.52	59.97	59.96
FeO^{tot}	18.12	18.14	18.08	18.16	17.89	18.29	17.71	17.42	18.18	17.75
MnO	0.29	0.29	0.28	0.29	0.28	0.28	0.25	0.28	0.27	0.27
MgO	12.94	12.73	12.60	12.84	12.78	12.90	12.77	12.61	12.79	12.85
NiO	0.14	0.14	0.09	0.09	0.11	0.14	0.12	0.12	0.13	0.13
Cr#	0.81	0.80	0.81	0.81	0.81	0.80	0.80	0.80	0.81	0.81
Mg#	0.62	0.61	0.61	0.62	0.62	0.62	0.62	0.61	0.62	0.62
Cr/Fe^{2+}	4.04	3.94	3.93	4.01	3.99	3.95	3.96	3.95	3.98	4.03

Sample	C595									
Analysis#	1	2	3	4	5	6	7	8	9	10
TiO_2	0.13	0.13	0.13	0.11	0.11	0.11	0.13	0.14	0.11	0.12
V_2O_5	0.19	0.16	0.24	0.22	0.21	0.22	0.20	0.23	0.21	0.20
Al_2O_3	14.94	15.48	15.13	15.09	15.65	15.35	15.21	15.18	15.86	15.41
Cr_2O_3	56.45	56.38	56.72	56.76	56.34	55.93	56.34	55.93	55.59	55.50
FeO^{tot}	14.51	14.67	14.59	14.46	14.47	14.35	14.53	14.43	14.19	14.59
MnO	0.26	0.26	0.25	0.23	0.25	0.23	0.28	0.25	0.26	0.26
MgO	14.00	14.17	14.11	14.12	14.21	13.71	13.58	13.93	13.85	13.80
NiO	0.09	0.10	0.11	0.10	0.07	0.13	0.10	0.10	0.11	0.10
Cr#	0.72	0.71	0.72	0.72	0.71	0.71	0.71	0.71	0.70	0.71
Mg#	0.66	0.66	0.66	0.66	0.66	0.65	0.64	0.65	0.65	0.65
Cr/Fe^{2+}	4.07	4.05	4.06	4.08	4.05	3.94	3.89	4.02	3.95	3.95

Sample	C104									
Analysis#	1	2	3	4	5	6	7	8	9	10
TiO_2	0.09	0.10	0.10	0.12	0.10	0.08	0.11	0.11	0.10	0.08
V_2O_5	0.07	0.06	0.06	0.04	0.05	0.07	0.08	0.04	0.04	0.05
Al_2O_3	6.89	7.25	7.16	7.12	7.24	7.20	7.07	6.92	7.24	7.05
Cr_2O_3	64.23	64.79	65.32	63.92	64.39	64.72	64.29	64.28	64.54	63.84
FeO^{tot}	16.00	15.79	15.89	15.81	16.09	16.15	15.73	16.42	15.72	16.64
MnO	0.29	0.28	0.30	0.27	0.27	0.25	0.26	0.31	0.29	0.33
MgO	12.47	12.54	12.46	12.77	12.78	12.52	12.43	12.47	12.57	12.00
NiO	0.04	0.06	0.07	0.08	0.07	0.06	0.07	0.09	0.07	0.08
Cr#	0.86	0.86	0.86	0.86	0.86	0.86	0.86	0.86	0.86	0.86
Mg#	0.61	0.61	0.61	0.63	0.62	0.61	0.61	0.61	0.62	0.59
Cr/Fe^{2+}	4.35	4.33	4.30	4.47	4.40	4.29	4.33	4.32	4.37	4.14

Sample	C670									
Analysis#	1	2	3	4	5	6	7	8	9	10
TiO_2	0.08	0.08	0.09	0.08	0.09	0.09	0.10	0.08	0.08	0.09
V_2O_5	0.06	0.06	0.07	0.05	0.04	0.04	0.04	0.06	0.07	0.05
Al_2O_3	7.03	7.01	7.05	7.12	6.68	6.98	7.06	6.95	6.84	7.01
Cr_2O_3	64.96	66.02	65.64	66.06	66.39	67.28	65.94	65.57	65.74	65.67
FeO^{tot}	13.30	12.99	12.85	12.92	12.91	12.86	13.01	13.16	13.21	13.16
MnO	0.23	0.25	0.26	0.24	0.25	0.26	0.27	0.25	0.25	0.26
MgO	14.05	14.10	13.97	13.82	14.00	13.87	14.06	13.86	13.78	13.77
NiO	0.13	0.16	0.13	0.16	0.12	0.12	0.13	0.13	0.11	0.14
Cr#	0.86	0.86	0.86	0.86	0.87	0.87	0.86	0.86	0.87	0.86
Mg#	0.69	0.68	0.68	0.67	0.68	0.67	0.68	0.68	0.67	0.67
Cr/Fe^{2+}	5.38	5.40	5.35	5.23	5.40	5.23	5.37	5.28	5.23	5.21

Sample	C10							
Anl#	1	2	3	4	5	6	7	8
TiO_2	0.14	0.15	0.16	0.15	0.19	0.20	0.18	0.19
V_2O_5	0.13	0.12	0.13	0.16	0.13	0.08	0.12	0.09
Al_2O_3	10.34	10.45	10.74	10.44	11.89	13.55	13.74	13.51
Cr_2O_3	57.33	57.67	57.02	57.46	55.23	56.25	56.54	56.37
FeO^{tot}	18.82	19.08	19.06	19.16	18.00	16.23	15.67	15.39
MnO	0.24	0.28	0.26	0.28	0.24	0.26	0.24	0.21
MgO	12.41	12.14	12.48	12.33	12.77	12.88	13.22	12.94
NiO	0.17	0.17	0.18	0.15	0.15	0.15	0.12	0.14
Cr#	0.79	0.79	0.78	0.79	0.76	0.74	0.73	0.74
Mg#	0.60	0.59	0.61	0.60	0.62	0.62	0.63	0.62
Cr/Fe^{2+}	3.75	3.63	3.72	3.69	3.76	3.74	3.87	3.83

Sample	C10 continued							
Anl#	9	10	11	12	13	14	15	16
TiO_2	0.20	0.19	0.20	0.19	0.20	0.20	0.19	0.19
V_2O_5	0.08	0.07	0.08	0.09	0.11	0.08	0.11	0.11
Al_2O_3	13.98	13.95	14.07	14.00	13.21	12.99	13.18	13.28
Cr_2O_3	56.31	56.05	56.00	55.86	55.91	55.48	55.56	55.62
FeO^{tot}	15.75	15.49	15.73	15.68	16.50	16.44	16.75	16.38
MnO	0.24	0.22	0.22	0.23	0.25	0.23	0.24	0.23
MgO	13.35	13.17	13.38	13.01	12.85	12.84	12.89	12.82
NiO	0.15	0.13	0.11	0.14	0.14	0.16	0.12	0.15
Cr#	0.73	0.73	0.73	0.73	0.74	0.74	0.74	0.74
Mg#	0.63	0.63	0.64	0.62	0.62	0.62	0.62	0.62
Cr/Fe^{2+}	3.87	3.85	3.88	3.78	3.74	3.80	3.74	3.76

Sample	C655								
Analysis#	1	2	3	4	5	6	7	8	9
TiO_2	0.03	0.04	0.02	0.04	0.03	0.04	0.02	0.02	0.03
V_2O_5	0.10	0.10	0.10	0.09	0.09	0.09	0.07	0.08	0.10
Al_2O_3	4.03	4.12	3.97	4.04	3.78	3.99	3.61	3.58	3.97
Cr_2O_3	68.79	67.91	67.52	67.54	67.91	67.83	68.12	67.73	67.38
FeO^{tot}	14.59	14.39	14.68	14.57	14.34	14.32	13.95	14.18	14.49
MnO	0.29	0.28	0.28	0.26	0.29	0.29	0.26	0.31	0.29
MgO	12.83	12.51	12.92	12.89	12.79	12.79	12.62	12.77	12.44
NiO	0.09	0.09	0.07	0.05	0.07	0.06	0.08	0.08	0.08
Cr#	0.92	0.92	0.92	0.92	0.92	0.92	0.93	0.93	0.92
Mg#	0.64	0.63	0.65	0.64	0.64	0.64	0.64	0.65	0.63
Cr/Fe^{2+}	4.98	4.88	5.08	5.05	5.08	5.04	5.08	5.16	4.89

Sample	C123									
Analysis#	1	2	3	4	5	6	7	8	9	10
TiO_2	0.27	0.28	0.28	0.28	0.29	0.27	0.28	0.26	0.29	0.28
V_2O_5	0.05	0.07	0.09	0.10	0.08	0.06	0.11	0.09	0.07	0.11
Al_2O_3	12.03	12.18	12.24	12.54	12.28	12.21	11.99	11.82	12.60	12.62
Cr_2O_3	57.25	56.92	56.88	56.98	57.43	56.74	56.82	56.85	57.60	58.07
FeO^{tot}	16.47	16.70	16.12	16.08	16.64	16.38	16.53	16.43	15.79	15.34
MnO	0.21	0.24	0.23	0.21	0.22	0.23	0.23	0.21	0.22	0.24
MgO	14.54	14.44	14.56	14.37	14.12	14.04	14.54	14.28	14.26	14.41
NiO	0.22	0.23	0.22	0.18	0.23	0.25	0.24	0.22	0.20	0.20
Cr#	0.76	0.76	0.76	0.75	0.76	0.76	0.76	0.76	0.75	0.76
Mg#	0.68	0.68	0.69	0.68	0.66	0.67	0.69	0.68	0.67	0.67
Cr/Fe^{2+}	4.51	4.42	4.53	4.38	4.25	4.31	4.52	4.44	4.35	4.44

Sample	C205									
Analysis#	1	2	3	4	5	6	7	8	9	10
TiO_2	0.06	0.07	0.06	0.06	0.06	0.07	0.07	0.07	0.05	0.07
V_2O_5	0.10	0.07	0.07	0.06	0.08	0.10	0.08	0.11	0.05	0.06
Al_2O_3	6.76	6.85	6.58	6.62	6.60	6.63	6.55	6.80	6.44	6.50
Cr_2O_3	66.47	66.42	66.14	66.61	66.89	66.29	66.13	65.67	65.91	66.37
FeO^{tot}	12.52	12.40	12.44	12.62	12.27	12.17	12.02	12.13	12.09	12.21
MnO	0.26	0.23	0.24	0.22	0.25	0.22	0.23	0.21	0.25	0.24
MgO	14.99	14.81	14.96	14.93	14.89	14.99	14.89	14.87	14.97	14.95
NiO	0.13	0.17	0.15	0.16	0.17	0.17	0.14	0.15	0.15	0.14
Cr#	0.87	0.87	0.87	0.87	0.87	0.87	0.87	0.87	0.87	0.87
Mg#	0.72	0.71	0.72	0.72	0.72	0.72	0.72	0.72	0.73	0.72
Cr/Fe^{2+}	6.05	5.95	6.14	6.03	6.06	6.16	6.16	6.08	6.30	6.18

Sample	C206									
Analysis#	1	2	3	4	5	6	7	8	9	10
TiO_2	0.06	0.06	0.07	0.07	0.09	0.08	0.07	0.08	0.08	0.07
V_2O_5	0.08	0.06	0.08	0.08	0.09	0.07	0.06	0.08	0.08	0.09
Al_2O_3	6.73	6.82	6.70	6.87	6.96	6.67	6.90	6.75	6.89	6.66
Cr_2O_3	65.57	66.40	65.41	65.28	64.19	64.42	63.99	64.22	65.87	64.63
FeO^{tot}	12.57	12.24	12.35	12.42	12.45	12.19	12.26	12.29	12.26	12.24
MnO	0.26	0.25	0.25	0.21	0.26	0.25	0.25	0.24	0.24	0.24
MgO	14.93	15.03	14.90	14.68	14.42	14.72	14.71	14.71	14.61	14.78
NiO	0.17	0.15	0.16	0.13	0.18	0.17	0.17	0.18	0.16	0.16
Cr#	0.87	0.87	0.87	0.86	0.86	0.87	0.86	0.86	0.86	0.87
Mg#	0.72	0.72	0.73	0.71	0.71	0.73	0.73	0.73	0.71	0.73
Cr/Fe^{2+}	6.11	6.14	6.15	5.92	5.83	6.16	6.13	6.12	5.86	6.16

Sample	C207									
Analysis#	1	2	3	4	5	6	7	8	9	10
TiO_2	0.06	0.06	0.05	0.05	0.06	0.05	0.05	0.06	0.05	0.06
V_2O_5	0.09	0.09	0.11	0.07	0.09	0.08	0.07	0.07	0.08	0.09
Al_2O_3	5.89	6.07	6.10	5.88	5.94	5.78	5.77	5.78	6.15	5.98
Cr_2O_3	65.73	66.15	66.59	66.39	65.89	66.35	67.28	66.34	66.36	66.37
FeO^{tot}	12.65	12.87	13.03	13.09	12.69	12.66	12.92	12.80	12.74	12.97
MnO	0.25	0.23	0.23	0.25	0.25	0.26	0.27	0.23	0.23	0.22
MgO	14.14	14.06	14.39	14.26	14.45	14.21	14.14	14.14	14.39	14.23
NiO	0.11	0.14	0.14	0.15	0.15	0.13	0.14	0.12	0.13	0.14
Cr#	0.88	0.88	0.88	0.88	0.88	0.89	0.89	0.88	0.88	0.88
Mg#	0.70	0.69	0.70	0.70	0.71	0.70	0.69	0.70	0.70	0.70
Cr/Fe^{2+}	5.75	5.58	5.71	5.72	5.93	5.79	5.64	5.71	5.79	5.68

Sample	C210									
Analysis#	1	2	3	4	5	6	7	8	9	10
TiO_2	0.07	0.05	0.06	0.06	0.06	0.05	0.05	0.04	0.05	0.05
V_2O_5	0.05	0.09	0.09	0.10	0.10	0.11	0.07	0.06	0.08	0.09
Al_2O_3	6.13	5.88	6.02	5.99	5.84	5.85	5.95	6.01	5.80	5.67
Cr_2O_3	65.64	66.11	65.55	65.69	65.63	66.52	66.09	66.06	65.57	66.25
FeO^{tot}	13.45	13.46	13.02	13.40	13.26	13.22	13.22	13.59	13.10	13.12
MnO	0.25	0.24	0.25	0.27	0.24	0.26	0.25	0.28	0.26	0.25
MgO	14.08	14.06	13.68	13.89	13.89	14.40	13.73	13.88	14.08	13.57
NiO	0.13	0.15	0.12	0.13	0.14	0.16	0.14	0.15	0.13	0.14
Cr#	0.88	0.88	0.88	0.88	0.88	0.88	0.88	0.88	0.88	0.89
Mg#	0.69	0.69	0.68	0.69	0.69	0.70	0.68	0.68	0.70	0.67
Cr/Fe^{2+}	5.54	5.55	5.40	5.46	5.51	5.78	5.40	5.43	5.69	5.37

Sample	C211							
Analysis#	1	2	3	4	5	6	7	8
TiO_2	0.07	0.09	0.08	0.08	0.09	0.10	0.07	0.08
V_2O_5	0.12	0.06	0.08	0.04	0.07	0.08	0.11	0.09
Al_2O_3	6.42	6.71	6.45	6.64	6.55	6.80	6.33	6.56
Cr_2O_3	66.56	66.54	65.80	66.35	65.24	64.97	65.66	65.18
FeO^{tot}	13.00	12.81	12.76	12.95	12.89	12.73	12.65	12.68
MnO	0.27	0.25	0.26	0.27	0.25	0.24	0.27	0.25
MgO	14.33	14.33	14.29	14.58	14.40	14.20	14.32	14.22
NiO	0.13	0.18	0.16	0.16	0.17	0.17	0.15	0.14
Cr#	0.87	0.87	0.87	0.87	0.87	0.86	0.87	0.87
Mg#	0.69	0.69	0.70	0.70	0.71	0.70	0.70	0.70
Cr/Fe^{2+}	5.61	5.60	5.69	5.76	5.76	5.60	5.77	5.67

Sample	C212									
Analysis#	1	2	3	4	5	6	7	8	9	10
TiO_2	0.05	0.06	0.05	0.04	0.04	0.05	0.09	0.08	0.07	0.08
V_2O_5	0.10	0.09	0.08	0.09	0.09	0.08	0.09	0.08	0.11	0.08
Al_2O_3	6.78	6.79	6.32	6.26	6.24	6.58	7.84	7.85	7.45	7.15
Cr_2O_3	65.16	65.19	66.69	66.59	67.15	66.86	63.26	63.37	64.07	64.55
FeO^{tot}	13.65	13.46	13.19	13.38	13.12	13.20	13.30	13.67	13.35	13.39
MnO	0.25	0.24	0.20	0.22	0.23	0.26	0.26	0.27	0.27	0.26
MgO	14.20	14.07	14.17	14.38	14.35	14.03	14.03	13.92	13.96	14.11
NiO	0.11	0.14	0.13	0.13	0.16	0.16	0.16	0.12	0.16	0.18
Cr#	0.87	0.87	0.88	0.88	0.88	0.87	0.84	0.84	0.85	0.86
Mg#	0.69	0.69	0.69	0.70	0.69	0.68	0.69	0.68	0.68	0.69
Cr/Fe^{2+}	5.44	5.40	5.50	5.62	5.62	5.38	5.30	5.17	5.29	5.41

Sample	C213									
Analysis#	1	2	3	4	5	6	7	8	9	10
TiO_2	0.07	0.08	0.07	0.07	0.07	0.07	0.06	0.06	0.07	0.07
V_2O_5	0.10	0.09	0.07	0.09	0.11	0.11	0.08	0.07	0.09	0.07
Al_2O_3	6.43	6.58	6.08	6.31	6.58	6.64	5.81	6.22	6.39	6.52
Cr_2O_3	66.70	66.65	66.23	65.88	65.45	65.92	66.59	66.42	65.53	65.60
FeO^{tot}	12.96	12.96	12.69	13.00	12.64	12.81	13.16	13.07	13.09	13.07
MnO	0.28	0.26	0.26	0.22	0.28	0.25	0.30	0.26	0.26	0.26
MgO	14.27	14.17	14.04	14.03	14.13	14.10	14.17	14.14	14.36	14.35
NiO	0.13	0.14	0.15	0.12	0.12	0.15	0.12	0.14	0.12	0.17
Cr#	0.87	0.87	0.88	0.88	0.87	0.87	0.88	0.88	0.87	0.87
Mg#	0.69	0.69	0.69	0.69	0.69	0.69	0.69	0.69	0.70	0.70
Cr/Fe^{2+}	5.58	5.48	5.61	5.50	5.59	5.50	5.65	5.56	5.70	5.69

Sample	C214									
Analysis#	1	2	3	4	5	6	7	8	9	10
TiO_2	0.06	0.07	0.06	0.06	0.05	0.05	0.05	0.06	0.06	0.04
V_2O_5	0.07	0.11	0.09	0.10	0.10	0.08	0.09	0.10	0.10	0.09
Al_2O_3	5.99	5.96	6.12	6.12	5.93	5.86	5.97	6.13	5.84	5.98
Cr_2O_3	66.52	66.59	66.29	66.45	65.67	65.89	65.73	66.04	66.19	65.38
FeO^{tot}	12.47	12.71	13.21	12.61	12.92	12.52	13.08	13.03	12.55	12.67
MnO	0.27	0.29	0.27	0.25	0.27	0.24	0.24	0.25	0.25	0.23
MgO	14.23	14.06	14.37	14.45	14.16	13.90	14.20	14.17	14.22	14.35
NiO	0.15	0.13	0.13	0.15	0.14	0.15	0.16	0.16	0.14	0.12
Cr#	0.88	0.88	0.88	0.88	0.88	0.88	0.88	0.88	0.88	0.88
Mg#	0.70	0.69	0.70	0.71	0.70	0.69	0.70	0.69	0.70	0.71
Cr/Fe^{2+}	5.78	5.61	5.71	5.85	5.73	5.64	5.70	5.62	5.79	5.89

Sample	C215									
Analysis#	1	2	3	4	5	6	7	8	9	10
TiO_2	0.06	0.06	0.06	0.06	0.06	0.06	0.05	0.07	0.05	0.06
V_2O_5	0.06	0.06	0.07	0.07	0.12	0.09	0.10	0.09	0.09	0.08
Al_2O_3	6.33	6.13	5.87	6.04	6.66	6.45	6.65	6.66	5.98	6.24
Cr_2O_3	66.47	65.83	65.72	65.89	65.98	66.07	64.91	65.15	65.92	65.01
FeO^{tot}	13.19	13.32	13.20	13.31	13.17	12.96	13.33	13.10	13.32	13.62
MnO	0.26	0.27	0.24	0.29	0.27	0.27	0.28	0.26	0.26	0.26
MgO	14.27	14.18	14.16	13.88	14.10	14.35	14.21	14.11	14.14	13.97
NiO	0.10	0.12	0.13	0.13	0.13	0.11	0.11	0.12	0.11	0.10
Cr#	0.88	0.88	0.88	0.88	0.87	0.87	0.87	0.87	0.88	0.87
Mg#	0.69	0.69	0.70	0.68	0.69	0.70	0.70	0.69	0.69	0.69
Cr/Fe^{2+}	5.59	5.61	5.68	5.46	5.44	5.67	5.56	5.51	5.61	5.45

Shetland Chromitite Samples

Sample	CF1									
Analysis#	1	2	3	4	5	6	7	8	9	10
TiO_2	0.16	0.17	0.17	0.16	0.16	0.13	0.19	0.19	0.18	0.17
V_2O_5	0.13	0.16	0.13	0.13	0.12	0.13	0.12	0.14	0.14	0.12
Al_2O_3	17.94	17.92	17.90	18.14	18.20	18.29	17.90	18.14	18.17	18.48
Cr_2O_3	51.55	51.79	50.87	50.65	50.88	51.85	50.87	50.65	50.88	51.27
FeO^{tot}	15.10	14.88	15.15	15.10	14.54	14.86	15.15	15.10	15.43	15.35
MnO	0.24	0.24	0.24	0.22	0.22	0.26	0.24	0.22	0.25	0.24
MgO	15.54	15.39	15.13	15.25	15.76	15.64	15.13	15.25	15.67	15.63
NiO	0.14	0.13	0.15	0.14	0.14	0.14	0.15	0.14	0.12	0.13
Cr#	0.66	0.66	0.66	0.65	0.65	0.66	0.66	0.65	0.65	0.65
Mg#	0.71	0.70	0.70	0.70	0.72	0.71	0.70	0.70	0.71	0.71
Cr/Fe^{2+}	4.31	4.25	4.15	4.17	4.46	4.33	4.15	4.16	4.29	4.23

Sample	CF2									
Analysis#	1	2	3	4	5	6	7	8	9	10
TiO_2	0.17	0.17	0.17	0.16	0.15	0.14	0.16	0.15	0.16	0.17
V_2O_5	0.12	0.11	0.18	0.14	0.15	0.13	0.14	0.13	0.16	0.15
Al_2O_3	20.84	20.55	20.47	20.44	20.52	20.33	19.97	19.96	20.34	20.21
Cr_2O_3	48.30	47.89	47.99	47.61	47.94	48.10	48.32	48.00	47.53	48.36
FeO^{tot}	14.77	14.90	15.12	15.18	14.67	14.54	15.31	14.99	15.15	14.92
MnO	0.24	0.22	0.23	0.22	0.24	0.25	0.24	0.20	0.23	0.24
MgO	16.24	16.17	15.65	16.02	15.88	16.28	15.99	15.97	16.01	16.07
NiO	0.07	0.07	0.08	0.09	0.09	0.06	0.10	0.07	0.07	0.06
Cr#	0.61	0.61	0.61	0.61	0.61	0.61	0.62	0.62	0.61	0.62
Mg#	0.73	0.73	0.71	0.73	0.72	0.74	0.72	0.73	0.73	0.73
Cr/Fe^{2+}	4.25	4.27	4.00	4.19	4.16	4.41	4.22	4.26	4.19	4.25

Sample	CF3									
Analysis#	1	2	3	4	5	6	7	8	9	10
TiO_2	0.15	0.17	0.19	0.17	0.18	0.17	0.16	0.16	0.15	0.17
V_2O_5	0.14	0.13	0.11	0.14	0.11	0.15	0.11	0.12	0.15	0.14
Al_2O_3	19.58	19.81	19.99	20.22	20.07	20.04	19.90	20.05	20.08	19.81
Cr_2O_3	48.72	48.58	46.86	47.22	48.46	48.34	48.09	48.04	48.08	47.72
FeO^{tot}	16.34	16.33	16.33	16.34	16.12	15.76	15.91	15.84	15.60	15.65
MnO	0.23	0.25	0.20	0.22	0.28	0.25	0.23	0.22	0.22	0.23
MgO	14.90	14.87	14.89	14.96	15.11	15.37	15.30	15.27	15.48	15.37
NiO	0.17	0.16	0.26	0.21	0.20	0.21	0.09	0.10	0.08	0.09
Cr#	0.63	0.62	0.61	0.61	0.62	0.62	0.62	0.62	0.62	0.62
Mg#	0.68	0.68	0.69	0.69	0.69	0.70	0.70	0.70	0.71	0.71
Cr/Fe^{2+}	3.73	3.69	3.71	3.69	3.78	3.91	3.88	3.85	3.95	3.95

Sample	CF4								
Analysis#	1	2	3	4	5	6	7	8	9
TiO_2	0.18	0.17	0.19	0.18	0.17	0.19	0.18	0.18	0.18
V_2O_5	0.14	0.14	0.11	0.11	0.14	0.16	0.10	0.12	0.12
Al_2O_3	18.08	18.13	18.38	18.60	17.72	18.11	18.07	18.51	18.00
Cr_2O_3	50.07	50.81	48.82	49.13	50.51	50.93	50.78	50.32	50.81
FeO^{tot}	15.38	14.80	17.07	16.68	14.96	15.36	15.42	15.26	14.96
MnO	0.23	0.26	0.28	0.29	0.23	0.24	0.22	0.25	0.22
MgO	15.11	15.30	13.96	13.99	15.66	15.47	15.15	15.50	15.30
NiO	0.15	0.11	0.12	0.15	0.15	0.14	0.14	0.12	0.11
Cr#	0.65	0.65	0.64	0.64	0.66	0.65	0.65	0.65	0.65
Mg#	0.70	0.71	0.65	0.65	0.72	0.71	0.70	0.71	0.71
Cr/Fe^{2+}	4.10	4.22	3.50	3.52	4.46	4.22	4.10	4.21	4.22

Sample	CF5									
Analysis#	1	2	3	4	5	6	7	8	9	10
TiO_2	0.17	0.17	0.19	0.19	0.18	0.18	0.17	0.18	0.17	0.17
V_2O_5	0.17	0.13	0.17	0.13	0.12	0.14	0.11	0.12	0.12	0.12
Al_2O_3	17.68	17.35	17.58	17.78	18.19	18.20	17.52	17.40	17.49	17.62
Cr_2O_3	50.56	50.23	50.69	50.60	51.74	51.21	50.34	50.41	50.85	50.88
FeO^{tot}	15.27	15.11	14.95	14.98	14.51	14.52	15.17	15.10	14.87	14.69
MnO	0.25	0.23	0.22	0.22	0.21	0.19	0.24	0.26	0.23	0.23
MgO	15.65	15.40	15.16	15.48	15.81	15.67	15.34	15.24	15.60	15.21
NiO	0.15	0.17	0.12	0.13	0.10	0.11	0.15	0.17	0.10	0.13
Cr#	0.66	0.66	0.66	0.66	0.66	0.65	0.66	0.66	0.66	0.66
Mg#	0.72	0.72	0.70	0.71	0.72	0.72	0.71	0.71	0.72	0.71
Cr/Fe^{2+}	4.41	4.40	4.22	4.34	4.44	4.38	4.34	4.32	4.47	4.29

Sample	CF6									
Analysis#	1	2	3	4	5	6	7	8	9	10
TiO_2	0.14	0.15	0.15	0.15	0.16	0.17	0.16	0.16	0.16	0.16
V_2O_5	0.14	0.12	0.12	0.16	0.14	0.15	0.10	0.12	0.14	0.12
Al_2O_3	19.56	19.62	20.16	20.37	20.67	20.81	20.15	20.06	19.78	19.77
Cr_2O_3	48.76	49.24	47.83	47.75	48.42	48.68	47.33	47.54	46.79	47.69
FeO^{tot}	16.27	16.47	16.24	16.84	16.04	15.68	19.17	19.15	20.20	20.27
MnO	0.27	0.26	0.29	0.23	0.24	0.26	0.29	0.28	0.31	0.28
MgO	15.29	14.96	15.12	15.02	15.17	15.16	13.19	13.14	12.50	12.88
NiO	0.29	0.27	0.20	0.20	0.31	0.31	0.19	0.18	0.10	0.12
Cr#	0.63	0.63	0.61	0.61	0.61	0.61	0.61	0.61	0.61	0.62
Mg#	0.70	0.68	0.69	0.68	0.69	0.69	0.61	0.61	0.58	0.59
Cr/Fe^{2+}	3.93	3.76	3.78	3.63	3.74	3.74	2.97	2.96	2.77	2.85

Sample	CF8									
Analysis#	1	2	3	4	5	6	7	8	9	10
TiO_2	0.19	0.18	0.18	0.17	0.19	0.18	0.20	0.20	0.17	0.19
V_2O_5	0.13	0.13	0.13	0.11	0.14	0.11	0.11	0.12	0.13	0.10
Al_2O_3	17.50	17.66	18.18	18.02	18.12	18.27	18.33	18.46	18.31	18.13
Cr_2O_3	51.68	51.93	50.08	49.72	50.37	50.59	51.39	51.55	50.77	51.00
FeO^{tot}	14.56	14.61	14.99	14.93	14.55	14.76	14.42	14.25	14.37	14.55
MnO	0.23	0.23	0.23	0.25	0.23	0.26	0.23	0.22	0.26	0.19
MgO	15.28	15.16	15.34	15.44	15.63	15.68	15.72	15.70	15.45	15.17
NiO	0.13	0.14	0.13	0.10	0.15	0.13	0.11	0.16	0.14	0.15
Cr#	0.66	0.66	0.65	0.65	0.65	0.65	0.65	0.65	0.65	0.65
Mg#	0.71	0.70	0.71	0.72	0.72	0.72	0.72	0.72	0.71	0.70
Cr/Fe^{2+}	4.32	4.23	4.23	4.33	4.41	4.40	4.40	4.38	4.33	4.19

Sample	CF9								
Analysis#	1	2	3	4	5	6	7	8	9
TiO_2	0.05	0.04	0.04	0.05	0.06	0.06	0.05	0.06	0.05
V_2O_5	0.24	0.20	0.16	0.15	0.18	0.16	0.15	0.14	0.15
Al_2O_3	12.09	11.92	10.62	10.58	11.98	11.94	11.59	10.41	10.25
Cr_2O_3	57.58	57.31	59.96	59.85	57.98	57.98	57.94	57.60	57.61
FeO^{tot}	16.23	16.27	15.53	15.60	15.40	15.53	15.14	18.07	18.13
MnO	0.29	0.33	0.29	0.28	0.25	0.26	0.29	0.34	0.34
MgO	12.77	13.03	13.57	13.41	13.94	13.67	14.04	12.74	12.72
NiO	0.10	0.09	0.14	0.15	0.11	0.14	0.16	0.15	0.15
Cr#	0.76	0.76	0.79	0.79	0.76	0.76	0.77	0.79	0.79
Mg#	0.62	0.63	0.65	0.65	0.67	0.66	0.68	0.62	0.62
Cr/Fe^{2+}	3.86	3.99	4.41	4.35	4.40	4.29	4.57	3.94	3.95

Sample	CF10									
Analysis#	1	2	3	4	5	6	7	8	9	10
TiO_2	0.10	0.09	0.11	0.12	0.10	0.11	0.11	0.10	0.10	0.12
V_2O_5	0.11	0.13	0.16	0.13	0.18	0.12	0.10	0.13	0.14	0.11
Al_2O_3	17.97	18.12	18.13	18.24	18.63	18.46	18.27	18.08	18.09	18.26
Cr_2O_3	51.20	50.84	50.27	50.26	49.76	50.11	49.99	50.10	50.04	50.20
FeO^{tot}	14.23	14.61	14.57	14.34	14.49	14.00	14.41	14.27	14.50	14.57
MnO	0.23	0.23	0.21	0.22	0.22	0.24	0.25	0.21	0.23	0.22
MgO	15.47	15.60	15.47	15.49	15.83	15.63	15.59	15.65	15.40	15.29
NiO	0.13	0.13	0.14	0.16	0.08	0.11	0.18	0.17	0.14	0.11
Cr#	0.66	0.65	0.65	0.65	0.64	0.65	0.65	0.65	0.65	0.65
Mg#	0.72	0.72	0.72	0.72	0.73	0.72	0.72	0.73	0.72	0.71
Cr/Fe^{2+}	4.43	4.43	4.36	4.40	4.46	4.48	4.47	4.54	4.38	4.27

Sample	CF11									
Analysis#	1	2	3	4	5	6	7	8	9	10
TiO_2	0.08	0.08	0.08	0.10	0.06	0.06	0.04	0.03	0.08	0.09
V_2O_5	0.16	0.14	0.17	0.17	0.16	0.17	0.15	0.12	0.15	0.12
Al_2O_3	19.58	19.34	19.62	19.56	19.35	19.45	18.39	18.66	20.45	20.26
Cr_2O_3	50.07	50.45	50.13	50.25	50.87	50.84	50.93	50.54	49.10	49.43
FeO^{tot}	13.68	13.73	14.02	13.72	14.08	14.11	14.61	14.44	13.76	13.69
MnO	0.26	0.23	0.23	0.21	0.22	0.20	0.23	0.24	0.21	0.22
MgO	15.25	15.22	15.20	15.17	15.15	15.23	14.90	14.98	15.14	15.53
NiO	0.22	0.22	0.25	0.23	0.20	0.19	0.17	0.13	0.22	0.20
Cr#	0.63	0.64	0.63	0.63	0.64	0.64	0.65	0.64	0.62	0.62
Mg#	0.71	0.70	0.70	0.70	0.70	0.70	0.69	0.70	0.70	0.71
Cr/Fe^{2+}	4.17	4.18	4.10	4.10	4.09	4.09	4.09	4.12	3.99	4.19

Sample	CF12									
Analysis#	1	2	3	4	5	6	7	8	9	10
TiO_2	0.17	0.16	0.16	0.16	0.16	0.17	0.15	0.17	0.16	0.16
V_2O_5	0.14	0.12	0.13	0.14	0.13	0.14	0.13	0.12	0.16	0.17
Al_2O_3	20.11	20.10	19.91	20.24	20.29	20.23	20.29	20.37	20.45	20.20
Cr_2O_3	48.04	48.07	48.47	48.25	48.67	48.37	48.29	48.75	48.16	47.99
FeO^{tot}	15.40	15.04	15.38	15.91	15.56	15.87	15.35	15.21	15.10	15.16
MnO	0.24	0.22	0.23	0.24	0.25	0.22	0.24	0.21	0.23	0.22
MgO	15.43	15.45	15.07	15.62	15.56	15.58	15.74	15.68	15.68	15.53
NiO	0.11	0.13	0.11	0.09	0.11	0.11	0.10	0.11	0.14	0.14
Cr#	0.62	0.62	0.62	0.62	0.62	0.62	0.61	0.62	0.61	0.61
Mg#	0.71	0.71	0.69	0.71	0.70	0.70	0.71	0.71	0.71	0.71
Cr/Fe^{2+}	3.95	4.01	3.84	3.94	3.95	3.93	4.06	4.01	4.03	4.00

Sample	CF13								
Analysis#	1	2	3	4	5	6	7	8	9
TiO_2	0.17	0.16	0.17	0.17	0.15	0.17	0.16	0.17	0.15
V_2O_5	0.15	0.10	0.14	0.14	0.12	0.13	0.11	0.12	0.15
Al_2O_3	19.77	19.80	19.49	19.69	19.56	19.85	19.71	19.61	19.73
Cr_2O_3	47.87	47.89	48.06	48.02	47.97	48.24	48.26	47.73	47.89
FeO^{tot}	17.37	17.31	14.89	15.04	14.58	14.49	15.02	15.48	14.95
MnO	0.23	0.26	0.19	0.24	0.22	0.23	0.20	0.22	0.22
MgO	13.45	13.87	16.00	16.04	15.81	15.93	15.86	15.49	15.35
NiO	0.11	0.09	0.14	0.15	0.16	0.17	0.15	0.16	0.10
Cr#	0.62	0.62	0.62	0.62	0.62	0.62	0.62	0.62	0.62
Mg#	0.63	0.64	0.73	0.73	0.73	0.73	0.73	0.71	0.71
Cr/Fe^{2+}	3.16	3.30	4.38	4.36	4.35	4.35	4.27	4.08	4.03

Sample	CF14									
Analysis#	1	2	3	4	5	6	7	8	9	10
TiO_2	0.08	0.07	0.08	0.07	0.09	0.08	0.11	0.12	0.08	0.06
V_2O_5	0.14	0.15	0.14	0.12	0.16	0.15	0.14	0.15	0.14	0.13
Al_2O_3	14.68	14.72	14.69	14.79	15.22	15.00	16.92	17.10	14.45	14.56
Cr_2O_3	54.05	54.05	54.27	53.98	53.70	53.46	51.76	51.68	53.61	53.40
FeO^{tot}	15.75	16.28	15.18	15.43	15.23	15.27	15.49	14.92	16.76	16.75
MnO	0.26	0.27	0.27	0.24	0.21	0.26	0.24	0.26	0.27	0.30
MgO	13.84	13.84	14.43	14.35	14.57	14.46	14.37	14.53	13.21	13.20
NiO	0.17	0.12	0.15	0.16	0.09	0.12	0.08	0.08	0.10	0.12
Cr#	0.71	0.71	0.71	0.71	0.70	0.70	0.67	0.67	0.71	0.71
Mg#	0.66	0.66	0.68	0.68	0.69	0.69	0.67	0.68	0.63	0.64
Cr/Fe^{2+}	4.03	3.96	4.32	4.26	4.27	4.28	3.94	4.04	3.74	3.81

Sample	CF15									
Analysis#	1	2	3	4	5	6	7	8	9	10
TiO_2	0.16	0.19	0.19	0.17	0.17	0.16	0.17	0.16	0.17	0.18
V_2O_5	0.09	0.15	0.14	0.14	0.11	0.15	0.09	0.15	0.14	0.13
Al_2O_3	19.18	19.28	19.21	19.03	19.04	19.34	18.91	19.19	19.19	19.12
Cr_2O_3	48.09	48.58	48.76	49.11	48.62	48.90	48.42	48.64	48.72	48.42
FeO^{tot}	16.37	16.64	15.94	15.23	15.53	15.47	18.07	17.78	17.03	17.52
MnO	0.23	0.24	0.23	0.26	0.24	0.18	0.27	0.24	0.26	0.25
MgO	14.52	14.72	15.37	15.27	15.44	15.28	13.15	13.39	13.84	14.05
NiO	0.09	0.12	0.13	0.14	0.08	0.11	0.11	0.09	0.11	0.09
Cr#	0.63	0.63	0.63	0.63	0.63	0.63	0.63	0.63	0.63	0.63
Mg#	0.68	0.68	0.70	0.70	0.71	0.70	0.62	0.62	0.64	0.65
Cr/Fe^{2+}	3.66	3.66	3.99	4.06	4.10	3.97	3.14	3.18	3.37	3.45

Sample	CF16									
Analysis#	1	2	3	4	5	6	7	8	9	10
TiO_2	0.07	0.08	0.09	0.08	0.09	0.07	0.09	0.08	0.09	0.09
V_2O_5	0.16	0.18	0.17	0.13	0.20	0.11	0.13	0.15	0.16	0.15
Al_2O_3	16.15	15.83	16.08	15.89	15.66	15.59	16.01	16.05	15.64	15.62
Cr_2O_3	53.35	53.55	54.39	54.31	54.04	54.58	54.23	54.12	53.50	53.55
FeO^{tot}	14.48	14.60	14.46	14.52	14.86	14.64	14.19	14.07	14.54	14.77
MnO	0.24	0.27	0.24	0.24	0.27	0.23	0.25	0.28	0.23	0.25
MgO	14.46	14.59	14.42	14.48	14.24	14.18	14.47	14.61	14.40	14.58
NiO	0.08	0.07	0.08	0.11	0.11	0.07	0.11	0.10	0.09	0.07
Cr#	0.69	0.69	0.69	0.70	0.70	0.70	0.69	0.69	0.70	0.70
Mg#	0.68	0.69	0.67	0.68	0.67	0.67	0.68	0.69	0.68	0.69
Cr/Fe^{2+}	4.18	4.26	4.13	4.21	4.10	4.11	4.22	4.30	4.22	4.28

Sample	CF17										
Analysis#	1	2	3	4	5	6	7	8	9	10	11
TiO_2	0.19	0.18	0.18	0.17	0.17	0.16	0.16	0.17	0.17	0.16	0.17
V_2O_5	0.11	0.10	0.14	0.12	0.11	0.14	0.12	0.12	0.11	0.13	0.15
Al_2O_3	17.80	17.74	17.74	17.84	17.94	18.26	18.00	17.70	17.78	17.63	17.79
Cr_2O_3	50.27	50.28	50.54	51.37	50.77	50.67	50.07	50.52	50.06	49.89	49.79
FeO^{tot}	15.55	15.48	15.41	14.95	14.90	14.89	15.79	15.22	15.49	15.52	15.68
MnO	0.27	0.24	0.25	0.25	0.22	0.26	0.22	0.23	0.25	0.25	0.25
MgO	15.13	15.26	15.37	15.29	15.37	15.55	14.89	14.53	15.00	14.88	14.78
NiO	0.13	0.11	0.13	0.10	0.11	0.12	0.09	0.12	0.11	0.10	0.10
Cr#	0.65	0.66	0.66	0.66	0.65	0.65	0.65	0.66	0.65	0.65	0.65
Mg#	0.70	0.71	0.71	0.70	0.71	0.71	0.69	0.68	0.70	0.70	0.69
Cr/Fe^{2+}	4.14	4.21	4.26	4.23	4.28	4.31	3.98	3.94	4.10	4.07	3.98

Sample	CF18									
Analysis#	1	2	3	4	5	6	7	8	9	10
TiO_2	0.18	0.19	0.19	0.18	0.19	0.18	0.17	0.18	0.18	0.18
V_2O_5	0.12	0.12	0.10	0.09	0.13	0.11	0.13	0.11	0.11	0.13
Al_2O_3	17.67	17.35	17.68	17.74	17.77	17.35	17.41	17.48	17.36	17.48
Cr_2O_3	50.36	50.22	50.55	50.17	50.48	50.32	50.70	50.33	50.17	50.40
FeO^{tot}	14.74	14.68	14.37	14.22	14.44	14.59	13.96	14.05	14.73	14.78
MnO	0.23	0.23	0.22	0.25	0.22	0.23	0.23	0.24	0.23	0.25
MgO	15.95	15.90	16.12	16.10	16.24	16.10	16.05	16.25	15.84	16.09
NiO	0.15	0.15	0.18	0.20	0.20	0.18	0.20	0.16	0.13	0.14
Cr#	0.66	0.66	0.66	0.65	0.66	0.66	0.66	0.66	0.66	0.66
Mg#	0.74	0.74	0.74	0.75	0.75	0.75	0.75	0.75	0.74	0.74
Cr/Fe^{2+}	4.67	4.71	4.81	4.86	4.85	4.85	4.90	5.01	4.68	4.77

Sample	CL3							
An#	1	2	3	4	5	6	7	8
TiO_2	0.17	0.16	0.17	0.18	0.17	0.17	0.16	0.16
V_2O_5	0.11	0.13	0.14	0.10	0.12	0.10	0.15	0.13
Al_2O_3	20.10	19.96	20.01	20.13	19.53	19.29	19.69	19.34
Cr_2O_3	50.69	50.39	50.29	49.99	48.71	48.88	48.62	49.59
FeO^{tot}	15.02	14.81	15.13	14.91	17.26	17.64	17.37	17.30
MnO	0.24	0.22	0.25	0.24	0.29	0.29	0.30	0.29
MgO	14.78	14.63	14.66	14.37	12.65	12.82	12.64	12.95
NiO	0.07	0.10	0.08	0.10	0.06	0.07	0.07	0.05
Cr#	0.63	0.63	0.63	0.62	0.63	0.63	0.62	0.63
Mg#	0.67	0.67	0.67	0.66	0.60	0.60	0.59	0.60
Cr/Fe^{2+}	3.71	3.69	3.66	3.59	3.01	3.05	2.99	3.10

Sample	CL3 continued ...							
An#	9	10	11	12	13	14	15	16
TiO_2	0.14	0.18	0.18	0.17	0.18	0.16	0.17	0.17
V_2O_5	0.11	0.13	0.14	0.15	0.12	0.11	0.15	0.13
Al_2O_3	18.78	19.03	18.65	19.18	19.26	20.07	19.92	20.31
Cr_2O_3	49.49	49.90	49.99	49.49	49.93	50.91	51.01	50.65
FeO^{tot}	17.77	15.16	15.61	15.47	15.23	14.60	14.68	14.53
MnO	0.34	0.29	0.28	0.26	0.26	0.26	0.24	0.26
MgO	12.33	14.38	14.48	14.01	13.96	15.19	15.15	14.99
NiO	0.05	0.06	0.09	0.10	0.08	0.09	0.06	0.08
Cr#	0.64	0.64	0.64	0.63	0.63	0.63	0.63	0.63
Mg#	0.58	0.67	0.67	0.65	0.65	0.69	0.69	0.68
Cr/Fe^{2+}	2.98	3.71	3.77	3.55	3.55	3.91	3.89	3.80

Sample	1349 – part 1								
Analysis#	1	2	3	4	5	6	7	8	9
TiO_2	0.18	0.18	0.17	0.19	0.17	0.18	0.17	0.18	0.17
V_2O_5	0.11	0.14	0.11	0.12	0.13	0.15	0.17	0.10	0.14
Al_2O_3	19.63	19.38	19.67	19.75	20.06	19.83	20.13	20.10	20.08
Cr_2O_3	48.46	48.72	48.47	48.38	48.82	49.40	48.57	48.78	48.35
FeO^{tot}	16.27	15.94	16.29	16.33	15.12	14.79	15.11	14.99	15.74
MnO	0.23	0.24	0.23	0.24	0.26	0.22	0.23	0.22	0.23
MgO	13.82	13.80	13.77	13.85	14.44	14.61	14.62	14.37	14.11
NiO	0.08	0.08	0.09	0.12	0.07	0.10	0.09	0.07	0.07
Cr#	0.62	0.63	0.62	0.62	0.62	0.63	0.62	0.62	0.62
Mg#	0.65	0.65	0.64	0.65	0.67	0.67	0.68	0.67	0.66
Cr/Fe^{2+}	3.38	3.41	3.36	3.37	3.61	3.71	3.66	3.61	3.46

Sample	1349 – part 2								
Analysis#	10	11	12	13	14	15	16	17	18
TiO_2	0.18	0.18	0.17	0.18	0.17	0.17	0.16	0.16	0.18
V_2O_5	0.15	0.14	0.16	0.14	0.16	0.13	0.12	0.15	0.13
Al_2O_3	19.93	20.11	20.26	20.29	20.28	20.24	20.02	20.23	20.12
Cr_2O_3	48.50	49.62	49.59	49.84	49.10	48.82	48.82	48.95	48.74
FeO^{tot}	15.71	15.56	15.38	15.52	15.24	14.79	14.71	14.61	14.70
MnO	0.26	0.22	0.20	0.24	0.25	0.22	0.21	0.23	0.25
MgO	14.02	14.45	14.51	14.61	14.61	14.64	14.60	14.78	14.78
NiO	0.08	0.08	0.13	0.09	0.09	0.06	0.08	0.08	0.11
Cr#	0.62	0.62	0.62	0.62	0.62	0.62	0.62	0.62	0.62
Mg#	0.65	0.66	0.66	0.66	0.67	0.68	0.68	0.68	0.68
Cr/Fe^{2+}	3.45	3.55	3.58	3.58	3.62	3.68	3.72	3.76	3.76

Sample	Q1 pod									
Analysis#	1	2	3	4	5	6	7	8	9	10
TiO_2	0.17	0.18	0.18	0.15	0.19	0.17	0.15	0.17	0.17	0.17
V_2O_5	0.23	0.20	0.23	0.24	0.26	0.24	0.25	0.20	0.25	0.19
Al_2O_3	18.00	18.12	18.50	18.33	17.90	18.10	18.23	17.65	18.07	18.07
Cr_2O_3	49.82	49.28	49.66	50.08	49.44	49.16	50.26	50.61	50.21	50.63
FeO^{tot}	18.64	19.01	19.17	18.70	18.45	18.83	19.10	18.82	19.01	18.75
MnO	0.23	0.23	0.26	0.22	0.26	0.27	0.23	0.23	0.25	0.28
MgO	12.01	12.10	12.41	12.46	12.12	12.24	11.92	12.17	11.79	11.81
NiO	0.10	0.08	0.09	0.09	0.11	0.13	0.12	0.10	0.09	0.09
Cr#	0.65	0.65	0.64	0.65	0.65	0.65	0.65	0.66	0.65	0.65
Mg#	0.57	0.57	0.58	0.58	0.58	0.58	0.56	0.57	0.55	0.56
Cr/Fe^{2+}	2.89	2.88	2.90	2.95	2.93	2.93	2.83	2.95	2.82	2.85

Sample	Q2 pod									
Analysis#	1	2	3	4	5	6	7	8	9	10
TiO_2	0.17	0.16	0.17	0.19	0.16	0.16	0.15	0.17	0.20	0.20
V_2O_5	0.21	0.20	0.22	0.19	0.22	0.22	0.23	0.23	0.20	0.26
Al_2O_3	15.39	14.88	15.66	15.92	15.32	15.30	15.25	15.31	15.68	15.93
Cr_2O_3	50.85	51.89	52.10	52.35	52.22	51.75	52.31	52.57	53.18	51.86
FeO^{tot}	22.94	23.48	21.61	21.28	21.06	20.99	19.72	20.06	19.65	19.48
MnO	0.39	0.46	0.36	0.35	0.31	0.26	0.27	0.25	0.25	0.27
MgO	9.30	9.52	9.94	10.32	10.91	10.98	11.67	11.63	11.39	11.46
NiO	0.08	0.08	0.11	0.11	0.11	0.12	0.11	0.09	0.12	0.12
Cr#	0.69	0.70	0.69	0.69	0.70	0.69	0.70	0.70	0.69	0.69
Mg#	0.45	0.46	0.48	0.49	0.52	0.53	0.56	0.55	0.54	0.55
Cr/Fe^{2+}	2.41	2.47	2.56	2.62	2.77	2.78	3.00	2.96	2.90	2.90

Sample	Q3 pod 1									
Analysis#	1	2	3	4	5	6	7	8	9	10
TiO_2	0.24	0.23	0.23	0.24	0.25	0.26	0.23	0.23	0.24	0.24
V_2O_5	0.20	0.20	0.23	0.23	0.21	0.18	0.23	0.23	0.20	0.22
Al_2O_3	13.86	14.13	13.63	13.71	14.05	14.08	13.44	13.68	14.06	14.52
Cr_2O_3	54.27	54.17	54.50	53.94	53.91	53.58	54.52	54.28	52.66	52.73
FeO^{tot}	20.84	20.95	20.06	19.43	18.81	19.19	18.99	18.93	23.53	23.11
MnO	0.34	0.31	0.31	0.25	0.29	0.29	0.28	0.28	0.36	0.33
MgO	10.86	10.54	11.30	11.20	11.51	11.59	11.09	11.12	9.48	9.12
NiO	0.05	0.05	0.08	0.08	0.09	0.09	0.07	0.09	0.04	0.07
Cr#	0.72	0.72	0.73	0.73	0.72	0.72	0.73	0.73	0.72	0.71
Mg#	0.52	0.51	0.54	0.54	0.56	0.56	0.54	0.54	0.46	0.44
Cr/Fe^{2+}	2.87	2.79	3.02	3.02	3.10	3.10	3.05	3.04	2.49	2.43

Sample	Q3 pod 2 – part 1									
Analysis#	1	2	3	4	5	6	7	8	9	10
TiO_2	0.22	0.24	0.23	0.24	0.26	0.24	0.27	0.24	0.22	0.23
V_2O_5	0.21	0.23	0.23	0.16	0.28	0.26	0.27	0.26	0.22	0.24
Al_2O_3	14.33	14.28	14.36	14.53	15.12	14.91	14.97	14.59	13.72	13.90
Cr_2O_3	55.23	54.31	54.38	55.12	53.10	52.84	52.96	53.30	52.39	52.87
FeO^{tot}	19.16	19.22	19.05	19.27	19.44	19.67	19.52	20.62	22.64	22.27
MnO	0.31	0.27	0.31	0.27	0.30	0.27	0.27	0.34	0.38	0.36
MgO	10.78	11.40	10.96	11.41	11.73	11.38	11.21	10.54	8.78	8.96
NiO	0.10	0.06	0.09	0.09	0.11	0.11	0.09	0.10	0.06	0.07
Cr#	0.72	0.72	0.72	0.72	0.70	0.70	0.70	0.71	0.72	0.72
Mg#	0.52	0.55	0.53	0.54	0.56	0.55	0.54	0.51	0.44	0.44
Cr/Fe^{2+}	2.93	3.05	2.96	3.03	3.02	2.96	2.92	2.78	2.46	2.49

Sample	Q3 pod 2 – part 2									
Analysis#	11	12	13	14	15	16	17	18	19	20
TiO_2	0.24	0.24	0.23	0.23	0.22	0.23	0.22	0.23	0.23	0.22
V_2O_5	0.18	0.24	0.21	0.24	0.24	0.21	0.20	0.25	0.22	0.21
Al_2O_3	13.81	13.97	13.95	14.06	13.71	14.00	13.67	13.95	13.99	14.56
Cr_2O_3	53.34	53.21	53.10	53.46	53.92	54.43	54.01	53.77	53.40	52.86
FeO^{tot}	22.82	21.62	23.13	22.75	22.48	22.25	23.28	23.23	23.25	23.56
MnO	0.40	0.34	0.40	0.40	0.41	0.36	0.44	0.42	0.42	0.41
MgO	8.97	9.80	8.80	8.95	8.64	9.03	8.30	8.57	8.45	8.62
NiO	0.06	0.06	-	-	-	-	0.06	0.04	0.04	0.06
Cr#	0.72	0.72	0.72	0.72	0.73	0.72	0.73	0.72	0.72	0.71
Mg#	0.44	0.48	0.43	0.44	0.43	0.44	0.41	0.42	0.42	0.42
Cr/Fe^{2+}	2.48	2.64	2.43	2.46	2.46	2.51	2.39	2.41	2.39	2.36

Sample	QX13								
Analysis#	1	2	3	4	5	6	7	8	9
TiO_2	0.32	0.32	0.29	0.29	0.35	0.32	0.41	0.32	0.40
V_2O_5	0.22	0.22	0.23	0.23	0.25	0.23	0.21	0.24	0.24
Al_2O_3	20.24	20.86	20.69	20.87	21.07	20.97	21.14	21.28	20.72
Cr_2O_3	44.82	45.51	45.80	46.04	45.57	45.21	45.43	45.97	44.79
FeO^{tot}	20.56	20.78	20.23	20.16	20.73	20.78	20.03	19.72	19.80
MnO	0.25	0.22	0.23	0.22	0.21	0.19	0.23	0.21	0.20
MgO	12.18	12.12	12.59	12.72	12.35	12.29	12.44	12.92	12.51
NiO	0.15	0.16	0.19	0.17	0.16	0.13	0.17	0.15	0.16
Cr#	0.60	0.59	0.60	0.60	0.59	0.59	0.59	0.59	0.59
Mg#	0.57	0.56	0.58	0.58	0.57	0.57	0.57	0.59	0.58
Cr/Fe^{2+}	2.59	2.53	2.67	2.68	2.55	2.54	2.59	2.70	2.64

Sample	Q3PX									
Analysis#	1	2	3	4	5	6	7	8	9	10
TiO_2	0.17	0.18	0.15	0.16	0.16	0.17	0.22	0.18	0.20	0.18
V_2O_5	0.26	0.20	0.20	0.21	0.22	0.25	0.21	0.23	0.25	0.21
Al_2O_3	16.45	16.58	16.37	16.24	15.55	15.77	16.23	16.37	16.48	16.97
Cr_2O_3	51.93	52.17	52.74	52.17	52.27	52.47	51.45	51.28	51.97	51.69
FeO^{tot}	20.96	21.12	19.18	18.66	19.19	19.11	19.14	19.32	19.06	19.78
MnO	0.35	0.34	0.25	0.25	0.24	0.23	0.23	0.27	0.27	0.24
MgO	10.38	10.75	11.76	11.85	11.52	11.41	12.08	11.72	12.23	12.17
NiO	0.09	0.06	0.13	0.04	0.11	0.09	0.12	0.11	0.10	0.13
Cr#	0.68	0.68	0.68	0.68	0.69	0.69	0.68	0.68	0.68	0.67
Mg#	0.49	0.51	0.55	0.56	0.55	0.55	0.57	0.56	0.57	0.57
Cr/Fe^{2+}	2.60	2.65	2.96	3.01	2.97	2.92	3.02	2.93	3.04	2.95

Sample	HG1									
Analysis#	1	2	3	4	5	6	7	8	9	10
TiO_2	0.19	0.19	0.21	0.21	0.22	0.22	0.19	0.21	0.20	0.20
V_2O_5	0.25	0.26	0.24	0.23	0.22	0.24	0.25	0.26	0.23	0.24
Al_2O_3	19.05	19.21	19.76	19.97	19.38	19.03	19.72	19.91	19.43	19.79
Cr_2O_3	48.89	49.18	48.59	48.28	48.26	47.95	47.38	47.48	47.97	47.49
FeO^{tot}	19.43	19.30	19.08	18.73	18.72	18.91	18.79	18.81	18.56	18.98
MnO	0.25	0.25	0.22	0.24	0.25	0.22	0.24	0.23	0.25	0.25
MgO	12.53	12.33	12.57	12.56	12.47	12.49	12.32	12.25	12.57	12.49
NiO	0.12	0.10	0.12	0.13	0.14	0.16	0.17	0.12	0.12	0.13
Cr#	0.63	0.63	0.62	0.62	0.63	0.63	0.62	0.62	0.62	0.62
Mg#	0.58	0.57	0.58	0.58	0.58	0.59	0.58	0.57	0.59	0.58
Cr/Fe^{2+}	2.90	2.81	2.82	2.83	2.86	2.88	2.80	2.75	2.89	2.81

Sample	HG4									
Analysis#	1	2	3	4	5	6	7	8	9	10
TiO_2	0.15	0.16	0.18	0.19	0.19	0.19	0.17	0.18	0.19	0.19
V_2O_5	0.21	0.26	0.22	0.24	0.20	0.24	0.21	0.22	0.25	0.20
Al_2O_3	20.61	20.87	21.10	21.26	21.00	21.22	20.98	20.88	21.00	21.04
Cr_2O_3	48.28	48.15	47.78	47.49	48.17	48.37	47.83	48.34	48.63	48.68
FeO^{tot}	16.90	17.05	17.67	18.31	17.35	17.15	17.74	17.57	17.39	17.36
MnO	0.24	0.26	0.25	0.26	0.25	0.24	0.28	0.24	0.25	0.26
MgO	13.00	13.45	12.97	13.08	13.52	13.26	13.31	13.33	13.54	13.36
NiO	0.08	0.10	0.08	0.09	0.13	0.11	0.10	0.09	0.10	0.12
Cr#	0.61	0.61	0.60	0.60	0.61	0.60	0.60	0.61	0.61	0.61
Mg#	0.61	0.62	0.60	0.60	0.62	0.61	0.61	0.61	0.61	0.61
Cr/Fe^{2+}	3.04	3.06	2.89	2.86	3.05	2.97	2.98	2.99	3.04	3.01

Sample	HG5									
Analysis#	1	2	3	4	5	6	7	8	9	10
TiO_2	0.19	0.19	0.18	0.20	0.21	0.22	0.22	0.21	0.21	0.21
V_2O_5	0.24	0.25	0.24	0.23	0.26	0.26	0.25	0.25	0.26	0.25
Al_2O_3	21.72	22.00	22.60	22.89	22.12	22.28	22.06	22.37	23.00	22.74
Cr_2O_3	46.66	46.43	46.12	46.39	46.60	46.55	45.96	46.33	45.95	45.44
FeO^{tot}	18.12	18.32	16.64	16.84	17.72	17.49	17.59	17.30	17.29	17.30
MnO	0.30	0.29	0.26	0.25	0.24	0.25	0.25	0.24	0.23	0.23
MgO	12.87	12.59	13.64	13.76	13.59	13.58	13.29	13.32	13.57	13.62
NiO	0.07	0.05	0.14	0.10	0.11	0.15	0.12	0.11	0.10	0.11
Cr#	0.59	0.59	0.58	0.58	0.59	0.58	0.58	0.58	0.57	0.57
Mg#	0.59	0.58	0.62	0.62	0.62	0.62	0.61	0.61	0.61	0.62
Cr/Fe^{2+}	2.78	2.68	2.97	2.95	2.92	2.92	2.87	2.86	2.86	2.90

Sample	HG6									
Analysis#	1	2	3	4	5	6	7	8	9	10
TiO_2	0.18	0.17	0.20	0.19	0.20	0.22	0.20	0.20	0.20	0.20
V_2O_5	0.21	0.21	0.23	0.22	0.20	0.21	0.22	0.21	0.19	0.20
Al_2O_3	15.31	15.06	14.53	14.22	15.62	15.93	15.50	15.41	14.42	14.60
Cr_2O_3	52.89	52.89	54.02	53.58	52.72	52.56	52.18	51.83	53.11	53.45
FeO^{tot}	19.27	19.13	18.82	19.57	18.83	18.83	19.65	19.82	18.82	18.98
MnO	0.24	0.25	0.25	0.28	0.26	0.25	0.29	0.27	0.26	0.25
MgO	11.55	11.35	11.65	11.77	11.86	12.10	11.23	11.29	11.55	11.85
NiO	0.13	0.07	0.09	0.11	0.09	0.09	0.09	0.08	0.11	0.11
Cr#	0.70	0.70	0.71	0.72	0.69	0.69	0.69	0.69	0.71	0.71
Mg#	0.55	0.55	0.56	0.56	0.56	0.57	0.54	0.54	0.56	0.57
Cr/Fe^{2+}	2.99	2.97	3.09	3.11	3.05	3.07	2.91	2.89	3.09	3.17

Sample	HG7									
Analysis#	1	2	3	4	5	6	7	8	9	10
TiO_2	0.14	0.14	0.13	0.14	0.13	0.13	0.13	0.14	0.14	0.14
V_2O_5	0.25	0.23	0.24	0.23	0.23	0.19	0.23	0.22	0.19	0.22
Al_2O_3	22.84	22.87	22.56	22.79	22.25	22.28	22.76	23.09	22.82	22.50
Cr_2O_3	45.91	46.28	45.96	46.06	46.71	46.59	46.33	46.32	45.91	46.06
FeO^{tot}	16.41	16.76	17.14	17.29	16.69	16.58	16.45	17.09	16.56	16.32
MnO	0.21	0.23	0.25	0.26	0.23	0.24	0.24	0.25	0.20	0.21
MgO	14.34	14.21	13.82	13.79	14.29	14.05	13.88	13.98	14.20	14.18
NiO	0.15	0.15	0.15	0.12	0.16	0.16	0.15	0.13	0.13	0.14
Cr#	0.57	0.58	0.58	0.58	0.58	0.58	0.58	0.57	0.57	0.58
Mg#	0.65	0.64	0.63	0.62	0.65	0.64	0.63	0.63	0.64	0.65
Cr/Fe^{2+}	3.15	3.09	3.00	2.95	3.18	3.14	3.04	2.99	3.11	3.15

Sample	HG8									
Analysis#	1	2	3	4	5	6	7	8	9	10
TiO_2	0.17	0.18	0.18	0.20	0.17	0.17	0.18	0.19	0.14	0.17
V_2O_5	0.25	0.22	0.24	0.23	0.24	0.19	0.24	0.22	0.20	0.22
Al_2O_3	18.64	18.57	19.29	19.21	18.50	18.80	18.38	18.78	18.04	18.23
Cr_2O_3	48.58	48.97	48.44	48.38	48.79	48.65	49.64	48.98	50.19	50.34
FeO^{tot}	19.26	19.23	19.11	19.20	19.63	19.88	18.85	19.23	19.31	19.27
MnO	0.27	0.25	0.24	0.25	0.30	0.28	0.23	0.25	0.29	0.25
MgO	12.34	12.18	12.59	12.43	11.95	11.85	12.59	12.60	12.05	12.36
NiO	0.11	0.11	0.17	0.12	0.09	0.11	0.11	0.12	0.10	0.13
Cr#	0.64	0.64	0.63	0.63	0.64	0.63	0.64	0.64	0.65	0.65
Mg#	0.58	0.57	0.58	0.58	0.56	0.56	0.59	0.59	0.57	0.57
Cr/Fe^{2+}	2.87	2.84	2.88	2.84	2.78	2.73	2.97	2.91	2.87	2.91

Sample	HG9									
Analysis#	1	2	3	4	5	6	7	8	9	10
TiO_2	0.27	0.27	0.28	0.28	0.29	0.28	0.27	0.29	0.28	0.28
V_2O_5	0.26	0.22	0.22	0.19	0.20	0.21	0.25	0.20	0.21	0.20
Al_2O_3	19.89	19.76	19.99	19.82	20.08	20.38	20.22	20.19	19.91	19.80
Cr_2O_3	47.28	47.90	47.74	47.64	47.36	47.17	47.17	47.53	46.90	47.17
FeO^{tot}	19.11	18.89	18.77	18.81	19.21	18.59	18.46	18.75	18.81	18.79
MnO	0.23	0.25	0.24	0.23	0.23	0.23	0.26	0.24	0.25	0.22
MgO	12.65	13.01	12.85	12.60	12.95	12.99	12.45	13.08	12.48	12.74
NiO	0.13	0.14	0.13	0.10	0.12	0.14	0.13	0.13	0.13	0.11
Cr#	0.61	0.62	0.62	0.62	0.61	0.61	0.61	0.61	0.61	0.62
Mg#	0.59	0.60	0.59	0.59	0.60	0.60	0.58	0.60	0.58	0.59
Cr/Fe^{2+}	2.81	2.92	2.87	2.83	2.86	2.88	2.78	2.91	2.80	2.86

Sample	HG11									
Analysis#	1	2	3	4	5	6	7	8	9	10
TiO_2	0.19	0.19	0.21	0.21	0.20	0.19	0.22	0.23	0.21	0.20
V_2O_5	0.27	0.23	0.28	0.27	0.23	0.27	0.21	0.25	0.27	0.25
Al_2O_3	19.03	18.88	19.19	19.22	18.92	18.59	19.12	19.22	18.05	18.18
Cr_2O_3	48.80	48.86	48.95	49.01	48.19	48.43	49.19	49.20	50.96	50.93
FeO^{tot}	18.13	18.50	18.28	18.09	18.66	18.25	19.33	19.56	18.40	18.70
MnO	0.22	0.23	0.25	0.24	0.25	0.25	0.26	0.28	0.25	0.22
MgO	13.22	13.14	12.70	12.87	12.58	12.47	12.33	12.37	12.54	12.66
NiO	0.17	0.14	0.16	0.15	0.15	0.15	0.13	0.13	0.14	0.16
Cr#	0.63	0.63	0.63	0.63	0.63	0.64	0.63	0.63	0.65	0.65
Mg#	0.61	0.61	0.59	0.60	0.59	0.59	0.57	0.57	0.58	0.59
Cr/Fe^{2+}	3.10	3.07	2.95	3.00	2.93	2.96	2.82	2.81	3.01	3.01

Sample	QY1									
Analysis#	1	2	3	4	5	6	7	8	9	10
TiO_2	0.12	0.11	0.12	0.12	0.12	0.13	0.11	0.11	0.13	0.11
V_2O_5	0.10	0.14	0.12	0.15	0.15	0.18	0.12	0.12	0.08	0.11
Al_2O_3	14.36	14.18	14.50	14.47	14.25	14.31	14.16	14.15	14.13	14.35
Cr_2O_3	55.88	55.76	55.64	55.45	55.73	55.53	57.07	56.70	55.71	55.64
FeO^{tot}	14.83	14.72	16.01	16.01	14.52	14.85	15.24	14.97	15.46	15.70
MnO	0.25	0.25	0.28	0.27	0.24	0.29	0.23	0.25	0.26	0.25
MgO	14.37	14.13	13.39	13.11	13.91	13.82	14.01	14.08	14.00	13.95
NiO	0.08	0.09	0.06	0.08	0.09	0.08	0.08	0.08	0.09	0.10
Cr#	0.72	0.73	0.72	0.72	0.72	0.72	0.73	0.73	0.73	0.72
Mg#	0.68	0.67	0.63	0.62	0.66	0.66	0.66	0.66	0.66	0.66
Cr/Fe^{2+}	4.32	4.26	3.81	3.72	4.17	4.09	4.12	4.19	4.14	4.06

Sample	QY2									
Analysis#	1	2	3	4	5	6	7	8	9	10
TiO_2	0.15	0.14	0.13	0.13	0.14	0.14	0.16	0.17	0.16	0.16
V_2O_5	0.10	0.08	0.12	0.12	0.15	0.13	0.11	0.16	0.13	0.12
Al_2O_3	15.34	15.54	14.73	14.90	15.05	15.10	15.60	15.60	15.85	15.82
Cr_2O_3	54.30	54.40	53.63	54.01	54.22	53.92	54.80	54.53	54.72	54.52
FeO^{tot}	16.15	16.14	17.68	18.08	16.65	16.59	15.57	15.72	15.12	15.03
MnO	0.28	0.27	0.29	0.27	0.29	0.28	0.27	0.26	0.28	0.22
MgO	13.69	13.64	12.86	12.89	13.77	13.41	14.63	14.41	14.10	14.32
NiO	0.10	0.11	0.07	0.08	0.12	0.14	0.14	0.13	0.10	0.09
Cr#	0.70	0.70	0.71	0.71	0.71	0.71	0.70	0.70	0.70	0.70
Mg#	0.64	0.64	0.61	0.61	0.65	0.64	0.68	0.67	0.66	0.67
Cr/Fe^{2+}	3.81	3.78	3.51	3.46	3.83	3.72	4.17	4.05	3.97	4.05

Sample	QY5									
Analysis#	1	2	3	4	5	6	7	8	9	10
TiO_2	0.09	0.08	0.09	0.09	0.09	0.09	0.09	0.10	0.08	0.09
V_2O_5	0.15	0.15	0.14	0.12	0.11	0.12	0.12	0.13	0.11	0.12
Al_2O_3	15.71	15.83	15.27	15.31	15.58	15.77	15.72	15.99	15.44	15.32
Cr_2O_3	55.06	54.91	55.73	55.31	54.52	55.52	55.12	55.06	54.96	54.72
FeO^{tot}	15.93	15.85	15.67	15.38	14.61	14.71	15.26	15.07	15.84	15.90
MnO	0.31	0.31	0.23	0.28	0.23	0.25	0.28	0.29	0.27	0.28
MgO	14.05	13.65	14.19	14.35	14.84	14.84	14.33	14.21	14.36	14.20
NiO	0.11	0.09	0.10	0.14	0.10	0.11	0.08	0.10	0.09	0.11
Cr#	0.70	0.70	0.71	0.71	0.70	0.70	0.70	0.70	0.70	0.71
Mg#	0.65	0.64	0.66	0.67	0.69	0.69	0.67	0.66	0.67	0.66
Cr/Fe^{2+}	3.91	3.77	4.02	4.14	4.39	4.32	4.07	4.01	4.08	4.03

Sample	QY6									
Analysis#	1	2	3	4	5	6	7	8	9	10
TiO_2	0.09	0.10	0.12	0.11	0.11	0.10	0.13	0.12	0.09	0.09
V_2O_5	0.14	0.12	0.10	0.12	0.12	0.11	0.11	0.12	0.12	0.07
Al_2O_3	15.98	15.98	16.37	16.10	15.46	15.70	16.60	16.18	15.26	15.11
Cr_2O_3	55.76	56.13	54.18	54.60	54.86	54.30	55.20	54.71	55.30	55.61
FeO^{tot}	14.12	13.77	13.12	13.40	13.34	13.46	13.45	13.14	13.88	14.07
MnO	0.24	0.22	0.23	0.23	0.20	0.20	0.25	0.24	0.24	0.23
MgO	14.92	15.00	15.05	15.16	14.95	14.79	15.31	14.85	14.66	14.68
NiO	0.09	0.13	0.08	0.10	0.10	0.07	0.11	0.10	0.09	0.07
Cr#	0.70	0.70	0.69	0.69	0.70	0.70	0.69	0.69	0.71	0.71
Mg#	0.69	0.69	0.70	0.71	0.70	0.70	0.70	0.70	0.69	0.69
Cr/Fe^{2+}	4.36	4.43	4.54	4.59	4.59	4.49	4.53	4.46	4.43	4.44

Sample	QY8									
Analysis#	1	2	3	4	5	6	7	8	9	10
TiO_2	0.06	0.06	0.06	0.06	0.07	0.08	0.06	0.07	0.08	0.08
V_2O_5	0.15	0.13	0.15	0.13	0.10	0.11	0.13	0.11	0.11	0.13
Al_2O_3	16.90	16.77	16.90	16.77	17.03	16.66	16.35	16.74	16.06	16.02
Cr_2O_3	54.04	54.02	54.04	54.02	53.49	53.56	54.16	54.72	54.51	54.66
FeO^{tot}	14.65	14.25	14.65	14.25	13.97	13.72	14.04	14.03	14.20	14.02
MnO	0.23	0.22	0.23	0.22	0.25	0.21	0.24	0.25	0.24	0.21
MgO	14.83	14.68	14.83	14.68	14.84	14.84	14.81	14.97	14.34	14.55
NiO	0.08	0.13	0.08	0.13	0.10	0.11	0.14	0.10	0.11	0.13
Cr#	0.68	0.68	0.68	0.68	0.68	0.68	0.69	0.69	0.69	0.70
Mg#	0.68	0.68	0.68	0.68	0.69	0.69	0.69	0.69	0.67	0.68
Cr/Fe^{2+}	4.17	4.20	4.17	4.20	4.27	4.35	4.34	4.33	4.16	4.26

Sample	QY9									
Analysis#	1	2	3	4	5	6	7	8	9	10
TiO_2	0.09	0.08	0.08	0.10	0.09	0.10	0.09	0.08	0.09	0.09
V_2O_5	0.06	0.10	0.11	0.11	0.07	0.09	0.10	0.11	0.09	0.07
Al_2O_3	15.45	15.33	15.00	15.15	15.17	15.22	15.46	15.24	14.61	14.78
Cr_2O_3	55.82	56.09	55.77	56.25	55.65	55.31	55.17	55.19	55.99	55.54
FeO^{tot}	14.52	14.12	14.34	14.46	15.55	15.73	14.40	14.46	14.33	14.30
MnO	0.26	0.26	0.26	0.26	0.28	0.25	0.27	0.26	0.25	0.24
MgO	14.37	14.50	14.36	14.17	13.50	13.53	14.19	14.12	13.79	13.79
NiO	0.05	0.09	0.10	0.06	0.08	0.08	0.08	0.08	0.07	0.06
Cr#	0.71	0.71	0.71	0.71	0.71	0.71	0.71	0.71	0.72	0.72
Mg#	0.67	0.68	0.68	0.66	0.64	0.64	0.67	0.67	0.66	0.66
Cr/Fe^{2+}	4.19	4.31	4.28	4.14	3.83	3.81	4.15	4.15	4.11	4.10

Sample	QY10									
Analysis#	1	2	3	4	5	6	7	8	9	10
TiO_2	0.15	0.15	0.17	0.17	0.16	0.15	0.17	0.16	0.16	0.17
V_2O_5	0.12	0.10	0.13	0.13	0.09	0.12	0.10	0.10	0.11	0.12
Al_2O_3	12.81	12.45	14.50	14.65	14.37	14.29	14.28	14.44	14.18	14.38
Cr_2O_3	58.17	58.31	56.11	55.67	55.84	56.00	55.72	56.49	56.78	56.52
FeO^{tot}	15.01	14.81	15.08	14.75	15.06	14.93	15.19	14.51	14.92	14.88
MnO	0.25	0.26	0.23	0.23	0.22	0.23	0.24	0.25	0.24	0.24
MgO	14.39	14.65	14.48	14.53	14.71	14.83	15.01	14.53	14.49	14.76
NiO	0.12	0.09	0.11	0.12	0.13	0.11	0.13	0.13	0.15	0.14
Cr#	0.75	0.76	0.72	0.72	0.72	0.72	0.72	0.72	0.73	0.72
Mg#	0.68	0.69	0.68	0.68	0.69	0.69	0.70	0.68	0.68	0.69
Cr/Fe^{2+}	4.47	4.67	4.27	4.32	4.42	4.49	4.55	4.38	4.35	4.43

Sample	NKE-1									
Analysis#	1	2	3	4	5	6	7	8	9	10
TiO_2	0.21	0.22	0.22	0.21	0.22	0.21	0.22	0.21	0.23	0.22
V_2O_5	0.14	0.17	0.16	0.15	0.15	0.17	0.14	0.14	0.16	0.16
Al_2O_3	26.46	26.61	26.31	26.81	26.35	26.64	26.43	26.10	26.22	26.44
Cr_2O_3	42.90	42.71	42.87	42.39	43.24	43.08	42.27	42.59	42.40	42.03
FeO^{tot}	13.99	13.84	14.08	14.10	14.32	14.11	14.13	13.52	13.90	13.99
MnO	0.23	0.21	0.21	0.18	0.20	0.20	0.22	0.21	0.20	0.18
MgO	15.43	15.74	15.61	15.86	15.59	15.93	15.66	15.59	15.78	15.89
NiO	0.18	0.19	0.15	0.17	0.16	0.16	0.17	0.16	0.16	0.16
Cr#	0.52	0.52	0.52	0.51	0.52	0.52	0.52	0.52	0.52	0.52
Mg#	0.69	0.70	0.70	0.70	0.69	0.70	0.70	0.70	0.71	0.71
Cr/Fe^{2+}	3.27	3.35	3.33	3.35	3.29	3.39	3.33	3.41	3.41	3.41

Sample	NKE-2									
Analysis#	1	2	3	4	5	6	7	8	9	10
TiO_2	0.14	0.12	0.13	0.14	0.13	0.14	0.13	0.15	0.12	0.15
V_2O_5	0.15	0.13	0.13	0.14	0.13	0.15	0.13	0.16	0.15	0.14
Al_2O_3	25.00	25.02	24.73	24.72	25.58	25.24	25.32	25.03	24.85	25.28
Cr_2O_3	42.66	43.17	42.71	43.24	42.60	42.86	42.44	42.90	42.69	42.65
FeO^{tot}	15.22	14.83	14.98	14.66	15.02	15.02	15.05	14.61	14.98	14.90
MnO	0.22	0.22	0.23	0.18	0.21	0.21	0.23	0.23	0.23	0.21
MgO	15.40	15.43	15.60	15.24	15.67	15.36	15.33	15.69	15.56	15.59
NiO	0.18	0.18	0.15	0.17	0.17	0.17	0.17	0.19	0.16	0.16
Cr#	0.53	0.54	0.54	0.54	0.53	0.53	0.53	0.53	0.54	0.53
Mg#	0.70	0.70	0.71	0.69	0.70	0.69	0.69	0.71	0.70	0.70
Cr/Fe^{2+}	3.36	3.41	3.49	3.38	3.40	3.33	3.32	3.51	3.46	3.41

Sample	NKE-3									
Analysis#	1	2	3	4	5	6	7	8	9	10
TiO_2	0.12	0.13	0.12	0.13	0.11	0.14	0.13	0.12	0.13	0.13
V_2O_5	0.15	0.17	0.17	0.18	0.17	0.16	0.14	0.14	0.16	0.15
Al_2O_3	25.64	26.11	25.67	25.84	26.28	25.73	25.56	25.75	25.69	25.37
Cr_2O_3	42.74	42.53	42.86	42.86	42.09	42.22	42.75	42.35	42.67	42.54
FeO^{tot}	15.30	15.04	15.61	15.26	15.37	15.80	15.08	15.48	15.08	14.62
MnO	0.23	0.22	0.22	0.23	0.24	0.23	0.20	0.23	0.21	0.21
MgO	15.80	15.06	14.64	15.73	15.44	15.31	15.30	15.69	15.31	15.91
NiO	0.13	0.17	0.16	0.17	0.15	0.13	0.19	0.16	0.16	0.15
Cr#	0.53	0.52	0.53	0.53	0.52	0.52	0.53	0.52	0.53	0.53
Mg#	0.70	0.68	0.66	0.70	0.69	0.68	0.69	0.70	0.69	0.71
Cr/Fe^{2+}	3.40	3.13	3.02	3.35	3.20	3.18	3.27	3.34	3.25	3.54

Sample	NKE-4									
Analysis#	1	2	3	4	5	6	7	8	9	10
TiO_2	0.17	0.17	0.16	0.18	0.15	0.15	0.15	0.16	0.17	0.15
V_2O_5	0.17	0.16	0.20	0.20	0.20	0.19	0.18	0.20	0.17	0.16
Al_2O_3	23.50	23.33	23.49	23.54	23.99	23.81	23.55	23.66	23.86	23.76
Cr_2O_3	45.93	45.21	45.72	45.53	46.44	46.20	46.05	46.41	45.97	46.11
FeO^{tot}	14.95	15.17	14.59	14.78	14.93	15.34	15.62	15.29	15.04	14.63
MnO	0.25	0.24	0.22	0.22	0.21	0.23	0.24	0.25	0.23	0.23
MgO	14.86	14.91	15.11	15.28	15.22	14.87	14.85	15.35	15.40	15.17
NiO	0.15	0.15	0.14	0.16	0.12	0.17	0.14	0.13	0.14	0.15
Cr#	0.57	0.57	0.57	0.56	0.56	0.57	0.57	0.57	0.56	0.57
Mg#	0.67	0.68	0.68	0.69	0.68	0.67	0.67	0.68	0.69	0.68
Cr/Fe^{2+}	3.36	3.38	3.46	3.49	3.39	3.29	3.29	3.45	3.47	3.45

Sample	NKE-5									
Analysis#	1	2	3	4	5	6	7	8	9	10
TiO_2	0.17	0.17	0.18	0.18	0.18	0.19	0.17	0.17	0.18	0.18
V_2O_5	0.17	0.16	0.16	0.14	0.17	0.15	0.16	0.14	0.15	0.14
Al_2O_3	26.53	26.30	26.63	26.77	26.42	26.82	26.31	26.13	26.42	26.16
Cr_2O_3	43.05	43.36	43.37	43.14	43.12	42.75	42.21	42.25	42.26	42.63
FeO^{tot}	14.48	14.79	14.27	14.59	15.00	14.62	14.72	14.35	14.38	14.20
MnO	0.21	0.20	0.23	0.21	0.23	0.23	0.21	0.24	0.21	0.22
MgO	16.28	15.72	15.84	16.11	15.67	15.70	15.82	15.67	15.74	15.76
NiO	0.18	0.18	0.16	0.18	0.18	0.17	0.13	0.18	0.20	0.17
Cr#	0.52	0.53	0.52	0.52	0.52	0.52	0.52	0.52	0.52	0.52
Mg#	0.71	0.69	0.70	0.71	0.69	0.69	0.70	0.70	0.70	0.70
Cr/Fe^{2+}	3.50	3.31	3.35	3.40	3.26	3.26	3.36	3.38	3.35	3.41

Sample	NKE-6									
Analysis#	1	2	3	4	5	6	7	8	9	10
TiO_2	0.17	0.17	0.17	0.18	0.16	0.18	0.17	0.16	0.17	0.16
V_2O_5	0.15	0.15	0.16	0.15	0.10	0.19	0.16	0.16	0.14	0.12
Al_2O_3	25.74	25.73	25.91	25.26	25.79	25.67	24.80	25.34	25.55	25.97
Cr_2O_3	42.32	43.16	43.21	42.70	42.83	42.00	42.47	41.60	42.96	42.53
FeO^{tot}	15.29	14.55	14.67	14.74	14.21	14.83	14.69	14.75	14.26	14.31
MnO	0.22	0.22	0.26	0.22	0.21	0.20	0.22	0.22	0.21	0.21
MgO	15.63	16.64	15.76	16.11	15.83	15.88	15.85	16.31	16.28	16.11
NiO	0.17	0.16	0.14	0.16	0.17	0.18	0.16	0.16	0.19	0.17
Cr#	0.52	0.53	0.53	0.53	0.53	0.52	0.53	0.52	0.53	0.52
Mg#	0.70	0.73	0.70	0.72	0.71	0.71	0.72	0.73	0.72	0.72
Cr/Fe^{2+}	3.32	3.76	3.39	3.60	3.50	3.45	3.59	3.69	3.69	3.56

Sample	NKE-7									
Analysis#	1	2	3	4	5	6	7	8	9	10
TiO_2	0.21	0.22	0.23	0.23	0.22	0.22	0.21	0.19	0.21	0.23
V_2O_5	0.12	0.17	0.14	0.16	0.17	0.16	0.13	0.13	0.14	0.16
Al_2O_3	26.60	26.26	26.75	26.18	25.80	25.80	26.06	25.56	25.47	25.68
Cr_2O_3	42.56	42.87	42.78	42.97	42.19	42.58	42.85	42.02	42.50	41.92
FeO^{tot}	14.46	14.39	14.31	14.42	14.25	14.78	14.22	14.17	13.83	14.45
MnO	0.21	0.23	0.21	0.21	0.18	0.21	0.22	0.19	0.20	0.20
MgO	16.58	16.16	16.09	16.14	16.38	16.16	15.95	16.51	16.13	16.02
NiO	0.17	0.17	0.18	0.18	0.20	0.17	0.21	0.19	0.17	0.16
Cr#	0.52	0.52	0.52	0.52	0.52	0.53	0.52	0.52	0.53	0.52
Mg#	0.73	0.71	0.71	0.71	0.73	0.72	0.71	0.74	0.72	0.72
Cr/Fe^{2+}	3.61	3.49	3.41	3.49	3.67	3.52	3.48	3.80	3.67	3.52

Sample	NKS-1								
Analysis#	1	2	3	4	5	6	7	8	9
TiO_2	0.10	0.09	0.10	0.09	0.11	0.09	0.10	0.10	0.11
V_2O_5	0.15	0.17	0.19	0.18	0.17	0.17	0.17	0.15	0.16
Al_2O_3	23.31	23.02	23.44	23.81	24.04	23.64	23.34	23.31	23.67
Cr_2O_3	45.97	46.04	46.47	46.19	45.68	45.51	45.97	45.17	45.69
FeO^{tot}	14.48	14.26	13.76	13.61	13.93	13.78	14.21	13.95	14.18
MnO	0.21	0.24	0.23	0.21	0.23	0.21	0.23	0.25	0.23
MgO	15.24	15.10	15.74	15.31	15.39	15.59	15.42	15.37	15.23
NiO	0.20	0.18	0.19	0.22	0.19	0.20	0.25	0.24	0.21
Cr#	0.57	0.57	0.57	0.57	0.56	0.56	0.57	0.57	0.56
Mg#	0.69	0.69	0.71	0.69	0.69	0.71	0.70	0.70	0.69
Cr/Fe^{2+}	3.57	3.59	3.80	3.62	3.58	3.74	3.67	3.71	3.56

Sample	NKS-2								
Analysis#	1	2	3	4	5	6	7	8	9
TiO_2	0.17	0.16	0.16	0.16	0.17	0.19	0.19	0.20	0.19
V_2O_5	0.14	0.10	0.12	0.17	0.15	0.15	0.15	0.14	0.16
Al_2O_3	24.80	24.21	24.75	24.75	24.83	24.69	24.43	25.02	24.92
Cr_2O_3	44.53	43.94	44.76	44.14	45.49	45.17	45.19	45.09	44.60
FeO^{tot}	13.91	14.46	14.33	14.67	14.49	14.75	14.87	14.66	14.33
MnO	0.21	0.21	0.25	0.21	0.24	0.23	0.21	0.22	0.21
MgO	15.60	15.47	15.61	14.85	15.62	15.40	15.67	15.48	15.29
NiO	0.18	0.22	0.19	0.18	0.15	0.19	0.20	0.19	0.19
Cr#	0.55	0.55	0.55	0.54	0.55	0.55	0.55	0.55	0.55
Mg#	0.70	0.70	0.70	0.67	0.69	0.69	0.70	0.69	0.69
Cr/Fe^{2+}	3.55	3.56	3.53	3.24	3.48	3.40	3.51	3.39	3.37

Sample	NKS-3									
Analysis#	1	2	3	4	5	6	7	8	9	10
TiO_2	0.07	0.07	0.08	0.06	0.07	0.08	0.08	0.07	0.09	0.06
V_2O_5	0.19	0.17	0.18	0.16	0.19	0.17	0.18	0.17	0.17	0.18
Al_2O_3	24.15	23.85	24.06	24.51	24.37	24.12	24.35	24.36	24.03	24.42
Cr_2O_3	45.80	45.70	45.89	45.71	45.49	45.05	45.04	45.24	45.67	45.41
FeO^{tot}	14.26	14.38	14.39	14.60	14.26	14.13	13.97	14.24	13.97	14.06
MnO	0.22	0.20	0.20	0.18	0.19	0.20	0.20	0.19	0.22	0.20
MgO	15.79	15.53	15.74	15.56	15.75	15.75	15.64	15.87	15.94	15.93
NiO	0.20	0.18	0.21	0.21	0.19	0.24	0.20	0.19	0.21	0.20
Cr#	0.56	0.56	0.56	0.56	0.56	0.56	0.55	0.55	0.56	0.55
Mg#	0.71	0.70	0.70	0.69	0.70	0.71	0.70	0.71	0.71	0.71
Cr/Fe^{2+}	3.68	3.62	3.66	3.52	3.64	3.70	3.64	3.69	3.80	3.72

Sample	NKS-4									
Analysis#	1	2	3	4	5	6	7	8	9	10
TiO_2	0.09	0.08	0.07	0.08	0.08	0.07	0.08	0.09	0.08	0.08
V_2O_5	0.19	0.18	0.16	0.17	0.19	0.17	0.15	0.18	0.20	0.17
Al_2O_3	20.56	20.54	20.60	20.58	20.60	20.29	20.67	20.52	20.73	20.82
Cr_2O_3	48.94	48.75	48.58	48.74	48.43	48.73	48.44	48.54	48.20	48.57
FeO^{tot}	15.67	15.49	14.64	14.86	15.24	14.46	14.66	14.67	14.85	14.86
MnO	0.21	0.21	0.22	0.21	0.23	0.20	0.21	0.23	0.22	0.24
MgO	14.50	14.30	14.37	14.66	14.44	14.58	14.52	14.13	14.62	14.50
NiO	0.19	0.17	0.18	0.17	0.20	0.18	0.18	0.16	0.19	0.17
Cr#	0.61	0.61	0.61	0.61	0.61	0.62	0.61	0.61	0.61	0.61
Mg#	0.66	0.66	0.67	0.68	0.67	0.68	0.67	0.66	0.68	0.67
Cr/Fe^{2+}	3.53	3.49	3.60	3.67	3.56	3.72	3.64	3.51	3.64	3.59

Sample	NKS-5									
Analysis#	1	2	3	4	5	6	7	8	9	10
TiO_2	0.08	0.10	0.11	0.10	0.11	0.11	0.08	0.09	0.10	0.10
V_2O_5	0.15	0.14	0.14	0.15	0.15	0.14	0.16	0.13	0.16	0.16
Al_2O_3	24.30	24.73	25.18	24.69	24.67	24.89	23.17	23.31	24.29	24.15
Cr_2O_3	46.48	46.32	45.51	45.25	45.88	45.43	47.90	47.86	45.13	45.27
FeO^{tot}	14.21	14.00	13.92	13.85	14.23	14.10	14.03	13.79	13.82	13.87
MnO	0.23	0.21	0.23	0.20	0.21	0.22	0.24	0.21	0.22	0.21
MgO	15.12	15.17	15.74	15.58	15.47	15.38	14.92	14.84	15.13	15.11
NiO	0.14	0.15	0.16	0.14	0.16	0.15	0.15	0.14	0.16	0.17
Cr#	0.56	0.56	0.55	0.55	0.55	0.55	0.58	0.58	0.55	0.56
Mg#	0.68	0.68	0.70	0.70	0.69	0.69	0.67	0.67	0.69	0.69
Cr/Fe^{2+}	3.43	3.40	3.55	3.56	3.49	3.45	3.50	3.48	3.47	3.48

Sample	NKS-6							
Analysis#	1	2	3	4	5	6	7	8
TiO_2	0.12	0.13	0.14	0.14	0.12	0.12	0.13	0.12
V_2O_5	0.14	0.14	0.16	0.14	0.15	0.11	0.13	0.15
Al_2O_3	21.33	21.57	21.33	21.42	20.64	20.57	22.64	22.75
Cr_2O_3	47.64	46.96	47.81	47.12	48.47	47.84	47.53	47.10
FeO^{tot}	15.80	15.86	15.83	15.54	16.07	15.99	15.04	15.08
MnO	0.23	0.24	0.24	0.24	0.25	0.24	0.23	0.21
MgO	14.01	14.10	14.22	14.40	13.91	13.61	15.00	14.90
NiO	0.13	0.13	0.13	0.13	0.12	0.12	0.17	0.14
Cr#	0.60	0.59	0.60	0.60	0.61	0.61	0.58	0.58
Mg#	0.65	0.65	0.65	0.66	0.64	0.64	0.68	0.67
Cr/Fe^{2+}	3.29	3.28	3.34	3.42	3.31	3.25	3.50	3.45

Sample	KH1									
Analysis#	1	2	3	4	5	6	7	8	9	10
TiO_2	0.21	0.20	0.20	0.20	0.20	0.20	0.18	0.19	0.20	0.20
V_2O_5	0.12	0.13	0.13	0.15	0.13	0.17	0.15	0.13	0.13	0.12
Al_2O_3	23.18	22.99	22.81	23.36	23.15	22.90	23.46	23.21	22.91	23.03
Cr_2O_3	43.26	43.39	43.72	42.98	43.73	43.82	43.33	43.48	43.07	43.52
FeO^{tot}	16.94	16.63	16.40	16.54	16.39	16.65	16.80	16.47	16.83	16.62
MnO	0.23	0.21	0.23	0.23	0.25	0.20	0.20	0.19	0.24	0.21
MgO	15.21	15.79	15.33	15.14	14.81	14.81	15.34	14.78	15.03	14.81
NiO	0.11	0.17	0.15	0.13	0.12	0.13	0.14	0.11	0.14	0.13
Cr#	0.56	0.56	0.56	0.55	0.56	0.56	0.55	0.56	0.56	0.56
Mg#	0.69	0.71	0.70	0.69	0.68	0.68	0.69	0.67	0.69	0.68
Cr/Fe^{2+}	3.34	3.61	3.49	3.34	3.27	3.26	3.36	3.24	3.34	3.26

Sample	KH2									
Analysis#	1	2	3	4	5	6	7	8	9	10
TiO_2	0.19	0.21	0.22	0.19	0.20	0.19	0.20	0.20	0.19	0.19
V_2O_5	0.11	0.13	0.14	0.14	0.15	0.15	0.11	0.13	0.14	0.13
Al_2O_3	23.37	23.25	23.25	23.36	23.15	23.11	23.23	22.75	23.43	23.68
Cr_2O_3	43.88	43.15	43.56	43.78	43.87	43.66	43.34	43.53	42.99	43.58
FeO^{tot}	16.58	17.03	16.49	16.61	16.91	16.83	16.44	16.11	15.80	16.16
MnO	0.23	0.25	0.19	0.23	0.26	0.22	0.22	0.22	0.25	0.20
MgO	15.05	14.96	15.28	15.46	15.38	15.04	15.52	15.49	15.05	15.45
NiO	0.17	0.13	0.11	0.16	0.14	0.14	0.15	0.11	0.17	0.14
Cr#	0.56	0.55	0.56	0.56	0.56	0.56	0.56	0.56	0.55	0.55
Mg#	0.68	0.68	0.69	0.70	0.69	0.68	0.70	0.71	0.69	0.70
Cr/Fe^{2+}	3.31	3.25	3.38	3.44	3.40	3.31	3.50	3.57	3.38	3.43

Sample	RLM053							
Analysis#	1	2	3	4	5	6	7	8
TiO_2	0.16	0.17	0.17	0.14	0.18	0.17	0.17	0.16
V_2O_5	0.15	0.16	0.14	0.17	0.16	0.15	0.15	0.17
Al_2O_3	20.59	20.24	20.36	20.31	20.15	19.74	19.87	19.52
Cr_2O_3	49.94	49.60	50.23	49.84	49.97	49.77	50.19	49.62
FeO^{tot}	15.47	15.28	15.37	15.31	15.36	15.36	14.84	14.79
MnO	0.25	0.23	0.24	0.23	0.24	0.22	0.25	0.24
MgO	14.38	14.57	14.29	14.55	14.28	14.45	14.65	14.39
NiO	0.20	0.15	0.15	0.13	0.17	0.16	0.15	0.15
Cr#	0.62	0.62	0.62	0.62	0.62	0.63	0.63	0.63
Mg#	0.65	0.67	0.65	0.66	0.65	0.66	0.67	0.67
Cr/Fe^{2+}	3.49	3.60	3.49	3.58	3.51	3.62	3.72	3.68

Sample	RLM058							
Analysis#	1	2	3	4	5	6	7	8
TiO_2	0.22	0.22	0.24	0.23	0.24	0.24	0.25	0.23
V_2O_5	0.16	0.14	0.15	0.13	0.16	0.14	0.17	0.16
Al_2O_3	24.87	24.84	24.71	24.45	26.44	26.70	25.09	25.12
Cr_2O_3	43.66	44.20	43.85	43.57	43.56	43.65	44.55	44.36
FeO^{tot}	15.44	15.34	15.07	15.18	13.77	14.09	14.72	14.60
MnO	0.23	0.23	0.21	0.22	0.22	0.22	0.24	0.22
MgO	14.46	14.47	14.83	14.80	14.67	15.24	14.49	14.86
NiO	0.19	0.16	0.16	0.16	0.17	0.14	0.19	0.23
Cr#	0.54	0.54	0.54	0.54	0.52	0.52	0.54	0.54
Mg#	0.66	0.65	0.67	0.67	0.66	0.68	0.65	0.67
Cr/Fe^{2+}	3.05	3.06	3.19	3.21	3.05	3.16	3.08	3.20

Sample	LQ1									
Analysis#	1	2	3	4	5	6	7	8	9	10
TiO_2	0.17	0.16	0.18	0.17	0.15	0.16	0.15	0.17	0.16	0.16
V_2O_5	0.11	0.15	0.16	0.15	0.14	0.12	0.12	0.13	0.13	0.18
Al_2O_3	19.72	19.67	19.56	19.83	19.57	19.49	19.84	19.75	19.74	19.89
Cr_2O_3	48.35	48.62	48.53	48.34	48.28	48.38	48.44	47.97	48.51	48.56
FeO^{tot}	13.92	13.78	14.24	14.30	14.44	14.53	14.20	14.21	14.48	14.36
MnO	0.23	0.20	0.22	0.25	0.20	0.24	0.22	0.26	0.23	0.21
MgO	16.11	16.26	15.80	16.00	15.78	15.86	15.90	16.12	15.71	15.65
NiO	0.13	0.13	0.14	0.13	0.18	0.13	0.15	0.17	0.15	0.16
Cr#	0.62	0.62	0.62	0.62	0.62	0.62	0.62	0.62	0.62	0.62
Mg#	0.74	0.74	0.73	0.73	0.73	0.73	0.73	0.74	0.72	0.72
Cr/Fe^{2+}	4.54	4.62	4.34	4.39	4.33	4.37	4.37	4.52	4.25	4.19

Sample	LQ2									
Analysis#	1	2	3	4	5	6	7	8	9	10
TiO_2	0.18	0.19	0.18	0.18	0.18	0.18	0.19	0.19	0.19	0.19
V_2O_5	0.10	0.12	0.12	0.12	0.12	0.16	0.14	0.12	0.16	0.11
Al_2O_3	16.58	16.99	16.51	17.15	16.91	16.81	16.53	17.10	16.93	16.83
Cr_2O_3	52.53	52.39	51.97	52.96	51.67	51.93	51.92	52.24	53.48	52.72
FeO^{tot}	14.92	15.32	14.55	14.68	15.35	15.24	15.34	15.12	14.62	15.16
MnO	0.22	0.21	0.26	0.24	0.24	0.23	0.25	0.24	0.29	0.22
MgO	14.94	15.03	15.28	15.78	15.17	15.28	15.52	15.14	14.99	15.34
NiO	0.26	0.22	0.17	0.16	0.21	0.17	0.15	0.16	0.15	0.15
Cr#	0.68	0.67	0.68	0.67	0.67	0.67	0.68	0.67	0.68	0.68
Mg#	0.70	0.69	0.71	0.72	0.70	0.71	0.72	0.70	0.69	0.71
Cr/Fe^{2+}	4.29	4.20	4.52	4.57	4.30	4.35	4.51	4.25	4.23	4.36

Sample	LQ3									
Analysis#	1	2	3	4	5	6	7	8	9	10
TiO_2	0.16	0.16	0.16	0.16	0.15	0.16	0.14	0.13	0.15	0.14
V_2O_5	0.12	0.14	0.15	0.19	0.15	0.14	0.14	0.13	0.14	0.14
Al_2O_3	19.97	20.40	20.66	19.88	20.07	20.35	18.50	18.26	18.82	19.80
Cr_2O_3	49.37	49.49	49.40	49.15	49.88	48.93	51.54	51.67	49.17	50.24
FeO^{tot}	14.79	14.89	14.01	14.71	14.72	14.82	14.44	14.37	14.83	14.65
MnO	0.25	0.24	0.25	0.23	0.23	0.21	0.25	0.24	0.22	0.25
MgO	15.82	15.58	15.70	16.19	15.50	16.08	15.69	15.83	15.90	15.99
NiO	0.22	0.19	0.16	0.20	0.18	0.18	0.10	0.10	0.18	0.15
Cr#	0.62	0.62	0.62	0.62	0.62	0.62	0.65	0.65	0.64	0.63
Mg#	0.72	0.70	0.71	0.73	0.70	0.72	0.71	0.72	0.73	0.72
Cr/Fe^{2+}	4.21	4.01	4.11	4.40	4.04	4.25	4.36	4.48	4.45	4.30

Berit Chromitite Samples

Sample	MBD-4									
Analysis#	1	2	3	4	5	6	7	8	9	10
TiO_2	0.20	0.22	0.22	0.19	0.22	0.21	0.21	0.22	0.21	0.21
V_2O_5	0.15	0.15	0.18	0.17	0.18	0.18	0.14	0.16	0.17	0.17
Al_2O_3	15.44	15.60	16.11	15.84	16.11	16.23	15.90	15.98	15.45	15.73
Cr_2O_3	49.89	50.18	50.03	49.98	49.11	49.40	49.59	49.47	49.70	49.81
FeO^{tot}	23.12	23.11	23.14	22.76	22.99	23.22	22.94	23.09	22.95	22.92
MnO	0.35	0.38	0.39	0.34	0.35	0.36	0.35	0.33	0.38	0.33
MgO	10.86	10.85	11.14	11.24	10.97	10.91	11.01	10.86	11.09	10.83
NiO	0.09	0.09	0.11	0.08	0.07	0.12	0.10	0.11	0.08	0.11
Cr#	0.68	0.68	0.68	0.68	0.67	0.67	0.68	0.67	0.68	0.68
Mg#	0.52	0.52	0.53	0.53	0.52	0.52	0.53	0.52	0.53	0.52
Cr/Fe^{2+}	2.64	2.63	2.64	2.70	2.60	2.59	2.64	2.60	2.69	2.62

Sample	MBD-7									
Analysis#	1	2	3	4	5	6	7	8	9	10
TiO_2	0.42	0.40	0.40	0.39	0.44	0.40	0.45	0.45	0.40	0.37
V_2O_5	0.23	0.23	0.23	0.18	0.23	0.19	0.21	0.23	0.21	0.18
Al_2O_3	29.75	29.93	30.23	30.00	29.45	30.13	30.24	30.50	30.95	30.78
Cr_2O_3	34.97	34.85	35.47	35.26	35.17	35.51	34.39	34.24	34.44	34.84
FeO^{tot}	18.53	18.59	18.62	18.84	18.98	19.07	18.72	18.58	18.25	18.42
MnO	0.25	0.23	0.23	0.26	0.24	0.22	0.21	0.24	0.21	0.23
MgO	15.46	15.30	15.47	15.68	15.53	15.45	15.78	15.41	16.08	15.74
NiO	0.11	0.12	0.12	0.13	0.11	0.13	0.13	0.08	0.13	0.14
Cr#	0.44	0.44	0.44	0.44	0.44	0.44	0.43	0.43	0.43	0.43
Mg#	0.67	0.67	0.67	0.68	0.68	0.67	0.68	0.67	0.69	0.68
Cr/Fe^{2+}	2.49	2.43	2.45	2.52	2.50	2.44	2.49	2.39	2.54	2.49

Sample	MBD-8											
Analysis#	1	2	3	4	5	6	7	8	9	10	11	12
TiO_2	0.45	0.67	0.31	0.34	0.42	0.43	0.46	0.52	0.42	0.51	0.54	0.38
V_2O_5	0.18	0.18	0.18	0.17	0.17	0.21	0.19	0.18	0.19	0.15	0.19	0.21
Al_2O_3	28.99	28.83	29.41	29.77	30.09	30.20	29.75	29.47	29.20	29.27	28.91	28.99
Cr_2O_3	36.06	35.86	36.67	36.69	35.67	35.76	36.28	36.17	35.79	35.74	36.62	36.49
FeO^{tot}	17.52	17.32	18.36	18.32	17.79	17.91	18.19	18.38	18.28	18.12	18.00	17.82
MnO	0.24	0.22	0.23	0.23	0.23	0.23	0.22	0.24	0.25	0.24	0.21	0.22
MgO	15.67	15.81	15.78	15.62	16.03	15.55	15.70	15.64	15.56	15.88	15.78	15.41
NiO	0.20	0.22	0.18	0.20	0.19	0.21	0.20	0.19	0.20	0.19	0.18	0.19
Cr#	0.45	0.45	0.46	0.45	0.44	0.44	0.45	0.45	0.45	0.45	0.46	0.46
Mg#	0.69	0.69	0.68	0.68	0.69	0.67	0.68	0.68	0.68	0.69	0.68	0.68
Cr/Fe^{2+}	2.70	2.71	2.66	2.59	2.67	2.53	2.58	2.57	2.60	2.67	2.67	2.63

Sample	MBD-8A									
Analysis#	1	2	3	4	5	6	7	8	9	10
TiO_2	0.11	0.11	0.11	0.22	0.29	0.48	0.31	0.14	0.17	0.16
V_2O_5	0.13	0.13	0.16	0.17	0.18	0.18	0.15	0.18	0.16	0.16
Al_2O_3	35.78	36.41	35.48	35.69	34.06	33.97	35.15	35.51	36.53	36.65
Cr_2O_3	32.58	33.20	33.05	33.31	34.93	34.43	33.53	33.61	32.88	32.59
FeO^{tot}	13.75	13.75	14.00	14.10	14.66	14.49	14.15	13.81	13.71	13.85
MnO	0.18	0.19	0.19	0.22	0.18	0.20	0.21	0.21	0.18	0.22
MgO	16.94	16.86	16.76	16.78	16.23	16.22	16.42	16.77	17.06	17.07
NiO	0.11	0.14	0.11	0.08	0.10	0.11	0.12	0.10	0.11	0.11
Cr#	0.38	0.38	0.38	0.38	0.41	0.40	0.39	0.39	0.38	0.37
Mg#	0.72	0.71	0.71	0.71	0.69	0.69	0.70	0.71	0.72	0.72
Cr/Fe^{2+}	2.65	2.58	2.62	2.57	2.55	2.52	2.52	2.63	2.60	2.58

Sample	MBD-8B									
Analysis#	1	2	3	4	5	6	7	8	9	10
TiO_2	0.32	0.31	0.34	0.36	0.39	0.34	0.33	0.34	0.64	0.37
V_2O_5	0.17	0.20	0.16	0.21	0.18	0.18	0.20	0.22	0.18	0.18
Al_2O_3	29.73	30.06	30.21	30.43	30.71	30.59	30.35	30.88	30.83	30.84
Cr_2O_3	36.76	36.34	37.01	37.00	36.12	36.65	36.95	36.80	36.94	36.61
FeO^{tot}	15.86	15.75	15.89	15.97	16.35	16.80	16.11	16.15	16.00	16.27
MnO	0.23	0.23	0.24	0.23	0.24	0.23	0.24	0.25	0.23	0.25
MgO	16.63	16.33	16.51	16.44	16.55	16.33	16.47	16.39	16.42	16.34
NiO	0.19	0.21	0.22	0.21	0.17	0.19	0.23	0.22	0.22	0.23
Cr#	0.45	0.45	0.45	0.45	0.44	0.45	0.45	0.44	0.45	0.44
Mg#	0.72	0.71	0.71	0.71	0.71	0.70	0.71	0.70	0.70	0.70
Cr/Fe^{2+}	3.06	2.94	2.97	2.90	2.85	2.79	2.91	2.83	2.77	2.80

Sample	MBD-11									
Analysis#	1	2	3	4	5	6	7	8	9	10
TiO_2	0.42	0.43	0.46	0.47	0.46	0.45	0.45	0.48	0.34	0.32
V_2O_5	0.18	0.17	0.18	0.18	0.18	0.19	0.20	0.20	0.19	0.18
Al_2O_3	29.86	29.38	30.22	30.35	29.86	30.41	30.29	30.21	31.39	31.02
Cr_2O_3	34.95	34.95	34.76	35.59	34.70	35.18	34.92	34.97	34.74	34.75
FeO^{tot}	18.85	18.78	18.83	18.77	18.91	19.09	18.73	18.91	18.15	17.98
MnO	0.25	0.26	0.25	0.26	0.26	0.26	0.24	0.25	0.25	0.25
MgO	15.27	15.11	15.25	15.05	15.30	15.16	15.36	15.19	15.60	15.64
NiO	0.08	0.10	0.14	0.14	0.12	0.12	0.14	0.17	0.12	0.14
Cr#	0.44	0.44	0.44	0.44	0.44	0.44	0.44	0.44	0.43	0.43
Mg#	0.67	0.67	0.66	0.65	0.67	0.66	0.67	0.66	0.67	0.68
Cr/Fe^{2+}	2.42	2.44	2.39	2.35	2.42	2.34	2.41	2.37	2.42	2.48

Sample	MBD-13										
Analysis#	1	2	3	4	5	6	7	8	9	10	11
TiO_2	0.11	0.09	0.14	0.14	0.12	0.12	0.12	0.16	0.14	0.21	0.21
V_2O_5	0.10	0.12	0.14	0.17	0.14	0.16	0.14	0.16	0.16	0.15	0.14
Al_2O_3	35.89	35.54	35.75	35.23	35.30	35.08	34.90	34.83	34.47	33.15	33.24
Cr_2O_3	32.91	32.87	33.31	32.95	33.11	32.83	32.41	32.64	32.75	32.30	32.79
FeO^{tot}	14.53	14.56	14.85	14.49	14.83	14.13	14.29	14.03	14.43	16.86	16.75
MnO	0.18	0.15	0.20	0.19	0.18	0.19	0.19	0.19	0.19	0.18	0.19
MgO	17.15	17.03	16.92	17.01	16.90	16.77	16.77	16.43	16.55	16.24	16.48
NiO	0.08	0.12	0.12	0.10	0.11	0.08	0.10	0.12	0.09	0.13	0.11
Cr#	0.38	0.38	0.38	0.39	0.39	0.39	0.38	0.39	0.39	0.40	0.40
Mg#	0.72	0.72	0.71	0.72	0.72	0.72	0.72	0.71	0.71	0.70	0.71
Cr/Fe^{2+}	2.65	2.65	2.57	2.66	2.61	2.65	2.66	2.59	2.63	2.49	2.56

Sample	Ader-2									
Analysis#	1	2	3	4	5	6	7	8	9	10
TiO_2	0.22	0.24	0.21	0.20	0.20	0.20	0.21	0.19	0.20	0.19
V_2O_5	0.23	0.24	0.21	0.23	0.23	0.24	0.23	0.23	0.19	0.20
Al_2O_3	25.38	25.33	25.32	25.42	26.10	26.09	25.81	25.67	25.59	25.64
Cr_2O_3	41.76	41.98	42.17	42.83	42.37	42.20	42.17	42.63	42.74	42.98
FeO^{tot}	14.83	14.84	15.00	15.17	15.25	15.37	15.30	14.86	15.12	15.21
MnO	0.22	0.23	0.21	0.22	0.21	0.19	0.21	0.19	0.23	0.23
MgO	16.22	15.94	15.82	16.27	16.03	16.15	16.09	15.98	15.87	16.00
NiO	0.12	0.11	0.10	0.07	0.12	0.11	0.10	0.10	0.12	0.10
Cr#	0.52	0.53	0.53	0.53	0.52	0.52	0.52	0.53	0.53	0.53
Mg#	0.72	0.71	0.71	0.72	0.71	0.71	0.71	0.71	0.70	0.71
Cr/Fe^{2+}	3.58	3.47	3.43	3.54	3.37	3.40	3.42	3.44	3.41	3.43

Sample	Ader-3									
Analysis#	1	2	3	4	5	6	7	8	9	10
TiO_2	0.19	0.18	0.22	0.22	0.27	0.25	0.19	0.19	0.29	0.26
V_2O_5	0.25	0.23	0.23	0.22	0.23	0.23	0.21	0.23	0.22	0.23
Al_2O_3	24.16	23.96	23.91	23.60	24.42	24.47	24.11	24.32	25.21	25.16
Cr_2O_3	43.65	42.63	43.31	42.98	43.19	42.55	42.44	42.57	42.92	42.78
FeO^{tot}	16.40	16.77	17.14	17.23	16.03	15.80	18.24	18.11	15.12	15.05
MnO	0.26	0.24	0.23	0.24	0.25	0.25	0.24	0.28	0.25	0.25
MgO	16.07	15.67	15.72	15.64	16.20	15.73	15.46	15.41	16.37	16.09
NiO	0.10	0.11	0.08	0.09	0.11	0.11	0.09	0.10	0.10	0.12
Cr#	0.55	0.54	0.55	0.55	0.54	0.54	0.54	0.54	0.53	0.53
Mg#	0.71	0.70	0.70	0.70	0.72	0.70	0.69	0.68	0.72	0.71
Cr/Fe^{2+}	3.53	3.40	3.36	3.38	3.56	3.42	3.18	3.15	3.60	3.52

Sample	Ader-4									
Analysis#	1	2	3	4	5	6	7	8	9	10
TiO_2	0.16	0.16	0.18	0.18	0.20	0.17	0.19	0.19	0.18	0.18
V_2O_5	0.24	0.21	0.24	0.25	0.23	0.26	0.23	0.23	0.21	0.25
Al_2O_3	23.90	23.74	24.35	24.29	24.34	23.90	24.08	24.03	23.80	24.04
Cr_2O_3	43.74	43.82	44.24	44.32	43.92	43.02	43.33	42.90	43.26	43.74
FeO^{tot}	16.95	17.21	16.09	16.40	16.53	16.80	17.01	16.86	17.11	16.97
MnO	0.27	0.27	0.26	0.27	0.25	0.27	0.27	0.28	0.29	0.27
MgO	15.56	15.40	15.83	15.56	15.82	15.54	15.38	15.45	15.22	15.25
NiO	0.10	0.11	0.10	0.13	0.09	0.10	0.12	0.10	0.08	0.09
Cr#	0.55	0.55	0.55	0.55	0.55	0.55	0.55	0.54	0.55	0.55
Mg#	0.69	0.69	0.70	0.69	0.70	0.70	0.69	0.69	0.68	0.68
Cr/Fe^{2+}	3.35	3.30	3.44	3.34	3.40	3.35	3.26	3.30	3.24	3.23

Sample	Ader-5									
Analysis#	1	2	3	4	5	6	7	8	9	10
TiO_2	0.23	0.22	0.15	0.17	0.22	0.22	0.22	0.21	0.20	0.19
V_2O_5	0.24	0.24	0.22	0.21	0.22	0.26	0.22	0.22	0.21	0.22
Al_2O_3	25.02	24.99	23.59	23.81	23.88	23.90	24.40	24.50	23.77	23.94
Cr_2O_3	42.74	42.30	42.92	43.28	43.21	42.82	43.06	42.99	42.71	43.03
FeO^{tot}	17.20	17.21	18.09	18.02	18.22	18.46	17.59	17.69	18.30	18.15
MnO	0.28	0.26	0.27	0.28	0.25	0.25	0.25	0.26	0.28	0.28
MgO	15.56	15.32	15.37	15.31	15.20	15.21	15.16	15.06	15.09	15.03
NiO	0.11	0.12	0.09	0.10	0.10	0.12	0.08	0.13	0.12	0.12
Cr#	0.53	0.53	0.55	0.55	0.55	0.55	0.54	0.54	0.55	0.55
Mg#	0.69	0.68	0.69	0.68	0.67	0.67	0.67	0.67	0.67	0.67
Cr/Fe^{2+}	3.18	3.11	3.24	3.20	3.12	3.10	3.10	3.07	3.11	3.09

Sample	DMK-9									
Analysis#	1	2	3	4	5	6	7	8	9	10
TiO_2	0.16	0.15	0.16	0.15	0.15	0.17	0.16	0.15	0.16	0.15
V_2O_5	0.16	0.18	0.19	0.16	0.16	0.19	0.15	0.16	0.16	0.19
Al_2O_3	27.97	27.31	27.57	27.22	27.23	28.41	27.70	27.42	27.28	27.09
Cr_2O_3	38.69	38.20	38.94	38.76	39.14	38.86	38.43	38.44	39.61	39.65
FeO^{tot}	17.53	17.27	17.67	17.51	17.34	17.34	17.22	17.05	17.06	17.16
MnO	0.25	0.28	0.25	0.24	0.26	0.27	0.26	0.28	0.27	0.26
MgO	15.33	15.22	15.11	14.97	15.41	15.20	15.12	15.11	15.35	14.91
NiO	0.17	0.16	0.14	0.16	0.15	0.14	0.15	0.15	0.17	0.14
Cr#	0.48	0.48	0.49	0.49	0.49	0.48	0.48	0.48	0.49	0.50
Mg#	0.68	0.68	0.67	0.67	0.68	0.67	0.68	0.68	0.68	0.67
Cr/Fe^{2+}	2.81	2.87	2.77	2.79	2.92	2.74	2.80	2.84	2.92	2.81

Sample	DMK-12									
Analysis#	1	2	3	4	5	6	7	8	9	10
TiO_2	0.24	0.24	0.25	0.24	0.23	0.22	0.25	0.26	0.24	0.24
V_2O_5	0.20	0.21	0.18	0.17	0.20	0.21	0.21	0.21	0.18	0.20
Al_2O_3	24.19	24.05	24.91	24.64	24.50	24.22	23.61	23.19	24.58	24.58
Cr_2O_3	42.91	42.16	41.70	41.32	42.08	41.91	42.45	42.68	42.34	42.34
FeO^{tot}	18.44	18.18	18.40	17.94	17.94	17.67	18.24	17.96	18.47	18.16
MnO	0.27	0.26	0.27	0.27	0.24	0.26	0.23	0.24	0.25	0.23
MgO	15.09	14.99	15.20	14.87	14.61	14.65	14.70	14.16	15.03	14.95
NiO	0.14	0.14	0.15	0.12	0.16	0.14	0.16	0.14	0.14	0.16
Cr#	0.54	0.54	0.53	0.53	0.54	0.54	0.55	0.55	0.54	0.54
Mg#	0.67	0.67	0.67	0.67	0.66	0.66	0.66	0.65	0.67	0.67
Cr/Fe^{2+}	3.05	3.05	3.01	2.98	2.93	2.99	3.01	2.93	2.99	2.99

Sample	DMK-16									
Analysis#	1	2	3	4	5	6	7	8	9	10
TiO_2	0.23	0.22	0.24	0.22	0.24	0.23	0.22	0.22	0.22	0.22
V_2O_5	0.15	0.15	0.16	0.19	0.15	0.15	0.14	0.13	0.16	0.14
Al_2O_3	27.68	27.63	27.88	27.98	28.58	27.78	27.51	27.61	27.52	27.13
Cr_2O_3	39.17	39.32	39.32	39.02	38.90	39.15	39.08	38.97	38.98	38.42
FeO^{tot}	16.99	17.08	17.17	17.26	17.67	17.16	17.12	17.79	17.04	17.26
MnO	0.23	0.23	0.22	0.21	0.21	0.22	0.24	0.22	0.23	0.21
MgO	15.15	15.19	15.14	15.09	15.22	14.95	14.95	14.96	14.81	15.04
NiO	0.16	0.16	0.17	0.17	0.15	0.18	0.14	0.14	0.14	0.16
Cr#	0.49	0.49	0.49	0.48	0.48	0.49	0.49	0.49	0.49	0.49
Mg#	0.49	0.49	0.49	0.48	0.48	0.49	0.49	0.49	0.49	0.49
Cr/Fe^{2+}	2.81	2.82	2.77	2.74	2.69	2.74	2.77	2.72	2.74	2.82

Sample	DMK-17									
Analysis#	1	2	3	4	5	6	7	8	9	10
TiO_2	0.15	0.15	0.15	0.16	0.16	0.14	0.15	0.14	0.15	0.15
V_2O_5	0.15	0.16	0.17	0.17	0.17	0.18	0.14	0.17	0.15	0.13
Al_2O_3	27.22	26.93	27.94	27.60	27.65	27.04	27.27	27.43	27.26	27.05
Cr_2O_3	41.10	40.80	40.82	40.57	39.79	39.66	40.37	40.21	40.24	40.41
FeO^{tot}	15.69	15.58	15.71	15.56	15.36	15.53	15.59	15.39	15.04	15.07
MnO	0.23	0.21	0.23	0.23	0.22	0.20	0.23	0.22	0.21	0.21
MgO	15.60	15.74	15.65	15.68	15.53	15.80	15.48	15.59	15.91	15.71
NiO	0.17	0.15	0.12	0.14	0.16	0.16	0.17	0.13	0.15	0.14
Cr#	0.50	0.50	0.49	0.50	0.49	0.50	0.50	0.50	0.50	0.50
Mg#	0.69	0.70	0.69	0.69	0.69	0.71	0.69	0.69	0.71	0.70
Cr/Fe^{2+}	3.11	3.19	3.03	3.09	3.06	3.20	3.08	3.10	3.25	3.21

Sample	DMK-18									
Analysis#	1	2	3	4	5	6	7	8	9	10
TiO_2	0.16	0.16	0.18	0.16	0.17	0.17	0.17	0.16	0.17	0.17
V_2O_5	0.14	0.17	0.15	0.15	0.17	0.14	0.16	0.15	0.15	0.15
Al_2O_3	27.57	27.46	27.57	27.40	26.38	26.56	27.19	26.94	26.73	27.04
Cr_2O_3	40.94	40.91	40.14	40.59	41.09	40.99	40.39	40.06	40.54	40.64
FeO^{tot}	16.05	16.00	15.88	16.09	16.19	15.97	16.17	15.70	16.16	16.10
MnO	0.23	0.22	0.24	0.22	0.24	0.23	0.21	0.22	0.23	0.22
MgO	15.69	15.65	15.78	15.73	15.42	15.06	15.58	15.63	15.53	15.51
NiO	0.16	0.15	0.15	0.17	0.15	0.15	0.16	0.15	0.19	0.19
Cr#	0.50	0.50	0.49	0.50	0.51	0.51	0.50	0.50	0.50	0.50
Mg#	0.69	0.69	0.70	0.69	0.69	0.68	0.69	0.70	0.69	0.69
Cr/Fe^{2+}	3.07	3.06	3.10	3.09	3.10	3.00	3.05	3.15	3.11	3.07

Sample	DMK-28									
Analysis#	1	2	3	4	5	6	7	8	9	10
TiO_2	0.17	0.17	0.18	0.19	0.20	0.19	0.18	0.17	0.19	0.17
V_2O_5	0.15	0.14	0.16	0.14	0.15	0.13	0.15	0.13	0.13	0.17
Al_2O_3	29.02	28.80	26.98	27.14	27.00	26.98	27.11	27.34	26.68	27.31
Cr_2O_3	39.20	39.09	40.52	40.26	40.38	40.44	40.22	40.71	40.68	40.18
FeO^{tot}	14.78	14.70	14.84	14.95	15.50	15.08	15.15	15.36	15.22	15.42
MnO	0.20	0.23	0.21	0.22	0.24	0.21	0.21	0.23	0.20	0.22
MgO	16.64	16.56	15.84	16.04	15.79	15.92	16.22	16.00	15.95	15.68
NiO	0.16	0.17	0.14	0.17	0.14	0.19	0.16	0.13	0.17	0.18
Cr#	0.48	0.48	0.50	0.50	0.50	0.50	0.50	0.50	0.51	0.50
Mg#	0.73	0.73	0.71	0.71	0.70	0.71	0.72	0.71	0.71	0.70
Cr/Fe^{2+}	3.30	3.32	3.27	3.32	3.20	3.29	3.37	3.24	3.32	3.14

Sample	KBK-2									
Analysis#	1	2	3	4	5	6	7	8	9	10
TiO_2	0.35	0.36	0.35	0.34	0.36	0.33	0.37	0.36	0.36	0.37
V_2O_5	0.23	0.21	0.21	0.22	0.21	0.21	0.24	0.22	0.20	0.22
Al_2O_3	25.27	24.87	25.25	25.02	24.56	24.31	23.57	23.30	24.22	23.81
Cr_2O_3	41.85	41.93	41.00	41.32	41.66	42.22	42.30	42.14	42.16	41.69
FeO^{tot}	18.09	17.92	17.36	17.00	17.65	17.72	17.59	17.73	17.57	17.95
MnO	0.26	0.26	0.26	0.25	0.28	0.27	0.26	0.26	0.27	0.27
MgO	14.65	14.78	14.87	14.60	14.72	14.22	14.51	14.48	14.42	14.20
NiO	0.19	0.17	0.18	0.18	0.16	0.16	0.17	0.17	0.17	0.18
Cr#	0.53	0.53	0.52	0.53	0.53	0.54	0.55	0.55	0.54	0.54
Mg#	0.65	0.66	0.67	0.66	0.66	0.64	0.66	0.66	0.65	0.65
Cr/Fe^{2+}	2.82	2.90	2.93	2.91	2.94	2.84	2.98	3.00	2.91	2.86

Sample	KBK-16									
Analysis#	1	2	3	4	5	6	7	8	9	10
TiO_2	0.17	0.16	0.16	0.15	0.16	0.17	0.16	0.16	0.16	0.16
V_2O_5	0.20	0.18	0.20	0.20	0.18	0.17	0.18	0.18	0.19	0.19
Al_2O_3	26.82	26.69	27.35	27.33	26.92	26.86	26.59	26.75	26.25	26.38
Cr_2O_3	39.22	39.42	39.68	39.50	39.09	39.54	39.21	39.63	39.67	39.67
FeO^{tot}	16.42	16.50	16.08	16.00	15.68	15.40	16.08	16.26	16.48	16.16
MnO	0.25	0.25	0.26	0.24	0.24	0.22	0.24	0.22	0.26	0.24
MgO	16.15	15.93	15.97	15.92	16.09	16.04	16.16	15.86	16.02	16.11
NiO	0.20	0.14	0.14	0.16	0.13	0.15	0.16	0.16	0.16	0.13
Cr#	0.50	0.50	0.49	0.49	0.49	0.50	0.50	0.50	0.50	0.50
Mg#	0.72	0.71	0.71	0.71	0.72	0.72	0.72	0.71	0.71	0.72
Cr/Fe^{2+}	3.27	3.20	3.16	3.16	3.30	3.31	3.34	3.19	3.29	3.33

Sample	KBK-17									
Analysis#	1	2	3	4	5	6	7	8	9	10
TiO_2	0.17	0.16	0.17	0.18	0.16	0.15	0.16	0.16	0.17	0.18
V_2O_5	0.18	0.20	0.19	0.21	0.16	0.19	0.17	0.18	0.16	0.19
Al_2O_3	26.47	26.63	27.44	27.33	27.00	26.64	27.44	27.41	26.37	25.94
Cr_2O_3	40.39	40.53	39.47	38.72	39.34	39.62	38.43	37.47	39.38	39.44
FeO^{tot}	19.56	19.44	18.88	18.76	19.34	19.10	19.25	19.42	19.13	19.29
MnO	0.27	0.27	0.27	0.28	0.27	0.27	0.27	0.26	0.27	0.25
MgO	14.13	13.94	14.85	14.96	14.24	14.39	14.39	14.47	13.82	13.68
NiO	0.15	0.15	0.14	0.13	0.16	0.12	0.15	0.14	0.11	0.11
Cr#	0.51	0.51	0.49	0.49	0.49	0.50	0.48	0.48	0.50	0.50
Mg#	0.63	0.62	0.65	0.66	0.63	0.64	0.64	0.65	0.62	0.62
Cr/Fe^{2+}	2.55	2.50	2.65	2.68	2.53	2.61	2.52	2.52	2.51	2.50

Sample	KBK-18									
Analysis#	1	2	3	4	5	6	7	8	9	10
TiO_2	0.20	0.20	0.19	0.19	0.19	0.19	0.19	0.19	0.18	0.19
V_2O_5	0.19	0.20	0.21	0.21	0.20	0.20	0.19	0.22	0.20	0.21
Al_2O_3	26.53	26.21	26.32	26.13	26.49	26.40	26.73	25.92	26.27	26.56
Cr_2O_3	39.72	40.01	40.05	39.70	39.26	39.12	39.78	39.53	39.70	39.58
FeO^{tot}	18.60	18.84	18.83	18.20	18.51	18.75	18.10	18.10	18.83	18.29
MnO	0.30	0.26	0.26	0.26	0.28	0.27	0.26	0.26	0.29	0.27
MgO	14.28	14.55	14.40	14.18	14.20	14.88	14.59	14.50	14.40	14.18
NiO	0.13	0.12	0.11	0.12	0.12	0.12	0.13	0.12	0.12	0.12
Cr#	0.50	0.51	0.51	0.50	0.50	0.50	0.50	0.51	0.50	0.50
Mg#	0.64	0.65	0.64	0.64	0.64	0.66	0.65	0.65	0.64	0.64
Cr/Fe^{2+}	2.62	2.69	2.64	2.65	2.60	2.75	2.70	2.74	2.65	2.61

Sample	KBK-19									
Analysis#	1	2	3	4	5	6	7	8	9	10
TiO_2	0.23	0.23	0.23	0.24	0.23	0.24	0.23	0.22	0.23	0.23
V_2O_5	0.18	0.18	0.20	0.18	0.17	0.18	0.17	0.19	0.17	0.20
Al_2O_3	26.62	27.21	27.19	26.88	27.16	27.37	27.15	26.57	26.61	26.42
Cr_2O_3	40.69	40.15	41.01	40.24	40.36	40.34	40.78	40.28	40.97	40.62
FeO^{tot}	15.88	16.02	15.82	16.04	16.03	16.12	15.62	15.76	15.72	15.76
MnO	0.24	0.20	0.23	0.26	0.25	0.21	0.24	0.23	0.23	0.23
MgO	15.38	15.38	15.67	15.27	15.68	15.40	15.70	15.72	15.91	15.86
NiO	0.13	0.14	0.14	0.13	0.15	0.14	0.15	0.14	0.15	0.13
Cr#	0.51	0.50	0.50	0.50	0.50	0.50	0.50	0.50	0.51	0.51
Mg#	0.69	0.68	0.69	0.68	0.69	0.68	0.69	0.70	0.70	0.70
Cr/Fe^{2+}	3.07	2.98	3.08	2.99	3.09	2.96	3.12	3.18	3.24	3.24

Sample	KBK-20									
Analysis#	1	2	3	4	5	6	7	8	9	10
TiO_2	0.22	0.22	0.23	0.24	0.22	0.21	0.21	0.20	0.22	0.22
V_2O_5	0.16	0.17	0.16	0.20	0.20	0.19	0.17	0.17	0.18	0.19
Al_2O_3	27.45	27.19	27.16	26.97	26.92	26.62	27.87	27.49	26.47	26.34
Cr_2O_3	40.04	39.35	39.68	40.18	40.67	40.68	39.73	39.45	41.26	40.74
FeO^{tot}	16.11	15.85	15.68	15.67	15.85	16.06	15.93	15.48	15.95	15.84
MnO	0.26	0.25	0.25	0.26	0.25	0.28	0.26	0.23	0.26	0.24
MgO	15.44	15.57	15.38	15.41	14.99	15.28	15.67	15.61	15.33	15.48
NiO	0.14	0.16	0.15	0.14	0.12	0.15	0.15	0.14	0.14	0.13
Cr#	0.49	0.49	0.49	0.50	0.50	0.51	0.49	0.49	0.51	0.51
Mg#	0.68	0.70	0.69	0.69	0.67	0.68	0.69	0.70	0.68	0.69
Cr/Fe^{2+}	2.98	3.07	3.03	3.05	2.93	3.03	3.02	3.08	3.07	3.13

Sample	KBK-21									
Analysis#	1	2	3	4	5	6	7	8	9	10
TiO_2	0.27	0.27	0.28	0.28	0.28	0.30	0.30	0.29	0.29	0.29
V_2O_5	0.18	0.18	0.21	0.17	0.21	0.17	0.20	0.19	0.20	0.21
Al_2O_3	27.37	27.62	26.28	26.66	26.83	26.79	26.86	26.51	26.84	26.80
Cr_2O_3	40.18	39.86	41.32	41.20	41.69	41.47	41.36	41.47	40.93	40.79
FeO^{tot}	15.02	14.65	15.28	15.14	15.67	15.47	15.48	15.27	15.79	15.18
MnO	0.21	0.21	0.20	0.20	0.21	0.19	0.21	0.21	0.22	0.21
MgO	16.02	16.01	15.66	15.69	15.66	15.59	15.78	15.52	15.33	15.63
NiO	0.16	0.17	0.17	0.13	0.14	0.15	0.13	0.14	0.13	0.12
Cr#	0.50	0.49	0.51	0.51	0.51	0.51	0.51	0.51	0.51	0.51
Mg#	0.71	0.71	0.70	0.70	0.69	0.69	0.69	0.69	0.68	0.69
Cr/Fe^{2+}	3.24	3.24	3.22	3.19	3.11	3.12	3.16	3.14	3.01	3.15

Sample	KBK-22									
Analysis#	1	2	3	4	5	6	7	8	9	10
TiO_2	0.29	0.29	0.30	0.29	0.29	0.28	0.27	0.29	0.30	0.29
V_2O_5	0.20	0.18	0.18	0.17	0.19	0.19	0.17	0.18	0.19	0.19
Al_2O_3	26.02	26.09	26.48	26.06	25.61	25.57	26.40	26.47	26.09	26.02
Cr_2O_3	42.07	41.49	40.91	41.05	42.25	42.43	41.47	41.14	41.85	41.68
FeO^{tot}	15.83	15.24	15.09	15.41	16.37	15.82	15.75	15.71	15.99	15.99
MnO	0.22	0.22	0.23	0.22	0.22	0.22	0.23	0.22	0.24	0.22
MgO	15.75	15.74	15.89	15.78	15.74	15.65	15.58	15.99	15.60	15.49
NiO	0.14	0.16	0.12	0.14	0.15	0.12	0.16	0.15	0.17	0.15
Cr#	0.52	0.52	0.51	0.51	0.53	0.53	0.51	0.51	0.52	0.52
Mg#	0.69	0.70	0.71	0.70	0.69	0.69	0.69	0.71	0.69	0.69
Cr/Fe^{2+}	3.22	3.27	3.29	3.28	3.23	3.25	3.15	3.27	3.16	3.13

Sample	KBK-37									
Analysis#	1	2	3	4	5	6	7	8	9	10
TiO_2	0.22	0.23	0.21	0.20	0.22	0.23	0.22	0.22	0.23	0.23
V_2O_5	0.17	0.15	0.17	0.16	0.16	0.19	0.18	0.17	0.17	0.18
Al_2O_3	28.74	29.16	30.01	29.97	29.07	29.62	28.71	28.65	29.86	29.47
Cr_2O_3	39.29	39.01	38.89	38.77	38.77	38.53	39.08	39.29	38.28	38.49
FeO^{tot}	14.99	15.08	14.31	14.18	14.78	15.00	15.24	15.00	15.20	15.25
MnO	0.23	0.23	0.22	0.21	0.22	0.21	0.23	0.21	0.21	0.22
MgO	16.67	16.62	17.31	17.06	16.69	16.56	16.53	16.28	16.18	16.60
NiO	0.14	0.15	0.13	0.15	0.18	0.16	0.15	0.16	0.15	0.16
Cr#	0.48	0.47	0.46	0.46	0.47	0.47	0.48	0.48	0.46	0.47
Mg#	0.73	0.72	0.74	0.74	0.73	0.72	0.72	0.71	0.70	0.72
Cr/Fe^{2+}	3.30	3.22	3.42	3.36	3.30	3.14	3.24	3.18	2.99	3.15

Sample	KBK-38									
Analysis#	1	2	3	4	5	6	7	8	9	10
TiO_2	0.23	0.25	0.23	0.24	0.23	0.23	0.24	0.24	0.23	0.25
V_2O_5	0.17	0.18	0.17	0.17	0.15	0.17	0.17	0.16	0.14	0.16
Al_2O_3	29.24	28.60	28.65	28.91	28.86	28.41	29.07	28.75	29.58	28.96
Cr_2O_3	38.86	38.61	38.38	38.34	38.49	38.26	38.61	38.95	39.05	38.67
FeO^{tot}	15.25	15.23	15.40	15.27	15.61	15.39	15.07	15.32	14.99	14.84
MnO	0.20	0.21	0.20	0.22	0.23	0.23	0.23	0.22	0.21	0.20
MgO	16.69	16.40	16.41	16.41	16.44	16.42	16.87	16.72	17.10	17.05
NiO	0.19	0.17	0.17	0.17	0.19	0.17	0.18	0.18	0.16	0.17
Cr#	0.47	0.48	0.47	0.47	0.47	0.47	0.47	0.48	0.47	0.47
Mg#	0.72	0.72	0.72	0.72	0.72	0.72	0.73	0.73	0.73	0.74
Cr/Fe^{2+}	3.22	3.20	3.19	3.17	3.16	3.23	3.32	3.29	3.34	3.42

Sample	KBK-39									
Analysis#	1	2	3	4	5	6	7	8	9	10
TiO_2	0.24	0.24	0.23	0.23	0.23	0.24	0.24	0.24	0.23	0.23
V_2O_5	0.16	0.19	0.18	0.18	0.18	0.18	0.18	0.16	0.17	0.16
Al_2O_3	28.34	27.88	28.34	28.18	28.44	28.15	28.61	28.14	28.16	28.07
Cr_2O_3	38.12	38.49	39.26	38.65	39.19	38.62	39.28	39.27	39.09	39.05
FeO^{tot}	15.48	15.56	15.38	15.53	15.49	15.07	14.89	15.08	15.21	15.23
MnO	0.24	0.22	0.22	0.22	0.22	0.23	0.21	0.22	0.22	0.21
MgO	16.20	16.00	16.56	16.22	16.27	16.16	16.26	16.48	16.55	16.49
NiO	0.16	0.12	0.15	0.15	0.16	0.15	0.16	0.17	0.15	0.14
Cr#	0.47	0.48	0.48	0.48	0.48	0.48	0.48	0.48	0.48	0.48
Mg#	0.72	0.71	0.72	0.71	0.71	0.72	0.71	0.72	0.73	0.72
Cr/Fe^{2+}	3.16	3.12	3.27	3.17	3.15	3.20	3.18	3.31	3.31	3.31

Sample	MBI-2									
Analysis#	1	2	3	4	5	6	7	8	9	10
TiO_2	0.27	0.27	0.27	0.25	0.27	0.23	0.27	0.27	0.25	0.25
V_2O_5	0.20	0.17	0.15	0.17	0.17	0.19	0.16	0.19	0.15	0.17
Al_2O_3	27.87	27.77	27.58	28.41	28.30	28.86	27.92	27.79	28.10	28.49
Cr_2O_3	38.45	38.98	39.27	38.62	38.66	37.78	39.67	39.10	39.09	39.09
FeO^{tot}	16.11	15.56	16.03	15.34	15.47	15.26	15.94	16.24	15.45	15.98
MnO	0.21	0.23	0.24	0.22	0.22	0.22	0.22	0.21	0.23	0.21
MgO	15.66	15.77	15.50	15.98	15.82	15.83	15.82	16.01	16.13	15.84
NiO	0.20	0.17	0.19	0.23	0.16	0.19	0.22	0.20	0.21	0.19
Cr#	0.48	0.48	0.49	0.48	0.48	0.47	0.49	0.49	0.48	0.48
Mg#	0.70	0.70	0.69	0.71	0.70	0.70	0.70	0.70	0.71	0.69
Cr/Fe^{2+}	2.98	3.07	2.98	3.09	3.03	3.00	3.04	3.08	3.17	2.98

Sample	MBI-5									
Analysis#	1	2	3	4	5	6	7	8	9	10
TiO_2	0.19	0.21	0.20	0.18	0.19	0.20	0.20	0.20	0.19	0.20
V_2O_5	0.18	0.16	0.18	0.15	0.18	0.17	0.20	0.17	0.19	0.19
Al_2O_3	27.34	27.42	27.49	27.81	27.87	27.63	27.89	27.81	26.89	27.29
Cr_2O_3	41.04	40.36	41.11	40.94	40.99	40.96	40.43	40.54	40.70	40.86
FeO^{tot}	14.34	14.11	14.32	14.37	13.97	14.37	14.33	14.18	14.19	14.21
MnO	0.22	0.18	0.22	0.23	0.20	0.22	0.21	0.22	0.21	0.22
MgO	17.28	17.51	17.12	17.28	17.68	17.37	17.47	17.42	17.12	16.99
NiO	0.13	0.14	0.13	0.12	0.12	0.15	0.16	0.17	0.15	0.15
Cr#	0.50	0.50	0.50	0.50	0.50	0.50	0.49	0.49	0.50	0.50
Mg#	0.75	0.76	0.74	0.75	0.76	0.75	0.76	0.76	0.75	0.74
Cr/Fe^{2+}	3.81	3.94	3.71	3.74	3.93	3.79	3.80	3.83	3.84	3.70

Sample	MBI-9									
Analysis#	1	2	3	4	5	6	7	8	9	10
TiO_2	0.26	0.25	0.25	0.24	0.24	0.25	0.24	0.23	0.23	0.24
V_2O_5	0.17	0.15	0.15	0.18	0.18	0.20	0.15	0.13	0.14	0.17
Al_2O_3	28.49	28.02	28.81	28.52	28.56	28.64	28.88	29.05	28.81	28.36
Cr_2O_3	38.82	39.00	37.71	38.08	38.64	38.55	38.21	38.12	38.62	38.81
FeO^{tot}	15.62	15.65	15.24	15.13	15.25	15.48	15.97	15.90	15.66	15.76
MnO	0.23	0.22	0.21	0.23	0.21	0.21	0.22	0.22	0.21	0.23
MgO	16.02	16.11	16.13	16.51	16.38	16.42	16.42	16.55	15.80	16.06
NiO	0.22	0.20	0.19	0.23	0.22	0.17	0.20	0.19	0.20	0.19
Cr#	0.48	0.48	0.47	0.47	0.48	0.47	0.47	0.47	0.47	0.48
Mg#	0.70	0.71	0.71	0.73	0.72	0.72	0.72	0.72	0.70	0.71
Cr/Fe^{2+}	3.07	3.15	3.10	3.28	3.21	3.17	3.12	3.16	2.97	3.09

Sample	MBK-2									
Analysis#	1	2	3	4	5	6	7	8	9	10
TiO_2	0.11	0.12	0.11	0.11	0.10	0.11	0.11	0.12	0.11	0.12
V_2O_5	0.09	0.07	0.08	0.05	0.09	0.07	0.09	0.05	0.04	0.06
Al_2O_3	18.02	17.83	16.89	17.71	18.27	17.70	17.46	17.49	18.17	17.59
Cr_2O_3	46.05	46.41	46.84	46.39	46.32	46.27	47.06	47.25	46.41	46.77
FeO^{tot}	25.97	25.97	26.52	26.83	25.27	25.65	24.80	25.31	24.79	24.86
MnO	0.38	0.37	0.39	0.36	0.35	0.36	0.39	0.37	0.34	0.36
MgO	8.59	8.35	8.28	7.98	8.74	8.58	8.33	8.46	8.32	8.51
NiO	0.08	0.10	0.10	0.08	0.09	0.05	0.07	0.06	0.11	0.07
Cr#	0.63	0.64	0.65	0.64	0.63	0.64	0.64	0.64	0.63	0.64
Mg#	0.42	0.41	0.41	0.39	0.42	0.42	0.41	0.41	0.41	0.42
Cr/Fe^{2+}	2.04	2.03	2.05	1.97	2.07	2.07	2.09	2.09	2.05	2.10

Sample	MBK-14									
Analysis#	1	2	3	4	5	6	7	8	9	10
TiO_2	0.12	0.13	0.12	0.12	0.11	0.12	0.09	0.12	0.11	0.12
V_2O_5	0.12	0.11	0.11	0.10	0.10	0.09	0.11	0.09	0.09	0.09
Al_2O_3	8.66	8.90	8.83	8.86	8.57	8.44	8.23	8.62	8.38	8.28
Cr_2O_3	57.55	57.79	57.81	57.34	57.99	58.02	57.24	57.14	57.50	57.85
FeO^{tot}	24.94	24.86	24.32	24.04	24.40	24.64	23.93	24.64	22.91	22.51
MnO	0.44	0.42	0.42	0.43	0.45	0.42	0.43	0.44	0.41	0.40
MgO	8.83	8.92	9.05	8.96	8.60	8.84	8.62	8.44	9.85	9.89
NiO	0.07	0.06	0.07	0.05	0.05	0.07	0.08	0.04	0.07	0.09
Cr#	0.82	0.81	0.81	0.81	0.82	0.82	0.82	0.82	0.82	0.82
Mg#	0.44	0.44	0.45	0.45	0.43	0.44	0.44	0.43	0.50	0.50
Cr/Fe^{2+}	2.73	2.73	2.78	2.78	2.73	2.76	2.77	2.68	3.04	3.08

Sample	MBS-1									
Analysis#	1	2	3	4	5	6	7	8	9	10
TiO_2	0.16	0.18	0.15	0.15	0.15	0.16	0.17	0.16	0.17	0.16
V_2O_5	0.23	0.22	0.20	0.24	0.22	0.23	0.24	0.22	0.22	0.18
Al_2O_3	26.61	26.27	25.66	26.10	25.88	25.35	24.23	24.13	25.87	26.16
Cr_2O_3	41.10	40.55	40.41	40.28	41.12	41.14	41.39	41.60	40.82	41.03
FeO^{tot}	16.91	16.76	16.58	16.79	16.43	16.58	16.97	17.00	16.22	15.88
MnO	0.22	0.21	0.21	0.22	0.23	0.19	0.26	0.24	0.18	0.22
MgO	15.94	16.19	15.58	15.45	15.58	15.39	15.41	15.56	15.95	16.09
NiO	0.16	0.14	0.14	0.17	0.14	0.12	0.16	0.11	0.12	0.16
Cr#	0.51	0.51	0.51	0.51	0.52	0.52	0.53	0.54	0.51	0.51
Mg#	0.70	0.71	0.70	0.69	0.69	0.69	0.70	0.70	0.71	0.71
Cr/Fe^{2+}	3.16	3.29	3.20	3.08	3.18	3.16	3.28	3.34	3.30	3.37

Sample	MBA-6									
Analysis#	1	2	3	4	5	6	7	8	9	10
TiO_2	0.38	0.37	0.34	0.33	0.34	0.32	0.37	0.39	0.34	0.29
V_2O_5	0.25	0.24	0.26	0.23	0.26	0.26	0.21	0.20	0.23	0.21
Al_2O_3	24.41	24.04	24.30	23.93	24.16	23.81	23.75	23.89	24.87	25.03
Cr_2O_3	41.94	41.82	42.19	41.60	42.08	41.92	41.48	41.33	41.06	41.17
FeO^{tot}	19.86	19.93	19.33	19.83	19.77	19.56	19.61	20.02	18.81	18.76
MnO	0.26	0.25	0.25	0.25	0.28	0.29	0.27	0.28	0.25	0.26
MgO	14.13	14.05	14.16	14.49	14.21	14.36	14.18	13.97	14.33	14.61
NiO	0.14	0.12	0.14	0.14	0.12	0.12	0.16	0.16	0.14	0.15
Cr#	0.54	0.54	0.54	0.54	0.54	0.54	0.54	0.54	0.53	0.52
Mg#	0.63	0.63	0.63	0.65	0.63	0.64	0.64	0.63	0.64	0.65
Cr/Fe^{2+}	2.65	2.67	2.71	2.79	2.70	2.79	2.75	2.66	2.73	2.80

Sample	MBP-3									
Analysis#	1	2	3	4	5	6	7	8	9	10
TiO_2	0.34	0.31	0.41	0.41	0.55	0.40	0.38	0.38	0.38	0.36
V_2O_5	0.27	0.22	0.25	0.26	0.24	0.28	0.23	0.24	0.21	0.26
Al_2O_3	24.27	23.98	24.40	24.38	24.65	24.36	24.27	24.09	24.70	24.30
Cr_2O_3	43.57	43.65	43.06	43.42	43.76	42.93	43.41	43.36	42.62	42.59
FeO^{tot}	16.68	16.51	16.67	17.03	16.31	16.09	16.61	16.62	17.00	16.81
MnO	0.25	0.24	0.23	0.27	0.26	0.26	0.26	0.26	0.25	0.26
MgO	15.04	14.76	15.18	15.32	15.42	15.48	15.77	15.16	14.78	14.82
NiO	0.21	0.19	0.19	0.20	0.19	0.18	0.19	0.20	0.17	0.16
Cr#	0.55	0.55	0.54	0.54	0.54	0.54	0.55	0.55	0.54	0.54
Mg#	0.67	0.66	0.68	0.68	0.68	0.69	0.70	0.68	0.66	0.67
Cr/Fe^{2+}	3.12	3.11	3.13	3.15	3.16	3.27	3.35	3.18	2.98	3.04

Sample	MBT-15									
Analysis#	1	2	3	4	5	6	7	8	9	10
TiO_2	0.15	0.16	0.14	0.16	0.16	0.18	0.14	0.14	0.17	0.19
V_2O_5	0.13	0.16	0.15	0.11	0.13	0.09	0.15	0.15	0.12	0.12
Al_2O_3	10.40	10.35	10.76	10.39	10.52	10.42	10.55	10.57	10.64	10.67
Cr_2O_3	57.35	56.49	57.56	57.12	57.02	57.01	57.19	56.83	57.39	56.70
FeO^{tot}	22.84	22.44	22.52	22.81	22.65	22.67	22.96	23.25	22.66	22.73
MnO	0.37	0.38	0.38	0.37	0.40	0.37	0.37	0.36	0.38	0.38
MgO	9.70	9.83	9.88	9.90	10.06	10.12	9.78	9.81	9.96	9.93
NiO	0.07	0.08	0.04	0.07	0.08	0.06	0.06	0.04	0.07	0.06
Cr#	0.79	0.79	0.78	0.79	0.78	0.79	0.78	0.78	0.78	0.78
Mg#	0.48	0.49	0.48	0.49	0.49	0.49	0.48	0.48	0.49	0.49
Cr/Fe^{2+}	2.85	2.89	2.87	2.88	2.92	2.93	2.84	2.83	2.88	2.86

Appendix 3 - Chromite Analysis from Dunite and Harzburgite Samples

Shetland Chromite Analyses

Sample	MR6					
Analysis#	1	2	3	4	5	6
TiO_2	0.04	0.04	0.04	0.04	0.03	0.04
V_2O_5	0.27	0.28	0.26	0.23	0.26	0.26
Al_2O_3	10.11	9.96	10.01	9.67	10.75	10.90
Cr_2O_3	60.46	60.68	61.86	61.90	59.35	59.40
FeO^{tot}	21.04	21.16	18.95	19.16	20.58	20.72
MnO	0.40	0.40	0.39	0.35	0.36	0.36
MgO	8.90	8.94	9.91	10.02	9.34	9.12
NiO	0.00	0.00	0.00	0.04	0.00	0.05
Cr#	0.80	0.80	0.81	0.81	0.79	0.79
Mg#	0.44	0.44	0.48	0.49	0.46	0.45
Cr/Fe^{2+}	2.82	2.83	3.12	3.16	2.87	2.82

Sample	MR12							
Analysis#	1	2	3	4	5	6	7	8
TiO_2	0.06	0.07	0.06	0.07	0.07	0.05	0.05	0.07
V_2O_5	0.21	0.24	0.23	0.23	0.23	0.24	0.25	0.26
Al_2O_3	13.23	13.31	13.80	14.31	14.64	12.78	12.58	14.61
Cr_2O_3	55.07	54.67	53.49	53.75	53.77	54.61	53.31	53.56
FeO^{tot}	22.55	22.83	23.86	23.97	21.83	24.77	24.22	21.39
MnO	0.43	0.38	0.40	0.39	0.33	0.42	0.41	0.37
MgO	8.80	8.81	8.88	8.67	10.26	7.86	8.12	9.84
NiO	0.07	0.00	0.07	0.05	0.07	0.04	0.03	0.05
Cr#	0.74	0.73	0.72	0.72	0.71	0.74	0.74	0.71
Mg#	0.43	0.43	0.43	0.42	0.49	0.39	0.41	0.48
Cr/Fe^{2+}	2.53	2.50	2.44	2.38	2.68	2.34	2.39	2.63

Sample	RL007							
Analysis#	1	2	3	4	5	6	7	8
TiO_2	0.13	0.13	0.14	0.14	0.13	0.14	0.15	0.15
V_2O_5	0.39	0.34	0.33	0.35	0.35	0.34	0.36	0.33
Al_2O_3	19.02	19.00	19.00	19.44	17.95	18.15	17.46	17.58
Cr_2O_3	49.46	49.85	49.30	49.14	49.09	49.02	49.67	49.65
FeO^{tot}	21.27	21.46	21.33	21.31	22.48	22.72	22.79	22.45
MnO	0.35	0.34	0.36	0.37	0.37	0.37	0.39	0.39
MgO	10.01	10.19	10.02	9.99	9.75	9.75	9.68	9.35
NiO	0.04	0.04	0.05	0.07	0.05	0.06	0.05	0.05
Cr#	0.64	0.64	0.63	0.63	0.65	0.64	0.66	0.65
Mg#	0.47	0.48	0.47	0.47	0.46	0.46	0.46	0.45
Cr/Fe^{2+}	2.34	2.37	2.34	2.32	2.32	2.30	2.33	2.29

Sample	RL011									
Analysis#	1	2	3	4	5	6	7	8	9	10
TiO_2	0.25	0.25	0.23	0.25	0.23	0.24	0.25	0.26	0.26	0.27
V_2O_5	0.23	0.20	0.20	0.16	0.18	0.17	0.18	0.20	0.19	0.18
Al_2O_3	27.18	27.37	26.93	26.92	27.24	27.26	26.41	26.37	26.70	26.87
Cr_2O_3	36.69	36.36	36.81	37.11	36.79	37.01	37.26	37.52	36.90	37.09
FeO^{tot}	23.63	23.74	22.58	22.58	23.34	22.90	23.11	23.01	23.09	23.36
MnO	0.26	0.28	0.28	0.28	0.27	0.29	0.28	0.26	0.29	0.26
MgO	12.32	12.14	12.76	12.47	12.46	12.39	12.28	12.41	12.63	12.43
NiO	0.14	0.15	0.12	0.13	0.12	0.14	0.14	0.13	0.12	0.13
Cr#	0.48	0.47	0.48	0.48	0.48	0.48	0.49	0.49	0.48	0.48
Mg#	0.55	0.55	0.57	0.56	0.56	0.56	0.56	0.56	0.57	0.56
Cr/Fe^{2+}	1.95	1.91	2.07	2.04	1.98	1.99	2.02	2.04	2.04	2.00

Sample	RL016							
Analysis#	1	2	3	4	5	6	7	8
TiO_2	0.09	0.09	0.10	0.09	0.10	0.10	0.10	0.10
V_2O_5	0.20	0.20	0.19	0.21	0.21	0.20	0.22	0.16
Al_2O_3	34.54	34.36	34.64	34.98	33.47	33.81	33.61	33.85
Cr_2O_3	30.57	30.05	29.04	29.35	30.67	30.24	30.52	30.99
FeO^{tot}	21.19	21.13	21.63	22.03	21.30	21.01	21.47	21.12
MnO	0.22	0.22	0.22	0.21	0.21	0.23	0.20	0.21
MgO	14.48	14.31	14.24	14.16	13.77	13.98	14.37	14.18
NiO	0.13	0.15	0.15	0.12	0.16	0.15	0.14	0.13
Cr#	0.37	0.37	0.36	0.36	0.38	0.37	0.38	0.38
Mg#	0.62	0.62	0.62	0.61	0.60	0.61	0.62	0.61
Cr/Fe^{2+}	1.83	1.81	1.74	1.70	1.79	1.80	1.85	1.84

Sample	RL019							
Analysis#	1	2	3	4	5	6	7	8
TiO_2	0.16	0.16	0.15	0.17	0.15	0.15	0.16	0.15
V_2O_5	0.21	0.21	0.20	0.20	0.20	0.17	0.23	0.22
Al_2O_3	27.09	27.07	26.24	26.19	27.38	27.57	27.66	27.28
Cr_2O_3	37.87	38.18	38.21	37.97	37.91	37.76	37.80	37.81
FeO^{tot}	22.42	21.95	22.26	22.30	22.33	22.39	22.30	22.24
MnO	0.28	0.26	0.26	0.28	0.28	0.29	0.27	0.26
MgO	12.82	12.58	12.24	12.36	12.70	12.69	12.85	12.78
NiO	0.10	0.09	0.09	0.12	0.13	0.09	0.10	0.12
Cr#	0.48	0.49	0.49	0.49	0.48	0.48	0.48	0.48
Mg#	0.57	0.56	0.56	0.56	0.57	0.57	0.57	0.57
Cr/Fe^{2+}	2.10	2.09	2.08	2.09	2.08	2.06	2.07	2.09

Sample	CF19							
Analysis#	1	2	3	4	5	6	7	8
TiO_2	0.09	0.08	0.08	0.07	0.08	0.08	0.07	0.07
V_2O_5	0.22	0.16	0.23	0.17	0.17	0.18	0.16	0.19
Al_2O_3	15.29	15.03	15.35	15.27	15.08	15.37	15.23	15.10
Cr_2O_3	52.18	51.57	52.66	52.72	53.46	52.85	53.47	53.57
FeO^{tot}	22.86	22.92	20.65	20.74	20.03	20.23	20.36	20.35
MnO	0.39	0.42	0.39	0.38	0.34	0.35	0.37	0.38
MgO	9.69	9.37	10.92	10.62	10.85	10.76	10.89	10.93
NiO	0.04	b.d.l.	0.05	b.d.l.	0.04	0.06	0.04	0.04
Cr#	0.70	0.70	0.70	0.70	0.70	0.70	0.70	0.70
Mg#	0.47	0.46	0.52	0.51	0.52	0.52	0.52	0.52
Cr/Fe^{2+}	2.50	2.46	2.81	2.76	2.85	2.80	2.84	2.85

Sample	CF20							
Analysis#	1	2	3	4	5	6	7	8
TiO_2	0.08	0.08	0.08	0.08	0.07	0.08	0.08	0.08
V_2O_5	0.21	0.17	0.14	0.18	0.19	0.18	0.18	0.18
Al_2O_3	15.62	15.22	15.61	15.28	15.40	15.40	15.43	15.16
Cr_2O_3	53.79	53.09	52.48	52.89	52.96	53.14	52.61	52.51
FeO^{tot}	20.20	20.36	19.87	19.94	21.19	21.20	21.50	21.09
MnO	0.34	0.32	0.37	0.33	0.34	0.34	0.33	0.35
MgO	10.90	11.09	10.97	11.06	10.53	10.29	9.95	10.19
NiO	0.08	0.08	0.03	0.06	0.07	0.07	0.06	0.07
Cr#	0.70	0.70	0.69	0.70	0.70	0.70	0.70	0.70
Mg#	0.52	0.53	0.53	0.53	0.50	0.49	0.48	0.49
Cr/Fe^{2+}	2.81	2.87	2.85	2.88	2.71	2.67	2.59	2.67

Sample	CF23							
Analysis#	1	2	3	4	5	6	7	8
TiO_2	0.06	0.09	0.07	0.07	0.07	0.08	0.08	0.08
V_2O_5	0.20	0.23	0.23	0.18	0.17	0.18	0.23	0.19
Al_2O_3	15.37	15.52	14.80	14.97	15.14	14.88	15.04	15.01
Cr_2O_3	54.07	53.72	52.91	53.22	53.88	53.51	52.72	53.01
FeO^{tot}	19.46	19.61	21.43	21.33	19.44	19.19	20.45	20.36
MnO	0.35	0.37	0.43	0.42	0.39	0.36	0.35	0.39
MgO	11.44	11.23	9.99	10.26	11.20	11.18	10.42	10.27
NiO	0.05	0.05	0.06	0.04	0.05	0.04	0.07	0.07
Cr#	0.70	0.70	0.71	0.70	0.70	0.71	0.70	0.70
Mg#	0.54	0.53	0.49	0.49	0.54	0.54	0.51	0.50
Cr/Fe^{2+}	2.98	2.91	2.65	2.69	2.96	2.98	2.75	2.74

Sample	RLM001							
Analysis#	1	2	3	4	5	6	7	8
TiO_2	0.23	0.24	0.22	0.23	0.23	0.23	0.22	0.23
V_2O_5	0.13	0.15	0.13	0.11	0.15	0.12	0.14	0.11
Al_2O_3	23.17	23.24	23.06	23.02	23.25	22.73	22.80	22.87
Cr_2O_3	44.91	45.15	44.56	44.16	44.62	44.12	44.65	44.62
FeO^{tot}	18.20	18.28	18.17	18.60	18.52	18.57	18.27	18.32
MnO	0.31	0.29	0.28	0.26	0.28	0.24	0.28	0.25
MgO	13.83	13.98	13.47	13.41	13.67	13.56	13.59	13.62
NiO	0.14	0.15	0.13	0.11	0.14	0.11	0.16	0.13
Cr#	0.57	0.57	0.56	0.56	0.56	0.57	0.57	0.57
Mg#	0.63	0.63	0.61	0.61	0.62	0.62	0.62	0.62
Cr/Fe^{2+}	2.87	2.89	2.80	2.76	2.80	2.81	2.85	2.84

Sample	MR267							
Analysis#	1	2	3	4	5	6	7	8
TiO_2	0.03	0.05	0.03	0.05	0.03	0.04	0.04	0.04
V_2O_5	0.24	0.20	0.18	0.19	0.18	0.21	0.17	0.18
Al_2O_3	18.61	18.75	18.78	18.50	17.88	18.17	19.12	18.75
Cr_2O_3	51.81	51.57	51.11	51.48	50.76	51.04	49.18	48.61
FeO^{tot}	18.89	18.56	18.59	18.90	18.77	19.36	22.39	22.95
MnO	0.36	0.32	0.34	0.36	0.35	0.38	0.48	0.47
MgO	11.31	11.60	11.50	11.44	10.89	10.18	7.94	7.62
NiO	0.07	0.05	0.06	0.05	0.06	b.d.l	0.04	0.06
Cr#	0.65	0.65	0.65	0.65	0.66	0.65	0.63	0.63
Mg#	0.53	0.54	0.54	0.54	0.52	0.49	0.39	0.38
Cr/Fe^{2+}	2.73	2.79	2.78	2.77	2.72	2.55	2.08	2.04

Sample	MR35			
Analysis#	1	2	3	4
TiO_2	0.08	0.08	0.07	0.06
V_2O_5	0.25	0.23	0.24	0.24
Al_2O_3	15.27	15.07	15.92	15.61
Cr_2O_3	51.14	50.98	49.15	49.18
FeO^{tot}	21.93	21.89	24.21	24.93
MnO	0.34	0.33	0.39	0.37
MgO	10.22	10.44	8.57	8.89
NiO	0.10	0.08	0.09	0.08
Cr#	0.69	0.69	0.67	0.68
Mg#	0.50	0.51	0.42	0.44
Cr/Fe^{2+}	2.61	2.67	2.23	2.26

Sample	MR256							
Analysis#	1	2	3	4	5	6	7	8
TiO_2	0.02	0.03	0.02	0.02	0.03	0.02	0.02	0.02
V_2O_5	0.25	0.26	0.24	0.25	0.29	0.25	0.24	0.26
Al_2O_3	25.23	25.33	25.17	25.43	25.53	25.38	25.46	25.62
Cr_2O_3	44.75	44.96	45.10	44.78	45.20	45.12	44.23	44.32
FeO^{tot}	14.99	15.23	16.25	16.07	13.16	13.07	16.59	16.51
MnO	0.25	0.29	0.27	0.27	0.30	0.25	0.30	0.27
MgO	13.80	13.92	13.23	13.31	16.51	16.98	12.89	13.21
NiO	0.11	0.09	0.11	0.09	0.09	0.08	0.09	0.07
Cr#	0.54	0.54	0.55	0.54	0.54	0.54	0.54	0.54
Mg#	0.63	0.63	0.60	0.60	0.73	0.74	0.59	0.60
Cr/Fe^{2+}	2.90	2.91	2.71	2.71	3.87	4.12	2.60	2.64

Sample	MR1									
Analysis#	1	2	3	4	5	6	7	8	9	10
TiO_2	0.04	0.04	0.03	0.03	0.03	0.04	0.03	0.03	0.02	0.03
V_2O_5	0.26	0.24	0.24	0.26	0.26	0.25	0.26	0.25	0.25	0.21
Al_2O_3	16.23	15.97	16.21	16.22	16.47	16.62	16.41	16.84	16.10	16.47
Cr_2O_3	53.57	53.11	51.68	52.67	51.37	51.59	52.50	52.61	53.13	53.64
FeO^{tot}	19.43	19.32	21.00	20.64	22.79	21.75	20.50	20.84	19.07	18.79
MnO	0.39	0.39	0.53	0.51	0.54	0.50	0.49	0.48	0.36	0.34
MgO	10.62	10.38	8.95	9.60	8.66	8.86	9.37	9.53	10.70	10.66
NiO	0.05	0.06	0.04	0.05	0.06	b.d.l	0.06	0.07	0.03	b.d.l
Cr#	0.69	0.69	0.68	0.69	0.68	0.68	0.68	0.68	0.69	0.69
Mg#	0.51	0.50	0.44	0.47	0.42	0.43	0.46	0.46	0.52	0.51
Cr/Fe^{2+}	2.76	2.74	2.42	2.54	2.30	2.35	2.50	2.48	2.80	2.78

Sample	MR254							
Analysis#	1	2	3	4	5	6	7	8
TiO_2	b.d.l	0.02	0.02	0.03	0.02	0.02	0.03	b.d.l
V_2O_5	0.31	0.30	0.34	0.32	0.30	0.27	0.32	0.31
Al_2O_3	24.15	23.92	24.69	24.72	24.60	24.68	24.45	24.16
Cr_2O_3	45.46	45.61	43.74	43.96	45.75	46.22	45.14	45.11
FeO^{tot}	17.56	17.65	17.13	17.28	17.02	16.91	16.70	16.35
MnO	0.31	0.29	0.29	0.27	0.28	0.27	0.28	0.29
MgO	12.00	12.33	12.36	12.13	12.74	12.57	12.70	12.37
NiO	0.05	0.05	0.06	0.05	0.06	0.07	0.06	0.05
Cr#	0.56	0.56	0.54	0.54	0.56	0.56	0.55	0.56
Mg#	0.55	0.56	0.57	0.56	0.58	0.57	0.58	0.57
Cr/Fe^{2+}	2.48	2.55	2.51	2.46	2.61	2.58	2.62	2.61

Sample	MR276							
Analysis#	1	2	3	4	5	6	7	8
TiO_2	0.04	0.04	0.04	0.04	0.04	0.03	0.03	0.04
V_2O_5	0.16	0.18	0.15	0.15	0.15	0.17	0.17	0.17
Al_2O_3	40.95	41.00	41.28	41.54	41.57	41.69	42.40	42.03
Cr_2O_3	28.03	27.91	26.76	27.05	26.62	26.35	26.34	26.00
FeO^{tot}	13.81	13.68	13.55	13.46	13.62	13.98	13.59	13.87
MnO	0.20	0.19	0.19	0.22	0.18	0.19	0.17	0.18
MgO	16.81	16.77	16.93	16.78	16.86	16.74	17.15	17.03
NiO	0.20	0.18	0.18	0.18	0.18	0.19	0.18	0.20
Cr#	0.31	0.31	0.30	0.30	0.30	0.30	0.29	0.29
Mg#	0.70	0.70	0.71	0.70	0.71	0.70	0.71	0.71
Cr/Fe^{2+}	2.10	2.08	2.08	2.04	2.03	1.98	2.02	2.00

Sample	NB2a							
Analysis#	1	2	3	4	5	6	7	8
TiO_2	0.22	0.22	0.20	0.20	0.23	0.22	0.22	0.22
V_2O_5	0.20	0.19	0.20	0.20	0.17	0.21	0.21	0.16
Al_2O_3	24.21	24.02	24.49	24.21	24.91	24.70	24.17	24.10
Cr_2O_3	40.92	41.20	41.63	41.47	40.40	40.35	41.00	41.21
FeO^{tot}	20.88	21.03	21.11	20.68	21.88	21.64	22.07	21.72
MnO	0.28	0.30	0.30	0.31	0.28	0.27	0.30	0.29
MgO	12.94	13.17	13.03	12.71	12.49	12.82	12.29	12.71
NiO	0.12	0.12	0.15	0.10	0.12	0.08	0.10	0.08
Cr#	0.53	0.53	0.53	0.53	0.52	0.52	0.53	0.53
Mg#	0.59	0.60	0.59	0.58	0.57	0.58	0.56	0.58
Cr/Fe^{2+}	2.41	2.47	2.41	2.39	2.24	2.31	2.25	2.34

Sample	NB2b							
Analysis#	1	2	3	4	5	6	7	8
TiO_2	0.20	0.22	0.21	0.21	0.23	0.23	0.20	0.21
V_2O_5	0.21	0.19	0.20	0.22	0.20	0.20	0.18	0.17
Al_2O_3	24.04	23.82	24.00	24.42	24.28	24.37	24.51	24.21
Cr_2O_3	41.58	41.57	41.01	40.99	41.22	40.99	41.18	40.70
FeO^{tot}	21.30	21.13	21.34	21.06	21.42	21.50	21.17	21.23
MnO	0.28	0.27	0.28	0.30	0.28	0.31	0.33	0.27
MgO	12.84	13.09	12.87	12.86	12.99	12.96	12.80	13.03
NiO	0.11	0.10	0.15	0.11	0.11	0.11	0.14	0.12
Cr#	0.54	0.54	0.53	0.53	0.53	0.53	0.53	0.53
Mg#	0.58	0.59	0.59	0.58	0.59	0.59	0.58	0.59
Cr/Fe^{2+}	2.39	2.46	2.40	2.37	2.39	2.37	2.37	2.41

Sample	RLM026							
Analysis#	1	2	3	4	5	6	7	8
TiO_2	0.22	0.20	0.21	0.20	0.19	0.20	0.22	0.23
V_2O_5	0.17	0.16	0.18	0.18	0.14	0.18	0.18	0.19
Al_2O_3	16.67	16.84	17.24	16.99	16.51	16.10	16.70	16.88
Cr_2O_3	48.32	48.13	47.53	47.67	48.62	48.28	47.60	47.23
FeO^{tot}	22.58	22.66	22.82	22.90	23.46	22.80	22.82	23.16
MnO	0.34	0.31	0.33	0.30	0.32	0.33	0.34	0.34
MgO	11.55	11.48	11.94	12.13	11.71	11.21	11.48	11.58
NiO	0.10	0.10	0.10	0.10	0.10	0.10	0.09	0.11
Cr#	0.66	0.66	0.65	0.65	0.66	0.67	0.66	0.65
Mg#	0.55	0.54	0.56	0.57	0.55	0.54	0.55	0.55
Cr/Fe^{2+}	2.69	2.66	2.70	2.75	2.69	2.66	2.65	2.64

Sample	RLM057							
Analysis#	1	2	3	4	5	6	7	8
TiO_2	0.20	0.21	0.20	0.22	0.22	0.21	0.23	0.23
V_2O_5	0.18	0.19	0.18	0.19	0.18	0.15	0.17	0.17
Al_2O_3	25.70	26.05	25.57	25.52	25.42	25.10	25.85	25.84
Cr_2O_3	40.85	40.45	40.89	40.97	40.85	40.41	40.58	40.56
FeO^{tot}	19.79	19.96	19.60	19.61	19.21	19.50	19.10	19.38
MnO	0.31	0.28	0.27	0.28	0.26	0.27	0.30	0.28
MgO	13.88	13.67	14.02	13.92	13.66	13.60	13.94	14.04
NiO	0.16	0.15	0.17	0.15	0.13	0.14	0.15	0.16
Cr#	0.52	0.51	0.52	0.52	0.52	0.52	0.51	0.51
Mg#	0.62	0.61	0.63	0.62	0.62	0.62	0.63	0.63
Cr/Fe^{2+}	2.55	2.46	2.59	2.57	2.55	2.55	2.58	2.58

Berit Chromite Samples

Sample	Ader-1									
Analysis#	1	2	3	4	5	6	7	8	9	10
TiO_2	0	0	0	0	0	0	0	0	0	0
V_2O_5	0.27	0.27	0.27	0.26	0.31	0.30	0.23	0.25	0.29	0.28
Al_2O_3	8.13	7.75	7.06	6.64	5.31	4.49	7.99	7.94	6.78	6.84
Cr_2O_3	40.31	40.62	40.81	40.75	39.96	38.98	41.82	42.27	37.45	37.52
FeO^{tot}	44.58	44.36	44.55	44.87	49.20	49.92	43.61	43.36	48.51	48.35
MnO	0.48	0.49	0.50	0.50	0.54	0.53	0.52	0.49	0.46	0.48
MgO	5.85	5.81	5.55	5.69	4.98	4.82	5.79	5.63	5.44	5.37
NiO	0.22	0.21	0.21	0.21	0.22	0.24	0.19	0.19	0.32	0.29
Cr#	0.77	0.78	0.79	0.80	0.83	0.85	0.78	0.78	0.79	0.79
Mg#	0.30	0.30	0.29	0.29	0.26	0.25	0.29	0.29	0.28	0.28
Cr/Fe^{2+}	1.55	1.57	1.56	1.58	1.46	1.44	1.60	1.60	1.42	1.42

Sample	Ader-9					
Analysis#	1	2	3	4	5	6
TiO_2	0.13	0.11	0.13	0.14	0.11	0.09
V_2O_5	0.40	0.44	0.40	0.38	0.44	0.44
Al_2O_3	23.83	23.25	20.94	20.86	24.51	24.59
Cr_2O_3	36.59	36.69	38.77	38.25	37.91	37.80
FeO^{tot}	29.76	29.76	30.80	30.80	27.07	26.84
MnO	0.38	0.38	0.39	0.37	0.33	0.34
MgO	9.85	9.59	9.26	9.10	10.74	10.84
NiO	0.14	0.16	0.17	0.18	0.18	0.17
Cr#	0.51	0.51	0.55	0.55	0.51	0.51
Mg#	0.45	0.45	0.43	0.43	0.49	0.49
Cr/Fe^{2+}	1.64	1.64	1.71	1.68	1.80	1.81

Sample	Ader-12									
Analysis#	1	2	3	4	5	6	7	8	9	10
TiO_2	0.07	0.05	0.05	0.05	0.05	0.07	0.05	0.05	0.05	0.06
V_2O_5	0.23	0.22	0.21	0.24	0.24	0.22	0.22	0.24	0.26	0.23
Al_2O_3	21.53	21.45	21.41	21.48	21.16	21.41	20.45	20.55	20.78	20.92
Cr_2O_3	42.12	42.02	40.71	40.93	42.44	42.32	42.52	41.98	40.81	40.66
FeO^{tot}	23.38	23.22	25.19	24.90	24.56	24.50	26.62	26.59	26.41	26.44
MnO	0.35	0.32	0.34	0.35	0.32	0.33	0.34	0.34	0.34	0.32
MgO	12.70	12.66	11.35	11.36	12.34	12.13	11.21	11.05	11.47	11.42
NiO	0.14	0.10	0.11	0.12	0.12	0.13	0.12	0.11	0.12	0.12
Cr#	0.57	0.57	0.56	0.56	0.57	0.57	0.58	0.58	0.57	0.57
Mg#	0.58	0.59	0.53	0.53	0.57	0.56	0.52	0.51	0.53	0.53
Cr/Fe^{2+}	2.48	2.48	2.17	2.18	2.38	2.33	2.17	2.13	2.17	2.15

Sample	Ader-13					
Analysis#	1	2	3	4	5	6
TiO_2	0.44	0.45	0.48	0.47	0.49	0.45
V_2O_5	0.32	0.34	0.36	0.36	0.32	0.31
Al_2O_3	5.31	5.17	4.59	4.68	4.67	4.74
Cr_2O_3	38.01	38.02	38.71	38.81	40.63	41.01
FeO^{tot}	49.97	49.74	50.00	50.11	48.11	48.02
MnO	0.54	0.52	0.51	0.50	0.53	0.52
MgO	4.41	4.22	4.53	4.66	4.85	4.83
NiO	0.29	0.26	0.30	0.28	0.24	0.25
Cr#	0.83	0.83	0.85	0.85	0.85	0.85
Mg#	0.23	0.22	0.24	0.24	0.25	0.25
Cr/Fe^{2+}	1.37	1.37	1.41	1.41	1.50	1.51

Sample	DMK-13									
Analysis#	1	2	3	4	5	6	7	8	9	10
TiO_2	0	0	0	0	0	0	0	0	0	0
V_2O_5	0.18	0.20	0.19	0.18	0.19	0.18	0.18	0.18	0.20	0.18
Al_2O_3	22.39	22.25	22.54	22.41	21.65	21.66	23.48	23.39	22.45	22.86
Cr_2O_3	39.49	39.28	39.09	38.84	38.76	38.02	37.95	38.40	37.69	38.02
FeO^{tot}	26.20	26.02	26.58	26.22	27.12	27.09	26.84	26.75	27.82	27.78
MnO	0.33	0.33	0.34	0.34	0.33	0.34	0.30	0.33	0.34	0.35
MgO	11.69	11.44	11.23	10.91	10.75	10.80	11.88	11.78	10.75	11.10
NiO	0.14	0.13	0.14	0.13	0.13	0.11	0.13	0.12	0.15	0.10
Cr#	0.54	0.54	0.54	0.54	0.55	0.54	0.52	0.52	0.53	0.53
Mg#	0.54	0.53	0.52	0.51	0.50	0.51	0.54	0.54	0.50	0.51
Cr/Fe^{2+}	2.08	2.06	1.99	1.96	1.95	1.94	2.00	2.00	1.87	1.90

Sample	DMK-14					
Analysis#	1	2	3	4	5	6
TiO_2	0.37	0.39	0.30	0.28	0.32	0.31
V_2O_5	0.17	0.15	0.18	0.18	0.16	0.16
Al_2O_3	23.01	23.52	23.75	23.65	23.06	22.78
Cr_2O_3	36.03	36.42	36.19	35.57	36.50	36.36
FeO^{tot}	30.01	29.72	28.92	29.05	30.23	30.30
MnO	0.35	0.37	0.33	0.34	0.36	0.36
MgO	10.45	10.50	11.11	11.01	10.25	10.08
NiO	0.14	0.11	0.16	0.16	0.15	0.14
Cr#	0.51	0.51	0.51	0.50	0.51	0.52
Mg#	0.48	0.48	0.51	0.51	0.47	0.47
Cr/Fe^{2+}	1.70	1.70	1.78	1.76	1.69	1.68

Sample	DMK-15									
Analysis#	1	2	3	4	5	6	7	8	9	10
TiO_2	0.22	0.22	0.18	0.17	0.15	0.16	0.23	0.23	0.24	0.24
V_2O_5	0.26	0.24	0.25	0.26	0.26	0.25	0.27	0.29	0.36	0.39
Al_2O_3	17.07	17.10	16.78	16.83	13.86	14.23	15.53	15.33	14.78	15.20
Cr_2O_3	40.17	40.10	41.52	41.24	44.55	44.57	40.30	40.08	40.43	40.65
FeO^{tot}	33.91	33.54	30.95	31.32	32.91	32.72	35.66	35.41	35.76	35.70
MnO	0.39	0.44	0.42	0.43	0.48	0.48	0.49	0.48	0.51	0.47
MgO	7.62	7.55	8.32	8.41	7.63	7.28	6.92	7.17	6.82	6.82
NiO	0.17	0.18	0.15	0.14	0.11	0.12	0.15	0.16	0.16	0.18
Cr#	0.61	0.61	0.62	0.62	0.68	0.68	0.64	0.64	0.65	0.64
Mg#	0.37	0.37	0.41	0.41	0.38	0.36	0.34	0.35	0.34	0.34
Cr/Fe^{2+}	1.65	1.65	1.83	1.82	1.87	1.83	1.60	1.63	1.61	1.60

Sample	DMK-29									
Analysis#	1	2	3	4	5	6	7	8	9	10
TiO_2	0.51	0.49	0.44	0.43	0.48	0.44	0.41	0.38	0.45	0.45
V_2O_5	0.25	0.23	0.20	0.19	0.21	0.22	0.17	0.19	0.23	0.20
Al_2O_3	18.00	18.13	18.87	18.77	18.78	18.42	19.88	19.79	19.00	18.80
Cr_2O_3	36.92	36.65	36.40	36.61	37.20	37.00	37.32	37.71	37.37	37.37
FeO^{tot}	34.24	34.33	33.06	32.84	33.58	33.13	32.43	32.38	33.63	34.25
MnO	0.40	0.40	0.37	0.39	0.39	0.38	0.40	0.38	0.39	0.39
MgO	8.75	8.91	9.41	9.22	9.60	9.40	9.88	9.60	9.23	8.93
NiO	0.22	0.19	0.21	0.20	0.22	0.20	0.19	0.19	0.21	0.20
Cr#	0.58	0.58	0.56	0.57	0.57	0.57	0.56	0.56	0.57	0.57
Mg#	0.42	0.43	0.45	0.44	0.45	0.45	0.46	0.45	0.44	0.42
Cr/Fe^{2+}	1.62	1.62	1.68	1.68	1.70	1.70	1.73	1.71	1.66	1.62

Sample	KBK-1											
Analysis#	1	2	3	4	5	6	7	8	9	10	11	12
TiO_2	0.29	0.30	0.37	0.38	0.32	0.30	0.38	0.38	0.39	0.40	0.04	0.03
V_2O_5	0.20	0.22	0.25	0.24	0.21	0.23	0.25	0.24	0.26	0.29	0.33	0.30
Al_2O_3	21.65	21.53	20.48	20.40	20.37	19.95	19.97	20.49	18.23	18.32	19.64	19.51
Cr_2O_3	38.82	38.77	38.41	38.48	41.02	40.40	39.18	38.16	40.54	39.88	36.40	36.30
FeO^{tot}	29.07	29.21	30.05	30.19	28.54	29.09	31.15	31.41	32.13	31.38	32.45	32.94
MnO	0.35	0.34	0.38	0.36	0.35	0.35	0.38	0.37	0.38	0.41	0.42	0.44
MgO	10.19	10.70	10.01	10.29	10.29	10.54	9.71	9.93	9.23	9.17	9.02	8.75
NiO	0.13	0.15	0.17	0.18	0.14	0.15	0.17	0.16	0.13	0.12	0.40	0.00
Cr#	0.55	0.55	0.56	0.56	0.57	0.58	0.57	0.56	0.60	0.59	0.55	0.56
Mg#	0.47	0.49	0.47	0.48	0.48	0.49	0.45	0.46	0.43	0.44	0.44	0.42
Cr/Fe^{2+}	1.82	1.87	1.80	1.83	1.94	1.96	1.77	1.75	1.79	1.78	1.68	1.63

Sample	KBK-3									
Analysis#	1	2	3	4	5	6	7	8	9	10
TiO_2	0.21	0.21	0.21	0.21	0.22	0.21	0.22	0.24	0.22	0.22
V_2O_5	0.20	0.22	0.20	0.23	0.23	0.20	0.22	0.22	0.22	0.21
Al_2O_3	20.66	20.50	21.25	20.59	21.03	20.84	20.67	20.46	21.34	21.26
Cr_2O_3	38.25	38.17	37.31	38.03	38.21	37.85	38.43	38.14	37.43	37.67
FeO^{tot}	29.71	30.15	30.59	30.16	29.11	29.76	30.12	29.72	29.64	29.39
MnO	0.35	0.34	0.34	0.35	0.36	0.33	0.36	0.34	0.36	0.34
MgO	10.35	10.51	10.46	10.39	10.51	10.55	10.23	10.60	10.35	10.45
NiO	0.20	0.18	0.20	0.18	0.19	0.18	0.18	0.17	0.19	0.18
Cr#	0.55	0.56	0.54	0.55	0.55	0.55	0.55	0.56	0.54	0.54
Mg#	0.49	0.49	0.49	0.49	0.49	0.49	0.48	0.50	0.49	0.49
Cr/Fe^{2+}	1.86	1.87	1.80	1.84	1.88	1.86	1.83	1.89	1.81	1.84

Sample	KBK-36									
Analysis#	1	2	3	4	5	6	7	8	9	10
TiO_2	0	0	0	0	0	0	0	0	0	0
V_2O_5	0.19	0.15	0.20	0.18	0.19	0.18	0.20	0.17	0.19	0.19
Al_2O_3	23.06	22.91	21.43	21.17	19.58	19.45	18.51	18.27	21.49	21.15
Cr_2O_3	37.41	37.35	38.05	38.14	37.65	37.92	37.22	37.07	36.98	36.81
FeO^{tot}	27.80	27.39	29.41	29.21	31.76	31.53	34.01	33.52	29.29	29.63
MnO	0.35	0.35	0.39	0.38	0.40	0.38	0.40	0.41	0.37	0.34
MgO	11.40	11.25	10.54	10.34	9.41	9.60	8.98	8.98	10.72	10.71
NiO	0.12	0.17	0.16	0.14	0.17	0.15	0.20	0.20	0.14	0.15
Cr#	0.52	0.52	0.54	0.55	0.56	0.57	0.57	0.58	0.54	0.54
Mg#	0.52	0.52	0.49	0.48	0.45	0.46	0.43	0.43	0.50	0.50
Cr/Fe^{2+}	1.91	1.92	1.84	1.84	1.72	1.75	1.64	1.67	1.84	1.84

Sample	KBK-41									
Analysis#	1	2	3	4	5	6	7	8	9	10
TiO_2	0	0	0	0	0	0	0	0	0	0
V_2O_5	0.37	0.38	0.39	0.41	0.38	0.36	0.38	0.38	0.38	0.38
Al_2O_3	23.30	23.04	22.88	22.96	22.52	22.25	22.93	23.16	23.48	23.48
Cr_2O_3	36.79	37.14	36.34	36.02	36.92	36.36	36.90	36.21	36.88	36.88
FeO^{tot}	28.21	27.86	30.17	30.39	28.90	28.86	28.35	27.72	28.18	28.18
MnO	0.30	0.32	0.37	0.37	0.35	0.32	0.32	0.33	0.33	0.33
MgO	10.71	10.90	9.65	9.61	10.43	10.47	10.72	11.11	11.17	11.17
NiO	0.17	0.18	0.17	0.16	0.19	0.20	0.19	0.17	0.17	0.17
Cr#	0.51	0.52	0.52	0.51	0.52	0.52	0.52	0.51	0.51	0.51
Mg#	0.50	0.51	0.45	0.45	0.49	0.49	0.50	0.52	0.51	0.51
Cr/Fe^{2+}	1.80	1.85	1.65	1.62	1.79	1.80	1.82	1.86	1.85	1.85

Sample	KBK-42									
Analysis#	1	2	3	4	5	6	7	8	9	10
TiO_2	0.04	0.03	0.10	0.10	0.04	0.04	0.03	0.04	0.04	0.03
V_2O_5	0.36	0.33	0.39	0.39	0.30	0.32	0.32	0.35	0.33	0.30
Al_2O_3	19.14	19.05	15.83	15.55	20.19	20.11	20.29	20.31	19.64	19.51
Cr_2O_3	36.76	36.46	35.70	35.48	36.75	36.86	36.84	36.62	36.40	36.30
FeO^{tot}	33.60	33.54	38.45	39.69	31.68	31.43	32.01	31.98	32.45	32.94
MnO	0.41	0.42	0.44	0.44	0.41	0.38	0.46	0.48	0.42	0.44
MgO	8.87	8.62	7.58	7.26	9.39	9.11	8.36	8.36	9.02	8.75
NiO	0.17	0.20	0.26	0.24	0.18	0.16	0.17	0.14	0.19	0.18
Cr#	0.56	0.56	0.60	0.60	0.55	0.55	0.55	0.55	0.55	0.56
Mg#	0.43	0.42	0.37	0.36	0.45	0.44	0.41	0.41	0.44	0.42
Cr/Fe^{2+}	1.64	1.62	1.50	1.45	1.70	1.68	1.60	1.59	1.66	1.63

Appendix 4 - Olivine analyses from chromitite, dunite and harzburgite samples

Shetland Olivine Analyses

Sample	MR6					
Analysis#	1	2	3	4	5	6
SiO_2	41.10	41.16	41.91	41.65	41.74	41.59
TiO_2	0.00	0.00	0.00	0.00	0.00	0.00
V_2O_5	0.00	0.00	0.00	0.00	0.00	0.00
Al_2O_3	0.00	0.00	0.00	0.00	0.00	0.00
Cr_2O_3	0.00	0.00	0.00	0.00	0.00	0.00
FeO^{tot}	7.64	7.53	7.39	7.21	7.90	7.80
MnO	0.11	0.13	0.11	0.11	0.11	0.13
MgO	50.42	50.42	51.29	51.07	50.95	51.30
NiO	0.38	0.37	0.37	0.37	0.38	0.40
Fo#	0.92	0.92	0.93	0.93	0.92	0.92

Sample	MR12					
Analysis#	1	2	3	4	5	6
SiO_2	41.63	41.26	41.54	41.59	41.65	40.80
TiO_2	0.00	0.00	0.00	0.00	0.00	0.00
V_2O_5	0.00	0.00	0.00	0.00	0.00	0.00
Al_2O_3	0.00	0.00	0.00	0.00	0.00	0.00
Cr_2O_3	0.00	0.00	0.00	0.00	0.00	0.00
FeO^{tot}	7.75	7.56	7.74	7.56	8.17	8.44
MnO	0.13	0.13	0.12	0.13	0.11	0.11
MgO	50.48	50.32	50.03	49.75	49.73	49.46
NiO	0.31	0.30	0.54	0.48	0.36	0.31
Fo#	0.92	0.92	0.92	0.92	0.92	0.91

Sample	RL007					
Analysis#	1	2	3	4	5	6
SiO_2	40.51	40.68	39.91	40.51	41.16	41.21
TiO_2	0.00	0.00	0.00	0.00	0.00	0.00
V_2O_5	0.00	0.00	0.00	0.00	0.03	0.00
Al_2O_3	0.00	0.00	0.00	0.00	0.00	0.00
Cr_2O_3	0.00	0.00	0.00	0.00	0.00	0.00
FeO^{tot}	11.08	11.07	11.32	11.50	11.09	10.96
MnO	0.15	0.18	0.16	0.17	0.17	0.15
MgO	48.41	48.15	48.41	47.95	48.53	48.81
NiO	0.24	0.23	0.22	0.24	0.22	0.26
Fo#	0.89	0.89	0.88	0.88	0.89	0.89

Sample	RL011					
Analysis#	1	2	3	4	5	6
SiO_2	41.00	40.88	40.77	40.74	41.03	40.78
TiO_2	0.00	0.00	0.00	0.00	0.00	0.00
V_2O_5	0.00	0.00	0.00	0.00	0.00	0.00
Al_2O_3	0.00	0.00	0.00	0.00	0.00	0.00
Cr_2O_3	0.00	0.00	0.00	0.00	0.00	0.00
FeO^{tot}	10.49	10.48	10.49	10.28	10.91	10.80
MnO	0.16	0.14	0.17	0.17	0.16	0.18
MgO	48.02	48.04	47.98	47.58	47.89	47.92
NiO	0.30	0.26	0.30	0.24	0.28	0.28
Fo#	0.89	0.89	0.89	0.89	0.89	0.89

Sample	RL016								
Analysis#	1	2	3	4	5	6	7	8	9
SiO_2	40.32	40.28	40.41	40.40	40.46	40.52	40.50	40.60	41.17
TiO_2	0.00	0.00	0.00	0.00	0.00	0.00	0.00	0.00	0.00
V_2O_5	0.00	0.00	0.00	0.00	0.00	0.00	0.00	0.03	0.00
Al_2O_3	0.00	0.00	0.00	0.00	0.00	0.00	0.00	0.00	0.00
Cr_2O_3	0.00	0.00	0.00	0.00	0.00	0.00	0.00	0.00	0.00
FeO^{tot}	10.39	10.21	10.50	10.36	10.80	10.59	10.51	9.85	9.60
MnO	0.13	0.11	0.10	0.10	0.07	0.13	0.13	0.15	0.14
MgO	47.56	47.54	48.27	47.45	47.93	48.44	48.97	49.12	49.37
NiO	0.24	0.22	0.18	0.18	0.11	0.25	0.24	0.24	0.25
Fo#	0.89	0.89	0.89	0.89	0.89	0.89	0.89	0.90	0.90

Sample	RL019					
Analysis#	1	2	3	4	5	6
SiO_2	40.79	41.55	40.73	40.63	41.24	41.05
TiO_2	0.00	0.00	0.00	0.00	0.00	0.00
V_2O_5	0.00	0.00	0.00	0.00	0.00	0.00
Al_2O_3	0.00	0.00	0.00	0.00	0.00	0.00
Cr_2O_3	0.00	0.00	0.00	0.00	0.00	0.00
FeO^{tot}	10.09	10.53	10.41	10.23	10.41	10.55
MnO	0.15	0.14	0.17	0.13	0.15	0.17
MgO	48.04	47.98	48.48	48.07	49.00	48.54
NiO	0.27	0.30	0.32	0.23	0.25	0.24
Fo#	0.89	0.89	0.89	0.89	0.89	0.89

Sample	CF19					
Analysis#	1	2	3	4	5	6
SiO_2	41.37	41.23	40.88	40.89	41.55	41.39
TiO_2	0.00	0.00	0.00	0.00	0.00	0.00
V_2O_5	0.00	0.00	0.00	0.00	0.00	0.00
Al_2O_3	0.00	0.00	0.00	0.00	0.00	0.00
Cr_2O_3	0.00	0.00	0.00	0.00	0.00	0.00
FeO^{tot}	7.50	7.39	7.74	8.15	7.70	8.01
MnO	0.13	0.13	0.14	0.13	0.14	0.12
MgO	51.23	51.02	50.74	51.01	51.17	51.29
NiO	0.34	0.33	0.38	0.36	0.34	0.33
Fo#	0.92	0.92	0.92	0.92	0.92	0.92

Sample	CF20					
Analysis#	1	2	3	4	5	6
SiO_2	41.21	40.88	41.02	41.12	41.17	41.02
TiO_2	0.00	0.00	0.00	0.00	0.00	0.00
V_2O_5	0.00	0.00	0.00	0.00	0.00	0.00
Al_2O_3	0.00	0.00	0.00	0.00	0.00	0.00
Cr_2O_3	0.00	0.00	0.00	0.00	0.00	0.00
FeO^{tot}	7.53	7.70	8.08	8.11	8.13	7.90
MnO	0.12	0.14	0.14	0.12	0.13	0.12
MgO	51.32	50.80	50.87	51.18	51.00	49.87
NiO	0.38	0.39	0.30	0.33	0.33	0.34
Fo#	0.92	0.92	0.92	0.92	0.92	0.92

Sample	CF23					
Analysis#	1	2	3	4	5	6
SiO_2	40.83	40.77	41.01	40.63	40.63	40.44
TiO_2	0.00	0.00	0.00	0.00	0.00	0.00
V_2O_5	0.00	0.00	0.00	0.00	0.00	0.00
Al_2O_3	0.00	0.00	0.00	0.00	0.00	0.00
Cr_2O_3	0.00	0.00	0.00	0.00	0.00	0.00
FeO^{tot}	7.46	7.74	7.52	7.88	7.55	7.53
MnO	0.13	0.12	0.15	0.13	0.13	0.14
MgO	50.51	50.42	50.53	51.03	50.22	50.29
NiO	0.34	0.33	0.31	0.32	0.34	0.31
Fo#	0.92	0.92	0.92	0.92	0.92	0.92

Sample	MR267							
Analysis#	1	2	3	4	5	6	7	8
SiO_2	41.48	41.56	40.61	40.65	41.61	41.57	40.98	41.06
TiO_2	0.00	0.00	0.00	0.00	0.00	0.00	0.00	0.00
V_2O_5	0.00	0.00	0.00	0.00	0.00	0.00	0.00	0.00
Al_2O_3	0.00	0.00	0.00	0.00	0.00	0.00	0.00	0.00
Cr_2O_3	0.00	0.00	0.00	0.00	0.00	0.00	0.00	0.00
FeO^{tot}	9.39	8.93	10.74	10.91	11.16	11.08	9.89	10.06
MnO	0.15	0.12	0.20	0.19	0.23	0.19	0.16	0.20
MgO	49.08	48.61	46.85	47.62	47.56	47.43	48.33	48.17
NiO	0.43	0.40	0.41	0.40	0.41	0.41	0.40	0.41
Fo#	0.90	0.91	0.89	0.89	0.88	0.88	0.90	0.90

Sample	MR35			
Analysis#	1	2	3	4
SiO_2	41.45	41.08	41.42	41.35
TiO_2	0.00	0.00	0.00	0.00
V_2O_5	0.00	0.00	0.00	0.00
Al_2O_3	0.00	0.00	0.00	0.00
Cr_2O_3	0.00	0.00	0.00	0.00
FeO^{tot}	8.31	8.47	8.20	8.20
MnO	0.12	0.14	0.13	0.14
MgO	49.14	49.24	49.78	49.20
NiO	0.39	0.38	0.39	0.40
Fo#	0.91	0.91	0.92	0.91

Sample	MR256					
Analysis#	1	2	3	4	5	6
SiO_2	41.82	42.16	41.70	41.96	42.12	41.95
TiO_2	0.00	0.00	0.00	0.00	0.00	0.00
V_2O_5	0.00	0.00	0.00	0.00	0.00	0.00
Al_2O_3	0.00	0.00	0.00	0.00	0.00	0.00
Cr_2O_3	0.00	0.00	0.00	0.00	0.00	0.00
FeO^{tot}	9.00	8.49	8.41	8.66	8.74	8.72
MnO	0.14	0.12	0.11	0.12	0.13	0.14
MgO	49.68	49.67	49.75	49.82	49.83	49.70
NiO	0.43	0.43	0.41	0.41	0.42	0.40
Fo#	0.91	0.91	0.91	0.91	0.91	0.91

Sample	MR1					
Analysis#	1	2	3	4	5	6
SiO_2	41.52	41.79	41.84	42.00	41.01	41.16
TiO_2	0.00	0.00	0.00	0.00	0.00	0.00
V_2O_5	0.00	0.00	0.00	0.00	0.00	0.00
Al_2O_3	0.00	0.00	0.00	0.00	0.00	0.00
Cr_2O_3	0.00	0.00	0.00	0.00	0.00	0.00
FeO^{tot}	8.57	8.70	8.73	8.51	8.44	8.27
MnO	0.13	0.13	0.15	0.14	0.16	0.14
MgO	49.99	50.13	50.07	49.95	49.18	49.56
NiO	0.41	0.43	0.40	0.38	0.42	0.41
Fo#	0.91	0.91	0.91	0.91	0.91	0.91

Sample	MR254					
Analysis#	1	2	3	4	5	6
SiO_2	41.26	41.17	40.95	40.97	41.87	41.26
TiO_2	0.00	0.00	0.00	0.00	0.00	0.00
V_2O_5	0.00	0.00	0.00	0.00	0.00	0.00
Al_2O_3	0.00	0.00	0.00	0.00	0.00	0.00
Cr_2O_3	0.00	0.00	0.00	0.00	0.00	0.00
FeO^{tot}	8.82	8.64	8.71	8.77	9.08	8.92
MnO	0.13	0.13	0.14	0.12	0.16	0.12
MgO	48.60	48.54	49.36	49.10	49.33	49.21
NiO	0.43	0.43	0.46	0.40	0.42	0.40
Fo#	0.91	0.91	0.91	0.91	0.91	0.91

Sample	MR276					
Analysis#	1	2	3	4	5	6
SiO_2	41.00	41.11	41.06	40.83	41.16	40.78
TiO_2	0.00	0.00	0.00	0.00	0.00	0.00
V_2O_5	0.00	0.00	0.00	0.00	0.00	0.00
Al_2O_3	0.00	0.00	0.00	0.00	0.00	0.00
Cr_2O_3	0.00	0.00	0.00	0.00	0.00	0.00
FeO^{tot}	9.04	9.04	9.17	8.96	8.99	8.83
MnO	0.14	0.13	0.15	0.13	0.16	0.13
MgO	50.10	50.47	50.06	50.12	50.26	49.40
NiO	0.45	0.43	0.45	0.43	0.41	0.42
Fo#	0.91	0.91	0.91	0.91	0.91	0.91

Sample	NB2a					
Analysis#	1	2	3	4	5	6
SiO_2	41.29	40.79	41.13	41.37	41.11	40.32
TiO_2	0.00	0.00	0.00	0.00	0.00	0.00
V_2O_5	0.00	0.00	0.00	0.00	0.00	0.00
Al_2O_3	0.00	0.00	0.00	0.00	0.00	0.00
Cr_2O_3	0.00	0.00	0.00	0.00	0.00	0.00
FeO^{tot}	9.24	9.83	9.05	9.03	9.48	9.22
MnO	0.14	0.16	0.14	0.16	0.13	0.14
MgO	49.94	50.14	50.09	50.14	50.13	49.65
NiO	0.35	0.30	0.34	0.30	0.34	0.33
Fo#	0.91	0.90	0.91	0.91	0.90	0.91

Sample	NB2b					
Analysis#	1	2	3	4	5	6
SiO_2	41.35	40.98	41.29	40.78	41.25	40.69
TiO_2	0.00	0.00	0.00	0.00	0.00	0.00
V_2O_5	0.00	0.00	0.00	0.00	0.00	0.00
Al_2O_3	0.00	0.00	0.00	0.00	0.00	0.00
Cr_2O_3	0.00	0.00	0.00	0.00	0.00	0.00
FeO^{tot}	9.52	9.38	9.45	9.39	9.22	9.35
MnO	0.17	0.13	0.16	0.14	0.16	0.14
MgO	50.07	50.00	49.16	49.45	49.99	49.60
NiO	0.33	0.29	0.31	0.31	0.35	0.33
Fo#	0.90	0.90	0.90	0.90	0.91	0.90

Sample	RLM026	
Analysis#	1	2
SiO_2	41.01	40.88
TiO_2	0.00	0.00
V_2O_5	0.00	0.00
Al_2O_3	0.00	0.00
Cr_2O_3	0.00	0.00
FeO^{tot}	7.10	6.88
MnO	0.11	0.14
MgO	50.34	50.80
NiO	0.35	0.37
Fo#	0.93	0.93

Sample	RLM057					
Analysis#	1	2	3	4	5	6
SiO_2	41.27	41.12	41.29	41.69	41.24	41.64
TiO_2	0.00	0.00	0.00	0.00	0.00	0.00
V_2O_5	0.00	0.00	0.00	0.00	0.00	0.00
Al_2O_3	0.00	0.00	0.00	0.00	0.00	0.00
Cr_2O_3	0.00	0.00	0.00	0.00	0.00	0.00
FeO^{tot}	8.45	8.44	8.67	8.45	8.36	8.12
MnO	0.14	0.15	0.14	0.15	0.15	0.14
MgO	50.01	49.90	50.41	50.53	50.47	49.93
NiO	0.44	0.43	0.37	0.44	0.42	0.43
Fo#	0.91	0.91	0.91	0.91	0.92	0.92

Berit Olivine Analyses

Sample	MBD-11					
Analysis#	1	2	3	4	5	6
SiO_2	42.33	41.76	42.06	41.92	41.98	41.51
TiO_2	0.00	0.00	0.00	0.00	0.00	0.01
V_2O_5	0.00	0.00	0.03	0.00	0.00	0.00
Al_2O_3	0.00	0.00	0.00	0.00	0.00	0.00
Cr_2O_3	0.00	0.00	0.00	0.00	0.00	0.00
FeO^{tot}	6.67	6.48	6.59	6.55	6.21	6.42
MnO	0.10	0.09	0.11	0.07	0.07	0.05
MgO	51.93	51.12	51.39	50.94	51.32	50.91
NiO	0.35	0.36	0.28	0.17	0.16	0.13
Fo#	0.93	0.93	0.93	0.93	0.94	0.93

Sample	Ader-1							
Analysis#	1	2	3	4	5	6	7	8
SiO_2	40.97	41.00	41.31	40.99	41.87	41.84	42.12	41.68
TiO_2	0.00	0.00	0.00	0.00	0.00	0.00	0.00	0.00
V_2O_5	0.00	0.00	0.00	0.00	0.00	0.00	0.00	0.00
Al_2O_3	0.00	0.00	0.00	0.00	0.00	0.00	0.00	0.00
Cr_2O_3	0.00	0.00	0.00	0.00	0.00	0.00	0.00	0.00
FeO^{tot}	8.05	8.07	7.85	7.84	8.17	7.99	7.93	8.17
MnO	0.13	0.12	0.11	0.12	0.12	0.10	0.12	0.11
MgO	49.55	49.94	49.83	49.72	50.64	50.79	50.95	50.78
NiO	0.31	0.35	0.35	0.34	0.36	0.38	0.35	0.36
Fo#	0.92	0.92	0.92	0.92	0.92	0.92	0.92	0.92

Sample	Ader-9							
Analysis#	1	2	3	4	5	6	7	8
SiO_2	41.45	41.10	41.08	41.28	40.76	40.79	40.70	40.72
TiO_2	0.00	0.00	0.00	0.00	0.00	0.00	0.00	0.00
V_2O_5	0.00	0.00	0.00	0.00	0.00	0.00	0.00	0.00
Al_2O_3	0.00	0.00	0.00	0.00	0.00	0.00	0.00	0.00
Cr_2O_3	0.00	0.00	0.00	0.00	0.00	0.00	0.00	0.00
FeO^{tot}	9.22	9.20	9.29	9.33	9.36	9.48	9.12	8.94
MnO	0.15	0.11	0.14	0.13	0.15	0.12	0.14	0.14
MgO	49.76	49.10	49.16	49.53	48.94	48.82	48.61	48.71
NiO	0.42	0.40	0.41	0.36	0.38	0.41	0.40	0.43
Fo#	0.91	0.90	0.90	0.90	0.90	0.90	0.90	0.91

Sample	Ader-12							
Analysis#	1	2	3	4	5	6	7	8
SiO_2	41.53	41.33	41.26	40.83	41.69	41.55	41.28	41.05
TiO_2	0.00	0.00	0.00	0.00	0.00	0.00	0.00	0.00
V_2O_5	0.00	0.00	0.00	0.00	0.00	0.00	0.00	0.00
Al_2O_3	0.00	0.00	0.00	0.00	0.00	0.00	0.00	0.00
Cr_2O_3	0.00	0.00	0.00	0.00	0.00	0.00	0.00	0.00
FeO^{tot}	7.07	7.05	7.20	7.14	7.71	7.71	7.28	7.46
MnO	0.08	0.13	0.11	0.11	0.08	0.11	0.12	0.12
MgO	50.77	51.13	50.25	50.32	50.65	50.70	50.45	50.64
NiO	0.30	0.31	0.29	0.29	0.33	0.34	0.32	0.29
Fo#	0.93	0.93	0.93	0.93	0.92	0.92	0.93	0.92

Sample	Ader-13							
Analysis#	1	2	3	4	5	6	7	8
SiO_2	40.81	41.05	41.20	41.18	41.27	41.55	41.01	40.71
TiO_2	0.00	0.00	0.00	0.00	0.00	0.00	0.00	0.00
V_2O_5	0.00	0.03	0.00	0.00	0.00	0.00	0.00	0.00
Al_2O_3	0.00	0.00	0.00	0.00	0.00	0.00	0.00	0.00
Cr_2O_3	0.00	0.00	0.00	0.00	0.00	0.00	0.00	0.00
FeO^{tot}	8.21	8.33	8.50	8.62	8.44	8.44	8.47	8.23
MnO	0.10	0.10	0.09	0.10	0.09	0.11	0.12	0.13
MgO	49.12	49.13	49.76	49.70	49.76	49.68	49.18	49.13
NiO	0.33	0.27	0.34	0.30	0.31	0.30	0.29	0.31
Fo#	0.91	0.91	0.91	0.91	0.91	0.91	0.91	0.91

Sample	DMK-9	
Analysis#	1	2
SiO_2	42.01	41.96
TiO_2	0.00	0.00
V_2O_5	0.00	0.00
Al_2O_3	0.00	0.38
Cr_2O_3	0.00	0.00
FeO^{tot}	5.63	5.67
MnO	0.11	0.07
MgO	53.11	52.75
NiO	0.52	0.50
Fo#	0.94	0.94

Sample	DMK-12					
Analysis#	1	2	3	4	5	6
SiO_2	41.67	41.92	41.71	41.34	41.67	41.68
TiO_2	0.00	0.00	0.00	0.00	0.00	0.00
V_2O_5	0.00	0.00	0.00	0.00	0.00	0.00
Al_2O_3	0.00	0.00	0.00	0.00	0.00	0.00
Cr_2O_3	0.00	0.00	0.00	0.00	0.00	0.00
FeO^{tot}	4.92	4.83	5.52	5.63	4.89	4.73
MnO	0.07	0.09	0.10	0.10	0.09	0.11
MgO	53.05	52.73	52.75	52.18	53.19	52.75
NiO	0.51	0.54	0.51	0.48	0.52	0.49
Fo#	0.95	0.95	0.94	0.94	0.95	0.95

Sample	DMK-13							
Analysis#	1	2	3	4	5	6	7	8
SiO_2	39.16	38.85	39.22	39.02	38.49	38.36	38.25	38.55
TiO_2	0.00	0.00	0.00	0.00	0.00	0.00	0.00	0.00
V_2O_5	0.00	0.00	0.00	0.00	0.00	0.00	0.00	0.00
Al_2O_3	0.00	0.00	0.00	0.00	0.00	0.00	0.00	0.00
Cr_2O_3	0.00	0.00	0.00	0.00	0.00	0.00	0.00	0.00
FeO^{tot}	8.18	8.56	7.38	7.41	8.28	8.28	7.90	8.02
MnO	0.14	0.13	0.11	0.09	0.12	0.14	0.12	0.12
MgO	52.40	52.07	53.01	53.25	51.67	51.59	52.58	52.41
NiO	0.35	0.35	0.27	0.27	0.40	0.35	0.31	0.30
Fo#	0.92	0.92	0.93	0.93	0.92	0.92	0.92	0.92

Sample	DMK-14							
Analysis#	1	2	3	4	5	6	7	8
SiO_2	37.99	38.02	38.80	38.49	38.81	38.22	38.64	38.48
TiO_2	0.00	0.00	0.00	0.00	0.00	0.00	0.00	0.00
V_2O_5	0.00	0.00	0.00	0.00	0.00	0.00	0.00	0.00
Al_2O_3	0.00	0.00	0.00	0.00	0.00	0.00	0.00	0.00
Cr_2O_3	0.00	0.00	0.00	0.00	0.00	0.00	0.00	0.00
FeO^{tot}	9.38	9.40	9.52	9.26	9.58	9.28	9.51	9.52
MnO	0.14	0.15	0.15	0.12	0.13	0.15	0.15	0.14
MgO	50.95	51.12	51.87	51.73	51.36	51.23	51.84	51.72
NiO	0.31	0.29	0.34	0.36	0.29	0.29	0.33	0.28
Fo#	0.91	0.91	0.91	0.91	0.91	0.91	0.91	0.91

Sample	DMK-15							
Analysis#	1	2	3	4	5	6	7	8
SiO_2	38.78	38.66	38.91	38.64	39.04	38.55	39.03	39.01
TiO_2	0.00	0.00	0.00	0.00	0.00	0.00	0.00	0.00
V_2O_5	0.00	0.00	0.00	0.00	0.00	0.00	0.00	0.00
Al_2O_3	0.00	0.00	0.00	0.00	0.00	0.00	0.00	0.00
Cr_2O_3	0.00	0.00	0.00	0.00	0.00	0.00	0.00	0.00
FeO^{tot}	9.48	9.39	9.16	9.08	9.47	9.42	9.46	9.36
MnO	0.13	0.14	0.13	0.12	0.14	0.15	0.12	0.12
MgO	52.17	51.44	52.06	52.04	52.13	52.28	52.17	52.04
NiO	0.38	0.37	0.38	0.39	0.41	0.39	0.42	0.41
Fo#	0.91	0.91	0.91	0.91	0.91	0.91	0.91	0.91

Sample	DMK-18					
Analysis#	1	2	3	4	5	6
SiO_2	41.84	42.03	41.97	41.23	42.23	41.91
TiO_2	0.00	0.00	0.00	0.00	0.00	0.00
V_2O_5	0.00	0.00	0.00	0.00	0.00	0.00
Al_2O_3	0.00	0.00	0.00	0.00	0.00	0.00
Cr_2O_3	0.00	0.00	0.00	0.00	0.00	0.00
FeO^{tot}	4.92	4.95	5.49	5.22	5.22	5.26
MnO	0.06	0.07	0.07	0.07	0.11	0.08
MgO	52.98	52.66	52.77	52.46	52.83	52.96
NiO	0.52	0.54	0.52	0.50	0.51	0.52
Fo#	0.95	0.95	0.94	0.95	0.95	0.95

Sample	DMK-28					
Analysis#	1	2	3	4	5	6
SiO_2	42.25	42.18	42.05	42.06	42.25	42.39
TiO_2	0.00	0.00	0.00	0.00	0.00	0.00
V_2O_5	0.00	0.00	0.00	0.00	0.00	0.00
Al_2O_3	0.00	0.00	0.00	0.00	0.00	0.00
Cr_2O_3	0.00	0.00	0.00	0.00	0.00	0.00
FeO^{tot}	4.41	4.53	4.31	4.20	4.53	4.54
MnO	0.09	0.07	0.10	0.07	0.07	0.07
MgO	52.57	52.52	53.18	52.95	52.69	52.91
NiO	0.60	0.53	0.57	0.57	0.57	0.53
Fo#	0.96	0.95	0.96	0.96	0.95	0.95

Sample	DMK-29							
Analysis#	1	2	3	4	5	6	7	8
SiO_2	39.03	38.59	38.38	38.81	38.24	38.15	38.47	38.03
TiO_2	0.00	0.00	0.02	0.02	0.00	0.00	0.00	0.00
V_2O_5	0.00	0.00	0.00	0.00	0.00	0.00	0.00	0.00
Al_2O_3	0.00	0.00	0.00	0.00	0.00	0.00	0.00	0.00
Cr_2O_3	0.00	0.00	0.00	0.00	0.00	0.00	0.00	0.00
FeO^{tot}	8.74	9.02	9.19	9.11	9.04	8.80	8.76	8.85
MnO	0.14	0.13	0.15	0.15	0.13	0.13	0.15	0.12
MgO	51.79	52.51	52.31	52.24	51.87	51.89	51.44	51.61
NiO	0.35	0.34	0.36	0.34	0.35	0.33	0.35	0.33
Fo#	0.91	0.91	0.91	0.91	0.91	0.91	0.91	0.91

Sample	KBK-1							
Analysis#	1	2	3	4	5	6	7	8
SiO_2	41.63	41.33	41.49	41.34	41.34	41.56	41.67	41.53
TiO_2	0.00	0.01	0.00	0.00	0.00	0.00	0.00	0.00
V_2O_5	0.00	0.00	0.00	0.00	0.00	0.00	0.00	0.00
Al_2O_3	0.00	0.00	0.00	0.00	0.00	0.00	0.00	0.00
Cr_2O_3	0.00	0.00	0.00	0.00	0.00	0.00	0.00	0.00
FeO^{tot}	8.25	8.30	8.38	8.29	8.41	8.40	8.24	8.46
MnO	0.16	0.14	0.14	0.13	0.11	0.14	0.12	0.12
MgO	50.75	50.42	50.43	50.82	50.46	50.23	50.53	50.61
NiO	0.37	0.39	0.38	0.40	0.40	0.38	0.37	0.41
Fo#	0.92	0.92	0.91	0.92	0.91	0.91	0.92	0.91

Sample	KBK-3					
Analysis#	1	2	3	4	5	6
SiO_2	41.83	41.27	41.35	41.17	41.65	41.68
TiO_2	0.00	0.00	0.00	0.00	0.00	0.00
V_2O_5	0.00	0.00	0.00	0.00	0.00	0.00
Al_2O_3	0.00	0.00	0.00	0.00	0.00	0.00
Cr_2O_3	0.00	0.00	0.00	0.00	0.00	0.00
FeO^{tot}	8.64	8.68	8.30	8.41	8.40	8.55
MnO	0.12	0.14	0.14	0.11	0.13	0.13
MgO	50.01	50.32	49.73	49.91	50.27	50.35
NiO	0.40	0.39	0.39	0.38	0.41	0.37
Fo#	0.91	0.91	0.91	0.91	0.91	0.91

Sample	KBK-16					
Analysis#	1	2	3	4	5	6
SiO_2	42.25	41.96	41.92	41.57	42.55	42.43
TiO_2	0.00	0.00	0.00	0.00	0.00	0.00
V_2O_5	0.00	0.00	0.00	0.00	0.00	0.00
Al_2O_3	0.00	0.00	0.00	0.00	0.00	0.00
Cr_2O_3	0.00	0.00	0.00	0.00	0.00	0.00
FeO^{tot}	4.41	4.49	4.41	4.50	5.10	4.93
MnO	0.05	0.07	0.09	0.08	0.10	0.10
MgO	53.51	52.82	52.84	52.81	52.43	52.75
NiO	0.49	0.49	0.47	0.46	0.50	0.52
Fo#	0.96	0.95	0.96	0.95	0.95	0.95

Sample	KBK-17							
Analysis#	1	2	3	4	5	6	7	8
SiO_2	40.94	41.29	42.52	42.36	41.76	41.82	41.65	41.89
TiO_2	0.00	0.00	0.00	0.00	0.00	0.00	0.00	0.01
V_2O_5	0.00	0.00	0.00	0.00	0.00	0.00	0.00	0.03
Al_2O_3	0.00	0.00	0.00	0.00	0.00	0.00	0.00	0.00
Cr_2O_3	0.00	0.00	0.00	0.00	0.00	0.00	0.00	0.00
FeO^{tot}	6.41	6.80	6.13	6.07	6.70	6.62	6.52	6.36
MnO	0.09	0.07	0.09	0.09	0.10	0.10	0.09	0.09
MgO	50.93	50.67	52.28	52.48	51.54	51.05	51.28	51.34
NiO	0.41	0.36	0.39	0.35	0.39	0.36	0.38	0.37
Fo#	0.93	0.93	0.94	0.94	0.93	0.93	0.93	0.94

Sample	KBK-18					
Analysis#	1	2	3	4	5	6
SiO_2	41.14	41.89	41.69	41.28	41.12	41.27
TiO_2	0.00	0.00	0.00	0.00	0.00	0.00
V_2O_5	0.00	0.00	0.00	0.00	0.00	0.00
Al_2O_3	0.00	0.00	0.00	0.00	0.00	0.00
Cr_2O_3	0.00	0.00	0.00	0.00	0.00	0.00
FeO^{tot}	6.40	6.56	6.10	5.77	5.93	6.06
MnO	0.10	0.13	0.11	0.10	0.09	0.11
MgO	51.58	51.62	52.13	51.26	51.10	51.15
NiO	0.42	0.41	0.43	0.43	0.44	0.39
Fo#	0.93	0.93	0.94	0.94	0.94	0.94

Sample	KBK-21					
Analysis#	1	2	3	4	5	6
SiO_2	41.63	41.58	41.86	41.64	41.89	41.64
TiO_2	0.00	0.00	0.00	0.00	0.00	0.00
V_2O_5	0.00	0.00	0.00	0.00	0.00	0.00
Al_2O_3	0.00	0.00	0.00	0.00	0.00	0.00
Cr_2O_3	0.00	0.00	0.00	0.00	0.00	0.00
FeO^{tot}	5.02	4.90	4.67	4.78	4.80	5.12
MnO	0.08	0.08	0.05	0.06	0.07	0.05
MgO	51.94	51.60	52.19	52.29	51.42	51.42
NiO	0.54	0.54	0.52	0.51	0.50	0.50
Fo#	0.95	0.95	0.95	0.95	0.95	0.95

Sample	KBK-22					
Analysis#	1	2	3	4	5	6
SiO_2	41.90	41.47	41.58	41.30	41.77	41.41
TiO_2	0.00	0.00	0.00	0.01	0.00	0.00
V_2O_5	0.00	0.00	0.00	0.00	0.00	0.00
Al_2O_3	0.00	0.00	0.00	0.00	0.00	0.00
Cr_2O_3	0.00	0.00	0.00	0.00	0.00	0.00
FeO^{tot}	4.99	4.84	5.09	4.85	4.92	5.04
MnO	0.07	0.08	0.07	0.10	0.09	0.08
MgO	53.31	52.64	52.45	52.16	52.43	52.01
NiO	0.50	0.54	0.52	0.53	0.50	0.52
Fo#	0.95	0.95	0.95	0.95	0.95	0.95

Sample	KBK-36							
Analysis#	1	2	3	4	5	6	7	8
SiO_2	42.02	41.53	41.68	41.45	41.01	41.56	41.46	41.46
TiO_2	0.00	0.00	0.00	0.00	0.00	0.00	0.00	0.00
V_2O_5	0.00	0.00	0.00	0.00	0.00	0.00	0.00	0.00
Al_2O_3	0.00	0.00	0.00	0.00	0.00	0.00	0.00	0.00
Cr_2O_3	0.00	0.00	0.00	0.00	0.00	0.00	0.00	0.00
FeO^{tot}	9.26	9.02	8.75	8.99	8.83	8.94	9.08	9.04
MnO	0.14	0.12	0.14	0.15	0.16	0.10	0.15	0.15
MgO	50.01	49.73	49.87	49.82	49.86	49.97	50.31	49.48
NiO	0.32	0.34	0.31	0.33	0.30	0.32	0.35	0.35
Fo#	0.91	0.91	0.91	0.91	0.91	0.91	0.91	0.91

Sample	KBK-37					
Analysis#	1	2	3	4	5	6
SiO_2	14.31	14.28	14.24	14.29	14.36	14.41
TiO_2	0.00	0.00	0.00	0.00	0.00	0.00
V_2O_5	0.00	0.00	0.00	0.00	0.00	0.00
Al_2O_3	0.00	0.00	0.00	0.00	0.00	0.00
Cr_2O_3	0.00	0.00	0.00	0.00	0.00	0.00
FeO^{tot}	1.29	1.26	1.37	1.32	1.21	1.20
MnO	0.02	0.03	0.02	0.02	0.03	0.03
MgO	27.08	27.15	27.10	27.07	27.07	27.02
NiO	0.14	0.14	0.15	0.15	0.15	0.15
Fo#	0.95	0.96	0.95	0.95	0.96	0.96

Sample	KBK-38					
Analysis#	1	2	3	4	5	6
SiO_2	42.64	42.32	41.54	42.10	41.53	41.76
TiO_2	0.00	0.00	0.00	0.00	0.00	0.00
V_2O_5	0.00	0.00	0.00	0.00	0.00	0.00
Al_2O_3	0.00	0.00	0.00	0.00	0.17	0.27
Cr_2O_3	0.00	0.00	0.00	0.00	0.00	0.00
FeO^{tot}	4.14	4.15	4.42	4.39	4.63	4.32
MnO	0.06	0.08	0.05	0.07	0.08	0.07
MgO	53.98	53.49	52.98	52.87	53.01	52.47
NiO	0.55	0.53	0.53	0.57	0.52	0.57
Fo#	0.96	0.96	0.96	0.96	0.95	0.96

Sample	KBK-39					
Analysis#	1	2	3	4	5	6
SiO_2	41.69	41.61	41.75	41.60	41.36	41.67
TiO_2	0.00	0.00	0.00	0.00	0.00	0.00
V_2O_5	0.00	0.00	0.00	0.00	0.00	0.00
Al_2O_3	0.00	0.00	0.00	0.00	0.00	0.00
Cr_2O_3	0.00	0.00	0.00	0.00	0.00	0.00
FeO^{tot}	4.73	4.55	4.65	4.69	4.76	4.52
MnO	0.07	0.09	0.07	0.06	0.09	0.06
MgO	52.42	51.88	51.83	52.42	52.40	52.15
NiO	0.47	0.51	0.53	0.53	0.50	0.53
Fo#	0.95	0.95	0.95	0.95	0.95	0.95

Sample	KBK-41					
Analysis#	1	2	3	4	5	6
SiO_2	40.83	41.00	40.63	40.20	41.24	41.05
TiO_2	0.00	0.00	0.00	0.00	0.00	0.00
V_2O_5	0.00	0.00	0.00	0.00	0.00	0.00
Al_2O_3	0.00	0.00	0.00	0.00	0.00	0.00
Cr_2O_3	0.00	0.00	0.00	0.00	0.00	0.00
FeO^{tot}	8.71	9.02	8.66	9.00	8.88	8.93
MnO	0.14	0.15	0.14	0.11	0.15	0.14
MgO	49.18	49.17	48.81	48.84	49.31	49.78
NiO	0.43	0.41	0.43	0.39	0.41	0.37
Fo#	0.91	0.91	0.91	0.91	0.91	0.91

Sample	KBK-42									
Analysis#	1	2	3	4	5	6	7	8	9	10
SiO_2	41.47	41.42	41.32	41.21	40.87	41.45	41.13	41.28	41.16	40.82
TiO_2	0.00	0.00	0.00	0.00	0.00	0.00	0.00	0.00	0.00	0.00
V_2O_5	0.00	0.00	0.00	0.00	0.00	0.00	0.00	0.03	0.00	0.00
Al_2O_3	0.00	0.00	0.00	0.00	0.00	0.00	0.00	0.00	0.00	0.00
Cr_2O_3	0.00	0.00	0.00	0.00	0.00	0.00	0.00	0.00	0.00	0.00
FeO^{tot}	8.96	8.72	8.99	9.13	8.57	8.88	9.15	9.13	9.04	9.16
MnO	0.13	0.14	0.15	0.13	0.13	0.13	0.12	0.13	0.12	0.14
MgO	50.44	50.38	50.11	50.11	50.10	50.24	50.33	49.82	49.33	49.46
NiO	0.43	0.43	0.43	0.40	0.41	0.40	0.41	0.39	0.40	0.39
Fo#			0.91	0.91						

Appendix 5 - Laser ICP-MS data

Al'Ays Laser ICP-MS data

Stratigraphic Group 1

Sample	C205			C206			C207	
Analysis#	1	2	3	1	2	3	1	2
Al_2O_3	5.82	6.28	6.579	6.68	7.03	6.87	7.27	7.08
Cr_2O_3	70.77	67.07	69.65	66.65	66.62	68.2	69.89	68.21
FeO	13.10	13.10	11.24	11.41	11.67	11.44	12.17	11.92
TiO_2	0.07	0.07	0.05	0.08	0.09	0.07	0.06	0.06
V	396	394	356	404	416	424	467	458
Ni	1759	1733	1854	1524	1560	1619	1173	1261
Co	188	185	192	162	162	171	174	173
Zn	146	143	139	111	102	122	122	114
Ga	11	10	10	11	11	12	11	10

Sample	C213			C214			C215		
Analysis#	1	2	3	1	2	3	1	2	3
Al_2O_3	3.82	3.33	6.09	5.05	5.42	5.727	5.48	6.39	6.90
Cr_2O_3	64.41	64.33	72.12	64.17	67.61	62.48	69.53	69.13	74.13
FeO	12.53	12.98	12.69	12.78	13.84	10.7	14.15	14.40	13.28
TiO_2	0.07	0.07	0.06	0.06	0.06	0.044	0.06	0.07	0.07
V	400	401	472	414	440	353.2	463	451	524
Ni	1303	1352	1402	1364	1698	1734	1396	1586	1431
Co	170	185	183	171	203	180	208	203	215
Zn	134	148	142	138	162	142	147	144	132
Ga	10	10	13	9	11	10	10	10	13

Stratigraphic Group 2

Sample	C670			C655			C10		
Analysis#	1	2	3	1	2	3	1	2	3
Al_2O_3	6.88	6.94	6.68	3.57	3.49	3.888	20.38	20.59	18.76
Cr_2O_3	66.47	65.73	61.88	71.61	72.27	56.73	48.60	48.13	50.42
FeO	13.29	13.08	10.95	15.10	16.38	11.44	12.32	12.21	10.82
TiO_2	0.10	0.09	0.074	0.03	0.03	0.022	0.04	0.04	0.035
V	291	299	275	453	476	353	892	919	994
Ni	1467	1544	1681	814	757	829	1684	1552	1511
Co	181	170	185	265	331	218	171	169	162
Zn	162	158	185	334	323	207	193	182	195
Ga	12	12	9	8	8	6	34	34	31

Sample	C123		
Analysis#	1	2	3
Al_2O_3	11.07	10.51	12.41
Cr_2O_3	57.11	58.05	60.60
FeO	14.46	14.59	14.52
TiO_2	0.27	0.29	0.25
V	359	373	384
Ni	2262	2147	2378
Co	168	165	175
Zn	138	143	146
Ga	20	20	25

Stratigraphic Group 3

Sample	C60			C40			C33		
Analysis#	1	2	3	1	2	3	1	2	3
Al_2O_3	11.41	11.71	11.36	14.15	13.34	12.09	12.05	12.25	13.78
Cr_2O_3	60.17	60.23	62.93	55.67	58.03	44.08	55.3	56.46	51.97
FeO	16.24	16.47	15.15	14.83	16.56	11.77	15.98	16.03	13.23
TiO_2	0.03	0.03	0.03	0.05	0.05	0.033	0.10	0.11	0.084
V	931	941	1038	1135	1140	740	460	515	425
Ni	639	710	703	786	910	897	1203	1303	1350
Co	234	240	238	220	232	196	204	210	197
Zn	250	262	260	226	242	228	150	241	212
Ga	21	21	20	15	19	13	23	25	22

Sample	C46		
Analysis#	1	2	3
Al_2O_3	12.57	12.80	12.94
Cr_2O_3	57.11	58.67	55.65
FeO	19.03	16.25	13.87
TiO_2	0.20	0.20	0.18
V	531	436	466
Ni	1776	1557	1292
Co	205	204	179
Zn	204	203	177
Ga	38	29	21

Stratigraphic Group 4

Sample	C63			C533			C54		
Analysis#	1	2	3	1	2	3	1	2	3
Al_2O_3	18.25	21.22	21.67	21.26	20.83	22.29	17.74	18.66	18.78
Cr_2O_3	46.65	47.45	48.94	47.47	48.67	47.26	46.97	48.75	50.18
FeO	17.42	16.26	14.70	13.73	13.68	12.40	16.43	15.46	15.45
TiO_2	0.13	0.14	0.13	0.12	0.12	0.10	0.13	0.13	0.12
V	856	878	878	790	823	807	825	830	848
Ni	3004	3403	3815	3386	1799	2827	1589	1049	1889
Co	262	246	249	193	201	194	227	225	255
Zn	249	232	251	208	214	192	228	220	230
Ga	27	31	37	26	29	33	26	26	35

Sample	C238			C413			C328		
Analysis#	1	2	3	1	2	3	1	2	3
Al_2O_3	17.72	17.65	18.74	17.44	17.62	19.14	15.28	14.81	16.81
Cr_2O_3	52.37	53.46	54.89	53.69	49.05	50.57	54.30	52.23	50.23
FeO	14.41	13.86	13.46	15.76	15.62	14.13	18.58	18.43	16.31
TiO_2	0.10	0.10	0.09	0.16	0.16	0.14	0.10	0.10	0.09
V	616	602	627	609	612	606	1134	1118	1157
Ni	1715	1710	1791	1659	1529	1623	1135	1185	1187
Co	187	184	189	202	186	189	247	247	215
Zn	179	178	166	251	217	201	316	346	291
Ga	23	23	29	29	27	34	31	30	35

Sample	C559			C51			C462		
Analysis#	1	2	3	1	2	3	1	2	3
Al_2O_3	22.18	22.06	21.36	23.48	23.23	22.72	14.46	15.73	15.85
Cr_2O_3	45.86	46.43	48.13	44.99	44.8	44.4	55.93	53.56	53.96
FeO	19.28	17.29	15.27	15.37	15.08	14.77	15.01	14.05	13.02
TiO_2	0.14	0.13	0.12	0.12	0.12	0.12	0.11	0.10	0.09
V	882	871	874	751	729	731	628	620	637
Ni	763	951	809	1377	1436	1555	1316	1239	1178
Co	219	214	211	211	212	235	200	192	181
Zn	238	240	236	211	211	229	218	200	189
Ga	40	39	35	34	34	37	25	22	25

Stratigraphic Group 5

Sample	C580			C278			C262		
Analysis#	1	2	3	1	2	3	1	2	3
Al_2O_3	10.09	11.04	12.31	22.96	23.37	23.23	20.80	21.10	20.96
Cr_2O_3	56.98	55.05	58.23	47.13	45.89	47.97	47.23	53.52	48.44
FeO	18.73	18.4	16.84	19.84	19.02	18.26	14.66	14.84	12.95
TiO_2	0.09	0.10	0.079	0.17	0.16	0.15	0.11	0.11	0.09
V	1052	1139	963.1	839	814	864	748	743	762
Ni	981	894	1151	1176	1129	1101	1024	1067	953
Co	223	234	252	281	269	267	204	215	192
Zn	255	298	316	406	367	348	200	227	180
Ga	25	27	23	40	40	46	27	29	31

Sample	C590			C311		
Analysis#	1	2	3	1	2	3
Al_2O_3	8.00	8.19	10.09	18.72	18.55	18.65
Cr_2O_3	56.39	56.96	55.27	45.73	53.34	56.50
FeO	19.36	21.48	17.08	16.96	17.01	18.09
TiO_2	0.10	0.11	0.084	0.14	0.14	0.13
V	1162	1216	1065	1082	1107	1196
Ni	989	993	1279	1027	1007	942
Co	220	245	247	223	250	263
Zn	273	297	312	266	313	286
Ga	20	21	20	31	34	44

Stratigraphic Group 6

Sample	C382			C498		
Analysis#	1	2	3	1	2	3
Al_2O_3	8.29	8.23	8.86	13.64	14.10	13.88
Cr_2O_3	57.21	55.24	63.28	55.49	58.43	59.67
FeO	17.60	17.21	18.97	16.28	16.65	16.42
TiO_2	0.09	0.09	0.07	0.08	0.08	0.07
V	1075	987	1063	889	935	975
Ni	875	806	941	828	737	763
Co	232	232	248	228	233	241
Zn	319	312	333	259	288	310
Ga	18	17	25	37	37	43

Shetland Laser ICP-MS data

Harold's Grave

Sample	HG1			HG4			HG5		
Analysis#	1	2	3	1	2	3	1	2	3
Al_2O_3	20.96	21.12	19.35	21.65	22.19	21.15	23.39	22.90	23.34
Cr_2O_3	49.04	50.15	49.70	48.77	49.48	54.52	41.65	43.29	48.56
FeO	18.60	19.17	17.34	17.06	18.40	17.16	15.67	15.85	16.00
TiO_2	0.21	0.21	0.21	0.17	0.17	0.20	0.17	0.17	0.20
V	1237	1310	1241	1160	1226	1321	1052	1092	1195
Ni	1417	1385	1323	1086	1081	1127	1083	1063	1099
Co	235	248	233	254	268	264	232	230	266
Zn	337	368	330	400	398	376	374	398	376
Ga	48	48	48	45	43	52	48	46	56

Sample	HG6			HG8			HG9		
Analysis#	1	2	3	1	2	3	1	2	3
Al_2O_3	14.49	15.90	16.60	20.58	20.58	19.85	20.17	20.81	20.54
Cr_2O_3	54.48	59.68	70.12	52.26	52.34	51.38	46.87	48.32	49.60
FeO	19.27	22.04	25.20	21.40	20.48	17.91	19.19	19.60	16.93
TiO_2	0.20	0.22	0.23	0.17	0.17	0.19	0.30	0.32	0.28
V	1007	1109	1355	1285	1277	1160	1025	1057	1091
Ni	1017	999	984	1214	1133	1133	1447	1338	1345
Co	232	284	369	275	262	256	250	230	229
Zn	338	430	553	389	364	371	381	317	323
Ga	39	41	37	45	46	46	56	53	49

Sample	HG11		
Analysis#	1	2	3
Al_2O_3	19.53	19.85	19.33
Cr_2O_3	43.27	45.98	49.88
FeO	16.22	17.23	16.63
TiO_2	0.16	0.19	0.19
V	1070	1181	1183
Ni	1357	1632	1442
Co	205	217	218
Zn	355	388	340
Ga	41	49	47

Quoys

Sample	QY1			QY2			QY5		
Analysis#	1	2	3	1	2	3	1	2	3
Al_2O_3	13.86	14.81	14.46	14.66	15.21	15.36	16.42	15.71	15.39
Cr_2O_3	52.32	56.26	57.51	53.07	52.73	54.95	51.10	55.67	55.43
FeO	15.62	15.93	13.11	14.46	15.07	13.29	14.36	15.15	14.56
TiO_2	0.09	0.11	0.11	0.13	0.13	0.14	0.09	0.09	0.09
V	559	626	665	595	606	573	535	585	580
Ni	847	714	887	1113	1281	1202	976	1113	1075
Co	191	214	199	198	204	198	198	208	204
Zn	187	200	189	196	203	189	194	200	211
Ga	25	17	19	19	25	25	20	24	24

Sample	QY8			QY9			QY10		
Analysis#	1	2	3	1	2	3	1	2	3
Al_2O_3	16.88	16.73	16.62	16.73	15.95	15.01	15.05	14.67	14.37
Cr_2O_3	46.64	47.39	55.82	59.58	59.36	56.97	58.00	59.24	57.31
FeO	11.55	11.83	12.82	15.74	14.57	12.62	13.94	14.31	13.73
TiO_2	0.06	0.06	0.07	0.09	0.09	0.08	0.16	0.17	0.15
V	504	506	591	551	538	525	544	566	532
Ni	975	934	1057	694	796	825	1175	1269	1169
Co	167	166	189	274	253	223	189	185	186
Zn	169	168	175	146	175	172	155	144	171
Ga	21	21	29	19	20	21	21	22	25

Cliff

Sample	CF2			CF3			CF5		
Analysis#	1	2	3	1	2	3	1	2	3
Al_2O_3	21.65	21.48	21.37	21.33	21.17	21.24	18.76	19.14	18.99
Cr_2O_3	50.08	49.40	51.59	52.56	48.58	53.59	54.89	53.75	54.97
FeO	15.58	14.39	13.73	15.34	15.71	15.59	15.05	14.67	13.2
TiO_2	0.17	0.17	0.15	0.19	0.18	0.16	0.19	0.18	0.16
V	658	644	659	642	625	674	583	581	614
Ni	941	839	886	1396	2123	1604	1298	1326	1316
Co	196	196	198	244	226	299	204	190	189
Zn	183	184	196	175	176	214	190	166	144
Ga	36	37	35	32	32	30	36	32	30

Sample	CF8			CF13			CF14		
Analysis#	1	2	3	1	2	3	1	2	3
Al_2O_3	19.74	19.65	18.86	21.16	21.05	19.96	18.45	19.90	17.88
Cr_2O_3	52.31	54.72	54.51	54.11	53.09	49.82	69.88	56.51	72.72
FeO	17.33	14.87	12.19	15.56	14.87	12.74	22.08	15.79	22.54
TiO_2	0.19	0.19	0.16	0.17	0.17	0.14	0.10	0.12	0.09
V	619	595	604	654	656	610	870	717	878
Ni	1432	1432	1133	1394	1384	1241	1076	875	901
Co	207	197	184	205	208	180	282	224	296
Zn	199	183	172	191	184	168	249	176	223
Ga	39	35	28	31	31	32	25	27	29

Nikkavord East

Sample	NKE-1			NKE-2			NKE-3		
Analysis#	1	2	3	1	2	3	1	2	3
Al_2O_3	26.24	25.81	26.85	24.68	25.56	26.06	25.44	25.98	26.44
Cr_2O_3	47.26	48.08	48.19	45.07	48.73	48.80	46.81	48.85	49.21
FeO	13.80	13.95	14.22	14.13	14.31	14.48	14.72	15.57	15.13
TiO_2	0.21	0.21	0.22	0.13	0.13	0.13	0.13	0.13	0.13
V	834	835	859	789	830	825	857	880	894
Ni	1853	1818	1811	1693	1796	1737	1602	1779	1655
Co	237	240	249	196	202	208	213	213	219
Zn	222	230	211	198	200	209	216	209	216
Ga	44	44	45	41	43	44	49	47	47

Sample	NKE-4			NKE-5		
Analysis#	1	2	3	1	2	3
Al_2O_3	24.13	22.31	23.78	25.86	26.23	26.14
Cr_2O_3	44.65	49.45	52.06	45.45	47.59	48.30
FeO	13.07	14.31	14.84	13.75	14.55	13.93
TiO_2	0.14	0.16	0.16	0.16	0.18	0.17
V	874	989	1034	797	829	835
Ni	1440	1533	1553	1651	1682	1803
Co	219	236	248	190	205	216
Zn	179	200	207	181	203	211
Ga	34	38	39	43	44	45

Nikkavord South

Sample	NKS-1			NKS-2			NKS-3		
Analysis#	1	2	3	1	2	3	1	2	3
Al_2O_3	26.25	25.68	23.62	25.53	26.44	24.70	26.06	25.71	23.71
Cr_2O_3	48.54	48.00	48.22	41.26	44.04	47.06	44.82	45.21	47.89
FeO	13.93	13.61	12.69	12.23	13.88	12.87	13.62	13.77	12.73
TiO_2	0.11	0.11	0.09	0.15	0.17	0.17	0.07	0.07	0.07
V	811	825	781	610	644	698	832	862	909
Ni	2032	1860	1994	1399	1758	1781	1849	1954	1916
Co	197	199	191	172	182	181	186	186	181
Zn	183	168	153	180	195	190	207	191	193
Ga	37	32	34	31	35	45	34	35	39

Sample	NKS-4		
Analysis#	1	2	3
Al_2O_3	21.51	21.62	21.42
Cr_2O_3	48.12	50.04	49.79
FeO	13.87	14.51	13.30
TiO_2	0.07	0.08	0.06
V	807	833	800
Ni	1772	1865	1879
Co	209	224	198
Zn	219	245	190
Ga	36	39	41

Keen of Hamar

Sample	KH1			KH2		
Analysis#	1	2	3	1	2	3
Al_2O_3	25.56	25.55	24.25	25.52	25.12	24.25
Cr_2O_3	49.09	50.11	49.61	49.54	49.45	49.61
FeO	16.77	17.07	15.92	16.64	16.70	15.92
TiO_2	0.22	0.23	0.22	0.23	0.23	0.22
V	774	796	731	788	789	731
Ni	1476	1493	1560	1500	1506	1560
Co	245	246	251	242	247	252
Zn	213	212	249	212	209	253
Ga	36	37	41	36	36	41

Long Quarry

Sample	LQ1			LQ2			LQ3		
Analysis#	1	2	3	1	2	3	1	2	3
Al_2O_3	21.62	21.67	20.23	18.97	18.37	18.48	21.42	22.19	21.49
Cr_2O_3	55.62	54.87	54.50	59.72	60.30	59.37	56.19	58.09	54.71
FeO	14.60	14.19	12.98	15.64	15.97	14.69	14.23	14.51	13.82
TiO_2	0.16	0.17	0.17	0.19	0.19	0.18	0.16	0.16	0.15
V	704	720	708	695	715	632	763	793	671
Ni	1705	1516	1356	1467	2151	1636	1476	1561	1820
Co	194	191	188	211	215	211	191	202	186
Zn	182	170	174	159	168	146	177	191	189
Ga	33	32	33	29	31	31	27	31	43

Berit Laser ICP-MS data

Dereagzi

Sample	MBD-4			MBD-8			MBD-11		
Analysis#	1	2	3	1	2	3	1	2	3
Al_2O_3	14.37	17.25	11.76	30.68	30.35	28.78	30.44	31.66	30.77
Cr_2O_3	67.08	56.67	58.88	37.10	34.55	29.33	35.29	35.86	35.64
FeO	27.44	25.16	21.17	16.77	16.31	11.55	18.13	19.40	19.6
TiO_2	0.20	0.22	0.17	0.43	0.45	0.277	0.35	0.37	0.45
V	902	949	536	816	794	625	815	863	830
Ni	844	990	906	2258	2090	1907	1035	1140	1161
Co	460	428	443	223	220	185	226	237	231
Zn	762	776	777	300	276	235	313	349	303
Ga	24	29	15	60	58	32	61	71	62

Sample	MBD-13			Ader-2			Ader-4		
Analysis#	1	2	3	1	2	3	1	2	3
Al_2O_3	35.35	36.95	36.49	25.96	26.13	24.77	25.34	23.62	23.71
Cr_2O_3	32.25	30.48	31.55	44.16	46.37	39.73	41.53	42.26	38.48
FeO	10.89	10.45	10.58	14.73	16.40	11.96	16.24	16.38	12.76
TiO_2	0.11	0.13	0.13	0.20	0.23	0.162	0.14	0.15	0.14
V	677	653	662	1246	1308	951	1076	1152	903
Ni	973	1275	1197	1083	1155	1197	1097	1111	1155
Co	205	198	203	224	253	220	247	264	245
Zn	299	281	291	315	393	357	393	411	357
Ga	38	37	38	39	39	32	37	35	28

Demerlik

Sample	DMK-9			DMK-12			DMK-18		
Analysis#	1	2	3	1	2	3	1	2	3
Al_2O_3	28.48	28.17	27.57	25.82	24.47	23.61	29.38	28.38	23.84
Cr_2O_3	38.22	38.07	38.54	40.39	41.12	34.95	39.80	42.57	36.53
FeO	15.74	16.04	14.53	16.82	17.77	13.47	15.09	16.38	12.23
TiO_2	0.14	0.14	0.13	0.19	0.20	0.163	0.14	0.16	0.13
V	812	828	699	905	986	696	797	853	637
Ni	1558	1550	1909	1381	1463	1502	1556	1686	1738
Co	279	284	254	273	280	214	209	234	209
Zn	290	282	293	256	305	281	219	234	215
Ga	43	43	38	37	40	29	43	45	33

Sample	DMK-28		
Analysis#	1	2	3
Al_2O_3	28.46	29.30	26.65
Cr_2O_3	42.90	42.83	37.87
FeO	15.04	14.88	12.21
TiO_2	0.16	0.17	0.14
V	810	812	620
Ni	1699	1602	1800
Co	200	197	195
Zn	227	208	238
Ga	45	45	35

Kabakteppe

Sample	KBK-2			KBK-21			KBK-22		
Analysis#	1	2	3	1	2	3	1	2	3
Al_2O_3	24.55	24.40	24.07	28.45	26.66		27.83	28.27	25.73
Cr_2O_3	42.90	44.26	46.43	40.57	45.80		43.06	46.28	39.55
FeO	15.68	15.35	17.11	14.98	15.31		15.54	15.65	12.98
TiO_2	0.30	0.30	0.32	0.24	0.26		0.26	0.27	0.242
V	958	975	1034	872	954		941	987	770
Ni	1638	1749	1784	1356	1502		1379	1624	1727
Co	215	243	246	205	212		200	214	212
Zn	328	377	410	209	216		234	247	244
Ga	43	45	47	40	41		41	42	35

Sample	KBK-37			KBK-38			KBK-39		
Analysis#	1	2	3	1	2	3	1	2	3
Al_2O_3	31.14	31.31	27.56	29.97	30.73	29.88	29.22	29.18	27.61
Cr_2O_3	38.83	41.57	31.06	38.34	41.17	38.45	40.05	41.89	35.6
FeO	14.86	14.54	10.84	14.32	15.05	12.9	14.90	14.97	11.85
TiO_2	0.20	0.20	0.16	0.20	0.22	0.201	0.20	0.21	0.18
V	828	836	566	774	837	686	838	859	688
Ni	1642	1587	1595	1651	1801	2064	1563	1501	1807
Co	212	219	185	212	224	226	215	216	214
Zn	249	253	208	236	257	241	257	241	253
Ga	47	46	32	45	46	38	44	44	35

Other

Sample	MBK-2			MBK-14			MBA-6		
Analysis#	1	2	3	1	2	3	1	2	3
Al_2O_3	18.84	18.52	18.10	9.53	9.08	8.82	23.99	25.92	26.09
Cr_2O_3	46.51	47.20	47.28	53.38	56.75	58.33	38.47	40.13	41.21
FeO	23.80	23.63	22.56	21.11	21.47	22.13	13.82	13.98	15.21
TiO_2	0.10	0.10	0.10	0.11	0.11	0.11	0.24	0.24	0.329
V	366	377	374	478	463	485	835	911	946
Ni	867	798	760	818	956	993	1566	1480	1602
Co	403	400	390	453	419	421	201	216	221
Zn	2091	2108	2033	1185	1012	906	292	297	283
Ga	60	57	52	16	15	15	35	37	39

Sample	MBT-15		
Analysis#	1	2	3
Al_2O_3	10.09	10.61	10.59
Cr_2O_3	55.19	57.67	56.24
FeO	18.63	20.19	20.34
TiO_2	0.15	0.16	0.141
V	545	640	614
Ni	820	898	827
Co	407	450	424
Zn	750	795	770
Ga	15	16	16

Appendix 6 - Al'Ays Chromitite Pod Dimensions

A table showing the physical dimensions and orientation of the Al'Ays chromitite pods. All data are taken from Neary, 1974. Questions marks indicate that the values are not known.

Site No	Strat.	Length (m)	Breadth (m)	Depth (m)	Strike	Dip
C215	1	15.00	8.00	?	155	62W
C214	1	15.00	8.00	?	155	62W
C213	1	15.00	8.00	?	155	62W
C212	1	15.00	8.00	?	155	62W
C211	1	15.00	8.00	?	155	62W
C210	1	15.00	8.00	?	155	62W
C207	1	15.00	8.00	?	155	62W
C206	1	15.00	8.00	?	155	62W
C205	1	15.00	8.00	?	155	62W
C670	2	10.00	1.50	?	180	90
C655	2	?	?	?	35	90
C595	2	0.75	0.38	?	?	?
C123	2	?	?	?	?	?
C104	2	?	?	?	?	?
C10	2	?	?	?	?	?
650	2	16.00	3.00	?	?	?
645	2	0.50	0.03	?	180	90
640	2	?	?	?	?	?
636	2	7.00	0.10	?	170	65W
573	2	?	?	?	?	?
133	2	1.25	0.04	?	?	?
132	2	1.00	0.01	?	?	?
C60	3	?	?	?	?	?
C46	3	?	?	?	?	?
C44	3	?	?	?	?	?
C40	3	?	?	?	?	?
C33	3	?	?	?	?	?
598	3	?	?	?	?	?
597	3	?	?	?	?	?
596	3	5.00	1.00	?	?	?
527	3	?	?	?	?	?
89	3	1.00	1.00	0.10	?	?
45	3	?	?	?	?	?
42	3	?	?	?	?	?

Site No	Strat.	Length (m)	Breadth (m)	Depth (m)	Strike	Dip
C318	4	1.00	0.10	?	150	55E
C63	4	?	?	?	?	?
C559	4	10.00	1.50	?	?	?
C54	4	?	?	?	?	?
C533	4	?	?	?	?	?
C51	4	?	?	?	?	?
C484	4	?	?	?	?	?
C463	4	1.00	0.30	?	?	?
C462	4	1.00	0.30	?	?	?
C413	4	?	?	?	90	90
C328	4	7.00	0.40	?	110	80S
C238	4	10.00	1.50	?	?	?
557	4	0.25	0.20	?	12	65E
536	4	4.00	1.00	?	40	90
504	4	2.00	0.10	?	?	?
483	4	?	?	?	?	?
461	4	19.00	1.50	?	?	?
321	4	1.00	0.10	?	?	?
271	4	3.00	0.05	?	95	66S
C590	5	1.00	0.25	?	?	?
C580	5	2.00	1.00	?	?	?
C365	5	0.30	0.30	?	?	?
C362	5	1.00	0.10	?	?	?
C311	5	2.00	0.10	?	?	?
C278	5	1.00	0.30	?	?	?
C262	5	?	?	?	85	62S
591	5	?	?	?	?	?
469	5	25.00	4.00	?	?	?
340	5	0.40	0.04	?	?	?
302	5	2.00	1.00	?	63	70S
280	5	1.50	0.30	?	166	35E
255	5	?	?	?	?	?
218	5	?	?	?	?	?
C498	6	0.20	0.10	?	?	?
C382	6	2.00	0.30	?	120	90
C375	6	0.50	0.20	?	?	?
C178	6	3.00	0.02	?	15	90
514	6	?	?	?	?	?
494	6	?	?	?	?	?
489	6	?	?	?	?	?
477	6	4.00	0.30	?	?	?
459	6	4.00	1.00	?	?	?
161	6	2.00	1.00	0.00	?	?
159	6	?	?	?	?	?

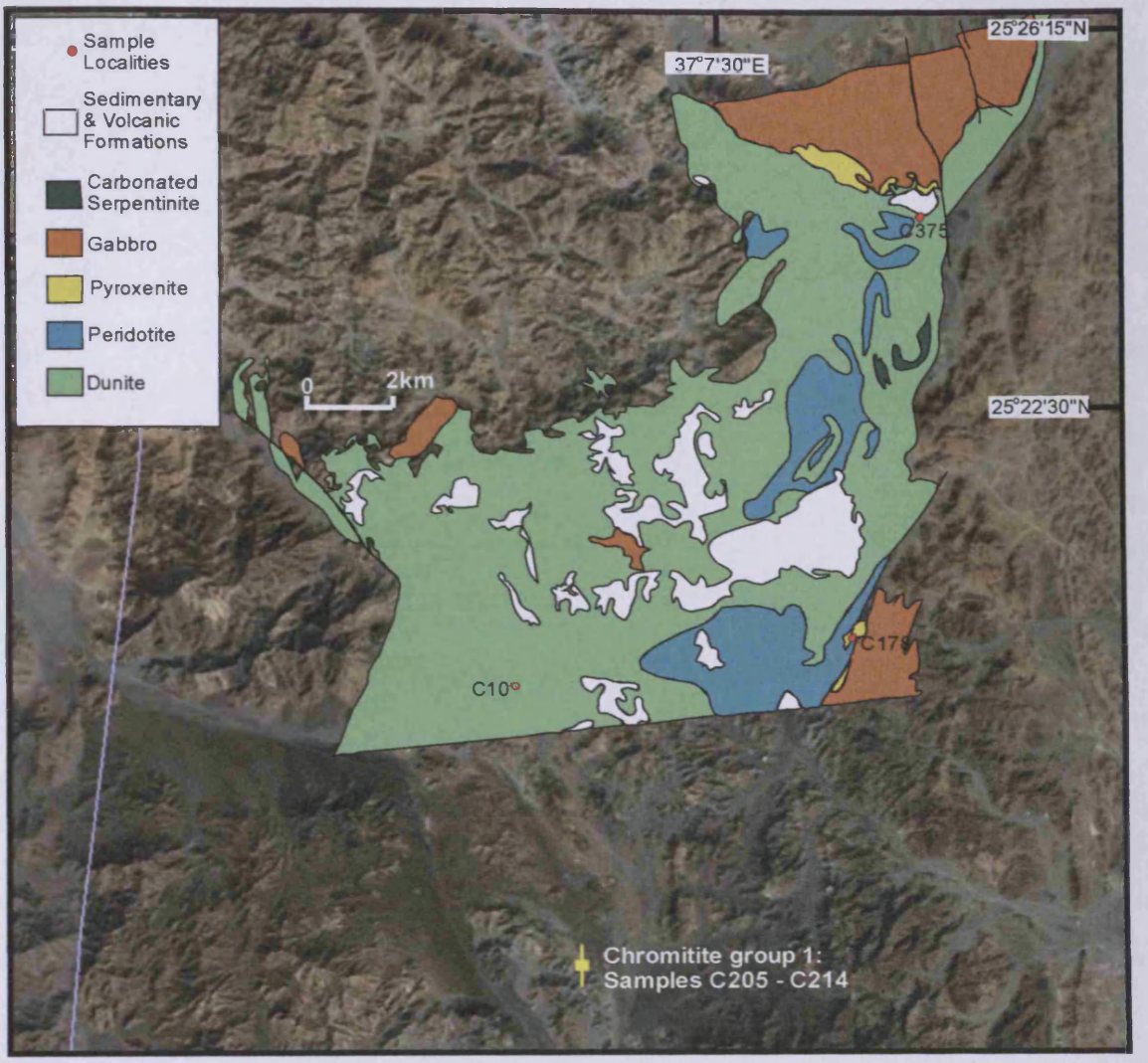

Figure A6.1: *Topographical map of the Al 'Ays area overlain with the geological map of the studied area and showing the location of the group 1 chromitites (sample C204 – C215). Location of the group 1 chromitites taken from Henry & Lefevre, (1966).*

Appendix 7 – Mineral Analyses

All mineral analyses were collected as atomic spectra to determine the mineral speciation. The data are therefore presented as qualitative and are <u>not</u> taken as quantitative results

Cluster analyses – Al 'Ays Ophiolite

Sample	Site of Interest	Analysis #	Mineral	O	Na	Mg	Al	Si	Ca	Cr	Fe
C262	1	i	*Edenite*	58.3	2.7	10.5	5.7	16.0	5.0	0.9	0.8
		ii	*Diopside*	59.3		9.5	0.5	19.9	9.9	0.4	0.4
		iii	*Edenite*	58.5	2.6	10.5	5.7	16.0	5.0	0.9	0.7
		iv	*Diopside*	59.1		9.7	0.7	19.9	9.8	0.4	0.4
		v	*Diopside*	58.7		9.6	0.7	20.2	9.9	0.5	0.5
	2	i	*Edenite*	58.6	2.7	10.6	5.4	16.0	5.1	0.9	0.6
		ii	*Diopside*	59.2		9.6	0.6	20.1	9.7	0.4	0.5
		iii	*Diopside*	59.4		9.9	0.6	19.8	9.7	0.3	0.3
		iv	*Edenite*	58.5	2.9	10.6	5.5	16.0	5.0	0.9	0.7
		v	*Pumpellyite - Mg*	60.8		5.3	8.6	14.1	10.0	0.8	0.5
	3	i	*Diopside*	56.7		10.0	0.7	21.2	10.4	0.5	0.5
		ii	*Edenite*	58.6	2.6	10.7	5.5	16.1	4.9	0.9	0.6
		iii	*Edenite*	56.8	2.8	11.1	6.0	15.8	4.7	1.9	1.0
	4	i	*Diopside*	59.6		9.4	0.6	19.6	9.7	0.4	0.4
		ii	*Diopside*	59.4		9.6	0.6	19.9	9.9	0.3	0.4
	5	i	*Edenite*	58.7	2.8	10.6	5.3	16.0	4.9	1.1	0.6
		ii	*Edenite*	59.0	2.5	10.5	5.3	16.0	4.9	1.1	0.6
		iii	*Edenite*	58.2	2.8	10.5	6.3	14.9	4.4	2.0	0.9
		iv	*Edenite*	58.9	2.6	10.5	5.5	15.8	4.9	1.0	0.6

Sample	Site of Interest	Analysis No.	Mineral	O	Mg	Al	Si	Cr	Fe
C375	1	i	*Cr-Clinochlore*	58.5	19.7	5.3	13.9	1.1	1.2
		ii	*Cr-Clinochlore*	63.6	19.7	1.9	12.9	1.0	0.9
		iii	*Cr-Clinochlore*	60.9	18.9	5.0	12.9	0.7	1.2

Sample	Site of Interest	Analysis #	Mineral	O	Na	Mg	Al	Si	K	Ca	Cr
C498	1	i	~*Potassicrichterite*	64.0	1.0	13.2	6.2	13.4	0.4	0.6	0.8
		ii	~*Potassicrichterite*	60.2	0.9	14.1	6.4	15.1	2.2	0.1	0.8
		iii	~*Potassicrichterite*	59.4	1.1	15.3	6.2	15.1	0.3	0.7	1.2
	2	i	~*Potassicrichterite*	63.3	1.1	13.7	6.1	13.5	0.9	0.2	0.9
		ii	~*Potassicrichterite*	63.3	1.3	13.1	5.2	13.9	1.7	0.4	0.7
		iii	~*Potassicrichterite*	63.6	0.8	13.5	6.1	13.6	0.5	0.7	0.9
	3	i	*Cr - Grossular*	61.7			2.5	14.0		14.2	7.0
		ii	*Edenite*	61.5	2.3	10.6	3.7	16.2		4.4	0.9
		iii	*Sodicgedrite*	59.6	4.1	13.7	6.5	14.5	0.3		0.8
	4	i	*Edenite*	60.7	2.2	10.5	3.9	16.6		4.6	0.9
	5	ii	*Diopside*	60.9	0.6	8.0	2.4	18.3		8.3	0.5

Sample	Site of Interest	Analysis No.	Mineral	O	Na	Mg	Al	Si	Ca	Cr	Fe
C413	1	i	*Edenite*	59.4	2.4	10.6	5.1	16.0	4.7	0.8	0.6
		ii	*Edenite*	59.5	2.4	10.5	4.9	16.2	4.8	0.9	0.7
		iii	*Edenite*	58.7	2.6	10.7	5.1	16.7	4.9	0.8	0.6
		iv	*Cr-Clinochlore*	61.1		17.3	8.8	11.2		1.0	0.4
		v	*Edenite*	60.3	2.5	10.5	4.6	16.0	4.6	0.9	0.5
		vi	*Edenite*	60.1	2.5	10.7	4.6	16.2	4.5	0.8	0.6
	2	i	*Edenite*	59.7	2.6	10.9	4.6	16.3	4.6	0.7	0.5
		ii	*Edenite*	58.4	2.5	10.4	5.3	16.3	5.0	1.0	0.7
		iii	*Edenite*	59.6	2.5	10.5	5.1	15.9	4.7	0.9	0.7
	3	i	*Edenite*	60.3	2.2	10.7	4.2	16.2	4.6	1.0	0.7
		ii	*Edenite*	58.9	2.3	11.1	4.6	16.9	4.7	0.9	0.6
		iii	*Edenite*	58.3	2.3	11.3	4.6	17.2	4.8	0.8	0.6
		iv	*Edenite*	55.6	2.6	11.3	4.6	18.7	5.5	0.9	0.7
	4	i	*Edenite*	58.5	2.6	10.8	4.8	17.1	4.8	0.8	0.6
		ii	*Cr - Grossular*	63.0		0.6	5.1	13.5	13.2	3.7	0.7
		iii	*Cr - Grossular*	62.6		0.9	4.9	13.4	13.1	4.4	0.6

Sample	Site of Interest	Analysis No.	Mineral	O	Na	Mg	Al	Si	Ca	Cr	Fe
C51	1	i	*Diopside*	60.7		9.3	0.7	19.2	9.4	0.3	0.4
	2	i	*Edenite*	59.3	2.5	10.0	5.8	15.6	4.9	1.0	0.8
		ii	*Edenite*	60.3	2.4	9.9	5.7	15.2	4.9	0.9	0.7
		iii	*Edenite*	59.8	2.9	10.0	5.7	15.1	4.7	0.9	0.7
	3	i	*Edenite*	59.6	2.7	9.9	5.7	15.2	5.0	1.0	0.7
		ii	*Edenite*	60.0	2.6	10.0	5.6	15.3	4.8	0.9	0.8
		iii	*Edenite*	59.8	2.8	9.9	5.7	14.8	4.9	1.1	0.8
	4	i	*Edenite*	59.5	2.8	10.2	5.5	15.3	4.8	0.9	0.8
		ii	*Edenite*	60.4	2.5	9.9	5.4	15.7	4.6	0.9	0.6
		iii	*Edenite*	60.6	2.5	9.8	5.4	15.0	4.9	1.0	0.8

Sample	Site of Interest	Analysis #	Mineral	O	Na	Mg	Al	Si	Ca	Cr	Fe
C61	1	i	*Edenite*	59.5	2.7	10.4	5.2	15.7	4.8	1.0	0.7
		ii	*Wollastonite*	61.5		2.4	3.0	13.4	12.1	4.9	2.3
	2	i	*Wollastonite*	60.4		1.2	2.6	14.3	13.3	4.9	3.3
		ii	*Wollastonite*	65.1		5.4	4.4	11.6	8.7	3.9	0.9
		iii	*Cr-Grossular*	61.9			3.7	13.6	14.1	5.4	1.1
	3	i	*Edenite*	59.0	2.9	10.5	5.3	15.9	4.8	1.0	0.7
		ii	*Edenite*	59.3	3.0	10.4	5.3	15.8	4.6	0.9	0.7
		iii	*Edenite*	57.8	2.9	10.7	5.6	15.0	4.5	2.3	1.2
	4	i	*Edenite*	59.4	2.8	10.4	5.3	15.6	4.9	0.9	0.8
		ii	*Edenite*	59.4	2.9	10.3	5.4	15.4	4.9	0.9	0.8
	5	i	*Wollastonite*	60.9		1.7	6.8	14.0	14.5	1.0	0.8
		ii	*Edenite*	58.1	2.9	10.5	5.5	16.2	5.0	1.0	0.7
		iii	*Diopside*	59.6	0.5	9.0	0.7	19.8	9.4	0.4	0.5
		iv	*Edenite*	58.2	3.0	10.6	5.4	15.9	5.0	1.0	0.8
		v	*Edenite*	59.7	3.1	10.3	5.1	15.5	4.7	0.9	0.7
		vi	*Edenite*	64.3	1.2	8.1	5.5	10.2	3.8	4.8	2.1
	6	i	*Wollastonite*	62.5			1.3	13.4	13.6	3.7	4.6
		ii	*Wollastonite*	67.0		1.1	2.1	12.0	10.5	2.6	4.4
	7	i	*Diopside*	59.4	0.5	9.3	0.6	19.9	9.3	0.4	0.6
		ii	*Diopside*	59.6	0.5	9.4	0.6	19.4	9.4	0.6	0.5
		iii	*Edenite*	59.2	2.9	10.6	5.1	15.7	4.8	1.1	0.6
		iv	*Cr-Clinochlore*	63.1		18.0	5.7	11.1		1.6	0.6
		v	*Edenite*	59.7	2.7	10.4	5.3	15.4	4.8	0.9	0.6
		vi	*Edenite*	59.5	2.9	10.4	5.2	15.5	4.7	1.1	0.7
		vii	*Edenite*	59.4	2.8	10.5	5.0	15.7	4.9	1.0	0.7
		viii	*Diopside*	59.7		9.6	0.6	19.7	9.5	0.5	0.5

Sample	Site of Interest	Analysis #	Mineral	O	Na	Mg	Al	Si	Ca	Cr	Fe
C559	1	i	*Edenite*	58.8	2.8	10.9	4.7	16.6	4.7	0.7	0.8
		ii	*Diopside*	59.5		10.0	0.5	19.8	9.4	0.3	0.5
		iii	*Andradite*	59.4		0.8	0.8	15.2	13.9	0.7	9.3
	2	i	*Cr - Grossular*	60.7			5.3	14.7	14.5	4.4	0.4
		ii	*Edenite*	59.2	2.6	10.5	5.0	16.3	4.8	0.8	0.7
	3	i	*Cr - Grossular*	60.5			4.6	14.6	14.5	4.8	1.0
		ii	*Diopside*	59.8		9.7	0.5	19.7	9.4	0.2	0.5
		iii	*Cr - Grossular*	60.4			8.0	14.2	14.7	2.4	0.3
		iv	*Cr - Grossular*	58.6			5.0	15.2	14.8	4.4	2.0
	4	i	*Cr - Grossular*	61.0			3.9	14.4	14.4	5.3	1.1
		ii	*Cr - Grossular*	60.9			3.7	14.4	14.4	5.7	0.7
		iii	*Cr-Clinochlore*	64.4		17.2	5.2	10.7		1.5	0.9
	5	i	*Wollastonite*	56.2		1.7	6.9	12.0	10.2	9.3	3.7

Cluster analyses – Berit Ophiolite

Sample	Site of Interest	Analysis #	Mineral	O	Na	Mg	Al	Si	Ca	Cr	Fe
Ader-12	1	i	*Diopside*	60.5	0.2	9.2	0.5	19.1	9.3	0.6	0.6
		ii	*Edenite*	60.0	2.6	9.8	5.7	15.3	4.8	0.6	1.2
		iii	*Edenite*	60.0	2.6	9.9	5.6	15.3	4.8	0.7	1.2
		iv	*Edenite*	60.2	2.6	9.7	5.7	15.1	4.6	0.7	1.3
		v	*Calcite*	70.7					28.3	0.3	
		vi	*Edenite*	60.5	2.7	9.6	5.5	15.0	4.7	0.7	1.3
	2	i	*Cr-Clinochlore*	63.7	0.5	13.9	6.6	9.7	1.0	2.5	2.0
		ii	*Edenite*	61.1	2.6	9.6	5.5	14.3	4.6	0.8	1.4
		iii	*Edenite*	59.9	2.9	9.8	5.7	14.9	4.6	0.8	1.4
		iv	*Edenite*	60.0	2.7	8.9	5.5	12.5	4.1	3.2	3.2
		v	*Edenite*	66.3	0.4	9.9	3.7	8.2	3.9	2.9	4.6
		vi	*Edenite*	60.5	2.4	9.1	5.5	12.7	4.4	2.6	2.7
		vii	*~Richterite*	63.5	0.4	13.6	3.9	11.1	2.0	1.6	3.9
	3	i	*Diopside*	61.5	0.5	9.3	1.0	18.1	8.6	0.4	0.6
		ii	*Edenite*	59.9	2.5	9.8	5.9	15.0	4.8	0.7	1.4
		iii	*Edenite*	61.8	2.3	9.2	5.5	13.6	5.1	0.6	1.7
		iv	*Calcite*	73.8		3.4	1.0	1.5	19.3	0.4	0.4

Sample	Site of Interest	Analysis #	Mineral	O	Na	Mg	Al	Si	Ca	Cr	Fe
KBK-21	1	i	*Edenite*	61.5	1.5	10.6	3.8	16.5	4.6	0.6	0.6
		ii	*Edenite*	61.2	1.6	10.6	4.0	16.5	4.6	0.6	0.6
		iii	*Edenite*	61.5	1.5	10.4	4.1	16.2	4.6	0.6	0.6
	2	i	*Edenite*	61.4	1.6	10.4	4.4	16.0	4.6	0.6	0.6
		ii	*Serpentine*	64.6	0.2	20.8	0.3	13.1	0.0	0.2	0.5
		iii	*Edenite*	60.0	1.6	10.5	4.3	16.9	5.0	0.6	0.6
		iv	*Edenite*	61.0	1.7	10.6	4.3	16.2	4.6	0.5	0.6
		v	*Edenite*	60.8	1.6	10.6	4.2	16.4	4.7	0.6	0.7
		vi	*Edenite*	61.0	1.6	10.6	4.3	16.1	4.7	0.5	0.7
	3	i	*Edenite*	61.1	1.4	10.4	4.3	16.5	4.7	0.5	0.7
		ii	*Edenite*	60.9	1.4	10.6	4.1	16.7	4.8	0.6	0.6
		iii	*Edenite*	60.6	1.5	10.7	4.2	16.8	4.7	0.5	0.6
		iv	*Edenite*	60.6	1.4	10.7	4.1	16.9	4.7	0.6	0.7
		v	*Edenite*	61.4	1.4	10.2	4.4	16.4	4.7	0.5	0.6
		vi	*Edenite*	61.0	1.5	10.7	3.9	16.7	4.7	0.5	0.6
	4	i	*Edenite*	61.6	1.3	10.7	3.7	16.5	4.7	0.6	0.6
		ii	*Edenite*	61.4	1.3	10.7	3.7	16.6	4.7	0.6	0.6
		iii	*Edenite*	61.2	1.4	10.6	4.1	16.4	4.7	0.6	0.6
		iv	*Enstatite*	60.4	0.0	18.6	0.4	19.4	0.1	0.2	0.9
		v	*Edenite*	61.7	1.4	10.6	3.6	16.6	4.7	0.5	0.6
		vi	*Edenite*	61.4	1.3	10.6	3.9	16.5	4.8	0.6	0.6
	5	i	*Edenite*	61.3	1.6	10.4	4.0	16.2	4.9	0.6	0.6
		ii	*Enstatite*	61.2	0.0	18.1	0.0	18.9	0.1	0.3	1.0
		iii	*Edenite*	62.2	1.4	10.1	4.1	15.5	4.7	0.7	0.8
		iv	*Edenite*	61.9	1.5	10.6	3.7	16.0	4.7	0.6	0.7
		v	*Enstatite*	61.1	0.1	18.1	0.0	18.8	0.1	0.4	0.9
	6	i	*Edenite*	61.9	1.3	10.5	3.6	15.3	4.4	1.7	0.9
		ii	*Edenite*	61.7	1.3	10.6	3.6	16.4	4.6	0.8	0.7
		iii	*Edenite*	61.5	1.2	10.8	3.6	16.8	4.7	0.5	0.6

Sample	Site of Interest	Analysis #	Mineral	O	Na	Mg	Al	Si	Ca	Cr	Fe
MBD-13	1	i	*Edenite*	59.2	1.4	10.1	5.4	17.0	5.2	0.6	0.7
		ii	*Edenite*	60.6	1.5	10.0	5.2	16.2	4.8	0.6	0.8
		iii	*Edenite*	61.2	1.4	10.1	4.5	16.4	4.8	0.5	0.6
		iv	*Edenite*	61.0	1.5	10.0	4.9	16.3	4.8	0.5	0.7
		v	*Edenite*	60.5	1.4	10.3	4.9	16.3	4.6	0.6	0.9
		vi	*Edenite*	61.8	1.4	10.0	4.5	16.1	4.7	0.5	0.7
	2	i	*Edenite*	59.9	1.8	10.4	4.7	16.5	4.8	0.7	0.8
		ii	*Edenite*	60.4	1.7	10.4	4.7	16.5	4.7	0.6	0.7
		iii	*Edenite*	60.3	1.8	10.3	4.6	16.7	4.8	0.6	0.7
		iv	*Edenite*	60.2	1.8	10.5	4.5	16.5	4.8	0.6	0.7
		v	*Edenite*	59.7	1.8	10.5	4.8	16.8	4.7	0.6	0.8
		vi	*Edenite*	59.5	1.9	10.5	4.9	16.4	4.7	0.9	0.8
		vii	*Edenite*	57.8	1.7	11.2	5.4	15.4	3.9	1.5	1.2
	3	i	*Edenite*	59.5	1.8	10.6	4.8	16.8	4.9	0.6	0.7
		ii	*Edenite*	60.8	1.6	10.1	5.2	14.9	4.6	1.4	1.1
		iii	*Edenite*	60.7	1.6	10.4	4.7	15.9	4.7	0.8	0.8
	4	i	*Edenite*	60.2	1.6	10.3	4.9	16.6	4.7	0.6	0.9
		ii	*Edenite*	60.3	1.6	10.3	4.7	16.6	4.8	0.6	0.7
		iii	*Edenite*	59.9	1.7	10.6	4.5	16.9	4.8	0.6	0.7
		iv	*Edenite*	60.1	1.7	10.4	4.6	16.6	4.8	0.7	0.8
		v	*Edenite*	60.3	1.6	10.6	4.4	16.8	4.8	0.6	0.7
		vi	*Edenite*	60.1	1.7	10.5	4.5	16.6	4.9	0.6	0.8
	5	i	*Edenite*	60.7	1.4	10.3	4.7	16.4	4.9	0.6	0.7
		ii	*Edenite*	60.5	1.6	10.2	4.7	16.6	4.9	0.5	0.7
		iii	*Edenite*	59.9	1.5	10.5	4.6	16.8	5.0	0.6	0.7

Sulphide and Alloy analyses – Al 'Ays Ophiolite

Sample	Site of Interest	Analysis No.	Mineral	O	S	Fe	Ni
C559	1	i	*Millerite*		48.7		51.3
		ii	*Millerite*		47.8		52.2
	2	i	*Heazlewoodite*	0.0	38.8		60.8
		ii	*Oxidised Millerite*	21.2	36.6		41.7
		iii	*Millerite*	2.6	44.2		52.4
		iv	*Oxidised Millerite*	25.5	34.1		39.4
	3	i	*Millerite*	0.0	45.6		53.9
		ii	*Millerite*	5.1	45.1		49.4
		iii	*Millerite*	7.2	44.2		48.6
	4	i	*Heazlewoodite*		38.3		61.0
		ii	*Millerite*		45.5		53.4
		iii	*Millerite*		45.2		54.3
		iv	*Heazlewoodite*		38.8		60.8
	5	i	*Awaruite*			26.7	72.3
	6	i	*Millerite*	4.3	46.5	0.0	48.9
		ii	*Millerite*	3.6	46.3	0.0	50.1
		iii	*Millerite*	0.0	46.1	0.5	53.4
	7	i	*Awaruite*	7.5		22.3	67.8
	8	i	*Awaruite*			26.5	72.5
		ii	*Awaruite*			25.7	73.2
		iii	*Awaruite*			25.6	73.2
		iv	*Awaruite*			26.0	72.7

Sample	Site of Interest	Analysis No.	Mineral	O	S	Fe	Ni
C581	1	i	*Heazlewoodite*	1.7	39.3	1.3	55.3
		ii	*Heazlewoodite*	0.0	40.1	1.1	57.2
		iii	*Heazlewoodite*	1.4	39.7	1.4	55.2
	2	i	*Millerite*	0.0	47.8	0.3	51.7
		ii	*Heazlewoodite*	1.2	40.7	0.4	57.3
		iii	*Heazlewoodite*	4.0	38.4	0.8	54.5
	3	i	*Heazlewoodite*	0.0	40.9	0.3	58.3
		ii	*Millerite*	8.0	43.8	0.3	47.2
		iii	*Millerite*	10.5	43.1	0.7	44.4

Sample	Site of Interest	Analysis #	Mineral	O	S	Fe	Co	Ni	Ag
C51	1	i	*Awaruite*			24.4		73.8	
		ii	*Awaruite*			23.5		75.2	
	2	i	*Awaruite*			23.7		74.7	
		ii	*Awaruite*			23.5		75.1	
	3	i	*Awaruite*			24.3		74.1	
	4	I	*Awaruite*			23.1		73.9	
		ii	*Awaruite*			23.1		74.4	
	5	I	*Awaruite*	6.2		26.8	2.1	61.0	
		ii	*Awaruite*	4.5		27.1	1.9	64.3	
	6	I	*Acanthite*	29.1	20.5				39.1
		ii	*Acanthite*	8.7	29.3				56.3
	7	i	*Millerite*	9.2	39.8			46.0	
	8	i	*Awaruite*			23.4	0.9	74.5	
	9	i	*Awaruite*			23.2	0.8	75.3	
	10	i	*Awaruite*			22.9	1.1	75.2	
	11	i	*Awaruite*			22.8	0.9	75.1	
	12	i	*Awaruite*			23.8	0.8	74.2	

Sample	Site of Interest	Analysis #	Mineral	O	S	Fe	Ni	Cu	As
C63	1	i	*Awaruite - (Cu)*	6.1		20.7	65.5	3.9	
		ii	*Awaruite - (Cu)*	5.5		21.1	68.0	2.2	
	2	i	*Millerite*	5.0	45.2		49.5		
	3	i	*Heazlewoodite*	4.1	38.6	0.4	56.6		
	4	i	*Awaruite*	4.1	1.1	21.2	68.9	1.1	
		ii	*Heazlewoodite*	3.3	38.7	0.8	55.1	0.0	
	5	i	*Oxidised Millerite*	14.9	40.7	0.1	44.2		
		ii	*Oxidised Orcelite*	14.9	0.3	0.4	55.2		29.0
	6	i	*Heazlewoodite*	3.3	38.4	1.4	54.4	0.0	
		ii	*Awaruite - (Cu)*	3.3	0.0	19.4	62.7	10.5	
		iii	*Awaruite - (Cu)*	3.9	0.4	19.7	66.9	5.3	
	7	i	*Orcelite*	3.4	0.0	0.6	63.5		31.7
		ii	*Heazlewoodite*	1.8	39.6	0.4	57.4		
	8	i	*Native Cu + Ni*	5.4	0.0	1.4	11.4	77.0	
		ii	*Heazlewoodite*	4.4	37.3	1.2	54.1	0.0	
	9	i	*Heazlewoodite*	1.3	39.0	1.1	55.4	0.0	0.0
		ii	*Awaruite*	5.1	0.0	20.4	69.0	1.4	0.6
		iii	*Awaruite*	4.8	0.0	19.4	67.9	1.7	2.0
		iv	*Heazlewoodite*	1.8	38.8	1.3	54.9	0.0	0.0

Sample	Site of Interest	Analysis #	Mineral	S	Fe	Ni
C250	1	i	*Millerite*	46.9	0.4	52.4
		ii	*Heazlewoodite*	40.2	0.5	59.0
		iii	*Heazlewoodite*	40.4	0.5	58.8
		iv	*Millerite*	49.5	0.8	49.3
	2	i	*Heazlewoodite*	40.5	0.3	59.0
		ii	*Heazlewoodite*	40.5	0.3	58.8
		iii	*Heazlewoodite*	40.6	0.2	58.9
	3	i	*Millerite*	46.2	0.3	53.1
		ii	*Heazlewoodite*	40.3	0.3	59.0
		iii	*Heazlewoodite*	40.4	0.3	58.7
	4	i	*Heazlewoodite*	39.9	0.9	57.7
		ii	*Heazlewoodite*	39.6	0.8	58.1
	5	i	*Heazlewoodite*	39.9	0.7	58.1
		ii	*Heazlewoodite*	40.5	0.4	58.4
		iii	*Millerite*	47.0	0.5	51.1

Sample	Site of Interest	Analysis #	Mineral	O	S	Fe	Ni	Cu
C262	1	i	*Oxidised Heazlewoodite*	12.8	36.0	0.4	49.9	
		ii	*Heazlewoodite*	3.7	39.6	0.4	55.4	
	2	i	*Millerite*	3.5	46.4	0.3	49.2	
		ii	*Heazlewoodite*	0.0	40.2	0.6	57.7	
	3	i	*Chalcocite*	2.2	33.3			60.7
	4	i	*Millerite*	2.6	47.8	0.8	47.8	
		ii	*Millerite*	4.0	45.4	1.4	47.0	
		iii	*Millerite*	8.6	43.5	1.0	45.5	
	5	i	*Oxidised Millerite*	12.2	42.7	0.8	43.0	
		ii	*Millerite*	0.0	47.4	1.1	50.1	

Sulphide and Alloy analyses – Berit Ophiolite

Sample	Site of Interest	Analysis #	Mineral	O	S	Fe	Co	Ni
Ader-2	1	i	*Pentlandite*		46.9	26.6	1.2	24.2
		ii	*Millerite*		49.6	0.1		50.0
		iii	*Heazlewoodite*		40.2			59.4
		iv	*Millerite*		48.6			51.2
	2	i	*Heazlewoodite*		40.2	0.4		59.0
		ii	*Pentlandite*		47.1	27.1		25.0
		iii	*Pentlandite*		47.1	26.3		24.8
	3	i	*Heazlewoodite*		39.9	0.9		56.9
		ii	*Millerite*		47.0	0.8		50.4
		iii	*Pentlandite*		46.6	25.6		25.6
	4	i	*Pentlandite*	3.7	44.7	25.2		23.9
		ii	*Oxi - Heazlewoodite*	25.1	24.4	1.7		37.7
		iii	*Oxi - Heazlewoodite*	6.2	37.0	1.4		51.6
	5	i	*Pentlandite*		46.7	25.0		25.4
		ii	*Pentlandite*		47.2	26.0		24.2
		iii	*Pentlandite*		46.2	25.4		25.4
		iv	*Pentlandite*		46.3	26.1		24.8

Sample	Site of Interest	Analysis #	Mineral	S	Fe	Co	Ni
Ader-3	1	i	*Pentlandite*	47.3	26.6		25.7
		ii	*Pentlandite*	46.9	25.0		27.3
		iii	*Millerite*	47.2	0.4		51.7
	2	i	*Pentlandite*	46.8	26.4		25.4
		ii	*Pentlandite*	47.4	26.0		25.0
		iii	*Pentlandite*	46.8	26.4		25.0
	3	i	*Pentlandite*	45.3	24.9	1.1	26.4
		ii	*Pentlandite*	46.6	25.4	1.0	25.5
		iii	*Pentlandite*	46.4	25.5	1.0	25.8
	4	i	*Pentlandite*	46.0	25.0	1.2	24.6
		ii	*Pentlandite*	46.0	25.3	1.3	24.7
	5	i	*Pentlandite*	46.5	26.1	0.8	25.2
		ii	*Pentlandite*	46.6	26.1	0.9	25.7

Sample	Site of Interest	Analysis #	Mineral	O	S	Fe	Ni
Ader-12	1	i	*Pentlandite*	4.4	44.8	28.0	22.0
		ii	*Pentlandite*	4.3	44.9	27.6	22.4
	2	i	*Pentlandite*	3.1	45.2	26.6	23.1
		ii	*Pentlandite*	2.6	45.6	26.6	23.5
	3	i	*Pentlandite*		46.7	28.5	24.2
		ii	*Pentlandite*		47.0	27.9	23.9
	4	i	*Pentlandite*		47.1	28.9	23.4
		ii	*Pentlandite*		46.9	28.8	23.6
	5	i	*Pentlandite*	3.7	45.3	24.9	25.5

Sample	Site of Interest	Analysis #	Mineral	O	S	Fe	Ni
DMK-14	1	i	*Oxi - Horomanite*	7.6	43.7	31.3	16.2
		ii	*Oxi - Horomanite*	14.9	37.6	29.6	16.4
	2	i	*Oxi - Horomanite*	6.9	43.9	32.7	16.4
		ii	*Oxi - Horomanite*	15.6	38.0	29.3	17.1
	3	i	*Oxi - Horomanite*	10.7	40.2	29.8	18.7
		ii	*Oxi - Horomanite*	5.0	45.4	33.0	16.1
	4	i	*Horomanite?*		47.5	34.0	17.3
		ii	*Horomanite?*		48.3	34.5	15.8
	5	i	*Horomanite?*		48.0	32.2	18.7
		ii	*Horomanite?*		47.6	34.9	16.3

Sample	Site of Interest	Analysis #	Mineral	S	Fe	Ni
KBK-21	1	i	*Pentlandite*	46.8	27.4	24.7
		ii	*Pentlandite*	46.8	27.5	24.7
	2	i	*Millerite*	49.2	0.9	49.4
		ii	*Pentlandite*	46.9	28.0	24.4
		iii	*Pentlandite*	46.8	27.7	24.2
	3	i	*Pentlandite*	46.9	27.7	24.5
		ii	*Pentlandite*	46.7	27.8	24.9
	4	i	*Pentlandite*	46.8	27.6	25.0
		ii	*Pentlandite*	46.5	27.5	25.3
		iii	*Pentlandite*	46.6	27.4	25.3
	5	i	*Pentlandite*	46.9	27.9	24.4
		ii	*Pentlandite*	46.8	27.4	24.9

Sample	Site of Interest	Analysis #	Mineral	O	Si	S	Fe	Ni	Cu
MBD-13	1	i	*Pentlandite*			46.4	22.1	29.5	0.0
		ii	*Horomanite?*			55.7	26.4	16.1	0.0
		iii	*Pentlandite*			53.1	25.2	19.7	0.2
		iv	*Pentlandite*			47.1	23.3	28.0	0.0
		v	*Chalcopyrite*			49.0	25.2	0.2	23.9
	2	i	*Chalcopyrite*			48.7	25.4	0.5	23.7
		ii	*Pentlandite*			46.3	24.7	27.0	0.0
		iii	*Pentlandite*			46.8	20.1	31.2	0.0
	3	i	*Violarite*	2.5		45.4	19.5	31.3	0.0
		ii	*Chalcopyrite*	1.8		48.0	24.8	0.4	23.4
		iii	*Oxidised Pentlandite*	7.8		50.5	16.7	22.2	0.3
	4	i	*Oxidised Copper*	54.1			1.2		43.7
		ii	*Oxidised Copper*	63.6	2.5		15.0	3.2	14.3
	5	i	*Chalcopyrite*			47.6	24.3	2.3	21.7
		ii	*Pentlandite*			47.3	23.7	28.7	0.0
		iii	*Pyrite*			65.0	30.4	4.4	0.0

Sample	Site of Interest	Analysis No.	Mineral	S	Fe	Ni
MBD-7	1	i	*Pyrite*	65.9	32.1	1.7
		ii	*Smythite?*	55.6	28.6	15.5
		iii	*Pentlandite*	47.1	24.6	27.9

Sulphide and Alloy analyses – Shetland Ophiolite

Sample	Site of Interest	Analysis #	Mineral	O	S	Fe	Ni	As
QY1	1	i	*Maucherite*				58.2	41.8
	2	i	*Violarite*	6.8	44.7	14.1	33.8	
		ii	*Violarite*		46.3	18.6	34.2	
	3	i	*Maucherite*				57.4	41.9

Sample	Site of Interest	Analysis #	Mineral	O	Si	S	Fe	Ni	Cu
NB2b	1	i	*Awaruite*				26.0	72.7	
		ii	*Oxidised Awaruite*	23.8			20.6	46.5	
	2	i	*Awaruite*				28.4	71.2	
		ii	*Pentlandite*			46.8	28.7	23.3	
		iii	*Haematite*	58.3			40.7	0.3	
	3	i	*Pentlandite*			47.0	27.0	26.0	
		ii	*Oxidised Awaruite*	7.8		5.9	24.6	60.6	
	4	i	*Pentlandite*			46.8	29.2	22.8	
		ii	*Haematite*	58.4			40.6	0.3	
		iii	*Oxidised Awaruite*	8.6		5.6	25.2	59.6	
		iv	*Pentlandite*			46.2	26.8	26.7	
	5	i	*Pentlandite*			47.1	28.5	23.7	
		ii	*Heazlewoodite*			39.9	0.9	58.8	
		iii	*Oxidised Awaruite*	5.4		0.5	24.1	65.0	4.6
		iv	*Oxidised Awaruite*	16.0	1.5	0.8	22.8	55.5	

Sample	Site of Interest	Analysis #	Mineral	O	S	Fe	Ni	Cu	As	Sb
CF21	1	i	*Orcelite*	2.8	0.6		63.9		31.6	1.1
		ii	*Heazlewoodite*	3.3	38.8		57.9			
		iii	*Heazlewoodite*		40.0		60.0			
		iv	*Pentlandite*		47.0	23.1	29.4			
		v	*Orcelite*	4.0	0.6	1.2	64.2		28.8	1.3
		vi	*Orcelite*	2.7	0.9	1.1	63.0		31.0	1.3
	2	i	*Chalcocite*	4.8	32.0	2.2		60.3		
		ii	*Heazlewoodite*	1.8	39.5	3.1	55.5			
	3	i	*Violarite*		38.0	16.6	38.5	6.3		
		ii	*Heazlewoodite*		39.4		60.6			
		iii	*Pentlandite*		46.9	23.1	29.5			
		iv	*Orcelite*		0.8	0.5	67.3		30.4	1.1

Sample	Site of Interest	Analysis #	Mineral	S	Fe	Ni
RLM053	1	i	*Millerite*	46.3		53.1
		ii	*Heazlewoodite*	40.0		59.4
	2	i	*Heazlewoodite*	39.1	0.4	59.1
		ii	*Millerite*	48.2	0.7	49.7

Sample	Site of Interest	Analysis #	Mineral	O	S	Fe	Ni	Cu	As	Sb
CF20	1	i	*Breithauptite*			2.7	50.3		1.6	45.4
		ii	*Heazlewoodite*		39.1		60.9			
		iii	*Orcelite*		0.8		69.5		28.3	1.4
		iv	*Pentlandite*		46.8	23.1	30.0			
		v	*Pentlandite*		46.6	23.5	29.8			
	2	i	*Pentlandite*		46.1	21.9	28.7	2.6		
		ii	*Orcelite*		0.5	3.5	66.1		28.5	1.3
		iii	*Pentlandite*		39.3		60.7			
		iv	*Breithauptite*	6.9		0.9	47.0			41.6
		v	*Orcelite*		8.7	0.4	64.8		25.4	0.7

Sample	Site of Interest	Analysis #	Mineral	O	S	Fe	Co	Ni	Cu	As
CF2	1	i	*Pentlandite*		46.6	22.3		29.4		
		ii	*Orcelite*					68.6		31.4
	2	i	*Maucherite*			0.4		57.3		41.7
		ii	*Heazlewoodite*		38.6	0.4		60.2		
	3	i	*Pentlandite*		45.0	20.2	1.5	29.8		
		ii	*Heazlewoodite*		38.7	1.0		58.8		
		iii	*Chalcocite*	2.4	32.5	1.3			62.3	
		iv	*Oxidised Maucherite*	7.7		1.7		51.0		37.5
		v	*Heazlewoodite*		38.6	1.4		57.5		0.4
	4	i	*Orcelite*	10.9				63.1		26.0
		ii	*Orcelite*					66.7		33.3
	5	i	*Millerite*		46.7			53.3		
		ii	*Heazlewoodite*		39.0			61.0		
		iii	*Maucherite*					57.1		42.9

Sample	Site of Interest	Analysis #	Mineral	S	Fe	Co	Ni
HG8	1	i	*Millerite*	46.5			53.5
	2	i	*Pentlandite*	47.0	23.9	2.0	26.8
	3	i	*Heazlewoodite*	38.5	0.9		59.1
		ii	*Millerite*	46.5	0.9		51.0
		iii	*Heazlewoodite*	39.0	0.7		58.9

Sample	Site of Interest	Analysis #	Mineral	O	S	Fe	Co	Ni
LQ3	1	i	*Millerite*		46.8			52.9
		ii	*Heazlewoodite*		40.0			60.0
		iii	*Heazlewoodite*		40.2			59.8
	2	i	*Heazlewoodite*		39.2			60.8
		ii	*Millerite*		46.9			53.1
	3	i	*Heazlewoodite*		40.1			59.9
		ii	*Millerite*		46.2			53.6
	4	i	*Millerite*		47.6	0.3		51.5
		ii	*Heazlewoodite*		39.6			60.0
	5	i	*Oxidised Pentlandite*	16.2	35.4	19.8	1.7	20.7
		ii	*Pentlandite*		45.6	24.3	2.2	26.6

Sample	Site of Interest	Analysis #	Mineral	S	Ni
HG11	1	i	*Heazlewoodite*	40.0	60.0

Sample	Site of Interest	Analysis #	Mineral	O	S	Fe	Co	Ni	Cu	As	Te
CF3	1	i	*Maucherite*		1.2			57.9		40.9	
		ii	*Maucherite*		0.9			57.3		41.9	
	2	i	*Maucherite*			0.7		55.6		42.4	
		ii	*Heazlewoodite*		39.4			60.6			
	3	i	*Orcelite*	2.8	0.6			67.0		29.6	
		ii	*Heazlewoodite*		40.5			59.1		0.4	
		iii	*Orcelite*		1.1			67.7		31.2	
	4	i	*Polydymite?*		53.6	0.6		40.7	3.9		
		ii	*Chalcocite*	3.7	32.2	0.6		1.5	60.0		3.8
		iii	*Millerite*		46.6	0.8		51.0			
	5	i	*Maucherite*		1.0			56.7		42.3	
		ii	*Maucherite*		0.7			57.0		41.8	
		iii	*Pentlandite*		46.2	21.7	1.1	30.6			
		iv	*Maucherite*		0.7			57.7		41.7	
		v	*Millerite*		47.8	0.9		51.1			

Appendix 8 – Microprobe Analyses

Sample C462

The first 7 analyses are those with higher Cr#. Totals include trace element values.

Analysis# (C462)	Mg#	Cr#	Cr/ Fe^{2+}	Fe^{3+}#	Al_2O_3	Cr_2O_3	FeO	MgO	Fe_2O_3	Total
1	0.60	0.81	4.01	0.01	9.39	61.31	14.45	12.01	1.20	98.79
2	0.63	0.75	3.99	0.02	12.54	57.60	13.65	12.91	1.73	98.84
3	0.62	0.73	3.78	0.02	13.75	56.71	14.19	12.85	1.63	99.62
4	0.64	0.73	3.95	0.02	14.20	56.42	13.49	13.38	1.69	99.62
5	0.65	0.72	4.06	0.02	14.64	55.76	12.99	13.62	1.63	99.12
6	0.62	0.72	3.77	0.02	14.68	55.82	14.00	13.09	1.46	99.53
7	0.63	0.72	3.82	0.02	14.68	55.68	13.79	13.18	1.68	99.45
8	0.63	0.70	3.79	0.01	15.85	55.15	13.74	13.39	1.18	99.77
9	0.64	0.70	3.85	0.02	15.87	55.00	13.51	13.56	1.41	99.88
10	0.64	0.70	3.83	0.02	15.86	54.89	13.55	13.55	1.53	99.81
11	0.64	0.70	3.84	0.02	15.94	54.43	13.41	13.58	1.75	99.50
12	0.64	0.69	3.77	0.02	16.11	54.72	13.71	13.45	1.32	99.79
13	0.65	0.69	3.89	0.02	16.03	54.16	13.15	13.69	1.71	99.18
14	0.64	0.69	3.82	0.01	16.23	54.64	13.52	13.56	1.12	99.54
15	0.65	0.69	3.89	0.03	15.96	53.67	13.04	13.70	2.11	98.91
16	0.64	0.69	3.80	0.01	16.30	54.74	13.63	13.53	1.09	99.78
17	0.65	0.69	3.88	0.02	16.06	53.92	13.13	13.66	1.79	99.01
18	0.65	0.69	3.89	0.02	16.14	54.18	13.15	13.74	1.73	99.42
19	0.65	0.69	3.92	0.03	15.94	53.49	12.91	13.74	2.28	98.71
20	0.64	0.69	3.79	0.02	16.13	54.12	13.51	13.51	1.75	99.48
21	0.66	0.69	4.03	0.03	16.01	53.71	12.61	13.95	2.11	98.80
22	0.63	0.69	3.71	0.02	16.22	54.43	13.85	13.36	1.42	99.76
23	0.64	0.69	3.78	0.02	16.19	54.28	13.57	13.57	1.72	99.81
24	0.65	0.69	3.89	0.02	16.10	53.97	13.11	13.74	1.88	99.23
25	0.64	0.69	3.77	0.02	16.30	54.62	13.69	13.58	1.43	100.05
26	0.65	0.69	3.87	0.03	15.99	53.59	13.08	13.66	2.20	98.87
27	0.64	0.69	3.79	0.01	16.35	54.75	13.65	13.57	1.21	100.01
28	0.65	0.69	3.90	0.02	16.02	53.63	13.01	13.73	1.96	98.80
29	0.65	0.69	3.94	0.02	16.21	54.27	13.03	13.81	1.63	99.39
30	0.64	0.69	3.77	0.02	16.21	54.26	13.61	13.53	1.50	99.58
31	0.65	0.69	3.90	0.02	16.18	53.99	13.08	13.84	1.82	99.38
32	0.64	0.69	3.81	0.02	16.20	54.06	13.42	13.64	1.83	99.63
33	0.64	0.69	3.81	0.02	16.15	53.85	13.35	13.55	1.89	99.37
34	0.65	0.69	3.84	0.02	16.16	53.86	13.25	13.65	1.86	99.20
35	0.63	0.69	3.73	0.02	16.26	54.19	13.73	13.39	1.34	99.40
36	0.65	0.69	3.86	0.02	16.37	54.53	13.34	13.72	1.35	99.79
37	0.65	0.69	3.92	0.01	16.36	54.52	13.16	13.81	1.24	99.58
38	0.66	0.69	3.92	0.03	16.05	53.48	12.91	13.76	2.11	98.73
39	0.64	0.69	3.83	0.02	16.20	53.90	13.30	13.56	1.48	98.87
40	0.64	0.69	3.78	0.02	16.32	54.30	13.56	13.52	1.38	99.58

Analysis# (C462)	Mg#	Cr#	Cr/ Fe^{2+}	Fe^{3+}#	Al_2O_3	Cr_2O_3	FeO	MgO	Fe_2O_3	Total
41	0.66	0.69	3.95	0.02	16.18	53.79	12.87	13.80	1.82	98.86
42	0.64	0.69	3.83	0.01	16.47	54.68	13.51	13.69	1.06	100.03
43	0.65	0.69	3.87	0.02	16.24	53.91	13.18	13.73	1.81	99.26
44	0.65	0.69	3.87	0.03	16.10	53.43	13.04	13.73	2.22	98.96
45	0.64	0.69	3.76	0.02	16.28	53.99	13.57	13.53	1.78	99.59
46	0.65	0.69	3.87	0.02	16.27	53.98	13.19	13.69	1.54	99.18
47	0.65	0.69	3.82	0.02	16.21	53.75	13.30	13.68	2.04	99.38
48	0.64	0.69	3.80	0.01	16.45	54.54	13.58	13.60	1.14	99.78
49	0.63	0.69	3.71	0.02	16.36	54.25	13.84	13.41	1.42	99.75
50	0.66	0.69	3.97	0.02	16.18	53.62	12.78	13.87	1.88	98.75
51	0.64	0.69	3.78	0.02	16.28	53.94	13.48	13.56	1.76	99.48
52	0.63	0.69	3.70	0.02	16.30	54.00	13.79	13.35	1.47	99.35
53	0.64	0.69	3.80	0.02	16.41	54.38	13.53	13.59	1.37	99.74
54	0.65	0.69	3.84	0.02	16.37	54.22	13.34	13.70	1.61	99.69
55	0.64	0.69	3.79	0.02	16.40	54.20	13.53	13.60	1.56	99.75
56	0.65	0.69	3.89	0.02	16.33	53.97	13.11	13.75	1.51	99.17
57	0.65	0.69	3.85	0.02	16.32	53.91	13.23	13.66	1.54	99.13
58	0.67	0.69	4.07	0.03	16.07	53.06	12.33	14.02	2.20	98.07
59	0.65	0.69	3.84	0.02	16.41	54.19	13.33	13.71	1.49	99.57
60	0.65	0.69	3.91	0.02	16.30	53.82	13.01	13.81	1.76	99.15
61	0.64	0.69	3.81	0.02	16.35	53.97	13.38	13.62	1.72	99.50
62	0.66	0.69	3.91	0.02	16.22	53.50	12.95	13.79	2.00	98.89
63	0.64	0.69	3.79	0.01	16.56	54.64	13.62	13.58	0.94	99.84
64	0.64	0.69	3.79	0.02	16.39	54.06	13.49	13.58	1.46	99.45
65	0.65	0.69	3.87	0.02	16.41	54.09	13.21	13.73	1.45	99.46
66	0.65	0.69	3.90	0.02	16.30	53.72	13.01	13.79	1.72	98.97
67	0.66	0.69	3.94	0.03	16.09	53.01	12.71	13.74	2.16	98.24
68	0.64	0.69	3.74	0.02	16.33	53.79	13.59	13.51	1.84	99.49
69	0.64	0.69	3.80	0.02	16.50	54.31	13.52	13.63	1.28	99.78
70	0.65	0.69	3.89	0.02	16.27	53.50	12.99	13.75	1.75	98.72
71	0.65	0.69	3.88	0.01	16.58	54.50	13.28	13.80	1.26	99.89
72	0.65	0.69	3.89	0.01	16.54	54.36	13.21	13.77	1.19	99.57
73	0.65	0.69	3.89	0.02	16.37	53.76	13.05	13.77	1.62	99.27
74	0.65	0.69	3.87	0.01	16.54	54.32	13.26	13.74	1.14	99.48
75	0.65	0.69	3.87	0.02	16.54	54.31	13.25	13.78	1.44	99.79
76	0.65	0.69	3.86	0.02	16.52	54.22	13.27	13.77	1.47	99.67
77	0.65	0.69	3.88	0.02	16.38	53.77	13.11	13.82	1.85	99.34
78	0.65	0.69	3.88	0.02	16.25	53.31	13.00	13.74	2.04	98.74
79	0.64	0.69	3.79	0.02	16.46	53.98	13.45	13.64	1.65	99.62
80	0.65	0.69	3.91	0.02	16.45	53.94	13.05	13.88	1.76	99.52

Analysis# (C462)	Mg#	Cr#	Cr/ Fe^{2+}	Fe^{3+}#	Al_2O_3	Cr_2O_3	FeO	MgO	Fe_2O_3	Total
81	0.64	0.69	3.78	0.02	16.47	54.00	13.52	13.59	1.61	99.68
82	0.63	0.69	3.70	0.02	16.53	54.10	13.82	13.47	1.47	99.84
83	0.64	0.69	3.73	0.02	16.45	53.82	13.64	13.49	1.72	99.54
84	0.65	0.69	3.85	0.01	16.62	54.40	13.35	13.76	1.25	99.87
85	0.64	0.69	3.76	0.02	16.46	53.84	13.52	13.59	1.82	99.66
86	0.64	0.69	3.79	0.02	16.47	53.89	13.45	13.64	1.82	99.69
87	0.66	0.69	3.90	0.02	16.38	53.58	12.97	13.85	1.92	99.14
88	0.64	0.69	3.79	0.02	16.51	54.00	13.47	13.58	1.50	99.55
89	0.65	0.69	3.83	0.02	16.61	54.33	13.42	13.71	1.29	99.86
90	0.65	0.69	3.81	0.02	16.53	54.07	13.42	13.68	1.53	99.73
91	0.65	0.69	3.88	0.02	16.46	53.82	13.12	13.82	1.84	99.48
92	0.65	0.69	3.82	0.02	16.61	54.28	13.42	13.74	1.42	99.92
93	0.65	0.69	3.84	0.02	16.58	54.18	13.32	13.75	1.39	99.72
94	0.66	0.69	3.94	0.02	16.42	53.60	12.86	13.92	2.01	99.18
95	0.65	0.69	3.86	0.02	16.49	53.82	13.19	13.73	1.57	99.26
96	0.64	0.69	3.76	0.02	16.59	54.12	13.61	13.56	1.39	99.68
97	0.64	0.69	3.72	0.02	16.48	53.76	13.65	13.49	1.66	99.53
98	0.64	0.69	3.77	0.02	16.53	53.92	13.53	13.56	1.49	99.47
99	0.65	0.69	3.81	0.02	16.55	53.96	13.37	13.69	1.57	99.60
100	0.64	0.69	3.76	0.01	16.74	54.54	13.71	13.54	0.78	99.83
101	0.64	0.69	3.80	0.02	16.61	54.04	13.45	13.63	1.39	99.56
102	0.65	0.69	3.85	0.02	16.62	54.07	13.28	13.74	1.48	99.67
103	0.64	0.69	3.77	0.02	16.60	53.96	13.52	13.61	1.48	99.60
104	0.64	0.69	3.76	0.02	16.59	53.95	13.55	13.61	1.65	99.78
105	0.64	0.69	3.78	0.02	16.57	53.88	13.47	13.63	1.63	99.60
106	0.65	0.69	3.86	0.02	16.61	53.98	13.23	13.77	1.39	99.45
107	0.65	0.69	3.81	0.02	16.57	53.83	13.34	13.69	1.53	99.47
108	0.65	0.69	3.84	0.02	16.57	53.81	13.26	13.80	1.79	99.66
109	0.65	0.69	3.83	0.02	16.62	53.98	13.31	13.72	1.41	99.49
110	0.65	0.69	3.80	0.02	16.64	54.00	13.42	13.73	1.57	99.80
111	0.64	0.69	3.81	0.01	16.69	54.13	13.43	13.66	1.25	99.69
112	0.66	0.69	3.95	0.02	16.52	53.58	12.82	13.88	1.64	98.94
113	0.65	0.69	3.90	0.02	16.63	53.93	13.07	13.86	1.48	99.40
114	0.64	0.68	3.81	0.01	16.74	54.27	13.45	13.67	1.16	99.79
115	0.66	0.68	3.90	0.02	16.56	53.67	13.02	13.89	1.90	99.50
116	0.65	0.68	3.86	0.02	16.51	53.49	13.10	13.69	1.61	98.86
117	0.65	0.68	3.80	0.02	16.60	53.80	13.37	13.69	1.79	99.69
118	0.64	0.68	3.76	0.02	16.61	53.82	13.53	13.56	1.50	99.50
119	0.65	0.68	3.85	0.02	16.63	53.88	13.22	13.80	1.56	99.61
120	0.65	0.68	3.87	0.02	16.56	53.62	13.11	13.70	1.49	98.92

Analysis# (C462)	Mg#	Cr#	Cr/ Fe^{2+}	Fe^{3+}#	Al_2O_3	Cr_2O_3	FeO	MgO	Fe_2O_3	Total
121	0.66	0.68	3.90	0.02	16.59	53.71	13.01	13.87	1.77	99.34
122	0.65	0.68	3.87	0.02	16.70	54.05	13.20	13.84	1.47	99.73
123	0.64	0.68	3.77	0.02	16.58	53.65	13.45	13.63	1.70	99.48
124	0.64	0.68	3.79	0.02	16.68	53.97	13.47	13.66	1.52	99.76
125	0.66	0.68	3.90	0.02	16.56	53.54	12.98	13.84	1.72	99.08
126	0.65	0.68	3.85	0.02	16.66	53.87	13.21	13.74	1.34	99.33
127	0.64	0.68	3.74	0.02	16.77	54.19	13.68	13.63	1.36	100.07
128	0.65	0.68	3.87	0.02	16.75	54.12	13.23	13.81	1.28	99.61
129	0.65	0.68	3.90	0.02	16.80	54.28	13.14	13.98	1.41	100.11
130	0.65	0.68	3.81	0.02	16.64	53.75	13.35	13.67	1.47	99.36
131	0.64	0.68	3.72	0.02	16.71	53.98	13.70	13.51	1.41	99.75
132	0.65	0.68	3.85	0.01	16.78	54.21	13.32	13.84	1.25	99.92
133	0.65	0.68	3.79	0.02	16.66	53.82	13.43	13.71	1.59	99.67
134	0.64	0.68	3.79	0.02	16.70	53.94	13.46	13.73	1.70	99.96
135	0.64	0.68	3.78	0.01	16.78	54.16	13.54	13.63	1.14	99.73
136	0.65	0.68	3.83	0.02	16.59	53.54	13.22	13.73	1.79	99.33
137	0.64	0.68	3.78	0.01	16.73	54.00	13.49	13.62	1.20	99.54
138	0.65	0.68	3.84	0.01	16.83	54.29	13.37	13.80	1.21	99.96
139	0.65	0.68	3.87	0.02	16.59	53.51	13.09	13.82	1.87	99.27
140	0.65	0.68	3.83	0.01	16.78	54.12	13.36	13.74	1.14	99.68
141	0.65	0.68	3.86	0.02	16.71	53.91	13.19	13.82	1.43	99.54
142	0.65	0.68	3.83	0.02	16.57	53.42	13.17	13.75	2.00	99.31
143	0.65	0.68	3.81	0.01	16.80	54.16	13.43	13.73	1.24	99.93
144	0.66	0.68	3.93	0.03	16.39	52.82	12.70	13.89	2.19	98.37
145	0.64	0.68	3.80	0.02	16.75	53.99	13.43	13.66	1.27	99.57
146	0.65	0.68	3.84	0.02	16.52	53.27	13.11	13.71	2.06	99.05
147	0.64	0.68	3.80	0.01	16.75	53.96	13.43	13.63	1.23	99.48
148	0.64	0.68	3.78	0.02	16.72	53.86	13.47	13.71	1.65	99.84
149	0.65	0.68	3.85	0.02	16.73	53.88	13.22	13.85	1.50	99.62
150	0.65	0.68	3.88	0.02	16.76	53.97	13.14	13.91	1.62	99.83
151	0.65	0.68	3.82	0.02	16.69	53.76	13.29	13.70	1.33	99.27
152	0.65	0.68	3.84	0.02	16.77	54.01	13.30	13.79	1.35	99.70
153	0.65	0.68	3.81	0.02	16.76	53.97	13.40	13.71	1.43	99.73
154	0.65	0.68	3.81	0.02	16.76	53.96	13.38	13.72	1.44	99.76
155	0.64	0.68	3.77	0.01	16.83	54.20	13.59	13.67	1.15	99.96
156	0.65	0.68	3.85	0.02	16.79	54.06	13.27	13.86	1.57	100.01
157	0.64	0.68	3.77	0.02	16.75	53.91	13.52	13.66	1.46	99.75
158	0.65	0.68	3.84	0.02	16.75	53.91	13.28	13.72	1.38	99.54
159	0.65	0.68	3.90	0.02	16.69	53.68	13.01	13.86	1.54	99.23
160	0.65	0.68	3.82	0.02	16.77	53.92	13.33	13.77	1.51	99.77

Analysis# (C462)	Mg#	Cr#	Cr/ Fe^{2+}	Fe^{3+}#	Al_2O_3	Cr_2O_3	FeO	MgO	Fe_2O_3	Total
161	0.65	0.68	3.85	0.02	16.77	53.90	13.25	13.78	1.30	99.50
162	0.65	0.68	3.86	0.02	16.75	53.78	13.18	13.84	1.60	99.73
163	0.65	0.68	3.85	0.02	16.80	53.94	13.26	13.78	1.31	99.52
164	0.64	0.68	3.77	0.01	16.85	54.08	13.55	13.65	1.17	99.84
165	0.64	0.68	3.78	0.01	16.81	53.94	13.51	13.61	1.26	99.53
166	0.65	0.68	3.83	0.03	16.49	52.90	13.05	13.80	2.39	99.05
167	0.65	0.68	3.83	0.02	16.75	53.74	13.28	13.77	1.46	99.47
168	0.65	0.68	3.82	0.02	16.88	54.16	13.39	13.76	1.36	100.06
169	0.65	0.68	3.84	0.02	16.79	53.85	13.25	13.78	1.31	99.42
170	0.65	0.68	3.78	0.02	16.77	53.79	13.44	13.71	1.67	99.76
171	0.65	0.68	3.81	0.02	16.85	54.04	13.40	13.78	1.37	99.95
172	0.64	0.68	3.78	0.02	16.77	53.76	13.44	13.65	1.48	99.57
173	0.65	0.68	3.87	0.02	16.83	53.95	13.18	13.87	1.34	99.65
174	0.65	0.68	3.84	0.02	16.81	53.86	13.27	13.81	1.58	99.76
175	0.64	0.68	3.75	0.02	16.77	53.74	13.54	13.68	1.62	99.78
176	0.65	0.68	3.81	0.02	16.74	53.62	13.31	13.73	1.74	99.56
177	0.64	0.68	3.73	0.02	16.63	53.24	13.47	13.56	1.88	99.24
178	0.65	0.68	3.86	0.02	16.81	53.80	13.18	13.86	1.53	99.61
179	0.65	0.68	3.81	0.02	16.79	53.73	13.33	13.78	1.76	99.87
180	0.65	0.68	3.87	0.02	16.88	54.00	13.19	13.95	1.44	99.97
181	0.65	0.68	3.85	0.02	16.86	53.93	13.26	13.79	1.35	99.67
182	0.65	0.68	3.78	0.02	16.77	53.62	13.40	13.67	1.59	99.47
183	0.64	0.68	3.74	0.02	16.66	53.26	13.45	13.58	1.85	99.25
184	0.65	0.68	3.84	0.02	16.76	53.60	13.19	13.72	1.44	99.19
185	0.65	0.68	3.84	0.02	16.82	53.79	13.25	13.80	1.42	99.60
186	0.65	0.68	3.87	0.02	16.81	53.73	13.11	13.93	1.78	99.80
187	0.65	0.68	3.87	0.02	16.87	53.89	13.17	13.85	1.37	99.64
188	0.65	0.68	3.84	0.02	16.82	53.72	13.23	13.76	1.35	99.34
189	0.64	0.68	3.68	0.02	16.88	53.89	13.84	13.53	1.52	100.16
190	0.65	0.68	3.88	0.02	16.72	53.39	13.00	13.84	1.60	99.05
191	0.65	0.68	3.80	0.02	16.90	53.94	13.43	13.73	1.39	99.88
192	0.65	0.68	3.83	0.02	16.83	53.71	13.25	13.78	1.45	99.48
193	0.65	0.68	3.80	0.02	16.84	53.74	13.38	13.75	1.52	99.71
194	0.65	0.68	3.81	0.02	16.84	53.74	13.33	13.70	1.30	99.31
195	0.65	0.68	3.80	0.01	16.95	54.08	13.45	13.74	1.23	99.91
196	0.65	0.68	3.84	0.02	16.72	53.36	13.15	13.76	1.73	99.18
197	0.65	0.68	3.86	0.02	16.81	53.62	13.13	13.81	1.32	99.87
198	0.64	0.68	3.78	0.01	16.93	54.00	13.49	13.70	1.22	99.79
199	0.66	0.68	3.93	0.02	16.77	53.44	12.87	13.93	1.71	99.13
200	0.64	0.68	3.75	0.01	16.93	53.96	13.61	13.61	1.14	99.70

Analysis# (C462)	Mg#	Cr#	Cr/ Fe^{2+}	Fe^{3+}#	Al_2O_3	Cr_2O_3	FeO	MgO	Fe_2O_3	Total
201	0.65	0.68	3.78	0.02	16.77	53.44	13.35	13.70	1.67	99.35
202	0.64	0.68	3.78	0.02	16.92	53.90	13.47	13.72	1.36	99.87
203	0.64	0.68	3.80	0.01	17.00	54.17	13.49	13.75	1.22	100.15
204	0.64	0.68	3.78	0.01	16.94	53.96	13.48	13.70	1.16	99.69
205	0.65	0.68	3.82	0.02	16.88	53.75	13.30	13.77	1.28	99.47
206	0.65	0.68	3.83	0.02	16.81	53.52	13.22	13.74	1.55	99.36
207	0.65	0.68	3.80	0.02	16.85	53.59	13.34	13.69	1.49	99.40
208	0.64	0.68	3.78	0.02	16.93	53.86	13.46	13.72	1.35	99.80
209	0.64	0.68	3.70	0.02	16.87	53.64	13.72	13.47	1.33	99.49
210	0.65	0.68	3.82	0.01	16.90	53.71	13.30	13.71	1.26	99.38
211	0.64	0.68	3.75	0.01	16.96	53.87	13.58	13.62	1.20	99.72
212	0.64	0.68	3.77	0.02	16.90	53.63	13.46	13.67	1.44	99.63
213	0.65	0.68	3.87	0.01	17.03	54.03	13.21	13.87	1.24	99.85
214	0.64	0.68	3.76	0.01	17.06	54.14	13.63	13.70	1.10	100.11
215	0.64	0.68	3.77	0.02	16.94	53.76	13.46	13.70	1.43	99.72
216	0.65	0.68	3.84	0.02	16.94	53.69	13.23	13.88	1.55	99.75
217	0.65	0.68	3.85	0.02	16.93	53.64	13.18	13.93	1.68	99.79
218	0.65	0.68	3.85	0.02	16.99	53.81	13.21	13.90	1.47	99.85
219	0.64	0.68	3.73	0.02	17.00	53.82	13.62	13.65	1.31	99.85
220	0.64	0.68	3.75	0.02	16.94	53.60	13.50	13.66	1.37	99.61
221	0.65	0.68	3.83	0.02	16.85	53.33	13.17	13.83	1.88	99.45
222	0.65	0.68	3.82	0.01	17.01	53.76	13.31	13.75	1.10	99.42
223	0.64	0.68	3.70	0.02	16.98	53.67	13.72	13.54	1.46	99.85
224	0.65	0.68	3.81	0.02	16.99	53.67	13.33	13.76	1.27	99.46
225	0.65	0.68	3.84	0.02	16.89	53.30	13.14	13.87	1.81	99.42
226	0.66	0.68	3.92	0.02	16.88	53.23	12.85	14.01	1.89	99.33
227	0.64	0.68	3.76	0.01	17.16	54.01	13.56	13.74	1.14	100.09
228	0.64	0.68	3.68	0.02	16.90	53.07	13.64	13.53	1.84	99.37
229	0.64	0.68	3.72	0.02	17.10	53.72	13.65	13.67	1.42	100.01
230	0.65	0.68	3.83	0.02	17.00	53.38	13.17	13.83	1.42	99.33
231	0.64	0.68	3.72	0.02	17.00	53.27	13.55	13.62	1.66	99.55
232	0.64	0.68	3.74	0.01	17.18	53.79	13.60	13.67	1.19	99.91
233	0.65	0.68	3.76	0.02	17.03	53.31	13.39	13.76	1.79	99.74
234	0.65	0.68	3.82	0.02	17.07	53.43	13.21	13.88	1.68	99.67
235	0.66	0.68	3.87	0.02	17.12	53.53	13.08	13.99	1.70	99.85
236	0.64	0.68	3.67	0.02	17.15	53.33	13.74	13.59	1.72	99.98
237	0.64	0.67	3.69	0.01	17.35	53.56	13.70	13.58	1.08	99.74
238	0.65	0.67	3.75	0.02	17.25	53.26	13.44	13.73	1.56	99.72
239	0.64	0.67	3.71	0.02	17.26	52.83	13.47	13.70	1.85	99.55

C462 – trace elements

Analysis# (C462)	Mg#	Cr#	Cr/ Fe^{2+}	Fe^{3+}#	SiO_2	TiO_2	V_2O_5	MnO	NiO
1	0.60	0.81	4.01	0.01	0.05	0.03	0.06	0.36	0.05
2	0.63	0.75	3.99	0.02	0.06	0.07	0.06	0.29	0.10
3	0.62	0.73	3.78	0.02	0.04	0.07	0.12	0.33	0.10
4	0.64	0.73	3.95	0.02	0.03	0.07	0.12	0.27	0.12
5	0.65	0.72	4.06	0.02	0.05	0.07	0.11	0.30	0.13
6	0.62	0.72	3.77	0.02	0.05	0.09	0.11	0.26	0.11
7	0.63	0.72	3.82	0.02	0.06	0.07	0.10	0.28	0.12
8	0.63	0.70	3.79	0.01	0.04	0.06	0.08	0.27	0.12
9	0.64	0.70	3.85	0.02	0.05	0.08	0.11	0.29	0.14
10	0.64	0.70	3.83	0.02	0.02	0.08	0.09	0.27	0.12
11	0.64	0.70	3.84	0.02	0.03	0.07	0.08	0.28	0.10
12	0.64	0.69	3.77	0.02	0.04	0.08	0.09	0.28	0.13
13	0.65	0.69	3.89	0.02	0.04	0.07	0.10	0.27	0.12
14	0.64	0.69	3.82	0.01	0.04	0.09	0.08	0.24	0.13
15	0.65	0.69	3.89	0.03	0.04	0.09	0.11	0.29	0.13
16	0.64	0.69	3.80	0.01	0.02	0.08	0.10	0.27	0.12
17	0.65	0.69	3.88	0.02	0.03	0.07	0.11	0.27	0.15
18	0.65	0.69	3.89	0.02	0.03	0.11	0.08	0.27	0.15
19	0.65	0.69	3.92	0.03	0.03	0.08	0.07	0.27	0.12
20	0.64	0.69	3.79	0.02	0.05	0.08	0.09	0.29	0.12
21	0.66	0.69	4.03	0.03	0.04	0.06	0.11	0.28	0.14
22	0.63	0.69	3.71	0.02	0.03	0.09	0.08	0.29	0.13
23	0.64	0.69	3.78	0.02	0.04	0.10	0.10	0.29	0.12
24	0.65	0.69	3.89	0.02	0.05	0.07	0.11	0.27	0.12
25	0.64	0.69	3.77	0.02	0.03	0.08	0.11	0.27	0.08
26	0.65	0.69	3.87	0.03	0.03	0.07	0.08	0.27	0.13
27	0.64	0.69	3.79	0.01	0.03	0.08	0.09	0.28	0.12
28	0.65	0.69	3.90	0.02	0.04	0.08	0.14	0.27	0.11
29	0.65	0.69	3.94	0.02	0.05	0.07	0.08	0.27	0.13
30	0.64	0.69	3.77	0.02	0.04	0.10	0.11	0.26	0.11
31	0.65	0.69	3.90	0.02	0.04	0.09	0.15	0.26	0.11
32	0.64	0.69	3.81	0.02	0.06	0.11	0.09	0.27	0.14
33	0.64	0.69	3.81	0.02	0.10	0.09	0.09	0.36	0.12
34	0.65	0.69	3.84	0.02	0.04	0.08	0.09	0.26	0.14
35	0.63	0.69	3.73	0.02	0.04	0.10	0.10	0.26	0.13
36	0.65	0.69	3.86	0.02	0.03	0.08	0.10	0.28	0.12
37	0.65	0.69	3.92	0.01	0.04	0.10	0.09	0.28	0.12
38	0.66	0.69	3.92	0.03	0.05	0.09	0.09	0.26	0.15
39	0.64	0.69	3.83	0.02	0.06	0.08	0.09	0.25	0.11
40	0.64	0.69	3.78	0.02	0.05	0.08	0.10	0.27	0.14

Analysis# (C462)	Mg#	Cr#	Cr/ Fe^{2+}	Fe^{3+}#	SiO_2	TiO_2	V_2O_5	MnO	NiO
41	0.66	0.69	3.95	0.02	0.03	0.06	0.10	0.26	0.16
42	0.64	0.69	3.83	0.01	0.11	0.10	0.12	0.24	0.14
43	0.65	0.69	3.87	0.02	0.03	0.08	0.10	0.26	0.11
44	0.65	0.69	3.87	0.03	0.05	0.10	0.10	0.28	0.14
45	0.64	0.69	3.76	0.02	0.03	0.08	0.11	0.28	0.14
46	0.65	0.69	3.87	0.02	0.08	0.10	0.09	0.29	0.11
47	0.65	0.69	3.82	0.02	0.05	0.09	0.10	0.27	0.11
48	0.64	0.69	3.80	0.01	0.04	0.09	0.09	0.27	0.10
49	0.63	0.69	3.71	0.02	0.04	0.10	0.10	0.27	0.12
50	0.66	0.69	3.97	0.02	0.05	0.09	0.09	0.26	0.11
51	0.64	0.69	3.78	0.02	0.04	0.08	0.11	0.28	0.13
52	0.63	0.69	3.70	0.02	0.04	0.10	0.07	0.27	0.12
53	0.64	0.69	3.80	0.02	0.04	0.07	0.09	0.27	0.13
54	0.65	0.69	3.84	0.02	0.03	0.07	0.10	0.28	0.13
55	0.64	0.69	3.79	0.02	0.04	0.08	0.10	0.27	0.12
56	0.65	0.69	3.89	0.02	0.06	0.10	0.09	0.28	0.11
57	0.65	0.69	3.85	0.02	0.07	0.08	0.09	0.25	0.13
58	0.67	0.69	4.07	0.03	0.04	0.10	0.09	0.26	0.12
59	0.65	0.69	3.84	0.02	0.05	0.09	0.08	0.28	0.09
60	0.65	0.69	3.91	0.02	0.07	0.08	0.10	0.26	0.12
61	0.64	0.69	3.81	0.02	0.07	0.07	0.09	0.28	0.14
62	0.66	0.69	3.91	0.02	0.05	0.09	0.10	0.27	0.13
63	0.64	0.69	3.79	0.01	0.02	0.09	0.08	0.26	0.12
64	0.64	0.69	3.79	0.02	0.04	0.09	0.11	0.26	0.13
65	0.65	0.69	3.87	0.02	0.13	0.07	0.12	0.26	0.13
66	0.65	0.69	3.90	0.02	0.05	0.09	0.10	0.25	0.12
67	0.66	0.69	3.94	0.03	0.21	0.06	0.08	0.28	0.11
68	0.64	0.69	3.74	0.02	0.02	0.09	0.11	0.27	0.13
69	0.64	0.69	3.80	0.02	0.09	0.10	0.09	0.27	0.12
70	0.65	0.69	3.89	0.02	0.03	0.10	0.12	0.27	0.12
71	0.65	0.69	3.88	0.01	0.02	0.07	0.09	0.27	0.12
72	0.65	0.69	3.89	0.01	0.05	0.08	0.09	0.27	0.14
73	0.65	0.69	3.89	0.02	0.28	0.09	0.09	0.26	0.13
74	0.65	0.69	3.87	0.01	0.03	0.08	0.10	0.26	0.13
75	0.65	0.69	3.87	0.02	0.05	0.07	0.08	0.29	0.12
76	0.65	0.69	3.86	0.02	0.04	0.07	0.09	0.27	0.12
77	0.65	0.69	3.88	0.02	0.03	0.10	0.11	0.27	0.11
78	0.65	0.69	3.88	0.02	0.03	0.10	0.09	0.26	0.12
79	0.64	0.69	3.79	0.02	0.04	0.09	0.09	0.25	0.13
80	0.65	0.69	3.91	0.02	0.04	0.08	0.11	0.28	0.11

Analysis# (C462)	Mg#	Cr#	Cr/ Fe^{2+}	Fe^{3+}#	SiO_2	TiO_2	V_2O_5	MnO	NiO
81	0.64	0.69	3.78	0.02	0.02	0.10	0.09	0.30	0.13
82	0.63	0.69	3.70	0.02	0.03	0.08	0.12	0.25	0.11
83	0.64	0.69	3.73	0.02	0.04	0.06	0.11	0.27	0.12
84	0.65	0.69	3.85	0.01	0.04	0.09	0.08	0.28	0.13
85	0.64	0.69	3.76	0.02	0.04	0.08	0.09	0.28	0.12
86	0.64	0.69	3.79	0.02	0.05	0.06	0.10	0.28	0.12
87	0.66	0.69	3.90	0.02	0.02	0.10	0.11	0.26	0.15
88	0.64	0.69	3.79	0.02	0.05	0.08	0.08	0.28	0.14
89	0.65	0.69	3.83	0.02	0.04	0.08	0.11	0.25	0.15
90	0.65	0.69	3.81	0.02	0.06	0.10	0.09	0.26	0.14
91	0.65	0.69	3.88	0.02	0.04	0.09	0.08	0.28	0.11
92	0.65	0.69	3.82	0.02	0.07	0.08	0.09	0.26	0.10
93	0.65	0.69	3.84	0.02	0.03	0.09	0.10	0.27	0.14
94	0.66	0.69	3.94	0.02	0.05	0.06	0.09	0.28	0.09
95	0.65	0.69	3.86	0.02	0.04	0.08	0.11	0.27	0.13
96	0.64	0.69	3.76	0.02	0.01	0.08	0.09	0.27	0.11
97	0.64	0.69	3.72	0.02	0.04	0.10	0.11	0.28	0.12
98	0.64	0.69	3.77	0.02	0.03	0.09	0.08	0.27	0.13
99	0.65	0.69	3.81	0.02	0.03	0.09	0.10	0.26	0.15
100	0.64	0.69	3.76	0.01	0.03	0.09	0.10	0.27	0.11
101	0.64	0.69	3.80	0.02	0.04	0.08	0.07	0.27	0.13
102	0.65	0.69	3.85	0.02	0.04	0.08	0.08	0.28	0.15
103	0.64	0.69	3.77	0.02	0.02	0.09	0.09	0.25	0.14
104	0.64	0.69	3.76	0.02	0.02	0.08	0.10	0.30	0.11
105	0.64	0.69	3.78	0.02	0.02	0.08	0.10	0.26	0.14
106	0.65	0.69	3.86	0.02	0.03	0.10	0.10	0.28	0.11
107	0.65	0.69	3.81	0.02	0.04	0.11	0.10	0.29	0.12
108	0.65	0.69	3.84	0.02	0.05	0.09	0.10	0.26	0.11
109	0.65	0.69	3.83	0.02	0.04	0.08	0.10	0.26	0.12
110	0.65	0.69	3.80	0.02	0.02	0.09	0.10	0.25	0.13
111	0.64	0.69	3.81	0.01	0.05	0.09	0.09	0.26	0.16
112	0.66	0.69	3.95	0.02	0.10	0.09	0.07	0.27	0.13
113	0.65	0.69	3.90	0.02	0.03	0.09	0.08	0.26	0.11
114	0.64	0.68	3.81	0.01	0.03	0.07	0.10	0.27	0.16
115	0.66	0.68	3.90	0.02	0.06	0.09	0.08	0.27	0.14
116	0.65	0.68	3.86	0.02	0.03	0.09	0.08	0.28	0.14
117	0.65	0.68	3.80	0.02	0.04	0.06	0.10	0.29	0.13
118	0.64	0.68	3.76	0.02	0.04	0.08	0.10	0.28	0.13
119	0.65	0.68	3.85	0.02	0.05	0.12	0.09	0.29	0.13
120	0.65	0.68	3.87	0.02	0.04	0.06	0.09	0.27	0.13

Analysis# (C462)	Mg#	Cr#	Cr/ Fe^{2+}	Fe^{3+}#	SiO_2	TiO_2	V_2O_5	MnO	NiO
121	0.66	0.68	3.90	0.02	0.04	0.07	0.08	0.27	0.12
122	0.65	0.68	3.87	0.02	0.02	0.09	0.10	0.26	0.14
123	0.64	0.68	3.77	0.02	0.05	0.10	0.10	0.28	0.10
124	0.64	0.68	3.79	0.02	0.03	0.08	0.09	0.27	0.13
125	0.66	0.68	3.90	0.02	0.04	0.08	0.10	0.27	0.12
126	0.65	0.68	3.85	0.02	0.02	0.10	0.10	0.28	0.14
127	0.64	0.68	3.74	0.02	0.04	0.10	0.08	0.26	0.11
128	0.65	0.68	3.87	0.02	0.02	0.07	0.09	0.27	0.10
129	0.65	0.68	3.90	0.02	0.07	0.09	0.10	0.27	0.12
130	0.65	0.68	3.81	0.02	0.04	0.09	0.11	0.28	0.11
131	0.64	0.68	3.72	0.02	0.03	0.08	0.08	0.27	0.14
132	0.65	0.68	3.85	0.01	0.03	0.11	0.11	0.26	0.12
133	0.65	0.68	3.79	0.02	0.05	0.10	0.10	0.26	0.11
134	0.64	0.68	3.79	0.02	0.03	0.08	0.11	0.27	0.13
135	0.64	0.68	3.78	0.01	0.03	0.09	0.09	0.28	0.12
136	0.65	0.68	3.83	0.02	0.03	0.08	0.11	0.28	0.14
137	0.64	0.68	3.78	0.01	0.04	0.09	0.10	0.28	0.12
138	0.65	0.68	3.84	0.01	0.04	0.08	0.09	0.25	0.12
139	0.65	0.68	3.87	0.02	0.04	0.08	0.09	0.25	0.12
140	0.65	0.68	3.83	0.01	0.05	0.11	0.09	0.28	0.13
141	0.65	0.68	3.86	0.02	0.05	0.10	0.09	0.26	0.12
142	0.65	0.68	3.83	0.02	0.05	0.06	0.10	0.27	0.13
143	0.65	0.68	3.81	0.01	0.10	0.09	0.11	0.28	0.13
144	0.66	0.68	3.93	0.03	0.03	0.10	0.10	0.24	0.12
145	0.64	0.68	3.80	0.02	0.03	0.07	0.11	0.27	0.12
146	0.65	0.68	3.84	0.02	0.04	0.06	0.08	0.31	0.10
147	0.64	0.68	3.80	0.01	0.05	0.06	0.10	0.25	0.14
148	0.64	0.68	3.78	0.02	0.03	0.08	0.11	0.26	0.11
149	0.65	0.68	3.85	0.02	0.04	0.09	0.12	0.25	0.10
150	0.65	0.68	3.88	0.02	0.04	0.08	0.09	0.27	0.12
151	0.65	0.68	3.82	0.02	0.03	0.10	0.12	0.28	0.11
152	0.65	0.68	3.84	0.02	0.06	0.09	0.11	0.27	0.11
153	0.65	0.68	3.81	0.02	0.03	0.08	0.08	0.27	0.14
154	0.65	0.68	3.81	0.02	0.05	0.08	0.11	0.27	0.15
155	0.64	0.68	3.77	0.01	0.04	0.10	0.11	0.26	0.12
156	0.65	0.68	3.85	0.02	0.03	0.07	0.11	0.27	0.13
157	0.64	0.68	3.77	0.02	0.05	0.10	0.08	0.24	0.13
158	0.65	0.68	3.84	0.02	0.05	0.06	0.10	0.28	0.14
159	0.65	0.68	3.90	0.02	0.03	0.08	0.09	0.27	0.14
160	0.65	0.68	3.82	0.02	0.03	0.08	0.10	0.27	0.14

Analysis# (C462)	Mg#	Cr#	Cr/ Fe^{2+}	Fe^{3+}#	SiO_2	TiO_2	V_2O_5	MnO	NiO
161	0.65	0.68	3.85	0.02	0.04	0.09	0.11	0.27	0.13
162	0.65	0.68	3.86	0.02	0.12	0.10	0.10	0.28	0.14
163	0.65	0.68	3.85	0.02	0.03	0.09	0.07	0.27	0.11
164	0.64	0.68	3.77	0.01	0.04	0.10	0.10	0.27	0.14
165	0.64	0.68	3.78	0.01	0.03	0.07	0.06	0.26	0.11
166	0.65	0.68	3.83	0.03	0.05	0.09	0.13	0.26	0.13
167	0.65	0.68	3.83	0.02	0.03	0.10	0.11	0.26	0.11
168	0.65	0.68	3.82	0.02	0.05	0.07	0.08	0.29	0.15
169	0.65	0.68	3.84	0.02	0.04	0.09	0.09	0.26	0.10
170	0.65	0.68	3.78	0.02	0.04	0.08	0.07	0.24	0.11
171	0.65	0.68	3.81	0.02	0.04	0.11	0.10	0.27	0.12
172	0.64	0.68	3.78	0.02	0.03	0.09	0.09	0.29	0.12
173	0.65	0.68	3.87	0.02	0.03	0.10	0.11	0.25	0.14
174	0.65	0.68	3.84	0.02	0.04	0.09	0.07	0.27	0.13
175	0.64	0.68	3.75	0.02	0.03	0.08	0.12	0.28	0.08
176	0.65	0.68	3.81	0.02	0.02	0.07	0.10	0.29	0.12
177	0.64	0.68	3.73	0.02	0.04	0.10	0.10	0.27	0.13
178	0.65	0.68	3.86	0.02	0.02	0.10	0.09	0.27	0.12
179	0.65	0.68	3.81	0.02	0.05	0.10	0.09	0.28	0.15
180	0.65	0.68	3.87	0.02	0.06	0.13	0.10	0.25	0.14
181	0.65	0.68	3.85	0.02	0.03	0.07	0.10	0.28	0.14
182	0.65	0.68	3.78	0.02	0.03	0.08	0.10	0.27	0.11
183	0.64	0.68	3.74	0.02	0.04	0.10	0.09	0.28	0.12
184	0.65	0.68	3.84	0.02	0.02	0.10	0.07	0.28	0.14
185	0.65	0.68	3.84	0.02	0.06	0.12	0.08	0.26	0.13
186	0.65	0.68	3.87	0.02	0.03	0.08	0.12	0.27	0.13
187	0.65	0.68	3.87	0.02	0.03	0.09	0.09	0.27	0.14
188	0.65	0.68	3.84	0.02	0.04	0.08	0.10	0.27	0.12
189	0.64	0.68	3.68	0.02	0.04	0.08	0.12	0.26	0.14
190	0.65	0.68	3.88	0.02	0.05	0.10	0.11	0.28	0.12
191	0.65	0.68	3.80	0.02	0.04	0.08	0.09	0.28	0.14
192	0.65	0.68	3.83	0.02	0.05	0.08	0.10	0.26	0.12
193	0.65	0.68	3.80	0.02	0.06	0.09	0.12	0.26	0.12
194	0.65	0.68	3.81	0.02	0.00	0.07	0.09	0.25	0.13
195	0.65	0.68	3.80	0.01	0.05	0.07	0.09	0.27	0.12
196	0.65	0.68	3.84	0.02	0.04	0.08	0.11	0.28	0.13
197	0.65	0.68	3.86	0.02	0.74	0.09	0.11	0.26	0.11
198	0.64	0.68	3.78	0.01	0.04	0.08	0.09	0.26	0.11
199	0.66	0.68	3.93	0.02	0.05	0.06	0.09	0.27	0.12
200	0.64	0.68	3.75	0.01	0.04	0.08	0.09	0.27	0.10

Analysis# (C462)	Mg#	Cr#	Cr/ Fe^{2+}	Fe^{3+}#	SiO_2	TiO_2	V_2O_5	MnO	NiO
201	0.65	0.68	3.78	0.02	0.02	0.09	0.10	0.26	0.11
202	0.64	0.68	3.78	0.02	0.04	0.09	0.11	0.28	0.12
203	0.64	0.68	3.80	0.01	0.06	0.09	0.08	0.28	0.14
204	0.64	0.68	3.78	0.01	0.03	0.08	0.10	0.26	0.10
205	0.65	0.68	3.82	0.02	0.04	0.09	0.13	0.27	0.10
206	0.65	0.68	3.83	0.02	0.06	0.09	0.10	0.28	0.15
207	0.65	0.68	3.80	0.02	0.03	0.07	0.10	0.26	0.14
208	0.64	0.68	3.78	0.02	0.03	0.10	0.09	0.28	0.11
209	0.64	0.68	3.70	0.02	0.04	0.08	0.09	0.28	0.10
210	0.65	0.68	3.82	0.01	0.08	0.06	0.10	0.27	0.12
211	0.64	0.68	3.75	0.01	0.04	0.08	0.09	0.27	0.12
212	0.64	0.68	3.77	0.02	0.07	0.09	0.12	0.28	0.12
213	0.65	0.68	3.87	0.01	0.02	0.05	0.11	0.27	0.15
214	0.64	0.68	3.76	0.01	0.04	0.08	0.11	0.25	0.12
215	0.64	0.68	3.77	0.02	0.03	0.06	0.11	0.28	0.09
216	0.65	0.68	3.84	0.02	0.03	0.10	0.10	0.26	0.12
217	0.65	0.68	3.85	0.02	0.04	0.11	0.09	0.25	0.12
218	0.65	0.68	3.85	0.02	0.03	0.09	0.11	0.28	0.12
219	0.64	0.68	3.73	0.02	0.03	0.09	0.10	0.26	0.10
220	0.64	0.68	3.75	0.02	0.06	0.12	0.10	0.26	0.15
221	0.65	0.68	3.83	0.02	0.05	0.07	0.09	0.27	0.11
222	0.65	0.68	3.82	0.01	0.03	0.09	0.09	0.26	0.11
223	0.64	0.68	3.70	0.02	0.04	0.07	0.10	0.28	0.14
224	0.65	0.68	3.81	0.02	0.02	0.09	0.10	0.26	0.10
225	0.65	0.68	3.84	0.02	0.02	0.09	0.11	0.25	0.11
226	0.66	0.68	3.92	0.02	0.04	0.10	0.10	0.26	0.14
227	0.64	0.68	3.76	0.01	0.04	0.08	0.10	0.28	0.09
228	0.64	0.68	3.68	0.02	0.02	0.09	0.10	0.28	0.10
229	0.64	0.68	3.72	0.02	0.03	0.07	0.12	0.27	0.09
230	0.65	0.68	3.83	0.02	0.07	0.09	0.13	0.27	0.11
231	0.64	0.68	3.72	0.02	0.03	0.08	0.12	0.28	0.12
232	0.64	0.68	3.74	0.01	0.02	0.10	0.09	0.26	0.14
233	0.65	0.68	3.76	0.02	0.05	0.10	0.10	0.26	0.14
234	0.65	0.68	3.82	0.02	0.03	0.09	0.09	0.28	0.11
235	0.66	0.68	3.87	0.02	0.03	0.09	0.08	0.27	0.13
236	0.64	0.68	3.67	0.02	0.05	0.09	0.09	0.26	0.13
237	0.64	0.67	3.69	0.01	0.03	0.08	0.08	0.25	0.14
238	0.65	0.67	3.75	0.02	0.07	0.09	0.09	0.27	0.14
239	0.64	0.67	3.71	0.02	0.04	0.10	0.10	0.27	0.13

Sample C559

Analysis# (C559)	Mg#	Cr#	Cr/ Fe^{2+}	Fe^{3+}#	Al_2O_3	Cr_2O_3	FeO	MgO	Fe_2O_3	Total
1	0.59	0.60	2.90	0.01	21.36	47.39	15.46	12.59	1.26	98.84
2	0.63	0.60	3.12	0.03	21.34	47.53	14.39	13.64	2.46	99.80
3	0.63	0.60	3.16	0.03	21.37	47.45	14.18	13.78	2.61	99.79
4	0.63	0.60	3.18	0.03	21.40	47.45	14.12	13.76	2.55	99.65
5	0.63	0.60	3.14	0.03	21.31	47.54	14.30	13.70	2.62	99.83
6	0.63	0.60	3.17	0.03	21.27	47.48	14.15	13.78	2.76	99.85
7	0.64	0.60	3.17	0.03	21.18	47.24	14.07	13.75	2.77	99.39
8	0.64	0.60	3.19	0.03	21.44	47.21	13.98	13.95	2.89	99.78
9	0.62	0.59	3.03	0.04	21.50	46.66	14.58	13.48	3.07	99.60
10	0.63	0.60	3.12	0.04	21.31	46.86	14.20	13.72	3.20	99.62
11	0.62	0.59	2.99	0.04	21.76	45.95	14.52	13.53	3.41	99.46
12	0.62	0.60	3.03	0.04	20.92	46.86	14.63	13.34	3.29	99.30
13	0.63	0.60	3.08	0.04	20.86	46.93	14.42	13.52	3.54	99.59
14	0.62	0.61	3.09	0.04	20.41	47.20	14.45	13.44	3.63	99.42
15	0.63	0.60	3.11	0.04	20.93	46.96	14.28	13.58	3.19	99.26
16	0.64	0.60	3.17	0.04	21.36	47.06	14.04	13.90	3.22	99.86
17	0.65	0.60	3.23	0.04	21.23	46.79	13.68	14.02	3.45	99.48
18	0.64	0.60	3.19	0.04	20.84	46.89	13.88	13.78	3.42	99.12
19	0.64	0.60	3.22	0.04	21.18	46.78	13.71	13.97	3.35	99.25
20	0.65	0.59	3.24	0.04	21.19	46.39	13.54	13.98	3.53	98.87
21	0.64	0.60	3.15	0.04	21.22	46.78	14.02	13.72	3.06	99.07
22	0.64	0.59	3.16	0.04	21.29	46.16	13.79	13.79	3.40	98.78
23	0.64	0.59	3.16	0.04	21.31	46.24	13.82	13.82	3.55	99.03
24	0.64	0.59	3.13	0.04	21.08	46.08	13.90	13.64	3.45	98.56
25	0.63	0.60	3.11	0.04	21.01	46.18	14.04	13.62	3.63	98.76
26	0.63	0.60	3.07	0.04	20.98	46.37	14.30	13.49	3.57	99.05
27	0.62	0.60	3.02	0.04	21.14	46.39	14.50	13.50	3.78	99.53
28	0.62	0.60	3.02	0.04	20.74	46.58	14.59	13.30	3.65	99.16
29	0.61	0.60	2.91	0.05	20.49	46.07	14.97	12.91	3.95	98.62
30	0.62	0.60	2.98	0.04	20.82	45.95	14.58	13.19	3.73	98.55
31	0.61	0.59	2.92	0.04	21.45	46.52	15.07	13.12	3.09	99.62
32	0.59	0.59	2.77	0.04	21.41	46.27	15.80	12.66	2.98	99.40
33	0.60	0.59	2.87	0.04	21.21	46.40	15.31	12.93	3.31	99.47
34	0.66	0.58	3.25	0.04	22.13	45.30	13.18	14.31	3.47	98.67
35	0.66	0.58	3.27	0.04	22.23	45.07	13.04	14.40	3.76	98.76
36	0.65	0.57	3.18	0.04	22.38	45.06	13.40	14.17	3.50	98.82
37	0.67	0.58	3.31	0.05	21.73	45.26	12.91	14.39	4.06	98.70
38	0.64	0.60	3.21	0.04	20.99	46.71	13.76	13.80	3.22	98.75
39	0.65	0.60	3.27	0.04	21.25	46.72	13.52	14.05	3.26	99.12
40	0.66	0.58	3.25	0.03	22.70	46.03	13.40	14.44	2.88	99.78

Analysis# (C559)	Mg#	Cr#	Cr/ Fe^{2+}	Fe^{3+}#	Al_2O_3	Cr_2O_3	FeO	MgO	Fe_2O_3	Total
41	0.66	0.58	3.29	0.04	22.35	45.99	13.22	14.45	3.20	99.54
42	0.66	0.58	3.25	0.04	22.19	45.96	13.36	14.30	3.17	99.29
43	0.66	0.58	3.25	0.04	22.35	45.88	13.33	14.34	3.10	99.38
44	0.65	0.58	3.22	0.03	22.44	46.16	13.55	14.25	2.94	99.68
45	0.66	0.58	3.25	0.04	22.33	46.09	13.39	14.35	3.15	99.61
46	0.66	0.58	3.25	0.04	22.24	45.62	13.27	14.25	3.02	98.76
47	0.67	0.58	3.32	0.04	22.26	45.66	12.99	14.54	3.45	99.25
48	0.66	0.58	3.28	0.03	22.26	46.09	13.30	14.36	3.01	99.32
49	0.64	0.58	3.13	0.03	22.34	46.15	13.96	13.99	2.91	99.75
50	0.65	0.58	3.20	0.04	22.25	46.31	13.66	14.15	3.03	99.77
51	0.64	0.58	3.13	0.03	22.31	46.00	13.90	13.98	2.98	99.50
52	0.65	0.58	3.19	0.03	22.18	46.22	13.68	14.08	2.79	99.30
53	0.64	0.58	3.16	0.03	22.21	46.26	13.83	14.06	2.99	99.68
54	0.64	0.58	3.12	0.03	22.41	46.21	13.99	13.99	2.77	99.70
55	0.65	0.58	3.18	0.04	22.10	46.20	13.75	14.07	3.08	99.51
56	0.65	0.58	3.17	0.03	22.10	46.32	13.81	14.09	3.02	99.74
57	0.62	0.58	3.00	0.03	22.03	46.17	14.53	13.45	2.55	99.12
58	0.63	0.59	3.09	0.03	21.76	46.46	14.23	13.71	3.00	99.50
59	0.63	0.58	3.03	0.03	22.09	46.12	14.41	13.60	2.81	99.39
60	0.64	0.57	3.05	0.03	22.72	45.54	14.11	13.90	3.02	99.59
61	0.64	0.58	3.09	0.04	22.25	45.82	14.01	13.92	3.20	99.50
62	0.65	0.58	3.17	0.04	22.15	46.25	13.80	14.14	3.25	99.95
63	0.65	0.58	3.16	0.04	22.21	46.04	13.79	14.07	3.15	99.60
64	0.63	0.59	3.10	0.03	21.47	46.75	14.27	13.64	2.92	99.44
65	0.63	0.60	3.12	0.04	21.17	46.77	14.19	13.63	3.26	99.35
66	0.64	0.59	3.14	0.04	21.41	46.74	14.06	13.81	3.32	99.71
67	0.63	0.59	3.08	0.04	21.44	46.68	14.32	13.63	3.05	99.47
68	0.63	0.59	3.06	0.04	21.45	46.44	14.34	13.62	3.38	99.55
69	0.63	0.59	3.07	0.04	21.35	46.66	14.35	13.63	3.33	99.59
70	0.62	0.60	3.06	0.03	21.27	46.69	14.43	13.49	2.95	99.22
71	0.63	0.59	3.04	0.03	21.95	47.00	14.61	13.67	2.71	100.26
72	0.63	0.59	3.08	0.03	21.72	46.85	14.39	13.66	2.93	99.90
73	0.63	0.59	3.08	0.03	21.59	46.99	14.42	13.66	2.87	99.87
74	0.62	0.59	3.03	0.03	21.71	47.10	14.71	13.50	2.59	99.98
75	0.63	0.60	3.10	0.03	21.49	47.35	14.43	13.65	2.68	100.01
76	0.63	0.59	3.12	0.03	21.66	47.04	14.24	13.82	2.93	100.05
77	0.64	0.59	3.14	0.03	21.79	46.98	14.15	13.84	2.71	99.88
78	0.63	0.59	3.11	0.03	21.77	46.94	14.28	13.72	2.61	99.65
79	0.63	0.59	3.05	0.03	21.76	47.00	14.55	13.64	2.86	100.15
80	0.61	0.59	2.90	0.04	21.46	46.19	15.05	13.21	3.38	99.62

Analysis# (C559)	Mg#	Cr#	Cr/ Fe^{2+}	Fe^{3+}#	Al_2O_3	Cr_2O_3	FeO	MgO	Fe_2O_3	Total
81	0.63	0.60	3.12	0.04	21.29	47.08	14.25	13.65	3.02	99.60
82	0.63	0.59	3.11	0.03	21.67	47.23	14.34	13.75	2.76	100.14
83	0.64	0.59	3.15	0.04	21.53	46.96	14.08	13.84	3.14	99.82
84	0.64	0.57	3.01	0.04	22.75	45.28	14.21	13.90	3.18	99.61
85	0.62	0.60	3.06	0.03	21.27	47.20	14.58	13.51	2.97	99.79
86	0.63	0.59	3.09	0.03	21.67	46.82	14.34	13.64	2.63	99.50
87	0.62	0.59	3.03	0.03	21.43	46.92	14.63	13.41	2.69	99.43
88	0.63	0.59	3.08	0.03	21.74	46.70	14.31	13.71	2.90	99.74
89	0.64	0.59	3.15	0.03	21.68	46.78	14.05	13.84	2.82	99.52
90	0.63	0.60	3.13	0.03	21.54	47.24	14.28	13.78	2.86	100.08
91	0.63	0.59	3.11	0.03	21.65	47.15	14.34	13.72	2.71	99.97
92	0.63	0.59	3.08	0.03	21.73	47.05	14.42	13.68	2.74	99.98
93	0.62	0.59	3.00	0.03	21.74	46.64	14.70	13.46	2.82	99.76
94	0.63	0.60	3.07	0.04	21.13	46.64	14.37	13.55	3.39	99.40
95	0.62	0.60	3.06	0.04	21.24	46.93	14.50	13.53	3.09	99.63
96	0.62	0.59	3.01	0.03	21.42	46.75	14.66	13.43	2.95	99.57
97	0.62	0.59	3.05	0.03	21.66	46.81	14.53	13.52	2.76	99.56
98	0.62	0.60	3.05	0.04	21.05	46.70	14.46	13.46	3.47	99.45
99	0.62	0.60	3.02	0.04	20.77	46.69	14.60	13.28	3.54	99.15
100	0.62	0.60	3.04	0.04	21.04	46.59	14.50	13.40	3.30	99.13
101	0.61	0.60	2.92	0.04	20.86	46.57	15.08	13.03	3.45	99.27
102	0.59	0.60	2.80	0.04	20.80	46.30	15.64	12.66	3.59	99.28
103	0.60	0.60	2.89	0.04	20.95	46.73	15.29	12.94	3.40	99.55
104	0.58	0.60	2.74	0.03	21.23	46.55	16.07	12.37	2.51	99.09
105	0.62	0.59	2.99	0.03	21.54	46.83	14.81	13.36	2.83	99.71
106	0.62	0.60	3.01	0.03	21.34	46.77	14.70	13.35	2.89	99.43
107	0.62	0.60	3.00	0.04	21.19	46.69	14.73	13.34	3.36	99.67
108	0.63	0.59	3.06	0.04	21.39	46.64	14.39	13.62	3.34	99.69
109	0.63	0.59	3.08	0.04	21.47	46.80	14.35	13.69	3.18	99.77
110	0.63	0.59	3.08	0.03	21.67	46.73	14.33	13.68	2.88	99.66
111	0.63	0.60	3.11	0.04	21.29	46.93	14.26	13.66	3.00	99.52
112	0.62	0.59	3.04	0.03	21.56	47.01	14.61	13.55	2.84	99.91
113	0.62	0.59	2.99	0.04	21.60	46.16	14.60	13.48	3.45	99.59
114	0.63	0.59	3.07	0.04	21.39	46.58	14.35	13.66	3.44	99.73
115	0.62	0.61	3.11	0.03	20.62	47.90	14.54	13.42	2.87	99.70
116	0.63	0.60	3.11	0.04	21.08	47.07	14.29	13.67	3.22	99.63
117	0.62	0.59	3.02	0.03	21.57	47.08	14.74	13.41	2.67	99.79
118	0.62	0.59	3.02	0.03	21.56	46.64	14.60	13.46	2.88	99.51
119	0.61	0.59	2.94	0.04	21.49	46.75	15.03	13.27	3.06	99.94
120	0.63	0.59	3.03	0.03	21.86	46.68	14.54	13.64	2.81	99.97

Analysis# (C559)	Mg#	Cr#	Cr/ Fe^{2+}	Fe^{3+}#	Al_2O_3	Cr_2O_3	FeO	MgO	Fe_2O_3	Total
121	0.63	0.59	3.05	0.03	21.84	46.69	14.48	13.56	2.65	99.61
122	0.63	0.59	3.07	0.03	21.66	47.11	14.51	13.63	2.65	99.96
123	0.62	0.59	3.00	0.03	21.70	46.79	14.76	13.48	2.93	99.99
124	0.63	0.59	3.04	0.04	21.78	46.55	14.46	13.75	3.30	100.17
125	0.63	0.60	3.09	0.04	20.76	46.86	14.34	13.54	3.72	99.45
126	0.62	0.59	3.01	0.04	21.40	46.65	14.65	13.39	3.12	99.50
127	0.63	0.59	3.09	0.04	21.62	46.61	14.26	13.76	3.32	99.88
128	0.62	0.59	3.01	0.04	21.66	46.41	14.60	13.51	3.07	99.61
129	0.63	0.59	3.06	0.03	21.87	46.81	14.45	13.70	2.89	100.05
130	0.63	0.59	3.07	0.03	21.83	46.50	14.31	13.69	2.81	99.59
131	0.63	0.59	3.05	0.04	21.76	46.61	14.44	13.72	3.21	100.07
132	0.63	0.59	3.08	0.04	21.42	46.55	14.28	13.72	3.50	99.81
133	0.63	0.60	3.08	0.04	21.08	46.64	14.32	13.57	3.55	99.42
134	0.63	0.59	3.06	0.03	21.47	46.90	14.48	13.56	2.85	99.62
135	0.62	0.60	2.98	0.04	21.05	46.65	14.79	13.28	3.40	99.49
136	0.64	0.59	3.14	0.04	21.56	46.78	14.10	13.81	3.08	99.63
137	0.64	0.59	3.11	0.04	21.66	46.30	14.06	13.81	3.26	99.36
138	0.63	0.59	3.07	0.04	21.27	46.23	14.25	13.56	3.45	99.02
139	0.64	0.59	3.14	0.04	21.22	46.40	13.97	13.72	3.29	99.13
140	0.64	0.59	3.15	0.04	21.42	46.65	14.02	13.81	3.18	99.43
141	0.64	0.59	3.21	0.04	21.35	46.64	13.75	13.91	3.30	99.28
142	0.64	0.60	3.17	0.03	21.44	47.10	14.04	13.84	2.94	99.69
143	0.64	0.60	3.16	0.04	21.36	46.91	14.02	13.81	3.11	99.57
144	0.63	0.59	3.13	0.04	21.45	46.75	14.11	13.77	3.10	99.52
145	0.62	0.59	3.02	0.03	21.76	46.79	14.66	13.48	2.62	99.65
146	0.64	0.60	3.17	0.04	21.20	46.72	13.92	13.76	3.15	99.08
147	0.64	0.60	3.18	0.04	21.28	46.70	13.88	13.87	3.17	99.18
148	0.64	0.60	3.20	0.03	21.33	46.74	13.82	13.89	2.98	99.12
149	0.64	0.59	3.17	0.04	21.38	46.63	13.89	13.83	3.25	99.28
150	0.64	0.56	3.02	0.04	23.09	44.41	13.91	14.09	3.76	99.54
151	0.64	0.59	3.17	0.03	21.61	46.98	14.03	13.89	2.99	99.85
152	0.63	0.59	3.08	0.03	21.76	46.69	14.33	13.69	2.99	99.79
153	0.62	0.60	3.00	0.04	20.85	46.97	14.82	13.29	3.50	99.69
154	0.63	0.60	3.08	0.04	21.02	46.88	14.39	13.61	3.48	99.64
155	0.64	0.59	3.17	0.04	21.47	46.90	13.99	13.85	3.02	99.57
156	0.63	0.59	3.10	0.03	21.55	46.89	14.31	13.71	2.98	99.76
157	0.64	0.59	3.13	0.04	21.67	46.77	14.14	13.86	3.09	99.85
158	0.63	0.59	3.12	0.03	21.58	46.96	14.24	13.72	2.79	99.63
159	0.58	0.60	2.80	0.01	21.36	47.35	15.98	12.40	1.25	98.87
160	0.64	0.59	3.13	0.04	21.39	46.64	14.07	13.78	3.32	99.53

Analysis# (C559)	Mg#	Cr#	Cr/ Fe^{2+}	Fe^{3+}#	Al_2O_3	Cr_2O_3	FeO	MgO	Fe_2O_3	Total
161	0.63	0.59	3.12	0.03	21.80	47.08	14.25	13.82	2.65	99.94
162	0.64	0.59	3.14	0.03	21.74	46.99	14.16	13.87	2.78	99.94
163	0.64	0.59	3.17	0.03	21.83	46.75	13.96	13.96	2.87	99.70
164	0.63	0.59	3.05	0.04	21.54	46.61	14.45	13.61	3.27	99.79
165	0.63	0.59	3.12	0.03	21.81	46.88	14.21	13.81	2.59	99.68
166	0.63	0.59	3.12	0.04	21.41	46.72	14.14	13.81	3.51	99.86
167	0.64	0.59	3.17	0.04	21.23	46.30	13.80	13.84	3.65	99.08
168	0.64	0.59	3.13	0.04	21.67	46.36	14.00	13.83	3.04	99.20
169	0.64	0.59	3.20	0.04	21.31	46.62	13.77	13.91	3.32	99.25
170	0.64	0.59	3.20	0.04	21.54	46.53	13.76	13.96	3.23	99.34
171	0.64	0.59	3.18	0.04	21.45	46.72	13.87	13.94	3.27	99.48
172	0.64	0.59	3.18	0.04	21.62	46.64	13.85	13.91	3.05	99.39
173	0.64	0.59	3.15	0.04	21.59	46.67	14.01	13.81	3.03	99.39
174	0.64	0.59	3.12	0.03	22.00	46.36	14.04	13.89	2.95	99.62
175	0.64	0.59	3.14	0.03	22.09	46.68	14.07	13.96	2.85	100.05
176	0.64	0.59	3.14	0.03	22.11	46.67	14.05	13.95	2.73	99.89
177	0.64	0.58	3.15	0.03	22.27	46.54	13.98	13.99	2.74	99.86
178	0.64	0.59	3.13	0.03	22.08	46.77	14.11	13.90	2.67	99.85
179	0.63	0.59	3.11	0.03	22.02	46.86	14.24	13.74	2.49	99.66
180	0.62	0.59	3.01	0.04	21.72	46.40	14.57	13.53	3.13	99.67
181	0.63	0.59	3.06	0.03	21.88	46.51	14.36	13.69	2.88	99.69
182	0.61	0.59	2.93	0.03	21.93	46.35	14.97	13.32	2.86	99.83
183	0.61	0.59	2.95	0.03	21.86	46.51	14.88	13.29	2.66	99.58
184	0.58	0.59	2.80	0.02	21.54	47.03	15.89	12.52	1.51	99.05
185	0.62	0.59	2.97	0.04	21.63	46.36	14.75	13.44	3.37	99.86
186	0.62	0.59	2.96	0.03	21.73	46.32	14.77	13.33	2.94	99.46
187	0.62	0.59	2.97	0.04	21.70	46.36	14.74	13.40	3.11	99.66
188	0.64	0.60	3.18	0.03	21.32	47.31	14.08	13.84	3.00	99.86
189	0.63	0.59	3.09	0.03	21.84	46.90	14.36	13.72	2.76	99.91
190	0.63	0.59	3.06	0.03	21.96	46.61	14.41	13.66	2.64	99.67
191	0.63	0.59	3.08	0.03	21.78	46.77	14.36	13.70	2.81	99.78
192	0.63	0.59	3.09	0.03	21.53	47.00	14.37	13.63	2.73	99.61
193	0.62	0.59	3.01	0.03	21.75	46.74	14.67	13.51	2.83	99.84
194	0.62	0.59	2.97	0.03	21.79	46.50	14.80	13.40	2.94	99.82
195	0.62	0.59	3.04	0.03	21.70	46.88	14.57	13.56	2.72	99.84
196	0.62	0.59	3.04	0.04	21.44	46.76	14.55	13.52	3.04	99.70
197	0.62	0.59	3.02	0.03	21.64	46.99	14.71	13.41	2.48	99.64
198	0.60	0.59	2.80	0.04	21.68	46.36	15.64	12.93	3.16	100.13
199	0.59	0.59	2.80	0.03	21.70	46.56	15.71	12.87	2.94	100.11
200	0.60	0.59	2.89	0.03	21.60	46.70	15.28	13.11	2.84	99.90

Analysis# (C559)	Mg#	Cr#	Cr/ Fe^{2+}	Fe^{3+}#	Al_2O_3	Cr_2O_3	FeO	MgO	Fe_2O_3	Total
201	0.60	0.59	2.83	0.03	21.66	46.51	15.51	12.89	2.67	99.64
202	0.61	0.59	2.93	0.03	21.50	46.86	15.13	13.18	2.97	99.98
203	0.61	0.60	2.95	0.03	21.41	47.16	15.13	13.22	2.70	99.97
204	0.61	0.59	2.88	0.04	21.86	46.27	15.18	13.19	3.06	99.91
205	0.62	0.59	2.97	0.04	21.73	46.53	14.79	13.45	3.22	100.04
206	0.61	0.59	2.95	0.03	21.86	46.74	14.99	13.34	2.79	100.05
207	0.61	0.59	2.91	0.03	21.45	46.69	15.16	13.12	2.83	99.65
208	0.61	0.59	2.89	0.04	21.85	46.16	15.07	13.27	3.21	99.89
209	0.61	0.59	2.95	0.04	21.64	46.95	15.03	13.36	3.04	100.30
210	0.61	0.60	2.94	0.04	21.16	46.80	15.05	13.21	3.37	99.87
211	0.62	0.59	3.02	0.03	21.58	47.11	14.74	13.50	2.94	100.28
212	0.63	0.59	3.09	0.03	21.70	47.03	14.39	13.64	2.61	99.73
213	0.63	0.60	3.14	0.03	21.49	47.56	14.33	13.71	2.53	99.92
214	0.63	0.59	3.15	0.03	21.60	47.25	14.16	13.82	2.57	99.76
215	0.62	0.60	3.02	0.04	21.16	46.83	14.68	13.36	3.18	99.59
216	0.63	0.60	3.08	0.04	21.14	47.00	14.45	13.57	3.28	99.77
217	0.61	0.60	2.96	0.04	21.01	46.55	14.86	13.19	3.47	99.37
218	0.63	0.59	3.11	0.04	21.61	46.53	14.17	13.77	3.26	99.69
219	0.63	0.59	3.06	0.04	21.41	46.57	14.37	13.61	3.23	99.53
220	0.63	0.59	3.04	0.04	21.49	46.60	14.47	13.62	3.15	99.69
221	0.62	0.59	2.99	0.04	21.61	46.13	14.58	13.52	3.54	99.65
222	0.65	0.59	3.22	0.03	21.59	46.97	13.77	14.06	2.96	99.74
223	0.64	0.59	3.19	0.04	21.61	46.81	13.86	13.99	3.10	99.69
224	0.64	0.59	3.20	0.03	21.73	46.84	13.85	14.00	2.75	99.56
225	0.65	0.59	3.22	0.04	21.58	46.67	13.70	14.05	3.06	99.41
226	0.63	0.59	3.06	0.04	21.61	46.30	14.29	13.65	3.25	99.42
227	0.62	0.59	3.02	0.04	21.59	46.32	14.49	13.49	3.12	99.35
228	0.63	0.59	3.08	0.04	21.50	46.71	14.34	13.66	3.20	99.72
229	0.63	0.59	3.05	0.03	21.79	46.66	14.45	13.59	2.72	99.60
230	0.62	0.59	3.05	0.03	21.83	46.89	14.52	13.58	2.57	99.72
231	0.63	0.59	3.12	0.03	21.83	46.88	14.21	13.85	2.99	100.15
232	0.63	0.59	3.12	0.04	21.49	46.78	14.18	13.71	3.06	99.53
233	0.63	0.59	3.10	0.03	21.69	47.07	14.37	13.68	2.56	99.75
234	0.63	0.59	3.09	0.03	21.51	46.76	14.32	13.64	3.00	99.55
235	0.64	0.59	3.17	0.03	21.84	46.93	13.98	13.99	2.84	99.97
236	0.63	0.59	3.11	0.03	21.92	46.82	14.24	13.84	2.95	100.09
237	0.63	0.59	3.10	0.03	21.97	46.64	14.22	13.80	2.81	99.82
238	0.64	0.59	3.17	0.03	21.75	46.83	13.97	13.91	2.86	99.71
239	0.64	0.59	3.15	0.03	21.83	46.71	14.03	13.93	2.88	99.70
240	0.64	0.59	3.14	0.03	21.80	46.53	14.01	13.88	2.96	99.51

Analysis# (C559)	Mg#	Cr#	Cr/ Fe^{2+}	Fe^{3+}#	Al_2O_3	Cr_2O_3	FeO	MgO	Fe_2O_3	Total
241	0.64	0.59	3.14	0.04	21.81	46.53	14.00	13.92	3.03	99.66
242	0.64	0.59	3.14	0.04	21.44	46.41	13.96	13.83	3.34	99.30
243	0.63	0.59	3.12	0.03	21.67	46.64	14.14	13.71	2.75	99.30
244	0.62	0.59	3.02	0.04	21.62	46.34	14.49	13.50	3.06	99.38
245	0.62	0.59	2.99	0.03	21.46	46.69	14.78	13.34	2.99	99.59
246	0.63	0.60	3.12	0.03	21.41	47.12	14.27	13.73	2.92	99.74
247	0.65	0.59	3.25	0.03	21.61	47.08	13.71	14.07	2.77	99.61
248	0.64	0.59	3.18	0.04	21.52	46.57	13.85	13.98	3.21	99.48
249	0.65	0.59	3.20	0.04	21.75	46.53	13.74	14.05	3.04	99.45
250	0.65	0.59	3.23	0.04	21.72	46.59	13.63	14.12	3.19	99.56
251	0.64	0.59	3.17	0.03	21.74	46.44	13.86	13.94	2.91	99.30
252	0.64	0.59	3.21	0.04	21.54	46.73	13.75	13.99	3.15	99.56
253	0.64	0.60	3.21	0.04	21.19	47.19	13.91	13.91	3.14	99.71
254	0.64	0.58	3.17	0.03	22.33	46.60	13.89	14.14	2.72	100.15
255	0.65	0.58	3.20	0.03	22.39	46.53	13.73	14.21	2.81	100.04
256	0.65	0.58	3.22	0.03	22.19	46.63	13.71	14.22	2.89	99.96
257	0.65	0.59	3.19	0.04	21.90	46.33	13.71	14.12	3.34	99.67
258	0.65	0.59	3.22	0.04	22.05	46.38	13.64	14.20	3.08	99.68
259	0.63	0.59	3.05	0.03	21.97	46.30	14.37	13.69	2.98	99.66
260	0.63	0.59	3.09	0.04	21.68	46.49	14.21	13.74	3.18	99.60
261	0.64	0.59	3.12	0.04	21.62	46.56	14.10	13.84	3.18	99.61
262	0.64	0.59	3.14	0.04	21.58	46.81	14.10	13.87	3.09	99.83
263	0.64	0.59	3.11	0.04	21.80	46.45	14.14	13.85	3.18	99.82
264	0.64	0.59	3.17	0.03	21.70	47.02	14.03	13.95	2.92	99.97
265	0.65	0.59	3.24	0.03	21.96	47.24	13.79	14.19	2.70	100.25
266	0.66	0.59	3.29	0.03	22.03	46.73	13.44	14.33	2.91	99.77
267	0.64	0.59	3.15	0.03	21.87	46.80	14.05	13.86	2.60	99.58
268	0.65	0.59	3.21	0.04	21.64	46.24	13.63	14.09	3.39	99.32
269	0.65	0.59	3.21	0.04	21.62	46.34	13.64	14.09	3.44	99.42
270	0.65	0.59	3.22	0.04	21.83	46.06	13.52	14.11	3.25	99.06
271	0.63	0.60	3.08	0.04	20.94	46.57	14.31	13.50	3.56	99.09
272	0.63	0.60	3.06	0.04	21.25	46.77	14.46	13.60	3.29	99.71
273	0.63	0.59	3.08	0.04	21.84	46.24	14.19	13.78	3.20	99.57
274	0.65	0.59	3.23	0.03	21.73	46.78	13.68	14.07	2.94	99.48
275	0.64	0.59	3.15	0.03	22.08	46.71	14.01	13.99	2.74	99.92
276	0.65	0.58	3.16	0.04	22.11	45.99	13.74	14.09	3.08	99.36
277	0.65	0.59	3.24	0.04	21.83	46.33	13.53	14.12	3.19	99.29
278	0.64	0.59	3.10	0.04	21.82	45.99	14.04	13.81	3.34	99.26
279	0.65	0.59	3.25	0.04	21.89	46.46	13.51	14.17	3.05	99.43
280	0.65	0.59	3.27	0.04	21.43	46.80	13.54	14.06	3.06	99.24

Analysis# (C559)	Mg#	Cr#	Cr/ Fe^{2+}	Fe^{3+}#	Al_2O_3	Cr_2O_3	FeO	MgO	Fe_2O_3	Total
281	0.65	0.59	3.27	0.03	21.58	47.00	13.57	14.14	2.82	99.49
282	0.65	0.60	3.30	0.03	21.52	47.41	13.60	14.18	2.93	99.98
283	0.65	0.59	3.27	0.03	21.53	47.01	13.60	14.13	2.88	99.52
284	0.64	0.59	3.18	0.03	21.68	46.94	13.93	13.98	2.82	99.70
285	0.64	0.59	3.14	0.03	21.95	46.56	14.00	13.95	2.78	99.64
286	0.65	0.59	3.24	0.04	21.48	46.81	13.67	14.09	3.13	99.47
287	0.64	0.59	3.21	0.04	21.44	46.95	13.83	14.00	3.10	99.61
288	0.65	0.59	3.25	0.04	21.53	46.76	13.62	14.07	3.08	99.40
289	0.64	0.60	3.18	0.04	21.44	47.17	14.00	13.95	3.11	100.02
290	0.61	0.58	2.93	0.01	22.49	47.13	15.20	13.14	0.95	99.46
291	0.62	0.59	3.01	0.01	22.33	47.11	14.81	13.36	1.23	99.36
292	0.62	0.58	3.00	0.02	22.49	47.17	14.85	13.43	1.33	99.72
293	0.64	0.59	3.13	0.03	22.14	46.66	14.11	13.88	2.56	99.69
294	0.65	0.60	3.27	0.03	21.16	47.42	13.71	14.01	2.96	99.57
295	0.64	0.60	3.21	0.04	21.24	46.71	13.76	13.94	3.35	99.27
296	0.65	0.60	3.31	0.03	21.12	47.35	13.52	14.07	2.91	99.30
297	0.65	0.60	3.29	0.03	21.50	47.20	13.56	14.11	2.64	99.38
298	0.65	0.60	3.35	0.04	20.66	47.06	13.30	14.11	3.49	98.92
299	0.64	0.59	3.22	0.03	21.62	47.23	13.85	13.98	2.67	99.72
300	0.63	0.61	3.21	0.03	20.60	48.16	14.18	13.70	2.81	99.75
301	0.63	0.59	3.08	0.04	21.87	46.30	14.19	13.81	3.17	99.63
302	0.65	0.59	3.21	0.04	21.73	46.72	13.78	14.11	3.19	99.83
303	0.64	0.59	3.14	0.04	21.63	46.76	14.09	13.87	3.11	99.77
304	0.64	0.58	3.11	0.04	22.00	46.18	14.05	13.96	3.40	99.88
305	0.64	0.58	3.18	0.03	22.48	46.66	13.88	14.13	2.38	99.96
306	0.65	0.58	3.24	0.03	22.18	46.43	13.54	14.22	2.72	99.48
307	0.65	0.58	3.19	0.03	22.23	46.65	13.81	14.11	2.60	99.81
308	0.65	0.58	3.16	0.03	22.26	46.10	13.79	14.07	2.85	99.41
309	0.64	0.59	3.14	0.04	21.75	46.47	13.97	13.89	3.10	99.50
310	0.65	0.59	3.24	0.04	21.72	46.21	13.47	14.11	3.14	98.96
311	0.63	0.60	3.20	0.03	21.00	47.77	14.12	13.74	2.49	99.51
312	0.65	0.59	3.23	0.03	21.83	46.97	13.76	14.07	2.72	99.75
313	0.65	0.58	3.18	0.04	22.11	46.16	13.71	14.10	3.11	99.49
314	0.65	0.58	3.21	0.03	22.28	46.24	13.63	14.13	2.79	99.43
315	0.65	0.58	3.21	0.03	22.38	46.18	13.61	14.26	2.95	99.71
316	0.64	0.59	3.14	0.04	21.79	46.21	13.90	13.90	3.19	99.31
317	0.64	0.58	3.12	0.04	21.95	46.07	13.98	13.88	3.09	99.30
318	0.65	0.58	3.16	0.04	21.96	45.99	13.74	14.02	3.32	99.32
319	0.64	0.58	3.19	0.03	22.12	46.50	13.80	14.06	2.84	99.70
320	0.65	0.58	3.21	0.03	22.19	46.51	13.70	14.20	2.87	99.80

Analysis# (C559)	Mg#	Cr#	Cr/ Fe^{2+}	Fe^{3+}#	Al_2O_3	Cr_2O_3	FeO	MgO	Fe_2O_3	Total
321	0.64	0.59	3.17	0.03	22.07	46.80	13.93	14.00	2.73	99.85
322	0.66	0.58	3.25	0.04	22.22	46.09	13.40	14.34	3.09	99.47
323	0.66	0.58	3.25	0.04	22.30	45.97	13.38	14.29	3.05	99.33
324	0.66	0.58	3.28	0.04	22.28	46.37	13.38	14.36	3.03	99.79
325	0.65	0.58	3.19	0.03	22.43	46.02	13.64	14.21	2.82	99.51
326	0.65	0.58	3.21	0.04	22.34	46.00	13.55	14.24	3.03	99.49
327	0.65	0.58	3.19	0.03	22.39	46.33	13.71	14.23	2.94	99.91
328	0.65	0.58	3.19	0.03	22.43	46.11	13.66	14.18	2.91	99.67
329	0.65	0.58	3.18	0.03	22.47	46.25	13.73	14.20	2.83	99.83

C559 – trace elements

Analysis# (C559)	Mg#	Cr#	Cr/ Fe^{2+}	Fe^{3+}#	SiO_2	TiO_2	V_2O_5	MnO	NiO
1	0.59	0.60	2.90	0.01	0.22	0.10	0.11	0.26	0.20
2	0.63	0.60	3.12	0.03	0.03	0.14	0.15	0.28	0.09
3	0.63	0.60	3.16	0.03	0.02	0.12	0.16	0.26	0.10
4	0.63	0.60	3.18	0.03	0.04	0.10	0.12	0.26	0.10
5	0.63	0.60	3.14	0.03	0.02	0.10	0.16	0.26	0.08
6	0.63	0.60	3.17	0.03	0.06	0.10	0.16	0.28	0.10
7	0.64	0.60	3.17	0.03	0.04	0.13	0.14	0.26	0.10
8	0.64	0.60	3.19	0.03	0.04	0.12	0.15	0.25	0.06
9	0.62	0.59	3.03	0.04	0.03	0.08	0.16	0.27	0.10
10	0.63	0.60	3.12	0.04	0.04	0.12	0.14	0.27	0.09
11	0.62	0.59	2.99	0.04	0.03	0.10	0.15	0.29	0.06
12	0.62	0.60	3.03	0.04	0.04	0.10	0.13	0.28	0.05
13	0.63	0.60	3.08	0.04	0.03	0.13	0.14	0.29	0.10
14	0.62	0.61	3.09	0.04	0.03	0.12	0.15	0.28	0.08
15	0.63	0.60	3.11	0.04	0.02	0.14	0.14	0.28	0.07
16	0.64	0.60	3.17	0.04	0.02	0.11	0.14	0.26	0.07
17	0.65	0.60	3.23	0.04	0.04	0.12	0.14	0.28	0.08
18	0.64	0.60	3.19	0.04	0.02	0.11	0.16	0.26	0.10
19	0.64	0.60	3.22	0.04	0.03	0.09	0.16	0.26	0.05
20	0.65	0.59	3.24	0.04	0.04	0.10	0.12	0.26	0.09
21	0.64	0.60	3.15	0.04	0.05	0.09	0.13	0.26	0.05
22	0.64	0.59	3.16	0.04	0.05	0.13	0.13	0.29	0.10
23	0.64	0.59	3.16	0.04	0.04	0.10	0.12	0.27	0.11
24	0.64	0.59	3.13	0.04	0.16	0.10	0.14	0.27	0.10
25	0.63	0.60	3.11	0.04	0.06	0.10	0.16	0.24	0.10
26	0.63	0.60	3.07	0.04	0.12	0.11	0.13	0.27	0.09
27	0.62	0.60	3.02	0.04	0.03	0.09	0.14	0.27	0.07
28	0.62	0.60	3.02	0.04	0.05	0.10	0.15	0.27	0.10
29	0.61	0.60	2.91	0.05	0.03	0.10	0.14	0.29	0.08
30	0.62	0.60	2.98	0.04	0.03	0.12	0.12	0.28	0.08
31	0.61	0.59	2.92	0.04	0.05	0.10	0.13	0.30	0.09
32	0.59	0.59	2.77	0.04	0.03	0.12	0.13	0.28	0.05
33	0.60	0.59	2.87	0.04	0.03	0.07	0.16	0.28	0.09
34	0.66	0.58	3.25	0.04	0.03	0.12	0.16	0.24	0.09
35	0.66	0.58	3.27	0.04	0.03	0.11	0.14	0.26	0.09
36	0.65	0.57	3.18	0.04	0.04	0.11	0.14	0.25	0.14
37	0.67	0.58	3.31	0.05	0.16	0.11	0.13	0.27	0.10
38	0.64	0.60	3.21	0.04	0.04	0.10	0.13	0.26	0.06
39	0.65	0.60	3.27	0.04	0.04	0.10	0.15	0.24	0.11
40	0.66	0.58	3.25	0.03	0.03	0.12	0.14	0.25	0.08

Analysis# (C559)	Mg#	Cr#	Cr/ Fe^{2+}	Fe^{3+}#	SiO_2	TiO_2	V_2O_5	MnO	NiO
41	0.66	0.58	3.29	0.04	0.02	0.12	0.15	0.27	0.10
42	0.66	0.58	3.25	0.04	0.01	0.10	0.17	0.26	0.09
43	0.66	0.58	3.25	0.04	0.04	0.12	0.16	0.26	0.11
44	0.65	0.58	3.22	0.03	0.03	0.10	0.13	0.28	0.10
45	0.66	0.58	3.25	0.04	0.02	0.11	0.14	0.27	0.10
46	0.66	0.58	3.25	0.04	0.04	0.12	0.14	0.26	0.10
47	0.67	0.58	3.32	0.04	0.04	0.13	0.15	0.26	0.11
48	0.66	0.58	3.28	0.03	0.02	0.11	0.13	0.25	0.08
49	0.64	0.58	3.13	0.03	0.03	0.09	0.18	0.27	0.12
50	0.65	0.58	3.20	0.04	0.06	0.09	0.13	0.26	0.13
51	0.64	0.58	3.13	0.03	0.03	0.11	0.13	0.26	0.09
52	0.65	0.58	3.19	0.03	0.03	0.10	0.15	0.25	0.09
53	0.64	0.58	3.16	0.03	0.04	0.09	0.15	0.27	0.09
54	0.64	0.58	3.12	0.03	0.02	0.09	0.15	0.27	0.08
55	0.65	0.58	3.18	0.04	0.03	0.10	0.14	0.25	0.10
56	0.65	0.58	3.17	0.03	0.04	0.14	0.16	0.26	0.11
57	0.62	0.58	3.00	0.03	0.04	0.10	0.15	0.26	0.11
58	0.63	0.59	3.09	0.03	0.03	0.11	0.14	0.28	0.09
59	0.63	0.58	3.03	0.03	0.02	0.10	0.15	0.28	0.09
60	0.64	0.57	3.05	0.03	0.06	0.10	0.11	0.24	0.10
61	0.64	0.58	3.09	0.04	0.01	0.12	0.14	0.26	0.09
62	0.65	0.58	3.17	0.04	0.05	0.14	0.13	0.28	0.08
63	0.65	0.58	3.16	0.04	0.05	0.12	0.13	0.27	0.09
64	0.63	0.59	3.10	0.03	0.05	0.10	0.17	0.28	0.10
65	0.63	0.60	3.12	0.04	0.05	0.10	0.13	0.27	0.10
66	0.64	0.59	3.14	0.04	0.03	0.11	0.15	0.29	0.11
67	0.63	0.59	3.08	0.04	0.04	0.12	0.15	0.28	0.08
68	0.63	0.59	3.06	0.04	0.03	0.12	0.13	0.27	0.09
69	0.63	0.59	3.07	0.04	0.03	0.10	0.14	0.25	0.08
70	0.62	0.60	3.06	0.03	0.03	0.13	0.16	0.30	0.08
71	0.63	0.59	3.04	0.03	0.01	0.12	0.13	0.26	0.07
72	0.63	0.59	3.08	0.03	0.03	0.09	0.14	0.28	0.10
73	0.63	0.59	3.08	0.03	0.04	0.11	0.14	0.26	0.09
74	0.62	0.59	3.03	0.03	0.03	0.10	0.15	0.27	0.08
75	0.63	0.60	3.10	0.03	0.04	0.10	0.16	0.28	0.10
76	0.63	0.59	3.12	0.03	0.02	0.13	0.14	0.26	0.11
77	0.64	0.59	3.14	0.03	0.04	0.12	0.13	0.27	0.11
78	0.63	0.59	3.11	0.03	0.03	0.11	0.12	0.25	0.09
79	0.63	0.59	3.05	0.03	0.02	0.11	0.13	0.28	0.07
80	0.61	0.59	2.90	0.04	0.03	0.14	0.15	0.27	0.08

Analysis# (C559)	Mg#	Cr#	Cr/ Fe^{2+}	Fe^{3+}#	SiO_2	TiO_2	V_2O_5	MnO	NiO
81	0.63	0.60	3.12	0.04	0.03	0.09	0.13	0.26	0.12
82	0.63	0.59	3.11	0.03	0.05	0.11	0.13	0.26	0.13
83	0.64	0.59	3.15	0.04	0.02	0.07	0.14	0.26	0.10
84	0.64	0.57	3.01	0.04	0.02	0.12	0.16	0.26	0.07
85	0.62	0.60	3.06	0.03	0.02	0.09	0.13	0.27	0.06
86	0.63	0.59	3.09	0.03	0.03	0.13	0.15	0.28	0.09
87	0.62	0.59	3.03	0.03	0.04	0.12	0.12	0.29	0.05
88	0.63	0.59	3.08	0.03	0.04	0.13	0.13	0.28	0.09
89	0.64	0.59	3.15	0.03	0.03	0.10	0.16	0.25	0.09
90	0.63	0.60	3.13	0.03	0.01	0.13	0.14	0.28	0.10
91	0.63	0.59	3.11	0.03	0.06	0.10	0.16	0.27	0.10
92	0.63	0.59	3.08	0.03	0.03	0.10	0.14	0.27	0.09
93	0.62	0.59	3.00	0.03	0.03	0.10	0.18	0.27	0.11
94	0.63	0.60	3.07	0.04	0.03	0.13	0.14	0.28	0.08
95	0.62	0.60	3.06	0.04	0.03	0.10	0.17	0.28	0.08
96	0.62	0.59	3.01	0.03	0.02	0.12	0.16	0.26	0.11
97	0.62	0.59	3.05	0.03	0.02	0.08	0.12	0.28	0.06
98	0.62	0.60	3.05	0.04	0.05	0.09	0.14	0.30	0.07
99	0.62	0.60	3.02	0.04	0.02	0.11	0.11	0.27	0.11
100	0.62	0.60	3.04	0.04	0.04	0.10	0.14	0.27	0.07
101	0.61	0.60	2.92	0.04	0.02	0.11	0.15	0.29	0.07
102	0.59	0.60	2.80	0.04	0.03	0.11	0.15	0.27	0.09
103	0.60	0.60	2.89	0.04	0.02	0.07	0.14	0.27	0.09
104	0.58	0.60	2.74	0.03	0.04	0.10	0.15	0.27	0.07
105	0.62	0.59	2.99	0.03	0.03	0.12	0.13	0.27	0.08
106	0.62	0.60	3.01	0.03	0.03	0.12	0.15	0.27	0.10
107	0.62	0.60	3.00	0.04	0.04	0.11	0.15	0.31	0.09
108	0.63	0.59	3.06	0.04	0.03	0.12	0.13	0.27	0.10
109	0.63	0.59	3.08	0.04	0.03	0.11	0.14	0.26	0.06
110	0.63	0.59	3.08	0.03	0.05	0.09	0.17	0.27	0.07
111	0.63	0.60	3.11	0.04	0.05	0.13	0.14	0.29	0.08
112	0.62	0.59	3.04	0.03	0.03	0.13	0.14	0.27	0.07
113	0.62	0.59	2.99	0.04	0.02	0.11	0.15	0.29	0.08
114	0.63	0.59	3.07	0.04	0.01	0.10	0.17	0.29	0.09
115	0.62	0.61	3.11	0.03	0.05	0.09	0.15	0.28	0.08
116	0.63	0.60	3.11	0.04	0.04	0.12	0.16	0.26	0.05
117	0.62	0.59	3.02	0.03	0.03	0.09	0.13	0.27	0.08
118	0.62	0.59	3.02	0.03	0.02	0.11	0.15	0.27	0.09
119	0.61	0.59	2.94	0.04	0.03	0.12	0.14	0.28	0.09
120	0.63	0.59	3.03	0.03	0.05	0.12	0.19	0.28	0.07

Analysis# (C559)	Mg#	Cr#	Cr/ Fe^{2+}	Fe^{3+}#	SiO_2	TiO_2	V_2O_5	MnO	NiO
121	0.63	0.59	3.05	0.03	0.03	0.10	0.14	0.28	0.10
122	0.63	0.59	3.07	0.03	0.02	0.13	0.16	0.26	0.11
123	0.62	0.59	3.00	0.03	0.03	0.11	0.14	0.28	0.08
124	0.63	0.59	3.04	0.04	0.01	0.13	0.18	0.27	0.07
125	0.63	0.60	3.09	0.04	0.02	0.11	0.12	0.27	0.07
126	0.62	0.59	3.01	0.04	0.02	0.09	0.13	0.28	0.08
127	0.63	0.59	3.09	0.04	0.02	0.11	0.15	0.28	0.09
128	0.62	0.59	3.01	0.04	0.05	0.12	0.15	0.28	0.07
129	0.63	0.59	3.06	0.03	0.02	0.10	0.15	0.27	0.08
130	0.63	0.59	3.07	0.03	0.02	0.12	0.18	0.28	0.12
131	0.63	0.59	3.05	0.04	0.04	0.10	0.17	0.27	0.08
132	0.63	0.59	3.08	0.04	0.05	0.13	0.15	0.29	0.10
133	0.63	0.60	3.08	0.04	0.02	0.09	0.14	0.26	0.10
134	0.63	0.59	3.06	0.03	0.05	0.11	0.14	0.28	0.06
135	0.62	0.60	2.98	0.04	0.03	0.11	0.16	0.28	0.08
136	0.64	0.59	3.14	0.04	0.02	0.10	0.15	0.26	0.09
137	0.64	0.59	3.11	0.04	0.03	0.11	0.14	0.25	0.07
138	0.63	0.59	3.07	0.04	0.03	0.12	0.12	0.26	0.08
139	0.64	0.59	3.14	0.04	0.21	0.13	0.14	0.30	0.08
140	0.64	0.59	3.15	0.04	0.03	0.12	0.15	0.28	0.09
141	0.64	0.59	3.21	0.04	0.04	0.08	0.15	0.29	0.11
142	0.64	0.60	3.17	0.03	0.02	0.10	0.13	0.27	0.09
143	0.64	0.60	3.16	0.04	0.04	0.11	0.14	0.28	0.11
144	0.63	0.59	3.13	0.04	0.04	0.11	0.15	0.26	0.09
145	0.62	0.59	3.02	0.03	0.02	0.10	0.14	0.26	0.07
146	0.64	0.60	3.17	0.04	0.03	0.11	0.13	0.28	0.09
147	0.64	0.60	3.18	0.04	0.03	0.12	0.14	0.25	0.06
148	0.64	0.60	3.20	0.03	0.04	0.12	0.16	0.27	0.08
149	0.64	0.59	3.17	0.04	0.03	0.10	0.12	0.27	0.10
150	0.64	0.56	3.02	0.04	0.04	0.12	0.15	0.25	0.10
151	0.64	0.59	3.17	0.03	0.03	0.11	0.14	0.28	0.09
152	0.63	0.59	3.08	0.03	0.03	0.10	0.12	0.27	0.09
153	0.62	0.60	3.00	0.04	0.03	0.11	0.13	0.26	0.08
154	0.63	0.60	3.08	0.04	0.03	0.11	0.16	0.27	0.05
155	0.64	0.59	3.17	0.04	0.04	0.12	0.13	0.28	0.09
156	0.63	0.59	3.10	0.03	0.02	0.11	0.14	0.26	0.08
157	0.64	0.59	3.13	0.04	0.04	0.10	0.15	0.26	0.06
158	0.63	0.59	3.12	0.03	0.03	0.10	0.14	0.27	0.09
159	0.58	0.60	2.80	0.01	0.02	0.12	0.16	0.27	0.09
160	0.64	0.59	3.13	0.04	0.03	0.10	0.15	0.27	0.11

Analysis# (C559)	Mg#	Cr#	Cr/ Fe^{2+}	Fe^{3+}#	SiO_2	TiO_2	V_2O_5	MnO	NiO
161	0.63	0.59	3.12	0.03	0.03	0.10	0.15	0.25	0.07
162	0.64	0.59	3.14	0.03	0.04	0.13	0.15	0.27	0.08
163	0.64	0.59	3.17	0.03	0.02	0.11	0.15	0.28	0.07
164	0.63	0.59	3.05	0.04	0.06	0.10	0.13	0.27	0.08
165	0.63	0.59	3.12	0.03	0.03	0.12	0.17	0.26	0.06
166	0.63	0.59	3.12	0.04	0.04	0.10	0.13	0.27	0.09
167	0.64	0.59	3.17	0.04	0.03	0.09	0.13	0.26	0.11
168	0.64	0.59	3.13	0.04	0.03	0.12	0.15	0.26	0.05
169	0.64	0.59	3.20	0.04	0.05	0.11	0.13	0.27	0.11
170	0.64	0.59	3.20	0.04	0.04	0.12	0.12	0.26	0.11
171	0.64	0.59	3.18	0.04	0.04	0.10	0.12	0.24	0.06
172	0.64	0.59	3.18	0.04	0.04	0.09	0.14	0.26	0.10
173	0.64	0.59	3.15	0.04	0.04	0.10	0.12	0.27	0.08
174	0.64	0.59	3.12	0.03	0.03	0.11	0.16	0.28	0.10
175	0.64	0.59	3.14	0.03	0.04	0.14	0.12	0.26	0.13
176	0.64	0.59	3.14	0.03	0.04	0.10	0.15	0.25	0.11
177	0.64	0.58	3.15	0.03	0.02	0.10	0.13	0.27	0.10
178	0.64	0.59	3.13	0.03	0.02	0.10	0.12	0.25	0.09
179	0.63	0.59	3.11	0.03	0.01	0.07	0.12	0.26	0.09
180	0.62	0.59	3.01	0.04	0.03	0.11	0.14	0.27	0.08
181	0.63	0.59	3.06	0.03	0.02	0.12	0.15	0.28	0.09
182	0.61	0.59	2.93	0.03	0.04	0.12	0.16	0.27	0.11
183	0.61	0.59	2.95	0.03	0.03	0.09	0.14	0.26	0.12
184	0.58	0.59	2.80	0.02	0.04	0.14	0.17	0.28	0.08
185	0.62	0.59	2.97	0.04	0.03	0.11	0.14	0.28	0.08
186	0.62	0.59	2.96	0.03	0.03	0.11	0.14	0.30	0.10
187	0.62	0.59	2.97	0.04	0.03	0.12	0.14	0.28	0.10
188	0.64	0.60	3.18	0.03	0.03	0.10	0.13	0.26	0.08
189	0.63	0.59	3.09	0.03	0.03	0.10	0.13	0.27	0.08
190	0.63	0.59	3.06	0.03	0.03	0.13	0.13	0.26	0.11
191	0.63	0.59	3.08	0.03	0.04	0.11	0.15	0.26	0.09
192	0.63	0.59	3.09	0.03	0.03	0.11	0.14	0.27	0.07
193	0.62	0.59	3.01	0.03	0.01	0.10	0.16	0.28	0.08
194	0.62	0.59	2.97	0.03	0.02	0.12	0.15	0.29	0.10
195	0.62	0.59	3.04	0.03	0.03	0.13	0.15	0.28	0.10
196	0.62	0.59	3.04	0.04	0.04	0.12	0.17	0.27	0.11
197	0.62	0.59	3.02	0.03	0.03	0.11	0.15	0.27	0.10
198	0.60	0.59	2.80	0.04	0.03	0.13	0.16	0.30	0.07
199	0.59	0.59	2.80	0.03	0.02	0.09	0.15	0.29	0.07
200	0.60	0.59	2.89	0.03	0.03	0.11	0.16	0.27	0.08

Analysis# (C559)	Mg#	Cr#	Cr/ Fe^{2+}	Fe^{3+}#	SiO_2	TiO_2	V_2O_5	MnO	NiO
201	0.60	0.59	2.83	0.03	0.03	0.10	0.16	0.29	0.08
202	0.61	0.59	2.93	0.03	0.03	0.10	0.13	0.28	0.09
203	0.61	0.60	2.95	0.03	0.03	0.12	0.15	0.27	0.05
204	0.61	0.59	2.88	0.04	0.04	0.10	0.15	0.28	0.07
205	0.62	0.59	2.97	0.04	0.05	0.09	0.14	0.27	0.09
206	0.61	0.59	2.95	0.03	0.01	0.09	0.16	0.29	0.08
207	0.61	0.59	2.91	0.03	0.05	0.13	0.14	0.27	0.08
208	0.61	0.59	2.89	0.04	0.01	0.12	0.16	0.27	0.08
209	0.61	0.59	2.95	0.04	0.04	0.09	0.14	0.27	0.05
210	0.61	0.60	2.94	0.04	0.00	0.12	0.14	0.28	0.09
211	0.62	0.59	3.02	0.03	0.05	0.10	0.15	0.30	0.10
212	0.63	0.59	3.09	0.03	0.04	0.08	0.15	0.27	0.08
213	0.63	0.60	3.14	0.03	0.01	0.11	0.09	0.24	0.10
214	0.63	0.59	3.15	0.03	0.04	0.11	0.15	0.26	0.08
215	0.62	0.60	3.02	0.04	0.04	0.12	0.14	0.30	0.10
216	0.63	0.60	3.08	0.04	0.03	0.10	0.16	0.28	0.09
217	0.61	0.60	2.96	0.04	0.03	0.10	0.15	0.30	0.09
218	0.63	0.59	3.11	0.04	0.04	0.10	0.16	0.29	0.09
219	0.63	0.59	3.06	0.04	0.03	0.12	0.15	0.27	0.09
220	0.63	0.59	3.04	0.04	0.04	0.14	0.17	0.25	0.08
221	0.62	0.59	2.99	0.04	0.05	0.11	0.13	0.28	0.07
222	0.65	0.59	3.22	0.03	0.04	0.11	0.17	0.27	0.09
223	0.64	0.59	3.19	0.04	0.03	0.09	0.16	0.27	0.07
224	0.64	0.59	3.20	0.03	0.03	0.12	0.17	0.26	0.09
225	0.65	0.59	3.22	0.04	0.04	0.15	0.13	0.26	0.09
226	0.63	0.59	3.06	0.04	0.03	0.11	0.15	0.26	0.09
227	0.62	0.59	3.02	0.04	0.04	0.12	0.12	0.28	0.09
228	0.63	0.59	3.08	0.04	0.02	0.11	0.14	0.28	0.09
229	0.63	0.59	3.05	0.03	0.02	0.10	0.17	0.28	0.09
230	0.62	0.59	3.05	0.03	0.02	0.09	0.15	0.27	0.08
231	0.63	0.59	3.12	0.03	0.05	0.09	0.16	0.27	0.11
232	0.63	0.59	3.12	0.04	0.04	0.10	0.12	0.27	0.09
233	0.63	0.59	3.10	0.03	0.02	0.11	0.15	0.27	0.08
234	0.63	0.59	3.09	0.03	0.04	0.10	0.14	0.26	0.10
235	0.64	0.59	3.17	0.03	0.04	0.11	0.16	0.24	0.12
236	0.63	0.59	3.11	0.03	0.03	0.10	0.13	0.26	0.09
237	0.63	0.59	3.10	0.03	0.03	0.09	0.17	0.28	0.10
238	0.64	0.59	3.17	0.03	0.05	0.12	0.13	0.29	0.10
239	0.64	0.59	3.15	0.03	0.05	0.12	0.13	0.26	0.05
240	0.64	0.59	3.14	0.03	0.00	0.10	0.16	0.26	0.09

Analysis# (C559)	Mg#	Cr#	Cr/ Fe^{2+}	Fe^{3+}#	SiO_2	TiO_2	V_2O_5	MnO	NiO
241	0.64	0.59	3.14	0.04	0.04	0.12	0.16	0.26	0.10
242	0.64	0.59	3.14	0.04	0.05	0.11	0.15	0.25	0.10
243	0.63	0.59	3.12	0.03	0.05	0.12	0.13	0.27	0.10
244	0.62	0.59	3.02	0.04	0.04	0.12	0.13	0.26	0.12
245	0.62	0.59	2.99	0.03	0.04	0.10	0.15	0.27	0.08
246	0.63	0.60	3.12	0.03	0.02	0.09	0.16	0.26	0.06
247	0.65	0.59	3.25	0.03	0.03	0.11	0.15	0.26	0.10
248	0.64	0.59	3.18	0.04	0.04	0.13	0.17	0.27	0.07
249	0.65	0.59	3.20	0.04	0.03	0.11	0.17	0.26	0.08
250	0.65	0.59	3.23	0.04	0.05	0.10	0.15	0.26	0.08
251	0.64	0.59	3.17	0.03	0.11	0.12	0.16	0.26	0.07
252	0.64	0.59	3.21	0.04	0.07	0.11	0.15	0.30	0.10
253	0.64	0.60	3.21	0.04	0.05	0.11	0.16	0.29	0.08
254	0.64	0.58	3.17	0.03	0.07	0.13	0.17	0.27	0.12
255	0.65	0.58	3.20	0.03	0.04	0.11	0.14	0.26	0.12
256	0.65	0.58	3.22	0.03	0.03	0.13	0.14	0.26	0.08
257	0.65	0.59	3.19	0.04	0.03	0.10	0.14	0.27	0.07
258	0.65	0.59	3.22	0.04	0.04	0.14	0.13	0.26	0.09
259	0.63	0.59	3.05	0.03	0.03	0.11	0.15	0.27	0.09
260	0.63	0.59	3.09	0.04	0.03	0.09	0.15	0.28	0.07
261	0.64	0.59	3.12	0.04	0.01	0.13	0.14	0.27	0.08
262	0.64	0.59	3.14	0.04	0.04	0.13	0.15	0.28	0.07
263	0.64	0.59	3.11	0.04	0.10	0.14	0.13	0.27	0.08
264	0.64	0.59	3.17	0.03	0.04	0.11	0.15	0.27	0.07
265	0.65	0.59	3.24	0.03	0.02	0.11	0.16	0.25	0.11
266	0.66	0.59	3.29	0.03	0.03	0.11	0.14	0.24	0.09
267	0.64	0.59	3.15	0.03	0.04	0.13	0.13	0.27	0.10
268	0.65	0.59	3.21	0.04	0.05	0.13	0.15	0.27	0.07
269	0.65	0.59	3.21	0.04	0.03	0.12	0.13	0.27	0.08
270	0.65	0.59	3.22	0.04	0.05	0.11	0.14	0.25	0.09
271	0.63	0.60	3.08	0.04	0.02	0.09	0.13	0.28	0.07
272	0.63	0.60	3.06	0.04	0.03	0.15	0.15	0.27	0.07
273	0.63	0.59	3.08	0.04	0.02	0.13	0.14	0.25	0.10
274	0.65	0.59	3.23	0.03	0.03	0.09	0.13	0.26	0.08
275	0.64	0.59	3.15	0.03	0.03	0.13	0.14	0.28	0.08
276	0.65	0.58	3.16	0.04	0.03	0.14	0.16	0.26	0.08
277	0.65	0.59	3.24	0.04	0.05	0.10	0.11	0.25	0.11
278	0.64	0.59	3.10	0.04	0.03	0.10	0.13	0.27	0.06
279	0.65	0.59	3.25	0.04	0.01	0.12	0.13	0.29	0.10
280	0.65	0.59	3.27	0.04	0.05	0.11	0.13	0.26	0.12

Analysis# (C559)	Mg#	Cr#	Cr/ Fe^{2+}	Fe^{3+}#	SiO_2	TiO_2	V_2O_5	MnO	NiO
281	0.65	0.59	3.27	0.03	0.03	0.11	0.17	0.25	0.09
282	0.65	0.60	3.30	0.03	0.04	0.09	0.13	0.27	0.11
283	0.65	0.59	3.27	0.03	0.03	0.13	0.15	0.27	0.09
284	0.64	0.59	3.18	0.03	0.04	0.11	0.16	0.27	0.04
285	0.64	0.59	3.14	0.03	0.06	0.15	0.14	0.26	0.06
286	0.65	0.59	3.24	0.04	0.03	0.12	0.16	0.25	0.06
287	0.64	0.59	3.21	0.04	0.03	0.12	0.13	0.23	0.09
288	0.65	0.59	3.25	0.04	0.04	0.12	0.13	0.29	0.08
289	0.64	0.60	3.18	0.04	0.04	0.10	0.17	0.26	0.09
290	0.61	0.58	2.93	0.01	0.02	0.11	0.15	0.27	0.08
291	0.62	0.59	3.01	0.01	0.04	0.12	0.15	0.26	0.08
292	0.62	0.58	3.00	0.02	0.02	0.10	0.13	0.26	0.07
293	0.64	0.59	3.13	0.03	0.00	0.11	0.14	0.27	0.09
294	0.65	0.60	3.27	0.03	0.04	0.09	0.14	0.25	0.10
295	0.64	0.60	3.21	0.04	0.03	0.10	0.15	0.26	0.08
296	0.65	0.60	3.31	0.03	0.02	0.11	0.13	0.25	0.10
297	0.65	0.60	3.29	0.03	0.03	0.11	0.15	0.27	0.09
298	0.65	0.60	3.35	0.04	0.02	0.11	0.15	0.26	0.10
299	0.64	0.59	3.22	0.03	0.03	0.10	0.15	0.27	0.10
300	0.63	0.61	3.21	0.03	0.03	0.10	0.13	0.26	0.06
301	0.63	0.59	3.08	0.04	0.03	0.11	0.14	0.26	0.06
302	0.65	0.59	3.21	0.04	0.03	0.13	0.14	0.27	0.06
303	0.64	0.59	3.14	0.04	0.02	0.12	0.14	0.27	0.09
304	0.64	0.58	3.11	0.04	0.03	0.13	0.13	0.27	0.08
305	0.64	0.58	3.18	0.03	0.03	0.12	0.17	0.26	0.09
306	0.65	0.58	3.24	0.03	0.04	0.12	0.15	0.26	0.09
307	0.65	0.58	3.19	0.03	0.04	0.12	0.15	0.27	0.08
308	0.65	0.58	3.16	0.03	0.04	0.12	0.15	0.25	0.07
309	0.64	0.59	3.14	0.04	0.02	0.10	0.15	0.26	0.11
310	0.65	0.59	3.24	0.04	0.04	0.12	0.12	0.24	0.09
311	0.63	0.60	3.20	0.03	0.04	0.13	0.14	0.25	0.08
312	0.65	0.59	3.23	0.03	0.02	0.10	0.16	0.27	0.12
313	0.65	0.58	3.18	0.04	0.03	0.10	0.14	0.25	0.10
314	0.65	0.58	3.21	0.03	0.03	0.10	0.13	0.27	0.10
315	0.65	0.58	3.21	0.03	0.02	0.14	0.14	0.24	0.10
316	0.64	0.59	3.14	0.04	0.04	0.10	0.15	0.26	0.10
317	0.64	0.58	3.12	0.04	0.04	0.10	0.16	0.26	0.08
318	0.65	0.58	3.16	0.04	0.02	0.12	0.12	0.27	0.09
319	0.64	0.58	3.19	0.03	0.03	0.13	0.12	0.29	0.11
320	0.65	0.58	3.21	0.03	0.04	0.11	0.15	0.24	0.09

Analysis# (C559)	Mg#	Cr#	Cr/ Fe^{2+}	Fe^{3+}#	SiO_2	TiO_2	V_2O_5	MnO	NiO
321	0.64	0.59	3.17	0.03	0.04	0.08	0.13	0.25	0.09
322	0.66	0.58	3.25	0.04	0.03	0.13	0.15	0.24	0.09
323	0.66	0.58	3.25	0.04	0.04	0.12	0.12	0.25	0.10
324	0.66	0.58	3.28	0.04	0.02	0.11	0.14	0.28	0.11
325	0.65	0.58	3.19	0.03	0.06	0.14	0.15	0.25	0.07
326	0.65	0.58	3.21	0.04	0.02	0.12	0.14	0.26	0.09
327	0.65	0.58	3.19	0.03	0.02	0.11	0.15	0.26	0.07
328	0.65	0.58	3.19	0.03	0.05	0.11	0.14	0.27	0.10
329	0.65	0.58	3.18	0.03	0.05	0.10	0.16	0.24	0.09